ANTI-OBESITY: TARGETING BROWN AND BEIGE ADIPOCYTES

EDITED BY: Jiqiu Wang, Karsten Kristiansen and Xinran Ma
PUBLISHED IN: Frontiers in Endocrinology

frontiers Research Topics

ISSN 1664-8714
ISBN 978-2-88974-341-4
DOI 10.3389/978-2-88974-341-4

About Frontiers

Frontiers is more than just an open-access publisher of scholarly articles: it is a pioneering approach to the world of academia, radically improving the way scholarly research is managed. The grand vision of Frontiers is a world where all people have an equal opportunity to seek, share and generate knowledge. Frontiers provides immediate and permanent online open access to all its publications, but this alone is not enough to realize our grand goals.

Frontiers Journal Series

The Frontiers Journal Series is a multi-tier and interdisciplinary set of open-access, online journals, promising a paradigm shift from the current review, selection and dissemination processes in academic publishing. All Frontiers journals are driven by researchers for researchers; therefore, they constitute a service to the scholarly community. At the same time, the Frontiers Journal Series operates on a revolutionary invention, the tiered publishing system, initially addressing specific communities of scholars, and gradually climbing up to broader public understanding, thus serving the interests of the lay society, too.

Dedication to Quality

Each Frontiers article is a landmark of the highest quality, thanks to genuinely collaborative interactions between authors and review editors, who include some of the world's best academicians. Research must be certified by peers before entering a stream of knowledge that may eventually reach the public - and shape society; therefore, Frontiers only applies the most rigorous and unbiased reviews.
Frontiers revolutionizes research publishing by freely delivering the most outstanding research, evaluated with no bias from both the academic and social point of view. By applying the most advanced information technologies, Frontiers is catapulting scholarly publishing into a new generation.

What are Frontiers Research Topics?

Frontiers Research Topics are very popular trademarks of the Frontiers Journals Series: they are collections of at least ten articles, all centered on a particular subject. With their unique mix of varied contributions from Original Research to Review Articles, Frontiers Research Topics unify the most influential researchers, the latest key findings and historical advances in a hot research area! Find out more on how to host your own Frontiers Research Topic or contribute to one as an author by contacting the Frontiers Editorial Office: frontiersin.org/about/contact

ANTI-OBESITY: TARGETING BROWN AND BEIGE ADIPOCYTES

Topic Editors:
Jiqiu Wang, Shanghai Jiao Tong University, China
Karsten Kristiansen, University of Copenhagen, Denmark
Xinran Ma, East China Normal University, China

Citation: Wang, J., Kristiansen, K., Ma, X., eds. (2022). Anti-Obesity: Targeting Brown and Beige Adipocytes. Lausanne: Frontiers Media SA.
doi: 10.3389/978-2-88974-341-4

Table of Contents

frontiers in Endocrinology

REVIEW
published: 23 September 2020
doi: 10.3389/fendo.2020.578830

AMPK in the Ventromedial Nucleus of the Hypothalamus: A Key Regulator for Thermogenesis

Hailan Liu[1,2], *Yong Xu*[2,3] *and Fang Hu*[1]*

[1] Department of Metabolism and Endocrinology, Metabolic Syndrome Research Center, National Clinical Research Center for Metabolic Diseases, The Second Xiangya Hospital of Central South University, Changsha, China, [2] Department of Pediatrics, Children's Nutrition Research Center, Baylor College of Medicine, Houston, TX, United States, [3] Department of Molecular and Cellular Biology, Baylor College of Medicine, Houston, TX, United States

Obesity has become a global health issue, but effective therapies remain very limited. Adaptive thermogenesis promotes weight loss by dissipating energy in the form of heat, thereby representing a promising target to counteract obesity. Notably, the regulation of thermogenesis is tightly orchestrated by complex neuronal networks, especially those in the hypothalamus. Recent evidence highlights the importance of adenosine monophosphate-activated protein kinase (AMPK) within the ventromedial nucleus of the hypothalamus (VMH) in modulating thermogenesis. Various molecules, such as GLP-1, leptin, estradiol, and thyroid hormones, have been reported to act on the VMH to inhibit AMPK, which subsequently increases thermogenesis through the activation of the sympathetic nervous system (SNS). In this review, we summarize the critical role of AMPK within the VMH in the control of energy balance, focusing on its contribution to thermogenesis and the associated mechanisms.

Keywords: AMPK, VMH, SNS, thermogenesis, obesity

OPEN ACCESS

Edited by:
Jiqiu Wang,
Shanghai Jiao Tong University, China

Reviewed by:
Andrew John Whittle,
Stanford University, United States
Miguel López,
University of Santiago de Compostela, Spain

***Correspondence:**
Fang Hu
hu_fang98@csu.edu.cn

Specialty section:
This article was submitted to Cellular Endocrinology, a section of the journal Frontiers in Endocrinology

Received: *01 July 2020*
Accepted: *24 August 2020*
Published: *23 September 2020*

Citation:
Liu H, Xu Y and Hu F (2020) AMPK in the Ventromedial Nucleus of the Hypothalamus: A Key Regulator for Thermogenesis. Front. Endocrinol. 11:578830. doi: 10.3389/fendo.2020.578830

INTRODUCTION

Obesity and its related metabolic disorders, including type 2 diabetes, cardiovascular diseases and cancer, are major health threats which cause thousands of deaths per year in the contemporary society (1). Given the current obesity epidemic, there is a pressing need for novel therapeutic interventions to help people manage their body weight more efficiently (1). Owing to their ability to trigger thermogenesis and enhance energy utilization, brown and beige adipose tissues have recently been identified as a promising target for obesity (2–4). More importantly, accumulating evidence suggests that brown adipocytes are also present in adult humans and are associated with improved metabolic profiles (5, 6). In this sense, therapies aimed at amplifying the thermogenic capabilities of brown and beige adipocytes are of great translational significance.

At the whole-body level, the hypothalamus plays a crucial role in controlling thermogenesis in brown and beige adipose tissues (7). Several hypothalamic nuclei, including the ventromedial (VMH), arcuate (ARH), dorsomedial (DMH), and paraventricular (PVH) nuclei, as well as the

preoptic (POA) and lateral hypothalamic (LHA) areas, have been demonstrated to participate in the regulation of adaptive thermogenesis (8). In particular, the VMH exerts a well-established action on brown adipose tissue (BAT) thermogenesis through its close link with the brainstem areas, including the rostral raphe pallidus (rRPa) and inferior olive (IO), which are involved in modulating BAT function through the SNS (9–11). Electrical stimulation of the VMH increases thermogenesis and BAT temperature, whereas lesions in the VMH inhibit thermogenesis and energy expenditure (12, 13).

As a highly conserved serine/threonine kinase, AMPK integrates peripheral and central metabolic signals to regulate energy homeostasis (14). In addition to its well-established effects on feeding, glucose control and insulin sensitivity, AMPK within the VMH regulates thermogenesis by manipulating the sympathetic firing to BAT and WAT (white adipose tissue) (15–17). For example, deletion of AMPK in the VMH ameliorates diet-induced obesity via exaggerating thermogenesis in BAT and WAT (18). This review intends to provide an insight on several hormonal signals acting on the VMH to control adaptive thermogenesis, with a particular focus on their influences on AMPK and downstream reactions.

THERMOGENIC CAPACITY OF BROWN AND BEIGE ADIPOCYTES: UNDER CONTROL OF THE HYPOTHALAMUS

Brown adipocytes, characterized by a great number of mitochondria and multilocular lipid droplets, are regarded as the major contributor to adaptive thermogenesis (4, 19). BAT has abundant expression of uncoupling protein 1 (UCP1), which dissipates the electrochemical proton gradient through a proton leak in the inner mitochondrial membrane, resulting in the uncoupling of oxidative phosphorylation from ATP synthesis to heat production (20). Sympathetic nerve releases norepinephrine (NE) to activate BAT via the widely distributed β3-adrenergic receptors (β3-ARs) in brown adipocytes, triggering lipolysis and thermogenesis (7, 21). Above all, functional brown adipocytes are found in discrete depots in adult humans and can be induced by sympathetic stimulus, such as cold (5, 6, 22). From this perspective, stimulation of BAT could have therapeutic potentials for long-term management of body weight in obese individuals (23).

In recent years, a novel type of adipocytes has been identified, termed beige adipocytes, which express the thermogenic genes characteristic of those typically associated with brown adipocytes (24). Beige adipocytes could be developed from white adipocytes through various stimulus, including cold, β3-AR agonists, and numerous circulating hormones, such as leptin and fibroblast growth factor 21 (25–27). The process through which white adipocytes turned into beige adipocytes is known as browning (28). Distinct from white adipocytes, which have a large lipid droplet for the storage of excess fat and few UCP1 and mitochondria, beige adipocytes own many similarities with brown adipocytes in both structure and function (29). Particularly, the amount of UCP1 and mitochondria is much more abundant in beige adipocytes than that in white adipocytes (29). In addition, beige adipocytes are densely innervated by sympathetic fibers and can be activated by the SNS (30). Furthermore, beige adipocytes share similar properties as brown adipocytes with respect to UCP1-mediated thermogenesis (31). Remarkably, clinical studies have revealed that chronic cold exposure promotes the recruitment of beige adipocytes in humans, which is associated with improved insulin sensitivity, glucose and lipid homeostasis (32–34). In particular, the increased glucose uptake ability and endocrine factors secreted by brown and beige fat are considered to play important roles in ameliorating the metabolic abnormalities in obese individuals (35).

Among numerous brain regions, the hypothalamus receives and integrates hormonal and neuronal signals that relay metabolic status of the body, hence plays a major role in controlling adaptive thermogenesis (36). The SNS mediates the crosstalk between the hypothalamus and adipose tissues (37). Anatomically, the POA, VMH, DMH, ARH, PVH, and LHA have direct or indirect connections with the sympathetic preganglionic neurons in the spinal cord (38). Stimulation of the aforementioned hypothalamic nuclei increases the sympathetic tone to BAT, and tonic inhibition of neurons in many of these areas reduces BAT activity (38). Specifically, the ARH contains proopiomelanocortin (POMC) and agouti-related-peptide (AgRP) expressing neurons, which are key components of the melanocortin system that accounts for the regulation of food intake and adaptive thermogenesis (39). POMC and AgRP neurons orchestrate feeding behavior and thermogenesis mainly by releasing several key neuropeptides or neurotransmitters, like α-melanocyte-stimulating hormone (α-MSH), AgRP, neuropeptide Y (NPY), and γ-aminobutyric acid (γ-GABA) (39, 40). These molecules act on their broadly distributed receptors in the central nervous system (CNS) to affect appetite and SNS-mediated thermogenesis (39, 41, 42). In parallel, the participation of the VMH in thermoregulation has been confirmed by emerging evidence. Ablation of steroidogenic factor-1 (SF-1), a transcription factor expressed exclusively in the VMH within the brain, impairs BAT thermogenesis without altering food intake (43). More remarkably, accumulating data point out that several key homeostatic signals act on the VMH to inhibit AMPK activity, which in turn stimulates BAT thermogenesis and WAT browning through the SNS (44).

HORMONAL REGULATION OF THERMOGENESIS THROUGH THE VMH: HIGHLIGHTING THE CANONICAL ROLE OF AMPK

The capacity of brown and beige adipocytes to increase adaptive thermogenesis is predominately governed by the hypothalamus through the regulation of the sympathetic outflows (8). Among various hypothalamic nuclei, the VMH plays a fundamental part in modulating BAT function given the fact that VMH neurons are anatomically linked to the rRPa and IO, which perform well-established actions on BAT thermogenesis through the SNS (10,

11, 45). Intra-VMH administration of glutamate or NE increases the activity of neurons in the rRPa and IO, leading to elevated BAT temperature. However, the increase in BAT temperature is abrogated by prior treatment with sympathetic ganglionic blockers or β-AR antagonists, confirming the functional significance of the SNS in mediating VMH stimulation-induced BAT thermogenesis (46–48). Additionally, mice lacking SF-1 or estrogen receptor α (ERα) in the VMH develop an obese phenotype characterized by significantly decreased UCP1 expression in BAT (43, 49). Peripheral signals, such as thyroid hormones (THs), glucagon-like peptide-1 (GLP-1), estradiol (E2), bone morphogenetic proteins (BMP8B), and leptin, act on the VMH to promote BAT thermogenesis and WAT browning (16, 17). Notably, the involvement of endoplasmic reticulum (ER) stress within the VMH in thermoregulation has been uncovered by increasing evidence. Pharmacological and genetic manipulations that exaggerate ER stress in the VMH impair BAT thermogenesis and accelerate the development obesity (50, 51). On the contrary, alleviating ER stress in the VMH is sufficient to improve BAT function and ameliorate diet-induced obesity (51–53). Taken together, these results indicate that the VMH plays an essential role in the regulation of adaptive thermogenesis.

AMPK, an intracellular energy sensor, is composed of a catalytic subunit, α (α1, α2), and two regulatory subunits, β (β1, β2) and γ (γ1, γ2, γ3) (54, 55). The catalytic activity of AMPK is triggered by the phosphorylation of Thr172 on the α subunit, a process initiated by ATP deprivation and inhibited by nutrient supplementation (56). AMPK can also be activated by several upstream kinases, such as liver kinase B1 (LKB1) and calmodulin-dependent kinase kinases (CaMKKs) (57–59). AMPK activation in the hypothalamus augments food intake and diminishes energy expenditure, whereas its inhibition suppresses appetite and increases energy utilization (7, 60, 61). Nevertheless, it is noteworthy that AMPK within the VMH mediates the thermogenic effects of numerous peripheral signals in a feeding independent manner (12, 62, 63). Many hormones, such as THs, GLP-1, E2, BMP8B, and leptin, amplify the sympathetic tone to BAT and WAT by inhibiting AMPK activity in the VMH, resulting in enhanced thermogenesis and energy dissipation independent on food intake (16, 52, 64–66). In stark contrast, constitutive activation of AMPK within the VMH reverses the thermogenic effects of these molecules without altering feeding behavior, verifying the important role of AMPK within the VMH in orchestrating BAT thermogenesis and WAT browning (62, 67). In the following sections of this review, we will discuss several key circulating hormones that act on the VMH to modulate AMPK activity, which subsequently contributes to the control of thermogenesis in BAT and WAT via the SNS.

Thyroid Hormones (THs)

THs, including triiodothyronine (T3) and thyroxine (T4), regulate a vast range of physiological activities, including growth, development, metabolism, and energy balance (68). The involvement of THs in energy balance has been clearly demonstrated by the phenomenon that the impairment in thyroid function is often accompanied by alterations in food intake and body weight. Hyperthyroidism is linked to hyperphagia and weight loss, whereas hypothyroidism causes appetite suppressing and weight gain (69). THs were originally thought to exert their effects on energy homeostasis by directly acting on peripheral tissues, such as the brown and white adipose tissues, muscle, heart, and liver (70). However, recent data indicate that THs modulate food intake, energy expenditure and body weight by acting, to a large extent, at the central level (70, 71). In support of this view, the α1, α2, β1, and β2 THs receptor (TR) isoforms were found to be widely distributed in the CNS, with the highest expression levels in metabolically active regions, such as the VMH, ARH, and PVH (72).

The significance of the CNS in mediating the effects of THs on energy balance was firstly confirmed by brain specific TRα1 mutant mice, which had elevated T3 concentrations in the hypothalamus and displayed higher food intake, metabolic rate and BAT thermogenic capability (73). In consistent with this, central injection of T3 increases energy expenditure by stimulating BAT thermogenesis and WAT browning (17, 52, 74). UCP1 plays an essential role in mediating T3-induced increase in energy expenditure, and deletion of UCP1 completely abolishes the thermogenic action of central T3 (15). Notably, inactivation of TR in the VMH of hyperthyroid rats blunts weight loss and decreases the expression of thermogenic markers in BAT without concomitant influences on food intake (74), suggesting that the VMH is a key region mediating the thermogenic effect of THs on BAT. Recently, the critical role of AMPK within the VMH in modulating T3-induced alterations in thermogenesis has been revealed by several studies. First, constitutive activation of AMPK within the VMH abrogates T3-induced weight loss and UCP1 expression in BAT and WAT (52). Second, pharmacological or genetic inactivation of AMPK in the VMH fully recapitulates the thermogenic actions of central T3 on BAT and WAT, and such effects could be abolished by application of the β3-AR antagonists (74). Third, ablation of AMPKα1 in SF-1 neurons mimics the actions of T3 in the VMH by enhancing BAT thermogenesis and WAT browning, which in turn protects mice from diet-induced obesity (18, 52). Remarkably, manipulation of AMPK in the VMH selectively impacts the thermogenic aspect of T3 without affecting food intake (18, 52). In brief, these data indicate that THs act centrally to promote BAT thermogenesis and WAT browning via suppressing AMPK activity in the VMH.

Interestingly, current work has demonstrated that ER stress in the VMH plays a role in THs-induced thermogenesis. Hyperthyroid rats exhibit lower hypothalamic ceramide and ER stress levels, which can be reversed by the activation of AMPK in the VMH (52). In contrast, increasing ceramide levels as well as pharmacologically or genetically inducing ER stress in the VMH blunts the effect of central THs on thermogenesis in BAT and WAT (52). This is in line with previous studies which found that alleviation of ER stress by overexpressing the glucose-regulated protein 78 (GRP78), a major ER chaperone protein, in the VMH is sufficient to ameliorate obesity by facilitating BAT thermogenesis and WAT browning (51). These findings support the notion that THs inhibits AMPK activity in the VMH, resulting in reduced ER stress levels, which in turn promotes BAT thermogenesis and WAT browning.

However, some critical limitations of these studies need to be taken into consideration. For example, given its diffusion property, it is likely that adenovirus-mediated manipulation of AMPK or TR or GRP78 is not restricted to the VMH. The involvement of other nuclei in thermoregulation requires more careful evaluation. VMH-specific drug delivery has the same issue. Furthermore, although deleting AMPKα1 in SF-1 neurons reflects functions of the AMPKα1 isoform in the majority of VMH neurons, the role of AMPKα1 deficiency-induced compensatory changes, such as elevated AMPKα2 levels, warrants further investigation.

Except for adipose tissues, THs act centrally to modulate lipid metabolism in the liver. Intra-VMH injection of T3 promotes hepatic lipid accumulation via c-JunN-terminal kinase 1 (cJNK1)-mediated activation of the vagus nerve innervation to liver, which is under control of AMPK but not ER stress (52). Whether AMPK within the VMH mediates the effects of THs on other organs remains to be determined.

Glucagon-Like Peptide-1 (GLP-1)

GLP-1 is primarily synthesized and secreted by the intestinal L-cells to increase glucose-induced insulin release and decrease glucagon secretion in response to a nutrient load (75). However, GLP-1 secretion is impaired in patients with T2D and obesity (76, 77). GLP-1 agonists are clinically used drugs for T2D, with additional benefits of weight loss and a low risk of hypoglycemia (78, 79). GLP-1 receptors (GLP-1Rs) are expressed in a broad range of neuronal populations, including in many hypothalamic nuclei crucial for the regulation of energy balance (80, 81). In addition, GLP-1 positive cells were found to be distributed in numerous human brain regions (82). Moreover, circulating GLP-1 and its analogs could be transported to the brain and activate neurons in various areas of the CNS (83). Interestingly, GLP-1 is also produced by a small population of preproglucagon neurons located in the brainstem nucleus of the solitary tract (NTS), which project to the hypothalamus to regulate appetite (84, 85).

Liraglutide, a long-acting GLP-1 analog, improves glucose homeostasis and reduces body weight in obese diabetic patients (79). Apart from its participation in glycemic control, liraglutide acts centrally to lower food intake and increase energy expenditure (16, 86). Central injection of liraglutide promotes weight loss via suppressing appetite and increasing energy dissipation, the latter is associated with enhanced lipolysis in WAT and thermogenesis in BAT (87, 88). Particularly, administrating liraglutide into the ARH, PVH or LH decreases food intake and body weight, but does not alter UCP1 expression in BAT and WAT. In opposite, intra-VMH injection of liraglutide has no significant influence on food intake but elevates UCP1 levels in BAT and WAT, resulting in obvious weight loss (16). Thus, central liraglutide participates in the regulation of food intake and energy expenditure by engaging in different hypothalamic nuclei (16, 89). Furthermore, β3-AR antagonists block central liraglutide-induced elevation of UCP1 in BAT and WAT, indicating that the SNS mediates the actions of liraglutide on BAT thermogenesis and WAT browning (16, 89). More importantly, central delivery of liraglutide decreases AMPK activity in the VMH (16). Pharmacological or genetic activation of AMPK in the VMH abolishes the actions of liraglutide on thermogenesis without corresponding alterations in feeding (16), verifying the importance of AMPK within the VMH in mediating liraglutide-induced thermogenesis. Nevertheless, potential engagement of AMPK in adjacent regions of VMH in thermoregulation should be assessed, given the inherent shortcomings of the studies that were analyzed earlier. The thermogenic effects of liraglutide rely on GLP-1Rs, mice lacking the GLP-1Rs in the CNS fail to show any obvious change in BAT temperature or thermogenic markers after the application of liraglutide (89). However, these mutant mice display a normal thermogenic response to cold exposure (89), indicating that endogenous GLP-1Rs are essential for liraglutide-induced thermogenesis but are dispensable for appropriate thermogenic response to cold.

On top of improving glucose control, liraglutide also reduces body weight in obese individuals (90). The weight reducing effects of liraglutide on human subjects have been confirmed by many clinical studies, although whether the decrease in body weight is linked to increased energy expenditure or not remains elusive (91, 92). Recently, the US Food and Drug Administration (FDA) committee has approved the application of liraglutide as an anti-obesity therapy. Other GLP-1 analogs, such as exendin-4, can act on the hypothalamus to inhibit AMPK, thereby suppressing appetite and body weight (93–95). However, the involvement of exendin-4 in the regulation of energy expenditure and the participation of AMPK within the VMH in this process are not clear, and additional work will be necessary to address these questions.

Estrogens

In addition to their critical role in the control of puberty, reproduction, growth, and development, estrogens act both centrally and peripherally to regulate energy balance (96, 97). Physiological, pathological, pharmacological, or genetically-induced estrogen deficiency promotes obesity by increasing appetite and reducing energy expenditure, which could be reversed by estrogen replacement (98, 99). Despite that E2 can modulate metabolism by directly acting on peripheral tissues, emerging evidence suggests that the hypothalamus mediates a large part of the actions of E2 on energy balance (100). For instance, estrogens receptors (ERs), including ERα and ERβ, are highly expressed in the hypothalamus (101, 102). ERα is believed to be the major mediator of the effects of estrogens on energy homeostasis. Food intake and body weight are suppressed by central administration of the ERα agonist propylpyrazole triol (PPT), but not by the selective ERβ agonist diarylpropionitrile (DPN) (103, 104). In addition, female mice with a targeted deletion of the ERα gene develop obesity, primarily due to decreased energy expenditure (99). Ablation of ERβ causes no obvious change in body weight under chow condition, but it promotes fat accumulation and improves insulin sensitivity after challenging with high fat diet (105).

Interestingly, estrogens participate in the regulation of food intake and energy expenditure by engaging in different hypothalamic neuronal populations. Disruption of ERα in POMC neurons augments food intake without affecting energy

expenditure (106). On the contrary, silencing ERα within the VMH suppresses energy expenditure with no concomitant alterations in feeding behavior. The same phenotype is recapitulated by ablating ERα in SF1 neurons of the VMH (49, 106). More specifically, the decreased energy expenditure in mice lacking ERα in SF-1 neurons is related to impaired BAT thermogenesis as demonstrated by reduced UCP1 levels in BAT. Administration of E2 into the VMH increases energy expenditure by amplifying the sympathetic outflow to BAT and WAT, which is associated with diminished AMPK activity in the VMH (64). Genetic activation of AMPK in the VMH blunts E2-induced weight loss and activation of thermogenesis in BAT and WAT (64), suggesting that E2 promotes BAT thermogenesis and WAT browning through suppressing AMPK in the VMH.

A recent study found that central injection of E2 alleviates ER stress levels in the hypothalamus through decreasing hypothalamic ceramide levels (53). Additionally, blocking ceramide synthesis in E2 deficient rats attenuates ER stress in the VMH and recapitulates the thermogenic effects of central E2 (53). Similarly, pharmacological or genetic inhibition of ER stress in the VMH of ovariectomized (OVX) rats increases BAT temperature and UCP1 expression, which mimics the outcome of E2 supplementation (53). Together, these findings support the notion that E2-induced decrease of ER stress in the VMH contributes to the maintenance of energy balance by modulating BAT thermogenesis. Considering that AMPK inactivation suppresses ER stress within the VMH, which also mediates the effects of central THs on BAT thermogenesis (52), it is possible that the AMPK (VMH)-ER stress-BAT axis might represent a canonical pathway that underlies hormonal and neuronal control of thermogenesis.

Except for ERα and SF-1 neurons, the role of AMPK in other VMH cell types in regulating E2-induced thermogenesis lacks thorough investigation. For example, it has been reported that hypothalamic kisspeptin/neurokinin B/dynorphin (KNDy) neurons are involved in the modulation of body temperature by E2, but whether AMPK in the VMH participates in this process remains to be clarified (107). Moreover, it is noteworthy that the thermogenic effects of E2 are diminished during gestation (108). Although hypothalamic AMPK signaling is inhibited by high circulating E2 levels, pregnant animals exhibit reduced temperature and BAT function (108). These observations raise the hypothesis that pregnancy promotes a state of resistance to the actions of E2, which may partially account for the gestational hyperphagia and fat accumulation to meet the metabolic demands of embryonic development (108). Unraveling the underlying mechanisms of E2 resistance may facilitate the development of new strategies to counteract obesity. Notably, the GLP-1-estrogen conjugate, which is designed to activate estrogen receptors in GLP-1 targeted tissues, has superior efficiency over either of the individual hormones to overcome obesity, hyperglycemia, and dyslipidemia while at the same time prevents hallmark side effects of estrogen such as reproductive toxicity and oncogenicity (109). GLP-1Rs deletion in the brain abrogates the beneficial metabolic consequences of the GLP-1-estrogen conjugate, indicating the CNS is a key action site for this chimera (109). Based on these findings, the use of peptide chimeras appears to be a promising approach in the context of overcoming obesity, but the underlying principles require further elucidation.

BMP8B

Bone morphogenetic proteins (BMPs) belong to the transforming growth factor β (TGFβ) superfamily and regulate a wide range of physiological processes from embryonic development to tissue homeostasis (110). In recent years, BMPs have been discovered to play a key role in the differentiation and development of BAT as well as in the maintenance of energy balance (110–112). Among the BMPs superfamily, BMP8B is expressed in BAT and the hypothalamus, and is involved in the regulation of BAT function and thermogenesis (113). Central administration of BMP8B increases BAT temperature and the activity of the SNS, resulting in reduced body weight (65). More specifically, intracerebroventricular injection of BMP8B stimulates neuronal activation in both the VMH and LHA (65). Nevertheless, injection of BMP8B into the VMH, rather than the LHA, promotes weight loss and enhances BAT thermogenesis and WAT browning without altering feeding behavior, suggesting the VMH is a direct targeting site for BPM8B (65, 114). Furthermore, the thermogenic action of central BMP8B is AMPK-dependent. BMP8B administration decreases AMPK activity in the VMH, while activation of AMPK within the VMH diminishes BMP8B-induced UCP1 expression in BAT and WAT (65, 114).

Interestingly, central injection of BMP8B stimulates UCP1 expression in brown and white adipocytes in females but not males, indicating that the thermogenic action of central BMP8B is sexually dimorphic (114). In addition, central administration of BMP8B fails to activate the thermogenic program in BAT and WAT in OVX female rats. E2 replacement restores the thermogenic response to BMP8B in OVX rats, further supporting that the presence of E2 is required for BMP8B to fully perform its function on thermogenesis (114). Nevertheless, it is not yet clear how E2 mediates the action of BMP8B, and future work is necessary for clarifying this issue.

Despite BMP8B cannot directly activate neurons in the LHA, central administration of BMP8B increases orexin (OX) levels in the LHA, which is relevant to the inhibition of AMPK within the VMH. Conversely, constitutive activation of AMPK within the VMH reduces BMP8B-induced elevation of OX in the LHA (114). Furthermore, rats pre-treated with SB-334867, an antagonist of OX receptor1 (OX1R), show significantly blunted thermogenic response to BMP8B without affecting AMPK signaling in the VMH, suggesting OX1R signaling is indispensable for the thermogenic actions of BMP8B and is a downstream mediator of AMPK (114). Suppressing glutamatergic signaling in the LHA by deleting GLUT2 (glutamate vesicular transporter 2) abolishes the effects of central BMP8B on BAT thermogenesis and reduces OX levels in the LHA, but has no significant influence on AMPK activity in the VMH, indicating that glutamatergic signaling acts downstream of AMPK to up-regulate OX expression in the LHA (114). Collectively, these results demonstrate that the thermogenic effects of BMP8B are mediated by the inhibition of AMPK in the VMH, the activation of glutamatergic signaling in the LHA, and the subsequent increase of OX levels (114).

Leptin

Leptin is a circulating hormone secreted by white adipocytes in proportion to fat mass and informs the brain the status of energy storage (115, 116). Leptin exerts its effects on energy balance mainly by acting on the long-form isoform of leptin receptor (LepRb), which is abundantly expressed in the hypothalamus, including the ARH and VMH (117–119). Mice lacking leptin or leptin receptor encoding genes exhibit morbid obesity associated with hyperphagia and low metabolic rate (115, 120). Re-expression of LepRb in the brain reverses obesity and its related metabolic disorders in LepRb null mutant mice, suggesting the metabolic actions of leptin are largely mediated by the central nervous system (121, 122).

LepRb is a member of the class 1 cytokine receptor superfamily that possesses endogenous tyrosine activity (117). The Janus kinase 2/signal transducer and activator of transcription 3 (JAK2/STAT3) pathway is considered as the central mediator of the weight-reducing effects of leptin (123, 124). Central injection of leptin promotes STAT3-dependent transcription of POMC gene, while at the same time inhibiting the expression of AgRP and NPY, thus suppressing appetite and enhancing thermogenesis and energy expenditure (124). Additionally, leptin recruits others signaling networks, such as the phosphatidylinositol 3 kinase/protein kinase B (PI3K/AKT), mammalian target of rapamycin complex 1 (mTORC1) and AMPK pathways to modulate food intake and energy expenditure (60, 125–127). Noticeably, AMPK coordinates with PI3K/AKT and mTORC1 signals to fully facilitate the functions of leptin in the hypothalamus (128, 129). For example, leptin stimulation promotes the phosphorylation of AMPK at ser485 and ser491 in the hypothalamus through the activation of the PI3K-AKT- mTORC1 pathway, which in turn attenuates AMPK activity, leading to reduced food intake (128).

The melanocortin system is believed to play indispensable roles in controlling leptin induced suppression of food intake and body weight (130). Deletion of lepRb in POMC or AgRP neurons results in hyperphagia and obesity (131, 132). Similarly, the VMH has been identified as a key reaction site for leptin, VMH specific SF-1 knockout mice display leptin resistance and are susceptible to diet-induced obesity (133). Leptin directly depolarizes SF-1 neurons in the VMH (134). Ablation of lepRb selectively in SF-1 neurons exaggerates diet-induced obesity, which is accompanied by impaired thermogenesis, indicating lepRb in SF-1 neurons is required for appropriate thermogenic response to overnutrition (134, 135). Furthermore, recent evidence has revealed the involvement of hypothalamic AMPK in mediating the thermogenic actions of leptin (136). Central injection of leptin inhibits hypothalamic AMPK activity and amplifies sympathetic drive to adipose tissues (137). In contrast, constitutive activation of AMPK in the hypothalamus prevents the ability of leptin to increase the sympathetic tone to BAT (60). More specifically, inhibition of the AMPK α2 isoform in the VMH mimics the thermogenic actions of leptin and prevents leptin to further enhance BAT activity, suggesting AMPK within the VMH is at least partially responsible for leptin-stimulated thermogenesis (137).

Additionally, mice lacking protein tyrosine phosphatase 1B (PTP1B), a negative regulator of leptin signaling, in the brain exhibit reduced UCP1 expression in BAT, which is associated with diminished AMPK activity in the hypothalamus (136). Nevertheless, whether AMPK within the VMH contributes to central PTP1B deficiency induced thermogenesis remains to be elucidated, creating and characterizing animal models with PTP1B deletion in the VMH may shed light on this question. Moreover, ablation of the suppressor of cytokine signaling 3 (SOCS3) in SF-1 neurons enhances leptin sensitivity and promotes modest weight loss during lactation, although food intake is not affected (138). However, the role of AMPK in this process warrants further investigation.

ER STRESS IN THE VMH: LINKING AMPK TO THERMOGENESIS?

The ER is a dynamic organ where proteins are matured, assembled and folded (139, 140). Improperly folded proteins are normally delivered to the ER for degradation (139). However, strong and prolonged cellular perturbations may alter ER homeostasis, leading to the accumulation of potentially toxic misfolded proteins and ER stress (141). Evidence accumulated in the past years has revealed a close relationship between ER stress and obesity (141). Particularly, genetic and diet-induced obesity models are associated with elevated ER stress levels in the hypothalamus (142). Central injection of ER stress inducers, such as tunicamycin or thapsigargin, accelerates the development of obesity (52, 143). In contrast, alleviating ER stress by treating obese animals with chemical chaperones, like tauroursodeoxycholic acid (TUDCA) or 4-phenylbutyrate (4-PBA), increases leptin sensitivity and attenuates the risk of obesity (53). Very recently, Contreras and colleagues found that the impaired thermogenesis in BAT and WAT of obese rats is closely related to the elevated ER stress levels in the VMH (51). Intra VMH injection of ceramide triggers ER stress, resulting in an obese phenotype characterized by decreased thermogenic markers in BAT and WAT (51). Inducing ER stress by inhibiting GRP78 in the VMH, but not in the ARH, increases body weight and decreases UCP1 concentrations in BAT (52). Conversely, overexpressing GRP78 in the VMH reduces ER stress, enhancing thermogenesis in BAT and WAT and improving metabolic profiles in obese animals (51, 144), suggesting that ER stress in the VMH plays a critical role in regulating thermogenesis and energy balance.

It is interesting that peripheral signals, such as THs, GLP-1, E2, BMP8B, and leptin, act on the VMH to inhibit AMPK, which subsequently enhances BAT thermogenesis through activating the SNS (16, 52, 64, 66, 114). Both THs and E2 have been reported to suppress AMPK in the VMH and alleviate ER stress in the hypothalamus (52, 53). Inactivation of AMPK within the VMH reduces ER stress levels, whereas constitutive activation of AMPK prevents T3-induced down-regulation of ER stress (52), indicating AMPK acts as an upstream regulator of ER stress in the VMH. Currently, the detailed mechanisms through

which AMPK affects ER stress are not fully understood. One acknowledged explanation is that AMPK alters cellular lipid composition by regulating its downstream mediator carnitine palmitoyltransferase 1 (CPT-1), resulting in elevated intracellular ceramide contents, which cause lipotoxicity and trigger the initiation of ER stress (52). In line with this observation, mice lacking CPT-1C display higher hypothalamic ER stress levels and body weight as well as impaired thermogenic response to short-term HFD exposure (145). Given the fact that THs, GLP-1, E2, BMP8B and leptin all stimulate BAT thermogenesis by inhibiting AMPK within the VMH and the close relationship between hypothalamic AMPK and ER stress (16, 52, 64, 66, 114), the VMH AMPK-ER stress-BAT axis may represent a canonical pathway for multiple peripheral signals that act on the VMH to control thermogenesis, although more studies are needed to further testify this hypothesis.

TARGETING AMPK WITHIN THE VMH TO COUNTERACT OBESITY

AMPK is a major energy regulator which exerts opposite actions regarding metabolism in the CNS and the periphery (146–148). On the one side, activation of AMPK promotes fatty acid oxidation and lipolysis in skeletal muscle, and diminishes glucose production in liver, contributing to the maintenance of lipid and glucose homeostasis (149, 150). On the other side, AMPK activation in the hypothalamus augments food intake and suppresses energy expenditure, promoting the development of obesity (146). Therefore, neither systematic activation nor inhibition of AMPK would be a good strategy for the treatment of obesity. In addition, although AMPK has been explored as a pharmacological target for years, the potential cardiac toxicity effects of systematically administrated AMPK activators prevent their clinical application. Therefore, site specific manipulation of AMPK is necessary in order to achieve better outcomes.

Both the VMH and LHA are important areas responsible for the control of food intake and adaptive thermogenesis (151–155). Previous virus tracing experiments have demonstrated that SF-1 neurons in the VMH project to and terminate in the LHA, providing evidence that these two nuclei are anatomically connected (10, 156). On the other hand, the AMPK (VMH)–glutamate- OX (LHA) pathway unravels a molecular basis for the functional interplay between these two major areas for the modulation of BAT thermogenic activity (114). It is of interest to test whether the AMPK (VMH)–glutamate- OX (LHA)-SNS-BAT axis is a universal determinant mechanism for peripheral hormones to regulate BAT thermogenesis (16, 52, 64, 65). Obviously, addressing this question is of considerable significance if we wish to fully understand the hormonal and neuronal control of BAT thermogenesis and may pave the way for developing novel therapies to overcome obesity.

Activation of rat-insulin-promoter-cre (RIP-Cre) neurons in the VMH preferentially promotes the recruitment of beige fat but has no effect on BAT (157). In contrast, inhibiting AMPKα1 activity in SF-1 neurons increases thermogenesis in both BAT and WAT (18). Additionally, central administration of BMP8B increases the sympathetic outflow to BAT but does not alter the sympathetic tone to kidney (114). These findings together indicate that the sympathetic innervations to different organs might be orchestrated by distinct subsets of neurons in the CNS. Notably, obesity is accompanied by elevated sympathetic tone to the cardiovascular system, which is a major contributor to obesity-related hypertension and heart disease (158). Hence, in order to stimulate thermogenesis specifically in adipocytes while circumventing detrimental cardiovascular effects, systematically examining the sympathetic connections between the VMH and peripheral tissues is necessary.

Furthermore, AMPK within the VMH plays a crucial role in the detection of acute hypoglycemia and the initiation of the glucose counter-regulatory response (159–162). Thereby, the potential hypoglycemic risk should be taken into consideration before the application of AMPK inhibitors. Nevertheless, it is noteworthy that the α1, but not the α2, isoform of AMPK within the VMH is mainly responsible for BAT thermogenesis and WAT browning (16, 18, 52). Conversely, the AMPK α2, but not the α1, isoform is a key contributor to the hypoglycemia regulation in the VMH (159–161). In this sense, delicately designed drugs that specifically inhibit the AMPK α1, but not the α2, isoform might be helpful to selectively enhance adaptive thermogenesis and at the same time circumvent the hypoglycemia issue.

Nevertheless, even though AMPK serves as a promising target for obesity in a number of animal models, plenty of difficulties need to be addressed before the clinical application of drugs that modify AMPK in treating human obesity. Firstly, due to the multifaceted actions of AMPK in different organs, site-specific manipulation of AMPK is required but hard to achieve in humans. Besides, the advancement of technology allows for region-selective or even neuron-selective gene manipulations in experimental animals, but targeting specific brain areas in humans remains challenging. In addition, central regulation of thermogenesis requires intact sympathetic innervations to adipocytes. Obesity is often accompanied by impaired sympathetic nerve distributions in fat tissues (163), which may jeopardize the anti-obesity effects of AMPK inhibition in the VMH. Moreover, while the β-AR agonist Mirabegron robustly stimulates glucose uptake in BAT of healthy adult humans (164), administration of a panadrenergic agonist Ephedrine produces minimal effects on BAT activity in obese subjects (165), suggesting the development of β-AR resistance in obesity. Finally, the distribution and regulation of brown and beige adipocytes in humans are not the same as that of rodents. Therefore, whether orchestrating AMPK within the VMH in humans would produce similar beneficial metabolic outcomes waits to be tested.

CONCLUDING REMARKS

As summarized in **Figure 1**, the importance of AMPK within the VMH in regulating thermogenesis is demonstrated by the fact that central THs, GLP-1, E2, BMP8B, and leptin all increase BAT thermogenesis and WAT browning by inhibiting AMPK in the VMH (16, 52, 64–66). Furthermore, ER stress in the

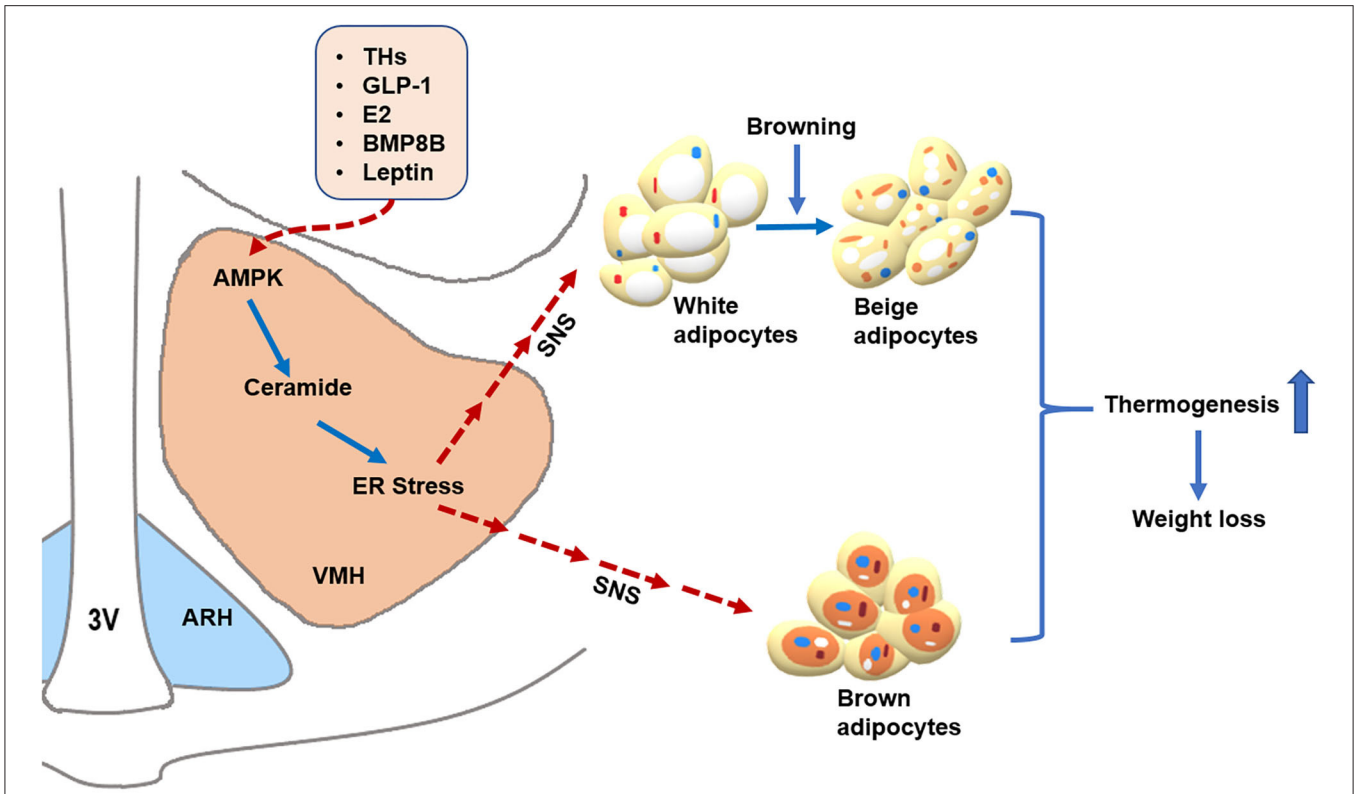

FIGURE 1 | AMPK within the VMH regulates BAT thermogenesis and WAT browning. Peripheral signals, such as THs, GLP-1, E2, BMP8B, and leptin, may act on the VMH to inhibit AMPK, which subsequently promotes BAT thermogenesis and WAT browning through activating the SNS, resulting in body weight loss. Additionally, THs and E2 may decrease ceramide and ER stress levels by suppressing AMPK in the VMH, leading to enhanced thermogenesis via the SNS. Alleviating ER stress in the VMH also increases hypothalamic leptin sensitivity. Whether ceramide and ER stress can mediate the thermogenic effects of GLP-1 and BMP8B warrant further investigation. The solid blue arrows represent activation, the dotted red arrows represent inhibition. 3V: third ventricle. ARH: arcuate nucleus of the hypothalamus. VMH: ventromedial nucleus of the hypothalamus. AMPK: adenosine monophosphate-activated protein kinase. ER stress: endoplasmic reticulum stress. SNS: sympathetic nervous system. THs: thyroid hormones. GLP-1: glucagon-like peptide-1. E2: estrogens. BMP8B: Bone morphogenetic protein 8B.

VMH mediates the effects of AMPK on thermogenesis (52), suggesting that ER stress is another useful target for obesity. Chemical chaperones, like TUDCA and 4-PBA, are sufficient to reduce hypothalamic ER stress and thereby decreases the risk of obesity (51, 52). More importantly, clinical evidence indicates that some of these chemical chaperones have high safety profiles in humans (166, 167). Thus, designing drugs that act specifically on the VMH to inhibit AMPK or ER stress might represent a promising approach for fighting against obesity.

Currently, there are still some fundamental questions that need to be addressed to fully uncover the role of AMPK in the VMH. First, although recent studies have demonstrated that SF-1 neurons are the key neuronal population which mediates the regulatory effect of AMPK on thermogenesis (18), the involvement of other neuronal populations in thermoregulation is poorly understood. Second, THs and E2 also reduce ER stress in the hypothalamus by inhibiting AMPK in the VMH, which contributes to the thermogenic actions of these hormones (52, 53). It is of significance to explore whether ER stress is a common downstream mediator for the thermogenic effects of THs, GLP-1, E2, BMP8B, and leptin. Third, how different hormones act on the VMH to inhibit AMPK is another question that warrants further investigation. Fourth, a better understanding of how VMH neurons regulate sympathetic outflow to different organs is required for avoiding undesirable side effects.

Overall, considering the critical role of AMPK within the VMH in regulating thermogenesis and the existence of brown and beige adipocytes in adult humans, more investigations are needed to expand our understanding of the neuronal and hormonal control of adaptive thermogenesis and the role of AMPK within the VMH in this process. Addressing these questions may facilitate the development of drugs that are specifically targeted at AMPK within the VMH to enhance thermogenesis and reduce body weight as well as bypass unexpected detrimental effects.

AUTHOR CONTRIBUTIONS

HL organized and wrote the manuscript. YX provided constructive comments. FH revised the manuscript.

All authors contributed to the article and approved the submitted version.

FUNDING

This work was supported by the National Natural Science Foundation of China (91957113, 31871180), the Nature Science Foundation of Hunan Province (2019JJ 40410) to FH, and by China Scholarship Council to HL (201906370218).

ACKNOWLEDGMENTS

We thank Dr. Hesong Liu's assistance in making the figure. We thank Shirley Pan for language editing.

REFERENCES

1. Collaborators GBDO, Afshin A, Forouzanfar MH, Reitsma MB, Sur P, Estep K, et al. Health effects of overweight and obesity in 195 countries over 25 years. *N Engl J Med*. (2017) 377:13–27. doi: 10.1056/NEJMoa1614362
2. Betz MJ, Enerback S. Targeting thermogenesis in brown fat and muscle to treat obesity and metabolic disease. *Nat Rev Endocrinol*. (2017) 14:77–87. doi: 10.1038/nrendo.2017.132
3. Castro E, Silva TEO, Festuccia WT. Critical review of beige adipocyte thermogenic activation and contribution to whole-body energy expenditure. *Horm Mol Biol Clin Investig*. (2017) 31. doi: 10.1515/hmbci-2017-0042
4. Cohen P, Spiegelman BM. Brown and beige fat: molecular parts of a thermogenic machine. *Diabetes*. (2015) 64:2346–51. doi: 10.2337/db15-0318
5. Cypess AM, Lehman S, Williams G, Tal I, Rodman D, Goldfine AB, et al. Identification and importance of brown adipose tissue in adult humans. *N Engl J Med*. (2009) 360:1509–17. doi: 10.1056/NEJMoa0810780
6. van Marken Lichtenbelt WD, Vanhommerig JW, Smulders NM, Drossaerts JM, Kemerink GJ, Bouvy ND, et al. Cold-activated brown adipose tissue in healthy men. *N Engl J Med*. (2009) 360:1500–8. doi: 10.1056/NEJMoa0808718
7. Morrison SF, Madden CJ, Tupone D. Central neural regulation of brown adipose tissue thermogenesis and energy expenditure. *Cell Metab*. (2014) 19:741–56. doi: 10.1016/j.cmet.2014.02.007
8. Contreras C, Nogueiras R, Dieguez C, Medina-Gomez G, Lopez M. Hypothalamus and thermogenesis: heating the BAT, browning the WAT. *Mol Cell Endocrinol*. (2016) 438:107–15. doi: 10.1016/j.mce.2016.08.002
9. Cano G, Passerin AM, Schiltz JC, Card JP, Morrison SF, Sved AF. Anatomical substrates for the central control of sympathetic outflow to interscapular adipose tissue during cold exposure. *J Comp Neurol*. (2003) 460:303–26. doi: 10.1002/cne.10643
10. Lindberg D, Chen P, Li C. Conditional viral tracing reveals that steroidogenic factor 1-positive neurons of the dorsomedial subdivision of the ventromedial hypothalamus project to autonomic centers of the hypothalamus and hindbrain. *J Comp Neurol*. (2013) 521:3167–90. doi: 10.1002/cne.23338
11. Uno T, Shibata M. Role of inferior olive and thoracic IML neurons in nonshivering thermogenesis in rats. *Am J Physiol Regul Integr Comp Physiol*. (2001) 280:R536–46. doi: 10.1152/ajpregu.2001.280.2.R536
12. Perkins MN, Rothwell NJ, Stock MJ, Stone TW. Activation of brown adipose tissue thermogenesis by the ventromedial hypothalamus. *Nature*. (1981) 289:401–2. doi: 10.1038/289401a0
13. Bernardis LL, Goldman JK. Origin of endocrine-metabolic changes in the weanling rat ventromedial syndrome. *J Neurosci Res*. (1976) 2:91–116. doi: 10.1002/jnr.490020202
14. Hardie DG, Ross FA, Hawley SA. AMPK: a nutrient and energy sensor that maintains energy homeostasis. *Nat Rev Mol Cell Biol*. (2012) 13:251–62. doi: 10.1038/nrm3311
15. Alvarez-Crespo M, Csikasz RI, Martinez-Sanchez N, Dieguez C, Cannon B, Nedergaard J, et al. Essential role of UCP1 modulating the central effects of thyroid hormones on energy balance. *Mol Metab*. (2016) 5:271–82. doi: 10.1016/j.molmet.2016.01.008
16. Beiroa D, Imbernon M, Gallego R, Senra A, Herranz D, Villarroya F, et al. GLP-1 agonism stimulates brown adipose tissue thermogenesis and browning through hypothalamic AMPK. *Diabetes*. (2014) 63:3346–58. doi: 10.2337/db14-0302
17. Martinez-Sanchez N, Moreno-Navarrete JM, Contreras C, Rial-Pensado E, Ferno J, Nogueiras R, et al. Thyroid hormones induce browning of white fat. *J Endocrinol*. (2017) 232:351–62. doi: 10.1530/JOE-16-0425
18. Seoane-Collazo P, Roa J, Rial-Pensado E, Linares-Pose L, Beiroa D, Ruiz-Pino F, et al. SF1-specific AMPKalpha1 deletion protects against diet-induced obesity. *Diabetes*. (2018) 67:2213–26. doi: 10.2337/db17-1538
19. Lowell BB, Spiegelman BM. Towards a molecular understanding of adaptive thermogenesis. *Nature*. (2000) 404:652–60. doi: 10.1038/35007527
20. Giralt M, Villarroya F. White, brown, beige/brite: different adipose cells for different functions? *Endocrinology*. (2013) 154:2992–3000. doi: 10.1210/en.2013-1403
21. Zeng W, Pirzgalska RM, Pereira MM, Kubasova N, Barateiro A, Seixas E, et al. Sympathetic neuro-adipose connections mediate leptin-driven lipolysis. *Cell*. (2015) 163:84–94. doi: 10.1016/j.cell.2015.08.055
22. Virtanen KA, Lidell ME, Orava J, Heglind M, Westergren R, Niemi T, et al. Functional brown adipose tissue in healthy adults. *N Engl J Med*. (2009) 360:1518–25. doi: 10.1056/NEJMoa0808949
23. Whittle AJ, Lopez M, Vidal-Puig A. Using brown adipose tissue to treat obesity-the central issue. *Trends Mol Med*. (2011) 17:405–11. doi: 10.1016/j.molmed.2011.04.001
24. Young P, Arch JR, Ashwell M. Brown adipose tissue in the parametrial fat pad of the mouse. *FEBS Lett*. (1984) 167:10–4. doi: 10.1016/0014-5793(84)80822-4
25. Bartness TJ, Liu Y, Shrestha YB, Ryu V. Neural innervation of white adipose tissue and the control of lipolysis. *Front Neuroendocrinol*. (2014) 35:473–93. doi: 10.1016/j.yfrne.2014.04.001
26. Fisher FM, Kleiner S, Douris N, Fox EC, Mepani RJ, Verdeguer F, et al. FGF21 regulates PGC-1alpha and browning of white adipose tissues in adaptive thermogenesis. *Genes Dev*. (2012) 26:271–81. doi: 10.1101/gad.177857.111
27. Commins SP, Watson PM, Levin N, Beiler RJ, Gettys TW. Central leptin regulates the UCP1 and ob genes in brown and white adipose tissue via different beta-adrenoceptor subtypes. *J Biol Chem*. (2000) 275:33059–67. doi: 10.1074/jbc.M006328200
28. Petrovic N, Walden TB, Shabalina IG, Timmons JA, Cannon B, Nedergaard J. Chronic peroxisome proliferator-activated receptor gamma (PPARgamma) activation of epididymally derived white adipocyte cultures reveals a population of thermogenically competent, UCP1-containing adipocytes molecularly distinct from classic brown adipocytes. *J Biol Chem*. (2010) 285:7153–64. doi: 10.1074/jbc.M109.053942
29. Cousin B, Cinti S, Morroni M, Raimbault S, Ricquier D, Penicaud L, et al. Occurrence of brown adipocytes in rat white adipose tissue: molecular and morphological characterization. *J Cell Sci*. (1992) 103(Pt 4):931–42.
30. Jiang H, Ding X, Cao Y, Wang H, Zeng W. Dense Intra-adipose sympathetic arborizations are essential for cold-induced beiging of mouse white adipose tissue. *Cell Metab*. (2017) 26:686–92.e3. doi: 10.1016/j.cmet.2017.08.016
31. Chouchani ET, Kazak L, Spiegelman BM. New advances in adaptive thermogenesis: UCP1 and beyond. *Cell Metab*. (2019) 29:27–37. doi: 10.1016/j.cmet.2018.11.002
32. Klepac K, Georgiadi A, Tschop M, Herzig S. The role of brown and beige adipose tissue in glycaemic control. *Mol Aspects Med*. (2019) 68:90–100. doi: 10.1016/j.mam.2019.07.001
33. Lee P, Smith S, Linderman J, Courville AB, Brychta RJ, Dieckmann W, et al. Temperature-acclimated brown adipose tissue modulates insulin sensitivity in humans. *Diabetes*. (2014) 63:3686–98. doi: 10.2337/db14-0513

34. Lee P, Werner CD, Kebebew E, Celi FS. Functional thermogenic beige adipogenesis is inducible in human neck fat. *Int J Obes*. (2014) 38:170–6. doi: 10.1038/ijo.2013.82
35. Kajimura S, Spiegelman BM, Seale P. Brown and beige fat: physiological roles beyond heat generation. *Cell Metab*. (2015) 22:546–59. doi: 10.1016/j.cmet.2015.09.007
36. Labbe SM, Caron A, Lanfray D, Monge-Rofarello B, Bartness TJ, Richard D. Hypothalamic control of brown adipose tissue thermogenesis. *Front Syst Neurosci*. (2015) 9:150. doi: 10.3389/fnsys.2015.00150
37. Bartness TJ, Vaughan CH, Song CK. Sympathetic and sensory innervation of brown adipose tissue. *Int J Obes*. (2010) 34(Suppl. 1):S36–42. doi: 10.1038/ijo.2010.182
38. Lage R, Ferno J, Nogueiras R, Dieguez C, Lopez M. Contribution of adaptive thermogenesis to the hypothalamic regulation of energy balance. *Biochem J*. (2016) 473:4063–82. doi: 10.1042/BCJ20160012
39. Xu Y, Elmquist JK, Fukuda M. Central nervous control of energy and glucose balance: focus on the central melanocortin system. *Ann N Y Acad Sci*. (2011) 1243:1–14. doi: 10.1111/j.1749-6632.2011.06248.x
40. Bagnol D, Lu XY, Kaelin CB, Day HE, Ollmann M, Gantz I, et al. Anatomy of an endogenous antagonist: relationship between agouti-related protein and proopiomelanocortin in brain. *J Neurosci*. (1999) 19:RC26. doi: 10.1523/JNEUROSCI.19-18-j0004.1999
41. Fan W, Voss-Andreae A, Cao WH, Morrison SF. Regulation of thermogenesis by the central melanocortin system. *Peptides*. (2005) 26:1800–13. doi: 10.1016/j.peptides.2004.11.033
42. Tong Q, Ye CP, Jones JE, Elmquist JK, Lowell BB. Synaptic release of GABA by AgRP neurons is required for normal regulation of energy balance. *Nat. Neurosci*. (2008) 11:998–1000. doi: 10.1038/nn.2167
43. Majdic G, Young M, Gomez-Sanchez E, Anderson P, Szczepaniak LS, Dobbins RL, et al. Knockout mice lacking steroidogenic factor 1 are a novel genetic model of hypothalamic obesity. *Endocrinology*. (2002) 143:607–14. doi: 10.1210/endo.143.2.8652
44. Wang B, Cheng KK. Hypothalamic AMPK as a mediator of hormonal regulation of energy balance. *Int J Mol Sci*. (2018) 19:3552. doi: 10.3390/ijms19113552
45. Zhang W, Bi S. Hypothalamic regulation of brown adipose tissue thermogenesis and energy homeostasis. *Front Endocrinol*. (2015) 6:136. doi: 10.3389/fendo.2015.00136
46. Amir S. Intra-ventromedial hypothalamic injection of glutamate stimulates brown adipose tissue thermogenesis in the rat. *Brain Res*. (1990) 511:341–4. doi: 10.1016/0006-8993(90)90181-A
47. Hugie T, Halvorson I, Thornhill J. Brown adipose tissue temperature responses following electrical stimulation of ventromedial hypothalamic and lateral preoptic areas or after norepinephrine infusion to long evans or sprague-dawley rats. *Brain Res*. (1992) 575:57–62. doi: 10.1016/0006-8993(92)90422-6
48. Yoshimatsu H, Egawa M, Bray GA. Sympathetic nerve activity after discrete hypothalamic injections of L-glutamate. *Brain Res*. (1993) 601:121–8. doi: 10.1016/0006-8993(93)91702-T
49. Musatov S, Chen W, Pfaff DW, Mobbs CV, Yang XJ, Clegg DJ, et al. Silencing of estrogen receptor alpha in the ventromedial nucleus of hypothalamus leads to metabolic syndrome. *Proc Natl Acad Sci USA*. (2007) 104:2501–6. doi: 10.1073/pnas.0610787104
50. Contreras C, Gonzalez-Garcia I, Martinez-Sanchez N, Seoane-Collazo P, Jacas J, Morgan DA, et al. Central ceramide-induced hypothalamic lipotoxicity and ER stress regulate energy balance. *Cell Rep*. (2014) 9:366–77. doi: 10.1016/j.celrep.2014.08.057
51. Contreras C, Gonzalez-Garcia I, Seoane-Collazo P, Martinez-Sanchez N, Linares-Pose L, Rial-Pensado E, et al. Reduction of hypothalamic endoplasmic reticulum stress activates browning of white fat and ameliorates obesity. *Diabetes*. (2017) 66:87–99. doi: 10.2337/db15-1547
52. Martinez-Sanchez N, Seoane-Collazo P, Contreras C, Varela L, Villarroya J, Rial-Pensado E, et al. Hypothalamic AMPK-ER stress-JNK1 axis mediates the central actions of thyroid hormones on energy balance. *Cell Metab*. (2017) 26:212–29.e12. doi: 10.1016/j.cmet.2017.06.014
53. Gonzalez-Garcia I, Contreras C, Estevez-Salguero A, Ruiz-Pino F, Colsh B, Pensado I, et al. Estradiol regulates energy balance by ameliorating hypothalamic ceramide-induced ER stress. *Cell Rep*. (2018) 25:413–23.e5. doi: 10.1016/j.celrep.2018.09.038
54. Xiao B, Heath R, Saiu P, Leiper FC, Leone P, Jing C, et al. Structural basis for AMP binding to mammalian AMP-activated protein kinase. *Nature*. (2007) 449:496–500. doi: 10.1038/nature06161
55. Carling D, Mayer FV, Sanders MJ, Gamblin SJ. AMP-activated protein kinase: nature's energy sensor. *Nat Chem Biol*. (2011) 7:512–8. doi: 10.1038/nchembio.610
56. Xiao B, Sanders MJ, Underwood E, Heath R, Mayer FV, Carmena D, et al. Structure of mammalian AMPK and its regulation by ADP. *Nature*. (2011) 472:230–3. doi: 10.1038/nature09932
57. Woods A, Johnstone SR, Dickerson K, Leiper FC, Fryer LG, Neumann D, et al. LKB1 is the upstream kinase in the AMP-activated protein kinase cascade. *Curr Biol*. (2003) 13:2004–8. doi: 10.1016/j.cub.2003.10.031
58. Hurley RL, Anderson KA, Franzone JM, Kemp BE, Means AR, Witters LA. The Ca2+/calmodulin-dependent protein kinase kinases are AMP-activated protein kinase kinases. *J Biol Chem*. (2005) 280:29060–6. doi: 10.1074/jbc.M503824200
59. Woods A, Dickerson K, Heath R, Hong SP, Momcilovic M, Johnstone SR, et al. Ca2+/calmodulin-dependent protein kinase kinase-beta acts upstream of AMP-activated protein kinase in mammalian cells. *Cell Metab*. (2005) 2:21–33. doi: 10.1016/j.cmet.2005.06.005
60. Minokoshi Y, Alquier T, Furukawa N, Kim YB, Lee A, Xue B, et al. AMP-kinase regulates food intake by responding to hormonal and nutrient signals in the hypothalamus. *Nature*. (2004) 428:569–74. doi: 10.1038/nature02440
61. Lopez M, Lage R, Saha AK, Perez-Tilve D, Vazquez MJ, Varela L, et al. Hypothalamic fatty acid metabolism mediates the orexigenic action of ghrelin. *Cell Metab*. (2008) 7:389–99. doi: 10.1016/j.cmet.2008.03.006
62. van Dam AD, Kooijman S, Schilperoort M, Rensen PC, Boon MR. Regulation of brown fat by AMP-activated protein kinase. *Trends Mol Med*. (2015) 21:571–9. doi: 10.1016/j.molmed.2015.07.003
63. Schneeberger M, Claret M. Recent Insights into the role of hypothalamic AMPK signaling cascade upon metabolic control. *Front Neurosci*. (2012) 6:185. doi: 10.3389/fnins.2012.00185
64. Martinez de Morentin PB, Gonzalez-Garcia I, Martins L, Lage R, Fernandez-Mallo D, Martinez-Sanchez N, et al. Estradiol regulates brown adipose tissue thermogenesis via hypothalamic AMPK. *Cell Metab*. (2014) 20:41–53. doi: 10.1016/j.cmet.2014.03.031
65. Whittle AJ, Carobbio S, Martins L, Slawik M, Hondares E, Vazquez MJ, et al. BMP8B increases brown adipose tissue thermogenesis through both central and peripheral actions. *Cell*. (2012) 149:871–85. doi: 10.1016/j.cell.2012.02.066
66. Martinez de Morentin PB, Whittle AJ, Ferno J, Nogueiras R, Dieguez C, Vidal-Puig A, et al. Nicotine induces negative energy balance through hypothalamic AMP-activated protein kinase. *Diabetes*. (2012) 61:807–17. doi: 10.2337/db11-1079
67. Lopez M. Hypothalamic AMPK and energy balance. *Eur J Clin Invest*. (2018) 48:e12996. doi: 10.1111/eci.12996
68. Obregon MJ. Adipose tissues and thyroid hormones. *Front Physiol*. (2014) 5:479. doi: 10.3389/fphys.2014.00479
69. Santini F, Marzullo P, Rotondi M, Ceccarini G, Pagano L, Ippolito S, et al. Mechanisms in endocrinology: the crosstalk between thyroid gland and adipose tissue: signal integration in health and disease. *Eur J Endocrinol*. (2014) 171:R137–52. doi: 10.1530/EJE-14-0067
70. Martinez-Sanchez N, Alvarez CV, Ferno J, Nogueiras R, Dieguez C, Lopez M. Hypothalamic effects of thyroid hormones on metabolism. *Best Pract Res Clin Endocrinol Metab*. (2014) 28:703–12. doi: 10.1016/j.beem.2014.04.004
71. Cannon B, Nedergaard J. Thyroid hormones: igniting brown fat via the brain. *Nat Med*. (2010) 16:965–7. doi: 10.1038/nm0910-965
72. Lopez M, Alvarez CV, Nogueiras R, Dieguez C. Energy balance regulation by thyroid hormones at central level. *Trends Mol Med*. (2013) 19:418–27. doi: 10.1016/j.molmed.2013.04.004
73. Sjogren M, Alkemade A, Mittag J, Nordstrom K, Katz A, Rozell B, et al. Hypermetabolism in mice caused by the central action of an unliganded thyroid hormone receptor alpha1. *EMBO J*. (2007) 26:4535–45. doi: 10.1038/sj.emboj.7601882
74. Lopez M, Varela L, Vazquez MJ, Rodriguez-Cuenca S, Gonzalez CR, Velagapudi VR, et al. Hypothalamic AMPK and fatty acid metabolism

mediate thyroid regulation of energy balance. *Nat Med*. (2010) 16:1001–8. doi: 10.1038/nm.2207
75. Mojsov S, Weir GC, Habener JF. Insulinotropin: glucagon-like peptide I (7–37) co-encoded in the glucagon gene is a potent stimulator of insulin release in the perfused rat pancreas. *J Clin Invest*. (1987) 79:616–9. doi: 10.1172/JCI112855
76. Campbell JE, Drucker DJ. Pharmacology, physiology, and mechanisms of incretin hormone action. *Cell Metab*. (2013) 17:819–37. doi: 10.1016/j.cmet.2013.04.008
77. Goke R, Fehmann HC, Goke B. Glucagon-like peptide-1(7–36) amide is a new incretin/enterogastrone candidate. *Eur J Clin Invest*. (1991) 21:135–44. doi: 10.1111/j.1365-2362.1991.tb01802.x
78. Marre M, Shaw J, Brandle M, Bebakar WM, Kamaruddin NA, Strand J, et al. Liraglutide, a once-daily human GLP-1 analogue, added to a sulphonylurea over 26 weeks produces greater improvements in glycaemic and weight control compared with adding rosiglitazone or placebo in subjects with Type 2 diabetes (LEAD-1 SU). *Diabet Med*. (2009) 26:268–78. doi: 10.1111/j.1464-5491.2009.02666.x
79. Astrup A, Rossner S, Van Gaal L, Rissanen A, Niskanen L, Al Hakim M, et al. Effects of liraglutide in the treatment of obesity: a randomised, double-blind, placebo-controlled study. *Lancet*. (2009) 374:1606–16. doi: 10.1016/S0140-6736(09)61375-1
80. Gu G, Roland B, Tomaselli K, Dolman CS, Lowe C, Heilig JS. Glucagon-like peptide-1 in the rat brain: distribution of expression and functional implication. *J Comp Neurol*. (2013) 521:2235–61. doi: 10.1002/cne.23282
81. Richards P, Parker HE, Adriaenssens AE, Hodgson JM, Cork SC, Trapp S, et al. Identification and characterization of GLP-1 receptor-expressing cells using a new transgenic mouse model. *Diabetes*. (2014) 63:1224–33. doi: 10.2337/db13-1440
82. Holst JJ. Incretin hormones and the satiation signal. *Int J Obes*. (2013) 37:1161–8. doi: 10.1038/ijo.2012.208
83. Skibicka KP, Alhadeff AL, Grill HJ. Hindbrain cocaine- and amphetamine-regulated transcript induces hypothermia mediated by GLP-1 receptors. *J Neurosci*. (2009) 29:6973–81. doi: 10.1523/JNEUROSCI.6144-08.2009
84. Trapp S, Richards JE. The gut hormone glucagon-like peptide-1 produced in brain: is this physiologically relevant? *Curr Opin Pharmacol*. (2013) 13:964–9. doi: 10.1016/j.coph.2013.09.006
85. Liu J, Conde K, Zhang P, Lilascharoen V, Xu Z, Lim BK, et al. Enhanced AMPA receptor trafficking mediates the anorexigenic effect of endogenous glucagon-like peptide-1 in the paraventricular hypothalamus. *Neuron*. (2017) 96:897–909.e5. doi: 10.1016/j.neuron.2017.09.042
86. Turton MD, O'Shea D, Gunn I, Beak SA, Edwards CM, Meeran K, et al. A role for glucagon-like peptide-1 in the central regulation of feeding. *Nature*. (1996) 379:69–72. doi: 10.1038/379069a0
87. Lutz TA. Gut hormones such as amylin and GLP-1 in the control of eating and energy expenditure. *Int J Obes Suppl*. (2016) 6(Suppl. 1):S15–21. doi: 10.1038/ijosup.2016.4
88. Lopez M, Dieguez C, Nogueiras R. Hypothalamic GLP-1: the control of BAT thermogenesis and browning of white fat. *Adipocyte*. (2015) 4:141–5. doi: 10.4161/21623945.2014.983752
89. Lockie SH, Heppner KM, Chaudhary N, Chabenne JR, Morgan DA, Veyrat-Durebex C, et al. Direct control of brown adipose tissue thermogenesis by central nervous system glucagon-like peptide-1 receptor signaling. *Diabetes*. (2012) 61:2753–62. doi: 10.2337/db11-1556
90. Calanna S, Christensen M, Holst JJ, Laferrere B, Gluud LL, Vilsboll T, et al. Secretion of glucagon-like peptide-1 in patients with type 2 diabetes mellitus: systematic review and meta-analyses of clinical studies. *Diabetologia*. (2013) 56:965–72. doi: 10.1007/s00125-013-2841-0
91. Iepsen EW, Zhang J, Thomsen HS, Hansen EL, Hollensted M, Madsbad S, et al. Patients with obesity caused by melanocortin-4 receptor mutations can be treated with a glucagon-like peptide-1 receptor agonist. *Cell Metab*. (2018) 28:23–32.e3. doi: 10.1016/j.cmet.2018.05.008
92. Torekov SS, Madsbad S, Holst JJ. Obesity-an indication for GLP-1 treatment? Obesity pathophysiology and GLP-1 treatment potential. *Obesity Rev*. (2011) 12:593–601. doi: 10.1111/j.1467-789X.2011.00860.x
93. DeFronzo RA, Ratner RE, Han J, Kim DD, Fineman MS, Baron AD. Effects of exenatide (exendin-4) on glycemic control and weight over 30 weeks in metformin-treated patients with type 2 diabetes. *Diabetes Care*. (2005) 28:1092–100. doi: 10.2337/diacare.28.5.1092
94. Buse JB, Drucker DJ, Taylor KL, Kim T, Walsh B, Hu H, et al. DURATION-1: exenatide once weekly produces sustained glycemic control and weight loss over 52 weeks. *Diabetes Care*. (2010) 33:1255–61. doi: 10.2337/dc09-1914
95. Burmeister MA, Ayala J, Drucker DJ, Ayala JE. Central glucagon-like peptide 1 receptor-induced anorexia requires glucose metabolism-mediated suppression of AMPK and is impaired by central fructose. *Am J Physiol Endocrinol Metab*. (2013) 304:E677–85. doi: 10.1152/ajpendo.00446.2012
96. Lopez M, Tena-Sempere M. Estradiol and brown fat. *Best Pract Res Clin Endocrinol Metab*. (2016) 30:527–36. doi: 10.1016/j.beem.2016.08.004
97. Sinchak K, Wagner EJ. Estradiol signaling in the regulation of reproduction and energy balance. *Front Neuroendocrinol*. (2012) 33:342–63. doi: 10.1016/j.yfrne.2012.08.004
98. Mauvais-Jarvis F, Clegg DJ, Hevener AL. The role of estrogens in control of energy balance and glucose homeostasis. *Endocr Rev*. (2013) 34:309–38. doi: 10.1210/er.2012-1055
99. Heine PA, Taylor JA, Iwamoto GA, Lubahn DB, Cooke PS. Increased adipose tissue in male and female estrogen receptor-alpha knockout mice. *Proc Natl Acad Sci USA*. (2000) 97:12729–34. doi: 10.1073/pnas.97.23.12729
100. Frank A, Brown LM, Clegg DJ. The role of hypothalamic estrogen receptors in metabolic regulation. *Front Neuroendocrinol*. (2014) 35:550–7. doi: 10.1016/j.yfrne.2014.05.002
101. Osterlund M, Kuiper GG, Gustafsson JA, Hurd YL. Differential distribution and regulation of estrogen receptor-alpha and -beta mRNA within the female rat brain. *Brain Res Mol Brain Res*. (1998) 54:175–80. doi: 10.1016/S0169-328X(97)00351-3
102. Merchenthaler I, Lane MV, Numan S, Dellovade TL. Distribution of estrogen receptor alpha and beta in the mouse central nervous system: *in vivo* autoradiographic and immunocytochemical analyses. *J Comp Neurol*. (2004) 473:270–91. doi: 10.1002/cne.20128
103. Roesch DM. Effects of selective estrogen receptor agonists on food intake and body weight gain in rats. *Physiol Behav*. (2006) 87:39–44. doi: 10.1016/j.physbeh.2005.08.035
104. Santollo J, Wiley MD, Eckel LA. Acute activation of ER alpha decreases food intake, meal size, and body weight in ovariectomized rats. *Am J Physiol Regul Integr Comp Physiol*. (2007) 293:R2194–201. doi: 10.1152/ajpregu.00385.2007
105. Foryst-Ludwig A, Clemenz M, Hohmann S, Hartge M, Sprang C, Frost N, et al. Metabolic actions of estrogen receptor beta (ERbeta) are mediated by a negative cross-talk with PPARgamma. *PLoS Genet*. (2008) 4:e1000108. doi: 10.1371/journal.pgen.1000108
106. Xu Y, Nedungadi TP, Zhu L, Sobhani N, Irani BG, Davis KE, et al. Distinct hypothalamic neurons mediate estrogenic effects on energy homeostasis and reproduction. *Cell Metab*. (2011) 14:453–65. doi: 10.1016/j.cmet.2011.08.009
107. Mittelman-Smith MA, Williams H, Krajewski-Hall SJ, Lai J, Ciofi P, McMullen NT, et al. Arcuate kisspeptin/neurokinin B/dynorphin (KNDy) neurons mediate the estrogen suppression of gonadotropin secretion and body weight. *Endocrinology*. (2012) 153:2800–12. doi: 10.1210/en.2012-1045
108. Martinez de Morentin PB, Lage R, Gonzalez-Garcia I, Ruiz-Pino F, Martins L, Fernandez-Mallo D, et al. Pregnancy induces resistance to the anorectic effect of hypothalamic malonyl-CoA and the thermogenic effect of hypothalamic AMPK inhibition in female rats. *Endocrinology*. (2015) 156:947–60. doi: 10.1210/en.2014-1611
109. Finan B, Yang B, Ottaway N, Stemmer K, Muller TD, Yi CX, et al. Targeted estrogen delivery reverses the metabolic syndrome. *Nat Med*. (2012) 18:1847–56. doi: 10.1038/nm.3009
110. Modica S, Wolfrum C. Bone morphogenic proteins signaling in adipogenesis and energy homeostasis. *Biochim Biophys Acta*. (2013) 1831:915–23. doi: 10.1016/j.bbalip.2013.01.010
111. Woods AJ, Stock MJ. Biphasic brown fat temperature responses to hypothalamic stimulation in rats. *Am J Physiol*. (1994) 266(Pt 2):R328–37. doi: 10.1152/ajpregu.1994.266.2.R328
112. Huang H, Song TJ, Li X, Hu L, He Q, Liu M, et al. BMP signaling pathway is required for commitment of C3H10T1/2 pluripotent stem cells to the adipocyte lineage. *Proc Natl Acad Sci USA*. (2009) 106:12670–5. doi: 10.1073/pnas.0906266106

113. Chen D, Zhao M, Mundy GR. Bone morphogenetic proteins. *Growth Factors*. (2004) 22:233–41. doi: 10.1080/08977190412331279890
114. Martins L, Seoane-Collazo P, Contreras C, Gonzalez-Garcia I, Martinez-Sanchez N, Gonzalez F, et al. A functional link between AMPK and orexin mediates the effect of BMP8B on energy balance. *Cell Rep*. (2016) 16:2231–42. doi: 10.1016/j.celrep.2016.07.045
115. Zhang Y, Proenca R, Maffei M, Barone M, Leopold L, Friedman JM. Positional cloning of the mouse obese gene and its human homologue. *Nature*. (1994) 372:425–32. doi: 10.1038/372425a0
116. Casanueva FF, Dieguez C. Neuroendocrine regulation and actions of leptin. *Front Neuroendocrinol*. (1999) 20:317–63. doi: 10.1006/frne.1999.0187
117. Tartaglia LA. The leptin receptor. *J Biol Chem*. (1997) 272:6093–6. doi: 10.1074/jbc.272.10.6093
118. Fei H, Okano HJ, Li C, Lee GH, Zhao C, Darnell R, et al. Anatomic localization of alternatively spliced leptin receptors (Ob-R) in mouse brain and other tissues. *Proc Natl Acad Sci USA*. (1997) 94:7001–5. doi: 10.1073/pnas.94.13.7001
119. Mercer JG, Hoggard N, Williams LM, Lawrence CB, Hannah LT, Trayhurn P. Localization of leptin receptor mRNA and the long form splice variant (Ob-Rb) in mouse hypothalamus and adjacent brain regions by *in situ* hybridization. *FEBS Lett*. (1996) 387:113–6. doi: 10.1016/0014-5793(96)00473-5
120. Chen H, Charlat O, Tartaglia LA, Woolf EA, Weng X, Ellis SJ, et al. Evidence that the diabetes gene encodes the leptin receptor: identification of a mutation in the leptin receptor gene in db/db mice. *Cell*. (1996) 84:491–5. doi: 10.1016/S0092-8674(00)81294-5
121. Kowalski TJ, Liu SM, Leibel RL, Chua SC Jr. Transgenic complementation of leptin-receptor deficiency. I. Rescue of the obesity/diabetes phenotype of LEPR-null mice expressing a LEPR-B transgene. *Diabetes*. (2001) 50:425–35. doi: 10.2337/diabetes.50.2.425
122. de Luca C, Kowalski TJ, Zhang Y, Elmquist JK, Lee C, Kilimann MW, et al. Complete rescue of obesity, diabetes, and infertility in db/db mice by neuron-specific LEPR-B transgenes. *J Clin Invest*. (2005) 115:3484–93. doi: 10.1172/JCI24059
123. Bates SH, Stearns WH, Dundon TA, Schubert M, Tso AW, Wang Y, et al. STAT3 signalling is required for leptin regulation of energy balance but not reproduction. *Nature*. (2003) 421:856–9. doi: 10.1038/nature01388
124. Piper ML, Unger EK, Myers MG Jr, Xu AW. Specific physiological roles for signal transducer and activator of transcription 3 in leptin receptor-expressing neurons. *Mol Endocrinol*. (2008) 22:751–9. doi: 10.1210/me.2007-0389
125. Hill JW, Williams KW, Ye C, Luo J, Balthasar N, Coppari R, et al. Acute effects of leptin require PI3K signaling in hypothalamic proopiomelanocortin neurons in mice. *J Clin Invest*. (2008) 118:1796–805. doi: 10.1172/JCI32964
126. Cota D, Matter EK, Woods SC, Seeley RJ. The role of hypothalamic mammalian target of rapamycin complex 1 signaling in diet-induced obesity. *J Neurosci*. (2008) 28:7202–8. doi: 10.1523/JNEUROSCI.1389-08.2008
127. Blouet C, Ono H, Schwartz GJ. Mediobasal hypothalamic p70 S6 kinase 1 modulates the control of energy homeostasis. *Cell Metab*. (2008) 8:459–67. doi: 10.1016/j.cmet.2008.10.004
128. Dagon Y, Hur E, Zheng B, Wellenstein K, Cantley LC, Kahn BB. p70S6 kinase phosphorylates AMPK on serine 491 to mediate leptin's effect on food intake. *Cell Metab*. (2012) 16:104–12. doi: 10.1016/j.cmet.2012.05.010
129. Watterson KR, Bestow D, Gallagher J, Hamilton DL, Ashford FB, Meakin PJ, et al. Anorexigenic and orexigenic hormone modulation of mammalian target of rapamycin complex 1 activity and the regulation of hypothalamic agouti-related protein mRNA expression. *Neurosignals*. (2013) 21:28–41. doi: 10.1159/000334144
130. Cowley MA, Smart JL, Rubinstein M, Cerdan MG, Diano S, Horvath TL, et al. Leptin activates anorexigenic POMC neurons through a neural network in the arcuate nucleus. *Nature*. (2001) 411:480–4. doi: 10.1038/35078085
131. Balthasar N, Coppari R, McMinn J, Liu SM, Lee CE, Tang V, et al. Leptin receptor signaling in POMC neurons is required for normal body weight homeostasis. *Neuron*. (2004) 42:983–91. doi: 10.1016/j.neuron.2004.06.004
132. Xu J, Bartolome CL, Low CS, Yi X, Chien CH, Wang P, et al. Genetic identification of leptin neural circuits in energy and glucose homeostases. *Nature*. (2018) 556:505–9. doi: 10.1038/s41586-018-0049-7
133. Kim KW, Zhao L, Donato J Jr, Kohno D, Xu Y, Elias CF, et al. Steroidogenic factor 1 directs programs regulating diet-induced thermogenesis and leptin action in the ventral medial hypothalamic nucleus. *Proc Natl Acad Sci USA*. (2011) 108:10673–8. doi: 10.1073/pnas.1102364108
134. Dhillon H, Zigman JM, Ye C, Lee CE, McGovern RA, Tang V, et al. Leptin directly activates SF1 neurons in the VMH, and this action by leptin is required for normal body-weight homeostasis. *Neuron*. (2006) 49:191–203. doi: 10.1016/j.neuron.2005.12.021
135. Bingham NC, Anderson KK, Reuter AL, Stallings NR, Parker KL. Selective loss of leptin receptors in the ventromedial hypothalamic nucleus results in increased adiposity and a metabolic syndrome. *Endocrinology*. (2008) 149:2138–48. doi: 10.1210/en.2007-1200
136. Xue B, Pulinilkunnil T, Murano I, Bence KK, He H, Minokoshi Y, et al. Neuronal protein tyrosine phosphatase 1B deficiency results in inhibition of hypothalamic AMPK and isoform-specific activation of AMPK in peripheral tissues. *Mol Cell Biol*. (2009) 29:4563–73. doi: 10.1128/MCB.01914-08
137. Tanida M, Yamamoto N, Shibamoto T, Rahmouni K. Involvement of hypothalamic AMP-activated protein kinase in leptin-induced sympathetic nerve activation. *PLoS ONE*. (2013) 8:e56660. doi: 10.1371/journal.pone.0056660
138. Ramos-Lobo AM, Teixeira PDS, Furigo IC, Donato J Jr. SOCS3 ablation in SF1 cells causes modest metabolic effects during pregnancy and lactation. *Neuroscience*. (2017) 365:114–24. doi: 10.1016/j.neuroscience.2017.09.048
139. Schroder M, Kaufman RJ. The mammalian unfolded protein response. *Ann Rev Biochem*. (2005) 74:739–89. doi: 10.1146/annurev.biochem.73.011303.074134
140. Ron D, Walter P. Signal integration in the endoplasmic reticulum unfolded protein response. *Nat Rev Mol Cell Biol*. (2007) 8:519–29. doi: 10.1038/nrm2199
141. Ozcan U, Cao Q, Yilmaz E, Lee AH, Iwakoshi NN, Ozdelen E, et al. Endoplasmic reticulum stress links obesity, insulin action, and type 2 diabetes. *Science*. (2004) 306:457–61. doi: 10.1126/science.1103160
142. Zhang X, Zhang G, Zhang H, Karin M, Bai H, Cai D. Hypothalamic IKKbeta/NF-kappaB and ER stress link overnutrition to energy imbalance and obesity. *Cell*. (2008) 135:61–73. doi: 10.1016/j.cell.2008.07.043
143. Won JC, Jang PG, Namkoong C, Koh EH, Kim SK, Park JY, et al. Central administration of an endoplasmic reticulum stress inducer inhibits the anorexigenic effects of leptin and insulin. *Obesity*. (2009) 17:1861–5. doi: 10.1038/oby.2009.194
144. Linares-Pose L, Rial-Pensado E, Estevez-Salguero A, Milbank E, Gonzalez-Garcia I, Rodriguez C, et al. Genetic targeting of GRP78 in the VMH improves obesity independently of food intake. *Genes*. (2018) 9:357. doi: 10.3390/genes9070357
145. Rodriguez-Rodriguez R, Miralpeix C, Fosch A, Pozo M, Calderon-Dominguez M, Perpinya X, et al. CPT1C in the ventromedial nucleus of the hypothalamus is necessary for brown fat thermogenesis activation in obesity. *Mol Metab*. (2019) 19:75–85. doi: 10.1016/j.molmet.2018.10.010
146. Lopez M. EJE PRIZE 2017: hypothalamic AMPK: a golden target against obesity? *Eur J Endocrinol*. (2017) 176:R235–46. doi: 10.1530/EJE-16-0927
147. Carling D. AMPK signalling in health and disease. *Curr Opin Cell Biol*. (2017) 45:31–7. doi: 10.1016/j.ceb.2017.01.005
148. Haslam D. Weight management in obesity-past and present. *Int J Clin Pract*. (2016) 70:206–17. doi: 10.1111/ijcp.12771
149. Minokoshi Y, Kim YB, Peroni OD, Fryer LG, Muller C, Carling D, et al. Leptin stimulates fatty-acid oxidation by activating AMP-activated protein kinase. *Nature*. (2002) 415:339–43. doi: 10.1038/415339a
150. Yamazaki S, Satoh H, Watanabe T. Liraglutide enhances insulin sensitivity by activating AMP-activated protein kinase in male wistar rats. *Endocrinology*. (2014) 155:3288–301. doi: 10.1210/en.2013-2157
151. Anand BK, Brobeck JR. Hypothalamic control of food intake in rats and cats. *Yale J Biol Med*. (1951) 24:123–40.
152. Brobeck JR, Tepperman J, Long CN. Experimental hypothalamic hyperphagia in the albino rat. *Yale J Biol Med*. (1943) 15:831–53.
153. Morrison SF, Madden CJ, Tupone D. An orexinergic projection from perifornical hypothalamus to raphe pallidus increases rat brown adipose tissue thermogenesis. *Adipocyte*. (2012) 1:116–20. doi: 10.4161/adip.19736

154. Madden CJ, Tupone D, Morrison SF. Orexin modulates brown adipose tissue thermogenesis. *Biomol Concepts*. (2012) 3:381–6. doi: 10.1515/bmc-2011-0066
155. Tupone D, Madden CJ, Cano G, Morrison SF. An orexinergic projection from perifornical hypothalamus to raphe pallidus increases rat brown adipose tissue thermogenesis. *J Neurosci*. (2011) 31:15944–55. doi: 10.1523/JNEUROSCI.3909-11.2011
156. Myers MG Jr, Olson DP. Central nervous system control of metabolism. *Nature*. (2012) 491:357–63. doi: 10.1038/nature11705
157. Wang B, Li A, Li X, Ho PW, Wu D, Wang X, et al. Activation of hypothalamic RIP-Cre neurons promotes beiging of WAT via sympathetic nervous system. *EMBO Rep*. (2018) 19:e44977. doi: 10.15252/embr.201744977
158. Saliba LJ, Maffett S. Hypertensive heart disease and obesity: a review. *Heart Fail Clin*. (2019) 15:509–17. doi: 10.1016/j.hfc.2019.06.003
159. McCrimmon RJ, Fan X, Ding Y, Zhu W, Jacob RJ, Sherwin RS. Potential role for AMP-activated protein kinase in hypoglycemia sensing in the ventromedial hypothalamus. *Diabetes*. (2004) 53:1953–8. doi: 10.2337/diabetes.53.8.1953
160. McCrimmon RJ, Fan X, Cheng H, McNay E, Chan O, Shaw M, et al. Activation of AMP-activated protein kinase within the ventromedial hypothalamus amplifies counterregulatory hormone responses in rats with defective counterregulation. *Diabetes*. (2006) 55:1755–60. doi: 10.2337/db05-1359
161. McCrimmon RJ, Shaw M, Fan X, Cheng H, Ding Y, Vella MC, et al. Key role for AMP-activated protein kinase in the ventromedial hypothalamus in regulating counterregulatory hormone responses to acute hypoglycemia. *Diabetes*. (2008) 57:444–50. doi: 10.2337/db07-0837
162. Hirschberg PR, Sarkar P, Teegala SB, Routh VH. Ventromedial hypothalamus glucose-inhibited neurones: a role in glucose and energy homeostasis? *J Neuroendocrinol*. (2020) 32:e12773. doi: 10.1111/jne.12773
163. Wang P, Loh KH, Wu M, Morgan DA, Schneeberger M, Yu X, et al. A leptin-BDNF pathway regulating sympathetic innervation of adipose tissue. *Nature*. (2020) 583:839–44. doi: 10.1038/s41586-020-2527-y
164. Cypess AM, Weiner LS, Roberts-Toler C, Franquet Elia E, Kessler SH, Kahn PA, et al. Activation of human brown adipose tissue by a beta3-adrenergic receptor agonist. *Cell Metab*. (2015) 21:33–8. doi: 10.1016/j.cmet.2014.12.009
165. Carey AL, Formosa MF, Van Every B, Bertovic D, Eikelis N, Lambert GW, et al. Ephedrine activates brown adipose tissue in lean but not obese humans. *Diabetologia*. (2013) 56:147–55. doi: 10.1007/s00125-012-2748-1
166. Maestri NE, Brusilow SW, Clissold DB, Bassett SS. Long-term treatment of girls with ornithine transcarbamylase deficiency. *N Engl J Med*. (1996) 335:855–9. doi: 10.1056/NEJM199609193351204
167. Chen WY, Bailey EC, McCune SL, Dong JY, Townes TM. Reactivation of silenced, virally transduced genes by inhibitors of histone deacetylase. *Proc Natl Acad Sci USA*. (1997) 94:5798–803. doi: 10.1073/pnas.94.11.5798

Conflict of Interest: The authors declare that the research was conducted in the absence of any commercial or financial relationships that could be construed as a potential conflict of interest.

frontiers in Endocrinology

ORIGINAL RESEARCH
published: 10 December 2020
doi: 10.3389/fendo.2020.592818

Diphyllin Improves High-Fat Diet-Induced Obesity in Mice Through Brown and Beige Adipocytes

Ya-Nan Duan[1,2†], Xiang Ge[3†], Hao-Wen Jiang[2], Hong-Jie Zhang[4], Yu Zhao[3], Jin-Long Li[3,4], Wei Zhang[5*] and Jing-Ya Li[2*]*

[1] Shanghai Engineering Research Center of Molecular Therapeutics and New Drug Development, School of Chemistry and Molecular Engineering, East China Normal University, Shanghai, China, [2] Shanghai Institute of Materia Medica, Chinese Academy of Sciences, Shanghai, China, [3] School of Pharmacy, Nantong University, Nantong, China, [4] School of Chinese Medicine, Hong Kong Baptist University, Kowloon, Hong Kong Special Administrative Region, People's Republic of China, [5] Kay Laboratory of Brain Functional Genomics, Ministry of Education, Shanghai Key Laboratory of Brain Functional Genomics, School of Life Science, East China Normal University, Shanghai, China

OPEN ACCESS

Edited by:
Jiqiu Wang,
Shanghai Jiao Tong University, China

Reviewed by:
Wanzhu Jin,
Chinese Academy of Sciences (CAS), China
Weiping Han,
*Singapore Bioimaging Consortium (A*STAR), Singapore*

***Correspondence:**
Jin-Long Li
jinlongli@ntu.edu.cn
Wei Zhang
wzhang@sat.ecnu.edu.cn
Jing-Ya Li
jyli@simm.ac.cn

[†]These authors have contributed equally to this work

Specialty section:
This article was submitted to Cellular Endocrinology, a section of the journal Frontiers in Endocrinology

Received: *08 August 2020*
Accepted: *22 October 2020*
Published: *10 December 2020*

Citation:
Duan Y-N, Ge X, Jiang H-W, Zhang H-J, Zhao Y, Li J-L, Zhang W and Li J-Y (2020) Diphyllin Improves High-Fat Diet-Induced Obesity in Mice Through Brown and Beige Adipocytes. Front. Endocrinol. 11:592818. doi: 10.3389/fendo.2020.592818

Brown adipose tissue (BAT) and beige adipose tissue dissipate metabolic energy and mediate nonshivering thermogenesis, thereby boosting energy expenditure. Increasing the browning of BAT and beige adipose tissue is expected to be a promising strategy for combatting obesity. Through phenotype screening of C3H10-T1/2 mesenchymal stem cells, diphyllin was identified as a promising molecule in promoting brown adipocyte differentiation. *In vitro* studies revealed that diphyllin promoted C3H10-T1/2 cell and primary brown/beige preadipocyte differentiation and thermogenesis, which resulted increased energy consumption. We synthesized the compound and evaluated its effect on metabolism *in vivo*. Chronic experiments revealed that mice fed a high-fat diet (HFD) with 100 mg/kg diphyllin had ameliorated oral glucose tolerance and insulin sensitivity and decreased body weight and fat content ratio. Adaptive thermogenesis in HFD-fed mice under cold stimulation and whole-body energy expenditure were augmented after chronic diphyllin treatment. Diphyllin may be involved in regulating the development of brown and beige adipocytes by inhibiting V-ATPase and reducing intracellular autophagy. This study provides new clues for the discovery of anti-obesity molecules from natural products.

Keywords: diphyllin, obesity, brown adipocyte, differentiation, thermogenesis, V-ATPase

INTRODUCTION

Obesity has reached epidemic proportions worldwide and is associated with an increased risk of metabolic, cardiovascular and chronic inflammatory diseases, such as type 2 diabetes, dyslipidemia, nonalcoholic fatty liver disease (NAFLD), hypertension, coronary heart disease and stroke (1). The fundamental cause of obesity is the chronic energy imbalance between caloric intake and consumption, where surplus energy is stored in adipose tissue (2). Dietary and lifestyle modifications can be effective for the treatment of obesity and the prevention of diabetes. However, these approaches are difficult to maintain in the long term. Efficient ways to increase energy expenditure are urgently needed to combat the escalating occurrence of obesity.

Adipose tissue is a key organ in the regulation of energy balance. Three functionally different types of adipose tissue are present in mammals: white adipose tissue (WAT), brown adipose tissue (BAT) and brown-like (beige) adipose tissue. White adipose tissue is the primary site of triglyceride storage, but BAT and beige adipose tissue are specialized in energy expenditure and adaptational thermogenesis (2). These three tissues differ in anatomical localization, abundance, maintenance throughout the life of the animal, morphology and mainly function (3). The functions of BAT and beige adipose tissue are mediated by uncoupling proteins (UCPs), which are located in the inner mitochondrial membrane. UCP1 uncouples the oxidative phosphorylation process, oxidizing fatty acids and glucose that are produced by triglyceride hydrolysis to generate heat (4). Thus, promoting brown/beige adipose browning is now considered a safe strategy to resist obesity and ameliorate metabolic syndromes, such as hyperglycemia and insulin resistance (5). Strategies to target the browning of brown/beige adipocytes can be divided into two directions according to the characteristics of brown/beige adipocytes: promoting brown/beige preadipocyte differentiation and increasing thermogenesis of brown/beige fat cells (6). After several decades of research, many transcriptional and epigenetic factors and small molecules have been reported to control brown adipose cell fate and function; these factors include PPARγ (7, 8), PRDM16 (9–12) and PGC1α (13–17), and external cues include PPARγ agonists (18), catecholamines, and polyphenols (19).

Natural products are major sources of new drug leads. Searching for molecules with medicinal value from traditional medicines and discovering new indications of bioactive natural products are important approaches in natural product research. Recently, through *in vitro* screening of compounds from natural sources that regulate energy balance, a variety of phytochemicals [e.g., resveratrol (20), quercetin (21), cyanidin-3-glucoside (22, 23), berberine (24), and gypenosides (25)] have been reported to be able to increase energy expenditure and curb obesity and its complications by promoting adipose tissue differentiation and/or thermogenesis capacity.

Aryl naphthalene lignans (ANLs) are widely distributed in dietary or medicinal plants and exhibit excellent biological activities, such as antibacterial, anti-inflammatory, antiviral and anticancer activities (26). In addition, some herbs with ANLs were used as folk medicine for adjuvant therapy of diabetes, such as *Cordia rufescens* (27, 28). Researchers of *Shionogi & Co., Ltd.* reported that S-8921 and S-8921G, two synthetic ANLs, exhibited significant hypocholesterolemic effects *in vivo*, which expanded the application of lignans to metabolic diseases (29). Inspired by the potential effects of these ANLs on glycolipid metabolism, an *in vitro* assay based on the effect of browning differentiation in C3H10-T1/2 mesenchymal stem cells were used to evaluate the glycolipid metabolism regulation effects of the ANLs in our natural product library. Interestingly, diphyllin, a common ANL, significantly promoted browning adipogenesis and thermogenesis in adipocytes and increased oxygen consumption under a nontoxic dosage in both C3H10-T1/2 mesenchymal stem cells and primary brown/beige adipocytes. Further investigations revealed that diphyllin reduced obesity and improved the glucose tolerance capacity in high-fat diet-fed C57BL/6J mice. There is less experimental research concerning the effects of these ANLs on glycolipid metabolism. This study may expand new applications of these lignans in metabolic diseases and provide an opportunity to develop a new class of agent against obesity or related diseases.

Abbreviations: BAT, brown adipose tissue; Cidea, cell death-inducing DFFA-like effector a; Cox7a1, cytochrome c oxidase polypeptide 7a1; Cox8b, cytochrome c oxidase polypeptide 8b; CPT1, carnitine palmitoyltransferase 1; Dio2, type II iodothyronine deiodinase; EE, energy expenditure; Elovl3, elongation of very long chain fatty acids protein 3; eWAT, epididymal white adipose tissue; FBG, fasting blood glucose; FCCP, carbonyl cyanide 4-(trifluoromethoxy) phenylhydrazone; H&E, hematoxylin and eosin; HFD, High-fat-diet; IBMX, 3-Isobutyl-1-methylxanthine; ITT, insulin tolerance test; iWAT, inguinal white adipose tissue; LC3, Microtubule-associated protein 1 light chain 3; NEFA, nonesterified fatty acid; NMR, 1H-nuclear magnetic resonance; OCR, oxygen consumption rates; P62, sequestosome 1; pH:pondus hydrogeni; PGC-1α, Peroxisome proliferator-activated receptor gamma coactivator 1-alpha; PRDM16, PR domain containing 16; RER, respiratory exchange rate; SVF, stromal vascular fraction; T3, 3,3′,5-Triiodo-L-thyronine; TC, total cholesterol; TG, triglyceride; UCP1, uncoupling protein 1; V-ATPase, vacuolar H^+-ATPase.

MATERIALS AND METHODS

Materials

The antibody sources were as follows: UCP-1 (Abclonal, A5857), PRDM16 (Abcam, ab106410), PGC-1α (Calbiochem, ST1202), β-actin (Abgent, AM1021B), Cide-A (Santa Cruz, sc-293289), PPARγ (Abcam, ab178860), adiponectin (AdipoQ) (Abcam, ab62551), FABP4 (Cell Signaling, #2120), LC3 (Proteintech, 14600-1-AP), and p62 (SQSTM1) (MBL, PM045). Rosiglitazone, dexamethasone, 3-Isobutyl-1-methylxanthine (IBMX), 3,3′,5-Triiodo-L-thyronine (T3), indomycine, oligomycin, carbonyl cyanide 4-(trifluoromethoxy) phenylhydrazone (FCCP), rotenone and antimycin A were purchased from Sigma-Aldrich. Recombinant human Insulin (Roche) was purchased from Changzheng Hospital (Shanghai, China). ELISA kits used in measurement of plasma parameters are as follows: TG (Shanghai Fosun Long March, 1.02.1801), TC (Shanghai Fosun Long March, 1.02.0401), NEFA (WAKO, 294-63601).

Chemical Synthesis of Diphyllin (1)

Diphyllin was prepared under the aldol reaction and Diels-Alder reaction (30). A schematic illustration of the synthesis of diphyllin is summarized in **Scheme S1**. Taking 3,4-dimethoxybenzaldehyde as a starting material, compound 2 was obtained after bromination. Glycolytic acetal 3 was synthesized from 2 and glycol by using p-TsOH as a catalyst in toluene under reflux. Under the condition of n-BuLi, the aldol reaction occurred with piperonal to obtain intermediate 3a, which was further dissolved in glacial acetic acid and reacted with diethyl acetylenedicarboxylate (DEADC) at 140°C under a nitrogen atmosphere to yield 4. The selective reduction of 4 by BH3.Me2S in THF led to diphyllin (**Scheme S1**, **Figures S1–S5**, Supporting Information).

The synthesis route was started with 3,4-dimethoxybenzaldehyde under bromination, aldol reaction, Diels-Alder reaction and selective reduction to obtain the target molecule.

6-Bromoveratrol (2). Br2 (11.26 ml, 220 mmol) was added to a solution of 3,4-dimethoxybenzaldehyde (33.2 g, 200 mmol) in MeOH (160 ml) in an ice bath over 1 h, and the mixture was stirred for 6 h at room temperature. After the completion of the reaction, as indicated by TLC, 300 ml of water was added, and the crystals were precipitated. To a suspension of the crystal was added aqueous NaOH to adjust it to a pH of approximately 9~10. The precipitate was collected by filtration, washed with water and dried under vacuum to give 49.1 g of 6-bromoveratrol (2) as a white solid (95%). 1H NMR (400 MHz, $CDCl_3$) δ 10.18 (1H, s), 7.41 (1H, s), 7.05 (1H, s), 3.96 (3H, s), 3.92 (3H, s).

2-(2-Bromo-4,5-dimethoxyphenyl)-1,3-dioxolane (3). To a flask containing dry toluene (150 ml), 6-bromoveratrol (2) (9.8 g, 40 mmol), glycol (6.5 ml, 48 mmol), and p-toluenesulfonic acid (0.6 g) were added as catalysts. The flask was connected to a Dean-Stark trap and refluxed for 3 h. The solvent was removed in vacuo, and the residue was partitioned between EA and 1 M NaOH (150 ml). The organic layer was washed with brine (250 ml) and dried over anhydrous Na_2SO_4. After the solvent was removed, the residue was recrystallized in EtOH to obtain 2-(2-bromo-4,5-dimethoxyphenyl)-1,3-dioxolane (3) (10.2 g, 89%). 1H NMR (400 MHz, $CDCl_3$) δ 7.11 (1H, s), 7.01 (1H, s), 5.99 (1H, s), 4.17 (2H, m), 4.06 (2H, m), 3.89 (3H, s), 3.88 (3H, s).

Diethyl 1-(3,4-methylenedioxyphenyl)-4-hydroxy-6,7-dimethoxynaphthalene-2,3-dicarboxylate (4). To a solution of the acetal (3) (2.9 g, 10 mmol) in dry THF (40 ml) was added n-BuLi (4.8 ml, 2.5 M solution in n-hexane, 12 mmol) dropwise at -78°C under N_2 atmosphere, and the mixture was stirred for 15 min. A solution of piperonal (1.5 g, 10 mmol) in anhydrous THF (10 ml) was added at -78°C. The mixture was stirred for 30 min and allowed to warm to rt for 2.5 h. The reaction was quenched with 50 ml of acetic acid below 0°C. DEADC (1.7 g, 10 mmol) was added to the solution and then heated at 140°C for 1 h in a N_2 atmosphere. After cooling to room temperature, the mixture was extracted with DCM. The organic layer was washed with brine 3 times and dried over anhydrous Na_2SO_4. The residue was purified by silica gel chromatography and eluted with PE/EA = 3:1 to afford 3.01 g of compound 4 as a yellow powder (64%). 1H NMR (400 MHz, Chloroform-d) δ 12.45 (1H, s), 7.74 (1H, s), 6.89 (1H, d, J = 7.8 Hz), 6.81 (1H, d, J = 1.6 Hz), 6.78 (1H, dd, J = 7.8, 1.6 Hz), 6.75 (1H, s), 6.06 (1H, d, J = 1.3 Hz), 6.01 (1H, d, J = 1.3 Hz, 1H), 4.41 (2H, q, J = 7.1 Hz), 4.06 (5H, m), 3.77 (3H, s), 1.36 (3H, t, J = 7.1 Hz), 1.06 (3H, t, J = 7.2 Hz).

Diphyllin (1). To a solution of compound 4 (3.0 g, 6.4 mmol) in THF (40 ml) was added $BH_3{\cdot}Me_2S$ (6.4 ml, 10.0 M solution in DMS, 64 mmol) in an ice bath, and the mixture was stirred overnight at room temperature. After the completion of the reaction, as indicated by TLC, 2 N HCl was added to the solution to adjust the pH to 2~3. Then, the solution was partitioned with DCM. The organic layer was washed with brine (250 ml) and dried over anhydrous Na_2SO_4. After the solvent was removed, the residue was recrystallized in MeOH to afford 0.866 g of diphyllin (1) as a yellow powder (36%). 1H NMR (400 MHz, DMSO-d6) δ 10.40 (1H, s), 7.62 (1H, s), 7.02 (1H, d, J = 7.9 Hz), 6.96 (1H, s), 6.86 (1H, d, J = 1.6 Hz), 6.75 (1H, dd, J = 7.9, 1.6 Hz), 6.11 (2H, s), 5.36 (2H, s), 3.94 (3H, s), 3.65 (3H, s). 13C NMR (100 MHz, DMSO-d6) δ 169.7, 150.5, 149.7, 146.8, 146.6, 144.9, 129.5, 129.5, 128.8, 123.8, 123.3, 121.7, 118.7, 111.1, 107.9, 105.4, 101.0, 100.7, 66.6, 55.6, 55.1.

Chemical Screening

Natural compounds were from Jing-Long Li laboratory, 36 molecules with different skeleton types of natural products (such as lignans, terpenoids, and alkaloids) were selected to treat the cells. For high-throughput chemical screenings, C3H10-T1/2 cells were differentiated in 48-well plates. At day 0 after 2 days of confluency, cells were treated with chemicals for 8 days with induction medium and maintenance medium and analyzed for mRNA levels using quantitative real-time PCR (qRT-PCR) and oil red O staining. The mRNA ratios of *Fapb4*, *Ucp1* and *Adiponectin* in each well were used to evaluate the effect of each chemical, and oil red O staining provided further confirmation. The chemical library was from the Jin-Long Li group and applied at a final concentration of 10 μM or 10 μg/ml of each chemical in screening. Cells treated with DMSO and 1 μM rosiglitazone were used as controls.

Sulforhodamine B Sodium Salt Assay

Cytotoxicity was determined by the sulforhodamine B sodium salt (SRB) cytotoxicity assay using 96-well microtiter plates as described (31). Cells were plated in duplicate wells (3,000 cells/well) and exposed to diphyllin at different concentrations. After 48 h of incubation, cells were fixed with 10% TCA (attached cells were fixed with 3.3% TCA) solution for 1 h, and 0.057% SRB (Sigma Chemical Co.) was added to each well. After a 30-min incubation, the plates were washed, and dye was dissolved in 10 mM Tris buffer (pH 10.5) and read at 570 nm on a microplate reader (Molecular Device). The wells with cells containing no drugs and wells with medium plus drugs but without cells were used as positive and negative controls, respectively. All of the reagents were purchased from Sigma-Aldrich.

Cell Culture

C3H10-T1/2 cells were a gift kindly given by Jiqiu Wang, Ruijin Hospital. All the cells were maintained in Dulbecco's modified Eagle's medium (DMEM) supplemented with 10% FBS (Gibco), 0.1 mg/ml streptomycin (Invitrogen) and 100 U/ml penicillin at 37°C in a 5% CO2 incubator. Adipocyte differentiation of C3H10-T1/2 cells were induced by treating confluent cells with DMEM containing 10% FBS, 0.5 mM isobutylmethylxanthine (IBMX), 125 nM indomethacin, 1 μM dexamethasone, 850 nM insulin and 1 nM T3. Two days after induction, cells were switched to maintenance medium containing 10% FBS, 850 nM insulin and 1 nM T3 for 6 days. For brown adipocyte differentiation, cells were incubated with diphyllin for 8 days at 5 and 10 μM. For adipocyte thermogenesis, cells were incubated with diphyllin for 24 h after differentiation.

Isolation of Adipose Stromal Vascular Fraction Cells and Differentiation *In Vitro*

Stromal vascular fraction (SVF) cells were isolated as described from 4- to 6-week-old male C57BL/6J mice previously (32). In brief, adipose tissue from inguinal area and interscapular area was minced on ice and digested with 2.4 mg/ml dispase II (Roche) and 10 mg/ml collagenase D (Roche) in phosphate-buffered saline (PBS) supplemented for 45 min at 37°C, followed by stopping digestion with complete medium and filtering through a 100 μm strainer (BD Biosciences). The cell suspensions were centrifuged at 4 °C for 10 min, 500g, then suspended and filtered through a 40 μm strainer (BD Biosciences) and then further centrifuged at 4 °C for 10 min, 500g, and suspended before plating onto 10 cm dishes. SVF cells were cultured in DMEM/F12 supplemented with 10% FBS and 0.1 mg/ml streptomycin (Invitrogen) and 100 U/ml penicillin (Invitrogen). Adipocyte differentiation was carried out by treating confluent cells in induction medium supplemented with 0.5 mM IBMX, 125 nM indomethacin, 1 μM dexamethasone, 850 nM insulin, and 10 nM T3 for 48 h. Next, the cells were maintained in maintenance medium supplemented with 850 nM insulin and 10 nM T3 for 6 days. To analyze the effects of diphyllin on differentiation, diphyllin was added throughout the differentiation. Experiments were performed on day 8 of differentiation. To analyze the effects of diphyllin on thermogenesis, diphyllin was added at day 7 for 24 h after differentiation.

Oil Red O Staining

Oil red O staining was performed according to standard protocols (33). Cells were washed twice with phosphate-buffered saline (PBS) and fixed with 4% paraformaldehyde for 30 min at room temperature, followed by oil red O (BBI, E607319) incubation for 60 min. The cells were washed with PBS 2~3 times before visualizing under a light microscope and image capture. Absorbance was measured with a Spectra Max M5 (Agilent Technologies) at 520 nm. The relative intracellular lipid content was expressed as the optical density at 520 nm relative to the solution control.

Quantitative RT-PCR Analysis

Total RNA was isolated from cells or homogenized tissues using TRIzol reagent (Invitrogen). Complementary DNA was prepared from 1 μg of total RNA using Prime Script Reverse Transcriptase (TaKaRa) according to the manufacturer's instructions. After 10-fold dilution, the cDNAs were amplified using 2 x SYBR Green qPCR Master Mix (Abclonal) and a Stratagene Mx3005P system (Agilent Technologies). Expression data were normalized to *36b4*. Sequences of primers used in this study are listed in **Table S1** (Supporting Information).

Western Blot Analysis

Cells were lysed with SDS-PAGE sample loading buffer (Beyotime) on ice and then denatured at 100°C for 10 min. Proteins were electrophoresed through SDS-PAGE and transferred to nitrocellulose filter membranes. Membranes were blocked with 5% skim milk at room temperature for 1 h and incubated with the indicated antibody overnight at 4°C, followed by incubation with secondary antibody at room temperature for 1 h. The expression signal of the indicated proteins was detected with enhanced chemiluminescence (GE Healthcare).

OCR Measurements

Cells were plated in an XF 96-well microplate (Seahorse Bioscience) and allowed to grow to confluency. The experiments were performed on day 8. For the analysis of diphyllin's effect on thermogenesis, diphyllin was added at day 7 and for 24 h to C3H10-T1/2 or primary brown/beige adipocytes. The cells were induced to undergo brown/beige adipogenesis for 8 days, followed by OCR measurement at 37°C using an XF96 analyzer (Seahorse Bioscience) according to the manufacturer's instructions. 2 μM oligomycin, 1 μM FCCP and 1 μM rotenone/antimycin A were used to detect uncoupled respiration, maximal respiration and nonmitochondrial respiration, respectively.

Chronic Efficacy Studies

All animal experiments were approved by the Animal Care and Use Committee of the Shanghai Institute of Materia Medica, where the experiments were conducted. Six-week-old male C57BL/6J mice (Shanghai SLAC Laboratory Animal Co., Shanghai, China) were housed in a temperature- and relative humidity-controlled room (22 ± 2°C, 55 ± 5%) with a 12-h light-dark cycle and free access to food and water. For chronic anti-obesity studies, mice were fed a high-fat diet (HFD) initiated at 6 weeks of age (60% calories from fat, 20% calories from protein, 20% calories from carbohydrate; Research Diets). At 22 weeks of age, HFD mice were randomly assigned to treatment groups. Vehicle and diphyllin (100 mg/kg) were given between 11:00 and 12:00 AM everyday for 9 weeks. Body weight and food intake were recorded daily. A glucose tolerance test (GTT) was performed in the 4th week. Cold exposure was tested in the 5th week. Metabolic analysis was performed in the 6th week. An insulin tolerance test (ITT) was conducted, and blood samples were collected in the 7th week of the study. Body composition measurements were performed in the 8th week. At the 9th week, tissues were dissected, weighed, immediately frozen in liquid nitrogen and stored at -80°C and fixed with 4% paraformaldehyde at room temperature for HE staining.

GTT and ITT Assays

The mice were fasted for 6 h and received a *p.o.* injection of glucose (2 g/kg) or *i.p.* injection of recombinant human insulin (0.75 U/kg). The glucose concentrations were measured in blood collected by venous bleeding from the tail vein immediately before and after 15, 30, 60, 90 and 120 min. The area under the curve was calculated for analysis.

Metabolic Analysis in the Animal Study

Oxygen consumption, carbon dioxide production and locomotor activity were measured using a sixteen-chamber indirect calorimeter (TSE PhenoMaster, TSE system) according to the manufacturer's instructions. The mice were maintained at 24°C

under a 12-h light-dark cycle. Food and water were available ad libitum. Locomotor activity was derived from the x-axis and y-axis beam breaks monitored every 17 min. Heat production as name as energy expenditure, oxygen expenditure, activity and RER were calculated as described previously. The total fat and lean masses of mice were assessed with the body composition in the 8th week of treatment using 1H-nuclear magnetic resonance spectroscopy (Minispec LF90 II, Bruker).

Cold Exposure

Mice were individually housed at 4°C for 8 h without food but with free access to water. Rectal temperature was measured every hour with a BAT-12 microprobe digital thermometer and RET-3 mouse rectal probe (Physitemp Instruments, Clifton, USA).

Lysosome Acidification Assays

Lysosomes were acidified using a LysoSensor™ Yellow/Blue DND-160 (Yeasen Biotechnology, 40768ES50) as reported before (34, 35). After diphyllin treatment, cells were incubated for 24 h with 2 μM LysoSensor™ Yellow/Blue DND-160 for 5 min before test. The OD value at 384 nm is used to indicate the pH of lysosomes.

Histology

Brown adipose tissue, white inguinal and epididymal adipose tissues were fixed in 4% formaldehyde overnight at room temperature, embedded in paraffin, and sectioned (6 μm) by a microtome. The slides were deparaffinized, rehydrated, and stained with hematoxylin and eosin (Sigma) according to a standard protocol. Images were viewed under a light microscope for image capture and cell surface was calculated by AdipoCount application, which was reported before (36).

Statistics

All the values represent the means ± SEM. Error bars represent SEM; significant differences compared to vehicle controls are indicated by *$p < 0.05$, **$p < 0.01$, and ***$p < 0.001$.

RESULTS

Diphyllin Is Identified as a Natural Inducer From Differentiation Screening of Natural Products on C3H10-T1/2 Cells

Activation of brown adipocytes contributes to total body fuel expenditure through energy dissipation as heat, which is considered an effective method for the treatment of obesity and related diseases. C3H10-T1/2 cells, which are mouse-derived mesenchymal stem cells, can differentiate into brown adipocytes by a browning cocktail. Based on natural molecules found to promote brown/beige browning, we performed a screening assay on C3H10-T1/2 mesenchymal stem cells, which can be induced into brown adipocytes. For each plate, DMSO and 1 μM rosiglitazone treatment were both included as internal controls. The Jin-long Li natural library was selected for C3H10-T1/2 differentiation, 36 molecules with different skeleton types of natural products (such as lignans, terpenoids, and alkaloids) were selected to treat the cells. Cells were treated with compounds throughout differentiation, and a schematic view of the strategy is shown in **Figure 1A**. The mRNA ratios of *Fapb4*, *Ucp1* and *Adiponectin* in each well were used to evaluate the effect of each chemical, and oil red O staining provided further confirmation. Consistent with many studies, the ratio of rosiglitazone treatment to the control group was significantly differentially promoted with respect to both mRNA (**Figures 1B, D**) and oil red O staining (**Figure 1E**). Fold changes upon treatment with respect to DMSO controls in each plate were then calculated for each compound at the mRNA level (**Figure 1B**). Diphyllin (1) (**Figure 1C**), an aryl naphthalene lignan and a natural compound that can activate *Ucp1*, *Fabp4* and *Adiponectin* expression, showed an mRNA ratio of more than 2-fold (**Figures 1B, D**) and promoted brown adipogenesis, showing more oil red O dye deposition (**Figure 1E**).

Diphyllin Promotes Differentiation and Thermogenesis of C3H10-T1/2 Cells, Primary Brown and Beige Adipocyte Preadipocytes

The cytotoxicity of diphyllin was initially evaluated in C3H10-T1/2 mesenchymal stem cells with a sulforhodamine B sodium salt (SRB) assay. As shown in **Figure S6** (Supporting Information), at a concentration of 10 μM for 48 h, diphyllin exhibited no apparent cytotoxicity.

Based on the *in vitro* screening experiment, we evaluated the effects of diphyllin on the browning of brown and beige adipocytes, including the differentiation stage and thermogenesis stage, using the stromal vascular fraction cells of brown fat and white inguinal fat, which could be induced to brown and beige adipocyte (37). For the late phase differentiation of brown and beige adipocyte, after the day 6, the brown and beige marker genes, such as *Adiponectin*, *Fabp4*, *Ucp1*, have reached a very high state, which means that adipocyte was mature (38–40). So, we choose day 7 to investigate the role of diphyllin on mature brown and beige fat, major in thermogenesis activation, except for the role of differentiation. The schematic view strategy is shown in **Figure 2A**. As shown in **Figure 2B**, diphyllin significantly promoted the differentiation of brown preadipocytes at concentrations of 5 and 10 μM by oil red O staining, with adipogenic genes, including *Pparγ*, *Fabp4*, *Adiponectin* and *Ucp1*, being significantly increased (**Figures 2C, D**). In addition, the same phenotypes were reproduced in primary brown and beige adipocyte precursors (**Figures 3A–D**, **Figures 3J–M**). The above data suggested that diphyllin promotes the differentiation of brown/beige adipocytes.

We then evaluated the effects of diphyllin on thermogenesis in differentiated C3H10-T1/2 cells. As shown in **Figures 2E, F**, the expression of thermogenic genes such as *Ucp1* and *Pgc1α* was upregulated in the presence of diphyllin at concentrations of 5 and 10 μM for 24 h. Consistently, the related thermogenic proteins, including UCP1, were also increased after treatment with diphyllin in comparison with the control group. In addition, the basal oxygen consumption rate (OCR) and uncoupling oxygen consumption rate were significantly induced in

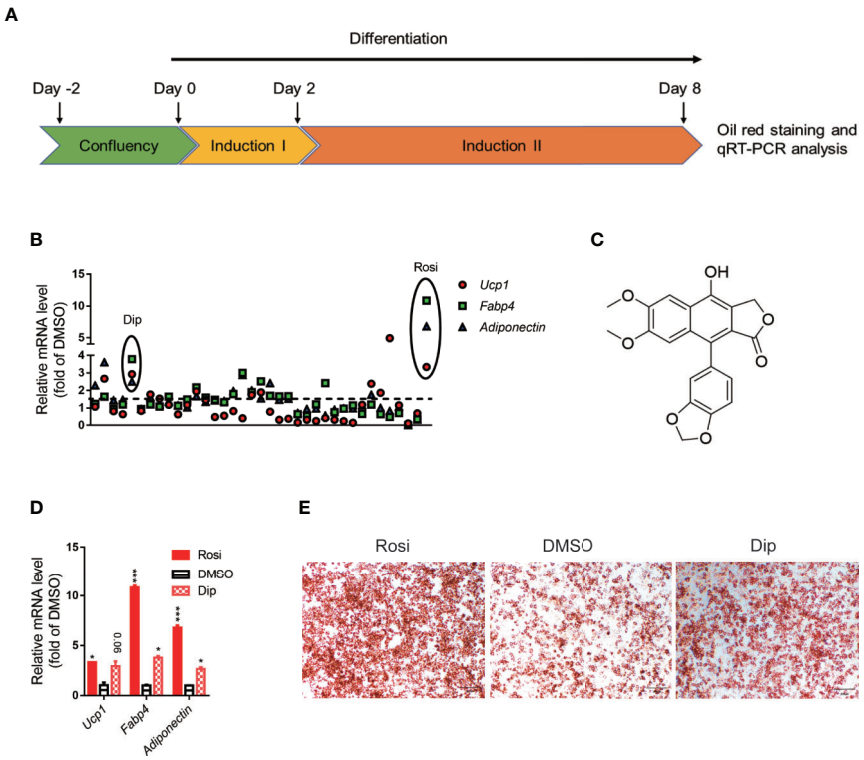

FIGURE 1 | Differentiation screening of natural products in C3H10-T1/2 cells. **(A)** Schematic view of the targeting strategy for natural product screening. **(B)** Relative gene mRNA expression in differentiated cells treated with natural products. **(C)** Structure of diphyllin (1). **(D)** Relative gene mRNA expression in differentiated cells treated with rosiglitazone and diphyllin. **(E)** Oil red O staining in differentiated cells treated with rosiglitazone or diphyllin. For oil red O staining, n=1; for mRNA expression, n=2. *p < 0.05 and ***p < 0.001.

differentiated C3H10-T1/2 brown adipocytes by coincubation with diphyllin for 24 h (**Figures 2G–I**). In addition, the same phenotypes were reproduced in primary mature brown and beige adipocytes (**Figures 3E–I**, **Figures 3N–R**). Collectively, these results indicated that diphyllin increased thermogenesis in brown/beige adipocytes.

Diphyllin Promotes Weight Loss With Increased Thermogenesis and Improves Metabolism *In Vivo*

On the basis of the aforementioned experiments, diphyllin was further evaluated for its effects on the metabolic characteristics of obese mice. After C57BL/6J mice were fed a high-fat diet (HFD-fed mice) for 16 weeks with insulin resistance and obvious obesity, diphyllin was administered orally once daily at a dose of 100 mg/kg for an additional 9 weeks. As shown in **Figure 4B**, significant weight loss of the mice was observed after 4 weeks of diphyllin treatment compared with the vehicle group, while total food intake did not differ between the two groups (**Figure 4A**). We analyzed the body composition of diphyllin-treated mice by NMR (**Figure 4C**). Compared with the control group, the diphyllin treatment group mice had a significantly reduced fat content ratio. In particular, diphyllin treatment significantly reduced the inguinal and epididymis white adipose tissue weights, which suggested that the decreasing weights of mice were mainly attributed to the lowered level of adiposity, since the weights of interscapular brown adipose tissues were similar between the two groups (**Figure 4D**). Consistent with the body weight change, diphyllin treatment resulted in modest improvement in both the glucose tolerance test (GTT) and insulin sensitivity test (ITT), suggesting improved metabolism (**Figures 4E–G**), and diphyllin was found to reduce plasma levels of free fatty acids and triglyceride but not sterol (**Figures 4H–J**).

Energy expenditure is an essential indicator of energy homeostasis, and increasing energy consumption is an important strategy to resist diet-induced obesity. To investigate how diphyllin administration reduced diet-induced obesity, the effects of diphyllin on whole-body energy expenditure were tested with the respiratory metabolic system in HFD-fed mice. After daily treatment for 6 weeks, oxygen consumption and energy expenditure during a 12-h light/dark cycle were higher in diphyllin-treated mice (*p.o.* 100 mg/kg) than control mice (**Figures 5A–D**), with basal respiratory exchange ratio (**Figure 5E**) and unchanged locomotor activity (RER) (**Figure 5F**), which showed that there was no bias in promoting diphyllin between glucose metabolism and lipid metabolism. These results indicated that diphyllin improved

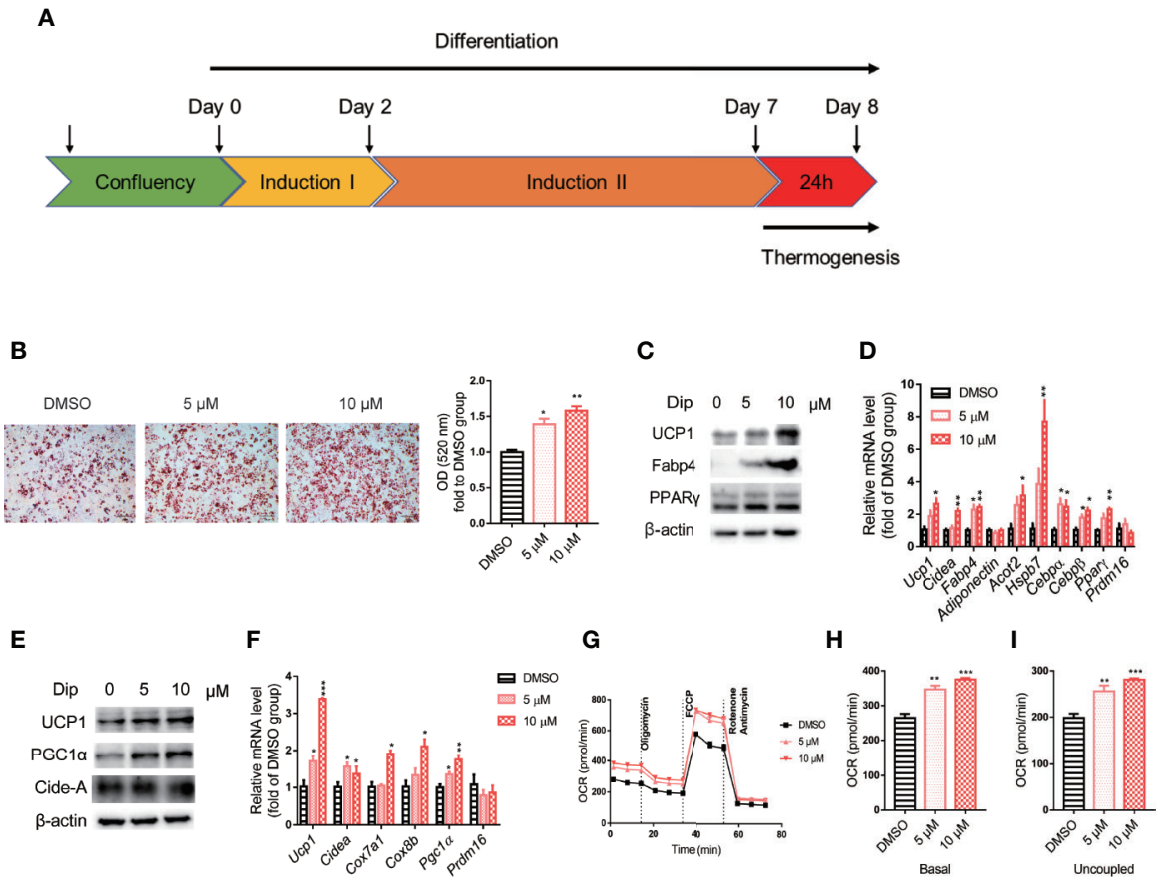

FIGURE 2 | Diphyllin promotes brown adipocyte differentiation and thermogenesis in C3H10-T1/2 cells. **(A)** Schematic view of the targeting strategy to evaluate the effect of diphyllin. **(B)** Oil red O staining in differentiated cells treated with diphyllin, N=3. **(C)** The protein levels in brown adipocytes after the differentiation test; **(D)** The relative gene mRNA levels in brown adipocytes after the differentiation test, n=3. **(E)** The protein levels in brown adipocytes after the thermogenesis test; **(F)** The relative gene mRNA levels in brown adipocytes after the thermogenesis test, n=3. **(G)** Oxygen consumption rates (OCR) of brown adipocytes after 5 and 10 μM diphyllin treatment for 24 h; **(H, I)**. The OCR-related basal metabolic rate and uncoupled oxygen consumption refer to **(C)**. *p < 0.05, **p < 0.01, and ***p < 0.001.

diet-induced obesity, which might be attributed to the higher energy expenditure in comparison to control mice. Brown adipose tissue is well known as an essential thermogenic organ that consumes abundant fuels to maintain basic body temperature by nonshivering thermogenesis under cold stimuli, called adaptive thermogenesis. As shown in **Figure 5G**, the mice treated with diphyllin had significantly increased rectal temperature after cold stimulation compared with the control group. All these above data showed that diphyllin treatment could improve glucose and lipid metabolism, resist diet-induced obesity and ameliorate insulin sensitivity.

Since activation of brown/beige adipocytes is one of the major ways to enhance energy expenditure, we tested whether diphyllin induces reprogramming to brown/beige in adipose tissues. Quantitative real-time PCR revealed that diphyllin upregulated thermogenic genes, including *Ucp1*, *Cox7a1* and *Pgc1α*; adipogenic genes, including *Ap2*, *Adiponectin* and *Pparγ*; and glucose uptake and lipolytic genes, including *Glut4*, *Hsl* and *Atgl*, in inguinal white adipose tissues, epididymal white adipose tissues and interscapular brown adipose tissues (**Figures 6A–C**). The upregulation of *Ucp1* expression in inguinal white adipose, epididymal white adipose and interscapular brown adipose tissues were also confirmed by immunoblotting of UCP1 proteins (**Figures 6D–F**). We also observed that the fat cell surface decreased after diphyllin administration compared to the control group in inguinal white adipose tissues, epididymal white adipose tissues and interscapular brown adipose tissues (**Figures 6G–I**). Based on the above results, we hypothesized that diphyllin augments whole-body energy expenditure to resist obesity by thermogenic activation of adipose tissue in HFD-fed mice.

DISCUSSION

The worldwide obesity epidemic makes developing a new strategy to combat obesity an urgent need. Few medicines are

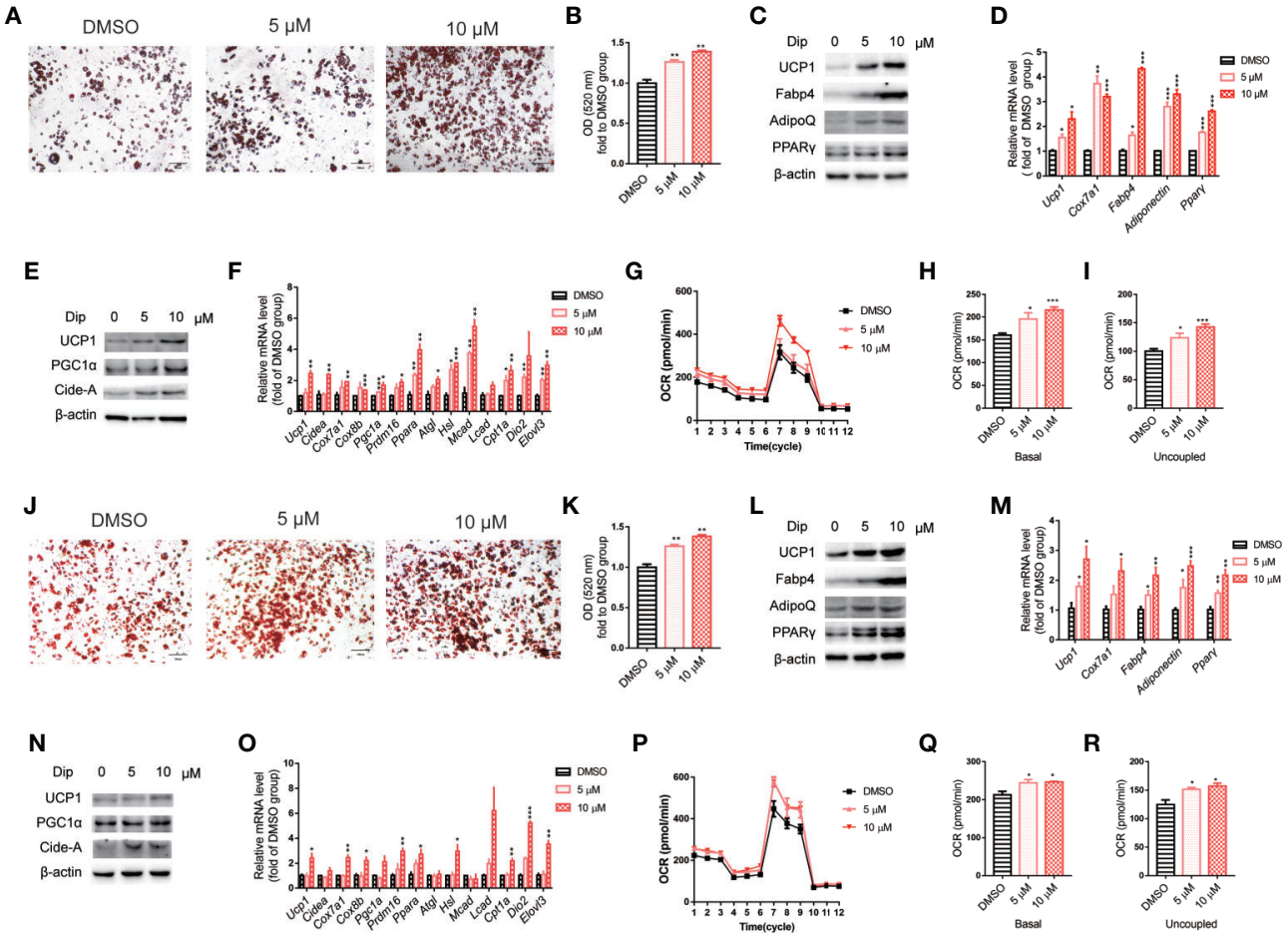

FIGURE 3 | Diphyllin promotes differentiation and thermogenesis in primary brown **(A–I)** and beige **(J–R)** adipocytes. **(A, J)** Oil red O staining of differentiated brown and beige adipocytes treated with diphyllin, N=4. **(B, K)** Quantitative statistics of oil red O staining. **(C, L)** The protein levels in brown adipocytes after the differentiation test; **(D, M)** The relative gene mRNA levels in brown adipocytes after the differentiation test, n=3. **(E, N)** The protein levels in brown adipocytes after the thermogenesis test; **(F, O)** The relative gene mRNA levels in brown adipocytes after the thermogenesis test, n=3. **(G, P)** Oxygen consumption rates (OCRs) of brown adipocytes after 5 and 10 μM diphyllin treatment for 24 h; **(H–I, Q–R)**. The OCR-related basal metabolic rate and uncoupled oxygen consumption. *$p < 0.05$, **$p < 0.01$, and ***$p < 0.001$.

currently available for the treatment of obesity on the market, and many that are have certain side effects, such as headache, depression and gastrointestinal reaction. Because of its properties, brown/beige adipocyte thermogenesis is considered a safe and effective strategy to combat obesity.

Natural products, owing to their structural and biological activity diversity, represent an important pool for the discovery of drug leads. In our continuing effort to find bioactive molecules that improve adipocyte browning from natural products, we obtained the natural compound diphyllin as a potentiator of brown adipose adipogenesis and thermogenesis by screening our natural product library. Our data showed that diphyllin promoted the thermogenesis and differentiation of brown/beige adipocytes and prevented diet-induced obesity and glycolipid metabolic syndrome in HFD-fed mice. The upregulation of UCP1 in white adipose tissues demonstrated that diphyllin could convert mature white adipocytes into beige adipocytes and promote thermogenesis *in vitro* and *in vivo*.

To determine the diphyllin-induced signaling pathway involved in differentiation and nonshivering thermogenesis, we next investigated the mechanism of diphyllin. Sørensen et al. found that diphyllin, as a novel and naturally potent vacuolar H+-ATPase (V-ATPase) inhibitor, abrogates acidification of the osteoclastic resorption lacunae and bone resorption (41). Diphyllin was previously reported as a V-ATPase inhibitor, which decreases the internal pH (pHi) and reverses the transmembrane pH gradient, inhibits the proliferation and induces the apoptosis of cancer cells and abrogates acidification of the osteoclastic resorption lacunae and bone resorption (42–45). V-ATPase activity as a proton pump is required for acidification of a wide array of different organelles in eukaryotes (46). In mammalian cells, V-ATPase proton pumps are the primary pH regulators that maintain intravascular and/or

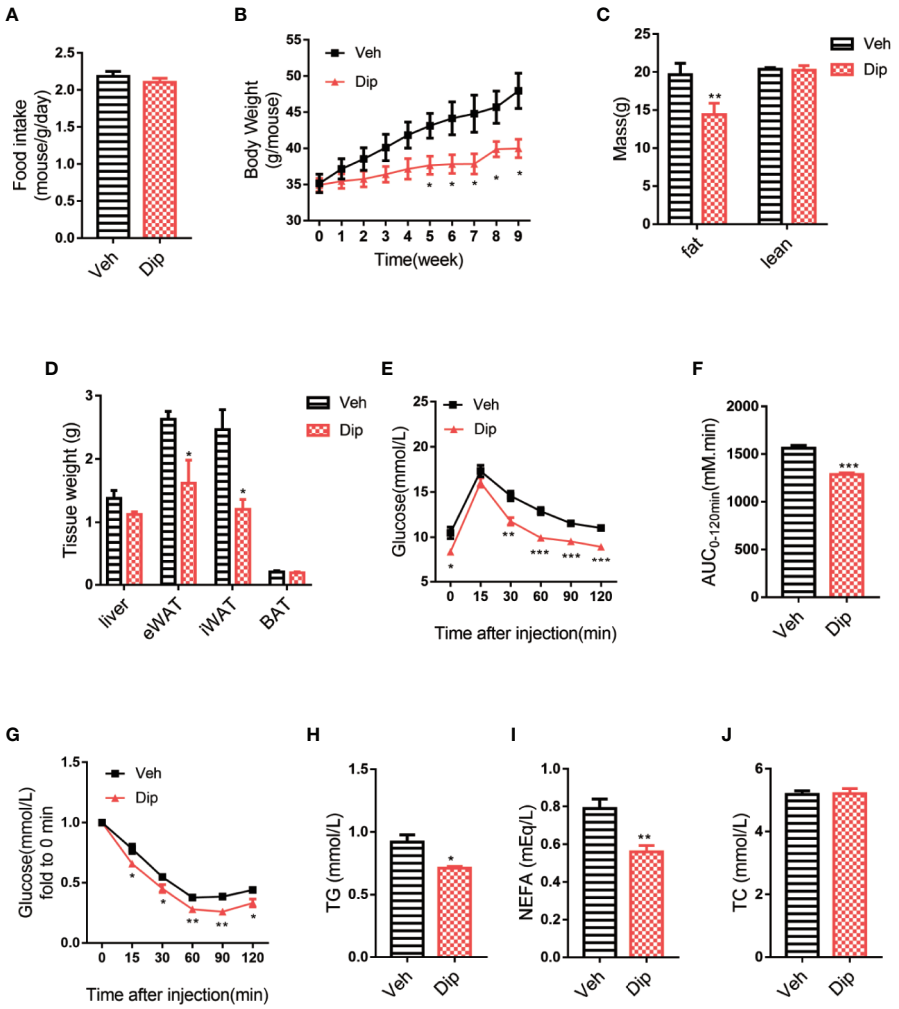

FIGURE 4 | Diphyllin protects mice against high-fat diet-induced obesity. **(A)** Food intake per mouse treated with diphyllin or vehicle. (n = 3). **(B)** Body weights of mice treated with diphyllin or vehicle. (n = 6). **(C)** Lean body mass and fat composition of mice determined by NMR after 5 weeks of treatment. (n = 6). **(D)** Tissue weights of mice determined by NMR after 5 weeks of treatment. (n = 6). **(E, F)** Glucose tolerance test (GTT) performed in mice after 4 weeks of treatment. (n = 6). **(G)** Insulin tolerance test (ITT) performed in mice after 6 weeks of treatment. (n = 6). **(H, I, J)** Plasma total triglyceride (TG), total cholesterol (TC), and nonesterified fatty acid (NEFA) contents of mice measured after 7 weeks of treatment. (n = 6). *$p < 0.05$, **$p < 0.01$, and ***$p < 0.001$.

extracellular pondus hydrogenii (pH). The V-ATPase complex is mainly responsible for lysosomal acidification. Recent reports implicate altered V-ATPase activity and lysosomal pH dysregulation in cellular aging, longevity, and adult-onset neurodegenerative diseases, including forms of Parkinson's disease and Alzheimer's disease (47). Ohsumi et al. tested whether vacuolar acidification was required for autophagy in yeast by following the accumulation of autophagic bodies in the vacuoles of wild-type and vma-mutant (V-ATPase deficient) cells and their subsequent degradation. This study confirmed that V-ATPase activity is required for the final step of autophagy, that is, the breakdown of cargo delivered to the vacuole (48). Genetic defects in V-ATPase subunits or V-ATPase-related proteins are increasingly seen in lipid metabolism dysregulation (49, 50) and in association with a decrease in autophagy in the late phase (51, 52). Lysosome-related autophagy regulates brown adipocyte function. Chloroquine, a weak lysosomotropic base that blocks the fusion of autophagosomes with lysosomes, blocked dexamethasone-induced brown adipose tissue whitening and decreased the fat mass content in dexamethasone-treated mice (53, 54). Bafilomycin, the autophagy repressor target of V-ATPase, increases UCP1 protein expression in primary preadipocytes (55). These studies reveal that V-ATPase activity and lysosomes regulate brown/beige cell fate and function.

As inhibiting V-ATPase causes lysosomal deacidification, leading to decreased autophagy flux through autophagosome-lysosome fusion (56), resulting in the accumulation of Microtubule-associated protein 1 light chain 3 (LC3) and sequestosome 1 (p62) (53). We tested the acidification of lysosomes using LysoSensor™ Yellow/Blue DND-160, an

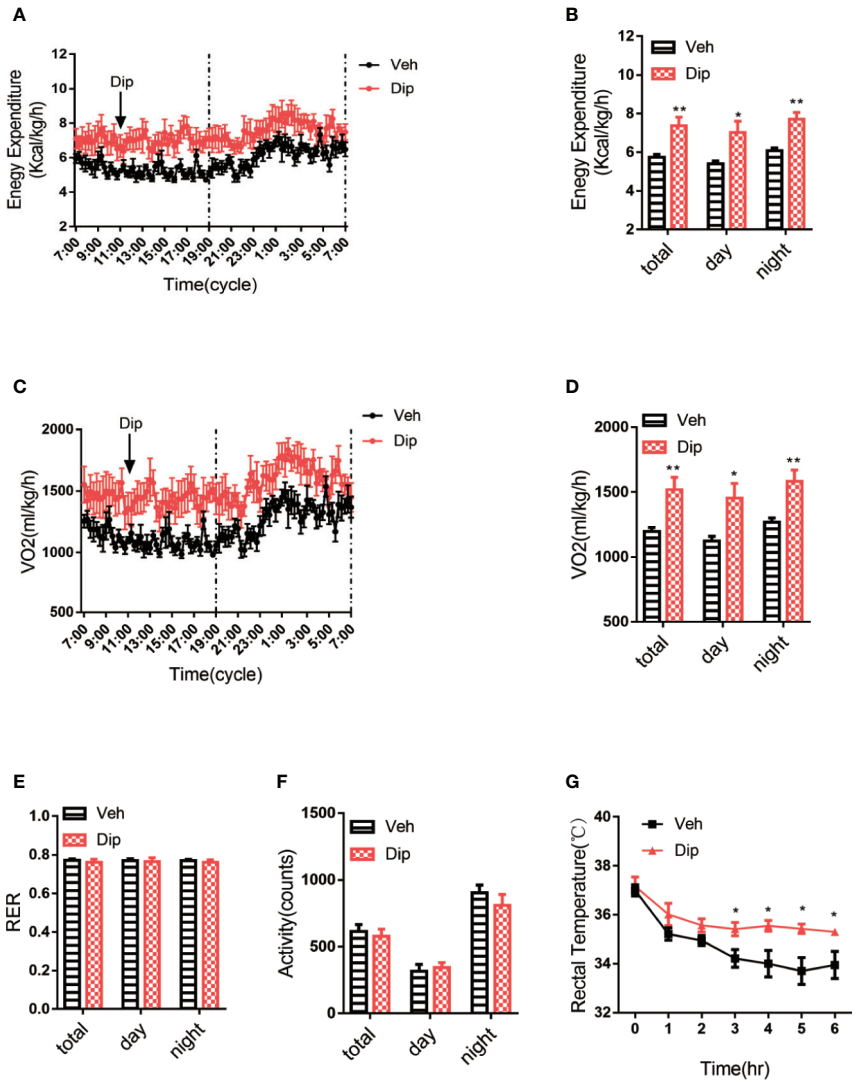

FIGURE 5 | Diphyllin increases energy expenditure and adaptive thermogenesis. **(A)** Energy expenditure and **(B)** statistics for different time periods in DIO mice after 6 weeks of diphyllin treatment (n=6). **(C)** Oxygen consumption (VO2) and **(D)** statistics for different time periods in DIO mice after 6 weeks of diphyllin treatment (n=6). **(E)** Statistics of the respiratory exchange ratio (RER) in DIO mice after 6 weeks of diphyllin treatment (n=6). **(F)** Statistics of the locomotor activity in DIO mice after 6 weeks of diphyllin treatment (n=6). **(G)** Rectal temperature during cold exposure was recorded in 1-h intervals in a cold room (n=6 mice). *$p < 0.05$ and **$p < 0.01$.

acidophilic lysosome shuttle probe, and diphyllin-treated cells showed lower yellow dye deposition than the controls (**Figure S7A**). Autophagy flux was tested with the tandem GFP-RFP-LC3 adenovirus, which represents autophagosome formation as previously described (57). We also observed decreased autophagy flux and an accumulation of LC3 and p62 (**Figures S7B, C**). This suggests that diphyllin may be involved in regulating the development of brown and beige adipocytes by inhibiting V-ATPase and reducing intracellular autophagy.

Autophagy for non-selective bulk degradation of proteins and lipids through the fusion of autophagosomes and lysosomes is suggested as one of the major types of autophagy in adipocytes (58–60). Many studies have shown that autophagy plays an important role in adipogenesis, activation and maintenance of brown/beige adipocytes. An adipocyte-specific mouse knockout of Atg7 increased features of brown adipocytes, which, along with an increase in normal brown adipose tissue, led to an elevated rate of fatty acid beta-oxidation and a lean body mass (60, 61). Inhibition of autophagy in brown adipocytes leads to an increase in UCP1 protein and mitochondrial density, causing more uncoupled respiration and OXPHOS, suggesting a repressing role for autophagy in the activity of the BAT thermogenic machinery (62). Autophagy is needed to convert beige adipocytes to WAT upon removal of β3-AR agonists or recovery from cold exposure, revealing that autophagy plays a negative role in beige adipocyte maintenance (63). It seems that

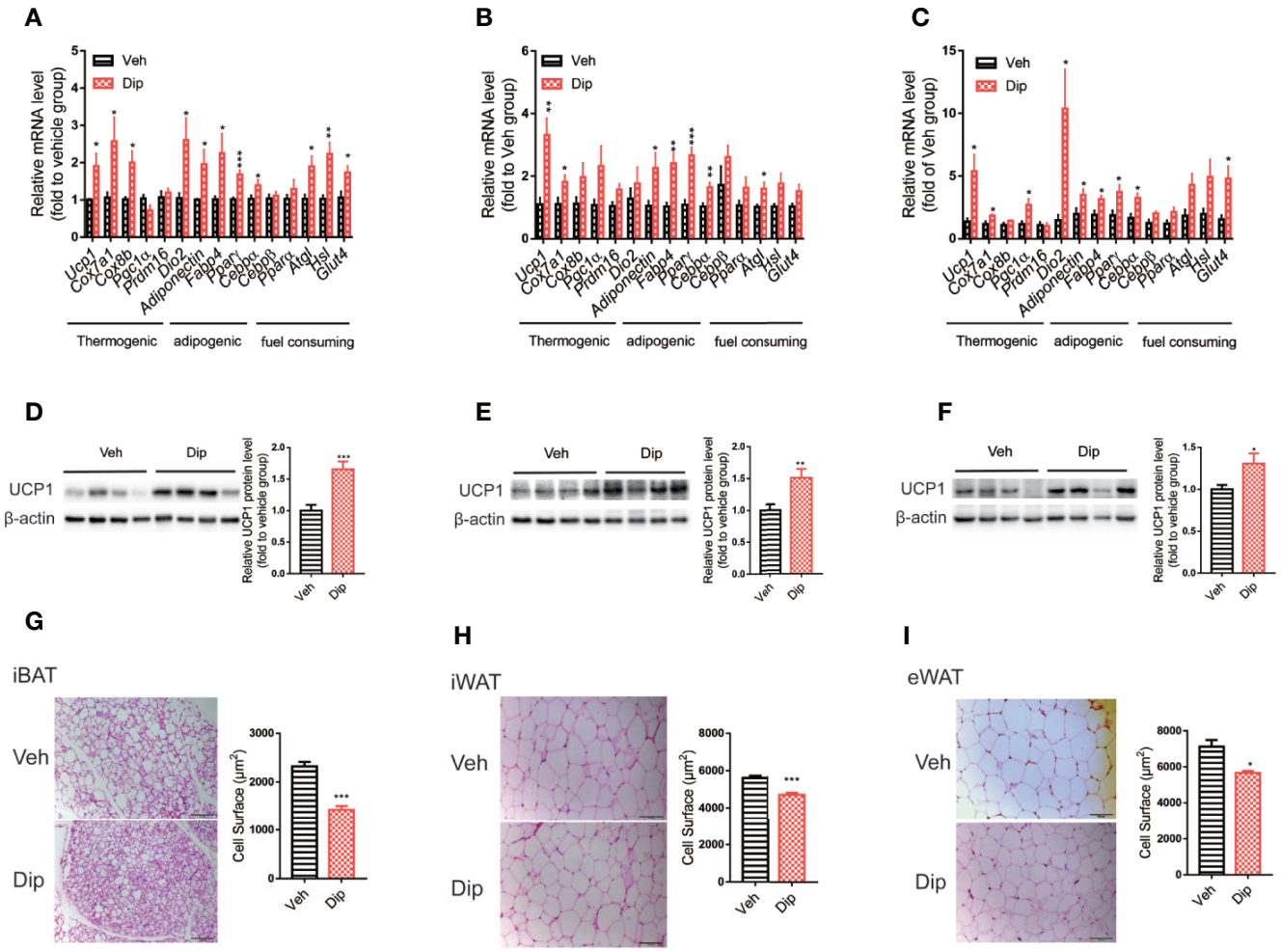

FIGURE 6 | Diphyllin enhances brown/beige thermogenesis and reduces adipocyte size in DIO mice. **(A–C)** Relative mRNA levels of the indicated genes after diphyllin treatment in iBAT, iWAT and eWAT (n=6). **(D–F)** Western blot analysis and relative integrated density of UCP1 protein in iBAT, iWAT, and eWAT of DIO mice after treatment (n=6). **(G–I)** Representative HE staining images and statistical diagram of the cell surface of BAT, iWAT, and eWAT. Scale bar = 100 μm for ×10. *p < 0.05, **p < 0.01, and ***p < 0.001.

a good anti-obesity strategy would be to inhibit autophagy, but due to inhibition of autophagy seeming detrimental in hypermetabolic conditions such as hepatic steatosis, atherosclerosis, thermal injury, sepsis, and cachexia through an increase in free fatty acid and glycerol release from WAT, the emerging concept of white fat browning–conversion to beige/brown fat has been controversial in its anti-obesity effect through facilitation of weight loss and improvement in metabolic health (64).

In summary, diphyllin improved brown and beige adipocyte differentiation and thermogenesis. Moreover, chronic diphyllin administration alleviated diet-induced obesity by promoting the browning process in brown adipose tissues, inguinal and epididymal white adipose tissues. These results revealed that diphyllin is a promising lead compound for the treatment of obesity and related diseases, and the lead molecule deserves to be further studied.

DATA AVAILABILITY STATEMENT

The original contributions presented in the study are included in the article/**Supplementary Material**, further inquiries can be directed to the corresponding author/s.

ETHICS STATEMENTS

The animal study was reviewed and approved by Animal Care and Use Committee of the Shanghai Institute of Materia Medica.

AUTHOR CONTRIBUTIONS

Y-ND and XG contributed to study design, data analyzing, discussion, and preparation of the manuscript. H-WJ, H-JZ,

and YZ contributed to conducting the experiments. J-LL, WZ, and J-YL contributed to the study design, discussion, reviewing, and editing the manuscript. All authors contributed to the article and approved the submitted version.

FUNDING

This work was supported by the National Natural Science Foundation of China (Nos. 81673493 and 81803384), the National Science and Technology Major Project (No. 2018ZX09711002-018), the Natural Science Foundation of Jiangsu Province, China (No. BK20180947), Strategic Priority Research Program of Chinese Academy of Sciences grant (XDA12050409), Strategic Pilot Program of the Chinese Academy of Sciences (XDA12040204), and the Hong Kong Scholars program (XJ2019054).

ACKNOWLEDGMENTS

We thank Dr. Jiqiu Wang from Ruijin Hospital, Shanghai Jiaotong University School of Medicine, for discussion and the guidance for SVFs isolation and differentiation.

SUPPLEMENTARY MATERIAL

The Supplementary Material for this article can be found online at: https://www.frontiersin.org/articles/10.3389/fendo.2020.592818/full#supplementary-material

REFERENCES

1. Wang YC, McPherson K, Marsh T, Gortmaker SL, Brown M. Health and economic burden of the projected obesity trends in the USA and the UK. *Lancet* (2011) 378(9793):815–25. doi: 10.1016/S0140-6736(11)60814-3
2. Gesta S, Tseng YH, Kahn CR. Developmental origin of fat: tracking obesity to its source. *Cell* (2007) 131(2):242–56. doi: 10.1016/j.cell.2007.10.004
3. Del Mar Gonzalez-Barroso M, Ricquier D, Cassard-Doulcier AM. The human uncoupling protein-1 gene (UCP1): present status and perspectives in obesity research. *Obes Rev* (2000) 1(2):61–72. doi: 10.1046/j.1467-789x.2000.00009
4. Alberdi G, Rodríguez VM, Miranda J, Macarulla MT, Churruca I, Portillo MP. Thermogenesis is involved in the body-fat lowering effects of resveratrol in rats. *Food Chem* (2013) 141(2):1530–5. doi: 10.1016/j.foodchem.2013.03.085
5. Fenzl A, Kiefer FW. Brown adipose tissue and thermogenesis. *Horm Mol Biol Clin Investig* (2014) 19(1):25–37. doi: 10.1515/hmbci-2014-0022
6. Rosenwald M, Perdikari A, Rülicke T, Wolfrum C. Bi-directional interconversion of brite and white adipocytes. *Nat Cell Biol* (2013) 15 (6):659–67. doi: 10.1038/ncb2740
7. Rosen ED, Sarraf P, Troy AE, Bradwin G, Moore K, Milstone DS, et al. PPAR gamma is required for the differentiation of adipose tissue in vivo and in vitro. *Mol Cell* (1999) 4(4):611–7. doi: 10.1016/s1097-2765(00)80211-7
8. Barak Y, Nelson MC, Ong ES, Jones YZ, Ruiz-Lozano P, Chien KR, et al. PPAR gamma is required for placental, cardiac, and adipose tissue development. *Mol Cell* (1999) 4(4):585–95. doi: 10.1016/s1097-2765(00)80209-9
9. Ohno H, Shinoda K, Ohyama K, Sharp LZ, Kajimura S. EHMT1 controls brown adipose cell fate and thermogenesis through the PRDM16 complex. *Nature* (2013) 504(7478):163–7. doi: 10.1038/nature12652
10. Kajimura S, Seale P, Kubota K, Lunsford E, Frangioni JV, Gygi SP, et al. Initiation of myoblast to brown fat switch by a PRDM16-C/EBP-beta transcriptional complex. *Nature* (2009) 460(7259):1154–8. doi: 10.1038/nature08262
11. Seale P, Kajimura S, Yang W, Chin S, Rohas LM, Uldry M, et al. Transcriptional control of brown fat determination by PRDM16. *Cell Metab* (2007) 6(1):38–54. doi: 10.1016/j.cmet.2007.06.001
12. Seale P, Bjork B, Yang W, Kajimura S, Chin S, Kuang S, et al. PRDM16 controls a brown fat/skeletal muscle switch. *Nature* (2008) 454(7207):961–7. doi: 10.1038/nature07182
13. Puigserver P, Wu Z, Park CW, Graves R, Wright M, Spiegelman BM. A cold-inducible coactivator of nuclear receptors linked to adaptive thermogenesis. *Cell* (1998) 92(6):829–39. doi: 10.1016/s0092-8674(00)81410-5
14. Tiraby C, Tavernier G, Lefort C, Larrouy D, Bouillaud F, Ricquier D, et al. Acquirement of brown fat cell features by human white adipocytes. *J Biol Chem* (2003) 278(35):33370–6. doi: 10.1074/jbc.M305235200
15. Iida S, Chen W, Nakadai T, Ohkuma Y, Roeder RG. PRDM16 enhances nuclear receptor-dependent transcription of the brown fat-specific Ucp1 gene through interactions with Mediator subunit MED1. *Genes Dev* (2015) 29 (3):308–21. doi: 10.1101/gad.252809.114
16. Chen W, Yang Q, Roeder RG. Dynamic interactions and cooperative functions of PGC-1alpha and MED1 in TRalpha-mediated activation of the brown-fat-specific UCP-1 gene. *Mol Cell* (2009) 35(6):755–68. doi: 10.1016/j.molcel.2009.09.015
17. Kong X, Banks A, Liu T, Kazak L, Rao RR, Cohen P, et al. IRF4 is a key thermogenic transcriptional partner of PGC-1α. *Cell* (2014) 158(1):69–83. doi: 10.1016/j.cell.2014.04.049
18. Sell H, Berger JP, Samson P, Castriota G, Lalonde J, Deshaies Y, et al. Peroxisome proliferator-activated receptor gamma agonism increases the capacity for sympathetically mediated thermogenesis in lean and ob/ob mice. *Endocrinology* (2004) 145(8):3925–34. doi: 10.1210/en.2004-0321
19. Li H, Qi J, Li L. Phytochemicals as potential candidates to combat obesity via adipose non-shivering thermogenesis. *Pharmacol Res* (2019) 147:104393. doi: 10.1016/j.phrs.2019.104393
20. Cho AS, Jeon SM, Kim MJ, Yeo J, Seo KI, Choi MS, et al. Chlorogenic acid exhibits anti-obesity property and improves lipid metabolism in high-fat diet-induced-obese mice. *Food Chem Toxicol* (2010) 48(3):937–43. doi: 10.1016/j.fct.2010.01.003
21. Lee SG, Parks JS, Kang HW. Quercetin, a functional compound of onion peel, remodels white adipocytes to brown-like adipocytes. *J Nutr Biochem* (2017) 42:62–71. doi: 10.1016/j.jnutbio.2016.12.018
22. You Y, Yuan X, Liu X, Liang C, Meng M, Huang Y, et al. Cyanidin-3-glucoside increases whole body energy metabolism by upregulating brown adipose tissue mitochondrial function. *Mol Nutr Food Res* (2017) 61(11):1–13. doi: 10.1002/mnfr.201700261
23. Pei L, Wan T, Wang S, Ye M, Qiu Y, Jiang R, et al. Cyanidin-3-O-β-glucoside regulates the activation and the secretion of adipokines from brown adipose tissue and alleviates diet induced fatty liver. *BioMed Pharmacother* (2018) 105:625–32. doi: 10.1016/j.biopha.2018.06.018
24. Zhang Z, Zhang H, Li B, Meng X, Wang J, Zhang Y, et al. Berberine activates thermogenesis in white and brown adipose tissue. *Nat Commun* (2014) 5:5493. doi: 10.1038/ncomms6493
25. Liu J, Li Y, Yang P, Wan J, Chang Q, Wang TTY, et al. Gypenosides Reduced the Risk of Overweight and Insulin Resistance in C57BL/6J Mice through Modulating Adipose Thermogenesis and Gut Microbiota. *J Agric Food Chem* (2017) 65(42):9237–46. doi: 10.1021/acs.jafc.7b03382
26. Zhao KP, Rakesh SM, Mumtaz S, Moku B, Asiri A, Marwani HM, et al. Arylnaphthalene lactone analogues: synthesis and development as excellent biological candidates for future drug discovery. *RSC Adv* (2018) 8:9487–502. doi: 10.1039/C7RA13754K
27. Souza da Silva SA, Souto AL, de Fatima Agra M, Leitao da-Cunha E, Barbosa-Filho JM, Sobral da Silva M, et al. A new arylnaphthalene type lignan from Cordia rufescens A. DC. (Boraginaceae). *ARKIVOC* (2004) 6:54–8. doi: 10.3998/ark.5550190.0005.607
28. Swami G, Nagpal N, Rahar S, Singh P, Porwal A, Manisha N, et al. Effect of aqueous leaves extract of Cordia dichotoma on blood glucose levels of normoglycemic & alloxan induced diabetic wister rats. *Int J Pharm Res Dev* (2010) 2:1–7.

29. Sakamoto S, Kusuhara H, Miyata K, Shimaoka H, Kanazu T, Matsuo Y, et al. Glucuronidation converting methyl 1-(3,4-dimethoxyphenyl)-3-(3-ethylvaleryl)-4-hydroxy-6,7,8-trimethoxy-2-naphthoate (S-8921) to a potent apical sodium-dependent bile acid transporter inhibitor, resulting in a hypocholesterolemic action. *J Pharmacol Exp Ther* (2007) 322(2):610–8. doi: 10.1124/jpet.106.116426
30. Charlton JL, Oleschuk CJ, Chee G-L. Hindered Rotation in Arylnaphthalene Lignans. *J Org Chem* (1996) 61:3452–7. doi: 10.1021/jo952048e
31. Skehan P, Storeng R, Scudiero D, Monks A, McMahon J, Vistica D, et al. New colorimetric cytotoxicity assay for anticancer-drug screening. *J Natl Cancer Inst* (1990) 82(13):1107–12. doi: 10.1093/jnci/82.13.1107
32. Wang J, Liu R, Wang F, Hong J, Li X, Chen M, et al. Ablation of LGR4 promotes energy expenditure by driving white-to-brown fat switch. *Nat Cell Biol* (2013) 15(12):1455–63. doi: 10.1038/ncb2867
33. Ramírez-Zacarías JL, Castro-Muñozledo F, Kuri-Harcuch W. Quantitation of adipose conversion and triglycerides by staining intracytoplasmic lipids with Oil red O. *Histochemistry* (1992) 97(6):493–7. doi: 10.1007/BF00316069
34. DePedro HM, Urayama P. Using LysoSensor Yellow/Blue DND-160 to sense acidic pH under high hydrostatic pressures. *Anal Biochem* (2009) 384(2):359–61. doi: 10.1016/j.ab.2008.10.007
35. Harris VM, Harley ITW, Kurien BT, Koelsch KA, Scofield RH. Lysosomal pH Is Regulated in a Sex Dependent Manner in Immune Cells Expressing CXorf21. *Front Immunol* (2019) 10:578. doi: 10.3389/fimmu.2019.00578
36. Zhi X, Wang J, Lu P, Jia J, Shen HB, Ning G. AdipoCount: A New Software for Automatic Adipocyte Counting. *Front Physiol* (2018) 9:85. doi: 10.3389/fphys.2018.00085
37. Wu J, Boström P, Sparks LM, Ye L, Choi JH, Giang AH, et al. Beige adipocytes are a distinct type of thermogenic fat cell in mouse and human. *Cell* (2012) 150(2):366–76. doi: 10.1016/j.cell.2012.05.016
38. Fu X, Jin L, Han L, Yuan Y, Mu Q, Wang H, et al. miR-129-5p Inhibits Adipogenesis through Autophagy and May Be a Potential Biomarker for Obesity. *Int J Endocrinol* (2019) 2019:5069578. doi: 10.1155/2019/5069578
39. Jun H, Yu H, Gong J, Jiang J, Qiao X, Perkey E, et al. An immune-beige adipocyte communication via nicotinic acetylcholine receptor signaling. *Nat Med* (2018) 24(6):814–22. doi: 10.1038/s41591-018-0032-8
40. Li S, Yu Q, Wang GX, Lin JD. The biological clock is regulated by adrenergic signaling in brown fat but is dispensable for cold-induced thermogenesis. *PloS One* (2013) 8(8):e70109. doi: 10.1371/journal.pone.0070109
41. Sørensen MG, Henriksen K, Neutzsky-Wulff AV, Dziegiel MH, Karsdal MA. Diphyllin, a novel and naturally potent V-ATPase inhibitor, abrogates acidification of the osteoclastic resorption lacunae and bone resorption. *J Bone Miner Res* (2007) 22(10):1640–8. doi: 10.1359/jbmr.070613
42. Chen H, Liu P, Zhang T, Gao Y, Zhang Y, Shen X, et al. Effects of diphyllin as a novel V-ATPase inhibitor on TE-1 and ECA-109 cells. *Oncol Rep* (2018) 39(3):921–8. doi: 10.3892/or.2018.6191
43. Zhao Y, Ni C, Zhang Y, Zhu L. Synthesis and bioevaluation of diphyllin glycosides as novel anticancer agents. *Arch Pharm (Weinheim)* (2012) 345(8):622–8. doi: 10.1002/ardp.201200035
44. Stransky L, Cotter K, Forgac M. The Function of V-ATPases in Cancer. *Physiol Rev* (2016) 96(3):1071–91. doi: 10.1152/physrev.00035.2015
45. Lu Y, Zhang R, Liu S, Zhao Y, Gao J, Zhu L. ZT-25, a new vacuolar H(+)-ATPase inhibitor, induces apoptosis and protective autophagy through ROS generation in HepG2 cells. *Eur J Pharmacol* (2016) 771:130–8. doi: 10.1016/j.ejphar.2015.12.026
46. Nishi T, Forgac M. The vacuolar (H+)-ATPases–nature's most versatile proton pumps. *Nat Rev Mol Cell Biol* (2002) 3(2):94–103. doi: 10.1038/nrm729
47. Bagh MB, Peng S, Chandra G, Zhang Z, Singh SP, Pattabiraman N, et al. Misrouting of v-ATPase subunit V0a1 dysregulates lysosomal acidification in a neurodegenerative lysosomal storage disease model. *Nat Commun* (2017) 8:14612. doi: 10.1038/ncomms14612
48. Nakamura N, Matsuura A, Wada Y, Ohsumi Y. Acidification of vacuoles is required for autophagic degradation in the yeast, Saccharomyces cerevisiae. *J Biochem* (1997) 121(2):338–44. doi: 10.1093/oxfordjournals.jbchem.a021592
49. Nakadera E, Yamashina S, Izumi K, Inami Y, Sato T, Fukushima H, et al. Inhibition of mTOR improves the impairment of acidification in autophagic vesicles caused by hepatic steatosis. *Biochem Biophys Res Commun* (2016) 469(4):1104–10. doi: 10.1016/j.bbrc.2015.12.010
50. Wilde L, Tanson K, Curry J, Martinez-Outschoorn U. Autophagy in cancer: a complex relationship. *Biochem J* (2018) 475(11):1939–54. doi: 10.1042/BCJ20170847
51. Xia Y, Liu N, Xie X, Bi G, Ba H, Li L, et al. The macrophage-specific V-ATPase subunit ATP6V0D2 restricts inflammasome activation and bacterial infection by facilitating autophagosome-lysosome fusion. *Autophagy* (2019) 15(6):960–75. doi: 10.1080/15548627.2019.1569916
52. Sasaki T, Lian S, Khan A, Llop JR, Samuelson AV, Chen W, et al. Autolysosome biogenesis and developmental senescence are regulated by both Spns1 and v-ATPase. *Autophagy* (2017) 13(2):386–403. doi: 10.1080/15548627.2016.1256934
53. Cypess AM, Chen YC, Sze C, Wang K, English J, Chan O, et al. Cold but not sympathomimetics activates human brown adipose tissue in vivo. *Proc Natl Acad Sci USA* (2012) 109:10001–5. doi: 10.1073/pnas.1207911109
54. Deng J, Guo Y, Yuan F, Chen S, Yin H, Jiang X, et al. Autophagy inhibition prevents glucocorticoid-increased adiposity via suppressing BAT whitening. *Autophagy* (2020) 16(3):451–65. doi: 10.1080/15548627.2019.1628537
55. Armani A, Cinti F, Marzolla V, Morgan J, Cranston GA, Antelmi A, et al. Mineralocorticoid receptor antagonism induces browning of white adipose tissue through impairment of autophagy and prevents adipocyte dysfunction in high-fat-diet-fed mice. *FASEB J* (2014) 28(8):3745–57. doi: 10.1096/fj.13-245415
56. Shen W, Zou X, Chen M, Liu P, Shen Y, Huang S, et al. Effects of diphyllin as a novel V-ATPase inhibitor on gastric adenocarcinoma. *Eur J Pharmacol* (2011) 667(1-3):330–8. doi: 10.1016/j.ejphar.2011.05.042
57. Han L, Zhang Y, Liu S, Zhao Q, Liang X, Ma Z, et al. Autophagy flux inhibition, G2/M cell cycle arrest and apoptosis induction by ubenimex in glioma cell lines. *Oncotarget* (2017) 8(64):107730–43. doi: 10.18632/oncotarget.22594
58. Singh R, Kaushik S, Wang Y, Xiang Y, Novak I, Komatsu M, et al. Autophagy regulates lipid metabolism. *Nature* (2009) 458:1131–5. doi: 10.1038/nature07976
59. Soler-Vazquez MC, Mera P, Zagmutt S, Serra D, Herrero L. New approaches targeting brown adipose tissue transplantation as a therapy in obesity. *Biochem Pharmacol* (2018) 155:346–55. doi: 10.1016/j.bcp.2018.07.022
60. Singh R, Xiang Y, Wang Y, Baikati K, Cuervo AM, Luu YK, et al. Autophagy regulates adipose mass and differentiation in mice. *J Clin Invest* (2009) 119(11):3329–39. doi: 10.1172/JCI39228
61. Zhang Y, Goldman S, Baerga R, Zhao Y, Komatsu M, Jin S. Adipose-specific deletion of autophagy-related gene 7 (atg7) in mice reveals a role in adipogenesis. *Proc Natl Acad Sci U S A* (2009) 106(47):19860–5. doi: 10.1073/pnas.0906048106
62. Cairó M, Villarroya J, Cereijo R, Campderrós L, Giralt M, Villarroya F. Thermogenic activation represses autophagy in brown adipose tissue. *Int J Obes (Lond)* (2016) 40(10):1591–9. doi: 10.1038/ijo.2016.115
63. Altshuler-Keylin S, Shinoda K, Hasegawa Y, Ikeda K, Hong H, Kang Q, et al. Beige Adipocyte Maintenance Is Regulated by Autophagy-Induced Mitochondrial Clearance. *Cell Metab* (2016) 24(3):402–19. doi: 10.1016/j.cmet.2016.08.002
64. Ro SH, Jang Y, Bae J, Kim IM, Schaecher C, Shomo ZD. Autophagy in Adipocyte Browning: Emerging Drug Target for Intervention in Obesity. *Front Physiol* (2019) 10:22. doi: 10.3389/fphys.2019.00022

Conflict of Interest: The authors declare that the research was conducted in the absence of any commercial or financial relationships that could be construed as a potential conflict of interest.

frontiers in Endocrinology

ORIGINAL RESEARCH
published: 11 January 2021
doi: 10.3389/fendo.2020.592154

Bola3 Regulates Beige Adipocyte Thermogenesis *via* Maintaining Mitochondrial Homeostasis and Lipolysis

Ningning Bai[1†], Jingyuan Ma[1†], Miriayi Alimujiang[1], Jun Xu[2], Fan Hu[1], Yuejie Xu[1], Qingyang Leng[3], Shuqing Chen[1], Xiaohua Li[3], Junfeng Han[1], Weiping Jia[1], Yuqian Bao[1] and Ying Yang[1*]*

[1] Department of Endocrinology and Metabolism, Shanghai Clinical Center for Diabetes, Shanghai Key Clinical Center for Metabolic Disease, Shanghai Diabetes Institute, Shanghai Key Laboratory of Diabetes Mellitus, Shanghai Jiao Tong University Affiliated Sixth People's Hospital, Shanghai, China, [2] Department of Geriatrics, Shanghai Jiao Tong University Affiliated Sixth People's Hospital, Shanghai, China, [3] Department of Endocrinology, Seventh People's Hospital of Shanghai University of TCM, Shanghai, China

OPEN ACCESS

Edited by:
Xinran Ma,
East China Normal University, China

Reviewed by:
Rita De Matteis,
University of Urbino Carlo Bo, Italy
Assunta Lombardi,
University of Naples Federico II, Italy

***Correspondence:**
Ying Yang
yangyingsh@sjtu.edu.cn
Yuqian Bao
yqbao@sjtu.edu.cn

[†]These authors have contributed equally to this work

Specialty section:
This article was submitted to Cellular Endocrinology, a section of the journal Frontiers in Endocrinology

Received: *06 August 2020*
Accepted: *19 November 2020*
Published: *11 January 2021*

Citation:
Bai N, Ma J, Alimujiang M, Xu J, Hu F, Xu Y, Leng Q, Chen S, Li X, Han J, Jia W, Bao Y and Yang Y (2021) Bola3 Regulates Beige Adipocyte Thermogenesis via Maintaining Mitochondrial Homeostasis and Lipolysis. Front. Endocrinol. 11:592154. doi: 10.3389/fendo.2020.592154

Mitochondrial iron-sulfur (Fe-S) cluster is an important cofactor for the maturation of Fe-S proteins, which are ubiquitously involved in energy metabolism; however, factors facilitating this process in beige fat have not been established. Here, we identified BolA family member 3 (Bola3), as one of 17 mitochondrial Fe-S cluster assembly genes, was the most significant induced gene in the browning program of white adipose tissue. Using lentiviral-delivered shRNA *in vitro*, we determined that Bola3 deficiency inhibited thermogenesis activity without affecting lipogenesis in differentiated beige adipocytes. The inhibition effect of Bola3 knockdown might be through impairing mitochondrial homeostasis and lipolysis. This was evidenced by the decreased expression of mitochondria related genes and respiratory chain complexes, attenuated mitochondrial formation, reduced mitochondrial maximal respiration and inhibited isoproterenol-stimulated lipolysis. Furthermore, BOLA3 mRNA levels were higher in human deep neck brown fat than in the paired subcutaneous white fat, and were positively correlated with thermogenesis related genes (UCP1, CIDEA, PRDM16, PPARG, COX7A1, and LIPE) expression in human omental adipose depots. This study demonstrates that Bola3 is associated with adipose tissue oxidative capacity both in mice and human, and it plays an indispensable role in beige adipocyte thermogenesis *via* maintaining mitochondrial homeostasis and adrenergic signaling-induced lipolysis.

Keywords: BolA family member 3, mitochondria, beige adipocyte, lipolysis, thermogenesis

INTRODUCTION

Obesity occurs when energy intake chronically exceeds energy expenditure, which increases the risk of developing metabolic disorders, such as insulin resistance, type 2 diabetes and cardiovascular diseases (1, 2). Adipose tissues play a pivotal role in systematic energy homeostasis through multiple functions (3). There are three functionally distinct adipocyte subtypes that have been identified in

mice. Classically, white adipocytes are responsible for triglyceride storage and mobilization as needed; brown adipocytes contain abundant uncoupling protein 1 (UCP1), which uncouples fuels oxidation from ATP production to heat generation; beige adipocytes are interspersed within white adipose tissue (WAT) and express UCP1 upon thermogenic activation (4). Although brown and beige adipocytes share many multilocular lipid droplets and densely packed mitochondria, they also have distinguishing developmental features. Unlike brown adipocytes, beige adipocytes originate from heterogeneous populations of adipogenic precursors with additional inducers (5). Thus, beige adipocytes have a flexible phenotype and can potentially carry out lipid turnover, either lipid storage or dissipation, depending on certain stimuli. Novel underlying mechanisms that promote beige adipocyte development need to be further defined to improve therapeutic avenues.

Beige adipocytes are highly inducible under both internal and external cues, including chronic cold exposure, PPARγ agonist, β_3-adrenergic agonists, and exercise training, resulting in an improvement of insulin sensitivity (6). Although the underlying molecular mechanisms are not fully understood, it is widely acknowledged that mitochondrial biogenesis is the key to beige adipocyte development (7). Mitochondria play a central role in adipocyte metabolism by switching fuels toward fat storage or β-oxidation, and the latter can drive heat production in the presence of UCP1 (8). Mitochondrial dynamics are regulated by a balance between mitochondrial biogenesis and degradation, and dysregulation of mitochondrial biogenesis in adipose tissue is associated with obesity and diabetes, which have been known to exhibit decreased activities of electron transport chain and oxidative enzymes (9, 10). Conversely, specific improvement of mitochondrial function in adipocytes ameliorates metabolic dysfunction. For instance, fat-specific overexpression of mitoNEET, an outer mitochondrial membrane protein that contains iron-sulfur (Fe-S) clusters, ameliorates obesity-associated adipose dysfunction and exhibits a browning signature in inguinal WAT (iWAT), and thereby mice display a healthy phenotype (11, 12). Due to containing Fe-S clusters, mitoNEET has been identified as a Fe-S protein (13). The mitochondrial Fe-S cluster is an important cofactor for Fe-S proteins, which are ubiquitously involved in a wide range of cellular processes, including mitochondrial electron transport, enzymatic catalysis and regulation (14). These observations highlight a tight connection between mitochondrial Fe-S proteins and adipose function, while factors that facilitate the synthesis of Fe-S clusters and the maturation of Fe-S proteins in beige fat have not been fully established.

Mitochondria are the primary site for the synthesis of Fe-S clusters and the maturation of Fe-S proteins, which are assisted by 17 proteins forming the Fe-S cluster assembly machinery (15). These 17 proteins are encoded by nuclear genes and evolutionarily conserved from bacteria to human (16). As one of them, BolA family member 3 (Bola3) encodes a mitochondrial protein that facilitates Fe-S clusters insertion into a subset of mitochondrial Fe-S proteins, such as enzymes involved in metabolism and energy production (17). Mutation in human BOLA3 causes multiple mitochondrial dysfunctions syndrome, accompanied by defects in 2-oxoacid dehydrogenases and mitochondrial respiratory chain complexes (18, 19). The BolA family contains two other members: Bola1, like Bola3, is located to mitochondria and performs overlapping roles during the maturation of specific Fe-S proteins; while Bola2 is present in the cytosol and its yeast homolog Bol2 regulates iron metabolism (17, 20). The potential molecular function of BolA proteins in functional cell types, particularly Bola3, remains to be resolved. Recently, Bola3 was reported to act a connective role between Fe-S-dependent oxidative respiration and glycine homeostasis in the process of endothelial metabolic re-programming, which is critical for pulmonary hypertension pathogenesis (21). Beige adipocyte is a re-programmed type of white adipocyte upon certain stimuli, and it largely depends on mitochondrial oxidative phosphorylation to drive thermogenesis (22). However, the potential role for Bola3 in beige adipocyte development remains undefined yet.

In the present study, we aimed to elucidate the role and possible mechanism of Bola3 in beige adipocyte by *in vitro* loss of function experiments. The association analysis between BOLA3 levels and thermogenic gene program in human adipose depots were performed. We found that Bola3 expression was significantly induced in iWAT of mice upon thermogenic activation, and Bola3 deficiency impaired the thermogenesis capacity in beige adipocytes. Furthermore, we demonstrated that BOLA3 mRNA levels were positively correlated with the expression of thermogenic genes in human omental adipose tissue samples. Thus, these findings may provide more extensive information on the regulatory role for Bola3 in beige adipocyte development.

MATERIALS AND METHODS

Data Processing

Transcriptome profiles of GSE86338 by high-throughput RNA sequencing (RNA-seq) were downloaded from Gene Expression Omnibus (GEO, https://www.ncbi.nlm.nih.gov/geo/). This dataset describes the transcriptional change during WAT browning induced by chronic cold exposure, β_3-adrenergic agonist and intensive exercise, and brown adipose tissue (BAT) activation by acute cold exposure (4 °C for 6 h) and inactivation by thermoneutrality (TN, 30 °C for 7 days) in C57BL/6J mice (23). The gene-expression change ($\log_2$FC) was identified by EBSeq algorithms. Genes cluster involved in the process of iWAT browning and BAT activation/inactivation were listed in the form of heatmap.

Another transcriptome data by microarray were also downloaded from GEO, and the accession number is GSE10246 (24). This dataset contains gene expression data from diverse tissues from mice. The gene-expression difference was represented as $\log_2$FC, where FC was expressed as fold over the median value in the selected metabolic tissues. The tissue-specific expression profiles of genes cluster were summarized in a heatmap form.

The transcriptome analysis of the omental adipose samples from lean and obese human subjects were described in our previous study (25). In brief, sequencing libraries were first constructed and then RNA-seq was performed with the Illumina instrument at Shanghai Biotechnology Corporation. After sequences were mapped to the human genome (hg19), the reads were converted to fragments per kilobase of exon per million mapped reads (FPKM), which were calculated as mRNA level of each gene.

Mice

Male C57BL/6 mice (SLAC, China) were bred on a chow diet with a 12-h light/dark cycle. For chronic cold exposure, 8-week-old mice were exposed to 4°C for 7 days; for β_3-adrenergic agonist treatment, CL-316243(Sigma, C5976, 1 mg/kg) were implanted subcutaneously with mini-pumps for 7 days; mouse swimming exercise was implemented according to a previously established program (23). Briefly, the protocol started at 10 mins **two** times daily, with 10 mins increase each day until 90 mins, two times per day was reached. After that, the training lasted for 2 weeks. The water temperature was kept at 30 °C to avoid the effect of cold exposure. For iWAT denervation, surgery was performed on 3-month-old mice. An abdominal midline incision was made to expose iWAT, and then 10 μl of 6-hydroxydopamine (Sigma, H4381, 10 μg/μl freshly dissolved in saline) was administrated along one side of fat pad, and the other side was injected with saline, after which the skin incision was sutured (26). Two weeks after denervation, the mice were utilized for 7-day cold exposure. All animal procedures were approved by the Animal Care Committee of Shanghai Jiao Tong University Affiliated Sixth People's Hospital.

Human Adipose Tissue Samples

Human deep neck fat and the paired subcutaneous fat samples were obtained from metabolically heathy patients who underwent thyroidectomy at Shanghai Jiao Tong University Affiliated Sixth People's Hospital. All patients had normal range of thyroid-stimulating hormone values and details on the collection were guided by the previous establishment (27). Human omental adipose tissue biopsies were collected from 10 (four men and six women) severely obese but metabolically healthy subjects with a BMI between 34 and 56, who underwent bariatric surgery at Shanghai Jiao Tong University Affiliated Sixth People's Hospital, and 11 (three men and eight women) lean controls with a BMI between 18.5 and 24.9, all without metabolic diseases, who underwent a laparoscopic cholecystectomy at Shanghai Seventh People's Hospital, as described in our recent study (25). This study was approved by the Human Research Ethics Committee of Shanghai Jiao Tong University Affiliated Sixth People's Hospital and Shanghai Seventh People's Hospital. All participants have signed written informed consent before taking part in this study.

Stromal Vascular Fraction (SVF) Isolation and Cell Culture

SVF cells were isolated from iWAT of 6-week-old male mice as previously described (28). For the differentiation of beige adipocyte, SVF were grown to confluence and induced to differentiate with 0.5 mM IBMX (Sigma, I7018), 1 μM rosiglitazone (Sigma, R2408), 1 nM T3 (Sigma, T2877), 1 μM dexamethasone (Sigma, D4902) and 5 μg/ml insulin (Lily, HI0240) for two days, and then maintained with rosiglitazone, T3 and insulin for another four days (29). In some experiments, the differentiated beige adipocytes were treated for 12h with 0.5 mM dibutyryl-cAMP (Sigma, D0627) or for 12h with 20 μM H-89 (Sigma, B1427) and 10 μM SB202190 (Sigma, S7067).

Gene Knock-Down by shRNA Lentivirus

Lentiviral shRNA clones for mouse Bola3 and a scrambled control were obtained from Shanghai GeneChem Corporation. For lentivirus production, 293T cells were transfected with 10 μg vectors. After 48h of incubation, the supernatant was collected. The SVF cells were infected with the virus supernatant to knock down Bola3, and the multiplicity of infection was 50. The efficiency of lentivirus infection was determined by the number of GFP-positive cells at 72h.

RNA Extraction and Real-Time Quantitative PCR (RT-qPCR)

Total RNA was isolated from cultured cells and tissues by the Trizol reagent (Invitrogen, 15596018). 1 μg of total RNA was then converted to cDNA using the PrimeScript RT reagent Kit (Takara, RR047B). RT-qPCR amplification was conducted using SYBR Premix Ex Taq (Takara, RR820A) with a LightCycler480 system (Roche, Germany). Quantitative expression of targeted genes was normalized to housekeeping gene 36B4 and calculated using the $2^{-\Delta\Delta CT}$ method. The primer sequences are summarized in **Table 1**.

Western Blot

Protein samples were extracted with RIPA lysis buffer supplemented with phosphatase inhibitor cocktail (Roche, 4906845001) and protease inhibitor cocktail (Roche, 04693132001) and then subjected to western blot analysis according to the standard protocol. Membranes were incubated overnight at 4 °C with the following antibodies: UCP1 (Abcam, ab10983), PPARγ (Cell Signaling Technology, 2443), Perilipin 1 (Cell Signaling Technology, 3470), C/EBPα (Cell Signaling Technology, 2295), total OXPHOS rodent WB cocktail (Abcam, ab110413), p HSL Ser563 (Cell Signaling Technology, 4139), HSL (Cell Signaling Technology, 4107), Tubulin (Sigma, T6199), and GAPDH (KANGCHEN, KC-5G4). The antibody against BOLA3 was custom-produced by GenScript. Subsequently the membranes were incubated with secondary antibodies for 1h at room temperature. Protein bands were visualized with ECL Western HRP Substrate (Millipore, WBKLS0500) using Image Quant LAS4000 Imaging Systems (GE Healthcare, USA).

Oil Red O Staining

After induction to mature beige adipocytes for six days, the differentiated cells underwent Red Oil O staining. In brief, cells were washed once with PBS, fixed in 4% paraformaldehyde for 15 mins, and stained with a filtered Oil Red O working solution

TABLE 1 | Primer Sequences Used in RT-qPCR.

Gene	Forward	Reverse
Mouse Bola3	CTGCGGGGCCATGTATGAAA	CCTGATTGACCATCTGGTGCT
Mouse Ucp1	AGGCTTCCAGTACCATTAGGT	CTGAGTGAGGCAAAGCTGATTT
Mouse Fabp4	AAGGTGAAGAGCATCATAACCCT	TCACGCCTTTCATAACACATTCC
Mouse Cidec	ATGGACTACGCCATGAAGTCT	CGGTGCTAACACGACAGGG
Mouse Pparg	TCGCTGATGCACTGCCTATG	GAGAGGTCCACAGAGCTGATT
Mouse Plin1	CTGTGTGCAATGCCTATGAGA	CTGGAGGGTATTGAAGAGCCG
Mouse 36B4	AAGCGCGTCCTGGCATTGTCT	CCGCAGGGGCAGCAGTGGT
Mouse Adipoq	TGTTCCTCTTAATCCTGCCCA	CCAACCTGCACAAGTTCCCTT
Mouse Glut4	GTGACTGGAACACTGGTCCTA	CCAGCCACGTTGCATTGTAG
Mouse Ppargc1a	TATGGAGTGACATAGAGTGTGCT	CCACTTCAATCCACCCAGAAAG
Mouse Cidea	TGACATTCATGGGATTGCAGAC	CATGGTTTGAAACTCGAAAAGGG
Mouse Cox7a1	CAGCGTCATGGTCAGTCTGT	AGAAAACCGTGTGGCAGAGA
Mouse Clstn3b	CTCCGCAGGAACAGCAGCCC	AGGATAACCATAAGCACCAG
Mouse Adrb3	TCTCTGGCTTTGTGGTCGGA	GTTGGTTATGGTCTGTAGTCTCG
Mouse Mfn1	CCTACTGCTCCTTCTAACCCA	AGGGACGCCAATCCTGTGA
Mouse Mfn2	AGAACTGGACCCGGTTACCA	CACTTCGCTGATACCCCTGA
Mouse Nrf1	AGCACGGAGTGACCCAAAC	TGTACGTGGCTACATGGACCT
Mouse Nrf2	CTTTAGTCAGCGACAGAAGGAC	AGGCATCTTGTTTGGGAATGTG
Mouse Tfam	ATTCCGAAGTGTTTTTCCAGCA	TCTGAAAGTTTTGCATCTGGGT
Mouse Fis1	TGTCCAAGAGCACGCAATTTG	CCTCGCACATACTTTAGAGCCTT
Human UCP1	GTGTGCCCAACTGTGCAATG	CCAGGATCCAAGTCGCAAGA
Human PPARGC1A	CAAGCCAAACCAACAACTTTATCTCT	CACACTTAAGGTGCGTTCAATAGTC
Human FABP4	CCTTTAAAAATACTGAGATTTCCTTCA	GGACACCCCCATCTAAGGTT
Human BOLA3	CACTTCACCATCGGATGTTTGC	GCTGTAGCTCGTGGAAACTTTT
Human RPLP0	AGCCCAGAACACTGGTCTC	ACTCAGGATTTCAATGGTGCC

(Sigma, O1391) for 20 mins. Subsequently, the stained cells were washed with PBS before imaging with microscope (Nikon Corp, Japan).

Mitochondrial DNA Content

Genomic DNA was isolated from cultured adipocytes by the Gentra Puregene Cell Kit following the manufacturer's instructions (Qiagen, 158745). The ratio of mitochondrial DNA (mtDNA) to genomic DNA was measured by performing qPCR. The following primers were used: mt-RNR1: forward 5'-AGGAGCCTGTTCTATAATCGATAAA-3'; reverse 5'-GATGGCGGTATATAGGCTGAA-3'. Genomic RBM15: forward 5'-GGACACTTTTCTTGGGCAAC-3'; reverse 5'-AGTTTGGCCCTGTGAGACAT-3'.

MitoTracker Staining

Adipocytes were stained with MitoTracker Red probes (Invitrogen, M7513) in DMEM containing 0.25% BSA at 37°C for 30 mins. Cells were gently washed twice with PBS. Images were obtained with a fluorescence microscope (Nikon Corp, Japan).

Cellular Triglyceride and Lipolysis Measurement

Triglyceride content in differentiated adipocytes was determined by kit (Shanghai Kehua Bio-Engineering, China) following manual instructions. For lipolysis measurement, adipocytes were pretreated with 1 μM isoproterenol (ISO) in DMEM containing 0.25% BSA for 3h. Glycerol content in the supernatant was measured using the reagent according to the manufacturer's protocols. Results were standardized to total cellular protein content.

Cellular Metabolic Rates

SVF cells were seeded on XF-24-well culture microplate (Seahorse Bioscience) pre-coated with poly-L-lysine and differentiated them into beige adipocytes for four days. Subsequently, Oxygen consumption rate (OCR) was measured using the Mito stress kit (Agilent, 103015) in an XF24 analyzer (Seahorse Bioscience). After measuring basal OCR, 2 μM oligomycin was added to measure the uncoupled respiration. Then, 1 μM FCCP was added to detect maximal respiration. Lastly, 1 μM rotenone/1 μM antimycin was added to measure non-mitochondrial respiration. Lastly, the final OCR results were standardized to total protein content.

Statistical Analysis

All results were presented as means ± SEM from at least three independent experiments. Statistical differences between groups were calculated by unpaired and paired two-side Student's t tests. Linear regression analysis was performed to examine the correlation between genes expression. $^{*}p < 0.05$, $^{**}p < 0.01$, and $^{***}p < 0.001$ compared with control group were considered as a statistical significance.

RESULTS

Bola3 Expression Was Induced in the Browning Program of iWAT in Mice

To identify the involvement of the mitochondrial Fe-S cluster assembly machinery in the browning program, we retrieved a transcriptome study (GSE86338) downloaded from GEO database and analyzed mRNA expression patterns of 17 Fe-S

cluster assembly genes during WAT browning and BAT activation/inactivation in male C57BL/6J mice. Among these, Bola3 was the most significantly induced gene in iWAT under multiple thermogenic stimuli, while remained unchanged in acute regulation of BAT thermogenesis (**Figure 1A**). We also examined the mRNA profiles of these 17 genes across several mouse tissues by analyzing GSE10246, and found that most of them were highly expressed in mitochondria-enriched tissues, such as BAT and muscle tissues (**Figure 1B**). Then, the expression of Bola3 was validated in epididymal WAT

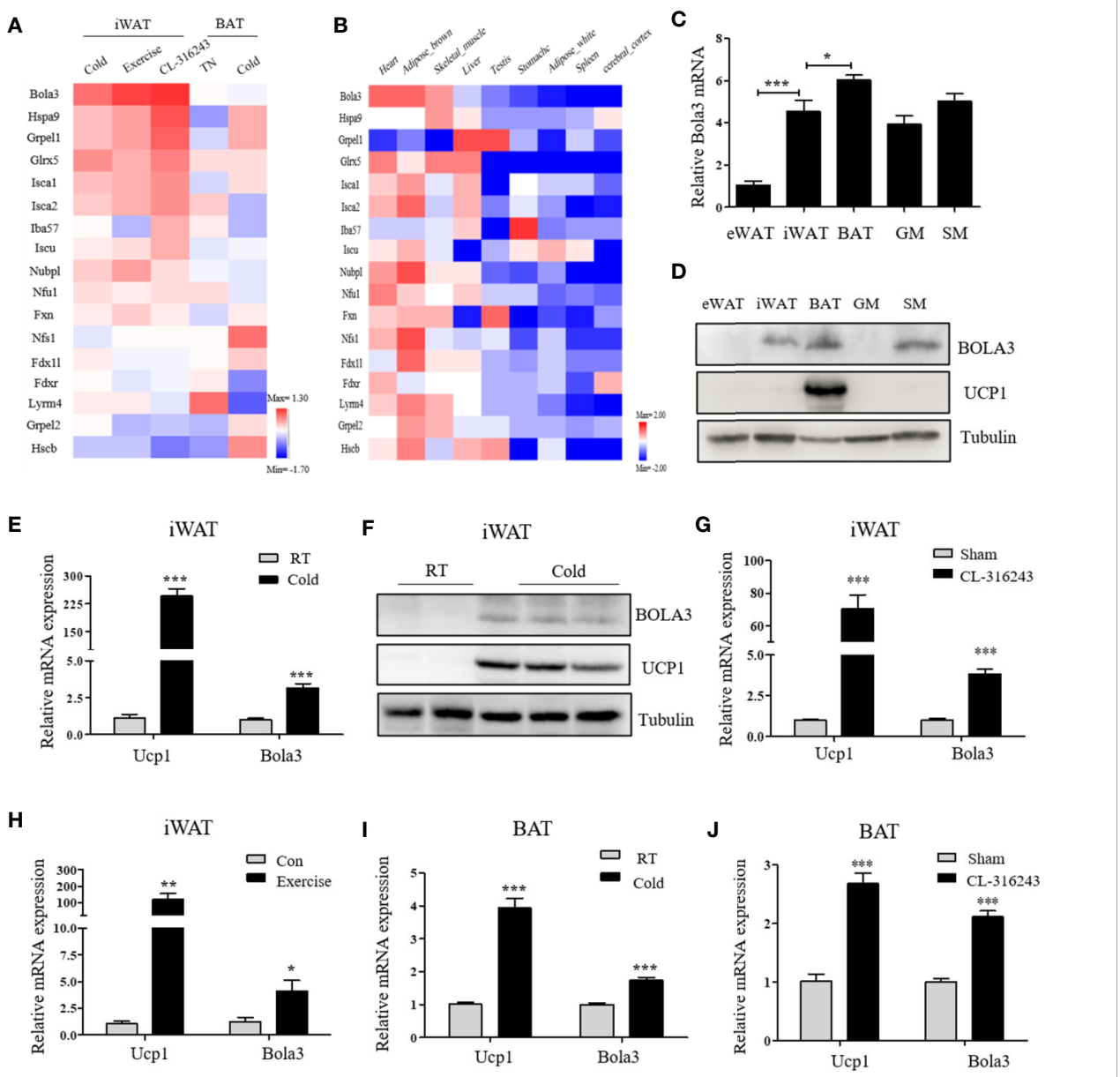

FIGURE 1 | Bola3 expression was induced in inguinal WAT (iWAT) upon thermogenic activation. **(A)** Heatmap summarizing expression profiles (log_2FC) of the mitochondrial Fe-S cluster assembly genes in the process of iWAT browning induced by cold exposure, exercise and CL-316243, and BAT activation/inactivation induced by acute cold and thermoneutrality (TN) respectively in C57BL/6J mice (GSE86338). **(B)** The expression patterns (log_2FC) of Fe-S cluster assembly genes across major metabolic tissues in mice (GSE10246). **(C, D)** Metabolic tissues from 6-week-old male mice were assessed for Bola3 mRNA (n=4) and protein expression by qPCR and western blot. eWAT (epididymal WAT), iWAT (inguinal WAT), BAT (interscapular BAT), GM (Gastrocnemius muscle) and SM (Soleus muscle). **(E, F)** Relative mRNA (n=5) and protein levels of Bola3 and Ucp1 in iWAT from mice exposed to cold (4 °C) for 7 days in an individual cage, and mice housed at room temperature (RT) served as controls. **(G)** Relative mRNA expression of Bola3 and Ucp1 in iWAT from mice subjected to CL-316243 treatment or the sham operation (n=4). **(H)** Relative mRNA levels of Bola3 and Ucp1 in iWAT from exercise-trained and sedentary control mice (n=6). **(I)** Relative mRNA levels of Bola3 and Ucp1 in BAT under 7-day cold exposure (n=7). **(J)** Relative mRNA levels of Bola3 and Ucp1 in BAT under CL-316243 injection (n=4). Data were presented as means ± SEM. *$p < 0.05$, **$p < 0.01$, and ***$p < 0.001$.

(eWAT), iWAT, BAT, gastrocnemius muscle (GM), and soleus muscle (SM). We found that Bola3 mRNA and protein levels were most highly expressed in BAT, followed by SM and iWAT (**Figures 1C, D**). Furthermore, we confirmed that long-term cold exposure induced a significant induction of Bola3 transcript and protein levels in iWAT, which was similar to the effect of chronic cold exposure on Ucp1 expression (**Figures 1E, F**). Similarly, higher Bola3 mRNA expression was observed in iWAT from CL-316243-injected mice and exercise-trained mice compared to the controls, which were in consistent with Ucp1 expression (**Figures 1G, H**). Furthermore, we also found that Bola3 was transcriptionally upregulated in BAT under chronic cold exposure and CL-316243 injection, which had some discrepancies with acute cold treatment (**Figures 1I, J**). As the patterns of Bola3 expression could indicate important clues about its function, we hypothesized that Bola3 might play a specific role in beige fat development.

Bola3 Expression in Beige Adipocytes Was Enhanced *via* Adrenergic Signaling Stimulation

Preadipocytes resided in SVFs cells from iWAT have the distinct capacity to differentiate into beige adipocytes (30). We next isolated SVF cells from iWAT of male C57BL/6J mice and differentiated them to examine Bola3 expression. After an 8-day induction with beige lipogenic procedures, we found that Bola3 mRNA expression was continuously increased (**Figure 2A**). Concomitantly, BOLA3 protein levels presented an increasing trend during the time course of beige adipocyte differentiation, which were similar to the induction of thermogenic marker UCP1(**Figure 2B**). We further isolated the SVF cells and mature adipocyte fraction (AF) from iWAT of male C57BL/6J mice, and found that Bola3 mRNA level was nearly 10-fold higher in AF than in SVF, indicating that Bola3 was predominantly expressed in mature adipocytes among all the resident cell types (**Figure 2C**). Furthermore, BOLA3 mRNA and protein levels were both significantly upregulated in AF isolated from iWAT of CL-316243-injected mice, a browning model with active adrenergic signaling (**Figures 2D, E**). These findings further supported the specific role of Bola3 on the browning program of white adipocytes.

To determine whether sympathetic signaling was required for Bola3 induction in thermogenic adipocytes, here we performed denervation studies in one side of iWAT to analyze Bola3 expression under basal and cold-induced state. Compared to the sham side, Bola3 mRNA levels were significantly decreased in the denervated side both at RT and chronic cold environment, which were in consistent with Ucp1, indicating that the sympathetic signaling was necessarily required for Bola3 expression in innervated beige fat (**Figure 2F**). Norepinephrine from sympathetic nerves can activate β_3-adrenergic receptor, increase cyclic adenosine monophosphate (cAMP) concentration, and enhance the activity of cAMP-dependent protein kinase A (PKA) pathway, thereby controlling the expression of thermogenic genes (31). To further investigate the modulation of Bola3 expression in differentiated beige adipocytes, we treated them with cAMP that enhanced the activity of PKA and p38 mitogen-activated protein kinase (p38 MAPK) pathway. Meanwhile, we assessed the effects of PKA antagonist (H-89) and p38 MAPK antagonist (SB202190) on BOLA3 modulation. Results showed that treatment of cAMP promoted a robust induction of BOLA3 protein level in beige adipocytes, while this effect was almost blocked by H-89 and SB202190, in parallel with UCP1, suggesting that Bola3 might be regulated through the cAMP/PKA/p38 MAPK pathway (**Figure 2G**). Overall, these findings might further support the potential role for Bola3 in the browning program as it responds to the adrenergic-induced, cAMP-mediated signaling.

Bola3 Deficiency Led to Impaired Thermogenesis in Normal Differentiated Beige Adipocytes

To reveal the role for Bola3 in WAT browning program, we performed *in vitro* loss of function experiments. Firstly, we efficiently knocked down Bola3 expression in SVF cells from iWAT with lentiviral-delivered shRNA and differentiated them into mature beige adipocytes (**Figures 3A, B**). Bola3 reduction did not affect lipid accumulation as determined by triglyceride quantification, cell morphology and Red Oil O staining (**Figures 3C–E**). Western blot analysis showed that the protein levels of adipocyte differentiation related genes such as PPARγ, C/EBPα, and Perilipin 1 remained unchanged with Bola3 knockdown (**Figure 3F**). In accordance with this, there were no significant difference of mRNA levels of lipogenesis related genes (Fabp4, Cidec, Glut4, Adipoq, Pparg, and Plin1) between the groups (**Figure 3G**). However, mRNA expression of thermogenic genes (Ucp1, Cidea, Cox7a1, and Clstn3b) were downregulated to a certain extend due to Bola3 deficiency (**Figure 4A**). UCP1 protein expression was likewise downregulated by Bola3 knockdown (**Figure 4B**). Furthermore, we observed that UCP1 protein levels in Bola3-deficient beige adipocytes were robustly inhibited in the presence of ISO, which activate thermogenesis *via* β_3-adrenergic signaling (**Figure 4C**). These results together suggest that Bola3 knockdown exhibits impaired thermogenic gene program while remains normal lipogenesis capacity in differentiated beige adipocytes.

Bola3 Mediated Browning Program by Regulating Mitochondrial Homeostasis and Lipolysis

As shown above, we found a suppression of thermogenic gene program in Bola3-deficient beige adipocytes. Next, we explored the possible insights underlying Bola3-mediated effects on thermogenic programming. Beige adipocyte is characterized by a sufficient number of functional mitochondria, which are essential for adaptive thermogenesis (32). As Bola3 was identified as a key regulator of Fe-S-specific mitochondrial respiratory chain, we investigated mitochondrial content and activity in Bola3-deficient beige adipocytes. Although mtDNA content had no difference between shBola3 infection and control group (**Figure 5A**), diminished fluorescence intensity *via* MitoTracker red-staining was observed in Bola3-deficient

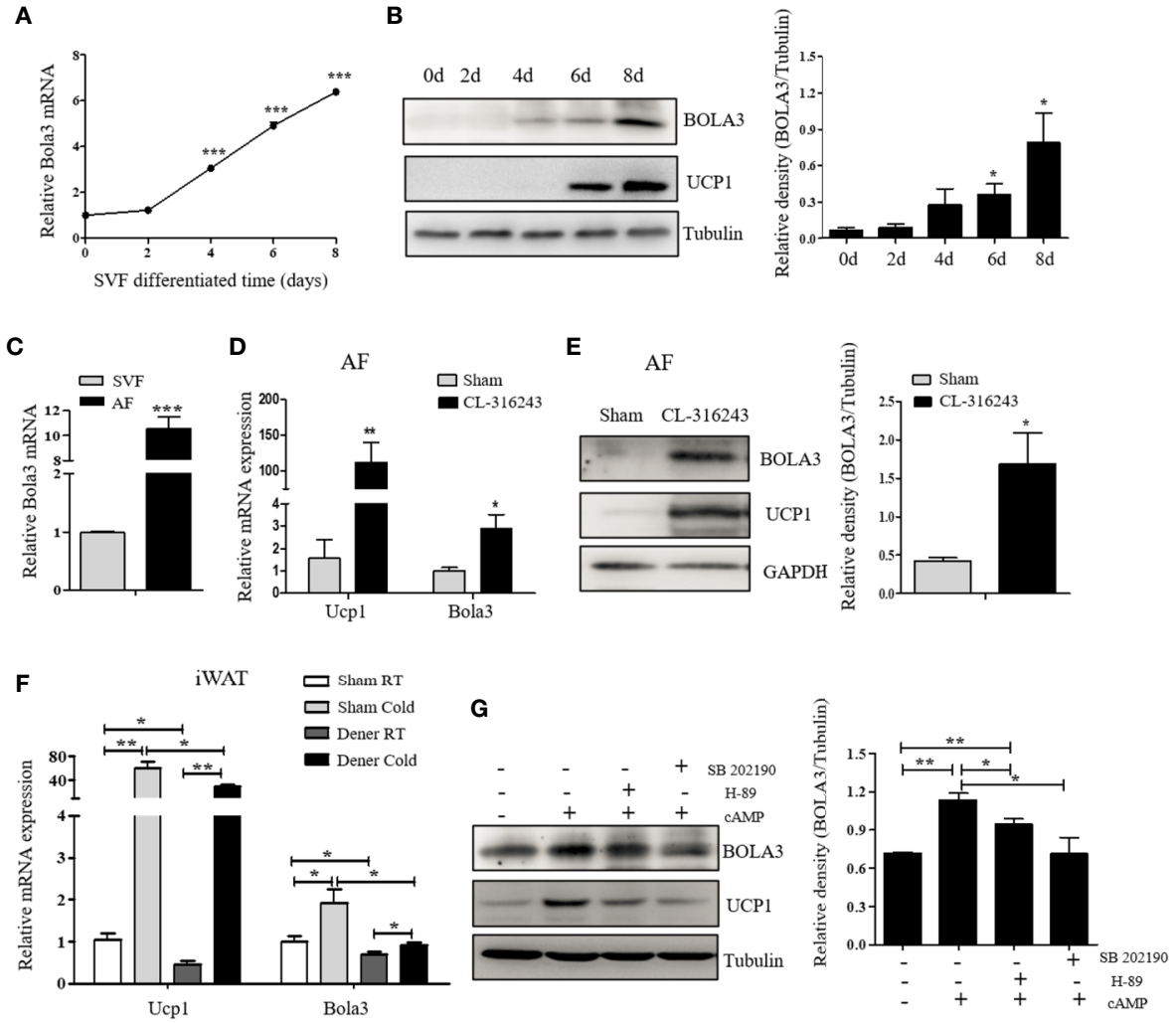

FIGURE 2 | The expression and modulation of Bola3 in thermogenic adipocytes. **(A, B)** SVF cells from inguinal WAT (iWAT) were induced to differentiate into beige adipocytes. Relative Bola3 mRNA (n=3) and protein levels during the time courses of beige adipocyte differentiation. **(C)** Relative Bola3 mRNA expression in SVF and AF isolated from iWAT of 6-week-old male mice (n=3). **(D, E)** Relative Bola3 mRNA (n=4) and protein levels of BOLA3 in AF isolated from iWAT of CL-316243-injected and the sham-operated mice. **(F)** Relative Bola3 and Ucp1 mRNA levels of the denervated and sham iWAT from mice housed at RT and cold environment (n=4). **(G)** Effects of 20 μM H-89 (PKA inhibitor) and 10 μM SB202190 (p38 MAPK inhibitor) on changes of BOLA3 and UCP1 protein levels induced by 0.5 mM dibutyryl-cAMP in differentiated beige adipocytes for 12 h. Data were presented as means ± SEM. $^{*}p < 0.05$, $^{**}p < 0.01$, and $^{***}p < 0.001$. The results are representative of at least three independent repeats in the cell experiments.

adipocytes, suggesting attenuated mitochondrial formation in beige adipocytes with Bola3 deletion (**Figure 5B**). Furthermore, quantitative PCR analysis showed that mitochondria related genes such as Mfn2, Nrf1, and Fis1, were inhibited by Bola3 reduction (**Figure 5C**). Consistent with the gene expression data, the protein levels of representative Complex I subunit, NDUFB8, and Complex II subunit, SDHB, were significantly decreased in Bola3-deficient beige adipocytes (**Figure 5D**), which was consistent with previous conclusion in other type of cells (18). In a mitochondrial stress test, basal respiration of beige adipocytes with Bola3 ablation was not altered, however Bola3 deficiency inhibited the ability to respond to FCCP, as demonstrated by the reduced maximal respiration, as well as the diminished spare respiratory capacity (**Figures 5E, F**). Overall, these data suggest that Bola3 plays an indispensable role in maintaining mitochondrial homeostasis, and thereby regulates beige adipocyte thermogenesis.

In addition to the effect of Bola3 knockdown on mitochondrial activity, we further explored its role in regulating the activity of lipolysis under basal and ISO-induced state. Activation of adrenergic signaling has been known to promote lipolysis *via* PKA-mediated phosphorylation of HSL (33). In beige or brown adipocytes, free fatty acids (FFAs) released by lipolysis can activate existing UCP1 and drive heat production in mitochondria (22). Results showed that there was no difference in glycerol concentration under basal state, while

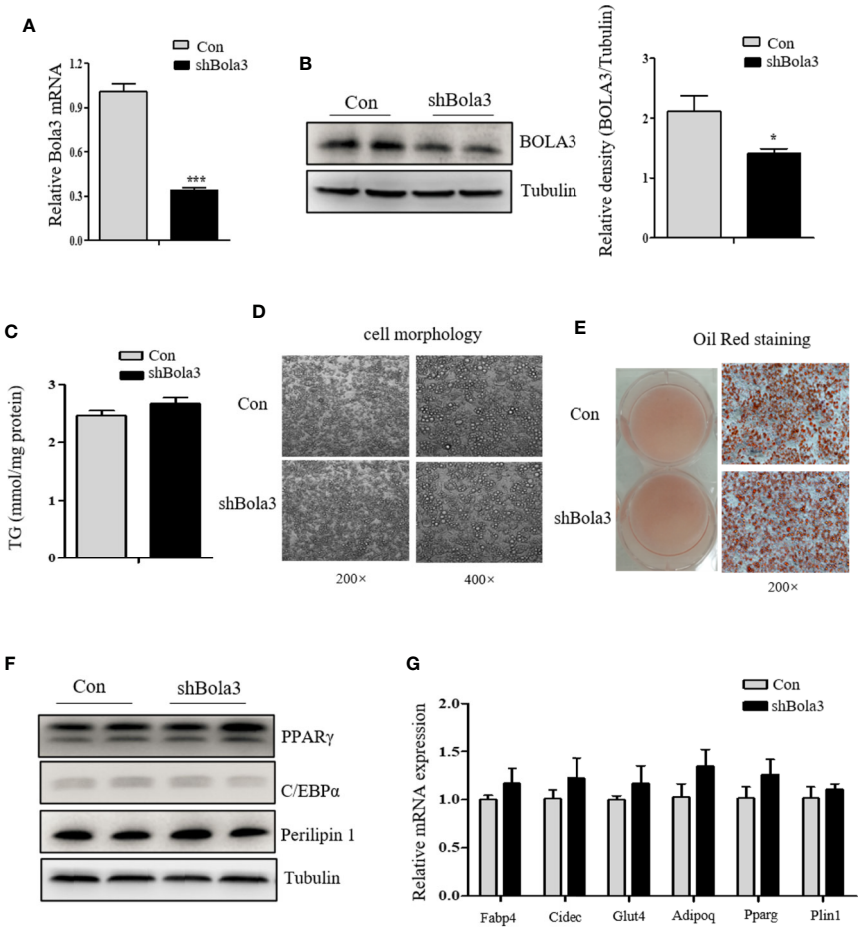

FIGURE 3 | Bola3 knockdown did not affect the lipogenesis process in differentiated beige adipocytes. **(A, B)** Relative Bola3 mRNA (n=4) and protein levels in beige adipocytes differentiated from inguinal WAT (iWAT) stromal vascular fraction (SVF) cells with infection of mouse Bola3 lentiviral shRNA. **(C–E)** TG concentration (n=4) and representative images of cell morphology and Oil Red O staining in beige adipocytes with Bola3 knockdown. **(F)** Protein levels of the lipogenic genes (PPARγ, C/EBPα and Perilipin 1) in beige adipocytes infected with mouse lentiviral Bola3 shRNA. **(G)** Quantitative PCR analysis of the lipogenic genes (Fabp4, Cidec, Glut4, Adipoq, Pparg and Plin1) expression in beige adipocytes infected with lentivirus expressing shBola3 or control (n=4). Data were presented as means ± SEM. $^{*}p < 0.05$ and $^{***}p < 0.001$. The results are representative of at least three independent repeats in the cell experiments.

Bola3 deficiency repressed ISO-induced glycerol release to a certain degree (**Figure 5G**). We next investigated the effect of Bola3 deletion on downstream intracellular signaling activation. It was found that ablation of Bola3 led to inhibited responses to adrenergic stimulation in beige adipocytes, as demonstrated by the decreased levels of HSL phosphorylation at S563 (**Figure 5H**). Hence, we demonstrated that Bola3 deficiency in beige adipocytes impairs isoproterenol-stimulated lipolysis, implying this might be another aspect by which Bola3 regulates beige adipocyte thermogenesis.

BOLA3 mRNA Levels in Human Adipose Depots Were Positively Correlated With Thermogenic Gene Program

Finally, we investigated whether the role for Bola3 in browning program that we observed in mice might occur in human subjects. We simultaneously obtained the subcutaneous and deep neck adipose depots from patients who underwent thyroidectomy. The subcutaneous fat and deep neck fat were regarded as white adipose and brown adipose respectively (27). RT-qPCR analysis confirmed that the thermogenesis marker genes, UCP1 and PPARGC1A, had higher transcript levels in deep neck fat compared to the paired subcutaneous fat, while the adipocyte differentiation marker FABP4, had no difference between groups (**Figure 6A**). We observed that BOLA3 mRNA levels were higher in human deep neck fat than in the paired subcutaneous fat, which demonstrated that higher BOLA3 levels were correlated with greater tissue oxidative capacity in human adipose tissue samples as well (**Figure 6B**). Furthermore, we investigated whether BOLA3 mRNA levels were correlated with genes which were involved in the process of thermogenesis and lipolysis in omental adipose depots from lean and obese human subjects. Association analysis showed that BOLA3 mRNA levels were positively correlated with the expression of thermogenesis

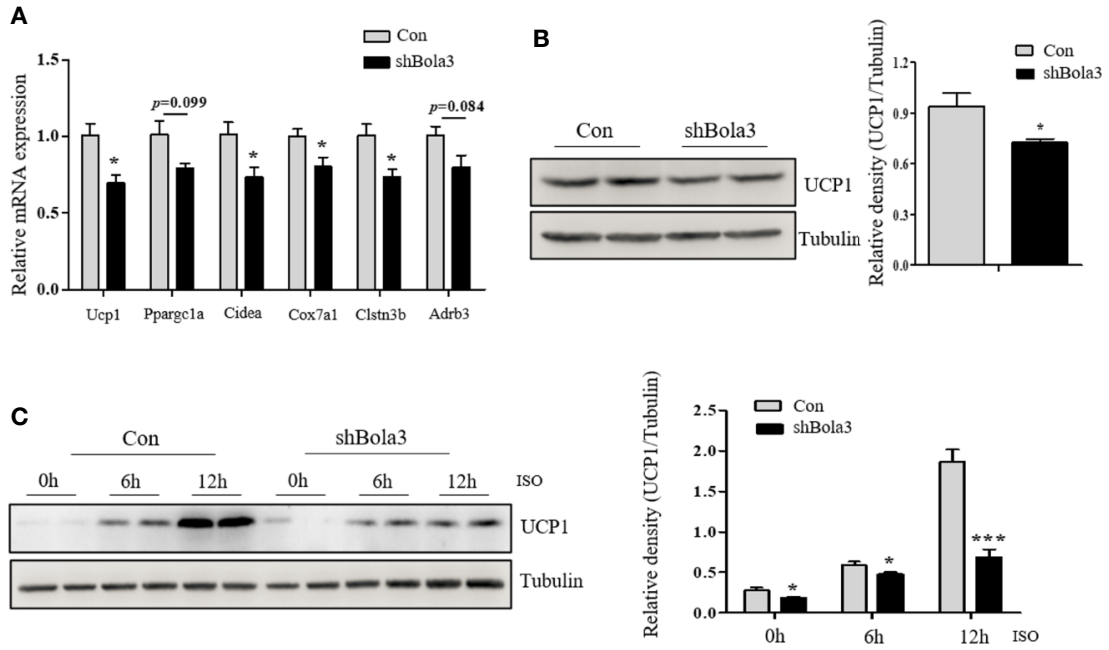

FIGURE 4 | Bola3 was required for maintaining beige adipocyte thermogenesis. **(A)** Quantitative PCR analysis of the thermogenic genes (Ucp1, Ppargc1a, Cidea, Cox7a1, Clstn3b and Adrb3) expression in beige adipocytes with the infection of mouse Bola3 lentiviral shRNA (n=4). **(B)** Western blot and quantification analysis of UCP1 protein levels in beige adipocytes infected with mouse lentiviral shRNA. **(C)** The protein levels of UCP1 were immunoblotted after 5 μM ISO treatment for 6 and 12 h. Data were presented as means ± SEM. $^{*}p < 0.05$ and $^{***}p < 0.001$. The results are representative of at least three independent repeats in the cell experiments.

related genes (UCP1, CIDEA, PRDM16, PPARG, and COX7A1) and lipolysis related gene LIPE, namely HSL (**Figures 6C–H**). Thus, we concluded that BOLA3 might play a regulatory role in thermogenic programming in human adipose depots as well.

DISCUSSION

In this study, we found that Bola3 expression was significantly induced in iWAT upon thermogenic activation, while Bola3 deficiency *in vitro* led to impaired thermogenesis activity of beige adipocytes. We further identified the positive correlation between BOLA3 expression and thermogenic gene program in human adipose depots. Taken together, we demonstrate that Bola3 plays a regulatory role in the thermogenic program of white fat in both mice and human subjects.

Beige fat has been regarded as a promising intervention target for obesity (34), because it is highly inducible under multiple stimuli, in the process, mitochondrial biogenesis is the key to beige adipocyte development. As mitochondria are involved in a complex communication network, continuously communicating and interacting with other organelles, even distinct tissues through multiple ways (35), hence the maintenance of mitochondrial homeostasis deserves to be further investigated in order to reveal the underlying pathologic mechanism and potential therapeutic interventions. The mitochondrial Fe-S cluster and its targeted Fe-S proteins are involved in a wide range of metabolic activities (36). The mitochondrial Fe-S cluster assembly machinery consists of about 17 proteins that operate in complex steps for the maturation process of Fe-S targeted proteins (16), while studies on the role of these genes in adipocyte metabolism are still lacking. Among 17 genes, Bola3 expression was most significantly induced in iWAT upon browning inputs. However, few studies have focused on Bola3 function, other than several case reports of multiple mitochondrial dysfunction syndrome due to BOLA3 gene mutation (19). Recently, the first mechanism study demonstrated that Bola3 acted as a crucial lynchpin in the process of endothelial metabolic re-programming in pulmonary hypertension (21). Hence, the dramatic induction of Bola3 expression in WAT browning program, clues that it may be involved in adipose tissue re-programming under thermogenic activation.

This observation promotes us to detect the modulation of Bola3 expression in thermogenic adipocytes. In response to cold exposure, the hormone norepinephrine released from sympathetic nerve system primarily acts on β_3-adrenergic receptor, leading to the activation of PKA and p38 MAPK signaling pathway. This adrenergic signaling is able to activate many thermogenesis related genes (31). We observed that Bola3 was predominantly enriched in mature adipocyte fraction, and thermogenic activation could further enhance its expression in this fraction. Furthermore, we found that Bola3 levels were diminished after iWAT denervation, likewise, block of PKA and p38 MAPK signaling pathway blunted cAMP-mediated induction of BOLA3 expression in differentiated beige

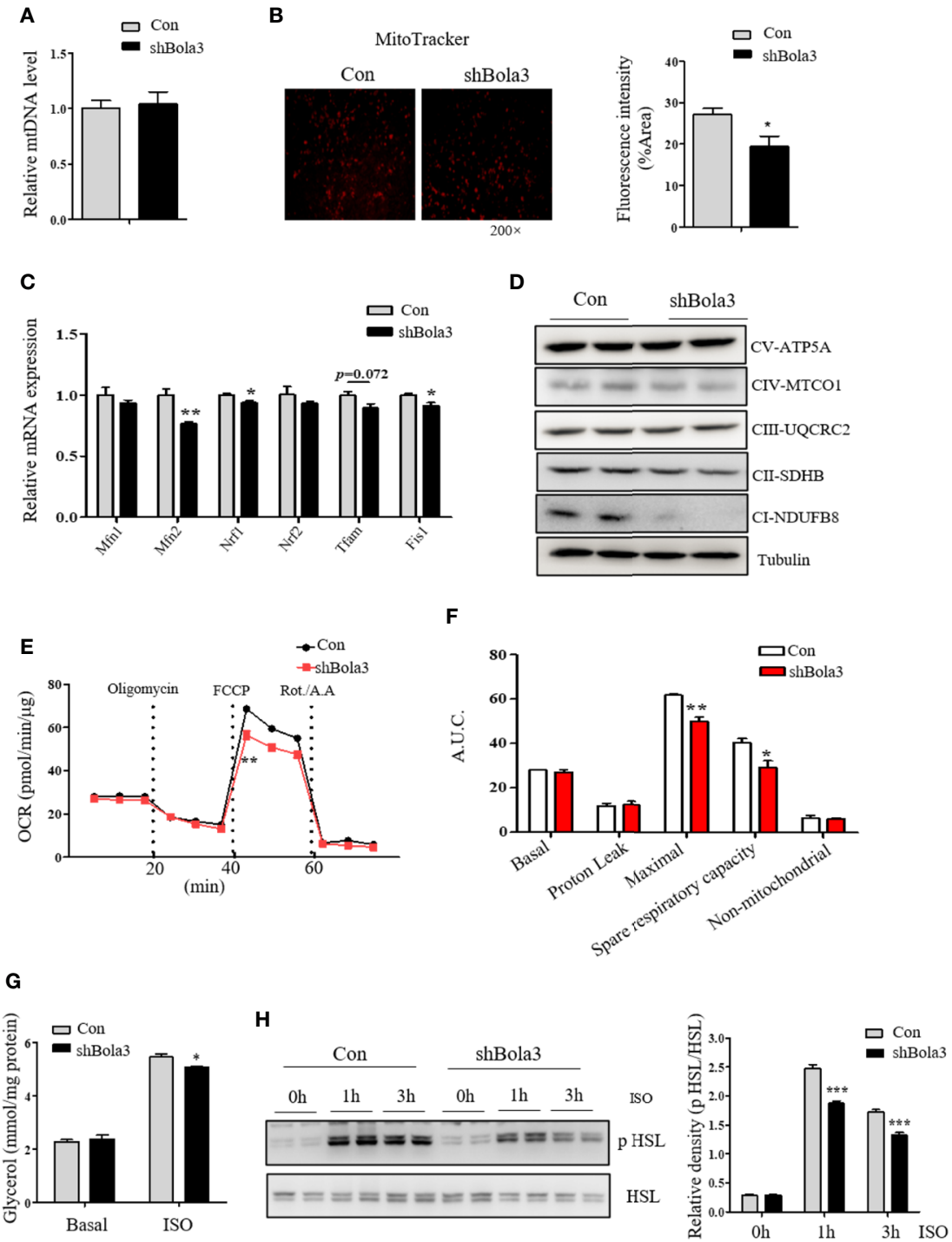

FIGURE 5 | Bola3 regulated thermogenic programming by maintaining mitochondrial homeostasis. **(A, B)** Mitochondrial DNA (mtDNA) levels (n=4) and representative fluorescent images, fluorescence intensity of MitoTracker staining in beige adipocytes differentiated from iWAT SVF cells infected with or without Bola3 lentiviral shRNA. **(C, D)** Quantitative PCR analysis of mitochondrial genes expression (n=3) and protein levels of mitochondrial OXPHOS complexes in beige adipocytes with Bola3 knockdown. **(E, F)** OCR measurement in Bola3-deficient beige adipocytes under 4-day differentiation. **(G, H)** Glycerol release (n=4) and p HSL 563, HSL protein levels in differentiated beige adipocytes infected with Bola3 lentiviral shRNA or control under basal and ISO-stimulated state. Data were presented as means ± SEM. $^{*}p < 0.05$, $^{**}p < 0.01$ and $^{***}p < 0.001$. The results are representative of at least three independent repeats in the cell experiments.

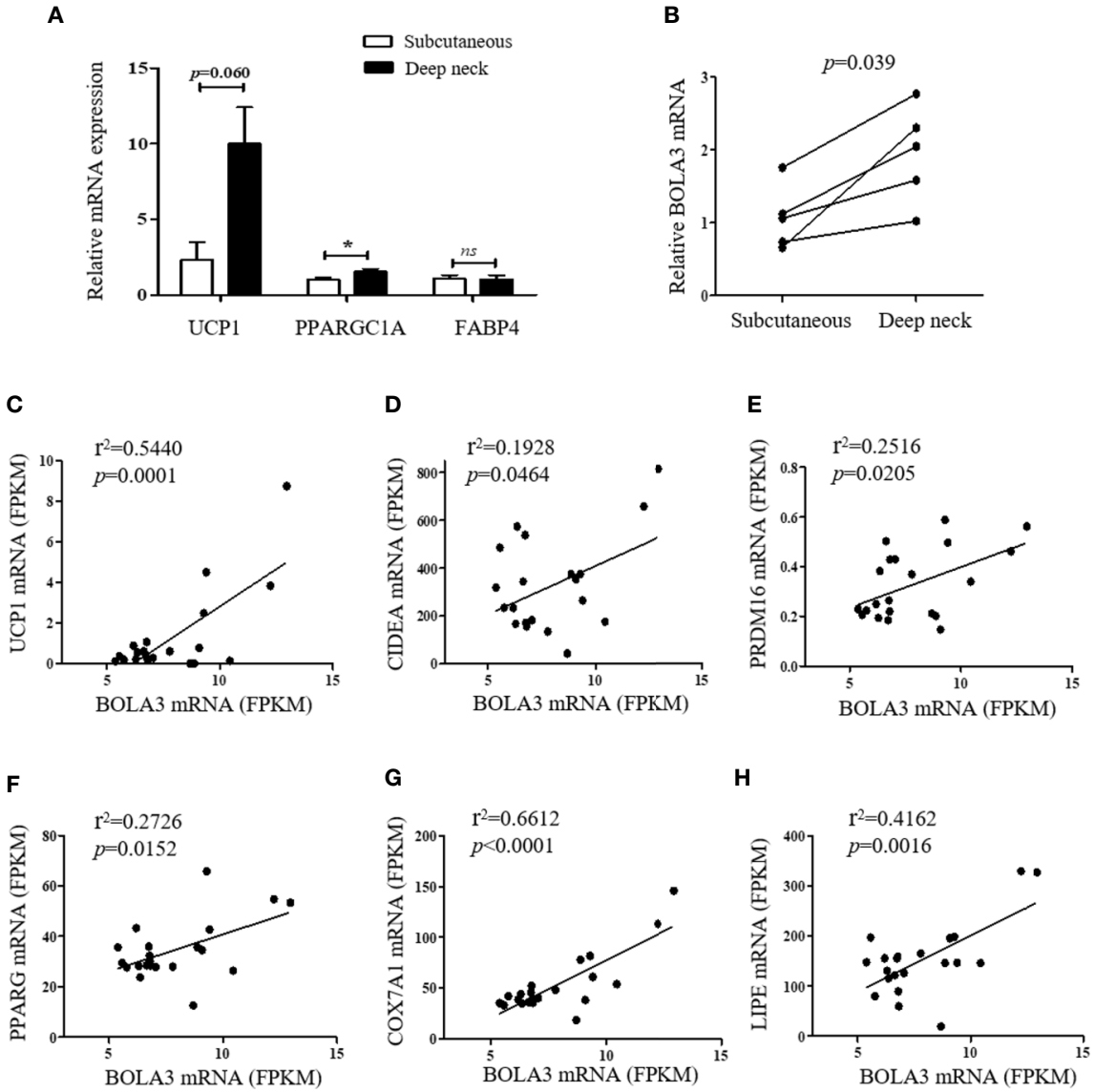

FIGURE 6 | BOLA3 mRNA levels were positively associated with thermogenic gene program in human adipose depots. **(A)** Quantitative PCR analysis of thermogenesis related genes (UCP1 and PPARGC1A) and lipogenesis related gene (FABP4) in human deep neck fat and the paired subcutaneous fat (n=5). **(B)** Gene expression analysis showed higher BOLA3 expression in human deep neck fat compared to the paired subcutaneous fat (p=0.039, n=5). Data were presented as means ± SEM. *$p < 0.05$, ns, not significant. **(C–G)** Relative BOLA3 expression is plotted against the expression of thermogenesis related genes (UCP1, CIDEA, PRDM16, PPARG, and COX7A1). **(H)** Relative BOLA3 expression is plotted against the expression of gene involved in lipolysis (LIPE, namely HSL). Gene expression levels are represented as fragments per kilobase of exon per million mapped reads (FPKM) value from RNA-seq; Linear regression analysis was performed; r^2 and p values were presented in the figure (n=21 omental fat samples from lean and obese human subjects).

adipocytes, which were similar to the pattern of UCP1 expression. Thus, Bola3 could be identified as an adrenergic signaling-targeted gene, which further indicates it may play a significant role in beige adipocyte development.

Next, our findings extend our understanding of the role for Bola3 in beige adipocyte development. It has been reported that BOLA3 mutant fibroblasts show ~30% (Complex I), 50% (complex II), and ~60% (complex III) of normal mitochondrial enzyme activity (18). Major functions of mitochondria in beige adipocytes include differentiation, fatty acid oxidation and thermogenesis (6). Our *in vitro* study demonstrated that Bola3 knockdown by lentivirus expressing shRNA impaired the thermogenic program by the following evidences: 1) Reduced expression of thermogenic genes, as represented by Ucp1, Cidea, Cox7a1, and Clstn3b, a new identified marker gene (37); 2) Disrupted mitochondrial homeostasis, including the decreased levels of mitochondrial components and impaired oxidative metabolism; 3) Inhibited responses to isoproterenol stimulation, in term of lipolysis and FFAs-driven thermogenesis. Collectively, these results suggest that Bola3 plays an indispensable role in regulation of beige adipocyte

thermogenesis, possibly by maintaining mitochondrial homeostasis and isoproterenol-mediated lipolysis.

In addition to mice study, we expect to verify our findings in human adipose tissue samples as well. Image-based studies with positron emission tomography-computed tomography (PET-CT) reveals that UCP1-expressing brown-like adipose depots are distributed in the supraspinal, pericardial, and neck regions of adult humans (38, 39). White adipose depots from human and mice have opposing patterns of "browning" gene program (40), showing that human omental fat displays a beige signature with higher expression of thermogenic genes (UCP1, PPARGC1A, TFAM, and TBX1) than the paired subcutaneous fat (41). Our results demonstrated that Bola3 mRNA levels were higher in human deep neck brown fat than in subcutaneous white fat, and they were strongly correlated with thermogenesis related genes (UCP1, CIDEA, PRDM16, PPARG, COX7A1, and LIPE) levels in the omental adipose depots from lean and obese human subjects. These results reinforce that BOLA3 may have a positive effect on regulating tissue oxidative capacity in human subjects as well.

Recently there is another independent study has demonstrated BOLA3 pathway-mediated mitochondrial lipoylation contributes to age-associated decline in brown adipose thermogenesis. As it mentions, there are no significant difference in Ucp1 transcript levels in BAT between the young and old mice (42). However, another study has shown that BAT from the aged mice has decreased Ucp1 mRNA levels (43). Therefore, the expression patterns of thermogenic gene program in BAT from the aged mice, remain to be further clarified. In our study, we found that Bola3 plays an indispensable role in WAT browning program. Obviously, there are two points that should be regarded as the novelty of our study. Firstly, although brown and beige fat are major tissues of adaptive thermogenesis, they also have distinguishing phenotypes and functional features. Brown adipocytes function well under basal conditions, while beige adipocytes express thermogenic components only under stimulation (32). Genetic studies show that genetic variation between mouse strains influence UCP1 levels in WAT but not in BAT under cold exposure, suggesting the different developmental and adaptive mechanism (44). Secondly, aging is a progressive and multifactorial process. In adipose tissue, mitochondrial dysfunction is one of the most highly investigated aging factors (42, 45), however, there exists some other factors as well. For instance, it was recently reported that adipocyte progenitors undergo an age-associated, senescence-like phenotype for age-dependent browning failure (46). Therefore, the pathogenetic mechanisms of age-associated reduction in brown fat thermogenesis will be much more complicated, or there may be different BOLA3 pathway-mediated mechanism involved in WAT browning program in our study.

However, there are some limitations to consider. First, the reason why Bola3 level fluctuation has such a great impact on mitochondrial activity remains unknown and there are several functional marks under thermogenic stimuli that we did not assess, such as mitochondrial morphology and oxygen consumption rate in Bola3-deficient beige adipocytes. The mechanistic roles of Bola3 in beige adipocyte-specific mitochondrial function need to be further explored. Second, our data from human adipose samples are limited to mRNA levels of BOLA3 and thermogenic genes. The correlation analysis between BOLA3 expression and clinical metabolic assessment will be strengthened within these or more human adipose samples. We hope future studies will provide a better understanding of Bola3's role on beige adipocyte metabolism.

DATA AVAILABILITY STATEMENT

The original contributions presented in the study are included in the article. Further inquiries can be directed to the corresponding authors.

ETHICS STATEMENT

The studies involving human participants were reviewed and approved by Human Research Ethics Committee of Shanghai Jiao Tong University Affiliated Sixth People's Hospital and Shanghai Seventh People's Hospital. The patients/participants provided their written informed consent to participate in this study. The animal study was reviewed and approved by Animal Care Committee of Shanghai Jiao Tong University Affiliated Sixth People's Hospital.

AUTHOR CONTRIBUTIONS

NB performed the experiments, analyzed the results, and wrote the manuscript. JM performed the experiments and analyzed the data. MA and JX assisted the RNA-seq data analysis. FH, YX, and SC assisted the experiments. QL, XL, JH, and WJ contributed the clinical samples. YB reviewed and edited the manuscript. YY conceived the study, wrote, and revised the manuscript. All authors contributed to the article and approved the submitted version.

FUNDING

This study was supported by grants from the National Natural Science Foundation of China (No. 82070896, No. 81974122, No. 81670778, No. 81603476).

ACKNOWLEDGMENTS

We thank members of Metabolic Disease Biobank Resource at Shanghai Jiao Tong University Affiliated Sixth People's Hospital for their technical support. We thank Professor Zhili Yang from Department of General Surgery at Shanghai Jiao Tong University Affiliated Sixth People's Hospital for kindly providing adult human neck brown fat and subcutaneous fat samples.

REFERENCES

1. Friedrich MJ. Global Obesity Epidemic Worsening. *Jama* (2017) 318:603. doi: 10.1001/jama.2017.10693
2. Van Gaal LF, Mertens IL, De Block CE. Mechanisms linking obesity with cardiovascular disease. *Nature* (2006) 444:875–80. doi: 10.1038/nature05487
3. Kusminski CM, Bickel PE, Scherer PE. Targeting adipose tissue in the treatment of obesity-associated diabetes. *Nat Rev Drug Discovery* (2016) 15:639–60. doi: 10.1038/nrd.2016.75
4. Peirce V, Carobbio S, Vidal-Puig A. The different shades of fat. *Nature* (2014) 510:76–83. doi: 10.1038/nature13477
5. Wang W, Seale P. Control of brown and beige fat development. *Nat Rev Mol Cell Biol* (2016) 17:691–702. doi: 10.1038/nrm.2016.96
6. Kajimura S, Spiegelman BM, Seale P. Brown and Beige Fat: Physiological Roles beyond Heat Generation. *Cell Metab* (2015) 22:546–59. doi: 10.1016/j.cmet.2015.09.007
7. Trevellin E, Scorzeto M, Olivieri M, Granzotto M, Valerio A, Tedesco L, et al. Exercise training induces mitochondrial biogenesis and glucose uptake in subcutaneous adipose tissue through eNOS-dependent mechanisms. *Diabetes* (2014) 63:2800–11. doi: 10.2337/db13-1234
8. Forner F, Kumar C, Luber CA, Fromme T, Klingenspor M, Mann M. Proteome differences between brown and white fat mitochondria reveal specialized metabolic functions. *Cell Metab* (2009) 10:324–35. doi: 10.1016/j.cmet.2009.08.014
9. Yin X, Lanza IR, Swain JM, Sarr MG, Nair KS, Jensen MD. Adipocyte mitochondrial function is reduced in human obesity independent of fat cell size. *J Clin Endocrinol Metab* (2014) 99:E209–16. doi: 10.1210/jc.2013-3042
10. Heinonen S, Buzkova J, Muniandy M, Kaksonen R, Ollikainen M. Impaired Mitochondrial Biogenesis in Adipose Tissue in Acquired Obesity. *Diabetes* (2015) 64:3135–45. doi: 10.2337/db14-1937
11. Kusminski CM, Park J, Scherer PE. MitoNEET-mediated effects on browning of white adipose tissue. *Nat Commun* (2014) 5:3962. doi: 10.1038/ncomms4962
12. Kusminski CM, Holland WL, Sun K, Park J, Spurgin SB, Lin Y, et al. MitoNEET-driven alterations in adipocyte mitochondrial activity reveal a crucial adaptive process that preserves insulin sensitivity in obesity. *Nat Med* (2012) 18:1539–49. doi: 10.1038/nm.2899
13. Wiley SE, Paddock ML, Abresch EC, Gross L, Van Der Geer P, Nechushtai R, et al. The outer mitochondrial membrane protein mitoNEET contains a novel redox-active 2Fe-2S cluster. *J Biol Chem* (2007) 282:23745–9. doi: 10.1074/jbc.C700107200
14. Rouault TA, Tong WH. Iron-sulphur cluster biogenesis and mitochondrial iron homeostasis. *Nat Rev Mol Cell Biol* (2005) 6:345–51. doi: 10.1038/nrm1620
15. Stehling O, Wilbrecht C, Lill R. Mitochondrial iron-sulfur protein biogenesis and human disease. *Biochimie* (2014) 100:61–77. doi: 10.1016/j.biochi.2014.01.010
16. Lill R, Hoffmann B, Molik S, Pierik AJ, Rietzschel N, Stehling O, et al. The role of mitochondria in cellular iron-sulfur protein biogenesis and iron metabolism. *Biochim Biophys Acta* (2012) 1823:1491–508. doi: 10.1016/j.bbamcr.2012.05.009
17. Uzarska MA, Nasta V, Weiler BD, Spantgar F, Ciofi-Baffoni S, Saviello MR, et al. Mitochondrial Bol1 and Bol3 function as assembly factors for specific iron-sulfur proteins. *Elife* (2016) 5:e16673. doi: 10.7554/eLife.16673
18. Cameron JM, Janer A, Levandovskiy V, Mackay N, Rouault TA, Tong WH, et al. Mutations in iron-sulfur cluster scaffold genes NFU1 and BOLA3 cause a fatal deficiency of multiple respiratory chain and 2-oxoacid dehydrogenase enzymes. *Am J Hum Genet* (2011) 89:486–95. doi: 10.1016/j.ajhg.2011.08.011
19. Haack TB, Rolinski B, Haberberger B, Zimmermann F, Schum J, Strecker V, et al. Homozygous missense mutation in BOLA3 causes multiple mitochondrial dysfunctions syndrome in two siblings. *J Inherit Metab Dis* (2013) 36:55–62. doi: 10.1007/s10545-012-9489-7
20. Banci L, Camponeschi F, Ciofi-Baffoni S, Muzzioli R. Elucidating the Molecular Function of Human BOLA2 in GRX3-Dependent Anamorsin Maturation Pathway. *J Am Chem Soc* (2015) 137:16133–43. doi: 10.1021/jacs.5b10592
21. Yu Q, Tai YY, Tang Y, Zhao J, Negi V, Culley MK, et al. BOLA (BolA Family Member 3) Deficiency Controls Endothelial Metabolism and Glycine Homeostasis in Pulmonary Hypertension. *Circulation* (2019) 139:2238–55. doi: 10.1161/circulationaha.118.035889
22. Chouchani ET, Kajimura S. Metabolic adaptation and maladaptation in adipose tissue. *Nat Metab* (2019) 1:189–200. doi: 10.1038/s42255-018-0021-8
23. Bai Z, Chai XR, Yoon MJ, Kim HJ, Lo KA, Zhang ZC, et al. Dynamic transcriptome changes during adipose tissue energy expenditure reveal critical roles for long noncoding RNA regulators. *PloS Biol* (2017) 15:e2002176. doi: 10.1371/journal.pbio.2002176
24. Lattin JE, Schroder K, Su AI, Walker JR, Zhang J, Wiltshire T, et al. Expression analysis of G Protein-Coupled Receptors in mouse macrophages. *Immunome Res* (2008) 4:5. doi: 10.1186/1745-7580-4-5
25. Ju L, Han J, Zhang X, Deng Y, Yan H, Wang C, et al. Obesity-associated inflammation triggers an autophagy-lysosomal response in adipocytes and causes degradation of perilipin 1. *Cell Death Dis* (2019) 10:121. doi: 10.1038/s41419-019-1393-8
26. Jiang H, Ding X, Cao Y, Wang H, Zeng W. Dense Intra-adipose Sympathetic Arborizations Are Essential for Cold-Induced Beiging of Mouse White Adipose Tissue. *Cell Metab* (2017) 26:686–92 e3. doi: 10.1016/j.cmet.2017.08.016
27. Cypess AM, White AP, Vernochet C, Schulz TJ, Xue R, Sass CA, et al. Anatomical localization, gene expression profiling and functional characterization of adult human neck brown fat. *Nat Med* (2013) 19:635–9. doi: 10.1038/nm.3112
28. Ju L, Zhang X, Deng Y, Han J, Yang J, Chen S, et al. Enhanced expression of Survivin has distinct roles in adipocyte homeostasis. *Cell Death Dis* (2017) 8:e2533. doi: 10.1038/cddis.2016.439
29. Zou Y, Lu P, Shi J, Liu W, Yang M, Zhao S, et al. IRX3 Promotes the Browning of White Adipocytes and Its Rare Variants are Associated with Human Obesity Risk. *EBioMedicine* (2017) 24:64–75. doi: 10.1016/j.ebiom.2017.09.010
30. Macotela Y, Emanuelli B, Mori MA, Gesta S, Schulz TJ, Tseng Y-H, et al. Intrinsic Differences in Adipocyte Precursor Cells From Different White Fat Depots. *Diabetes* (2012) 61:1691–9. doi: 10.2337/db11-1753
31. Collins S. beta-Adrenoceptor Signaling Networks in Adipocytes for Recruiting Stored Fat and Energy Expenditure. *Front Endocrinol (Lausanne)* (2011) 2:102. doi: 10.3389/fendo.2011.00102
32. Wu J, Bostrom P, Sparks LM, Ye L, Choi JH, Giang AH, et al. Beige adipocytes are a distinct type of thermogenic fat cell in mouse and human. *Cell* (2012) 150:366–76. doi: 10.1016/j.cell.2012.05.016
33. Duncan RE, Ahmadian M, Jaworski K, Sarkadi-Nagy E, Sul HS. Regulation of lipolysis in adipocytes. *Annu Rev Nutr* (2007) 27:79–101. doi: 10.1146/annurev.nutr.27.061406.093734
34. Sidossis L, Kajimura S. Brown and beige fat in humans: thermogenic adipocytes that control energy and glucose homeostasis. *J Clin Invest* (2015) 125:478–86. doi: 10.1172/JCI78362
35. Mottis A, Herzig S. Mitocellular communication: Shaping health and disease. *Science* (2019) 366:827–32. doi: 10.1126/science.aax3768
36. Rouault TA. Biogenesis of iron-sulfur clusters in mammalian cells: new insights and relevance to human disease. *Dis Model Mech* (2012) 5:155–64. doi: 10.1242/dmm.009019
37. Zeng X, Ye M, Resch JM, Jedrychowski MP, Hu B, Lowell BB, et al. Innervation of thermogenic adipose tissue via a calsyntenin 3beta-S100b axis. *Nature* (2019) 569:229–35. doi: 10.1038/s41586-019-1156-9
38. Cypess AM, Lehman S, Williams G, Tal I, Rodman D, Goldfine AB, et al. Identification and importance of brown adipose tissue in adult humans. *N Engl J Med* (2009) 360:1509–17. doi: 10.1056/NEJMoa0810780
39. Van Marken Lichtenbelt WD, Vanhommerig JW, Smulders NM, Drossaerts JM, Kemerink GJ, Bouvy ND, et al. Cold-activated brown adipose tissue in healthy men. *N Engl J Med* (2009) 360:1500–8. doi: 10.1056/NEJMoa0808718
40. Zuriaga MA, Fuster JJ, Gokce N, Walsh K. Humans and Mice Display Opposing Patterns of "Browning" Gene Expression in Visceral and Subcutaneous White Adipose Tissue Depots. *Front Cardiovasc Med* (2017) 4:27. doi: 10.3389/fcvm.2017.00027
41. Bettini S, Favaretto F, Compagnin C, Belligoli A, Sanna M, Fabris R, et al. Resting Energy Expenditure, Insulin Resistance and UCP1 Expression in Human Subcutaneous and Visceral Adipose Tissue of Patients With Obesity. *Front Endocrinol (Lausanne)* (2019) 10:548. doi: 10.3389/fendo.2019.00548

42. Tajima K, Ikeda K, Chang H-Y, Chang C-H, Yoneshiro T, Oguri Y, et al. Mitochondrial lipoylation integrates age-associated decline in brown fat thermogenesis. *Nat Metab* (2019) 1:886–98. doi: 10.1038/s42255-019-0106-z
43. Ma X, Xu L, Gavrilova O, Mueller E. Role of forkhead box protein A3 in age-associated metabolic decline. *Proc Natl Acad Sci U S A* (2014) 111:14289–94. doi: 10.1073/pnas.1407640111
44. Xue B, Rim JS, Hogan JC, Coulter AA, Koza RA, Kozak LP. Genetic variability affects the development of brown adipocytes in white fat but not in interscapular brown fat. *J Lipid Res* (2007) 48:41–51. doi: 10.1194/jlr.M600287-JLR200
45. Vernochet C, Kahn CR. Mitochondria, obesity and aging. *Aging (Albany NY)* (2012) 4:859–60. doi: 10.18632/aging.100518
46. Berry DC, Jiang Y, Arpke RW, Close EL, Uchida A, Reading D, et al. Cellular Aging Contributes to Failure of Cold-Induced Beige Adipocyte Formation in Old Mice and Humans. *Cell Metab* (2017) 25:481. doi: 10.1016/j.cmet.2017.01.011

Conflict of Interest: The authors declare that the research was conducted in the absence of any commercial or financial relationships that could be construed as a potential conflict of interest.

frontiers in Endocrinology

ORIGINAL RESEARCH
published: 10 March 2021
doi: 10.3389/fendo.2021.634191

IRX3 Overexpression Enhances *Ucp1* Expression *In Vivo*

Zhiyin Zhang[1,2†], *Qihan Wu*[1,2†], *Yang He*[1,2†], *Peng Lu*[1,2], *Danjie Li*[1,2], *Minglan Yang*[1,2], *Weiqiong Gu*[1,2], *Ruixin Liu*[1,2*], *Jie Hong*[1,2*] *and Jiqiu Wang*[1,2*]

[1] *Department of Endocrine and Metabolic Diseases, Shanghai Institute of Endocrine and Metabolic Diseases, Ruijin Hospital, Shanghai Jiao Tong University School of Medicine, Shanghai, China,* [2] *Shanghai National Clinical Research Center for Metabolic Diseases, Key Laboratory for Endocrine and Metabolic Diseases of the National Health Commission of the PR China, Shanghai National Center for Translational Medicine, Ruijin Hospital, Shanghai Jiao Tong University School of Medicine, Shanghai, China*

OPEN ACCESS

Edited by:
Jae B. Kim,
Seoul National University,
South Korea

Reviewed by:
Lei Sun,
National University of Singapore,
Singapore
Jong Bae Seo,
Mokpo National University,
South Korea

****Correspondence:***
Ruixin Liu
xiner198287@163.com
Jie Hong
hongjie@medmail.com.cn
Jiqiu Wang
wangjq@shsmu.edu.cn

[†]These authors have contributed equally to this work

Specialty section:
This article was submitted to Cellular Endocrinology, a section of the journal Frontiers in Endocrinology

Received: *27 November 2020*
Accepted: *04 February 2021*
Published: *10 March 2021*

Citation:
Zhang Z, Wu Q, He Y, Lu P, Li D, Yang M, Gu W, Liu R, Hong J and Wang J (2021) IRX3 Overexpression Enhances Ucp1 Expression In Vivo. Front. Endocrinol. 12:634191. doi: 10.3389/fendo.2021.634191

Objective: The Iroquois homeobox 3 (*IRX3*) gene was recently reported to be a functional downstream target of a common polymorphism in the *FTO* gene, which encodes an obesity-associated protein; however, the role of *IRX3* in energy expenditure remains unclear. Studies have revealed that the overexpression of a dominant–negative form of IRX3 in the mouse hypothalamus and adipose tissue promoted energy expenditure by enhancing brown/browning activities. Meanwhile, we and others recently demonstrated that *IRX3* knockdown impaired the browning program of primary preadipocytes *in vitro*. In this study, we aimed to further clarify the effects of overexpressing human *IRX3* (h*IRX3*) on brown/beige adipose tissues *in vivo*.

Methods: Brown/beige adipocyte-specific h*IRX3*-overexpressing mice were generated and the browning program of white adipose tissues was induced by both chronic cold stimulation and CL316,243 injection. Body weight, fat mass, lean mass, and energy expenditure were measured, while morphological changes and the expression of thermogenesis-related genes in adipose tissue were analyzed. Moreover, the browning capacity of primary preadipocytes derived from h*IRX3*-overexpressing mice was assessed. RNA sequencing was also employed to investigate the effect of h*IRX3* on the expression of thermogenesis-related genes.

Results: h*IRX3* overexpression in embryonic brown/beige adipose tissues (*Rosa26*^{hIRX3}; *Ucp1*-Cre) led to increased energy expenditure, decreased fat mass, and a lean body phenotype. After acute cold exposure or CL316,243 stimulation, brown/beige tissue h*IRX3*-overexpressing mice showed an increase in *Ucp1* expression. Consistent with this, induced h*IRX3* overexpression in adult mice (*Rosa26*^{hIRX3};*Ucp1*-Cre^{ERT2}) also promoted a moderate increase in *Ucp1* expression. *Ex vitro* experiments further revealed that h*IRX3* overexpression induced by *Ucp1*-driven Cre recombinase activity upregulated brown/beige adipocytes *Ucp1* expression and oxygen consumption rate (OCR). RNA sequencing analyses indicated that h*IRX3* overexpression in brown adipocytes enhanced brown fat cell differentiation, glycolysis, and gluconeogenesis.

Conclusion: Consistent with the *in vitro* findings, brown/beige adipocyte-specific overexpression of h*IRX3* promoted *Ucp1* expression and thermogenesis, while reducing fat mass.

Keywords: IRX3, Ucp1, thermogenesis, obesity, overexpression

INTRODUCTION

Iroquois homeobox gene 3 (*IRX3*) encodes a transcription factor of the Iroquois family of homeodomain-containing proteins (1). *IRX3* is initially expressed during embryogenesis, and is involved in the development and patterning of multiple tissues, including the nervous system, heart, and skeleton (2). Recent studies have indicated that *IRX3*, together with its homolog *IRX5*, may also have a role in energy balance and adiposity by regulating thermogenesis in brown adipose tissue (BAT) and the browning program in white adipose tissue (WAT). WAT stores energy in the form of triglycerides under excess caloric intake, whereas BAT dissipates energy through the activity of the inner mitochondrial membrane-localized uncoupled protein 1 (UCP1) to maintain body temperature hemostasis (3–5). Evidence for several genome-wide association studies (GWAS) has indicated that several common single nucleotide polymorphism (SNP) variants, such as rs1421085 and rs9930506, located in the first intron of fat mass and obesity associated (*FTO*) gene, are strongly associated with an increased risk of obesity (6–8), and the functional loci and biological targets associated with these variants are largely unknown.

Recently, *IRX3* and *IRX5*, but not *FTO*, were proposed to function as targets of the rs1421085 variant in thermogenesis (9). However, whether IRX3 acts as an activator or repressor of thermogenesis, where the functional target(s) are located, and whether other candidate genes including *FTO*, *IRX5*, and *Rpgrip1l* were involved in thermogenesis regulation of rs1421085 (10, 11), remain unclear. Another study reported that the hypothalamic overexpression of a dominant–negative form of IRX3 (EnR-*Irx3*) (12), which can increase instead of suppress the transcriptional activities of the IRX3 protein in certain contexts (13), induced a lean body phenotype accompanied by an enhanced WAT browning capacity and activation of BAT (12). Additionally, the overexpression of this "dominant–negative" form of IRX3 (EnR-*Irx3;aP2*-Cre) in adipose tissue also induced a lean body phenotype with marked browning changes in WATs (14). In contrast, a recent study demonstrated that partial (approximately 50%) inhibition of endogenous hypothalamic IRX3 expression reduced thermogenesis in peripheral BAT and increased diet-induced body mass gain, thereby exacerbating obesity (15). We have previously also provided evidence that *Irx3* knockdown can impair the thermogenic capacities of induced brown and beige adipocytes derived from preadipocytes of mouse inguinal WAT (iWAT) and BAT, and human subcutaneous WAT, respectively; and that missense mutations in *IRX3* identified in humans markedly reduced the transcription of *UCP1 in vitro* (16). Consistent with these observations, another group recently showed that *Irx3* knockout in mouse preadipocytes impaired both the early and late stages of adipogenic differentiation to beige adipocytes and preadipocyte mitochondrial respiration (17). These contradictory data highlight the importance of identifying the precise roles of human *IRX3* (wild type) in brown/beige adipocytes *in vivo*.

To this end, we generated two brown/beige adipocyte-specific h*IRX3*-overexpressing mouse models by crossing *Rosa26*^{hIRX3} knock-in mice with *Ucp1*-Cre mice, resulting in the continuous induced expression of h*IRX3* from the embryonic stage, as well as with *Ucp1*-Cre^{ERT2} mice, which expressed h*IRX3* from adulthood following tamoxifen (TMX) injection. In *Ucp1*-Cre mice, h*IRX3* overexpression in BAT led to increased energy expenditure, decreased fat mass, and a lean body phenotype, while h*IRX3* overexpression in adulthood induced a subtle increase in thermogenesis after stimulation with a β3-AR agonist. Furthermore, h*IRX3* overexpression significantly enhanced beige adipocyte differentiation concomitant with increased *Ucp1* expression. Together, our results revealed that h*IRX3* overexpression can promote thermogenesis in brown/beige adipose tissue *in vivo*, and provide a more comprehensive understanding of the role of IRX3 in energy balance and obesity.

MATERIALS AND METHODS

Animal Models

To generate *Rosa26*^{hIRX3} (h*IRX3* knock-in) mice, a human *IRX3* cDNA-polyA cassette (GenBank accession number: NM_024336.2; Ensembl: ENSG00000177508) was cloned into intron 1 of the *Rosa26* locus, and CAG-loxP-stop-loxP was inserted upstream of the cassette. *Ucp1*-Cre mice were obtained from the Jackson Laboratory (Jax no. 024670). To generate *Ucp1*-Cre^{ERT2} mice, a CreERT2-IRES-EGFP-PA cassette was knocked-in downstream of the ATG start codon of the m*Ucp1* gene such that the expression of CreERT2 and EGFP were under the control of m*Ucp1* regulatory sequences. Mouse genomic fragments were amplified with high-fidelity Taq DNA polymerase and were assembled into a targeting vector, together with recombination sites and selection markers, as indicated in the vector map in **Supplementary Figure 1A**. The final sequence of the targeting vector is shown in **Supplementary Figure 1B**. The constitutive h*IRX3* knock-in allele was obtained after Flp-mediated recombination (**Supplementary Figure 1C**). C57BL/6 embryonic stem cells were used for gene targeting. Genotypes were verified by PCR (**Supplementary Figure 1D**). Maximal Cre recombinase mRNA expression was seen in BAT (**Supplementary Figures 1E, F**). *Ucp1*-Cre;*Rosa26*^{hIRX3} (U-IRX3^{ov}) and *Ucp1*-Cre^{ERT2};*Rosa26*^{hIRX3} (iU-IRX3^{ov}) mice were

generated using the Cre/loxP system. *Rosa26*^{hIRX3} was used as a control with U-IRX3^{ov} mice. As *Ucp1*-Cre^{ERT2} showed an approximately 50% decrease in Ucp1 protein expression compared with that of endogenous *Ucp1* (**Supplementary Figure 1G**), we used *Rosa26*$^{wild\ type(WT)}$;*Ucp1*-Cre^{ERT2} as the control for iU-IRX3^{ov}. iU-IRX3^{ov} mice and control littermates were treated intraperitoneally with TMX at a dose of 100 mg/(kg·day^{-1}) to induce h*IRX3* expression (**Supplementary Figure 1H-K**). All animal procedures were approved by the Animal Care Committee of Shanghai Jiao Tong University School of Medicine and followed the guide for the care and use of laboratory animals.

Cold Exposure and CL316,243 Injection

For cold exposure, mice were placed individually in a room with the temperature set at 4°C for 7 days. The animals had free access to food and water during this period. Their core body temperature was measured using a rectal probe (Physitemp Instruments Inc., USA). CL316,243 (Sigma-Aldrich, USA) was injected interperitoneally at a dose of 1 mg/(kg·day^{-1}), and the injection protocol was described in the results part for details.

Measurement of Fat/Lean Mass and Whole-Body Energy Metabolism

The fat mass and lean mass of each mouse was measured using an EchoMRI-100H (EchoMRI, USA). The mice were placed in a Comprehensive Laboratory Animal Monitoring System (CLAMS, Columbus Instruments, USA) for the evaluation of whole-body energy metabolism. Oxygen and carbon dioxide consumption, as well as activity, was continuously measured for two days. The respiratory exchange ratio (RER) and energy expenditure were calculated based on the oxygen and carbon dioxide data and were normalized to body weight (18).

Morphological Analysis

BATs and WATs were isolated, fixed in 4% paraformaldehyde, embedded in paraffin, and sliced into 5-μm (iWAT, eWAT) or 3-μm (BAT) sections for hematoxylin and eosin (H&E) staining. Images were captured under a microscope (Olympus, Japan). Pictures were scanned by Digital Pathology Slide Scanner (KF-PRO-120).

Isolation of the Stromal Vascular Fraction and Brown/Beige Adipocyte Differentiation *In Vitro*

The stromal vascular fractions (SVFs) were isolated from the BAT and iWAT of five-week-old U-IRX3^{ov} and control mice and then induced to fully differentiate into brown/beige adipocytes as previously described (5). In brief, the fat pads were isolated, cut into pieces, and digested with type II collagenase (Sigma) at 37°C for 30 min followed by quenching with DMEM/F12 supplemented with 10% FBS. The suspended samples were filtered using a 40-μm strainer (BD, USA) and then plated on culture dishes. The SVFs were first grown to 100% confluence in DMEM/F12 supplemented with 10% FBS (plus 1% penicillin/streptomycin and 1 mM L-glutamine), and then these primary preadipocytes were differentiated into brown/beige adipocytes in a cocktail containing 5 μg/ml insulin (Eli Lilly, USA), 1 μM dexamethasone, 1 μM rosiglitazone, 1 μM triiodothyronine (T_3), and 0.5 mM IBMX (all Sigma–Aldrich, USA) for two days, and subsequently in medium with insulin, rosiglitazone, and T_3 for another six days.

Oil Red O Staining

After eight days of induction, mature adipocytes were stained with Oil Red O. In brief, the cells were fixed in 4% paraformaldehyde for 30 min, rinsed, air-dried, and incubated with Oil Red O (Nanjing Jiancheng Bioengineering Institute, China) for 30 min. Images were captured under a microscope (Olympus).

Measurement of the Oxygen Consumption Rate

SVFs were seeded in an XF24 V28 microplate (Agilent Technologies, USA) coated with poly-L-lysine. The induction protocol was as described in section 2.5. The oxygen consumption rate (OCR) was measured at induction day 4 using an XF24 analyzer (Agilent Technologies) following the manufacturer's instructions. Briefly, the induced brown/beige adipocytes were washed with Seahorse assay medium, consisting of XF DMEM supplemented with 10 mM XF glucose, 1 mM XF pyruvate, and 2 mM XF L-glutamine, followed by incubation with 525 μl of assay medium at 37°C in an incubator without CO_2 (Agilent Technologies) for 1 h. Respiratory inhibitors (75 μl) were loaded into the injection port to final concentrations of 1 mg/ml oligomycin, 2 mM FCCP, 0.5 mM antimycin A, and 0.5 mg/ml rotenone to detect uncoupled respiration, maximal respiration, and nonmitochondrial respiration, respectively. The final OCR results were standardized to the total protein content. The results are representative of at least three independent experiments.

RNA Extraction and Real-Time PCR Analysis

Total RNA was extracted from cultured cells or frozen adipose tissue using the Eastep Super Total RNA Extraction Kit (Promega (Beijing) Biotech Co., China). The absorbance ratio at 260/280 nm and the RNA concentration of each sample were detected using a NanoDrop ND2000 spectrophotometer (Thermo Scientific). Reverse transcription was performed using the PrimeScript Reverse Transcript Master Mix (TaKaRa, Japan). qPCR was performed using a QuantStudio Dx Real-Time PCR Instrument (Applied Biosystems). The comparative ΔΔCt method was used to evaluate the relative mRNA levels; 36B4 served as the reference gene (**Supplementary Table 1**).

RNA Sequencing and Analysis

RNA sequencing was performed by NovelBio, Shanghai, China. The RNA quality was assessed using an Agilent 2200 and the RNA was stored at −80°C. RNA with an RNA integrity number (RIN) >7 was considered acceptable for cDNA library construction. cDNA libraries were constructed for each RNA

sample using the TruSeq Stranded mRNA Library Prep Kit (Illumina) according to the manufacturer's instructions. The libraries were quality controlled with Agilent 2200 and sequenced by HiSeq X (Illumina) as 150-bp paired-end reads. For the analysis of differentially expressed genes, *P*-value and false discovery rate (FDR) analysis were subjected to the following criteria: i) Fold change (FC) >2 or <0.5; ii) *P*-value <0.05, FDR <0.05. Fisher's exact test was applied to identify significant GO categories and KEGG pathways (*P*-value <0.05). The approach for gene set enrichment analysis (GSEA) was in accordance with that previously reported (19). Genes were considered to be significantly differentially expressed when the FDR was less than 0.05 and the $\log_2$FC was more than 1.

Protein Preparation and Western Blot Analysis

Total protein was isolated using RIPA lysis buffer (Biocolors, China) with a protease inhibitor cocktail (Sigma). Western blotting was performed as previously described (5). The following antibodies were used: anti-IRX3 (ab174307, Abcam), anti-UCP1 (ab10983, Abcam), anti-Hsp90 (Cell Signaling Technology, 4877s), and anti-PGC-1α (Abcam, ab54481). The results are representative of at least three independent experiments.

Statistical Analysis

Data are shown as means ± S.E.M, and the results were compared by two-tailed *t*-tests. A *P*-value <0.05 was considered to be significantly different. Spearman's correlation analysis was performed to examine the associations between the expression of h*IRX3* and m*Ucp1*. For molecular experiments, data were generated from three independent experiments. Analyses were undertaken with GraphPad Prism version 8.2.1 (279) (GraphPad Software, Inc., La Jolla, CA, USA).

RESULTS

Brown/Beige Adipocyte-Specific Overexpression of h*IRX3* Increased Energy Expenditure and Induced a Lean Body Phenotype *In Vivo*

To clarify the physiological and biological roles of h*IRX3* in thermogenesis in brown/browning adipose tissues, we generated a *Ucp1*-Cre-driven h*IRX3* overexpression mouse model (*Ucp1*-Cre; *Rosa26*^{hIRX3}, referred to as U-IRX3^{ov}) (**Figure 1A**). When fed a normal chow diet, both male and female U-IRX3^{ov} mice gained substantially less body weight than the controls (*Rosa26*^{hIRX3}) at 10 weeks of age (**Figure 1B** and **Supplementary Figures 2A–C**). Body composition analysis revealed a lower fat mass percentage in U-IRX3^{ov} mice when compared with controls; however, there was no significant difference in lean mass percentage between the two genotypes (**Figures 1C, D** and **Supplementary Figures 2D, E**). To test for potential alterations in energy balance, we undertook a comprehensive evaluation of the food intake, physical activities, and energy expenditure of the mice. We found that, with comparable daily food intake (**Figure 1E** and **Supplementary Figure 2F**), U-IRX3^{ov} mice had greater O_2 consumption, increased CO_2 production, and greater total energy expenditure, especially at night, compared with controls (**Figures 1F–I**). U-IRX3^{ov} mice showed a slight increase in physical activities in few hours of a day (*X*-and *Y*-axis), although the total increase was not statistically significant (**Supplementary Figures 2G–I**). Importantly, U-IRX3^{ov} mice displayed higher average energy expenditure per hour compared with controls (**Figure 1J**). These findings suggested that U-IRX3^{ov} mice gained less fat mass, which was likely due to increased energy expenditure.

Overexpression of h*IRX3* Enhances Thermogenesis-Associated Gene Expression Following Chronic Cold or CL316,243 Stimulation

Next, to test the response of the mice to acute and chronic cold, we subjected the two groups of mice to cold treatment at 4°C. No significant differences in body temperature were observed during the first 6 h (**Supplementary Figure 2J**). However, after seven days of cold stimulation, the mice showed a subtle, but statistically insignificant, decrease in eWAT mass percentage (P = 0.08) (**Figure 2A**). With moderate h*IRX3* overexpression in inguinal WAT (iWAT) and BAT (**Figure 2B** and **Supplementary Figure 2K**), U-IRX3^{ov} mice showed marked morphological changes in iWAT, characterized by a more condensed texture with markedly increased number of smaller lipid droplets, as well as a significantly reduced droplet content in BAT, and an increase in the percentage of smaller adipocytes in eWAT compared with those in control mice (**Figures 2C, D**). We next examined the expression levels of thermogenesis-related genes in three adipose tissues, and found that the mRNA levels of *Pgc-1α* and *Dio2* were increased in the BAT of U-IRX3^{ov} mice (**Figure 2E**). Although the mRNA levels of *Ucp1* were unchanged, the BAT of U-IRX3^{ov} mice exhibited a small but substantial increase in UCP1 protein levels (**Figures 2F, G**). For iWAT, a marked increase in the mRNA expression levels of *Ucp1*, *Cidea*, *Dio2*, *Cox7a1*, and *Cox8b* was observed in U-IRX3^{ov} mice (**Figure 2H**). Consistent with our previous *in vitro* findings, h*IRX3* mRNA expression *in vivo* was also positively correlated with that of *Ucp1* (**Figure 2I**). The protein levels of UCP1 and PGC-1α in iWAT were also increased in the iWAT of U-IRX3^{ov} mice (**Figure 2J**). However, only the mRNA levels of *Ucp1* and *Cox8b*, and the protein levels of PGC-1α, showed increased expression in the eWAT of U-IRX3^{ov} mice (**Figures 2K, L**).

To further validate the promotive effect of h*IRX3* on thermogenesis in BAT, we intraperitoneally injected CL316,243, an agonist of the β3-adrenergic receptor (β3-AR), into female U-IRX3^{ov} and littermate control mice to activate BAT and induce the browning process. Male mice showed no significant change in mass under cold treatment; however, female U-IRX3^{ov} mice displayed a reduction in BAT, iWAT, and gWAT (gonadal WAT) content (**Supplementary Figure 3A**). Histomorphological analysis revealed that the adipocytes were smaller and more condensed in all these adipose tissues (**Supplementary Figures 3B–D**). Both the mRNA

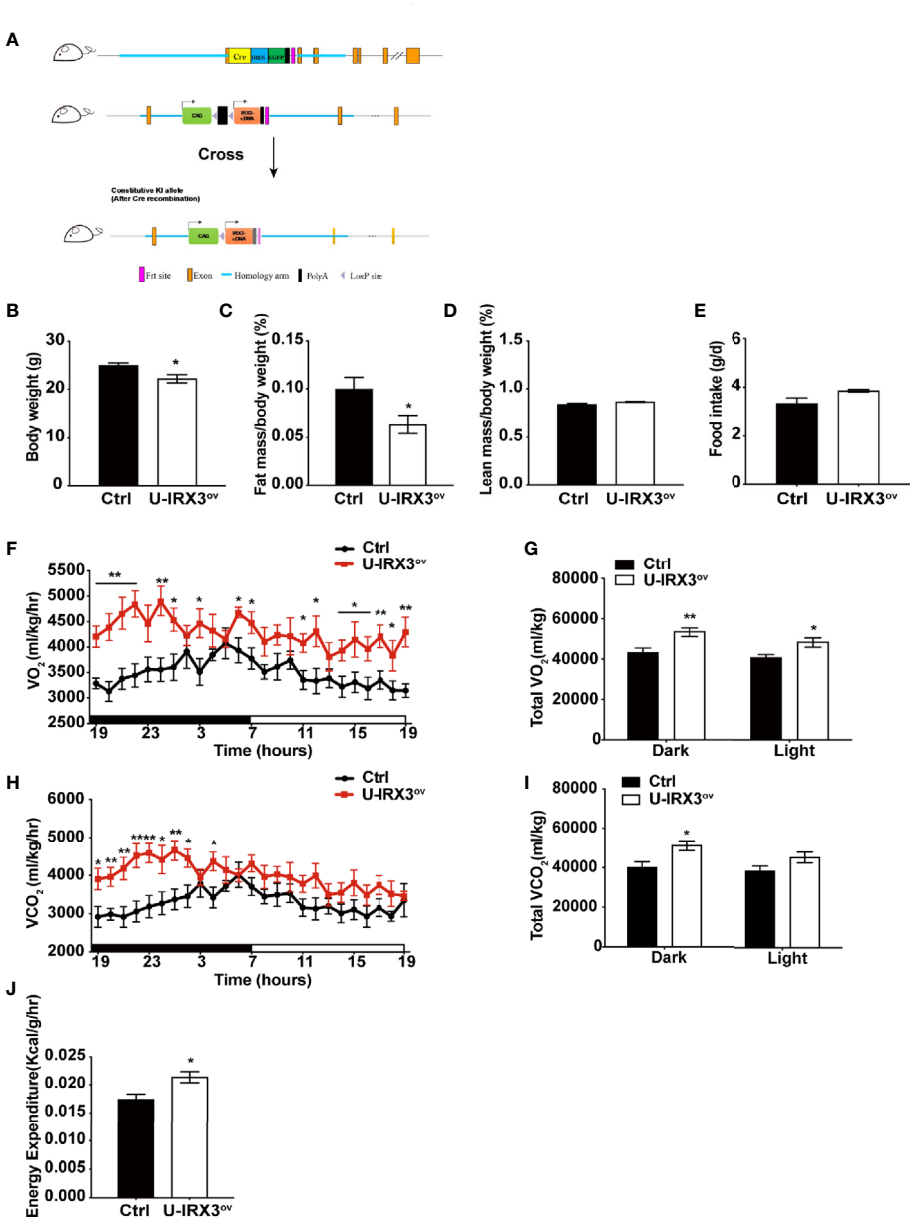

FIGURE 1 | Brown/beige adipocyte-specific h*IRX3* overexpression increases energy expenditure and induces a lean body phenotype in male mice. **(A)** Schematic diagram of the generation of U-IRX3^{ov} (*Rosa26*-loxP-stop-loxP-h*IRX3*;*Ucp1*-Cre) mice. **(B–D)** Body weight **(B)**, fat mass percentage **(C)**, and lean mass percentage **(D)** of male U-IRX3^{ov} and control mice at 10 weeks of age (n = 6~8). **(E)** Average daily food intake of male U-IRX3^{ov} and control mice at 10 weeks of age (average of 3 individual measurements). **(F–J)** Whole-body oxygen (O_2) consumption per hour **(F)** and per 12 h **(G)**, carbon dioxide (CO_2) production per hour **(H)** and per 12 h **(I)**, and energy expenditure **(J)** of 10-week-old U-IRX3^{ov} and control mice during a 24-h period (n = 6~8). Statistics were standardized by body weight. Data are shown as means ± SEM. *P < 0.05, **P < 0.01.

and protein expression levels of *Ucp1* and *Pgc-1α* were increased in the BAT of female U-IRX3^{ov} mice (**Supplementary Figures 3E, F**). The expression of thermogenesis-related genes, such as *Ucp1*, *Pgc-1α*, *Cidea*, and *Dio2*, was enhanced in the iWAT of U-IRX3^{ov} mice (**Supplementary Figure 3G**). Similarly, UCP1 protein levels showed an increasing trend in the iWAT of U-IRX3^{ov} mice (**Supplementary Figure 3H**). Collectively, these results indicated that the overexpression of h*IRX3* increased both cold treatment- and CL316,243-induced thermogenesis in brown/beige adipose tissues *in vivo*.

Overexpression of hIRX3 in Adulthood Enhanced β3-AR Agonist-Induced Thermogenesis

The protein expression of UCP1 in BAT first appears in late gestation and then rapidly increases at birth (20), allowing *Ucp1*

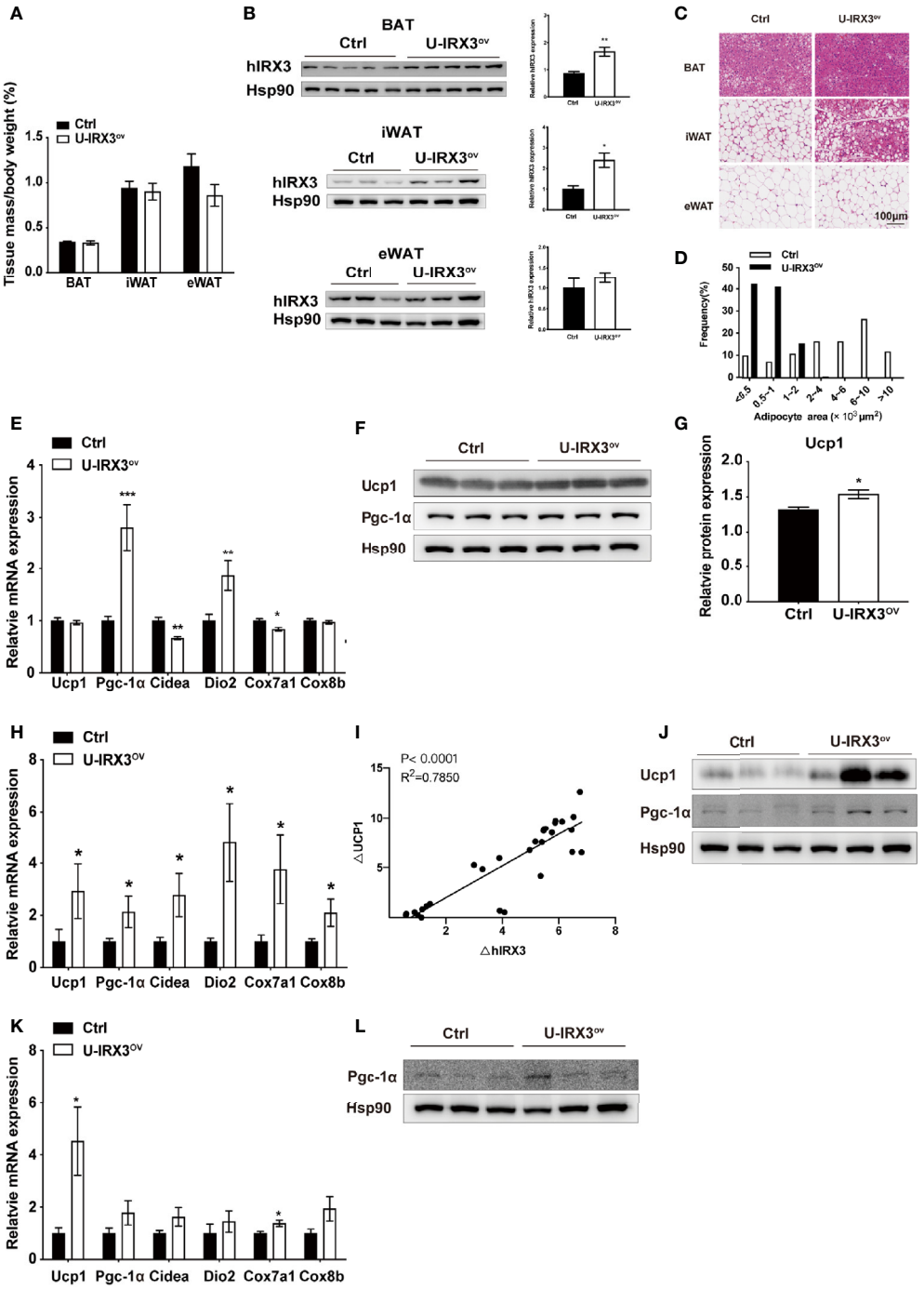

FIGURE 2 | The overexpression of h*IRX3* from the embryonic stage enhances cold-induced thermogenesis. **(A–L)** Ten-week-old U-IRX3^{OV} and control mice were placed in a cold room at 4°C for 7 days. Tissue mass percentage **(A)** and protein levels of overexpressed hIRX3 in BAT, iWAT, and eWAT of the two groups of mice (n = 3~5). **(B)** Representative images of hematoxylin and eosin (H&E) staining of BAT (top), iWAT (middle), and eWAT (bottom) for the two groups of mice **(C)**. **(D)** Adipocyte size distribution of the eWAT in **(C)**. Scale bars, 100 μm. **(E)** The mRNA expression levels of thermogenesis-related genes in the BAT of the two groups of mice (n = 6~8). **(F)** The protein levels of UCP1 and PGC-1α in the BAT of the two groups of mice (n = 3). **(G)** The UCP1 protein expression level relative to that of Hsp90 in **(F)**. **(H)** The mRNA expression levels of thermogenesis-related genes in the iWAT of the two groups of mice (n = 6~8). **(I)** Linear regression analyses of hIRX3 and Ucp1 RNA expression level of male (n=13) and female(n=16) U-IRX3^{OV} and control mice **(J)** The protein levels of UCP1 and PGC-1α in the iWAT of the two groups of mice (n = 3). **(K)** The mRNA expression levels of thermogenesis-related genes in the eWAT of the two groups of mice (n = 6~8). **(L)** The protein levels PGC-1α in the eWAT of the two groups of mice (n = 3). Data are shown as means ± SEM. *P < 0.05.

promoter-driven Cre recombinase to excise loxP-flanked (floxed) sequences (STOP in this study) and theoretically induce h*IRX3* overexpression prepartum. A recent study demonstrated that *Irx3* ablation in mouse preadipocytes attenuated the proliferation and early differentiation of beige adipocytes *in vitro* (17). To avoid the nonspecific consequences of overexpressing h*IRX3* in brown preadipocytes, and to investigate the effects of transient h*IRX3* overexpression in mature beige adipocytes in adult mice, we generated a TMX-inducible h*IRX3* overexpressing mouse line (*Ucp1*-Cre^{ERT2}; *Rosa26*^{hIRX3}, iU-IRX3^{ov}) by crossing *Rosa26*^{hIRX3} mice with *Ucp1*-Cre^{ERT2} mice (**Figure 3A**). Then, we treated eight-week-old male iU-IRX3^{ov} and control mice with TMX (i.p. once/day) for 5 days during the 10-days CL316,243 injection interval (**Figure 3B**). The overexpression of h*IRX3* in adipose tissue was validated by qPCR and Western-blot (**Supplementary Figures 1H–K**). No differences in body weight, fat mass percentage, lean mass percentage, or adipose tissue weight were observed between the two groups (**Figures 3C–F**). In the iWAT of iU-IRX3^{ov} mice, there was a small but significant increase in *Ucp1* mRNA and protein levels ($p<0.05$), while the expression of other thermogenesis-related genes showed an

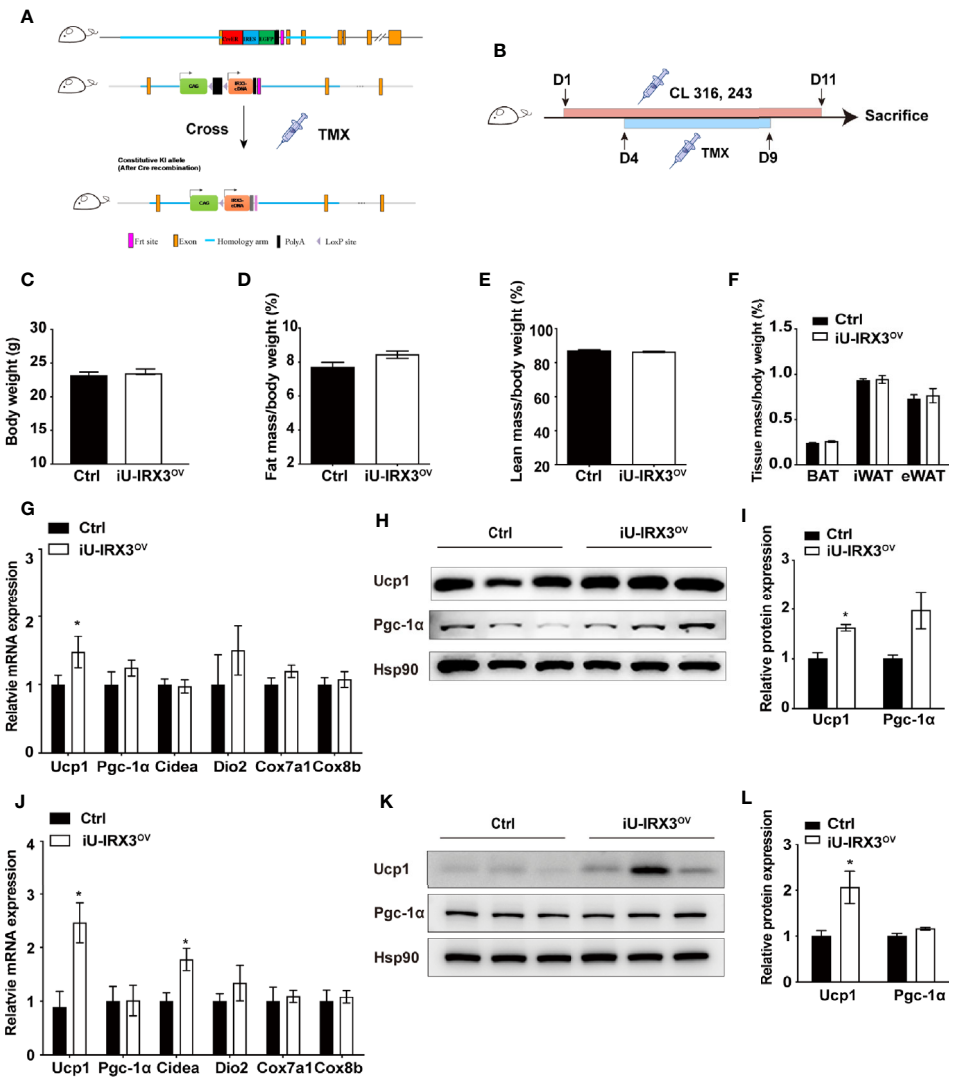

FIGURE 3 | Overexpressing hIRX3 after adulthood increased the expression of thermogenesis-related genes under β3-AR agonist (CL316,243) stimulation. **(A)** Schematic representation of the strategy to generate iU-IRX3^{ov} mice. **(B)** Timeline of CL316,243 and tamoxifen (TMX) injection in eight-week-old male iU-IRX3^{ov} and control mice (n = 9~10). **(C–F)** Body weight **(C)**, fat mass percentage **(D)**, lean mass percentage **(E)**, and tissue mass percentage of BAT, iWAT, and eWAT **(F)** in male iU-IRX3^{ov} and control mice. **(G)** The relative mRNA expression levels of *Ucp1* and other thermogenesis-related genes in the iWAT of iU-IRX3^{ov} mice(n = 9~10). **(H, I)** Images and quantitative values of UCP1 and PGC-1α protein levels in iWAT (n = 3). **(J)** The relative mRNA expression levels of *Ucp1* and other thermogenesis-related genes in eWAT (n = 9~10). **(K, L)** Images and quantitative values of UCP1 and PGC-1α protein levels in eWAT (n = 3). Data are shown as means ± SEM. *$P < 0.05$.

increasing, but insignificant, trend (**Figures 3G–I**). Interestingly, the mRNA expression of *Ucp1*, *Pgc-1α*, and *Cidea* was significantly increased in the eWAT of iU-IRX3^{ov} mice when compared with controls (**Figure 3J**), which was accompanied by an increase in UCP1 protein levels (**Figures 3K, L**). Combined, these results indicated that the temporary overexpression of h*IRX3* in WAT of adult mice, and especially in eWAT, can enhance thermogenesis, but with a relatively subtle effect when compared with that seen in U-IRX3^{ov} mice.

Overexpression of h*IRX3* Increases Thermogenesis in Brown/Beige Adipocytes *In Vitro*

We next investigated the effects of h*IRX3* overexpression on the differentiation and thermogenic capacities of induced brown and beige adipocytes obtained from primary preadipocyte SVFs. Over expression of hIRX3 was proved by qPCR and Western-blot (**Figures 4E, K** and **Supplementary Figure 3I**). BAT SVF derived from U-IRX3^{ov} mice showed markedly enhanced adipogenic differentiation capacity compared with controls, as evidenced by the increased number of multilocular lipid droplets in Oil Red O staining (**Figure 4A**). We also assessed the thermogenic capacity of induced brown adipocytes, represented by the mitochondrial OCR. Compared with controls, there was a significant increase in basal respiration and proton leak, as well as an increasing trend for the maximal respiration and ATP production capacity of the induced brown adipocytes derived from U-IRX3^{ov} mice. This suggested that h*IRX3* overexpression led to an increase in thermogenesis (**Figures 4B, C**). Meanwhile, the mRNA levels of thermogenesis-related genes, such as *Ucp1*, *Pgc-1α*, *Cidea*, *Cox7a1*, and *Cox8b*, were significantly increased in induced brown adipocytes derived from U-IRX3^{ov} mice (**Figure 4D**). Consistent with these results, the protein levels of UCP1 and PGC-1α were also enhanced by h*IRX3* overexpression (**Figures 4E, F**). Additionally, when the SVFs obtained from the iWAT of U-IRX3^{ov} and control mice were induced to beige adipocytes *in vitro*, we found that adipogenesis, thermogenic capacity, and expression of thermogenesis-related genes were all increased in the U-IRX3^{ov} group (**Figures 4G–L**). Together, these results indicated that the thermogenic capacity can be improved in brown and beige adipocytes following h*IRX3* overexpression mediated by *Ucp1* promoter-driven Cre recombinase activity *in vitro*.

h*IRX3* Enhances Thermogenesis Through Increasing *Ucp1* Expression

To further elucidate the effects of hIRX3 overexpression on thermogenesis, we performed RNA-seq analysis on induced brown adipocytes derived from the SVFs of U-IRX3^{ov} and control mice. In total, we identified 665 differentially expressed genes (FC <2, FDR <0.05) between the U-IRX3^{ov} and control groups, 248 of which were upregulated and 417 downregulated (**Supplementary Tables 2** and **3**). Notably, and consistent with the qPCR findings, several genes annotated as being positively related to the browning program, such as *Ucp1*, *Cidea*, *Pgc-1α*, *Cox7a1*, and *Cox8b*, were markedly upregulated in the U-IRX3^{ov} group (**Figure 5A**). Gene Ontology (GO) analysis revealed that the upregulated genes were enriched in biological processes involved in brown fat cell differentiation, glycolysis, gluconeogenesis, and other metabolic process associated with energy expenditure; meanwhile, the downregulated genes were mainly associated with immune system process, inflammatory response, and cell adhesion (**Figure 5B**), processes that are usually suppressed during brown adipogenesis or thermogenesis (21–23). Gene set enrichment analysis (GSEA) further indicated a marked overlap between enriched genes and the gene signature activated during brown adipogenesis (**Figure 5C**). We then explored protein–protein connection of upregulated genes, and clustered connected genes which classified into the same KEGG pathway. The results showed the upregulated genes were enriched in pathways related to thermogenesis, oxidative phosphorylation, glycolysis/gluconeogenesis, and PPAR signaling (**Figure 5D**). Collectively, these data suggested that h*IRX3* overexpression in induced brown adipocytes can promote *Ucp1* expression, brown cell adipocyte differentiation, and thermogenesis.

DISCUSSION

In this study, we generated two genetically modified mouse models to clarify the effects of h*IRX3* overexpression *in vivo*, and present evidence that h*IRX3* overexpression in mouse brown/beige adipocytes leads to an enhancement of thermogenesis. Using the U-IRX3^{ov} line, in which h*IRX3* is continuously expressed from an early stage of life, we found that the functional abilities of BAT and the browning program of WAT were both enhanced, which resulted in the increased expression of thermogenesis-related genes (including *Ucp1*), increased energy expenditure, smaller lipid droplets, and lower fat mass percentage. Using the iU-IRX3^{ov} mouse line, in which the expression of h*IRX3* is transiently induced in adulthood, we identified a weak but similar increase in the expression of thermogenesis-related genes in iWAT and eWAT.

Several GWAS studies have demonstrated that genetic variations (SNPs) within the first and second introns of the *FTO* gene are positively associated with an increased risk of obesity (6–8, 24–26). Among these SNPs, one variant—rs1421085—was recently identified as an underlying cause of adiposity through increasing *IRX3* expression *via* long-range chromatin interaction (9, 12). However, whether *IRX3* augments or attenuates the thermogenic capacities of brown/beige adipocytes remains unclear (27–29). In contrast to the findings that IRX3 is an inhibitor of the browning progress, we previously reported that *IRX3* expression is elevated in human and mouse brown/beige adipocytes, and that the browning program of adipocytes is repressed when *IRX3* is knockdown *in vitro* (16, 17). Importantly, we found that *IRX3* could upregulate the transcription of *Ucp1* by specific binding to the ACATGTGT motif (−3470 to −3463 bp) upstream of the transcription starting site of the mouse *Ucp1* gene. In this study, we aimed to further

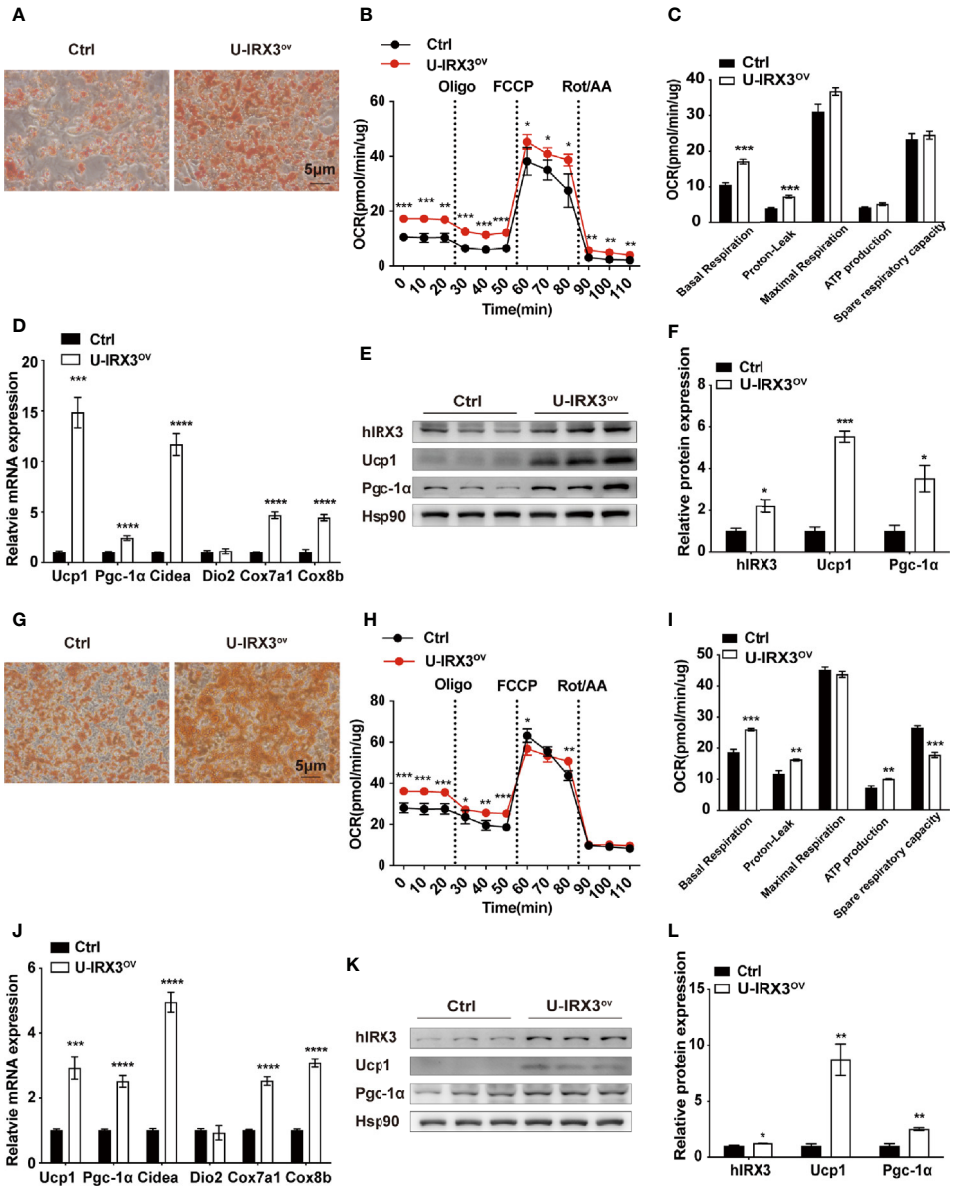

FIGURE 4 | The overexpression of h*IRX3* increases thermogenesis in brown/beige adipocytes *in vitro*. **(A–F)** The overexpression of h*IRX3* in stromal vascular fractions (SVFs) derived from BAT of U-IRX3^{ov} and control mice. Oil Red O staining **(A)**, oxygen consumption rate (OCR) **(B, C)**, mRNA expression levels of thermogenesis-related genes **(D)**, and the protein expression **(E)** and their quantitative values **(F)**, including hIRX3, PGC-1a, and UCP1, in induced brown adipocytes after five days of differentiation. **(G–L)** The overexpression of h*IRX3* in SVFs derived from the iWAT of U-IRX3^{ov} and control mice. Oil Red O staining of beige adipocytes after eight days of differentiation **(G)**; the OCR of beige adipocytes after eight days of differentiation **(H, I)**; the mRNA expression levels of thermogenesis-related genes **(J)**, and the protein expression **(K)** and their quantitative values **(L)**, including hIRX3, PGC-1a, and UCP1, in induced beige adipocytes after eight days of differentiation. Data are shown as means ± SEM. *$P < 0.05$, **$P < 0.01$, ***$P < 0.001$, ****$P < 0.0001$.

clarify the role of the human IRX3 in thermogenesis and its effect on *Ucp1* expression, especially in *Ucp1*-expressing brown/beige adipocytes. We found that h*IRX3* enhanced thermogenesis in both h*IRX3*-overexpression mouse models (noninducible and TMX-inducible). Of note, thermogenesis was more prominent in U-IRX3^{ov} (noninducible *Ucp1*-Cre) mice than in iU-IRX3^{ov} (inducible *Ucp1*-Cre^{ERT2}) mice. This difference could be attributed to the temporal, spatial, and dosage differences in h*IRX3* expression between the two models. First, h*IRX3* was expected to be expressed in brown adipocytes of U-IRX3^{ov} mice shortly after birth, similar to that observed for normal *Ucp1* expression (30), whereas h*IRX3* expression was only relatively weakly induced in brown adipocytes of adult iU-IRX3^{ov} mice after TMX injection. Second, there may be heterogeneity in the

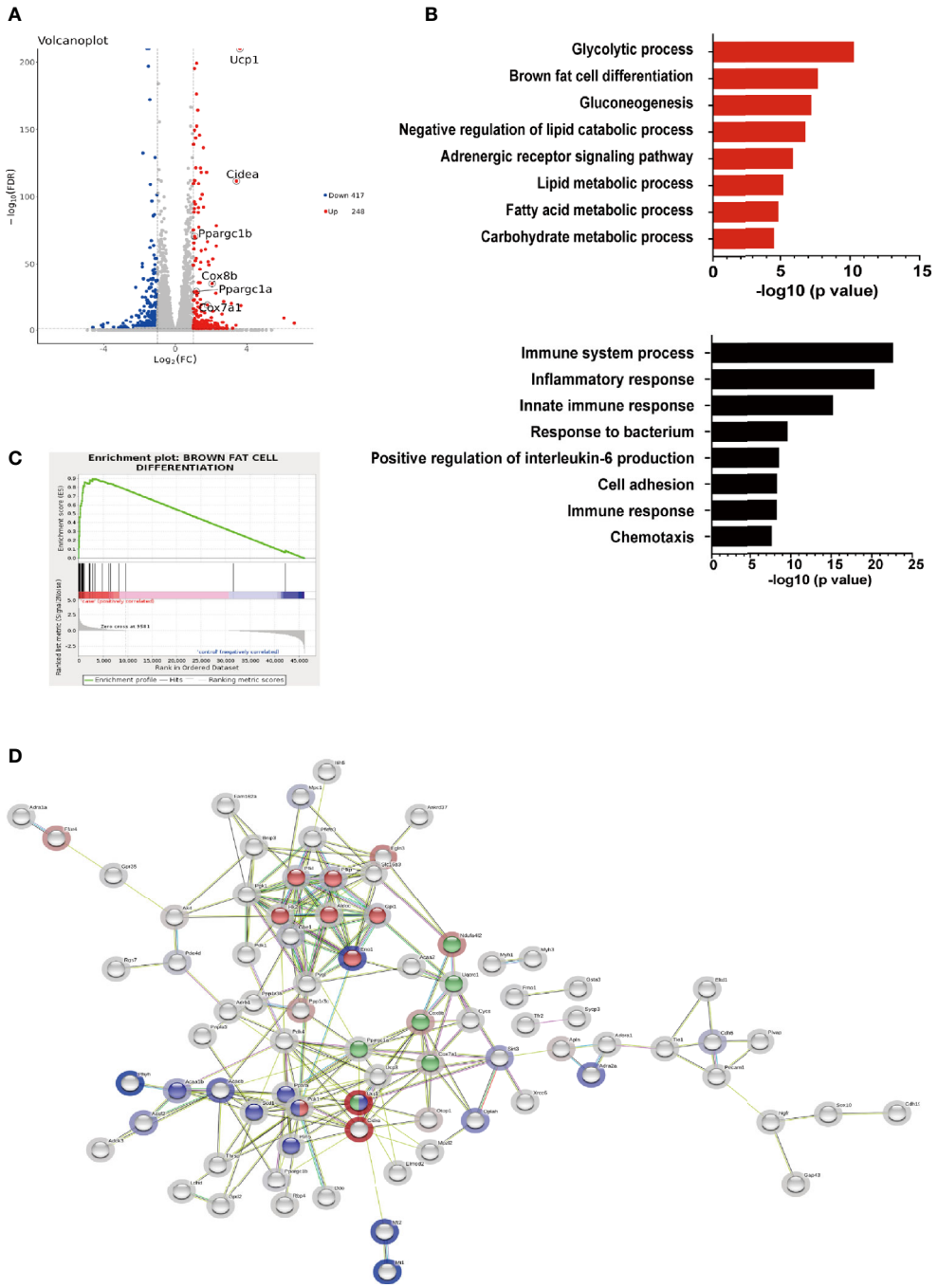

FIGURE 5 | The gene expression profile of h*IRX3*-overexpressing brown adipocytes. **(A–D)** After eight days of differentiation, RNA-seq analysis was performed on induced brown adipocytes derived from BAT of U-IRX3^{OV} and littermate control mice (n = 3). **(A)** Volcano plot of the differentially expressed genes; red: upregulated, blue: downregulated. The x-axis represents the log-fold change, and the y-axis represents the –log10 of the false discovery rate (FDR). Several key thermogenesis-related markers are circled. **(B)** The top gene ontology (GO) biological process terms enriched ($P < 0.05$, Fisher's test) among genes that show significantly higher (top 8, red) or lower (top 8, black) expression ($P < 0.05$, DESeq) in the U-IRX3^{OV} group relative to controls. **(C)** Gene set enrichment analysis (GSEA) of overlap between genes upregulated following h*IRX3* overexpression and the brown fat cell differentiation gene signature in the GO analysis. NES, normalized enrichment score; p, empirical p-value. **(D)** A protein–protein interaction network of the upregulated genes ($P < 0.05$, log2FC ≥1, group average count ≥50, n = 129) was constructed using the STRING database (https://string-db.org) applying an interaction score >0.4. The halo color represents the log2FC value from low (blue) to high (red). Gene clusters for the main KEGG pathways are shown based on node color (red for glycolysis/gluconeogenesis, blue for PPAR signaling pathway, green for thermogenesis).

spatial and quantitative expression of Cre recombinase: the ectogenic *Ucp1*-Cre construct was inserted spontaneously, thus Cre expression would have been extensively induced (might not restricted to brown and beige adipose tissue), whereas the endogenous expression of *Ucp1* would not be affected (31). On the other hand, in *Ucp1*-Cre^{ERT2}, the Cre sequence was directly inserted into exon 1 of *Ucp1*, which means the Cre only expressed where endogenous Ucp1 appeared, but at the same time impaired endogenous *Ucp1* expression and led to *Ucp1* protein reduced by half. Thus the Cre recombinase in the *Ucp1*-Cre^{ERT2} model likely showed weak gene-editing activity. Notably, the effect of *IRX3* on thermogenesis may change according to the stage of adipocyte development or differentiation status. By isolating preadipocytes from U-IRX3^{ov} mice and inducing brown/beige adipogenesis *in vitro*, we found that h*IRX3* overexpression following the initiation of *Ucp1* mRNA expression could effectively enhance the thermogenic capacity and *Ucp1* expression of mature brown/beige adipocytes. Nevertheless, the RNA-seq results showed that genes that were upregulated following h*IRX3* overexpression were primarily enriched in processes such as brown cell differentiation and oxidative phosphorylation, further supporting a promotive role for h*IRX3* in energy expenditure.

The overexpression of h*IRX3* either from an early stage of life or only in adulthood promoted the thermogenic potential of brown/beige adipocytes, which was consistent with our previous findings *in vitro* (16). However, other studies have indicated that IRX3 may be a negative regulator of thermogenesis through central or peripheral regulation (9, 12). Nobrega et al. previously demonstrated that obesity-associated *FTO* variants were positively associated with *IRX3* expression in the brain (12), and observed a 25%–30% decrease in body weight in *Irx3* global knockout mice fed a normocaloric diet (NCD) compared with wild-type controls, which was attributable to a significant increase in brown/beige adipocyte function. Additionally, the hypothalamic overexpression of a dominant–negative form of mouse *Irx3* (*Ins2*-Cre;*Irx3*DN) using EnR-*Irx3*, in which the EnR element was employed to inactivate *Irx3* expression, also resulted in a prominent increase in the thermogenic capacities of brown/beige adipocytes. A different group subsequently identified that rs1421085, a leading *FTO* gene variant, disrupted a conserved binding motif for the ARID5B repressor, leading to the specific disinhibition of *IRX3* expression in preadipocytes (not in mature white adipocytes) and, eventually, to the repression of preadipocyte thermogenic capacity or the impairment of adipocyte development at a very early stage of induction (day 2) *in vitro* (9). To support this, the authors generated adipose-specific *Irx3* dominant–negative (*aP2*-Cre;*Irx3*DN) mice and found phenotypes similar to those of *Ins2*-Cre;*Irx3*DN mice. Both studies supposed a negative role for *Irx3* in thermogenesis.

Interestingly, both groups crossed *Rosa26*-loxP-stop-loxP-EnR-*Irx3*DN (a theoretical dominant–negative form of Irx3) with corresponding Cre tool mice to produce the tissue-specific "knockout" models (9, 12), which could be intriguing and tricky. First, mice from both the *aP2*-Cre;*Irx3*DN and *Ins2*-Cre;*Irx3*DN lines appeared to be markedly smaller compared with controls in early life (even at three weeks), and showed a large difference (approximately 10 g) in body weight at eight weeks of age (9, 12). This indicated that these mice likely had growth impairment or developmental defects, and the increased thermogenic capacities of the evaluated adipose tissues might have been due to impaired development (32). Furthermore, the blotting of hypothalamic proteins showed concomitant similar expression levels of endogenous wild-type *Irx3* and exogenous EnR-*Irx3* in *Ins2*-Cre;EnR-*Irx3* mice. Indeed, the phenotypes of the *Ins2*-Cre;EnR-*Irx3* mice were similar to those of U-IRX3^{ov} mice, in which we employed *Rosa26*-loxP-stop-loxP-h*IRX3* using a similar strategy to that used by the Nobrega group, and where the mice displayed a reduced less body weight and increased thermogenesis in adipose tissue. However, no short stature was observed among either U-IRX3^{ov} or iU-IRX3^{ov} mice. Notably, in a different study, the authors infected isolated neonatal ventricular myocytes (NVMS) with adenovirus encoding wild-type *Irx3*, a dominant *Irx3* activator (VP16-*Irx3*), or a dominant *Irx3* repressor (EnR-*Irx3*), and found that *Cx40*/*Gja5*, an IRX3 target gene, was significantly upregulated following the overexpression of wild-type *Irx3* and EnR-*Irx3*, but not VP16-*Irx3* (13). These results raised the possibility that, under certain conditions, EnR-*Irx3* may exert a wild-type *Irx3*-like function. To address this, adipocyte-specific *Irx3* knockout models (without growth defects) using floxed *Irx3* would be beneficial for elucidating the roles of endogenous *Irx3* in thermogenesis.

Mellgren et al., who first identified a role for rs1421085 in the regulation of *IRX3* expression (9), further showed that the constitutive and complete absence of endogenous *Irx3* in embryonic fibroblasts leads to the loss of adipogenic differentiation capacity (17). ME3 cells lacking *Irx3* cannot initiate differentiation, and show profoundly inhibited mitochondrial respiration and a significant decrease in *Ucp1* and *Pgc-1α* levels when treating with brown adipocyte induction protocol (17). Accordingly, shRNA-induced *Irx3* knockdown in preadipocytes from both iWAT and BAT significantly repressed the thermogenic capacity and *Ucp1* expression in induced mature brown/beige adipocytes (at differentiation days 6–8) (16). However, the same group previously reported that silencing *Irx3* in wild-type preadipocytes derived from noncarriers (of rs1421085) did not inhibit *Ucp1* expression and thermogenic capacity at differentiation day 2, at which stage *Ucp1* expression and lipid droplet formation were almost undetectable (14). The thermogenesis phenotypes of preadipocytes on different induction day could be in different condition, which would be much essential and valuable, the detailed mechanism underlying these discrepancies was needed to be studied discreetly. Additionally, differences in species, cell lines, induction cocktail composition, *IRX3* dosage, and genetic background used by different groups are likely to lead to different outcomes.

In addition, another group presented evidence showing that partial inhibition of hypothalamic *Irx3* by lentiviral knockdown led to diet-induced adiposity, possibly through increasing caloric intake and reducing energy expenditure (15), in contrast to the metabolic phenotypes observed in *Ins2*-Cre;EnR-*Irx3* mice.

Further research using other neuron-specific *Irx3* knockout models is required to clarify the central regulatory roles of *Irx3* in peripheral brown/beige adipocyte thermogenesis.

We previously reported that IRX3 directly binds to the *Ucp1* promoter and enhances its transcription *in vitro*. Consistent with this result, in this study, we further showed that *Ucp1* expression was increased n h*IRX3*-overexpressing brown adipocytes *in vivo*, as was the expression of several other thermogenesis-related genes, including *Pgc-1α*, *Cidea*, and *Dio2*. Whether IRX3 can regulate other genes, including the above genes that form part of the transcription complex that binds to the enhancer region of *Ucp1* to increase thermogenesis, remains to be clarified. Moreover, RNA-seq analysis revealed a marked upregulation in the expression of mitochondria-related (such as *Cox7a1*, *Cox8b*, and *Uqcrb*) and lipid metabolism-related (such as *Scd1* and *Acaa2*) genes under the condition of h*IRX3* overexpression.

In summary, our research revealed that h*IRX3* exerts a regulatory role in energy homeostasis by promoting thermogenesis in brown/beige adipose tissues. Adult humans have active depots of BATs, while the size and activity of BAT depots in obese individuals are largely reduced (33–36). Whether *FTO* variants (including rs1421085) contribute to thermogenesis, and the exact role of *IRX3* in this process, merit further and urgent investigation.

DATA AVAILABILITY STATEMENT

The data presented in the study are deposited in online repositories, accession number can be found in the article/ **Supplementary Material**.

ETHICS STATEMENT

The animal study was reviewed and approved by Animal Care Committee of Shanghai Jiao Tong University School of Medicine.

AUTHOR CONTRIBUTIONS

JW, JH, and RL designed the experiments and supervised the study. ZZ, QW, YH, PL, DL, and MY carried out the animal and molecular experiments. ZZ analyzed the data. ZZ and JW wrote the manuscript. WG and JH contributed to text revision and discussion. All authors contributed to the article and approved the submitted version.

FUNDING

This work was supported by grants from National Key Research and Development Program of China (2018YFC1313802), the National Natural Science Foundation of China (91957124 and 81822009), and the Outstanding Academic Leader Project of Shanghai Municipal Health Commission (2018BR01).

ACKNOWLEDGMENTS

We thank Dr. Chi-Chuang Hui (from the Hospital for Sick Children, and Department of Molecular Genetics, University of Toronto) for his comments and suggestions to this project.

SUPPLEMENTARY MATERIAL

The Supplementary Material for this article can be found online at: https://www.frontiersin.org/articles/10.3389/fendo.2021.634191/full#supplementary-material

Supplementary Figure 1 | Generation of *Ucp1*-Cre^{ERT2}; *Rosa26*^{hIRX3}(iU-IRX3^{ov}) mouse model. **(A)** Final Targeting Vector. Linearization site: *Not*I. **(B)** The sequence of the final targeting vector. **(C)** Overview of the targeting strategy. **(D)** DNA PCR screen of *Ucp1*-Cre^{ERT2} mice. Recombinant allele target band: 413bp; WT allele target band: 139bp. **(E)** Cre mRNA expression in varies tissue (relative to 36B4, normalized to control mice, n=4~6). **(F)** IHC for BAT UCP1 expression in *Rosa26*$^{wild\ type(WT)}$;*Ucp1*-Cre^{ERT2} (control) male mice after 7-days cold exposure. GFP antibody (CST 2956s, 1:200). Photos were taken by LSM710 (Zeiss, 40×). **(G)** Ucp1 protein expression in BAT of control and *Ucp1*-Cre^{ERT2} mice (Het in 3rd lane, HO in 4th lane). **(H)** The mRNA expression levels of hIRX3(top) and mIRX3 (below) in BAT, iWAT, eWAT of male iU-IRX3^{ov} and control mice after CL316,243 and TMX injection (n = 9~10).**(I-K)** The protein expression levels of hIRX3 in BAT **(I)**, iWAT **(J)** and eWAT **(K)** of male iU-IRX3^{ov} and control mice after CL316,243 and TMX injection (n = 3~5).

Supplementary Figure 2 | Growth curve, body weight, physical activities and cold tolerance test in U-IRX3^{ov} mice. **(A, B)** Growth curve of NCD fed U-IRX3^{ov} and control from 4 weeks to 10 weeks. **(A)** Male body weight (n=6~8). **(B)** Female body weigth (n=9~11). **(C-F)** Body weight **(C)**, fat mass percentage **(D)**, lean mass percentage **(E)** and average food intake **(F)** of female U-IRX3^{ov} and Ctrl (n = 9~11, average of 3 individual measurements). **(G-I)** 24-hour (left) and total (right) physical activities on X-axis **(G)**, Y-axis **(H)** and Z-axis **(I)** of male U-IRX3^{ov} and control mice. **(J)** Body temperature changes of male U-IRX3^{ov} and control mice (n=9~10) for the first 6 h in 4°C cold room. **(K)** The mRNA expression levels of hIRX3 (left) and mIRX3 (right) in BAT, iWAT and eWAT of male U-IRX3^{ov} and control mice after cold stimulation (n = 9~10).

Supplementary Figure 3 | Overexpression of hIRX3 from the embryonic stage enhances β3-AR agonist-induced thermogenesis in female U-IRX3^{ov} mice **(A-H).** Tissue mass percentage **(A)**, representative images of HE staining of BAT (top), iWAT (middle) and gWAT (bottom) **(B)** and adipocyte size distribution of iWAT**(C)**, gWAT **(D)** of 10-week-old female U-IRX3^{ov} and control mice after 1-h CL 316,243 (1.5 mg/kg body weight) injection, the mRNA expression levels of thermogenesis-related genes (n = 9~11) **(E)**, the protein levels of Ucp1 and Pgc-1α in iWAT (n = 3) **(F)**, the mRNA expression levels of thermogenesis-related genes (n = 6~8) **(G)**, and the protein levels of Ucp1 and Pgc-1α in gWAT (n = 3) **(H)**. Expression level of hIRX3 mRNA **(I)** and mIRX3 mRNA **(J)** in SVF of male U-IRX3^{ov} mice BAT(n=6) and iWAT n=(4). Scale bars, 100 μm. Data are shown as mean ± SEM. *P < 0.05, **P < 0.01, ***P < 0.001.

Supplementary Table 1 | Mouse and human qPCR primers sequences.

Supplementary Table 2 | All down regulated genes in RNA-sequencing analysis in **Figure 5**.

Supplementary Table 3 | All up regulated genes in RNA-sequencing analysis **Figure 5**.

REFERENCES

1. Scarlett K, Pattabiraman V, Barnett P, Liu D, Anderson LM. The proangiogenic effect of iroquois homeobox transcription factor Irx3 in human microvascular endothelial cells. *J Biol Chem* (2015) 290:6303–15. doi: 10.1074/jbc.M114.601146
2. Holmquist Mengelbier L, Lindell-Munther S, Yasui H, Jansson C, Esfandyari J, Karlsson J, et al. The Iroquois homeobox proteins IRX3 and IRX5 have distinct roles in Wilms tumour development and human nephrogenesis. *J Pathol* (2019) 247:86–98. doi: 10.1002/path.5171
3. Shabalina IG, Petrovic N, deJong JMA, Kalinovich AV, Cannon B, Nedergaard J. UCP1 in Brite/Beige adipose tissue mitochondria is functionally thermogenic. *Cell Rep* (2013) 5:1196–203. doi: 10.1016/j.celrep.2013.10.044
4. Wang W, Seale P. Control of brown and beige fat development. *Nat Rev Mol Cell Biol* (2016) 17:691–702. doi: 10.1038/nrm.2016.96
5. Wang J, Liu R, Wang F, Hong J, Li X, Chen M, et al. Ablation of LGR4 Promotes Energy Expenditure by Driving White-To-Brown Fat Switch. *Nat Cell Biol* (2013) 15:1455–63. doi: 10.1038/ncb2867
6. Scuteri A, Sanna S, Chen WM, Uda M, Albai G, Strait J, et al. Genome-wide association scan shows genetic variants in the FTO gene are associated with obesity-related traits. *PloS Genet* (2007) 3:1200–10. doi: 10.1371/journal.pgen.0030115
7. Liu C, Mou S, Cai Y. FTO gene variant and risk of overweight and obesity among children and adolescents: a systematic review and meta-analysis. *PloS One* (2013) 8:e82133. doi: 10.1371/journal.pone.0082133
8. Dina C, Meyre D, Gallina S, Durand E, Körner A, Jacobson P, et al. Variation in FTO contributes to childhood obesity and severe adult obesity. *Nat Genet* (2007) 39:724–6. doi: 10.1038/ng2048
9. Claussnitzer M, Dankel SN, Kim K-H, Quon G, Meuleman W, Haugen C, et al. FTO obesity variant circuitry and adipocyte browning in humans. *N Engl J Med* (2015) 373:895–907. doi: 10.1056/NEJMoa1502214
10. Stratigopoulos G, Burnett LC, Rausch R, Gill R, Penn DB, Skowronski AA, et al. Hypomorphism of Fto and Rpgrip1l causes obesity in mice. *J Clin Invest* (2016) 126:1897–910. doi: 10.1172/JCI85526
11. Hunt LE, Noyvert B, Bhaw-Rosun L, Sesay AK, Paternoster L, Nohr EA, et al. Complete re-sequencing of a 2Mb topological domain encompassing the FTO/IRXB genes identifies a novel obesity-associated region upstream of IRX5. *Genome Med* (2015) 7:1–14. doi: 10.1186/s13073-015-0250-3
12. Smemo S, Tena JJ, Kim KH, Gamazon ER, Sakabe NJ, Gómez-Marín C, et al. Obesity-associated variants within FTO form long-range functional connections with IRX3. *Nature* (2014) 507:371–5. doi: 10.1038/nature13138
13. Zhang SS, Kim KH, Rosen A, Smyth JW, Sakuma R, Delgado-Olguiń P, et al. Iroquois homeobox gene 3 establishes fast conduction in the cardiac His-Purkinje network. *Proc Natl Acad Sci USA* (2011) 108:13576–81. doi: 10.1073/pnas.1106911108
14. Claussnitzer M, Dankel SN, Kim KH, Quon G, Meuleman W, Haugen C, et al. FTO obesity variant circuitry and adipocyte browning in humans. *N Engl J Med* (2015) 373:895–907. doi: 10.1056/NEJMoa1502214
15. de Araujo TM, Razolli DS, Correa-da-Silva F, de Lima-Junior JC, Gaspar RS, Sidarta-Oliveira D, et al. The partial inhibition of hypothalamic IRX3 exacerbates obesity. *EBioMedicine* (2019) 39:448–60. doi: 10.1016/j.ebiom.2018.11.048
16. Zou Y, Lu P, Shi J, Liu W, Yang M, Zhao S, et al. IRX3 Promotes the Browning of White Adipocytes and Its Rare Variants are Associated with Human Obesity Risk. *EBioMedicine* (2017) 24:64–75. doi: 10.1016/j.ebiom.2017.09.010
17. Bjune JI, Dyer L, Røsland GV, Tronstad KJ, Njølstad PR, Sagen JV, et al. The homeobox factor Irx3 maintains adipogenic identity. *Metabolism* (2020) 103:154014. doi: 10.1016/j.metabol.2019.154014
18. Tschöp MH, Speakman JR, Arch JRS, Auwerx J, Brüning JC, Chan L, et al. A guide to analysis of mouse energy metabolism. *Nat Methods* (2012) 9:57–63. doi: 10.1038/nmeth.1806
19. Subramaniana A, Tamayoa P, Moothaa VK, Mukherjeed S, Eberta BL, Gillettea MA, et al. Mesirova k aBroad. Gene set enrichment analysis: A knowledge-based approach for interpreting genome-wide expression profiles. *Proc Natl Acad Sci U.S.A.* (2005) 102:15545–50. doi: 10.3969/j.issn.0372-2112.2018.08.016
20. Symonds ME, Mostyn A, Pearce S, Budge H, Stephenson T. Endocrine and nutritional regulation of fetal adipose tissue development. *J Endocrinol* (2003) 179:293–9. doi: 10.1677/joe.0.1790293
21. Sun Y, Wang R, Zhao S, Li W, Liu W, Tang L, et al. FGF9 inhibits browning program of white adipocytes and associates with human obesity. *J Mol Endocrinol* (2019) 62:79–90. doi: 10.1530/JME-18-0151
22. Keipert S, Kutschke M, Ost M, Schwarzmayr T, van Schothorst EM, Lamp D, et al. Long-Term Cold Adaptation Does Not Require FGF21 or UCP1. *Cell Metab* (2017) 26:437–46. doi: 10.1016/j.cmet.2017.07.016
23. Zhao Y, Pan J, Wang Y, Zou Y, Guo L, Qian S, et al. Stimulation of histamine H4 receptor participates in cold-induced browning of subcutaneous white adipose tissue. *Am J Physiol Metab* (2019) 317(6):E1158–71. doi: 10.1152/ajpendo.00131.2019
24. Babenko V, Babenko R, Gamieldien J, Markel A. FTO haplotyping underlines high obesity risk for European populations. *BMC Med Genomics* (2019) 12:109–15. doi: 10.1186/s12920-019-0491-x
25. Peters U, North KE, Sethupathy P, Buyske S, Haessler J, Jiao S, et al. A systematic mapping approach of 16q12.2/FTO and BMI in more than 20,000 African Americans narrows in on the underlying functional variation: results from the Population Architecture using Genomics and Epidemiology (PAGE) study. *PloS Genet* (2013) 9:e1003171. doi: 10.1371/journal.pgen.1003171
26. Couto Alves A, De Silva NMG, Karhunen V, Sovio U, Das S, Taal HR, et al. GWAS on longitudinal growth traits reveals different genetic factors influencing infant, child, and adult BMI. *Sci Adv* (2019) 5:eaaw3095. doi: 10.1126/sciadv.aaw3095
27. Inagaki T. Regulations of Adipocyte Phenotype and Obesity by IRX3. Positive or Negative? *EBioMedicine* (2017) 24:7–8. doi: 10.1016/j.ebiom.2017.09.032
28. Tung YCL, Yeo GSH, O'Rahilly S, Coll AP. Obesity and FTO: Changing focus at a complex locus. *Cell Metab* (2014) 20:710–8. doi: 10.1016/j.cmet.2014.09.010
29. Cedernaes J, Benedict C. Human obesity: FTO, IRX3, or both? *Mol Metab* (2014) 3:505–6. doi: 10.1016/j.molmet.2014.05.003
30. Xue B, Rim JS, Hogan JC, Coulter AA, Koza RA, Kozak LP. Genetic variability affects the development of brown adipocytes in white fat but not in interscapular brown fat. *J Lipid Res* (2007) 48:41–51. doi: 10.1194/jlr.M600287-JLR200
31. Long JZ, Svensson KJ, Tsai L, Zeng X, Roh HC, Kong X, et al. Ribosomal Profiling Provides Evidence for a Smooth Muscle- Like Origin of Beige Adipocytes. *Cell Metab* (2014) 19:810–20. doi: 10.1016/j.cmet.2014.03.025.Ribosomal
32. Koizumi A, Sasano T, Kimura W, Miyamoto Y, Aiba T, Ishikawa T, et al. Genetic defects in a His-Purkinje system transcription factor, IRX3, cause lethal cardiac arrhythmias. *Eur Heart J* (2016) 37:1469–75. doi: 10.1093/eurheartj/ehv449
33. Somm E, Henry H, Bruce SJ, Aeby S, Rosikiewicz M, Sykiotis GP, et al. β-Klotho deficiency protects against obesity through a crosstalk between liver, microbiota, and brown adipose tissue. *JCI Insight* (2017) 2. doi: 10.1172/jci.insight.91809
34. Riis-Vestergaard MJ, Richelsen B, Bruun JM, Li W, Hansen JB, Pedersen SB. Beta-1 and not Beta-3 adrenergic receptors may be the primary regulator of human brown adipocyte metabolism. *J Clin Endocrinol Metab* (2020) 105:E994–E1005. doi: 10.1210/clinem/dgz298
35. Chevalier C, Stojanović O, Colin DJ, Suarez-Zamorano N, Tarallo V, Veyrat-Durebex C, et al. Gut Microbiota Orchestrates Energy Homeostasis during Cold. *Cell* (2015) 163:1360–74. doi: 10.1016/j.cell.2015.11.004
36. Worthmann A, John C, Rühlemann MC, Baguhl M, Heinsen FA, Schaltenberg N, et al. Cold-induced conversion of cholesterol to bile acids in mice shapes the gut microbiome and promotes adaptive thermogenesis. *Nat Med* (2017) 23:839–49. doi: 10.1038/nm.4357

Conflict of Interest: The authors declare that the research was conducted in the absence of any commercial or financial relationships that could be construed as a potential conflict of interest.

frontiers in Endocrinology

SYSTEMATIC REVIEW
published: 12 March 2021
doi: 10.3389/fendo.2021.599134

Beige Adipose Tissue Identification and Marker Specificity—Overview

Anna-Claire Pilkington[1], *Henry A. Paz*[1,2] *and Umesh D. Wankhade*[1,2*]

[1] *Arkansas Children's Nutrition Center, University of Arkansas for Medical Sciences, Little Rock, AR, United States,*
[2] *Department of Pediatrics, College of Medicine, University of Arkansas for Medical Sciences, Little Rock, AR, United States*

Adipose tissue (AT) is classified based on its location, physiological and functional characteristics. Although there is a clear demarcation of anatomical and molecular features specific to white (WAT) and brown adipose tissue (BAT), the factors that uniquely differentiate beige AT (BeAT) remain to be fully elaborated. The ubiquitous presence of different types of AT and the inability to differentiate brown and beige adipocytes because of similar appearance present a challenge when classifying them one way or another. Here we will provide an overview of the latest advances in BeAT, BAT, and WAT identification based on transcript markers described in the literature. The review paper will highlight some of the difficulties these markers pose and will offer new perspectives on possible transcript-specific identification of BeAT. We hope that this will advance the understanding of the biology of different ATs. In addition, concrete strategies to distinguish different types of AT may be relevant to track the efficacy and mechanisms around interventions aimed to improve metabolic health and thwart excessive weight gain.

Keywords: beige adipose tissue, brown adipose tissue, white adipose tissue, obesity, thermogenesis

OPEN ACCESS

Edited by:
Xinran Ma,
East China Normal University, China

Reviewed by:
Maoqing Ye,
Huadong Hospital Affiliated to Fudan University, Shanghai, China
Cheng-Chao Ruan,
Shanghai Jiao Tong University, China
Wanzhu Jin,
Chinese Academy of Sciences (CAS), China

***Correspondence:**
Umesh D. Wankhade
udwankhade@uams.edu

Specialty section:
This article was submitted to Cellular Endocrinology, a section of the journal Frontiers in Endocrinology

Received: *26 August 2020*
Accepted: *04 January 2021*
Published: *12 March 2021*

Citation:
Pilkington A-C, Paz HA and Wankhade UD (2021) Beige Adipose Tissue Identification and Marker Specificity—Overview. Front. Endocrinol. 12:599134. doi: 10.3389/fendo.2021.599134

INTRODUCTION

Adipose tissue (AT) is an integral component of increased weight gain and has garnered significant attention in the scientific community over the last few decades. White and brown ATs (WAT and BAT), being the two main types of AT in mammals, are the focus of most scientific studies. WAT stores excess energy as triglycerides, and BAT specializes in the dissipation of energy through the production of heat. In the last decade, a third and novel type of AT came to light. Because of appearance and location, these adipocytes have been deemed brite/beige adipocytes (BeATs). BeATs are brown-like adipocytes that reside in WAT depots. Chemical stimulation with β3-adrenergic agonists (CL316,243) or cold exposure is known to promote the development of BeAT.

The morphological, biochemical, and physiological characteristics of WAT and BAT are well described in the literature. White adipocytes are characterized by the presence of single lipid droplet consisting of triglycerides occupying 90% of the cell space. Mitochondria in white adipocytes are thin, elongated, and sparse in numbers. WAT is responsible for secretion of numerous hormones, growth factors, enzymes, cytokines, complement factors, and matrix proteins. These secretory

products are responsible for the regulation of healthy adipose mass maintenance, food intake, energy expenditure, metabolism, immunity, and blood pressure homeostasis (1). In contrast, brown adipocytes contain triglycerides in smaller and multiple vacuoles. BAT is highly vascularized and contains a large number of mitochondria that are large, spherical, and packed with laminar cristae. The brown color of BAT is attributable to its high mitochondrial density and vascularization. BAT has been reported to promote a 10–20% increase in energy expenditure when compared to basal metabolic rate with an estimated contribution of 100 kcal/day (2). Because of its relatively high tissue-specific metabolic rate, BAT demands increased oxygen and a denser neural supply when compared to WAT. A key component that differentiates BAT from WAT is BAT's physiological function of thermogenesis, which is aided mainly by the unique protein, uncoupling protein 1 (Ucp1) present in densely packed mitochondria in BAT. Stimulation by norepinephrine triggers a signaling cascade that activates Ucp1, which then uncouples aerobic respiration by dissipating the inter-membrane proton-motive force, creating a futile cycling of ions, thus generating a heat instead of ATPs (3). BeATs display characteristics of both brown and white fat cells and typically develop within subcutaneous WAT from a distinct subset of preadipocytes (4) or *via* the trans-differentiation of existing white adipocytes (5, 6). Beige adipocytes were originally observed to arise in response to cold exposure in rodents (7–9); however, studies have since identified that diet (10), exercise (11), pre-and probiotics (12), pharmaceutical agents, numerous plant-based bioactives, and even adipokines (13, 14), can also induce "beigeing" or "browning" of WAT. These regulators of BeAT are discussed in greater detail below.

BAT mass is very scarce in most adult humans (less than 1% of total body weight). Under conditions such as cold exposure, BAT can be activated, but even under these conditions, the amount of BAT remains small relative to WAT. Nevertheless, the BAT has the potential to significantly impact whole-body glucose homeostasis. This makes it appealing to consider if beige adipocytes can also play an important role in overall metabolism, even if BeAT abundance is small relative to WAT.

As alluded above, browning has been shown to occur with a variety of different stimulants. Diet has the potential to play a role in the beigeing process as different compounds, including capsinoids, polyphenolic compounds, green tea (specifically catechins), and fish oil, have been shown as promising but still need to undergo more extensive investigation (7). Certain plant bioactives, such as curcumin, may also contribute to beigeing (15). Exercise has been shown to promote beigeing by increasing the number of mitochondria in WAT and activating brown adipocyte genes, specifically Ucp1 (8). This phenomenon has been studied extensively in mice, where exercise consists of the mouse running on a treadmill. The microbiota has been of a growing interest over the years, and with its many implications into human health, it is not surprising that it may play a role in the browning process. Boosting the microbiota with pre- and probiotics, the host has demonstrated increased thermogenic capacity and therefore, an increase in energy expenditure of both BAT and subcutaneous WAT, indicative of browning assisted improved metabolism (9). Multiple pharmacological approaches have been studied to determine their efficacy in the browning process (16). These include Ppar agonists, SIRT-1, β-adrenergic receptor stimulation, thyroid hormone, Fgf21, and irisin (17). Each of these methods or compounds have been studied mainly in a mouse model so further research is needed to confirm the effectiveness of each strategy in the browning of human WAT and its clinical implications.

BAT is mostly located in neck and subscapular region whereas WAT is spread out in several parts of the body. Epicardial fat or fat layer underlying major blood vessels in the thoracic region tends to express BAT specific genes such Ucp1, Pgc1a, Prdm16, *etc* at high level giving it beige/bat like appearance (18–20). Beige adipocytes can be recruited or induced in WAT depots, leading to difficulties when trying to identify the exact type of AT that is present. In an attempt to overcome this challenge, multiple studies have been conducted to identify specific markers that allow for the characterization of the tissue present. Although we have come far in identifying molecular underpinnings of beige adipocyte formation in the last decade, the transcript marker identity of beige cells is still under question. Because of its similarity in appearance, location, and dubiousness of its origin, there are still no concrete measures to distinguish beige cells from classical brown fat cells.

Decades of research has provided us with a good outline to identify different adipose cell types. As lineage-tracing studies are impossible to perform in humans, there is a need for marker genes that allow distinction to be made between different classes of (human) adipocytes and adipose tissues. Such markers can thus be obtained only from animal studies and can be used to influence the development of strategies to promote recruitment of the tissues and activation of energy expenditure. This article therefore has two aims. The first is to provide an overview of transcript markers of identification laid out in literature to identify BAT, WAT, and BeAT. The second is to highlight some of the difficulties these markers pose and offer an opinion on possible transcript-specific identification of BeAT.

ORIGINS OF ADIPOSE TISSUES

In mammals, AT forms *in utero*, in the peripartum period, and throughout life. New adipocytes are generated continually in healthy and disease stages as physiological need arises (21). AT is composed of adipose stem cells that give rise to new adipocytes and immune cells. AT is located in several parts of the body and gets its name based on its location—in rodents, examples include inguinal, interscapular, perigonadal, retroperitoneal, and mesenteric depots. These various depots develop at specific and distinguishable pre- and postnatal times, and they have discrete, distinct morphologies (22, 23). While there is a long-standing belief that WAT is derived from the mesoderm germ layer, some studies indicate that adipose depots originate from neural crest cells which derived from the ectoderm (24). And in

mice, recent study had indicated that neural crest cells differentiate into both white and brown adipocytes (25). Multiple intrinsic factors play key roles in WAT formation, with distinct developmental cues and regulators determining adipose maturation and subsequent location. Pparγ and Cebpα have been deemed as key genetic components of WAT development during embryonic stages (26).

Brown adipocytes are derived from the dermomyotome, an engrailed 1 (EN1) (27) and myogenic factor 5 (myf5) positive cell lineage (28), which is the same lineage as that of myocytes. During the neonatal period in humans, BAT is commonly located in the dorsal region between the scapulae (29). In rodents such as rats and mice, BAT is located primarily in the back region. Despite differences in its reported origin, there are recent studies which demonstrate that a subset of white adipocytes also arises from myf5-positive cells (30), sharing this commonality with brown progenitor cells. Platelet-derived growth factor receptor alpha (PDGFRα)-positive lineage traces to BAT and WAT, and PDGFRα is present in proliferating brown and white adipose progenitors (31). Recently Oguri et al. reported expression of Pdgfrα, Sca1, and Cd81 on the surface of beige adipocyte progenitors (32). It is also known that there is some overlap in the transcriptional machinery utilized in the development of both WAT and BAT.

Within the last two decades, the discovery of and research focusing on beige adipocytes has taken off. In the early 2000s, Himms-Hagen et al. demonstrated the existence of brown-like adipocytes in WAT of rats treated with β-adrenergic agonist CL316,243 (5). Regardless of the morphological similarities between beige adipocytes and BAT, beige adipocytes originate from distinct precursor populations (4, 28). Beige adipocytes mostly emerge from a myf5 negative cell lineage, one that is similar to that of WAT. Specific groups of beige adipocytes seem to emerge from a smooth muscle-like precursor, driven by Myh11 (33). The variety of lineages for beige adipocytes leads to the conclusion that they stem from a heterogeneous population of cells. Beige cell recruitment and coincident expression of Ucp1 are dependent on external stimuli such as cold or other inducers such as β-adrenergic agonists or PPARγ activators (4, 34). By contrast, brown adipocytes express relatively high amounts of Ucp1 without stimulation. Classically, two external stimuli have been used to trigger a browning response: cold temperatures and CL316,243 [β3-adrenergic receptor (*Adrb3*) agonists]. Although these two treatments have known to be stronger triggers of beigeing and have been used interchangeably; however, whether these two stimuli may induce beigeing differently at the cellular and molecular levels remains unclear. Jiang et al. report that cold-induced beige adipocyte formation requires *Adrb*1, not activation. *Adrb*1 activation stimulates WAT resident perivascular (*Acta2*+) cells to form cold-induced beige adipocytes (35). In contrast, *Adrb3* activation CL316,243 stimulates mature white adipocytes to convert into beige adipocytes. The authors went on demonstrating it using mature adipocyte-specific *Prdm16* deletion strategies, which showed that adipocytes are required and are predominant source to generate *Adrb3*-induced, but not cold-induced, beige adipocytes (35). Stimulated beige adipocytes can undergo UCP1-mediated uncoupled respiration (4, 33, 36), but the relative magnitude per cell *versus* brown adipocytes remains to be established.

SELECTIVE MARKERS OF ADIPOSE TISSUES

White Adipose Tissue Markers

Being the largest AT in mass and having a distinct white/pink color makes it somewhat easy to identify WAT with the naked eye. Several marker genes have been classified to specifically identify WAT, including Ob (leptin), Hoxc8, and Hoxc9 (37). At the transcript level, leptin and adiponectin are other commonly used markers for WAT. Solute carrier family 7 member 10 (SLC7a10/Asc-1 neutral amino acid transporter, y+ system) is another more recently identified marker that was determined to be highly expressed in C57BL/6male mouse WAT while having low levels in BAT. It has been demonstrated to increase as mice gain white adipose mass, further supporting Asc-1 as a WAT marker (38, 39). In the same study conducted by Ussar et. al., Asc-1 had levels of expression similar to leptin. Garcia et al. observed higher expression of ASC-1 in mouse white adipocytes compared to beige adipocytes (40). This study also identified two other markers that have been associated with WAT, Serpina3k and Wdnm1-like (40). de Jong et al. analyzed Asc1 as a cell surface marker and, in sync with the other mentioned studies, found that its expression levels are higher in white than in brite and brown fat cells. However, they do acknowledge that complete exclusion of Asc1 being expressed in brite cells cannot be made based on their data alone (39).

Multiple studies have looked at anatomical groupings of AT and their subsequent markers. In subcutaneous white adipose sites, Ob and Hoxc9, along with Mpzl2, Ebf3, and Fbox31, were found to be the most prevalent genetic markers (41). In a study by Walden et al., specific WAT depot sites were analyzed and compared to the BAT and BeAT depot sites. They concluded that the Tcf21 gene had the greatest association with WAT (42). de Jong et al. further support the notion that Tcf21 mRNA expression levels are indicative of white adipocytes in both cell culture and tissue. However, when looking at adipose depots with the aim of identification based on validated markers, Tcf21 was expressed in epididymal WAT, as expected, but also in brite depots. This result is logical as BeAT is a mixture of WAT and BAT (39).

Brown Adipose Tissue Markers

As a greater understanding of beige AT is gained, a significant overlap in the markers for BAT and beige adipocytes is seen, making it important to identify those that are unique to each type. The overlap is expected due to the physiological similarities between brown and beige adipocytes, but there are also differences, likely due to their divergent developmental patterns.

Multiple studies have identified LHX8 and ZIC1 as strong markers of BAT (41–44). These studies demonstrated that these markers serve well as indicators of brown, and not BeAT. Further

evidence for the use of Zic1 as a BAT marker was found in an extensive study performed by de Jong et al. where all previously identified human adipose tissue markers were evaluated in cell lines and tissue. Zic1 mRNA was detectable only in interscapular BAT, both in tissue samples and cell cultures (39). However, when analyzing single adipose depots in a mouse model, only three of the five traditional BAT depots expressed Zic1. With further analysis, it appeared that the positional expression pattern of the gene was the explanation for this phenomenon, indicating that Zic1 expression is restricted to anterior depots. The absence seen in the two most posterior-like brown fat depots is indicative of them having different origins than classical BAT (39). This study gives evidence of Zic1 being a brown fat marker while also giving insight into the importance of understanding developmental origins. While this study provided evidence complementing other studies on the role of Zic1, it found conflicting evidence regarding Lhx8 as solely a BAT marker. The levels of Lhx8 mRNA were absent in WAT but found in nearly equal levels in beige adipocytes and BAT, indicating that Lhx8 mRNA may be a marker for either beige or BAT, not BAT alone (39). Eva1 (Mpzl2) is another genetic marker that has been proposed as a candidate for identifying BAT. Seale et al. determined that with Prdm16 stimulation, mRNA expression levels of Eva1 were significantly increased in BAT *versus* WAT (45). Wu et al. looked further into Eva1 by comparing expression levels in WAT, BAT, and beige adipocytes from mice and found a significantly higher expression in interscapular brown fat depots (4). In contrast to these studies, de Jong et al. found little to no difference in Eva1 mRNA levels between WAT, BAT, and beige adipocytes while also observing an increase in expression in all three tissues with cold exposure, indicating the possibility that Eva1 plays a role in functional adaptability to cold temperatures but not as a strong marker of BAT (39). Prex1, a possible BAT marker, is known for its role as a positive regulator of Ucp1-gene expression. Xue et al. found that Prex1 is present in brown adipocyte pre-cursor cells, indicating its importance in BAT development (46). There is little research that cites increased Prex1 expression levels in beige adipocytes so it is currently considered a unique marker for BAT.

As previously mentioned, brown and beige adipocytes arise from separate cell lines and are subsequently activated by different signals, so differentiating between the two tissue types can be made easier *via* their developmental histories. Ebf2 and BMP7 are two proteins that play pivotal roles in classical BAT development, with their expression being indicative of BAT presence (43). With increased awareness of BAT-specific markers along with the differences in developmental patterns, BAT and beige can be differentiated for the purposes of further research and the possibility of their metabolic implications.

Beige Adipose Tissue Markers

Identical appearance of brown and beige adipocytes makes it difficult to distinguish them one from another. In addition, similarities in physiological characteristics and marker expression make it even trickier to identify beige adipocytes. However, decade-long research of beige adipocyte development has provided some putative markers. The extensive research has allowed for the determination of markers overlapping between all three adipose tissues, along with the overlap seen between two of the types and of markers that seem to be unique to beige adipocytes. This overlap is outlined in the Venn diagram shown above with multiple of the genes of interest being discussed in this review (**Figure 1**).

Proposed Beige Adipose Tissue Markers

Tmem26, Tbx1, CD137, and CITED1: Several studies have shown that CD137, Tmem26, and Tbx1 could be used as beige adipocyte markers. These mRNA transcripts and subsequent proteins are expressed at significantly higher levels in the inguinal fat depot compared to the interscapular brown fat upon β-adrenergic stimulation or cold exposure (4). Upon differentiation, the cells containing higher levels of these proteins also expressed higher levels of Ucp1. Cd137 and Tmem26 were also identified as cell-surface markers for native beige precursors, allowing for the isolation of these cells from fat tissues (47). Cypess et al. identified Cd137 and Tmem26 to be the best markers for beige adipocyte identification after analysis of different AT groupings (41). Liang et al. further support these conclusions as an increase in Cd137 expression was recorded in 3T3-L1 cells differentiated into beige adipocytes (48). de Jong et al. suggest that Cd137 may be able to serve as a beige adipose tissue marker at the tissue level, but not at the cellular level. However, the data collected also shows that low expression levels of Cd137 alone cannot definitively exclude a tissue from being deemed beige (39). Tbx1 and Tmem26 displayed similar expression patterns to Cd137 in the de Jong et al. study. Both genes were expressed at significantly higher levels in BeAT compared to BAT but with much smaller differences between BeAT and WAT. It is possible that Tbx1 and Tmem26 may serve as beige markers in tissues but not in cell culture (39). When analyzing Cd137, Tbx1, and Tmem26 in single adipose depots, they were found to mark brite and WAT depots, indicating that there can be brite, but non-thermogenic depots. de Jong et al. presented these markers, plus Epsti1, to be necessary for a true brite tissue (39). Epsti1 is of note here—it had been previously suggested as a brown marker but in this study was found to be at much higher levels in BeAT than BAT, leading to its consideration as a beige adipose tissue marker (39).

In contrast to the evidence presented above, in the study conducted by Ussar et al., no change in expression of either Tbx or Tmem26 was found in mice exposed to chronic cold conditions or β3-adrenergic stimulation (38). Garcia et al. further solidified these findings as similar expression levels of Tmem26, Tbx1, and CD137 in the beige adipocytes and white adipocytes of mice exposed to cold temperatures were observed (40). When the cells were exposed to adrenergic stimulation, CD137 increased only in white adipocytes and CITED1 increased in WAT to such a degree that it was no longer distinguishable between beige and white cell types. There is also evidence that CD137 is not only an unreliable marker of beige AT but that it actually slows down the browning process and prevents the spread of beige adipocytes (49). de Jong et al.

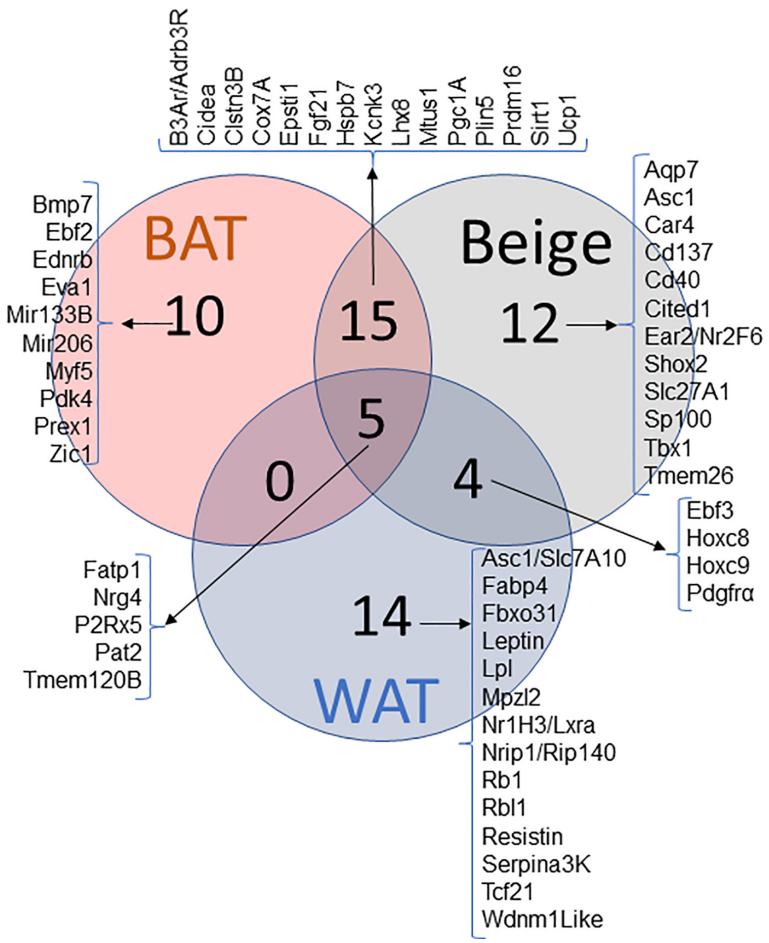

FIGURE 1 | Venn diagram of WAT, BAT and Beige markers and their pattern of expression. Genes reported in literature as a marker for WAT, BAT and BeAT. Venn diagram represents the commonality and uniqueness of certain transcripts.

found Cited1 mRNA to be expressed in extremely low levels in all three depots, excluding it as a marker of beige adipose tissue (39). These five markers need to be further studied to work out the discrepancies seen and to determine the relevance of these genes in accurately identifying beige AT.

Overlapping Markers

Markers found in WAT, BAT and BeAT

Pat2 and P2rx5: Ussar et al. identified Pat2 and P2rx5 as markers of beige and brown fat (38). The study induced the browning of WAT by exposing mice to chronic cold conditions and/or β3-adrenergic stimulation. P2rx5 expression increased both in BAT and subcutaneous WAT after both stimuli, while Pat2 had no change with cold but demonstrated a significant increase in subcutaneous WAT with β3-adrenergic stimulation. These mixed results led to the conclusion that each protein may be useful in marking brown or beige adipocyte populations, as they increased in the WAT with a browning stimulus (38). Consistent with previous results, Garcia et al. showed increased P2rx5 expression in beige adipocytes compared to white adipocytes upon differentiation *via* rosiglitazone, whereas adrenergic stimulation yielded a decrease in P2rx5 expression in both beige adipose cells and white adipose cells. Pat2, on the other hand, was decreased only in white adipocytes. Finally, with cold exposure, WAT showed an increase in both P2rx5 and Pat2 (40).

The results of both studies indicate that different stimulants of WAT browning, *i.e.* rosiglitazone, chronic cold or β3-adrenergic stimulation, can induce the expression of these different markers. The findings regarding Pat2 and P2rx5, while useful, are also vague and will need to be further studied to determine if they have a role in specific ATs or serve as a more general adipocyte marker. Both studies demonstrate Pat2 and P2rx5 expression in BAT and BeAT, along with data supporting the markers presence in WAT.

Nrg4: Nrg4 has been linked to BAT activity and the browning process. A recent study conducted by Comas et al. explored the expression pattern of Nrg4 as a marker of BAT or beige AT in humans. The putative beige adipocyte marker Tmem26 showed a

strong positive correlation with Nrg4 across individuals. While there are some conflicting data in regard to Nrg4's role in thermogenesis, the observations demonstrated that Nrg4 could be a possible beige AT marker and that further studies should be conducted to confirm. Another study conducted by Christian et al. categorizes Nrg4 as a cold-induced BAT gene. They found that while BAT did have the highest levels of Nrg4 expression, subcutaneous WAT also had significant increases in Nrg4 transcript with cold exposure (50). These results suggest that Nrg4 might play a role in the browning/beigeing process. Further research needs to be done to confirm the validity of Nrg4 as a marker of a specific type of AT.

Fgf21: Fgf21 is another putative beige AT marker and inducer that appears to be of importance. Garcia et al. suggest that Fgf21 matches the criteria necessary to be deemed as a possible beige adipocyte marker because of its inducible nature (compared to WAT) upon treatment with rosiglitazone (40). With adrenergic stimulation, Fgf21 displayed an eight-fold greater increase in mouse beige adipose cells compared to the change seen in white adipocytes. Fgf21 was expressed in high levels in the SVF cells of the mice at room temperature and then increased further when exposed to chronic cold temperatures. Findings from this study suggest Fgf21 is involved in the dynamics of the beigeing process because it is a factor that induces beige cell recruitment in WAT while also stimulating trans-differentiation of existing adipocytes to beige cells (51).

When comparing the expression of Fgf21 in WAT, BAT, and beige adipocytes, it is higher in beige and brown cells compared to WAT, indicating Fgf21 as a hormone present during browning but that it may not be indicative of beige adipocytes specifically (52). Soundarrajan et al. studied the correlation between active BAT and various markers, including Fgf21 (53). For this study, BAT was activated when the male human subjects were exposed to cold temperatures. A positive correlation was seen between the secretion of Fgf21 and BAT activity, determined using PET/CT scans, signifying that Fgf21 may play a positive role in the physiological response to cold exposure in BAT. Additional studies have demonstrated that Fgf21 and the molecular pathway by which it could be functioning in have the capacity of inducing beige adipocyte formation. As an endocrine regulator secreted from adipocytes, Fgf21 can increase the body's energy expenditure *via* paracrine signaling (54). Endocrine-like characteristics of Fgf21 contribute to the activation of Ucp1 and subsequently the thermogenic potential of brown and beige adipocytes (13). These properties are consistent with a connection between Fgf21 and beige function. The results also demonstrate that Fgf21 is not exclusively presented in beige adipocytes and may not serve as a marker for distinguishing between BAT and beige AT.

Markers Found in BAT and BeAT

There have been findings that human classical BAT is similar to mouse BeAT, leading to ambiguity in regard to identity. However, if the mouse is housed at thermoneutral conditions (30°C), such as those of humans, mouse BAT exhibits characteristics equivalent to human BAT. The seemingly small number of differential markers between BAT and BeAT can be compensated for by understanding their major differences (29). In an elegant study, Wu et al. observed that transcript signature of immortalized Ucp1+ cell line derived from inguinal AT from mouse was more similar to the expression pattern of transcripts expressed in human BAT (4). These findings were consistent with a study by Sharp et al. (39) suggesting that beige/brite cells that occur in inguinal WAT have more resemblance to classical human BAT.

CIDEA and Ucp1: Because of the physiological similarities between BAT and beige adipocytes, it is expected that they would have overlapping expression of CIDEA and Ucp1, two transcripts associated with the thermogenic responses of BAT. It has been proposed that these gene transcripts can be used to evaluate beigeing in mouse WAT (40). Mouse WAT exposed to chronic cold temperatures showed a significant increase in expression of both gene transcripts, with Ucp1 showing the most substantial increase. The gene transcripts do not act specifically as BAT *vs*. BeAT markers but are still valuable in terms of identifying and possibly inducing the beigeing of WAT. With the correlation seen in the increase of both Ucp1 and Cidea, it is also possible that Cidea plays a role in the thermogenicity of BeAT and BAT (39).

Ucp1 has been the focus of additional studies. It is well-known that Ucp1 is an indicator of BAT and therefore, the role that Ucp1 has in beige AT is a topic of interest. Wu et al. found that before inducing adipocyte differentiation, inguinal-derived cells from both beige and white adipose depots had low expression of Ucp1 transcript. After differentiation, with either cAMP or β-adrenergic agonist stimulation, the beige adipocytes had significantly increased Ucp1 expression compared to white adipocytes (4). In some cases, the Ucp1 mRNA levels in beige adipocytes were actually greater than seen in brown adipocytes. In response to high fat diet feeding Ucp1 expression tends to go up in BAT and Beige and diminishes in WAT (55). Another condition, aging is known to reduce the amount of BAT and consequently reduced Ucp1 expression (56). Thus, Ucp1 plays an important role in identifying beige AT. It may be possible that these gene transcripts will serve as better identifiers of beige AT *in vivo* compared to other proposed "beige-specific" markers.

Pgc1α: Pgc1α is known to be key in the regulation of a cascade of genes involved with energy metabolism in AT. Pgc1α serves as a master regulator of the thermogenic program in both BAT and beige ATs (57, 58). Mice lacking Pgc1α could still produce brown fat, but the thermogenic effects were diminished, indicating the indispensable role that Pgc1α plays in the physiological roles of BAT. Tiraby et al. demonstrated that when WAT has activated Pgc1α, as induced by rosiglitazone treatment, the WAT began to show characteristics of BAT, indicative of the browning process and the recruitment/trans-differentiating of beige adipocytes (59). Although several studies implicate Pgc1α as an important player in browning/beigeing, there is no distinction in the expression pattern in beige *versus* brown fat, making it a non-specific marker for BeAT identification.

Prdm16: Prdm16 has been identified as a transcriptional activator of the brown-fat selective gene program and also

repressor of the WAT-specific gene program (42, 45, 60). For both BAT and beige adipocyte development, research has shown that Prdm16 serves as a key transcriptional co-regulator and is needed for development. Prdm16 appears to be an inducer of BeAT differentiation and essential in BAT, but may not serve as a valid marker for AT that is already present.

Car4: In a comprehensive study of several possible beige adipocyte markers, Car4 came out as one of the most convincing (40). During beige adipocyte differentiation using rosiglitazone, there was a 23-fold increase of Car4 mRNA expression (30). Interestingly, with β-adrenergic stimulation of both white and beige adipocytes, Car4 expression levels increased in only white adipocytes suggesting formation of beige adipocytes upon β-adrenergic stimulation. Car4 showed a significant increase in the stromal vascular cell (SVC) fraction of WAT derived from mice exposed to chronic cold temperatures, suggesting the abundance of transcript increased due to beigeing (30). Jong et al., in support with the results from previous studies, demonstrated a significant increase in expression of Car4 after treatment with rosiglitazone in beige adipose cultures, but this increase was seen in BAT as well, possibly eliminating the exclusivity of Car4 being a marker of beige adipocytes (52). It is also of note that warm-acclimated mice in their study had the highest expression levels of Car4 in BAT (39). When analyzing adipose depots, Car4 was found to be expressed in similar levels in all adipose depots (39). These studies provide a wide array of information regarding Car4 and the possibility of it being identified as a beige adipocyte marker. Due to the mRNA expression seen in BAT and beige adipose tissue, specifically with rosiglitazone treatment, Car4 is a marker of interest for future studies to explore the possibility of its functional role in adipose development.

Markers Found in WAT and BeAT

Hoxc8 and Hoxc9: Overlap of markers between BeAT and WAT is expected because, as with BAT, beige adipocytes do have characteristics of white adipocytes. de Jong et al. report both Hoxc8 and Hoxc9 to have similar expression levels in both tissue and cultures of white and beige fat, with near absence from brown fat (39). However, when looking at single adipose depots, both Hoxc8 and Hoxc9 were expressed through the different depots. It is of note that Hoxc8 displayed a negative correlation with Ucp1 expression (39).

Aqp5, Aqp7, and Aqp9: The role of aquaglyceroporins in white AT differentiation has been well-studied, and it is known that Aqp7 is especially important for WAT. In a study conducted by Silva et al., aquaporin expression patterns were noted throughout beige adipocyte differentiation and were compared to other biomarkers to determine if they could be useful in denoting beige adipocytes (61). They determined that Aqp7 and Aqp9 mRNA expression levels were upregulated throughout the beigeing process, possibly indicating these proteins as markers of beige differentiation. In differentiated beige adipocytes, expression levels of Aqp7 and Aqp5 led to the conclusion that they are the most prominent aquaglyceroporins in beige adipocytes. It is interesting that Aqp7 was expressed at significantly lower levels in beige adipocytes compared to white adipocytes, leading to the possibility that Aqp7, while important in the beigeing process, may serve as a way of comparing WAT to beige adipocytes *via* level of expression.

CONCLUSION AND RELEVANCE

In conclusion, there are multiple markers that can possibly be used to identify the presence of BeAT. As made clear throughout this review, there is still conflicting evidence on the use of many of the genetic markers discussed. We now know that BeAT is derived from WAT but has similar properties to BAT, yet the full suite of regulators of BeAT and its metabolic properties, need to be better understood. The studies of BeAT have shown that cold temperature exposure and adrenergic stimulation are able to induce the beigeing of WAT in mice, and as the WAT is beiged, the presence of potential BeAT and BAT markers are increased. Expanding our current knowledge on the dynamics and identity of these factors is crucial for understanding the mechanisms that drive induction of BeAT and for considering nutritional, exercise, or pharmaceutical interventions that activate BeAT in order to improve metabolic health.

To make the best use of knowledge we gathered from previous studies, we can say two things for certain, 1) Beige cells reside and are recruited in typically subcutaneous WAT; using novel transcript markers such as Tmem26, Tbx1, CD137, or Car4 to identify BeAT is the best possible available strategy. 2) Because of the peculiar nature of recruiting sites/depots of BeAT, negative selection criteria such as expression of the above mentioned genes and in addition some of the BAT specific genes *e.g.* Ucp1, Cidea, and/or Pgc1a expression can also be used to classify the type of AT. *In vivo* imaging identifying the structural differences in adipocytes such as size of cells and number of lipid droplets in the cell can be used to aid the identification of BeAT.

Difficulties in using specific transcript expression solely has its own limitations. BeAT recruitment and expression pattern of these cells can be affected by physiological conditions (diet, age, and ambient temperature). Expression of BeAT in standard mouse models (chow-fed, young, and at 20°C) is different from those of humans. Ongoing studies from our lab are understanding the expression pattern of specific transcript under these certain conditions.

AUTHOR CONTRIBUTIONS

A-CP searched the literature and wrote the manuscript. UW prepared the figures and edited the manuscript. HP, revised the manuscript. All authors contributed to the article and approved the submitted version.

ACKNOWLEDGMENTS

The authors thank Drs. Craig Porter and Sean Adams for helpful comments and suggestions while drafting the manuscript. UW and HP is supported by USDA-ARS Project 6026-51000-012-06S.

REFERENCES

1. Matsuzawa Y. The metabolic syndrome and adipocytokines. *FEBS Lett* (2006) 580:2917–21. doi: 10.1016/j.febslet.2006.04.028
2. Carpentier AC, Blondin DP, Virtanen KA, Richard D, Haman F, Turcotte ÉE. Brown Adipose Tissue Energy Metabolism in Humans. *Front Endocrinol (Lausanne)* (2018) 9:447. doi: 10.3389/fendo.2018.00447
3. Cinti S. The adipose organ. *Prostaglandins Leukot Essent Fatty Acids* (2005) 73:9–15. doi: 10.1016/j.plefa.2005.04.010
4. Wu J, Boström P, Sparks LM, Ye L, Choi JH, Giang AH, et al. Beige adipocytes are a distinct type of thermogenic fat cell in mouse and human. *Cell* (2012) 150:366–76. doi: 10.1016/j.cell.2012.05.016
5. Himms-Hagen J, et al. Multilocular fat cells in WAT of CL-316243-treated rats derive directly from white adipocytes. *Am J Physiol Cell Physiol* (2000) 279:C670–81. doi: 10.1152/ajpcell.2000.279.3.C670
6. Barbatelli G, Murano I, Madsen L, Hao Q, Jimenez M, Kristiansen K, et al. The emergence of cold-induced brown adipocytes in mouse white fat depots is determined predominantly by white to brown adipocyte transdifferentiation. *Am J Physiol Endocrinol Metab* (2010) 298:E1244–53. doi: 10.1152/ajpendo.00600.2009
7. Young P, Arch JR, Ashwell M. Brown adipose tissue in the parametrial fat pad of the mouse. *FEBS Lett* (1984) 167:10–4. doi: 10.1016/0014-5793(84)80822-4
8. Loncar D, Afzelius BA, Cannon B. Epididymal white adipose tissue after cold stress in rats. II. Mitochondrial changes. *J Ultrastruct Mol Struct Res* (1988) 101:199–209. doi: 10.1016/0889-1605(88)90010-9
9. Wang QA, Tao C, Gupta RK, Scherer PE. Tracking adipogenesis during white adipose tissue development, expansion and regeneration. *Nat Med* (2013) 19:1338–44. doi: 10.1038/nm.3324
10. Okla M, Kim J, Koehler K, Chung S. Dietary Factors Promoting Brown and Beige Fat Development and Thermogenesis12. *Adv Nutr* (2017) 8:473–83. doi: 10.3945/an.116.014332
11. Mika A, Macaluso F, Barone R, Di Felice V, Sledzinski T. Effect of Exercise on Fatty Acid Metabolism and Adipokine Secretion in Adipose Tissue. *Front Physiol* (2019) 10:26. doi: 10.3389/fphys.2019.00026
12. Reynés B, Palou M, Rodríguez AM, Palou A. Regulation of Adaptive Thermogenesis and Browning by Prebiotics and Postbiotics. *Front Physiol* (2019) 9:1908. doi: 10.3389/fphys.2018.01908
13. Fisher FM, Kleiner S, Douris N, Fox EC, Mepani RJ, Verdeguer F, et al. FGF21 regulates PGC-1α and browning of white adipose tissues in adaptive thermogenesis. *Genes Dev* (2012) 26:271–81. doi: 10.1101/gad.177857.111
14. Kaisanlahti A, Glumoff T. Browning of white fat: agents and implications for beige adipose tissue to type 2 diabetes. *J Physiol Biochem* (2019) 75:1–10. doi: 10.1007/s13105-018-0658-5
15. Azhar Y, Parmar A, Miller CN, Samuels JS, Rayalam S. Phytochemicals as novel agents for the induction of browning in white adipose tissue. *Nutr Metab* (2016) 13:89. doi: 10.1186/s12986-016-0150-6
16. Thyagarajan B, Foster MT. Beiging of white adipose tissue as a therapeutic strategy for weight loss in humans. *Hormone Mol Biol Clin Invest* (2017) 1:13. doi: 10.1515/hmbci-2017-0016
17. Lee P, Linderman JD, Smith S, Brychta RJ, Wang J, Idelson C, et al. Irisin and FGF21 Are Cold-Induced Endocrine Activators of Brown Fat Function in Humans. *Cell Metab* (2014) 19:302–9. doi: 10.1016/j.cmet.2013.12.017
18. Sacks HS, et al. Adult Epicardial Fat Exhibits Beige Features. *J Clin Endocrinol Metab* (2013) 98:E1448–55. doi: 10.1210/jc.2013-1265
19. Gaborit B, Venteclef N, Ancel P, Pelloux V, Gariboldi V, Leprince P, et al. Human epicardial adipose tissue has a specific transcriptomic signature depending on its anatomical peri-atrial, peri-ventricular, or peri-coronary location. *Cardiovasc Res* (2015) 108:62–73. doi: 10.1093/cvr/cvv208
20. Chang L, Garcia-Barrio MT, Chen YE. Perivascular Adipose Tissue Regulates Vascular Function by Targeting Vascular Smooth Muscle Cells. *Arterioscler Thromb Vasc Biol* (2020) 40:1094–109. doi: 10.1161/ATVBAHA.120.312464
21. Spalding KL, Arner E, Westermark PO, Bernard S, Buchholz BA, Bergmann O, et al. Dynamics of fat cell turnover in humans. *Nature* (2008) 453:783–7. doi: 10.1038/nature06902
22. Gregoire FM, Smas CM, Sul HS. Understanding adipocyte differentiation. *Physiol Rev* (1998) 78:783–809. doi: 10.1152/physrev.1998.78.3.783
23. MacDougald OA, Mandrup S. Adipogenesis: forces that tip the scales. *Trends Endocrinol Metab* (2002) 13:5–11. doi: 10.1016/S1043-2760(01)00517-3
24. Berry DC, Stenesen D, Zeve D, Graff JM. The developmental origins of adipose tissue. *Development* (2013) 140:3939–49. doi: 10.1242/dev.080549
25. Fu M, Xu L, Chen X, Han W, Ruan C, Li J, et al. Neural Crest Cells Differentiate Into Brown Adipocytes and Contribute to Periaortic Arch Adipose Tissue Formation. *Arteriosclerosis Thrombosis Vasc Biol* (2019) 39:1629–44. doi: 10.1161/ATVBAHA.119.312838
26. Lefterova MII, et al. PPARγ and C/EBP factors orchestrate adipocyte biology via adjacent binding on a genome-wide scale. *Genes Dev* (2008) 22:2941–52. doi: 10.1101/gad.1709008
27. Atit R, et al. Beta-catenin activation is necessary and sufficient to specify the dorsal dermal fate in the mouse. *Dev Biol* (2006) 296:164–76. doi: 10.1016/j.ydbio.2006.04.449
28. Seale P, Bjork B, Yang W, Kajimura S, Chin S, Kuang S, et al. PRDM16 controls a brown fat/skeletal muscle switch. *Nature* (2008) 454:961–7. doi: 10.1038/nature07182
29. Cannon B, de Jong JMA, Fischer AW, Nedergaard J, Petrovic N. Human brown adipose tissue: Classical brown rather than brite/beige? *Exp Physiol* (2020) 105(8):1191–200. doi: 10.1113/EP087875
30. Sanchez-Gurmaches J, Hung CM, Sparks CA, Tang Y, Li H, Guertin DA. PTEN loss in the Myf5 lineage redistributes body fat and reveals subsets of white adipocytes that arise from Myf5 precursors. *Cell Metab* (2012) 16:348–62. doi: 10.1016/j.cmet.2012.08.003
31. Lee Y-H, Petkova AP, Mottillo EP, Granneman JG. In vivo identification of bipotential adipocyte progenitors recruited by β3-adrenoceptor activation and high-fat feeding. *Cell Metab* (2012) 15:480–91. doi: 10.1016/j.cmet.2012.03.009
32. Oguri Y, Shinoda K, Kim H, Alba DL, Bolus WR, Wang Q, et al. CD81 Controls Beige Fat Progenitor Cell Growth and Energy Balance via FAK Signaling. *Cell* (2020) 182:563–77.e20 doi: 10.1016/j.cell.2020.06.021.
33. Long JZ, Svensson KJ, Tsai L, Zeng X, Roh HC, Kong X, et al. A smooth muscle-like origin for beige adipocytes. *Cell Metab* (2014) 19:810–20. doi: 10.1016/j.cmet.2014.03.025
34. Ohno H, Shinoda K, Ohyama K, Sharp LZ, Kajimura S. EHMT1 controls brown adipose cell fate and thermogenesis through the PRDM16 complex. *Nature* (2013) 504:163–7. doi: 10.1038/nature12652
35. Jiang Y, Berry DC, Graff JM. Distinct cellular and molecular mechanisms for β3 adrenergic receptor-induced beige adipocyte formation. *eLife* (2017) 6: e30329. doi: 10.7554/eLife.30329
36. Shabalina IG, Petrovic N, de Jong JM, Kalinovich AV, Cannon B, Nedergaard J. UCP1 in brite/beige adipose tissue mitochondria is functionally thermogenic. *Cell Rep* (2013) 5:1196–203. doi: 10.1016/j.celrep.2013.10.044
37. Gesta S, Tseng Y-H, Kahn CR. Developmental origin of fat: tracking obesity to its source. *Cell* (2007) 131:242–56. doi: 10.1016/j.cell.2007.10.004
38. Ussar S, Lee KY, Dankel SN, Boucher J, Haering MF, Kleinridders A, et al. ASC-1, PAT2, and P2RX5 are cell surface markers for white, beige, and brown adipocytes. *Sci Trans Med* (2014) 6:247ra103. doi: 10.1126/scitranslmed.3008490
39. Sharp LZ, Shinoda K, Ohno H, Scheel DW, Tomoda E, Ruiz L, et al. Human BAT Possesses Molecular Signatures That Resemble Beige/Brite Cells. *PloS One* (2012) 7:e49452. doi: 10.1371/journal.pone.0049452
40. Garcia RA, Roemmich JN, Claycombe KJ. Evaluation of markers of beige adipocytes in white adipose tissue of the mouse. *Nutr Metab* (2016) 13:24. doi: 10.1186/s12986-016-0081-2
41. Cypess AM, White AP, Vernochet C, Schulz TJ, Xue R, Sass CA, et al. Anatomical localization, gene expression profiling and functional characterization of adult human neck brown fat. *Nat Med* (2013) 19:635–9 doi: 10.1038/nm.3112
42. Waldén TB, Hansen IR, Timmons JA, Cannon B, Nedergaard J. Recruited vs. nonrecruited molecular signatures of brown, "brite," and white adipose tissues. *Am J Physiol Endocrinol Metab* (2011) 302:E19–31. doi: 10.1152/ajpendo.00249.2011
43. Kajimura S, Spiegelman BM, Seale P. Brown and Beige Fat: Physiological Roles beyond Heat Generation. *Cell Metab* (2015) 22:546–59. doi: 10.1016/j.cmet.2015.09.007
44. Wankhade UD, Lee JH, Dagur PK, Yadav H, Shen M, Chen W, et al. TGF-β receptor 1 regulates progenitors that promote browning of white fat. *Mol Metab* (2018) 16:160–71. doi: 10.1016/j.molmet.2018.07.008
45. Seale P, et al. Transcriptional control of brown fat determination by PRDM16. *Cell Metab* (2007) 6:38–54. doi: 10.1016/j.cmet.2007.06.001

46. Xue R, Lynes MD, Dreyfuss JM, Shamsi F, Schulz TJ, Zhang H, et al. Clonal analyses and gene profiling identify genetic biomarkers of the thermogenic potential of human brown and white preadipocytes. *Nat Med* (2015) 21:760–8. doi: 10.1038/nm.3881
47. Harms M, Seale P. Brown and beige fat: development, function and therapeutic potential. *Nat Med* (2013) 19:1252–63. doi: 10.1038/nm.3361
48. Liang X, Pan J, Cao C, Zhang L, Zhao Y, Fan Y, et al. Transcriptional Response of Subcutaneous White Adipose Tissue to Acute Cold Exposure in Mice. *Int J Mol Sci* (2019) 20:3968. doi: 10.3390/ijms20163968
49. Srivastava RK, Moliner A, Lee ES, Nickles E, Sim E, Liu C, et al. CD137 negatively regulates "browning" of white adipose tissue during cold exposure. *J Biol Chem* (2020) 295(7):2034–42. doi: 10.1074/jbc.AC119.011795
50. Christian M. Transcriptional fingerprinting of 'browning' white fat identifies NRG4 as a novel adipokine. *Adipocyte* (2015) 4:50–4. doi: 10.4161/adip.29853
51. Cuevas-Ramos D, Mehta R, Aguilar-Salinas CA. Fibroblast Growth Factor 21 and Browning of White Adipose Tissue. *Front Physiol* (2019) 10:37. doi: 10.3389/fphys.2019.00037
52. de Jong JMA, Larsson O, Cannon B, Nedergaard J. A stringent validation of mouse adipose tissue identity markers. *Am J Physiol Endocrinol Metab* (2015) 308:E1085–1105. doi: 10.1152/ajpendo.00023.2015
53. Soundarrajan M, Deng J, Kwasny M, Rubert NC, Nelson PC, El-Seoud DA, et al. Activated brown adipose tissue and its relationship to adiposity and metabolic markers: an exploratory study. *Adipocyte* (2020) 9:87–95. doi: 10.1080/21623945.2020.1724740
54. Sidossis L, Kajimura S. Brown and beige fat in humans: thermogenic adipocytes that control energy and glucose homeostasis. *J Clin Invest* (2015) 125:478–86. doi: 10.1172/JCI78362
55. Fromme T, Klingenspor M. Uncoupling protein 1 expression and high-fat diets. *Am J Physiol Regul Integr Comp Physiol* (2011) 300:R1–8. doi: 10.1152/ajpregu.00411.2010
56. Zoico E, Rubele S, De Caro A, Nori N, Mazzali G, Fantin F, et al. Brown and Beige Adipose Tissue and Aging. *Front Endocrinol (Lausanne)* (2019) 10:368. doi: 10.3389/fendo.2019.00368
57. Puigserver P, Wu Z, Park CW, Graves R, Wright M, Spiegelman BM. A Cold-Inducible Coactivator of Nuclear Receptors Linked to Adaptive Thermogenesis. *Cell* (1998) 92:829–39. doi: 10.1016/S0092-8674(00)81410-5
58. Uldry M, et al. Complementary action of the PGC-1 coactivators in mitochondrial biogenesis and brown fat differentiation. *Cell Metab* (2006) 3:333–41. doi: 10.1016/j.cmet.2006.04.002
59. Tiraby C, Tavernier G, Lefort C, Larrouy D, Bouillaud F, Ricquier D, et al. Acquirement of Brown Fat Cell Features by Human White Adipocytes. *J Biol Chem* (2003) 278:33370–6. doi: 10.1074/jbc.M305235200
60. Inagaki T, Sakai J, Kajimura S. Transcriptional and epigenetic control of brown and beige adipose cell fate and function. *Nat Rev Mol Cell Biol* (2016) 17:480–95. doi: 10.1038/nrm.2016.62
61. da Silva IV, Díaz-Sáez F, Zorzano A, Gumà A, Camps M, Soveral G. Aquaglyceroporins Are Differentially Expressed in Beige and White Adipocytes. *Int J Mol Sci* (2020) 21:610. doi: 10.3390/ijms21020610

Conflict of Interest: The authors declare that the research was conducted in the absence of any commercial or financial relationships that could be construed as a potential conflict of interest.

frontiers in Endocrinology

REVIEW
published: 26 March 2021
doi: 10.3389/fendo.2021.595020

Signaling Pathways Regulating Thermogenesis

Chihiro Tabuchi and Hei Sook Sul *

Department of Nutritional Sciences and Toxicology, University of California, Berkeley, Berkeley, CA, United States

Obesity, an excess accumulation of white adipose tissue (WAT), has become a global epidemic and is associated with complex diseases, such as type 2 diabetes and cardiovascular diseases. Presently, there are no safe and effective therapeutic agents to treat obesity. In contrast to white adipocytes that store energy as triglycerides in unilocular lipid droplet, brown and brown-like or beige adipocytes utilize fatty acids (FAs) and glucose at a high rate mainly by uncoupling protein 1 (UCP1) action to uncouple mitochondrial proton gradient from ATP synthesis, dissipating energy as heat. Recent studies on the presence of brown or brown-like adipocytes in adult humans have revealed their potential as therapeutic targets in combating obesity. Classically, the main signaling pathway known to activate thermogenesis in adipocytes is β_3-adrenergic signaling, which is activated by norepinephrine in response to cold, leading to activation of the thermogenic program and browning. In addition to the β_3-adrenergic signaling, numerous other hormones and secreted factors have been reported to affect thermogenesis. In this review, we discuss several major pathways, β_3-adrenergic, insulin/IGF1, thyroid hormone and TGFβ family, which regulate thermogenesis and browning of WAT.

Keywords: thermogenesis, brown adipose tissue, browning/beiging, b3-adrenergic signaling, UCP1, insulin/IGF1 signaling, thyroid hormone, TGFβ superfamily

OPEN ACCESS

Edited by:
Jiqiu Wang,
Shanghai Jiao Tong University, China

Reviewed by:
Andreas Hoeflich,
Leibniz Institute for Farm Animal Biology (FBN), Germany
Rosalba Senese,
University of Campania Luigi Vanvitelli, Italy

***Correspondence:**
Hei Sook Sul
hsul@berkeley.edu

Specialty section:
This article was submitted to Cellular Endocrinology, a section of the journal Frontiers in Endocrinology

Received: *14 August 2020*
Accepted: *25 February 2021*
Published: *26 March 2021*

Citation:
Tabuchi C and Sul HS (2021) Signaling Pathways Regulating Thermogenesis. Front. Endocrinol. 12:595020. doi: 10.3389/fendo.2021.595020

INTRODUCTION

Brown adipose tissue (BAT) is specialized in heat production through non-shivering thermogenesis by burning fuels such as fatty acids (FA) and glucose (1). BAT is crucial for maintaining body temperature especially for infants who have limited ability to perform shivering thermogenesis, due to underdeveloped skeletal muscle (2). In adults, BAT contributes to energy expenditure as indicated by an inverse correlation between the presence of active BAT and central obesity (3, 4). In addition to numerous mitochondria, BAT possesses multilocular lipid droplets that provide FAs for β-oxidation, which drives tricarboxylic acid (TCA) cycle and electron transport chain (ETC) to create proton gradient (5). In contrast, white adipose tissue (WAT) serves as an energy storage and has a unilocular lipid droplet and fewer mitochondria.

Of all tissues, BAT expresses the highest levels of uncoupling protein 1 (UCP1) and UCP1 plays a central role in non-shivering thermogenesis (6). UCP1 acts as a proton transporter in the inner membrane of mitochondria, which allows protons to leak from intermembrane space into the mitochondrial matrix (7). This uncouples the proton gradient from ATP synthesis, dissipating the proton gradient in the form of heat. Therefore, having a large number of mitochondria and multilocular lipid droplets enables BAT to maximize its thermogenic capacity. Although WAT normally has little UCP1 expression, some cells in subcutaneous WAT depots display thermogenic

capacity with elevated UCP1 expression upon certain stimulations, the process so-called 'browning/beiging' (8). These thermogenic adipocytes are termed 'beige/brite' adipocytes, which seem to originate from different precursor cells than brown adipocytes, based on distinct gene signatures (9). However, transdifferentiation of mature white adipocytes to thermogenic beige adipocytes have also been reported (10). It is plausible that these thermogenic adipocytes can be generated by distinct mechanisms.

Classical brown adipocytes originate from a subset of multipotent stem cells in the dermomyotome that express engrailed 1 (EN1), paired box 7 (PAX7) and myogenic factor 5 (MYF5) (11). While the $MYF5^+/PAX7^+/EN1^+$ progenitor cells can give rise to other cell types, such as skeletal myocytes, they commit to brown adipocyte lineage upon early B cell factor 2 (EBF2) expression (12). Additionally, PR domain containing 16 (PRDM16) stimulates brown adipocyte differentiation over myoblast differentiation through the interaction with peroxisome proliferator activated receptor γ (PPARγ) (13). Ewing Sarcoma (EWS)/Y-box binding protein 1 (YBX1) complex promotes bone morphogenetic protein 7 (BMP7) transcription, which also determines brown adipocyte lineage during development (14). Committed brown precursor cells then differentiate into mature brown adipocytes through a series of transcriptional events (11, 15). ZFP516 stimulates thermogenic gene expression such as UCP1, DIO2 and CIDEA to promote brown adipocyte differentiation. ZFP516 interacts with not only PRDM16, but also with LSD1 in activating thermogenic gene program. ZC3H10 upregulates transcription of genes for mitochondrial biogenesis, such as NRF1 and TFAM (16, 17). EBF2 activates transcription of PPARγ, which promotes expression of numerous lipid metabolic genes, such as fatty acid binding protein (FABP4/aP2), cluster of differentiation 36 (CD36) and lipoprotein lipase (LPL) (18). In addition, EBF2 and PPARγ cooperatively activate transcription of PRDM16. CEBPβ also activates PPARγ transcription to promote adipogenic and thermogenic gene expression (19). PPARγ coactivator α (PGC1α) is another transcriptional co-regulator that interacts with many proteins including PPARγ, PRDM16 and IRF4 to promote BAT development, especially mitochondrial biogenesis through NRF1 and TFAM (15, 20). Some of the aforementioned transcription factors and co-activators such as ZFP516, ZC3H10 and PGC1α also induce thermogenic gene expression upon β_3-adrenergic stimuli in mature brown and white adipocytes, the latter of which leads to browning.

Environmental cues such as cold exposure, exercise and diet can trigger non-shivering thermogenesis in classical BAT and also browning of WAT, by activating specific signaling cascades within the cell (20, 21). For example, cold temperature stimulates the sympathetic nervous system to release norepinephrine, which then binds β_3-adrenergic receptor (15). β_3-adrenergic signaling has a wide range of downstream targets including numerous transcription factors and co-activators that can induce thermogenic genes (22). In addition to the transcriptional regulation, β_3-adrenergic signaling also increases lipolysis and glucose uptake to support thermogenesis (23). In this review, we discuss underlying signaling pathways that regulate thermogenesis in brown and beige adipocytes, as well as browning of WAT.

β_3-ADRENERGIC SIGNALING

The dominant signaling pathway that governs non-shivering thermogenesis in brown and beige adipocytes is β_3-adrenergic signaling. Upon cold exposure, norepinephrine released from the sympathetic nervous system binds mainly β_3-adrenergic receptor (β_3-AR) to induce adrenergic signaling (24, 25) (**Figure 1**). β_3-AR coupled with Gs activates AC, which in turn produces cAMP for PKA activation. A variety of downstream targets of PKA, such as p38, CREB and HSL, enhances thermogenesis by inducing thermogenic gene expression and/or mobilizing substrate to fuel thermogenesis (26, 27).

p38, a MAP kinase, phosphorylates multiple transcription factors/coregulators, including ATF2 and PGC1α, both of which promote UCP1 transcription (22). In addition, we recently found that ZC3H10, previously known to bind RNA, is phosphorylated by p38 upon cold, activating the thermogenic gene program in adipocytes (17). Specifically, ZC3H10 binds a distal upstream region of the UCP1 promoter for transcriptional activation. ZC3H10 also activates NRF1 and TFAM, which facilitate mitochondrial biogenesis to increase thermogenic capacity of adipocytes. Thus, transgenic mice overexpressing ZC3H10 exhibited increased oxygen consumption, higher BAT temperature and reduced body weight while ZC3H10 knockout mice displayed decreased oxygen consumption, lower BAT temperature and increased body weight. PGC1α, a downstream target of p38, serves as co-activator for PPARγ and NRF1 to induce expression of UCP1 and TFAM, respectively (27, 28). CREB was also shown to bind to the proximal promoter of UCP1 to potentially activate the transcription.

β_3-adrenergic signaling also increases the expression of ZFP516. ZFP516 recruits LSD1, which demethylases H3K9 at the proximal region of UCP1 promoter to induce UCP1 transcription. Furthermore, ZFP516 directly interacts with PRDM16 at the UCP1 promoter and potentially at other BAT gene promoters. ZFP516 depletion *in vivo* resulted in impaired BAT formation with decreased BAT gene expression and increased muscle gene expression in the presumptive BAT depot, while ZFP516 overexpression increased body temperature, oxygen consumption, browning of WAT, leading to lower body weight. Taken together, ZFP516 is required for BAT development in addition to promoting WAT browning.

Adipose thermogenesis can be enhanced by an increased supply of substrates such as FA and glucose. Upon β_3-AR activation, PKA phosphorylates HSL, now known as diacyl glycerol hydrolase, as well as PLIN on lipid droplets to promote lipolysis. FAs thus produced upon lipolysis can undergo β-oxidation to eventual production of NADH and FADH for ETC, during UCP1-mediated thermogenesis (5, 29). FA also directly binds UCP1 to assist proton influx into the mitochondrial matrix (30). In the fed state, however, FAs as substrates for thermogenesis seem to originate from white adipose tissue lipolysis, although it was also reported that

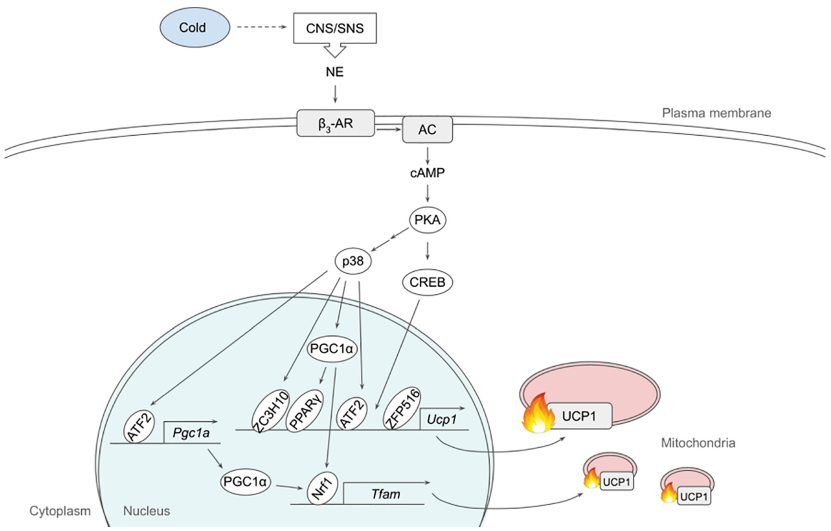

FIGURE 1 | Schematic model of β_3-adrenergic signaling pathway that promotes thermogenesis in adipocytes. Cold stimulates CNS/SNS to secrete NE that binds β_3-AR, which then activates AC producing cAMP. cAMP in turn activates PKA that has a variety of downstream targets, including transcription factors to upregulate thermogenic gene expression. See text for details. AC, adenylate cyclase; ATF2, activating transcription factor 2; β_3-AR, β_3-adrenergic receptor; CNS, central nervous system; CREB, cAMP response-element binding protein; ETC, electron transport chain; FFA, free fatty acid; IRF4, interferon regulatory factor 4; NE, norepinephrine; NRF1, nuclear respiratory factor 1; PGC1α, peroxisome proliferator activated receptor γ coactivator α; PKA, protein kinase A; PPARγ, peroxisome proliferator activated receptor γ; SNS sympathetic nervous system; TCA, tricarboxylic acid; TFAM, mitochondrial transcription factor A; UCP1, uncoupling protein 1; ZC3H10, zinc finger CCCH-type containing 10; ZFP516, zinc finger protein 516.

inhibition of intracellular lipolysis suppressed cold-induced non-shivering thermogenesis in BAT, which was compensated by an increased shivering in humans (31, 32). Of note, lipolysis can also be modulated non-adrenergically and this aspect has been extensively reviewed elsewhere (33).

We recently discovered a BAT-specific NADH oxidase, AIFM2, which is required for cold- and diet-induced thermogenesis (34). Upon cold or β_3-adrenergic stimuli, AIFM2 translocates from lipid droplet to the outer side of the inner membrane of mitochondria. AIFM2 oxidizes NADH to NAD, which is needed for glyceraldehyde-3 phosphate dehydrogenase (GAPDH) reaction, in supporting robust glycolysis. In addition, electrons generated from AIFM2 action are transferred to CoQ for ETC activity of mitochondria. AIFM2 KO mice exhibited higher body weight, lower oxygen consumption, and lower BAT temperature whereas AIFM2 overexpression resulted in the opposite phenotypes. In addition, the expression of AIFM2 was induced upon refeeding with high carb diet when examined at thermoneutrality, suggesting that glucose oxidation appears to be especially important in the fed state to promote thermogenesis when the blood glucose level is relatively high.

Collectively, there is no doubt that β_3-AR signaling plays a dominant role in regulating thermogenesis. Besides those mentioned above, there are many more proteins that are involved in and downstream of β_3-AR signaling. Further studies will elucidate more components related to β_3-AR signaling that regulate thermogenesis at various steps such as substrate metabolism, mitochondrial homeostasis, gene expression as well as signal transduction.

INSULIN/IGF1 SIGNALING

Insulin/IGF1 signaling plays important roles in adipose tissue development and thermogenesis. Mice with fat-specific double knockout of insulin receptor (IR) and IGF1 receptor (IGF1R) (FIGIRKO) exhibited decreased adiposity with more than 85% reduction in BAT, having lower body weight (35). Indeed, brown preadipocytes from FIGIRKO failed to differentiate *in vitro* with no increase in the expression of PPARγ and CEBPα, indicating that insulin/IGF-1 signaling is critical for BAT development. Since the addition of PPARγ agonist, rosiglitazone, did not rescue the impaired differentiation, insulin/IGF-1 signaling seemed to act on the upstream of PPARγ/CEBPα. Consistently, phosphorylation of CEBPβ at Thr188, which is required for DNA binding and therefore transcriptional activation of PPARγ/CEBPα, was reduced. FIGIRKO mice were also protected from diet-induced obesity, possibly due to impaired adipose development. FIGIRKO mice failed to maintain their body temperature during cold exposure, although they had higher energy expenditure/basal metabolic rate with no change in activity, this paradox remaining to be explained. In this regard, the study utilized aP2 promoter to express Cre recombinase for gene KO, which could have affected not only adipose tissues but also other cell types, such as macrophages.

The effects of insulin signaling and IGF-1 signaling were further investigated by comparing fat-specific IR single KO (F-IRKO) and IGF1R single KO (F-IGFRKO) to IR/IGF1R double KO (F-IR/IGFRKO), which were all generated by Cre driven by adiponectin promoter (36). F-IGFRKO only had a small

reduction in both WAT and BAT, while F-IR/IGFRKO had an almost complete loss of adipose tissue. Interestingly, F-IRKO had a large WAT reduction with an unexplainable 50% increase in BAT with large unilocular lipid droplet. BAT of F-IR/IGFRKO exhibited increased BAT gene expression and decreased WAT gene expression, whereas that of F-IRKO showed no change in BAT or WAT marker gene expression. Regardless, the expression of genes involved in BAT function, including UCP1 and other thermogenic genes, TFAM for example, was reduced in both F-IR/IGFRKO and F-IRKO, which could explain why both F-IR/IGFRKO and F-IRKO failed to maintain body temperature during the cold challenge. Indeed, F-IRKO had reduced mitochondrial content and oxygen consumption.

BAT-specific IR KO mice created by using UCP1 promoter-Cre, however, showed impaired BAT development (37). Since the expression of CEBPα, but not PPARγ, decreased in BAT of the KO mice, insulin signaling likely promotes brown adipogenesis mainly through CEBPα. Interestingly, UCP1 expression increased significantly in BAT and the KO mice even had leaner phenotype, possibly due to the remaining BAT compensating for the decreased thermogenesis. Another mechanism where insulin/IGF1 signaling can promote BAT development is by increasing proliferation. Insulin and IGF1, not only stimulated IRS1 and IRS2 tyrosine phosphorylation and their association with PI3K, but also enhanced IRS1-associated GRB2 phosphorylation, which can activate RAS-MAPK pathway for proliferation (38). BAT-specific IGF1R KO mice, on the other hand, had normal BAT size and normal body weight, while UCP1 expression in BAT was reduced and the KO mice were cold intolerant, suggesting that IGF1 signaling enhances BAT thermogenesis (39).

Insulin/IGF1 signaling plays a role in browning of WAT as well. PTEN antagonizes the action of PI3K by converting PIP3 back to PIP2 and, therefore, insulin/IGF1 signaling. PTEN knockdown (KD) by direct injection of Rec2-Cre in iWAT of PTEN floxed mice increased AKT signaling and induced browning (40). These effects were blocked by administration of an AKT inhibitor, indicating that the PI3K-AKT pathway promotes browning. Transgenic mice overexpressing PTEN were reported to have increased energy expenditure with hyperactivation of BAT. However, PTEN was overexpressed globally in these animals, making it difficult to interpret the exact contribution of PTEN in a tissue-specific manner (41).

Interestingly, insulin signaling can be modulated by β_3-adrenergic signaling. β_3-adrenergic signaling pretreatment reduced the activation of IR, IRS1 and IRS2. In addition, β_3-adrenergic signaling mitigated AKT activation and IRS1-associated activation of PI3K upon insulin treatment, while it did not affect MAPK activation and IRS2-associated activation of PI3K. Moreover, β_3-adrenergic signaling abolished insulin-mediated glucose uptake in brown adipocytes (42). In this regard, cold exposure has also been shown to alter the expression of many molecules involved in the insulin signaling pathway (43). Specifically, the expression of IRS1 and IRS2 as well as phosphorylation of AKT are upregulated. These discrepancies could be due to the differences in the methods used such as *in vitro* vs *in vivo*, mouse vs rat as well as protein phosphorylation vs transcriptome.

Taken together, IR/IGF1R signaling promotes adipose tissue thermogenesis by supporting BAT development, browning of WAT and BAT function. Some of those studies mentioned above are even conflicting, owing at least partly to the differences in promoters used to express Cre, which affects not only the efficiency of gene KO, but also tissue specificity. Even with a tissue-specific KO, some phenotypes could manifest because of secondary effects rather than direct, primary effects. Therefore, it would be important to recapitulate the results *in vitro* as well. Further research is needed to better clarify the role of IR and IGF1R signaling in adipose tissue thermogenesis.

THYROID HORMONE

Among various ligands/hormones that bind and function *via* nuclear hormone receptors, thyroid hormone (TH) is classically known to regulate thermogenesis (44). TH receptors (TR), TRα and TRβ, in adipocytes enhance BAT thermogenesis and WAT browning. TRs are activated by triiodothyronine (T3), an active form of TH produced from thyroxine (T4) by type II iodothyronine deiodinase (DIO2). Although TRα and TRβ may have overlapping functions, TRβ seems mainly responsible for UCP1 induction, whereas TRα might be more important for full β_3-adrenergic response. In hypothyroid mice, TRβ-selective ligand, GC-1, restored UCP1 expression to the same extent as T3, suggesting the significant role of TRβ in UCP1 upregulation (45). However, GC-1-treated mice failed to maintain body temperature during cold exposure, suggesting that UCP1 induction by TRβ alone is not sufficient to support thermogenesis. In agreement with this, GC-1 treatment did not restore cAMP production in isolated brown adipocytes of the hypothyroid mice, which suggests the involvement of TRα in β_3-adrenergic response. The same group later showed that hypothyroid mice with a dominant negative TRβ mutation failed to increase UCP1 expression in BAT (46). These hypothyroid TRβ mutant mice also had reduced cAMP production in BAT and lower body temperature upon T3 replacement and β_3-adrenergic stimulation, implying that TRβ might at least partly participate in β_3-adrenergic response. Although it has also been reported that TRα could bind UCP1 enhancer region for transcriptional activation, the results of the study were relied on *in vitro* experiments as opposed to the previously mentioned studies that investigated its role in animal models (47). DIO2 is another important TH/TR target that contributes to thermogenesis. GC-1 upregulated DIO2 mRNA and enzyme activity upon β_3-adrenergic stimulation, while TRα-selective ligand, CO23, increased DIO2 mRNA expression only (48). Indeed, DIO2 KO brown adipocytes exhibited reduced UCP1 expression, oxygen consumption and lipolysis in response to β3-adrenergic stimuli, which was reversed by T3 administration (49).

TH/TR can enhance BAT thermogenesis through regulation of mitochondrial homeostasis as well (50). Hyperthyroid mice showed increased expression of mitochondrial proteins including COX4I1 and TOMM20 and increased mitochondrial DNA copy number in BAT, implying that TH promoted mitochondrial biogenesis. On the

other hand, T3-treated brown adipocytes exhibited mitochondrial remnants inside autophagic vesicles, suggesting that T3 induced mitophagy. Inhibition of autophagy/mitophagy in hyperthyroid mice indeed increased mitochondrial proteins. Mitochondrial turnover was further assessed using MitoTimer, which showed upregulation of both clearance of mature mitochondria and generation of new mitochondria by T3 treatment. The importance of mitochondrial turnover for thermogenesis was confirmed by suppression of autophagy/mitophagy by ATG5 KD, which decreased oxygen consumption in brown adipocytes, and also conditional ATG5 KO in hyperthyroid mice that showed reduced body temperature.

T3 treatment has been shown to upregulate UCP1 and mitochondria-related genes in white adipocytes as well, by increasing mitochondrial biogenesis (51, 52). This was accompanied by elevated oxygen consumption and FA oxidation, indicating the role of T3 in WAT browning. Similar to that observed in brown adipocytes, UCP1 upregulation in WAT was mediated by TRβ rather than TRα since hyperthyroid TRβ KO mice failed to increase UCP1 expression in WAT (53). In addition to directly upregulating UCP1 transcription, T3 was reported also to trigger AMPK activation, which in turn activated the p38/ATF2 pathway to promote UCP1 expression in WAT, although the mechanism by which T3 could activate AMPK remains to be addressed (54).

Recently, a TH metabolite, 3,5 Diiodo-L-Thyronine (T2), was reported to affect thermogenesis as well (55). T2 administration restored lipid morphology, vascularization, innervation and mitochondrial content/activity in BAT of hypothyroid rats, which were accompanied by increased expression of UCP1 and PGC1α, leading to improved thermogenesis (56). Similarly, T2 seems to promote WAT browning in high fat diet-induced obese rats partly through upregulation of PRDM16 (57). Overall, it can be concluded that the TH/TR promotes BAT thermogenesis and WAT browning.

TRANSFORMING GROWTH FACTOR β SUPERFAMILY

Multiple members of the transforming growth factor beta (TGFβ) superfamily have been shown to regulate thermogenesis (**Figure 2**). In fact, bone morphogenetic protein 7 (BMP7), was reported first to trigger commitment of mesenchymal progenitor cells to brown adipocyte lineage by activating SMAD1/5/8 (58). Without the canonical differentiation induction cocktail, BMP7 induced the expression of both adipogenic and brown-adipocyte specific genes, such as CEBPs, PPARγ, PRDM16, PGC1α, and UCP1, while downregulating adipogenic suppressors such as Pref-1 and WNT10A. BMP7 KO mice exhibited reduced BAT mass that had almost undetectable UCP1 expression. In contrast, BMP7 overexpression *via* adenovirus injection increased the expression of PRDM16 and UCP1 in BAT, energy expenditure and body temperature, while decreasing body weight. In mature brown adipocytes, BMP7 increased mitochondrial activity through p38-ATF2 and SMAD1/5/8 pathways (59). BMP7-treated cells upregulated the expression of CD36 and CPT1 that transport FAs into the cells and mitochondria, respectively, resulting in increased citrate synthase activity and FA oxidation. Administration of BMP7 *in vivo* increased the expression of CD36 in BAT, which was accompanied by increased oxygen consumption. In addition, respiratory exchange ratio in these animals decreased, reflecting the substrate utilization switching towards fatty acids. Another study also confirmed the similar effects of BMP7, where BMP7 administration increased the expression of UCP1 and CD36 in BAT, BAT mass, energy expenditure and fat oxidation (60). Furthermore, these authors found that BMP7 induced the expression of BAT genes in WAT depots with overall reduced WAT size, suggesting that BMP7 promotes browning of WAT. This is supported by a finding that demonstrated BMP7 driving human adipogenic stem cells into beige adipocytes (61). BMP7 treatment promoted the expression of beige markers, such as CD137 and TMEM26, in addition to the expression of thermogenic genes, such as UCP1, CIDEA and DIO2.

BMP8b was found to be highly expressed in BAT and its expression increased during differentiation and during cold exposure (62). BMP8b KO mice exhibited lower energy expenditure, lower body temperature and higher body weight, which were exacerbated when these mice were on high fat diet (HFD). Although BMP8b KO mice showed normal BAT size and BAT gene expression, activation of thermogenic signaling pathways examined by phosphorylation of SMAD1/5/8/, p38 and CREB were impaired, indicating that BMP8b is indispensable for thermogenic activation of BAT, but not for BAT development. Consistently, BMP8b treatment increased phosphorylation of these proteins in differentiated brown adipocytes, as well as that of HSL and AMPK, resulting in increased lipolysis measured by glycerol release. In addition, BMP8b promoted the activation of AMPK in the central nervous system as well, increasing sympathetic output to BAT to support thermogenesis. In this regard, BMP8b was shown to stimulate sympathetic innervation and vascularization through NRG4 and VEGF, respectively, in both BAT and WAT as well as browning of WAT (63). Mice overexpressing BMP8b showed higher energy expenditure, lower body weight and fat mass, accompanied by decreased thermogenic gene expression in WAT that exhibited multilocular lipid droplets, whereas loss of BMP8b resulted in decreased nerve density.

TGFβ/SMAD3 signaling pathway has been reported to suppress browning of WAT (64). TGFβ treatment suppressed activation of PGC1α promoter-reporter in 3T3-L1 cells, which was abolished by SMAD3 KD, indicating that TGFβ represses PGC1α transcription through SMAD3. SMAD3 KO animals had higher body temperature, lower body weight, lower blood glucose, and better response to insulin. WAT of SMAD3 KO mice indeed expressed thermogenic genes, such as UCP1, and exhibited multilocular morphology. Similarly, adipose-specific TGFβ receptor 1 (TGFβR1) KO induced browning, as evidenced by increased UCP1 expression in WAT on HFD, which was accompanied by lower body weight (65). TGFβR1 inhibitor, SB431542, induced brown and beige genes during differentiation of WAT SVF cells, whereas TβR1 downregulated

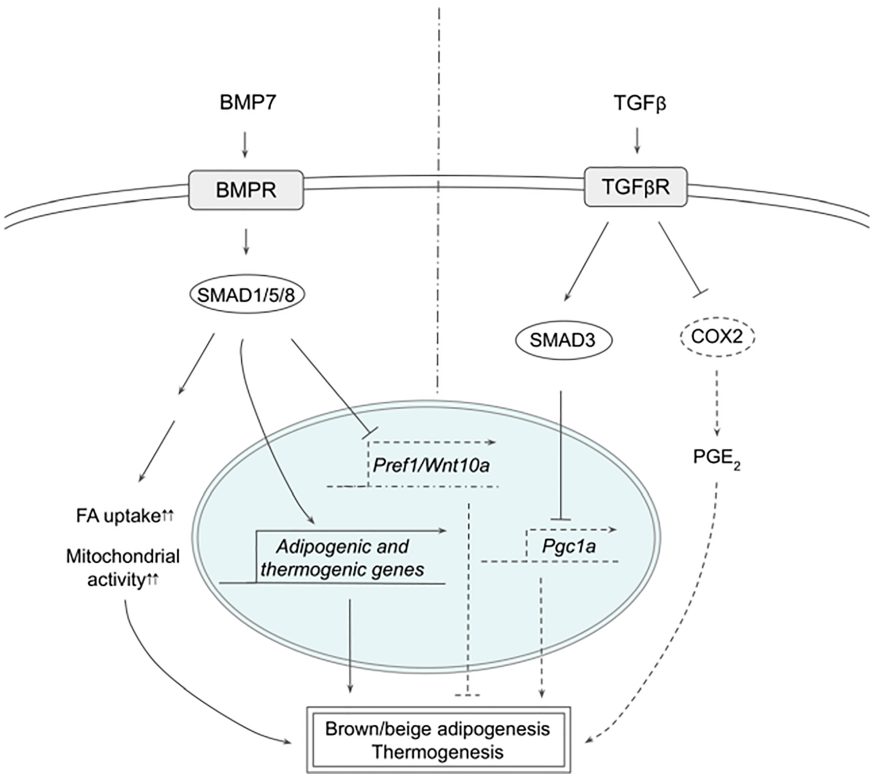

FIGURE 2 | Schematic models of BMP7 and TGFβ signaling pathways in thermogenesis. BMP7 binds TGFβR, which activates SMAD1/5/8, leading to expression of adipogenic and thermogenic genes as well as suppression of Pref1 and Wnt10a in precursor cells to promote brown and beige adipogenesis. In mature adipocytes, BMP7 signaling increases FA uptake and mitochondrial activity, resulting in enhanced thermogenesis. TGFβ activates SMAD2/3 that suppresses PGC1α expression and COX2/PGE2 pathway to reduce thermogenesis. See text for details. BMP7, bone morphogenetic protein 7; COX2, cyclooxygenase 2; FA, fatty acid; PGC1α, peroxisome proliferator activated receptor γ; PGE2, prostaglandin E2; PREF1, preadipocyte factor 1; SMAD, mothers against decapentaplegic homolog; TβR1, TGFβ receptor 1; TGFβ, Transforming growth factor beta; TGFβR, TGFβ receptor; WNT10a, Wnt family member 10A.

those genes. Interestingly, WAT of TGFβR1 KO also increased the expression of genes involved in prostaglandin pathways, such as COX2, implying that prostaglandin pathway might be involved in browning of WAT. SMAD3 KD in 3T3-L1 cells increased the expression of COX2 and other prostaglandin pathway-related proteins. Treatment with PGE_2, a product of COX2, upregulated thermogenic gene expression, such as CIDEA1 and PGC1α, in the presumptive beige precursor cells, which was further augmented by the addition of SB431542, implying the possible interaction between TGFβ/SMAD3 and COX2/PGE_2 pathways. These presumptive beige precursor cells were isolated and selected from WAT by FACS using a series of cell surface markers and were termed inducible beige stem/progenitor cells (iBSCs). iBSCs were then transplanted subcutaneously into immunodeficient nude mice on HFD with IPTT-300 transponder. During the cold exposure, iBSCs from TβR1 KO mice maintained higher temperature and showed higher expression of thermogenic genes with multilocular lipid droplet morphology, suggesting that the KO iBSCs underwent beige adipogenesis. Altogether, TGFβ/SMAD3 signaling negatively regulates WAT browning although further research will help to clarify the contributions of different downstream pathways.

CONCLUDING REMARK

The discovery of brown or brown-like adipocytes in human adults has made targeting adipocytes an attractive strategy to fight against obesity and its associated diseases. Activation of existing thermogenic adipocytes and/or induction of new thermogenic adipocytes can be mediated by various hormones and their signaling cascades, including those important pathways we describe in this review. Understanding the precise molecular mechanisms underlying regulation of thermogenesis and browning of WAT is critical for advancement of the future anti-obesity therapeutics.

AUTHOR CONTRIBUTIONS

CT drafted and HS revised the manuscript. All authors contributed to the article and approved the submitted version.

FUNDING

The work was supported in part by DK120075 to HSS.

REFERENCES

1. Nedergaard J, Cannon B. Brown adipose tissue as a heat-producing thermoeffector. *Handb Clin Neurol* (2018) 156:137–52. doi: 10.1016/B978-0-444-63912-7.00009-6
2. Lidell ME. Brown Adipose Tissue in Human Infants. In: A Pfeifer, M Klingenspor, S Herzig, editors. *Brown Adipose Tissue*. Cham: Springer International Publishing (2019). p. 107–23.
3. Wang Q, Zhang M, Xu M, Gu W, Xi Y, Qi L, et al. Brown adipose tissue activation is inversely related to central obesity and metabolic parameters in adult human. *PloS One* (2015) 10(4):e0123795. doi: 10.1371/journal.pone.0123795
4. Saito M. Brown adipose tissue as a regulator of energy expenditure and body fat in humans. *Diabetes Metab J* (2013) 37(1):22–9. doi: 10.4093/dmj.2013.37.1.22
5. Fenzl A, Kiefer FW. Brown adipose tissue and thermogenesis. *Hormone Mol Biol Clin Invest* (2014) 19(1):1868–91. doi: 10.1515/hmbci-2014-0022
6. Lattin JE, Schroder K, Su AI, Walker JR, Zhang J, Wiltshire T, et al. Expression analysis of G Protein-Coupled Receptors in mouse macrophages. *Immunome Res* (2008) 4:5. doi: 10.1186/1745-7580-4-5
7. Chouchani ET, Kazak L, Spiegelman BM. New Advances in Adaptive Thermogenesis: UCP1 and Beyond. *Cell Metab* (2018) 29(1):27–37. doi: 10.1016/j.cmet.2018.11.002
8. Herz CT, Kiefer FW. Adipose tissue browning in mice and humans. *J Endocrinol* (2019) 241(3):R97–109. doi: 10.1530/JOE-18-0598
9. Wu J, Boström P, Sparks LM, Ye L, Choi JH, Giang A-H, et al. Beige adipocytes are a distinct type of thermogenic fat cell in mouse and human. *Cell* (2012) 150(2):366–76. doi: 10.1016/j.cell.2012.05.016
10. Shao M, Wang QA, Song A, Vishvanath L, Busbuso NC, Scherer PE, et al. Cellular Origins of Beige Fat Cells Revisited. *Diabetes* (2019) 68(10):1874–85. doi: 10.2337/db19-0308
11. Wang W, Seale P. Control of brown and beige fat development. *Nat Rev Mol Cell Biol* (2016) 17(11):691–702. doi: 10.1038/nrm.2016.96
12. Rajakumari S, Wu J, Ishibashi J, Lim H-W, Giang A-H, Won K-J, et al. EBF2 determines and maintains brown adipocyte identity. *Cell Metab* (2013) 17(4):562–74. doi: 10.1016/j.cmet.2013.01.015
13. Seale P, Bjork B, Yang W, Kajimura S, Chin S, Kuang S, et al. PRDM16 controls a brown fat/skeletal muscle switch. *Nature* (2008) 454(7207):961–7. doi: 10.1038/nature07182
14. Park JH, Kang HJ, Kang SI, Lee JE, Hur J, Ge K, et al. A multifunctional protein, EWS, is essential for early brown fat lineage determination. *Dev Cell* (2013) 26(4):393–404. doi: 10.1016/j.devcel.2013.07.002
15. Inagaki T, Sakai J, Kajimura S. Transcriptional and epigenetic control of brown and beige adipose cell fate and function. *Nat Rev Mol Cell Biol* (2016) 17(8):480–95. doi: 10.1038/nrm.2016.62
16. Dempersmier J, Sambeat A, Gulyaeva O, Paul SM, Hudak CSS, Raposo HF, et al. Cold-inducible Zfp516 activates UCP1 transcription to promote browning of white fat and development of brown fat. *Mol Cell* (2015) 57(2):235–46. doi: 10.1016/j.molcel.2014.12.005
17. Yi D, Dempersmier JM, Nguyen HP, Viscarra JA, Dinh J, Tabuchi C, et al. Zc3h10 Acts as a Transcription Factor and Is Phosphorylated to Activate the Thermogenic Program. *Cell Rep* (2019) 29(9):2621–33.e4. doi: 10.1016/j.celrep.2019.10.099
18. Koppen A, Kalkhoven E. Brown vs white adipocytes: the PPARgamma coregulator story. *FEBS Lett* (2010) 584(15):3250–9. doi: 10.1016/j.febslet.2010.06.035
19. Kajimura S, Seale P, Kubota K, Lunsford E, Frangioni JV, Gygi SP, et al. Initiation of myoblast to brown fat switch by a PRDM16-C/EBP-beta transcriptional complex. *Nature* (2009) 460(7259):1154–8. doi: 10.1038/nature08262
20. Gill JA, La Merrill MA. An emerging role for epigenetic regulation of Pgc-1α expression in environmentally stimulated brown adipose thermogenesis. *Environ Epigenet* (2017) 3(2):dvx009. doi: 10.1093/eep/dvx009
21. Ikeda K, Maretich P, Kajimura S. The Common and Distinct Features of Brown and Beige Adipocytes. *Trends Endocrinol Metab* (2018) 29(3):191–200. doi: 10.1016/j.tem.2018.01.001
22. Yi D, Nguyen HP, Sul HS. Epigenetic dynamics of the thermogenic gene program of adipocytes. *Biochem J* (2020) 477(6):1137–48. doi: 10.1042/BCJ20190599
23. Reverte-Salisa L, Sanyal A, Pfeifer A. Brown Adipose Tissue: Role of cAMP and cGMP Signaling in Brown Fat. In: A Pfeifer, M Klingenspor, S Herzig, editors. *Brown Adipose Tissue*. Cham: Springer International Publishing (2019). p. 161–82.
24. Liu J, Wang Y, Lin L. Small molecules for fat combustion: targeting obesity. *Acta Pharm Sin B* (2019) 9(2):220–36. doi: 10.1016/j.apsb.2018.09.007
25. Schena G, Caplan MJ. Everything You Always Wanted to Know about β3-AR * (* But Were Afraid to Ask). *Cells* (2019) 8(4):357. doi: 10.3390/cells8040357
26. Shi F, Collins S. Second messenger signaling mechanisms of the brown adipocyte thermogenic program: an integrative perspective. *Hormone Mol Biol Clin Invest* (2017) 31(2):1868–91. doi: 10.1515/hmbci-2017-0062
27. Cao W, Daniel KW, Robidoux J, Puigserver P, Medvedev AV, Bai X, et al. p38 mitogen-activated protein kinase is the central regulator of cyclic AMP-dependent transcription of the brown fat uncoupling protein 1 gene. *Mol Cell Biol* (2004) 24(7):3057–67. doi: 10.1128/MCB.24.7.3057-3067.2004
28. Liang H, Ward WF. PGC-1alpha: a key regulator of energy metabolism. *Adv Physiol Educ* (2006) 30(4):145–51. doi: 10.1152/advan.00052.2006
29. Symonds ME. *Adipose Tissue Biology*. Cham: Springer (2017).
30. Kajimura S, Saito M. A new era in brown adipose tissue biology: molecular control of brown fat development and energy homeostasis. *Annu Rev Physiol* (2014) 76:225–49. doi: 10.1146/annurev-physiol-021113-170252
31. Blondin DP, Frisch F, Phoenix S, Guérin B, Turcotte ÉE, Haman F, et al. Inhibition of Intracellular Triglyceride Lipolysis Suppresses Cold-Induced Brown Adipose Tissue Metabolism and Increases Shivering in Humans. *Cell Metab* (2017) 25(2):438–47. doi: 10.1016/j.cmet.2016.12.005
32. Shin H, Ma Y, Chanturiya T, Cao Q, Wang Y, Kadegowda AKG, et al. Lipolysis in Brown Adipocytes Is Not Essential for Cold-Induced Thermogenesis in Mice. *Cell Metab* (2017) 26(5):764–77.e5. doi: 10.1016/j.cmet.2017.09.002
33. Braun K, Oeckl J, Westermeier J, Li Y, Klingenspor M. Non-adrenergic control of lipolysis and thermogenesis in adipose tissues. *J Exp Biol* (2018) 221(Pt Suppl 1):jeb165381. doi: 10.1242/jeb.165381
34. Nguyen HP, Yi D, Lin F, Viscarra JA, Tabuchi C, Ngo K, et al. Aifm2, a NADH Oxidase, Supports Robust Glycolysis and Is Required for Cold- and Diet-Induced Thermogenesis. *Mol Cell* (2020) 77(3):600–17.e4. doi: 10.1016/j.molcel.2019.12.002
35. Boucher J, Mori MA, Lee KY, Smyth G, Liew CW, Macotela Y, et al. Impaired thermogenesis and adipose tissue development in mice with fat-specific disruption of insulin and IGF-1 signalling. *Nat Commun* (2012) 3:902. doi: 10.1038/ncomms1905
36. Boucher J, Softic S, El Ouaamari A, Krumpoch MT, Kleinridders A, Kulkarni RN, et al. Differential Roles of Insulin and IGF-1 Receptors in Adipose Tissue Development and Function. *Diabetes* (2016) 65(8):2201–13. doi: 10.2337/db16-0212
37. Guerra C, Navarro P, Valverde AM, Arribas M, Brüning J, Kozak LP, et al. Brown adipose tissue-specific insulin receptor knockout shows diabetic phenotype without insulin resistance. *J Clin Invest* (2001) 108(8):1205–13. doi: 10.1172/JCI13103
38. Valverde AM, Lorenzo M, Pons S, White MF, Benito M. Insulin receptor substrate (IRS) proteins IRS-1 and IRS-2 differential signaling in the insulin/insulin-like growth factor-I pathways in fetal brown adipocytes. *Mol Endocrinol* (1998) 12(5):688–97. doi: 10.1210/mend.12.5.0106
39. Viana-Huete V, Guillén C, García-Aguilar A, García G, Fernández S, Kahn CR, et al. Essential Role of IGFIR in the Onset of Male Brown Fat Thermogenic Function: Regulation of Glucose Homeostasis by Differential Organ-Specific Insulin Sensitivity. *Endocrinology* (2016) 157(4):1495–511. doi: 10.1210/en.2015-1623
40. Huang W, Queen NJ, McMurphy TB, Ali S, Cao L. Adipose PTEN regulates adult adipose tissue homeostasis and redistribution via a PTEN-leptin-sympathetic loop. *Mol Metab* (2019) 30:48–60. doi: 10.1016/j.molmet.2019.09.008
41. Ortega-Molina A, Efeyan A, Lopez-Guadamillas E, Muñoz-Martin M, Gómez-López G, Cañamero M, et al. Pten positively regulates brown adipose function, energy expenditure, and longevity. *Cell Metab* (2012) 15(3):382–94. doi: 10.1016/j.cmet.2012.02.001
42. Klein J, Fasshauer M, Ito M, Lowell BB, Benito M, Kahn CR. β3-Adrenergic Stimulation Differentially Inhibits Insulin Signaling and Decreases Insulin-induced Glucose Uptake in Brown Adipocytes. *J Biol Chem* (1999) 274(49):34795–802. doi: 10.1074/jbc.274.49.34795

43. Wang X, Wahl R. Responses of the insulin signaling pathways in the brown adipose tissue of rats following cold exposure. *PloS One* (2014) 9(6):e99772. doi: 10.1371/journal.pone.0099772
44. Yau WW, Yen PM. Thermogenesis in Adipose Tissue Activated by Thyroid Hormone. *Int J Mol Sci* (2020) 21(8):3020. doi: 10.3390/ijms21083020
45. Ribeiro MO, Carvalho SD, Schultz JJ, Chiellini G, Scanlan TS, Bianco AC, et al. Thyroid hormone–sympathetic interaction and adaptive thermogenesis are thyroid hormone receptor isoform–specific. *J Clin Invest* (2001) 108 (1):97–105. doi: 10.1172/JCI200112584
46. Ribeiro MO, Bianco SDC, Kaneshige M, Schultz JJ, Cheng S-Y, Bianco AC, et al. Expression of uncoupling protein 1 in mouse brown adipose tissue is thyroid hormone receptor-beta isoform specific and required for adaptive thermogenesis. *Endocrinology* (2010) 151(1):432–40. doi: 10.1210/en.2009-0667
47. Chen W, Yang Q, Roeder RG. Dynamic interactions and cooperative functions of PGC-1alpha and MED1 in TRalpha-mediated activation of the brown-fat-specific UCP-1 gene. *Mol Cell* (2009) 35(6):755–68. doi: 10.1016/j.molcel.2009.09.015
48. Martinez de Mena R, Scanlan TS, Obregon M-J. The T3 receptor beta1 isoform regulates UCP1 and D2 deiodinase in rat brown adipocytes. *Endocrinology* (2010) 151(10):5074–83. doi: 10.1210/en.2010-0533
49. de Jesus LA, Carvalho SD, Ribeiro MO, Schneider M, Kim SW, Harney JW, et al. The type 2 iodothyronine deiodinase is essential for adaptive thermogenesis in brown adipose tissue. *J Clin Invest* (2001) 108(9):1379–85. doi: 10.1172/JCI200113803
50. Yau WW, Singh BK, Lesmana R, Zhou J, Sinha RA, Wong KA, et al. Thyroid hormone (T3) stimulates brown adipose tissue activation via mitochondrial biogenesis and MTOR-mediated mitophagy. *Autophagy* (2019) 15(1):131–50. doi: 10.1080/15548627.2018.1511263
51. Lee J-Y, Takahashi N, Yasubuchi M, Kim Y-I, Hashizaki H, Kim M-J, et al. Triiodothyronine induces UCP-1 expression and mitochondrial biogenesis in human adipocytes. *Am J Physiol Cell Physiol* (2012) 302(2):C463–72. doi: 10.1152/ajpcell.00010.2011
52. Krause K. Novel Aspects of White Adipose Tissue Browning by Thyroid Hormones. *Exp Clin Endocrinol Diabetes* (2020) 128(6-07):446–9. doi: 10.1055/a-1020-5354
53. Johann K, Cremer AL, Fischer AW, Heine M, Pensado ER, Resch J, et al. Thyroid-Hormone-Induced Browning of White Adipose Tissue Does Not Contribute to Thermogenesis and Glucose Consumption. *Cell Rep* (2019) 27 (11):3385–400.e3. doi: 10.1016/j.celrep.2019.05.054
54. Matesanz N, Bernardo E, Acín-Pérez R, Manieri E, Pérez-Sieira S, Hernández-Cosido L, et al. MKK6 controls T3-mediated browning of white adipose tissue. *Nat Commun* (2017) 8(1):856. doi: 10.1038/s41467-017-00948-z
55. Louzada RA, Carvalho DP. Similarities and Differences in the Peripheral Actions of Thyroid Hormones and Their Metabolites. *Front Endocrinol* (2018) 9:394. doi: 10.3389/fendo.2018.00394
56. Lombardi A, Senese R, De Matteis R, Busiello RA, Cioffi F, Goglia F, et al. 3,5-Diiodo-L-thyronine activates brown adipose tissue thermogenesis in hypothyroid rats. *PloS One* (2015) 10(2):e0116498. doi: 10.1371/journal.pone.0116498
57. Senese R, Cioffi F, De Matteis R, Petito G, de Lange P, Silvestri E, et al. 3,5 Diiodo-l-Thyronine (T_2) Promotes the Browning of White Adipose Tissue in High-Fat Diet-Induced Overweight Male Rats Housed at Thermoneutrality. *Cells* (2019) 8(3):256. doi: 10.3390/cells8030256
58. Tseng Y-H, Kokkotou E, Schulz TJ, Huang TL, Winnay JN, Taniguchi CM, et al. New role of bone morphogenetic protein 7 in brown adipogenesis and energy expenditure. *Nature* (2008) 454(7207):1000–4. doi: 10.1038/nature07221
59. Townsend KL, An D, Lynes MD, Huang TL, Zhang H, Goodyear LJ, et al. Increased mitochondrial activity in BMP7-treated brown adipocytes, due to increased CPT1- and CD36-mediated fatty acid uptake. *Antioxid Redox Signal* (2013) 19(3):243–57. doi: 10.1089/ars.2012.4536
60. Boon MR, van den Berg SAA, Wang Y, van den Bossche J, Karkampouna S, Bauwens M, et al. BMP7 activates brown adipose tissue and reduces diet-induced obesity only at subthermoneutrality. *PloS One* (2013) 8(9):e74083. doi: 10.1371/journal.pone.0074083
61. Okla M, Ha J-H, Temel RE, Chung S. BMP7 drives human adipogenic stem cells into metabolically active beige adipocytes. *Lipids* (2015) 50(2):111–20. doi: 10.1007/s11745-014-3981-9
62. Whittle AJ, Carobbio S, Martins L, Slawik M, Hondares E, Vázquez MJ, et al. BMP8B increases brown adipose tissue thermogenesis through both central and peripheral actions. *Cell* (2012) 149(4):871–85. doi: 10.1016/j.cell.2012.02.066
63. Pellegrinelli V, Peirce VJ, Howard L, Virtue S, Türei D, Senzacqua M, et al. Adipocyte-secreted BMP8b mediates adrenergic-induced remodeling of the neuro-vascular network in adipose tissue. *Nat Commun* (2018) 9(1):4974. doi: 10.1038/s41467-018-07453-x
64. Yadav H, Quijano C, Kamaraju AK, Gavrilova O, Malek R, Chen W, et al. Protection from obesity and diabetes by blockade of TGF-β/Smad3 signaling. *Cell Metab* (2011) 14(1):67–79. doi: 10.1016/j.cmet.2011.04.013
65. Wankhade UD, Lee J-H, Dagur PK, Yadav H, Shen M, Chen W, et al. TGF-β receptor 1 regulates progenitors that promote browning of white fat. *Mol Metab* (2018) 16:160–71. doi: 10.1016/j.molmet.2018.07.008

Conflict of Interest: The authors declare that the research was conducted in the absence of any commercial or financial relationships that could be construed as a potential conflict of interest.

frontiers in Endocrinology

CORRECTION
published: 22 June 2021
doi: 10.3389/fendo.2021.698619

Corrigendum: Signaling Pathways Regulating Thermogenesis

Chihiro Tabuchi and Hei Sook Sul *

Department of Nutritional Sciences and Toxicology, University of California, Berkeley, Berkeley, CA, United States

Keywords: thermogenesis, brown adipose tissue, browning/beiging, β3-adrenergic signaling, UCP1, insulin/IGF1 signaling, thyroid hormone, TGFβ superfamily

A Corrigendum on

Signaling Pathways Regulating Thermogenesis
By Tabuchi C and Sul HS (2021). Front. Endocrinol. 12:595020. doi: 10.3389/fendo.2021.595020

OPEN ACCESS

Edited and reviewed by:
Jiqiu Wang,
Shanghai Jiao Tong University, China

***Correspondence:**
Hei Sook Sul
hsul@berkeley.edu

Specialty section:
This article was submitted to Cellular Endocrinology, a section of the journal Frontiers in Endocrinology

Received: *21 April 2021*
Accepted: *02 June 2021*
Published: *22 June 2021*

Citation:
Tabuchi C and Sul HS (2021) Corrigendum: Signaling Pathways Regulating Thermogenesis. Front. Endocrinol. 12:698619. doi: 10.3389/fendo.2021.698619

In the original article, there were errors in **Figures 1** and **2**. In **Figure 1**, IRF4 had to be removed and the order of the transcription factors had to be reorganized during this correction**.** In **Figure 2**, SMAD2 needs to be removed. The corrected **Figures 1** and **2** are below.

In the original article, there were errors in the text. IRF4 needed to be replaced with PGC1α as a downstream target of p38. PGC1α and DIO needed to be removed as downstream targets of CREB, due to insufficient research.

A correction has been made to the section **β_3-Adrenergic Signaling**, the second paragraph:

"p38, a MAP kinase, phosphorylates multiple transcription factors/coregulators, including ATF2 and PGC1α, both of which promote UCP1 transcription (22). In addition, we recently found that ZC3H10, previously known to bind RNA, is phosphorylated by p38 upon cold, activating the thermogenic gene program in adipocytes (17). Specifically, ZC3H10 binds a distal upstream region of the UCP1 promoter for transcriptional activation. ZC3H10 also activates NRF1 and TFAM, which facilitate mitochondrial biogenesis to increase thermogenic capacity of adipocytes. Thus, transgenic mice overexpressing ZC3H10 exhibited increased oxygen consumption, higher BAT temperature and reduced body weight while ZC3H10 knockout mice displayed decreased oxygen consumption, lower BAT temperature and increased body weight. PGC1α, a downstream target of p38, serves as co-activator for PPARγ and NRF1 to induce expression of UCP1 and TFAM, respectively (27, 28). CREB was also shown to bind to the proximal promoter of UCP1 to potentially activate the transcription."

The authors apologize for these errors and state that this does not change the scientific conclusions of the article in any way. The original article has been updated.

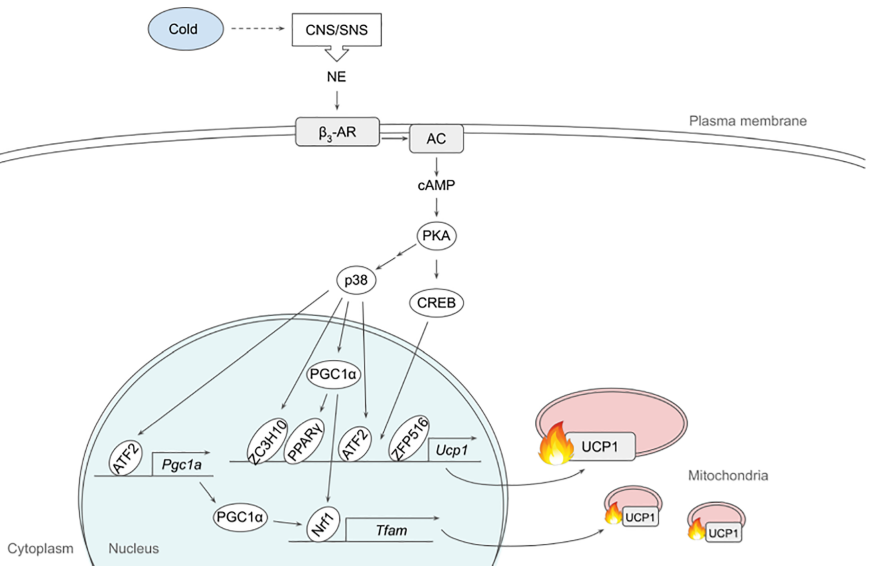

FIGURE 1 | Schematic model of β_3-adrenergic signaling pathway that promotes thermogenesis in adipocytes. Cold stimulates CNS/SNS to secrete NE that binds β_3-AR, which then activates AC producing cAMP. cAMP in turn activates PKA that has a variety of downstream targets, including transcription factors to upregulate thermogenic gene expression. See text for details. AC, adenylate cyclase; ATF2, activating transcription factor 2; β_3-AR, β_3-adrenergic receptor; CNS, central nervous system; CREB, cAMP response-element binding protein; ETC, electron transport chain; FFA, free fatty acid; IRF4, interferon regulatory factor 4; NE, norepinephrine; NRF1, nuclear respiratory factor 1; PGC1α, peroxisome proliferator activated receptor γ coactivator α; PKA, protein kinase A; PPARγ, peroxisome proliferator activated receptor γ; SNS sympathetic nervous system; TCA, tricarboxylic acid; TFAM, mitochondrial transcription factor A; UCP1, uncoupling protein 1; ZC3H10, zinc finger CCCH-type containing 10; ZFP516, zinc finger protein 516.

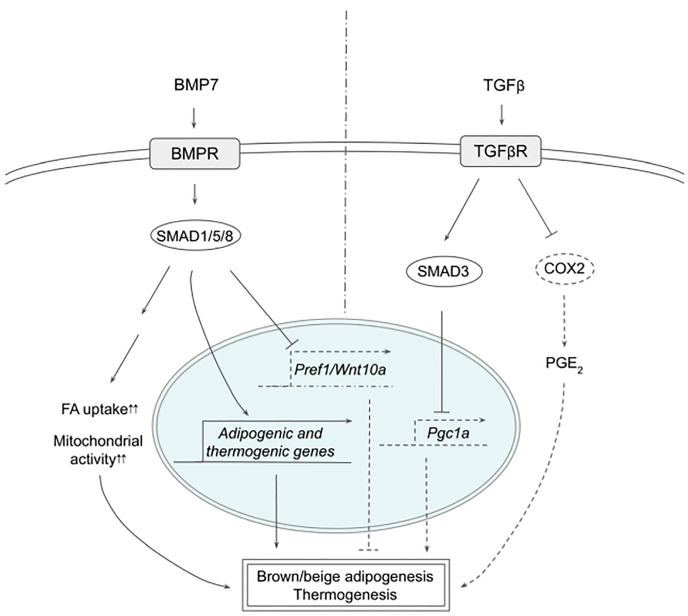

FIGURE 2 | Schematic models of BMP7 and TGFβ signaling pathways in thermogenesis. BMP7 binds TGFβR, which activates SMAD1/5/8, leading to expression of adipogenic and thermogenic genes as well as suppression of Pref1 and Wnt10a in precursor cells to promote brown and beige adipogenesis. In mature adipocytes, BMP7 signaling increases FA uptake and mitochondrial activity, resulting in enhanced thermogenesis. TGFβ activates SMAD2/3 that suppresses PGC1α expression and COX2/PGE2 pathway to reduce thermogenesis. See text for details. BMP7, bone morphogenetic protein 7; COX2, cyclooxygenase 2; FA, fatty acid; PGC1α, peroxisome proliferator activated receptor γ; PGE2, prostaglandin E2; PREF1, preadipocyte factor 1; SMAD, mothers against decapentaplegic homolog; TβR1, TGFβ receptor 1; TGFβ, Transforming growth factor beta; TGFβR, TGFβ receptor; WNT10a, Wnt family member 10A.

REFERENCES

17. Yi D, Dempersmier JM, Nguyen HP, Viscarra JA, Dinh J, Tabuchi C, et al. Zc3h10 Acts as a Transcription Factor and Is Phosphorylated to Activate the Thermogenic Program. *Cell Rep* (2019) 29(9):2621–33.e4. doi: 10.1016/j.celrep.2019.10.099
22. Yi D, Nguyen HP, Sul HS. Epigenetic Dynamics of the Thermogenic Gene Program of Adipocytes. *Biochem J* (2020) 477(6):1137–48. doi: 10.1042/BCJ20190599
27. Cao W, Daniel KW, Robidoux J, Puigserver P, Medvedev AV, Bai X, et al. p38 Mitogen-Activated Protein Kinase Is the Central Regulator of Cyclic AMP-Dependent Transcription of the Brown Fat Uncoupling Protein 1 Gene. *Mol Cell Biol* (2004) 24(7):3057–67. doi: 10.1128/MCB.24.7.3057-3067.2004
28. Liang H, Ward WF. PGC-1alpha: A Key Regulator of Energy Metabolism. *Adv Physiol Educ* (2006) 30(4):145–51. doi: 10.1152/advan.00052.2006

frontiers in Endocrinology

REVIEW
published: 31 March 2021
doi: 10.3389/fendo.2021.653972

The Role of Mondo Family Transcription Factors in Nutrient-Sensing and Obesity

Huiyi Ke†, *Yu Luan*†, *Siming Wu*†, *Yemin Zhu and Xuemei Tong**

Department of Biochemistry and Molecular Cell Biology, Shanghai Key Laboratory for Tumor Microenvironment and Inflammation, Key Laboratory of Cell Differentiation and Apoptosis of Chinese Ministry of Education, Shanghai Jiao Tong University School of Medicine, Shanghai, China

In the past several decades obesity has become one of the greatest health burdens worldwide. Diet high in fats and fructose is one of the main causes for the prevalence of metabolic disorders including obesity. Promoting brown or beige adipocyte development and activity is regarded as a potential treatment of obesity. Mondo family transcription factors including MondoA and carbohydrate response element binding protein (ChREBP) are critical for nutrient-sensing in multiple metabolic organs including the skeletal muscle, liver, adipose tissue and pancreas. Under normal nutrient conditions, MondoA and ChREBP contribute to maintaining metabolic homeostasis. When nutrient is overloaded, Mondo family transcription factors directly regulate glucose and lipid metabolism in brown and beige adipocytes or modulate the crosstalk between metabolic organs. In this review, we aim to provide an overview of recent advances in the understanding of MondoA and ChREBP in sensing nutrients and regulating obesity or related pathological conditions.

Keywords: MondoA, ChREBP, nutrient-sensing, obesity, brown and beige adipose tissue

OPEN ACCESS

Edited by:
Xinran Ma,
East China Normal University, China

Reviewed by:
Farnaz Shamsi,
Joslin Diabetes Center and Harvard Medical School, United States
Fang Hu,
Central South University, China

****Correspondence:***
Xuemei Tong
xuemeitong@shsmu.edu.cn

†These authors have contributed equally to this work and share first authorship

Specialty section:
This article was submitted to Cellular Endocrinology, a section of the journal Frontiers in Endocrinology

Received: *15 January 2021*
Accepted: *15 March 2021*
Published: *31 March 2021*

Citation:
Ke H, Luan Y, Wu S, Zhu Y and Tong X (2021) The Role of Mondo Family Transcription Factors in Nutrient-Sensing and Obesity. Front. Endocrinol. 12:653972. doi: 10.3389/fendo.2021.653972

INTRODUCTION

The epidemic of obesity has emerged as a worldwide public health issue. In 2017, the Global Burden of Disease Study estimated that high body mass index (BMI), one of the leading risk factors, accounted for 4.72 million deaths and 148 million disability-adjusted life-years (DALYs) (1). Excessive caloric intake mainly derived from the high-fat and high-fructose diet is a major cause for obesity (2–4). The urgent need for weight-loss treatments has given rise to multiple attempts to target cellular metabolism and restore systemic energy homeostasis, among which is the strategy of promoting brown and beige adipocyte activity and development. Brown adipocytes are essential for thermogenesis in mammals with their characteristic expression of uncoupling protein-1 (UCP1) in mitochondria, while beige adipocytes are inducible to express thermogenic genes in response to stimulus (5). Enhancing activities of brown and beige adipocytes not only promotes energy expenditure through heat generation, but also enhances glucose metabolism and protects against insulin resistance (6–11), which provides promising therapeutic effects to counteract obesity and related diseases.

The Mondo family transcription factors, comprised of MondoA (also known as MLXIP) and carbohydrate response element binding protein (ChREBP, also named MondoB and MLXIPL),

belong to the basic helix-loop-helix leucine zipper (bHLH/LZ) family (12, 13). Upon binding to their heteromeric partner MLX (Max-like protein X), Mondo and MLX translocate to the nucleus where they bind to carbohydrate response elements (ChoREs) on target gene promoters, and stimulate a transcriptional response to nutrients (12–14). As a structural basis of their nutrient-sensing and responsiveness, the glucose-sensing module (GSM) of Mondo proteins consists of a low-glucose inhibitory domain (LID) and a glucose-response activation conserved element (GRACE) (**Figure 1**). Under basal conditions, GRACE is repressed by the LID domain, which is relieved by alterations in nutrient levels such as the elevation of glucose concentration (15). An isoform of ChREBP, ChREBPβ, lacks the LID domain and is induced by the activation of the canonical isoform ChREBPα (16). Upon activation, MondoA and ChREBP bind to importin-α which mediates their nuclear entry (17), while their nuclear export and cytoplasmic retention are regulated by chromosome region maintenance protein 1 (CRM1) and 14–3-3 proteins (18–20). Though similar in structure, MondoA and ChREBP have distinct tissue distribution patterns, with MondoA predominantly in skeletal muscle and immune cells and ChREBP in liver and adipose tissue (12, 13), and our unpublished data.

Initially identified as glucose sensors, Mondo family has more extensive regulatory functions in metabolic homeostasis. Therefore, their role in physiological and pathological conditions has gained growing interest. In this review, we will discuss how MondoA and ChREBP sense and respond to nutrient availability, focusing on the involvement of Mondo family in obesity and related diseases.

NUTRIENT-SENSING BY MONDOA AND CHREBP

ChREBP in Metabolic Organs

ChREBP is widely expressed in metabolic organs, predominantly in liver, also in adipose tissues, pancreas, intestine, kidney, relatively low in skeletal muscle (21).

ChREBP is regulated by multiple nutrient molecules, among which glucose and its metabolites are major determinants. In the presence of high glucose, glucose 6-phosphate (G6P), the first intermediate in glycolysis binds to the GRACE domain of ChREBP (22, 23). Moreover, xylulose 5-phosphate (Xu5P), the metabolite generated through the pentose phosphate pathway, activates protein phosphatase 2A (PP2A), and the sequential

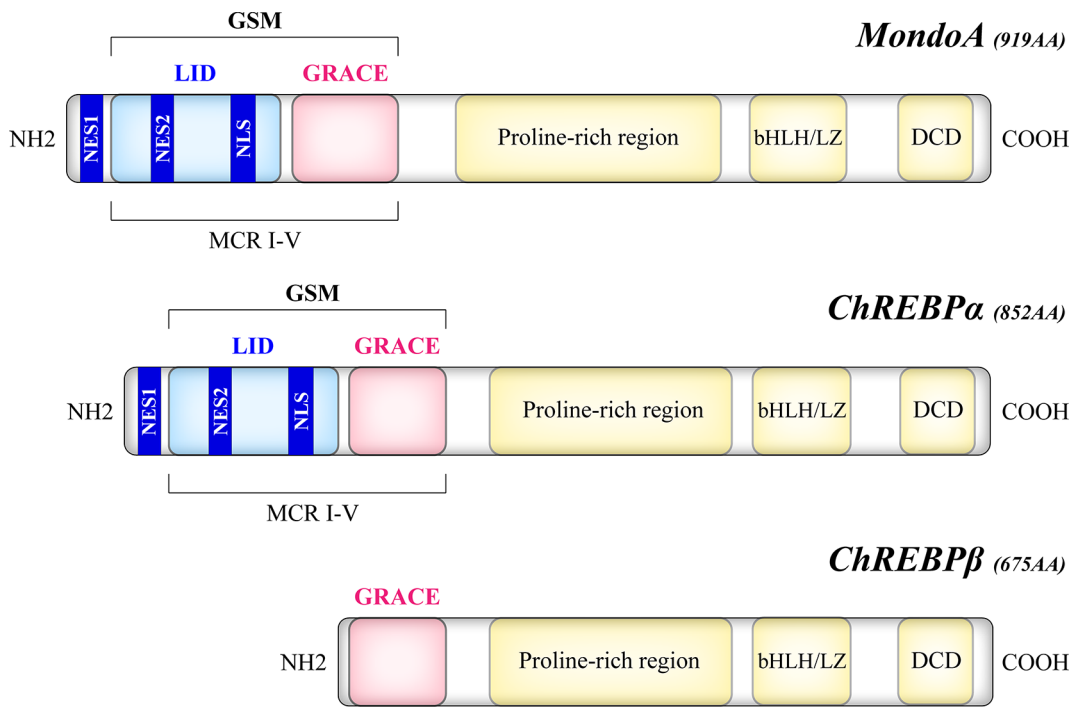

FIGURE 1 | Structural domains of the human Mondo proteins. MondoA and ChREBP contain homologous C-termini, where a bHLH/LZ region and a dimerization and cytoplasmic localization domain (DCD) mediate the heterodimerization process and DNA binding. On the other hand, the N-termini of MondoA and ChREBP determine their glucose responsiveness. The glucose-sensing module (GSM) lies within the N-terminal region of MondoA and ChREBPα and is composed of a low-glucose inhibitory domain (LID) and a glucose-response activation conserved element (GRACE). Compared with the canonical ChREBPα of 852 amino acids, the ChREBPβ isoform, a product of alternative splicing, is a 675-amino acid protein that lacks the LID domain. The N-terminal region also includes five Mondo conserved regions (MCR I-V), with LID spanning MCR I-IV and GRACE harboring MCR V. Two nuclear export signals (NES1, NES2) correspond to the binding site of CRM1, while a nuclear localization signal (NLS) allows the interaction with importin-α.

dephosphorylation of several residues activates ChREBP (24). Furthermore, fructose-2,6-bisphosphate (F2,6-BP) derived from fructose-6-phosphate (F6P) has been identified as another signaling metabolite responsible for glucose-induced recruitment of ChREBP to its target genes (25). On the other hand, when glucose is limited, branched chain keto-amino acids (BCKA) and fatty acids (FA) inhibit ChREBP activity (26, 27) (**Figure 2**).

ChREBP regulates many enzyme genes in glycolysis and lipogenesis, including liver type pyruvate kinase (L-PK), acetyl-CoA carboxylase (ACC), fatty acid synthase (FAS), ATP-citrate lyase (ACLY), stearoyl-CoA desaturase-1 (SCD1) and glycerol-3-phosphate dehydrogenase (GPDH) (28–30). In addition, ChREBP may control very low-density lipoprotein (VLDL) export by regulating microsomal triglyceride transfer protein (MTTP) transcription (31) (**Figure 3**).

Mouse models with knockout or overexpression of the ChREBP gene provide direct evidence for its role in glucose and lipid metabolism (**Table 1**). ChREBP global knockout mice show down-regulated pyruvate production and inhibited glycolysis, with lower mRNA levels of ACC, FAS, ACLY and SCD1 in liver than wild-type mice, leading to a significant decrease in lipids converted from glucose (32). ChREBP liver-specific knockout mice showed dysregulation of glucose response and impaired glucose homeostasis (34). Moreover, adenoviral overexpression of ChREBP caused higher liver triglyceride contents with increased FAS and ACC expression (35, 46). It is now believed that ChREBP and sterol regulatory element binding protein-1c (SREBP-1c) play a synergistic role in the regulation of lipogenesis in liver (47). Moreover, the expression of the ChREBPβ isoform is associated with the respective increase and repression of branched chain alpha-keto acid dehydrogenase kinase (BDK) and protein phosphatase Mg^{2+}/Mn^{2+}-dependent 1K (PPM1K) transcript levels in liver (48). In addition, the transcription of fibroblast growth factor 21 (FGF21) is regulated by ChREBP (49). FGF21 is involved in energy metabolism by regulating carbohydrate intake (50). Fructose ingestion increases FGF21 production in a ChREBP-dependent manner while FGF21 knockout attenuates ChREBP expression and *de novo* lipogenesis following fructose consumption, indicating that ChREBP and FGF21 constitute a signaling axis which mediates an adaptive hepatic metabolic response to fructose ingestion (51).

MondoA in Metabolic Organs

As another transcriptional biosensor of intracellular glucose concentration, MondoA contributes to more than 75% of glucose-induced transcription signature in HA1ER epithelial

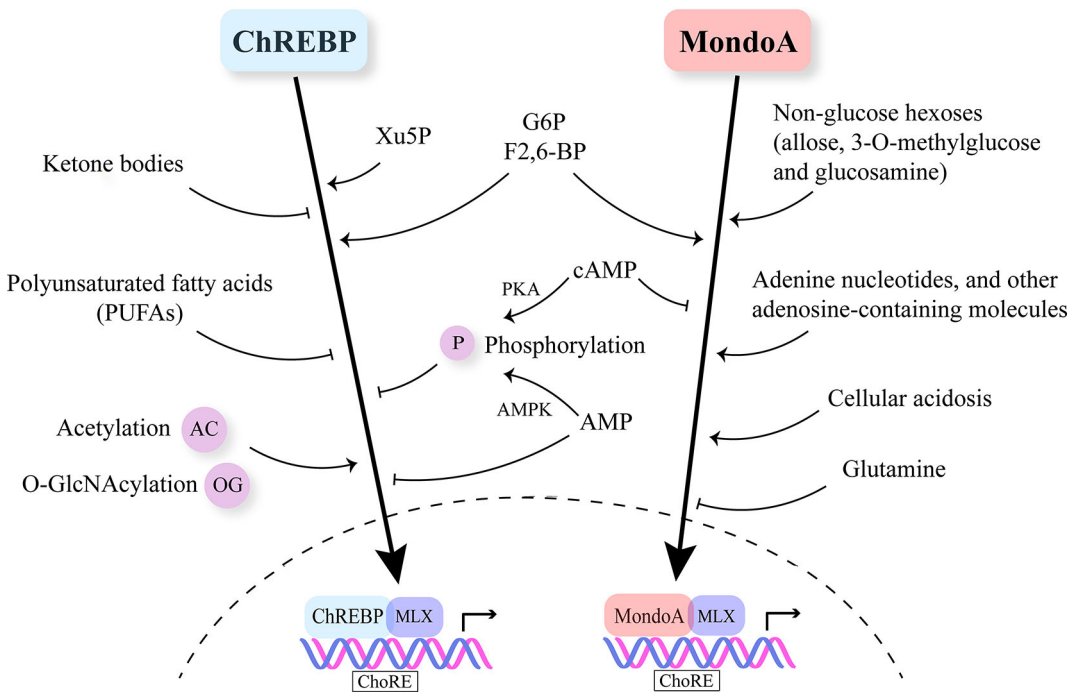

FIGURE 2 | Nutrient-sensing and regulation of Mondo family. Mondo family transcription factors sense multiple nutrients. G6P, F2,6-BP and Xu5P are considered the major metabolites through which glucose stimulates ChREBP and MondoA nuclear translocation and transcriptional activity. Ketone bodies and polyunsaturated fatty acids (PUFAs) are reported to inhibit ChREBP activity. MondoA activators include non-glucose hexoses, adenosine-containing molecules and cellular acidosis. Glutamine represses MondoA transcriptional activity. Post-transcriptional modifications (PTMs) including phosphorylation, acetylation and O-GlcNAcylation also play a role in regulating Mondo family, especially ChREBP. cAMP is a common inhibitor of ChREBP and MondoA. cAMP acts through PKA (protein kinase A) to promote the phosphorylation of ChREBP. Increased AMP levels lead to both retention of ChREBP in the cytosol and AMPK-induced phosphorylation of ChREBP, thus inhibiting ChREBP activity.

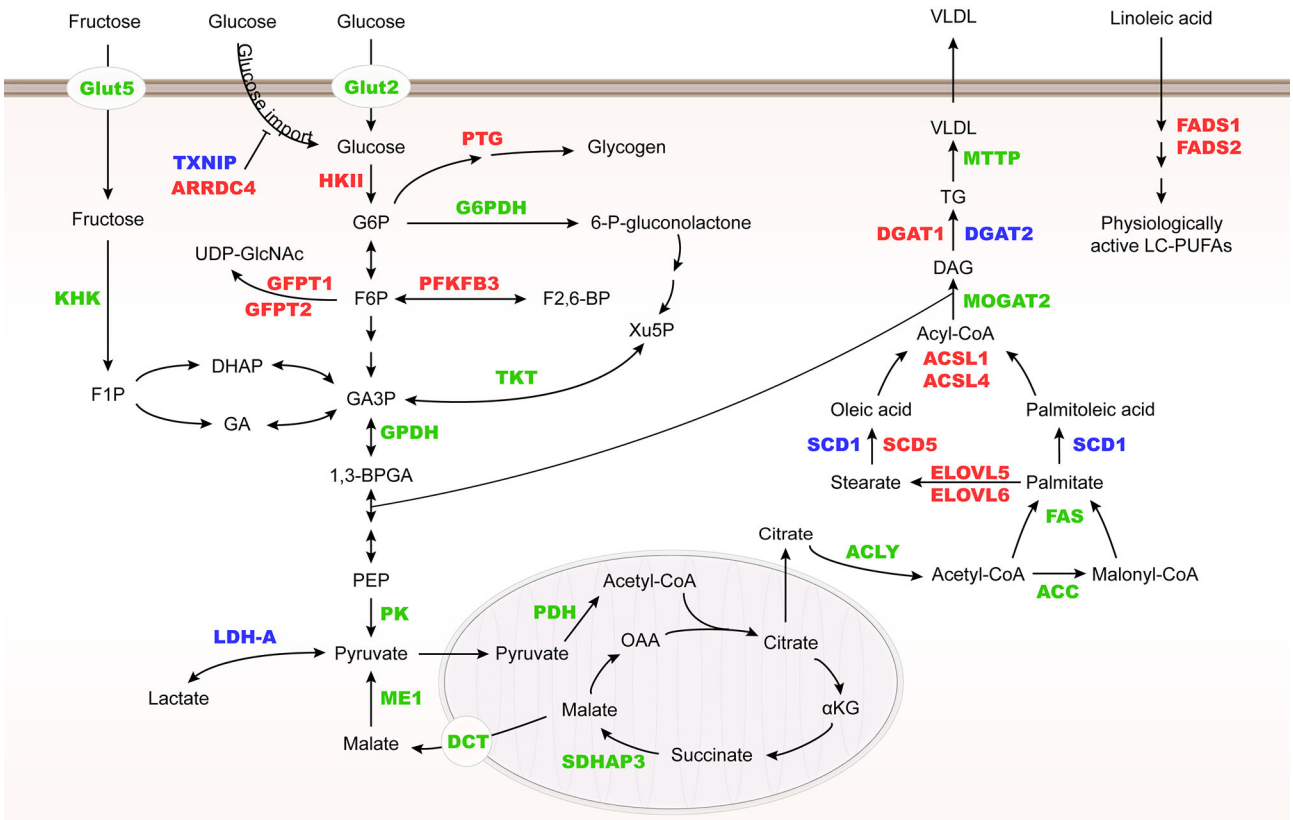

FIGURE 3 | Metabolic genes regulated by Mondo family. Metabolic genes regulated by MondoA and ChREBP at the transcriptional level are herein summarized. They are involved in glucose and fructose uptake, glycolysis, fructose metabolism, glycogenesis, hexosamine biosynthesis pathway (HBP), pentose phosphate pathway (PPP), and lipogenesis. MondoA targets are highlighted in red, ChREBP targets in green, and their common targets are in blue. HK II, hexokinase II; PTG, glycogen targeting protein; G6PDH, glucose-6-phosphate dehydrogenase; KHK, fructokinase; GFPT, glutamine:fructose-6-phosphate aminotransferase; PFKFB3, 6-phosphofructo-2-kinase/fructose-2,6-biphosphatase 3; TKT, transketolase; PK, pyruvate kinase; PDH, pyruvate dehydrogenase; SDHAP3, succinate dehydrogenase complex flavoprotein subunit A pseudogene 3; DCT, C4-dicarboxylate transport protein; ME1, malic enzyme; MOGAT2, monoacylglycerol O-acyltransferase 2; DGAT, diacylglycerol acyltransferase.

cells (52). By shuttling between mitochondria and nucleus, MondoA bridges cytoplasmic nutrient level to transcriptional adaptations. MondoA localizes to the outer mitochondrial membrane under basal conditions, and accumulates in the nucleus in response to nutrient signals such as high glucose (52, 53). In addition to nuclear accumulation, glucose triggers MondoA-MLX binding to target promoters, and activates gene expression through recruitment of histone H3 acetyltransferase as coactivators (54).

Similar to ChREBP, MondoA senses levels of G6P and F2,6-BP (52, 55) (**Figure 2**). Meanwhile, MondoA is responsive to non-glucose hexoses including allose and glucosamine (56). Intriguingly, glutamine recruits a histone deacetylase-dependent corepressor to MondoA, turning MondoA-MLX into a transcriptional repressor. Moreover, cellular acidosis drives MondoA transcriptional activity since low pH promotes the production of mitochondrial ATP, with which mitochondria-bound hexokinase generates G6P from cytoplasmic glucose (57). This finding has justified the special localization of MondoA-MLX and unraveled the mechanisms underlying the activation of MondoA by lactic acidosis. Other molecules reported to be sensed by MondoA include adenine nucleotides and other adenosine-containing molecules (58, 59). Furthermore, mTOR (mammalian target of rapamycin), another key nutrient sensor, interacts with MondoA with a suppressive effect on its transcriptional activity (60). Nonetheless, so far there is no report on fatty acids or amino acids regulating MondoA level or activity.

Different from ChREBP, MondoA is predominantly expressed in skeletal muscle and immune cells (12), and our unpublished data. MondoA-deficient mice show enhanced glycolytic rates probably because loss of MondoA in skeletal muscle increases glucose uptake (43) (**Table 1**). In response to glucose and fructose, MondoA activates transcription of thioredoxin interacting protein (TXNIP) and arrestin domain-containing 4 (ARRDC4), which inhibits glucose uptake (**Figure 3**) (56, 61). TXNIP, a dynamic sensor that modulates the energy demand of cells, plays a crucial role in the homeostasis of glucose.

TABLE 1 | Roles of Mondo family on body weight, hepatic steatosis and insulin sensitivity according to mouse models, depending on nutritional status, genetic background and drug administration.

Mondo family	Context	Modulation in Mouse Models	Body Weight	Fat Mass	Hepatic Steatosis	Insulin Sensitivity	Reference
ChREBP	Standard diet	Global knockout	=	↘	=	↘	(32, 33)
		Liver-specific knockout	=	↘	=	↘	(34)
		Liver-specific overexpression	=	↘	↗	=	(35)
		AT-specific knockout	=	=	↘	↘	(36)
		AT-specific overexpression	↘	↘	=	=	(37)
		Pancreatic β-cell-specific overexpression	↘	ND	ND	↘	(38)
	Standard diet in *ob/ob* mice background	Global knockout	↘	↘	↘	↗	(33)
		Liver-specific knockdown	↘	↘	↘	↗	(39)
	High-fat diet	Liver-specific knockout	=	=	=	↘	(34)
		Liver-specific overexpression	=	↘	↗	↗	(35)
		AT-specific knockout	=	=	=	↘	(36)
		AT-specific overexpression	↘	↘	↘	↗	(37)
	Western diet	Global knockout	↘	↘	↘	ND	(40)
	High-carbohydrate diet	Liver-specific knockout	↘	↘	↘	↘	(34)
	HFrD	Global knockout	↘	ND	↗	ND	(41)
		Liver-specific knockout	↘	↘	=	↗	(42)
MondoA	Standard diet	Global knockout	=	ND	ND	=	(43)
		Muscle-specific knockout	=	ND	ND	=	(44)
	High-fat diet	Muscle-specific knockout	=	ND	ND	↗	(44)
MondoA /ChREBP	High-fat diet	Administration of a compound (SBI-993) that deactivates MondoA/ChREBP signaling	↘	ND	↘	↗	(45)

"=" means not changed. ND, not determined. The upward and downward arrows indicate an increase and decrease in the level, respectively.

As a direct and glucose-responsive target of MondoA, TXNIP is upregulated when G6P level increases and concomitantly restricts glucose absorption, thus providing a negative feedback loop to prevent energy overload. Mechanisms underlying inhibition of glucose uptake regulated by TXNIP include the suppression of glucose transporter (GLUT) expression, GLUT vesicle transport and insulin signaling (44, 62–64). Moreover, MondoA enhances glycogen synthesis by activating the transcription of phosphoprotein phosphatase 1 regulatory subunit 3A (PPP1R3A), phosphoprotein phosphatase 1 regulatory subunit 3B (PPP1R3B) and genes encoding the glycogen targeting subunits of protein phosphatase 1 (PP1) for promoting glycogen synthesis (65, 66). Muscle-specific MondoA knockout decreases glycogen level in the skeletal muscle of mice (62) (**Table 1**). Hence, under physiological conditions, glucose homeostasis is maintained by the downstream effects of MondoA activation.

In addition to glucose metabolism, MondoA diverts nutrients to lipid metabolic pathways, including fatty acid thioesterification [acyl-CoA synthetase 1, 4 (ACSL1, 4)], desaturation [fatty acid desaturase 1,2 (FADS1, 2), SCD1, 5], elongation [elongation of very long chain fatty acids protein 5, 6 (ELOVL5, 6)], and triglyceride synthesis [diacylglycerol acyltransferase 1, 2 (DGAT1, 2)] (44) (**Figure 3**). Taken together, as a nutrient-regulated transcription factor, MondoA not only decreases glucose import but also diverts nutrients to storage in skeletal muscle. Although various posttranslational modifications of ChREBP have been revealed to regulate its activity in different conditions (67–69), there is so far no report on how MondoA is posttranslationally modified. Therefore, further mechanistic studies are needed to elucidate the interacting protein network of MondoA in response to nutrient level alterations.

THE ROLE OF MONDOA AND CHREBP IN OBESITY

ChREBP: From White to Brown and Beige Adipocytes

Obesity is the excessive accumulation of fat caused by imbalance between energy intake and consumption. It is the major risk factor for many metabolic disorders such as type 2 diabetes, fatty liver and cardiovascular diseases (70). Regarded as a crucial target for the prevention and treatment of obesity, the adipose tissue consists of white adipocytes which store energy, and brown and beige adipocytes which consume energy and produce heat (71). Inducing beige adipocytes from white adipose tissues (WAT) is known as browning, a process which improves glucose metabolism and insulin sensitivity (11). Various transcription and endocrine factors participate in this process by directly or indirectly stimulating UCP1 expression in adipose tissues, including peroxisome proliferator-activated receptor γ (PPARγ), PPARγ coactivator-1α (PGC-1α), silent information regulator type 1 (SIRT1) and FGF21 (72). The activation of brown and beige adipocytes is considered to be an attractive therapeutic strategy for obesity and its comorbidities. Brown and beige adipocytes serve as a sink for excessive nutrients by promoting energy expenditure in mitochondria (73).

ChREBP promotes lipogenesis in adipose tissues (36, 74). For high-carbohydrate diets, excessive fructose and glucose are converted to fatty acids, in which a series of enzymes including ACLY, ACC and FAS participate (75). The predominant destiny of the newly synthesized fatty acids is to become triglycerides for storage, which helps to maintain energy homeostasis (76). Adipocyte *de novo* lipogenesis is also involved in the regulation of systemic insulin sensitivity and thermogenesis, both of which

play key roles in mediating metabolic adaptations (21, 77). Overexpression of a constitutively active ChREBP isoform (caChREBP) in adipose tissues leads to an increase in expression of key enzymes involved in *de novo* lipogenesis (37). Conversely, adipocytes lacking ChREBP display impaired sucrose-induced lipogenesis (36). In WAT, Glut4-mediated glucose uptake induces ChREBP expression and activates the *de novo* lipogenic pathway. In Glut4 knockout mice, ChREBP expression in adipose tissues decreases by 50%. It is noteworthy that Glut4-mediated changes in glucose flux have a stronger effect on the transcriptional expression of ChREBPβ than ChREBPα in WAT (16). ChREBP activity in adipocytes depends on ACLY, one of its transcriptional targets. In the absence of ACLY, the expression of both ChREBP and its target genes is significantly suppressed. Consequently, ACLY and ChREBP form a positive feedback loop in adipocytes to foster dietary carbohydrates uptake, fatty acid synthesis and storage of lipids (78). Moreover, specific ablation of Rictor, the essential subunit of the mechanistic target of rapamycin complex 2 (mTORC2) in mature adipocytes reduces ChREBPβ expression and downregulates *de novo* lipogenesis in WAT and brown adipose tissue (BAT) (79). In mature brown adipocytes, AKT2, which can be phosphorylated by mTORC2, is required for lipogenesis driven by ChREBP activation (21, 80).

To date, the role of ChREBP in regulating thermogenic adipocyte function has been indicated in a growing body of literatures (**Figure 4**). Reduced brown fat mass and hypothermia in response to excess energy intake are observed in ChREBP-deficient mice (32). ChREBPβ and UCP1 expression levels positively correlate in human BAT, suggesting that ChREBPβ expression might indicate brown adipocyte activity (21). Under chronic cold exposure, specific impairment of ChREBP-driven lipogenesis in BAT promotes beige adipocyte development, which is probably a compensatory response (21). Moreover, studies in adipocytes exposed to high glucose show that ChREBP is a critical mediator in triiodothyronine-induced upregulation of UCP1 expression in brown adipocytes (81). However, there is no significant binding of ChREBP protein to the UCP1 promoter, indicating that ChREBP regulates UCP1 transcription indirectly (82), which awaits further study. In mice fed a chronic high sucrose diet, expression of UCP1 in BAT is significantly increased compared with controls, which is probably due to the activated ChREBP-FGF21 axis (83). Moreover, overexpression of constitutively active ChREBP in adipocytes induces PPARγ activity and upregulates its thermogenesis-related target genes including UCP1 that promotes browning of WAT, while depletion of endogenous ChREBP in adipocytes has reciprocal effects (84). Furthermore, adenoviral overexpression of ChREBP in mice increases mRNA level of white adipose tissue UCP1 with increased plasma FGF21 level (46). After ChREBPβ is identified, it is important to consider the functional difference between the two isoforms of ChREBP. Of note, overexpression of ChREBPβ in brown adipocytes leads to impaired BAT thermogenesis and WAT browning, reflecting the role of ChREBPβ as a feedback regulator upon cold exposure (82). Moreover, given the expression of ChREBP in metabolic organs and macrophages, global gain-of-function or loss-of-function mouse models of ChREBP may not be ideal for analyzing the role of ChREBP in adipose tissues. Additional studies will be needed to develop a full picture of the specific role and mechanism of the two isoforms of ChREBP in adipocyte thermogenesis.

MondoA: Inter-Organ Metabolic Crosstalk

MondoA is expressed predominantly in skeletal muscle which makes up ~40% of body weight and is responsible for ~80% of glucose uptake (62, 85). Therefore, as a transcriptional factor

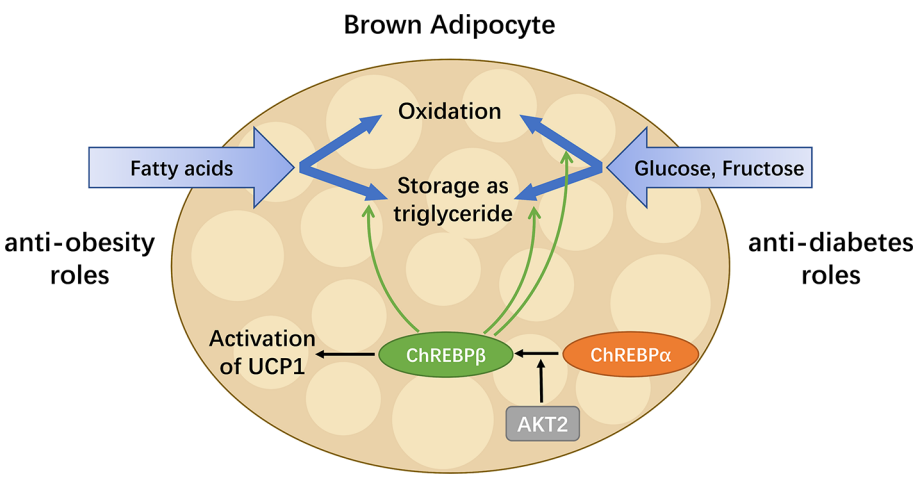

FIGURE 4 | ChREBP in BAT combats metabolic diseases. BAT has enormous promise for treating metabolic diseases including obesity and diabetes, as it is capable of taking up glucose, fructose and fatty acids, as well as oxidizing or storing them afterwards. ChREBPβ, a truncated isoform of ChREBP, is most highly expressed in BAT and induced by the activation of the canonical isoform ChREBPα. In addition to regulating key enzymes involved in metabolism pathways of glucose, fructose and fatty acids, ChREBP also mediates the activation of UCP1 in brown adipocytes. Thus, in BAT, ChREBP plays both anti-obesity and anti-diabetes roles by increasing energy expenditure, reducing circulating glucose and improving insulin sensitivity.

required for maintaining body homeostasis, MondoA plays a crucial part in inter-organ metabolic crosstalk.

In the context of chronic energy overload, MondoA is activated by glucose and fructose, which leads to the upregulation of TXNIP and ARRDC4, and concomitantly the impairment of glucose uptake in the skeletal muscle *via* suppression of insulin action (44, 45, 55). Additionally, the chronic activation of MondoA in skeletal muscle results in lipotoxicity, namely deleterious effects of ectopic triglyceride accumulation (44, 45, 55, 86). Therefore, MondoA activation results in myocellular insulin resistance and lipid accumulation (44), serving as an intriguing supplement to the well-known insulin resistance based on triglyceride accumulation (87). These defects, along with hyperglycemia and hyperlipidemia, contribute to obesity-induced type 2 diabetes (T2D) (88).

In obesity, pancreatic β cells adaptively produce more insulin to maintain blood glucose level, resulting in an amplified burden on β cells. Intriguingly, MondoA serves as a significant glucose-responsive transcription factor in β cells (89). Under high glucose conditions, MondoA shuttles to the nucleus to induce its targets TXNIP and ARRDC4 in β cells. TXNIP is a major factor promoting β cell apoptosis (89–93). Hence, impaired β cells might lead to progressive dysfunction of pancreas and even loss of its ability to produce and secrete insulin (94, 95).

All facts mentioned above will lead to an inter-organ vicious cycle of nutrient disposal and metabolism. The ideal solution is to limit energy intake while increasing the aerobic oxidation of fat in skeletal muscle by exercising (88). Therefore, to get out of the vicious cycle and regain the virtuous cycle, it is worthwhile to treat MondoA in skeletal muscle as a therapeutic target for obesity and insulin resistance.

MONDO FAMILY AS A TARGET FOR METABOLIC DISORDERS

In view of the central role of Mondo family in regulating energy homeostasis, the possibility to target MondoA or ChREBP in metabolic disorders has been explored.

As MondoA downregulates insulin sensitivity and promotes lipid storage in skeletal muscle (44, 45), it could be a promising therapeutic target for insulin resistance and lipotoxicity. For diet-induced obesity, muscle triglyceride accumulation and insulin resistance are partially relieved in muscle-specific MondoA knockout mice (44). MondoA deletion increases muscle glucose uptake and glycolytic capacity, resulting in enhanced sprint capacity (43). Moreover, SBI-477, a potent inhibitor of MondoA, alleviates muscle triglyceride levels and hepatic steatosis, thereby improving glucose tolerance in mice on a high-fat diet (45). However, the significant role of MondoA in skeletal muscle development has been recently revealed in mice (62). Therefore, in the development of MondoA as a novel therapeutic target, the timing for treatment is critical and the risk of interfering with normal myogenesis needs to be avoided.

Reducing ChREBP activity is considered as a promising target in the treatment of obesity according to studies utilizing *ob/ob* and ChREBP double knockout mice (33). Of note, ChREBP plays an important role in promoting white adipocyte browning (81). Therefore, ChREBP in brown and beige adipocytes can be regarded as a treatment option for obesity. In consideration of the well-established role of brown and beige adipocytes in counteracting obesity, we await further research in this respect.

SUMMARY

Mondo family transcription factors are critical for metabolic homeostasis, as they sense multiple nutrient molecules and regulate metabolic enzyme genes transcriptionally. MondoA limits glucose uptake and glycolysis mostly in skeletal muscle and immune cells, while ChREBP promotes *de novo* lipogenesis in liver and adipose tissue. In pathological states of nutrient overload, MondoA could interfere with insulin signaling, while adipose ChREBP is linked to systemic insulin sensitivity and its role extends from white to brown and beige adipose tissues. The role of ChREBP in browning of white adipocytes is especially worth further exploration. Targeting MondoA and ChREBP to counteract obesity and related diseases is an appealing strategy that requires further investigations. As the manipulation of Mondo family in different organs and tissues could yield distinct systemic metabolic consequences, future studies should be conducted using more specific and rigorous models in order to clarify the beneficial or deleterious effects of Mondo family in different contexts. Meanwhile, before the therapeutic approaches could be developed, it is noteworthy that MondoA and ChREBP could be involved in normal myogenesis and adipogenesis. Moreover, under certain circumstances, the target genes and metabolic pathways of MondoA and ChREBP are overlapping. In this regard, in the knockout phenotype of one of the two transcription factors, whether the other acts in a compensatory way requires special attention. Furthermore, increasing studies reveal the involvement of Mondo family in critical signaling pathways, which awaits mechanistic investigations to expand our understanding of the action and regulation of these transcription factors.

AUTHOR CONTRIBUTIONS

XT designed and revised the manuscript. HK, YL, SW, and YZ wrote the manuscript, made the figures and the table. All authors contributed to the article and approved the submitted version.

FUNDING

This work was supported by grants from the 14th Undergraduate Training Program for Innovation of Shanghai Jiao Tong University School of Medicine (1420Y002), from National Natural Science Foundation of China (81672322, 81972210 and 92057117); the Shanghai Municipal Science and Technology Major Project (19JC1410200); National Key R&D Program of China (2019YFA0906100); National Key Research and Development Program of China (No. 2016YFC1304800); Shanghai Jiao Tong

University School of Medicine and Innovative research team of high-level local universities in Shanghai (SSMU-ZDCX20180400); The Program for Professor of Special Appointment (Eastern Scholar) at Shanghai Institutions of Higher Learning and Construction; Plan of Laboratory Technical Team in Shanghai Universities (SYjdyx19019).

ACKNOWLEDGMENTS

We appreciate the useful suggestions from the members in the Tong laboratory. We apologize to those researchers whose work could not be cited or discussed in detail due to the space limitation.

REFERENCES

1. GBD 2017 Risk Factor Collaborators. Global, regional, and national comparative risk assessment of 84 behavioural, environmental and occupational, and metabolic risks or clusters of risks for 195 countries and territories, 1990-2017: a systematic analysis for the Global Burden of Disease Study 2017. *Lancet* (2018) 392:1923–94. doi: 10.1016/s0140-6736(18)32225-6
2. Ludwig DS, Peterson KE, Gortmaker SL. Relation between consumption of sugar-sweetened drinks and childhood obesity: a prospective, observational analysis. *Lancet* (2001) 357:505–8. doi: 10.1016/s0140-6736(00)04041-1
3. Schulze MB, Manson JE, Ludwig DS, Colditz GA, Stampfer MJ, Willett WC, et al. Sugar-sweetened beverages, weight gain, and incidence of type 2 diabetes in young and middle-aged women. *Jama* (2004) 292:927–34. doi: 10.1001/jama.292.8.927
4. Sievenpiper JL, de Souza RJ, Mirrahimi A, Yu ME, Carleton AJ, Beyene J, et al. Effect of fructose on body weight in controlled feeding trials: a systematic review and meta-analysis. *Ann Intern Med* (2012) 156:291–304. doi: 10.7326/0003-4819-156-4-201202210-00007
5. Harms M, Seale P. Brown and beige fat: development, function and therapeutic potential. *Nat Med* (2013) 19:1252–63. doi: 10.1038/nm.3361
6. Cederberg A, Grønning LM, Ahrén B, Taskén K, Carlsson P, Enerbäck S. FOXC2 is a winged helix gene that counteracts obesity, hypertriglyceridemia, and diet-induced insulin resistance. *Cell* (2001) 106:563–73. doi: 10.1016/s0092-8674(01)00474-3
7. Kopecky J, Clarke G, Enerbäck S, Spiegelman B, Kozak LP. Expression of the mitochondrial uncoupling protein gene from the aP2 gene promoter prevents genetic obesity. *J Clin Invest* (1995) 96:2914–23. doi: 10.1172/jci118363
8. Seale P, Conroe HM, Estall J, Kajimura S, Frontini A, Ishibashi J, et al. Prdm16 determines the thermogenic program of subcutaneous white adipose tissue in mice. *J Clin Invest* (2011) 121:96–105. doi: 10.1172/jci44271
9. Ortega-Molina A, Efeyan A, Lopez-Guadamillas E, Muñoz-Martin M, Gómez-López G, Cañamero M, et al. Pten positively regulates brown adipose function, energy expenditure, and longevity. *Cell Metab* (2012) 15:382–94. doi: 10.1016/j.cmet.2012.02.001
10. Vegiopoulos A, Müller-Decker K, Strzoda D, Schmitt I, Chichelnitskiy E, Ostertag A, et al. Cyclooxygenase-2 controls energy homeostasis in mice by *de novo* recruitment of brown adipocytes. *Science* (2010) 328:1158–61. doi: 10.1126/science.1186034
11. Lee P, Smith S, Linderman J, Courville AB, Brychta RJ, Dieckmann W, et al. Temperature-acclimated brown adipose tissue modulates insulin sensitivity in humans. *Diabetes* (2014) 63:3686–98. doi: 10.2337/db14-0513
12. Billin AN, Eilers AL, Coulter KL, Logan JS, Ayer DE. MondoA, a novel basic helix-loop-helix-leucine zipper transcriptional activator that constitutes a positive branch of a max-like network. *Mol Cell Biol* (2000) 20:8845–54. doi: 10.1128/mcb.20.23.8845-8854.2000
13. Yamashita H, Takenoshita M, Sakurai M, Bruick RK, Henzel WJ, Shillinglaw W, et al. A glucose-responsive transcription factor that regulates carbohydrate metabolism in the liver. *Proc Natl Acad Sci USA* (2001) 98:9116–21. doi: 10.1073/pnas.161284298
14. Stoeckman AK, Ma L, Towle HC. Mlx is the functional heteromeric partner of the carbohydrate response element-binding protein in glucose regulation of lipogenic enzyme genes. *J Biol Chem* (2004) 279:15662–9. doi: 10.1074/jbc.M311301200
15. Li MV, Chang B, Imamura M, Poungvarin N, Chan L. Glucose-dependent transcriptional regulation by an evolutionarily conserved glucose-sensing module. *Diabetes* (2006) 55:1179–89. doi: 10.2337/db05-0822
16. Herman MA, Peroni OD, Villoria J, Schön MR, Abumrad NA, Blüher M, et al. A novel ChREBP isoform in adipose tissue regulates systemic glucose metabolism. *Nature* (2012) 484:333–8. doi: 10.1038/nature10986
17. Ge Q, Nakagawa T, Wynn RM, Chook YM, Miller BC, Uyeda K. Importin-alpha protein binding to a nuclear localization signal of carbohydrate response element-binding protein (ChREBP). *J Biol Chem* (2011) 286:28119–27. doi: 10.1074/jbc.M111.237016
18. Eilers AL, Sundwall E, Lin M, Sullivan AA, Ayer DE. A novel heterodimerization domain, CRM1, and 14-3-3 control subcellular localization of the MondoA-Mlx heterocomplex. *Mol Cell Biol* (2002) 22:8514–26. doi: 10.1128/mcb.22.24.8514-8526.2002
19. Sakiyama H, Wynn RM, Lee WR, Fukasawa M, Mizuguchi H, Gardner KH, et al. Regulation of nuclear import/export of carbohydrate response element-binding protein (ChREBP): interaction of an alpha-helix of ChREBP with the 14-3-3 proteins and regulation by phosphorylation. *J Biol Chem* (2008) 283:24899–908. doi: 10.1074/jbc.M804308200
20. Li MV, Chen W, Poungvarin N, Imamura M, Chan L. Glucose-mediated transactivation of carbohydrate response element-binding protein requires cooperative actions from Mondo conserved regions and essential trans-acting factor 14-3-3. *Mol Endocrinol* (2008) 22:1658–72. doi: 10.1210/me.2007-0560
21. Sanchez-Gurmaches J, Tang Y, Jespersen NZ, Wallace M, Martinez Calejman C, Gujja S, et al. Brown Fat AKT2 Is a Cold-Induced Kinase that Stimulates ChREBP-Mediated De Novo Lipogenesis to Optimize Fuel Storage and Thermogenesis. *Cell Metab* (2018) 27:195–209. doi: 10.1016/j.cmet.2017.10.008
22. Dentin R, Tomas-Cobos L, Foufelle F, Leopold J, Girard J, Postic C, et al. Glucose 6-phosphate, rather than xylulose 5-phosphate, is required for the activation of ChREBP in response to glucose in the liver. *J Hepatol* (2012) 56:199–209. doi: 10.1016/j.jhep.2011.07.019
23. McFerrin LG, Atchley WR. A novel N-terminal domain may dictate the glucose response of Mondo proteins. *PloS One* (2012) 7:e34803. doi: 10.1371/journal.pone.0034803
24. Kabashima T, Kawaguchi T, Wadzinski BE, Uyeda K. Xylulose 5-phosphate mediates glucose-induced lipogenesis by xylulose 5-phosphate-activated protein phosphatase in rat liver. *Proc Natl Acad Sci USA* (2003) 100:5107–12. doi: 10.1073/pnas.0730817100
25. Arden C, Tudhope SJ, Petrie JL, Al-Oanzi ZH, Cullen KS, Lange AJ, et al. Fructose 2,6-bisphosphate is essential for glucose-regulated gene transcription of glucose-6-phosphatase and other ChREBP target genes in hepatocytes. *Biochem J* (2012) 443:111–23. doi: 10.1042/bj20111280
26. Sato S, Jung H, Nakagawa T, Pawlosky R, Takeshima T, Lee WR, et al. Metabolite Regulation of Nuclear Localization of Carbohydrate-response Element-binding Protein (ChREBP): ROLE OF AMP AS AN ALLOSTERIC INHIBITOR. *J Biol Chem* (2016) 291:10515–27. doi: 10.1074/jbc.M115.708982
27. Nakagawa T, Ge Q, Pawlosky R, Wynn RM, Veech RL, Uyeda K. Metabolite regulation of nucleo-cytosolic trafficking of carbohydrate response element-binding protein (ChREBP): role of ketone bodies. *J Biol Chem* (2013) 288:28358–67. doi: 10.1074/jbc.M113.498550
28. Postic C, Dentin R, Denechaud P-D, Girard J. ChREBP, a transcriptional regulator of glucose and lipid metabolism. *Annu Rev Nutr* (2007) 27:179–92. doi: 10.1146/annurev.nutr.27.061406.093618
29. Ishii S, Iizuka K, Miller BC, Uyeda K. Carbohydrate response element binding protein directly promotes lipogenic enzyme gene transcription. *Proc Natl Acad Sci USA* (2004) 101:15597–602. doi: 10.1073/pnas.0405238101
30. Ma L, Robinson LN, Towle HC. ChREBP*Mlx is the principal mediator of glucose-induced gene expression in the liver. *J Biol Chem* (2006) 281:28721–30. doi: 10.1074/jbc.M601576200
31. Niwa H, Iizuka K, Kato T, Wu W, Tsuchida H, Takao K, et al. ChREBP Rather Than SHP Regulates Hepatic VLDL Secretion. *Nutrients* (2018) 10:321. doi: 10.3390/nu10030321
32. Iizuka K, Bruick RK, Liang G, Horton JD, Uyeda K. Deficiency of carbohydrate response element-binding protein (ChREBP) reduces

lipogenesis as well as glycolysis. *Proc Natl Acad Sci USA* (2004) 101:7281–6. doi: 10.1073/pnas.0401516101
33. Iizuka K, Miller B, Uyeda K. Deficiency of carbohydrate-activated transcription factor ChREBP prevents obesity and improves plasma glucose control in leptin-deficient (ob/ob) mice. *Am J Physiol Endocrinol Metab* (2006) 291:E358–64. doi: 10.1152/ajpendo.00027.2006
34. Jois T, Chen W, Howard V, Harvey R, Youngs K, Thalmann C, et al. Deletion of hepatic carbohydrate response element binding protein (ChREBP) impairs glucose homeostasis and hepatic insulin sensitivity in mice. *Mol Metab* (2017) 6:1381–94. doi: 10.1016/j.molmet.2017.07.006
35. Benhamed F, Denechaud PD, Lemoine M, Robichon C, Moldes M, Bertrand-Michel J, et al. The lipogenic transcription factor ChREBP dissociates hepatic steatosis from insulin resistance in mice and humans. *J Clin Invest* (2012) 122:2176–94. doi: 10.1172/JCI41636
36. Vijayakumar A, Aryal P, Wen J, Syed I, Vazirani RP, Moraes-Vieira PM, et al. Absence of Carbohydrate Response Element Binding Protein in Adipocytes Causes Systemic Insulin Resistance and Impairs Glucose Transport. *Cell Rep* (2017) 21:1021–35. doi: 10.1016/j.celrep.2017.09.091
37. Nuotio-Antar AM, Poungvarin N, Li M, Schupp M, Mohammad M, Gerard S, et al. FABP4-Cre Mediated Expression of Constitutively Active ChREBP Protects Against Obesity, Fatty Liver, and Insulin Resistance. *Endocrinology* (2015) 156:4020–32. doi: 10.1210/en.2015-1210
38. Poungvarin N, Lee JK, Yechoor VK, Li MV, Assavapokee T, Suksaranjit P, et al. Carbohydrate response element-binding protein (ChREBP) plays a pivotal role in beta cell glucotoxicity. *Diabetologia* (2012) 55:1783–96. doi: 10.1007/s00125-012-2506-4
39. Dentin R, Benhamed F, Hainault I, Fauveau V, Foufelle F, Dyck JR, et al. Liver-specific inhibition of ChREBP improves hepatic steatosis and insulin resistance in ob/ob mice. *Diabetes* (2006) 55:2159–70. doi: 10.2337/db06-0200
40. Wu W, Tsuchida H, Kato T, Niwa H, Horikawa Y, Takeda J, et al. Fat and carbohydrate in western diet contribute differently to hepatic lipid accumulation. *Biochem Biophys Res Commun* (2015) 461:681–6. doi: 10.1016/j.bbrc.2015.04.092
41. Zhang D, Tong X, VanDommelen K, Gupta N, Stamper K, Brady GF, et al. Lipogenic transcription factor ChREBP mediates fructose-induced metabolic adaptations to prevent hepatotoxicity. *J Clin Invest* (2017) 127:2855–67. doi: 10.1172/jci89934
42. Kim M, Astapova II, Flier SN, Hannou SA, Doridot L, Sargsyan A, et al. Intestinal, but not hepatic, ChREBP is required for fructose tolerance. *JCI Insight* (2017) 2:e96703. doi: 10.1172/jci.insight.96703
43. Imamura M, Chang BH, Kohjima M, Li M, Hwang B, Taegtmeyer H, et al. MondoA deficiency enhances sprint performance in mice. *Biochem J* (2014) 464:35–48. doi: 10.1042/bj20140530
44. Ahn B, Wan S, Jaiswal N, Vega RB, Ayer DE, Titchenell PM, et al. MondoA drives muscle lipid accumulation and insulin resistance. *JCI Insight* (2019) 5: e129119. doi: 10.1172/jci.insight.129119
45. Ahn B, Soundarapandian MM, Sessions H, Peddibhotla S, Roth GP, Li JL, et al. MondoA coordinately regulates skeletal myocyte lipid homeostasis and insulin signaling. *J Clin Invest* (2016) 126:3567–79. doi: 10.1172/jci87382
46. Iizuka K, Takao K, Kato T, Horikawa Y, Takeda J. ChREBP Reciprocally Regulates Liver and Plasma Triacylglycerol Levels in Different Manners. *Nutrients* (2018) 10:1699. doi: 10.3390/nu10111699
47. Linden AG, Li S, Choi HY, Fang F, Fukasawa M, Uyeda K, et al. Interplay between ChREBP and SREBP-1c coordinates postprandial glycolysis and lipogenesis in livers of mice. *J Lipid Res* (2018) 59:475–87. doi: 10.1194/jlr.M081836
48. White PJ, McGarrah RW, Grimsrud PA, Tso SC, Yang WH, Haldeman JM, et al. and Lipid Metabolism *via* Regulation of ATP-Citrate Lyase. *Cell Metab* (2018) 27:1281–93.e7. doi: 10.1016/j.cmet.2018.04.015
49. Iizuka K, Takeda J, Horikawa Y. Glucose induces FGF21 mRNA expression through ChREBP activation in rat hepatocytes. *FEBS Lett* (2009) 583:2882–6. doi: 10.1016/j.febslet.2009.07.053
50. von Holstein-Rathlou S, BonDurant LD, Peltekian L, Naber MC, Yin TC, Claflin KE, et al. FGF21 Mediates Endocrine Control of Simple Sugar Intake and Sweet Taste Preference by the Liver. *Cell Metab* (2016) 23:335–43. doi: 10.1016/j.cmet.2015.12.003
51. Fisher FM, Kim M, Doridot L, Cunniff JC, Parker TS, Levine DM, et al. A critical role for ChREBP-mediated FGF21 secretion in hepatic fructose metabolism. *Mol Metab* (2017) 6:14–21. doi: 10.1016/j.molmet.2016.11.008
52. Stoltzman CA, Peterson CW, Breen KT, Muoio DM, Billin AN, Ayer DE. Glucose sensing by MondoA : Mlx complexes: a role for hexokinases and direct regulation of thioredoxin-interacting protein expression. *Proc Natl Acad Sci USA* (2008) 105:6912–7. doi: 10.1073/pnas.0712199105
53. Sans CL, Satterwhite DJ, Stoltzman CA, Breen KT, Ayer DE. MondoA-Mlx heterodimers are candidate sensors of cellular energy status: mitochondrial localization and direct regulation of glycolysis. *Mol Cell Biol* (2006) 26:4863–71. doi: 10.1128/mcb.00657-05
54. Peterson CW, Stoltzman CA, Sighinolfi MP, Han KS, Ayer DE. Glucose controls nuclear accumulation, promoter binding, and transcriptional activity of the MondoA-Mlx heterodimer. *Mol Cell Biol* (2010) 30:2887–95. doi: 10.1128/mcb.01613-09
55. Petrie JL, Al-Oanzi ZH, Arden C, Tudhope SJ, Mann J, Kieswich J, et al. Glucose induces protein targeting to glycogen in hepatocytes by fructose 2,6-bisphosphate-mediated recruitment of MondoA to the promoter. *Mol Cell Biol* (2013) 33:725–38. doi: 10.1128/mcb.01576-12
56. Stoltzman CA, Kaadige MR, Peterson CW, Ayer DE. MondoA senses non-glucose sugars: regulation of thioredoxin-interacting protein (TXNIP) and the hexose transport curb. *J Biol Chem* (2011) 286:38027–34. doi: 10.1074/jbc.M111.275503
57. Wilde BR, Ye Z, Lim TY, Ayer DE. Cellular acidosis triggers human MondoA transcriptional activity by driving mitochondrial ATP production. *Elife* (2019) 8:e40199. doi: 10.7554/eLife.40199
58. Yu FX, Goh SR, Dai RP, Luo Y. Adenosine-containing molecules amplify glucose signaling and enhance txnip expression. *Mol Endocrinol* (2009) 23:932–42. doi: 10.1210/me.2008-0383
59. Han KS, Ayer DE. MondoA senses adenine nucleotides: transcriptional induction of thioredoxin-interacting protein. *Biochem J* (2013) 453:209–18. doi: 10.1042/bj20121126
60. Kaadige MR, Yang J, Wilde BR, Ayer DE. MondoA-Mlx transcriptional activity is limited by mTOR-MondoA interaction. *Mol Cell Biol* (2015) 35:101–10. doi: 10.1128/mcb.00636-14
61. Parikh H, Carlsson E, Chutkow WA, Johansson LE, Storgaard H, Poulsen P, et al. TXNIP regulates peripheral glucose metabolism in humans. *PloS Med* (2007) 4:e158. doi: 10.1371/journal.pmed.0040158
62. Ran H, Lu Y, Zhang Q, Hu Q, Zhao J, Wang K, et al. MondoA Is Required for Normal Myogenesis and Regulation of the Skeletal Muscle Glycogen Content in Mice. *Diabetes Metab J* (2020). doi: 10.4093/dmj.2019.0212
63. Mandala A, Das N, Bhattacharjee S, Mukherjee B, Mukhopadhyay S, Roy SS. Thioredoxin interacting protein mediates lipid-induced impairment of glucose uptake in skeletal muscle. *Biochem Biophys Res Commun* (2016) 479:933–9. doi: 10.1016/j.bbrc.2016.09.168
64. Waldhart AN, Dykstra H, Peck AS, Boguslawski EA, Madaj ZB, Wen J, et al. Phosphorylation of TXNIP by AKT Mediates Acute Influx of Glucose in Response to Insulin. *Cell Rep* (2017) 19:2005–13. doi: 10.1016/j.celrep.2017.05.041
65. Delibegovic M, Armstrong CG, Dobbie L, Watt PW, Smith AJH, Cohen PTW. Disruption of the striated muscle glycogen targeting subunit PPP1R3A of protein phosphatase 1 leads to increased weight gain, fat deposition, and development of insulin resistance. *Diabetes* (2003) 52:596–604. doi: 10.2337/diabetes.52.3.596
66. Montori-Grau M, Guitart M, Lerin C, Andreu AL, Newgard CB, García-Martínez C, et al. Expression and glycogenic effect of glycogen-targeting protein phosphatase 1 regulatory subunit GL in cultured human muscle. *Biochem J* (2007) 405:107–13. doi: 10.1042/BJ20061572
67. Kawaguchi T, Takenoshita M, Kabashima T, Uyeda K. Glucose and cAMP regulate the L-type pyruvate kinase gene by phosphorylation/dephosphorylation of the carbohydrate response element binding protein. *Proc Natl Acad Sci USA* (2001) 98:13710–5. doi: 10.1073/pnas.231370798
68. Bricambert J, Miranda J, Benhamed F, Girard J, Postic C, Dentin R. Salt-inducible kinase 2 links transcriptional coactivator p300 phosphorylation to the prevention of ChREBP-dependent hepatic steatosis in mice. *J Clin Invest* (2010) 120:4316–31. doi: 10.1172/jci41624
69. Guinez C, Filhoulaud G, Rayah-Benhamed F, Marmier S, Dubuquoy C, Dentin R, et al. O-GlcNAcylation increases ChREBP protein content and

transcriptional activity in the liver. *Diabetes* (2011) 60:1399–413. doi: 10.2337/db10-0452
70. Carobbio S, Pellegrinelli V, Vidal-Puig A. Adipose Tissue Function and Expandability as Determinants of Lipotoxicity and the Metabolic Syndrome. *Adv Exp Med Biol* (2017) 960:161–96. doi: 10.1007/978-3-319-48382-5_7
71. Lynes MD, Tseng Y-H. Deciphering adipose tissue heterogeneity. *Ann N Y Acad Sci* (2018) 1411:5–20 doi: 10.1111/nyas.13398
72. Montanari T, Pošćić N, Colitti M. Factors involved in white-to-brown adipose tissue conversion and in thermogenesis: a review. *Obes Rev* (2017) 18:495–513. doi: 10.1111/obr.12520
73. Ricquier D. UCP1, the mitochondrial uncoupling protein of brown adipocyte: A personal contribution and a historical perspective. *Biochimie* (2017) 134:3–8. doi: 10.1016/j.biochi.2016.10.018
74. Song Z, Xiaoli AM, Yang F. Regulation and Metabolic Significance of Lipogenesis in Adipose Tissues. *Nutrients* (2018) 10:1383. doi: 10.3390/nu10101383
75. Ameer F, Scandiuzzi L, Hasnain S, Kalbacher H, Zaidi N. De novo lipogenesis in health and disease. *Metabolism* (2014) 63:895–902. doi: 10.1016/j.metabol.2014.04.003
76. Lodhi IJ, Wei X, Semenkovich CF. Lipoexpediency: *de novo* lipogenesis as a metabolic signal transmitter. *Trends Endocrinol Metab* (2011) 22:1–8. doi: 10.1016/j.tem.2010.09.002
77. Smith U, Kahn BB. Adipose tissue regulates insulin sensitivity: role of adipogenesis, *de novo* lipogenesis and novel lipids. *J Intern Med* (2016) 280:465–75. doi: 10.1111/joim.12540
78. Fernandez S, Viola JM, Torres A, Wallace M, Trefely S, Zhao S, et al. Adipocyte ACLY Facilitates Dietary Carbohydrate Handling to Maintain Metabolic Homeostasis in Females. *Cell Rep* (2019) 27:2772–84.e6. doi: 10.1016/j.celrep.2019.04.112
79. Tang Y, Wallace M, Sanchez-Gurmaches J, Hsiao WY, Li H, Lee PL, et al. Adipose tissue mTORC2 regulates ChREBP-driven *de novo* lipogenesis and hepatic glucose metabolism. *Nat Commun* (2016) 7:11365. doi: 10.1038/ncomms11365
80. Sanchez-Gurmaches J, Martinez Calejman C, Jung SM, Li H, Guertin DA. Brown fat organogenesis and maintenance requires AKT1 and AKT2. *Mol Metab* (2019) 23:60–74. doi: 10.1016/j.molmet.2019.02.004
81. Katz LS, Xu S, Ge K, Scott DK, Gershengorn MC. T3 and Glucose Coordinately Stimulate ChREBP-Mediated Ucp1 Expression in Brown Adipocytes From Male Mice. *Endocrinology* (2018) 159:557–69. doi: 10.1210/en.2017-00579
82. Wei C, Ma X, Su K, Qi S, Zhu Y, Lin J, et al. ChREBP-β regulates thermogenesis in brown adipose tissue. *J Endocrinol* (2020) 245:343–56. doi: 10.1530/JOE-19-0498
83. Maekawa R, Seino Y, Ogata H, Murase M, Iida A, Hosokawa K, et al. Chronic high-sucrose diet increases fibroblast growth factor 21 production and energy expenditure in mice. *J Nutr Biochem* (2017) 49:71–9. doi: 10.1016/j.jnutbio.2017.07.010
84. Witte N, Muenzner M, Rietscher J, Knauer M, Heidenreich S, Nuotio-Antar AM, et al. The Glucose Sensor ChREBP Links De Novo Lipogenesis to PPARgamma Activity and Adipocyte Differentiation. *Endocrinology* (2015) 156:4008–19. doi: 10.1210/EN.2015-1209
85. DeFronzo RA, Gunnarsson R, Björkman O, Olsson M, Wahren J. Effects of insulin on peripheral and splanchnic glucose metabolism in noninsulin-dependent (type II) diabetes mellitus. *J Clin Invest* (1985) 76:149–55. doi: 10.1172/JCI111938
86. Sartor F, Jackson MJ, Squillace C, Shepherd A, Moore JP, Ayer DE, et al. Adaptive metabolic response to 4 weeks of sugar-sweetened beverage consumption in healthy, lightly active individuals and chronic high glucose availability in primary human myotubes. *Eur J Nutr* (2013) 52:937–48. doi: 10.1007/s00394-012-0401-x
87. Pan DA, Lillioja S, Kriketos AD, Milner MR, Baur LA, Bogardus C, et al. Skeletal muscle triglyceride levels are inversely related to insulin action. *Diabetes* (1997) 46:983–8. doi: 10.2337/diab.46.6.983
88. Simonson DC, Halperin F, Foster K, Vernon A, Goldfine AB. Clinical and Patient-Centered Outcomes in Obese Patients With Type 2 Diabetes 3 Years After Randomization to Roux-en-Y Gastric Bypass Surgery Versus Intensive Lifestyle Management: The SLIMM-T2D Study. *Diabetes Care* (2018) 41:670–9. doi: 10.2337/dc17-0487
89. Richards P, Rachdi L, Oshima M, Marchetti P, Bugliani M, Armanet M, et al. MondoA Is an Essential Glucose-Responsive Transcription Factor in Human Pancreatic β-Cells. *Diabetes* (2018) 67:461–72. doi: 10.2337/db17-0595
90. Thielen L, Shalev A. Diabetes pathogenic mechanisms and potential new therapies based upon a novel target called TXNIP. *Curr Opin Endocrinol Diabetes Obes* (2018) 25:75–80. doi: 10.1097/MED.0000000000000391
91. Lerner AG, Upton J-P, Praveen PVK, Ghosh R, Nakagawa Y, Igbaria A, et al. IRE1α induces thioredoxin-interacting protein to activate the NLRP3 inflammasome and promote programmed cell death under irremediable ER stress. *Cell Metab* (2012) 16:250–64. doi: 10.1016/j.cmet.2012.07.007
92. Chen J, Hui ST, Couto FM, Mungrue IN, Davis DB, Attie AD, et al. Thioredoxin-interacting protein deficiency induces Akt/Bcl-xL signaling and pancreatic beta-cell mass and protects against diabetes. *FASEB J: Off Publ Fed Am Societies Exp Biol* (2008) 22:3581–94. doi: 10.1096/fj.08-111690
93. Saxena G, Chen J, Shalev A. Intracellular shuttling and mitochondrial function of thioredoxin-interacting protein. *J Biol Chem* (2010) 285:3997–4005. doi: 10.1074/jbc.M109.034421
94. Boland BB, Rhodes CJ, Grimsby JS. The dynamic plasticity of insulin production in β-cells. *Mol Metab* (2017) 6:958–73. doi: 10.1016/j.molmet.2017.04.010
95. Robertson RP. Chronic oxidative stress as a central mechanism for glucose toxicity in pancreatic islet beta cells in diabetes. *J Biol Chem* (2004) 279:42351–4. doi: 10.1074/jbc.R400019200

Conflict of Interest: The authors declare that the research was conducted in the absence of any commercial or financial relationships that could be construed as a potential conflict of interest.

frontiers in Endocrinology

REVIEW
published: 09 April 2021
doi: 10.3389/fendo.2021.653179

Novel Roles of Follistatin/Myostatin in Transforming Growth Factor-β Signaling and Adipose Browning: Potential for Therapeutic Intervention in Obesity Related Metabolic Disorders

Shehla Pervin[1,2], *Srinivasa T. Reddy*[3,4] *and Rajan Singh*[1,2,5]*

[1] Department of Obstetrics and Gynecology, David Geffen School of Medicine at University of California Los Angeles (UCLA), Los Angeles, CA, United States, [2] Division of Endocrinology and Metabolism, Charles R. Drew University of Medicine and Science, Los Angeles, CA, United States, [3] Department of Molecular and Medical Pharmacology, David Geffen School of Medicine at UCLA, Los Angeles, CA, United States, [4] Department of Medicine, Division of Cardiology, David Geffen School of Medicine, University of California Los Angeles, Los Angeles, CA, United States, [5] Department of Endocrinology, Men's Health: Aging and Metabolism, Brigham and Women's Hospital, Boston, MA, United States

OPEN ACCESS

Edited by:
Xinran Ma,
East China Normal University, China

Reviewed by:
Meng Dong,
Institute of Zoology, Chinese Academy of Sciences (CAS), China
Abir Mukherjee,
Royal Veterinary College (RVC), United Kingdom

***Correspondence:**
Rajan Singh
rajansingh@mednet.ucla.edu

Specialty section:
This article was submitted to Translational Endocrinology, a section of the journal Frontiers in Endocrinology

Received: 14 January 2021
Accepted: 19 March 2021
Published: 09 April 2021

Citation:
Pervin S, Reddy ST and Singh R (2021) Novel Roles of Follistatin/Myostatin in Transforming Growth Factor-β Signaling and Adipose Browning: Potential for Therapeutic Intervention in Obesity Related Metabolic Disorders. Front. Endocrinol. 12:653179. doi: 10.3389/fendo.2021.653179

Obesity is a global health problem and a major risk factor for several metabolic conditions including dyslipidemia, diabetes, insulin resistance and cardiovascular diseases. Obesity develops from chronic imbalance between energy intake and energy expenditure. Stimulation of cellular energy burning process has the potential to dissipate excess calories in the form of heat *via* the activation of uncoupling protein-1 (UCP1) in white and brown adipose tissues. Recent studies have shown that *activation* of transforming growth factor-β (TGF-β) signaling pathway significantly contributes to the development of obesity, and blockade or inhibition is reported to protect from obesity by promoting white adipose browning and increasing mitochondrial biogenesis. Identification of novel compounds that activate beige/brown adipose characteristics to burn surplus calories and reduce excess storage of fat are actively sought in the fight against obesity. In this review, we present recent developments in our understanding of key modulators of TGF-β signaling pathways including follistatin (FST) and myostatin (MST) in regulating adipose browning and brown adipose mass and activity. While MST is a key ligand for TGF-β family, FST can bind and regulate biological activity of several TGF-β superfamily members including activins, bone morphogenic proteins (BMP) and inhibins. Here, we review the literature supporting the critical roles for FST, MST and other proteins in modulating TGF-β signaling to influence beige and brown adipose characteristics. We further review the potential therapeutic utility of FST for the treatment of obesity and related metabolic disorders.

Keywords: follistatin, myostatin, obesity, transforming growth Factor β, UCP1, adipose tissue

INTRODUCTION

The obesity epidemic significantly affects every region and demographical group worldwide with no signs of abatement. Obesity substantially increases the risk for several chronic diseases including cardiovascular diseases, fatty liver, diabetes, insulin resistance and cancer. It has been estimated that by 2030 approximately 2.16 billion individuals will be overweight and 1.12 billion individuals will be obese as defined by body mass index (BMI) of 30 or higher (1). The economic impact of obesity and its related complications on United States has been estimated between 4-8% of gross domestic product and comparable to 2018 defense budget ($643 billion) and Medicare ($588 billion) (2), and significantly impacts low-income and economically disadvantaged populations. The strategies, to date, to combat the obesity epidemic have not been successful and there is an unmet need for the development of novel therapies to prevent and treat obesity and related metabolic complications. As obesity develops from surplus energy stored in adipose tissues, therapeutic approaches to reduce energy intake, increase energy expenditure, or both would provide attractive avenues for the fight against obesity and related diseases. Although thermogenic adipocytes and their precursors are composed of various distinct cell populations (3, 4), adipose tissue mass is composed mostly of white adipose tissue (WAT) and brown adipose tissue (BAT), which metabolically play opposing roles in regulating energy balance.

Recent clinical cross-sectional studies using [18F] FDG-PET/CT, suggest a clear decline in BAT activity and mass during aging that coincides with the development of obesity and insulin resistance. Several laboratories have presented evidence for expression of the thermogenic molecule UCP1 as well as its energy dissipating capacity in human BAT and contribute towards improved metabolic profiles (5–7). WAT, which is specialized for storage of energy could be manipulated *via* genetic or pharmacological means to promote browning. Such browning, also called as "beige" or "brite" (brown in white), is associated with increased expression of mitochondrial uncoupling protein-1 (UCP1) expression in response to external stimuli including chronic cold exposure, treatment with β-adrenergic agonists CL 316,243, exercise, and endocrine factors (8, 9). This type of adipose browning is also associated with increased thermogenic capacity of the cells since activation of UCP1 that uncouples mitochondrial respiration from ATP production provides significant metabolic benefits that are comparable to BAT (8, 9). Experimental mice with selective ablation of beige adipose cells are prone to obesity and metabolic dysfunction probably by reducing lipogenic capacity and energy expenditure as well as by modulating the inflammatory environment inside the WAT (10). Overexpression of Prdm16 (PR-domain containing 16) resulted in abundant beige adipocytes in subcutaneous adipose depots, associated with significantly increased energy expenditure and were resistant to weight gain in response to a high fat diet (HFD) (11). Similarly, CRISPR/CAS9-mediated reconstitution of UCP1 in WAT of pigs led to significantly decreased fat mass and improved energy expenditure (12), suggesting the therapeutic potential of modulating WAT phenotype by activation of key thermogenic genes for fighting obesity and metabolic syndrome. While implementation of findings from animal studies remains challenging to apply in humans, such studies have yielded novel insights into the molecular mechanisms underlying thermogenic regulation of brown and beige adipocytes and highlight their ability to reduce obesity and related metabolic disorders. Thus, further studies directed to translate the proofs of concept generated in animal models are crucial.

Transforming growth factor-beta (TGF-β) signaling has been shown to regulate glucose and energy homeostasis (13). TGF-β levels are reported to increase with adiposity in overweight (BMI between 25-29.9 kg/m^2) and obese (BMI ≥ 30 kg/m^2) subjects compared to the normal subjects with BMI less than 24.9 kg/m^2), and systemic blockade of TGF-β/SMAD3 signaling resulted in protection against diet-induced obesity in experimental mice (13). This effect was associated with acquisition of energy dissipating brown adipocyte phenotype in WAT. In this review, we will discuss the evidence for the novel role of FST, MST and other related proteins in modulating TGF-β signaling and adipocyte browning to explore possible therapeutic avenues for the treatment of obesity and associated metabolic disorders.

BEIGE AND BROWN ADIPOCYTE DEVELOPMENTAL ORIGIN AND MOLECULAR SIGNATURES

White, beige and brown adipocytes are three major types of adipocytes that have distinctly different fat morphology and differ in their developmental origin as well as function. During embryogenesis, BAT development precedes the formation of WAT, where it primarily contributes to non-shivering thermogenesis and maintain body temperature in newborns. Interscapular BAT mainly contributes to the temperature regulation during early stages of life and its levels slowly regress with age (14–16). Lineage-tracing studies demonstrated that classical brown adipocytes present in BAT depots originate from a sub-population of dermomyotome expressing specific transcription factors, including Pax7, engrailed 1, and Myf5 (17–20). Previously, these Myf5-expressing (Myf5+) precursors were assumed to be present exclusively in skeletal muscle precursors and absent in both in WAT and beige adipocytes (20, 21). Beige adipocytes present in the inguinal white adipose depots are reported to be derived from Myf5 negative (Myf5-) precursor pool (22). However, more recent lineage tracing studies have identified subsets of white adipocytes that are derived from both Myf5+ and Myf5- precursors (23–25), and beige adipocytes are derived from progenitor populations expressing Sma, Myh11 (a selective marker for smooth muscle cells), platelet-derived growth factor receptor (PDGFR)-α, or PDGFR-β in mice (26–29). Retinoic acid (RA)-induced adipose browning in endothelial cells and capillaries has also been reported *via* the activation of vascular endothelial growth factor (VEGF) A/VEGFR2 signaling that facilitate PDGFR-α-expressing adipocyte precursors (18). Beige cells could also appear as a result of trans-differentiation of

mature white adipocytes (15). Trans-differentiation of beige adipocytes to WAT has been reported during warm adaptations and aging (30, 31). Collectively, the above studies strongly suggest that beige adipocytes that emerge in WAT depots appear to have multiple origins compared to the brown adipocytes.

PGC-1α is a master regulator of adaptive thermogenesis that binds to PPAR-γ and coactivates PPAR-γ to stimulate the transcription of genes involved in the brown adipocyte differentiation process and acquisition of morphological and molecular features of brown and beige fat (32). PGC-1α expression is rapidly induced by cold exposure that turns on several key components of the adaptive thermogenic program including fatty acid oxidation, mitochondrial biogenesis, and increased oxygen consumption (33). The transcriptional factor PR domain zinc finger 16 (PRDM16) is selectively expressed in brown/beige compared to the visceral white fat cells and plays an important role in controlling the differentiation-linked brown adipose/skeletal muscle fate determination and gene expression program (34). Gain and loss-of-function studies of PRDM16 in various cell systems have clearly established its major role in brown adipose/skeletal muscle cell fate determination (35). Using analysis of clonal cell lines, Wu et al. also suggested that beige and brown adipose cells express related but distinctly different gene expression profiles (36). Beige cells are selectively enriched in Tmem26, Tbx1, and CD137 expression (36). The same study identified additional beige selective genes including Ear2, CD40, Sp100, Klh113, and Slc27a from interscapular BAT and inguinal fat. Wang et al. identified early B-cell factor 2 (Ebf2) as one of the most selective markers for brown and beige adipogenic precursor cells (37). More beige-selective genes including *HoxC8*, *HoxC9*, *Cited1*, and *Shox2* were identified using molecular profiling of human BAT (38, 39). On the other hand, epithelial V-like antigen (*Eva1*), *Lhx1*, *Zic1*, and *Epsti1* are selectively expressed in classical brown adipocytes (36–41). Additionally, *Ebf3*, *Pdk4*, *Fbxo31*, *Oplah*, and *Hsbp7* were also found to be highly enriched in interscapular BAT of 129SVE mice (36). Ussar et al. have reported few selective cell surface markers for white, beige and brown adipocytes that could provide unique tools to identify various adipocyte populations in both humans and rodents and potentially target them for therapy *in vivo* (42). The authors identified amino acid transporter *Asc1*, encoded by the SLC7A10 gene as a white adipocyte-specific cell surface protein, which was barely expressed in brown adipocytes (42). Expression level of purigenic receptor P2RX5, part of a seven-member family of ATP gated ion channels, was highest in brown adipocytes. Proton coupled amino acid transporter PAT2, another cell surface protein, show highest specificity for adipose tissue among all three markers identified in this study with significantly higher expression in brown fat compared to white fat. Better understanding of the gene expression pattern of such adipose-specific cell surface markers should provide novel tools to selectively mark and access intact white and brown adipocytes and could be used for diagnostic and therapeutic purposes. Analysis of microRNA (miRNA) between beige and brown fat have provided clear differences in their expression profile. Several miRNAs including miRNA-30, miRNA-182, and miRNA-203 are reported to positively regulate both beige and brown adipocytes (43, 44). On the other hand, miRNA-27 and miRNA-34a negatively regulator beige and brown adipogenesis (45, 46). Recent studies have also highlighted some specific miRNAs including miRNA-196b and miRNA-26 that positively and negatively regulate beige adipogenesis respectively (47, 48).

TRANSFORMING GROWTH FACTOR-BETA (TGF-β), ADIPOSE BROWNING AND OBESITY

The TGF-β superfamily consists of several members including TGFβ1, TGFβ2, and TGFβ3, bone morphogenetic proteins (BMPs), growth differentiation factors (GDFs), and activins that regulate diverse biological processes during embryogenesis, adult tissue homeostasis, and function of several cell types including adipocytes (49, 50). The pleiotropic effects of TGF-β/Smad3 signaling on cell metabolism and energy homeostasis plays an important part in the progression of obesity-linked diabetes; these include adipocyte differentiation, adipose browning, inflammation and regulation of insulin signaling amongst others. Members of TGF-β superfamily transmit their signals *via* dual serine/threonine kinase receptors and transcription factors called Smads. Recent studies have clearly established an essential role of TGF-β/Smad3 signaling in the pathogenesis of obesity and type 2 diabetes. Elevated levels of TGF-β has been reported in mice and human adipose tissue during hypertension and other cardiovascular diseases as well as in morbid obesity and diabetic neuropathy (51–53). Increased TGF-β levels have also been associated with a higher risk for type 2 diabetes in a prospective case-cohort study (54). Perry et al. identified Samd3 gene in a type2 diabetes genome-wide association study (55). Smad3 is known to bind to the PGC-1α promoter to repress its transcription (13). As PGC-1α is an important transcriptional coactivator for UCP1 gene induction, mitochondrial biogenesis, and fatty acid oxidation, it is not surprising that TGF-β/Smad3 signaling would inhibit beige/brown adipocyte differentiation and their thermogenic action. The discovery of TGF-β/Smad3 signaling as novel modifiers of beige adipocyte phenotype and metabolic characteristics by Yadav et al. has opened therapeutic avenues for identifying potent inhibitors of this signaling pathway for the treatment of obesity related complications (13). The authors observed significant positive correlation between TGF-β1 levels and adiposity in both rodents and human subjects. $Smad3^{-/-}$ mice displayed protection against diet-induced obesity and related metabolic syndromes. These effects were associated with significant induction of white to brown phenotype and increased mitochondrial biogenesis. Examination of a group of nondiabetic human subjects from diverse ethnic groups, the authors found direct relationship

between circulating TGF-β1 levels and BMI, fat mass, and oxygen consumption. The same group assessed the effect of blocking TGF-β/Smad3 signaling in two well-characterized mouse models of obesity and type 2 diabetes. Treatment with anti-TGF-β neutralizing antibody 1D11 resulted in significantly reduced body weight, improved glucose and insulin tolerance, as well as fasting glucose and insulin levels. These beneficial effects were associated with elevated expression of BAT and mitochondria-specific proteins including UCP1, COX-1 and PGC-1α as well as decreased phosphorylation of Smad3 in white adipose tissues. Such links between TGF-β signaling and mitochondrial energy metabolism pathway have also been reported by other laboratories (56). In addition, several studies have demonstrated extensive interaction between TGF-β and key energy sensors including adenosine monophosphate protein kinase (AMPK) and sirtuin family members (57, 58). Inhibition of activin receptor IIB (ActRIIB) responsible for integrating actions of TGF-β ligands promotes differentiation of primary brown adipocytes *in-vitro* and increases brown fat mass, but not white fat mass in mouse (59). Furthermore, inhibition of ActRIIB *via* a decoy receptor containing extracellular domain of ActRIIB fused with human Fc (ActRIIB-Fc) resulted in suppression of diet-induced obesity and related metabolic complications in mice (60). This blockade of ActRIIB was associated with increased browning and robust upregulation of UCP1 and PGC-1α expression in the epididymal white adipose fat and led to increased energy expenditure under ambient or cold temperature. Gene signature induced as result of ActRIIB inhibition, displayed an interesting similarity with PGC-1α overexpression *in-vivo*. Combined together, these studies provide significant insights into the role of TGF-β signaling in suppressing adipose browning program within white fat tissues in both mouse models and human subjects, suggesting that blockade of TGF-β activity could serve as an effective treatment strategy for obesity and diabetes.

Since bone morphogenic proteins (BMPs) belong to the same superfamily of growth factors as TGF-β, and regulate various aspects of white and brown adipocyte differentiation, we discussed below briefly their biological functions in modulating adipose tissue functions (61–66). BMP4 has been shown to promote differentiation of human adipose stem cells into beige adipocytes (61, 62). BMP4 overexpressing transgenic mice display reduced adiposity, improved insulin sensitivity, and induction of brown adipocytes within inguinal subcutaneous fat depots (63, 64). Interestingly, these transgenic mice display decreased expression of brown adipocyte markers including UCP1 and PGC-1α in the BAT (62). In spite of reduced BAT activity, these BMP4 overexpressing mice are protected from diet-induced obesity and insulin resistance perhaps due to increased WAT browning (63). It, therefore, appears that BMP4 may have opposite effects on the development of brown adipocytes in BAT and beige adipocytes in WAT *in-vivo*. BMP7 promotes the commitment of mesenchymal progenitor cells to a brown adipocyte lineage while it prevents osteogenesis by inhibiting the expression of runt-related transcription factor 2 (*Runx2*) (67). In C3H/10T1/2 cells, pretreatment with BMP7 results in brown adipogenesis with lipid accrual and expression of *Ucp1* (67). Tail vein injection of adenovirus expressing BMP7 increases BAT, without affecting the mass of WAT (67). Although BMP7 increases Prdm16 and Ucp1 expression in brown adipose, there are no changes in the expression of genes involved in energy metabolism in white adipose, muscle, or liver. The increase in BAT mass results in increased energy expenditure, higher basal body temperature, and decreased body weight attributes that clearly link BMP7 signaling to energy balance. BMP7 knockout mice show significant reduction of brown fat mass (67). Conversely, adenoviral-mediated expression of BMP7 in mice results in significant increase in brown fat mass, increased energy expenditure and reduction in weight gain and subcutaneous implantation of BMP7-treated MSCs into athymic nude mice results in ectopic brown adipose tissue formation (67). BMP8b promotes brown adipose tissue thermogenesis through both central and peripheral actions (65). This thermogenic effect of BMP8a is observed only in female mice and is thought to be mediated by estrogens (66). The molecular mechanisms responsible for such differential regulation of WAT, beige and BAT by various BMP members remains largely unknown.

MYOSTATIN, IRISIN, ADIPOSE BROWNING AND ENERGY METABOLISM

Myostatin (MST), also referred to as growth and differentiation factor 8 (GDF8), is a member of TGF-β superfamily. MST is synthesized as a precursor protein, which consists of a N-terminal propeptide domain that contains the signal sequence and a C-terminal domain that forms a disulfide-linked dimer and functions as the active ligand (68). MST requires release from the propeptide to be biologically active (69). MST binding to ActRIIB leads to the phosphorylation of Smad3 (70). Phosphorylated Smad3 can bind other Smad proteins and these complexes translocate into the nucleus, where they regulate the transcription of target genes (70). It is mainly expressed in skeletal muscle but is also detectable in cardiac muscle, blood, and to a limited extent in adipose cells. MST is known as the potent negative regulator of muscle mass as inactivation of *Mst* gene significantly accelerates muscle growth in cattle, sheep, fish and humans (71–75).

Recent studies from several laboratories have provided conclusive evidence that the effect of MST extends beyond its role in skeletal muscle, and it plays a significant role in the regulation of body fat and overall energy metabolism. Mst-knockout (*Mst*-KO) mice show significantly increased muscle mass, decreased fat mass, improved insulin sensitivity and resistance to diet-induced obesity (76, 77). On the other hand, overexpression of MST in mice has been shown to promote catabolic conditions and result in muscle wasting and cause insulin resistance (78). Since MST is expressed in very low amounts in fat tissues, it is not clear how lack of MST can

suppress fat accumulation in *Mst*-KO mice. Significantly increased energy expenditure and leptin sensitivity was observed in *Mst*-KO mice that could potentially explain reduced fat mass in these mice when compared to the WT mice (79). In primary cultures of mouse preadipocyte cells, Kim et al. reported decreased expression of key thermogenic genes *Ucp1*, *Prdm16*, and *Pgc-1a* and significant inhibition of brown adipogenic differentiation following treatment of the cells with recombinant MST protein (80). Using differentiating primary cultures of mouse embryonic fibroblast (MEF) isolated from *Mst*-KO and WT embryos, Braga et al. reported significant upregulation of key thermogenic markers in differentiating cultures of *Mst*-KO group compared to the WT group (81). In the same study, treatment with recombinant MST protein led to a significant decrease in Oil-Red O stained adipocytes and expression of key thermogenic genes in both WT and Mst-KO groups. Comparative analyses of epididymal (Epi) and subcutaneous (SC) adipose tissues isolated from WT and *Mst*-KO mice show clear induction of thermogenic proteins including UCP1, and PRDM16 along with C/EBPα. Gene expression analyses further confirmed significant upregulation of key adipogenic differentiation markers *Cebpα* and *Pparγ*, as well as key thermogenic genes including *Prdm16, Ucp1, Bmp7, PGC-1a/b* and *Cidea*, suggesting that loss of MST significantly promotes brown adipose-related markers in two main adipose depots in *Mst*-KO mice (81). Similar comparative analyses of muscle tissues from androgen-dependent (levator ani, LA) and independent (gastrocnemius, Gas) muscle tissues show upregulation of UCP1 and PRDM16 protein and several genes involved in the regulation of overall thermogenic program. These combined in-vitro and *in-vivo* approaches using differentiating MEF cultures, as well as *Mst*-KO and their WT littermates show that MST inhibition could not only promote white adipocyte browning in adipose depots but could also promote the conversion of inter-muscular white adipocytes into beige/brown adipocytes. Furthermore, protein expression analysis of energy-sensing adenosine monophosphate (AMP)-activated protein kinase (AMPK), a critical regulator of mitochondrial biogenesis that controls energy metabolism by acting in co-ordination with NAD+-dependent type III deacetylase sirtuin1 (Sirt1) was found to be significantly upregulated in differentiating *Mst*-KO MEF primary cultures compared to the WT group (81). Protein expression of adiponectin, a key protein secreted from adipocytes and regulator of adipocyte energy metabolism was also found to be upregulated in differentiating MEF cultures isolated from Mst-KO group compared to the WT (81). Adiponectin is reported to limit triglyceride (TG) accumulation in liver (82), increase glucose clearance and improve hepatic insulin action in adiponectin transgenic mice (82, 83). Zhang et al. also reported that inhibition of MST leads to increased skeletal muscle mass, slows down fat accumulation, lowers body weight and circulating levels of triacylglycerol in mice on high-fat diet (84). The authors reported that white adipose tissue of *Mst*-KO mouse express significantly higher levels of genes involved in lipid transport, synthesis, oxidation and hydrolysis. In addition, adipose tissues isolated from *Mst*-KO mice show increased expression of UCP1 and upregulation of AMPK signaling pathway when compared to the WT mice (84). Histological analysis of WAT isolated from Mst-KO revealed BAT-like cells filled with multilocular smaller lipid droplets and immunopositive for UCP1 (81), suggesting that MST deletion induced brown-like phenotype. Genetic loss of MST has also been reported to promote white adipose browning and improve insulin sensitivity by several other laboratories (85, 86). Shan et al. performed a thorough analysis of various muscle-derived circulatory factors to identify possible mediators of adipose browning phenotype in these Mst-KO mice (86). The authors reported that skeletal muscle derived irisin (encoded by *Fndc5* gene) plays a central role in promoting adipose browning in *Mst*-KO mice by activating AMPK-PGC-1α-Fndc5 signaling, providing an interesting involvement of muscle-adipose cross talk during adipose browning (86). Dong et al. also reported the involvement of Fndc5/irisin-mediated white adipose browning and improvement in insulin signaling in Mst-KO mice (87). *Mst*-KO Meishan pigs with functional deletion of Mst show increased insulin sensitivity, adipose browning and upregulation of several browning-like gene signature including *Ucp1, Prdm16, Pgc-1α, Cidea*, *Cd137* and *Tmem26* (85). Protein expression analysis of skeletal muscle in these *Mst*-KO pigs shows significantly increased levels of insulin receptor (IR) and insulin receptor substrate (IRS). Skeletal muscle protein expression of irisin precursor protein Fndc5 as well the serum irisin levels were significantly higher in Meishan *Mst*-KO pigs compared to the WT pigs. Activation of insulin signaling pathway could not be blocked *via* inhibition of irisin in this study, suggesting possible irisin independent activation of insulin signaling in MST deficient skeletal muscle (85). Reduction of interferon regulatory factor 4 (IRF4) leads to significantly reduced exercise capacity, mitochondrial function and ribosomal protein synthesis in brown fat, an effect that was associated with induction of MST levels (88). On the other hand, overexpression of IRF4 led to significantly reduced levels of serum MST and increased exercise capacity in muscle. IRF4 was shown to physically interact with PGC-1α and promote the thermogenic program by upregulating the transcription of UCP1 gene and driving mitochondrial biogenesis in BAT. In addition, IRF4 levels in BAT was found to be significantly induced following cold exposure and β3-adrenergic receptor (AR) agonist (88). These findings, therefore, suggest that IRF4 is a novel inducer of overall thermogenic program with the potential to inactivate MST bioactivity. Guo et al. reported additional role of MST regulation in the development of proatherogenic dyslipidemia, insulin-mediated glucose disposal as well as protection against hepatic steatosis (89). The authors show that administration of adeno-associated virus 9 (AAV9)-mediated MST pro-peptide significantly blocked the progression of atherosclerosis and development of hepatosteatosis in $LDLR^{-/-}$ mice on western diet. In this study, the beneficial effects of both *Mst* genetic ablation as well as its inactivation by MST pro-peptide were attributed to result from the enlarged muscle mass although the authors did not study its effect on adipose browning and brown fat activation. Several laboratories provided

compelling evidence to support the notion that brown fat activation could reduce hypercholesterolemia and elicit protection form atherosclerosis development (90–92). Most recently, Pydi et al. demonstrated that increased plasma MST levels in mice lacking β-arrestin 1 (barr1) (adipo-baar1-KO) led to impaired insulin signaling in multiple peripheral tissues (93). On the other hand, overexpression of baar1 in adipo-baar1-OE mice on high fat diet displayed pronounced improvements in glucose tolerance, insulin sensitivity, and displayed significant reduction in MST levels, suggesting that overexpression of baar1 in adipocytes protects mice from obesity-associated metabolic disorders. Collectively, these data provide strong evidence that inhibition of MST could provide justification not only for increased muscle mass but could also be beneficial for the treatment of obesity and associated metabolic disorders through activation of adipose browning.

Irisin is a key myokine and adipokine that is secreted following the proteolytic cleavage of its precursor fibronectin type III domain containing protein 5 (FNDC5). Secreted irisin exerts its major action by upregulating the expression of UCP1 and promoting browning of WAT (94). Circulating levels of irisin are regulated by various factors including diet, exercise, obesity and pharmacological agents (95). Bostrom et al. first isolated irisin from muscle tissues and performed its chemical characterization (96). Following exercise stimulation and activation of transcriptional co-activator PGC-1α, FNDC5 expression levels are increased in muscle, resulting in the secretion of irisin to induce adipose browning through activation of thermogenic genes (96). These findings provided strong evidence for the beneficial role of irisin in cardiovascular, obesity, diabetes, skeletal and other diseases. Cold activation and physical activity among several other factors are known to alter the level of circulating irisin (97, 98). Plasma irisin levels are reported to increase by 65% after 3 weeks of freewheel running, while in healthy humans irisin levels double after 10 weeks of endurance exercise (96). Several studies demonstrated that irisin improves glucose homeostasis, and its circulating levels are inversely associated with liver fat content (99–101). Based on these findings, irisin was revealed as a potential new target for the treatment of metabolic diseases. However, in contrast with the above reports, several other studies question the beneficial role of irisin and in some cases even its existence (101–104). There is also a disagreement regarding the induction of FNDC5/irisin by exercise (105, 106), and its association with markers of glucose and lipid homeostasis disturbance in obesity and metabolic syndrome (107–110). Such controversies could be explained by the fact that irisin levels increase only when muscle ATP concentration decreased in absence of physical activity during sedentary lifestyle (105). Perez-Sotelo et al. reported decreased browning capacity and increased adipogenesis of differentiating adipocytes by blocking adipose endogenous expression of FNDC5 (111). The authors reported that incubation of normal adipocytes with secreted factors from the WAT of obese patients resulted in significant reduction of FNDC5, PGC-1α and UCP1 expression. Irisin is also reported to influences glucose metabolism in skeletal muscle (112) and myocytes in-vitro *via* increased oxidative phosphorylation, mitochondrial biogenesis and upregulation of various genes involved in glucose transport as well as in mitochondrial uncoupling (113). Furthermore, exogenous FNDC5 induces UCP1 expression in subcutaneous white adipocytes in animal models, and FNDC5 overexpression in the liver prevented diet-induced weight gain, metabolic disturbances, and stimulation of oxygen consumption (114). Irisin administration was also found to increase the secretion of glycerol and decrease lipid accumulation *via* regulating the expression of hormone-sensitive lipase (HSL), adipose triglyceride lipase (ATGL) and fatty acid-binding protein 4 (FABP4) (115). Moreover, irisin was found to inhibit hepatic cholesterol synthesis through AMPK-SREBP2 signaling (116) in addition to its ability to lower plasma glucose levels and altered food intake in streptozotocin-induced diabetes mellitus model (117). Subcutaneous perfusion of irisin resulted in significantly increased energy expenditure, reduced hyperlipidemia and hyperglycemia, and improved insulin resistance (118). These beneficial effects of irisin were mediated *via* upregulation of cAMP/PKA/HSL-perilipin pathway (118). In a recent report, Li et al. provided supporting evidence for a critical role of irisin in mediating Fst-induced browning (119). They reported that Fst injection promoted increased secretion of irisin from the subcutaneous fat depots *via* AMPK-PGC1-α-irisin mediated signaling during adipose browning. In cardiomyocyte H9C2 cells, recombinant irisin (r-irisin) activated PI3K/AKT pathway, induced intracellular Ca^{2+} signaling, and increased cellular oxygen consumption (120). In primary adipocytes and 3T3-L1 cells, r-irisin significantly increased the expression levels of key thermogenic genes including *Ucp-1*, *Pgc-1a*, *Cox7a*, *Ebf3*, and *Elovl3* and phosphorylated forms of p38 MAPK and ERK1/2. Pharmacological inhibition of p38 MAPK and ERK1/2 phosphorylation significantly lowered irisin-induced UCP-1 expression (94). Collectively, these studies provide novel beneficial role of irisin in regulating key metabolic parameters associated with perturbed lipid, cholesterol and energy metabolism.

FOLLISTATIN

Follistatin and Follistatin-Like Proteins

Follistatin (FST) was initially identified as component of the follicular fluid capable of inhibiting follicle-stimulating hormone (FSH) (121). FST is a monomeric glycosylated protein that binds and neutralizes activins with high affinity and neutralizes their bioactivity (121). FST also binds with lower affinity to several other members of the TGF-β superfamily including MST and BMPs 2, 5, 7, and 8 (122–125). These reports highlight the potential for FST to modulate the biological activities of several TGFβ superfamily, particularly at higher concentrations. Two variants of FST are generated through alternate splicing at the C-terminus of the common precursor gene (126). A third isoform of approximately 300-303 amino acids (FST300 or FST303) is also reported to be produced by proteolytic cleavage of the C-terminus of FST315 (127). The shorter isoform FST288 is

capable of binding heparin-sulfated proteoglycans on the cell surface with high affinity. The longer isoform FST315 is localized primarily in the circulation and has reduced affinity for heparin as a result of masking of the heparin-binding site at the C-terminal (121). Another molecule related to FST, called follistatin-like 3 (FSTL3) has been identified (128). This protein lacks the heparin-binding sequence, but similar to Fst, it binds activin A with high affinity and activin B with relatively lower affinity (129). FSTL3 is relatively less effective in blocking endogenous activin A in various cells (130). It is, therefore, possible that the ability of FST to bind to the proteoglycan cell surface could be important for potent inhibition of activin A action. While Fst is expressed in several tissues including ovary, pituitary, muscle and adipose tissues, FSTL3 is distributed predominantly in testis, placenta, heart and pancreas (131). Moreover, unlike Fst, FSTL3 is located in the nucleus, though it is also secreted at a relatively slower rate (131). Based on the tissue distribution, subcellular localization and intracellular transport pattern of FST and FSTL3, it is evident that they are not functionally redundant. Glycosylation of these core proteins produces a number of protein variants ranging in size from 31 to 42 kDa in size. Human FST is glycosylated at two specific sites, but point mutation of these sites does not change the affinity of FS315 for activin A (132). It is important to note that FSTL3 along with GASP1 and MST-propeptide binds with MST in circulation, suggesting that FST might not be the sole physiological regulator of MST *in-vivo* (133–135).

Follistatin and Muscle Mass

Matzuk et al. elegantly assessed the role of FST in regulating muscle mass and reported that FST loss-of-function mutant (*Fst*-KO) mice show decreased diaphragm and intercostal muscles and die within hours of birth (136). Based on the role of MST in being the most potent negative regulator of muscle mass to date and its inhibition by FST, Amthor et al. explored the role of possible interaction between FST and MST during chick development using yeast and mammalian two-hybrid system (123). The authors demonstrated that FST and MST interact directly with a high affinity of 5.84×10^{-10} M, and are expressed in the overlapping domains during muscle development. Moreover, MST-induced decrease in the expression levels of key myogenic proteins Pax3 and MyoD was significantly blocked in the presence of FST, suggesting an important role of FST in antagonizing the inhibitory effect on muscle development. Subsequently, it was reported that FST-induced muscle hypertrophy was associated inhibition of both MST and activin A and induction of satellite cell proliferation (137). Fst gene delivery of AAV1-FST344 in normal and dystrophic mice as well as in non-human primates led to significant increase in muscle mass and strength (138, 139). Transgenic expression of *Fst* in mdx mice, a popular model for Duchenne muscular dystrophy (DMD), showed amelioration of dystrophic pathology and increase in skeletal muscle mass (140). Interestingly, in a gene therapy trial Mendell et al. demonstrated beneficial effects of FST344 direct delivery into intramuscular quadriceps in patients suffering from Becker Muscular Dystrophy without any apparent side effects (141). Initially, FST was identified as a direct downstream target of testosterone action during its pro-myogenic action in both mouse models (142) and cell-culture studies (143). Protein and gene expression of FST was significantly upregulated in mouse mesenchymal pluripotent C3H 10T1/2 cells following testosterone treatment (142). This upregulation of FST was associated with a parallel increase in key myogenic markers MyoD and myosin heavy chain (MHC) II proteins, and co-treatment of the testosterone treated C3H 10T1/2 cells with anti-FST antibody abolished the myogenic action of testosterone. Furthermore, castration-induced decrease in FST expression was normalized to basal levels following testosterone supplementation, suggesting an intermediate role of FST in mediating testosterone's promyogenic action on muscle mass (142). Subsequently, Braga et al. reported for the first time that FST is expressed in primary cultures of muscle satellite cells and respond to the myogenic action of testosterone (143). FST significantly antagonized the TGF-β-induced inhibition of MHC II expression and phosphorylation of Smad2/3 in satellite cells (143). Combined together, these findings provide conclusive support for a central role of FST in promoting muscle mass and function, and its potential therapeutic use for the treatment of muscle wasting cachexic conditions often associated with aging, HIV, and cancer.

Follistatin and Adipose Browning

Although the role of FST in regulating skeletal muscle mass has been supported by abundant literature, its potential role in lipid metabolism has not been thoroughly investigated. Based on the established role of FST in inhibiting TGF-β/MST signaling pathway known to inhibit adipose browning and thermogenic program, it is logical to hypothesize that FST may promote brown adipose characteristics and favorably alter overall lipid and energy metabolism (144). Since both skeletal muscle and brown adipose tissue share common Myf5+ precursor population, there is a possibility that severe musculoskeletal defects and death of *Fst*-KO newborn pups could also be complicated by their concomitant decrease of BAT mass and activity, resulting in their inability to maintain proper body temperature especially during the early neonatal life. Braga et al. provided the first evidence for a potential role of FST in regulating brown adipose metabolic characteristics and thermogenesis (144). First insight regarding a direct role for FST in adipose tissues was obtained from analysis of Fst gene expression of a tissue panel from C57BL6/J mice that included WAT (inguinal subcutaneous and epididymal) and BAT depots, as well as several other metabolic tissues including brain, heart, intestine, liver, skeletal muscle, and testis (144). Interestingly, Fst gene expression was highest in BAT and skeletal muscle, and at substantial levels in inguinal WAT and liver compared to other tissues where its expression was significantly low. This finding, therefore, suggested a possible novel role of FST in regulating WAT and BAT metabolic characteristics. Differentiated mouse brown preadipocyte primary cultures show significant upregulation of FST expression along with key thermogenic markers UCP1 and PRDM16, compared to the undifferentiated cells. Interestingly, *Fst* gene expression dramatically increased in mouse BAT following cold-exposure, suggesting a possible

functional role of FST during brown adipocyte differentiation and regulation of thermogenesis. Comparative analysis of mouse embryonic fibroblast (MEF) primary cultures isolated from WT and Fst-KO embryos, Braga et al. demonstrated significant inhibition of key brown adipogenic markers including PRDM16, UCP1 and PGC-1α in Fst-KO differentiating MEF cultures compared to the WT group (144). Treatment of these cells with recombinant FST protein (rFST) resulted in significant upregulation of BAT-related genes and proteins in both WT and *Fst*-KO MEF differentiated cultures. Comprehensive analysis of global gene expression profile revealed lipid metabolism pathways as the most significantly altered pathways between WT and *Fst*-KO groups. Furthermore, *Fst*-KO differentiating cultures displayed significantly compromised basal mitochondrial respiration compared to the WT group. Addition of exogenous rFST protein to the *Fst*-KO cultures rescued this respiration impairment by increasing the cellular respiration. In addition, expression level of phosphorylated adenosine monophosphate (pAMPK), a key energy sensor implicated in the regulation of cellular energy balance, was significantly down regulated in *Fst*-KO compared to the WT MEFs. More recently, Li et al. further confirmed FST-induced adipose browning in high fat diet (HFD)-fed obese mice (119). The authors demonstrated that intraperitoneal injection of FST increased thermogenesis, energy expenditure and browning of subcutaneous adipose fat in mice on HFD. FST injected mice had significantly higher body temperature 37.5^0C compared to the control group. This FST-induced thermogenesis was further confirmed by infrared imaging that demonstrated high-temperature areas in the FST injected group compared to the control group (119). In agreement with previous reports, a recent study reported that a single injection of AAV-mediated FST administration after several weeks of HFD feeding induced browning of subcutaneous WAT by upregulation of PGC-1α, PRDM16, UCP1 and beige-specific CD137, and decreased obesity-associated metabolic inflammation (145). Collectively, these data provided interesting novel insight regarding the importance of FST in modulating lipid and energy metabolism and suggest that overexpression of FST *in-vivo* may promote both beige and brown adipose tissue mass and activity.

Molecular Targets of FST During Adipose Browning

Using follistatin transgenic (*Fst*-Tg) mice (146), Singh et al. systematically analyzed the effect of FST in both WAT and interscapular classical BAT (147). These *Fst*-Tg mice express Fst under a muscle-specific promoter and have significantly elevated (1.5 fold) circulating levels of FST as well as interscapular BAT mass (70% higher) compared to age-matched WT control mice (147). Analysis of BAT signature genes important for differentiation (*Ucp1, Prdm16, Zic1, Myf5, Lhx8*), fatty acid oxidation (*Ascl1, Fabp3, Cidea*) and mitochondrial biogenesis and function (*Pgc1α, Cox7a1, Cox8*) as well key thermogenic proteins (UCP1, PRDM16, PGC1α) were significantly upregulated in the interscapular BAT of the *Fst*-Tg mice compared to the WT mice (147). Comparative analysis of epididymal and subcutaneous WAT between *Fst*-Tg and WT mice displayed similar upregulation of key BAT-related markers. These changes observed in both WAT obtained from *Fst*-Tg mice was associated with distinct adipose browning characteristics including increased UCP1 immunostating, and upregulation of key beige-specific *Cd137* gene in both WAT depots, with greater changes observed in subcutaneous WAT compared to the epididymal WAT. These findings provided the first line of evidence that Fst promotes adipose browning in both WAT depots and increase BAT mass *in-vivo*.

Analysis of molecular targets of FST in these two adipose depots identified two distinctly different mechanisms. While FST increased phosphorylation of p38 MAPK and ERK1/2 in both WAT depots, it increased Myf5 expression in BAT of Fst-Tg mice (147). The authors also utilized in- vitro model of differentiating 3T3-L1 cultures to confirm that recombinant FST (rFST) treatment led to significant upregulation of UCP1 and beige-specific CD137 protein and beige-selective genes *Cd137*, *Tbx1*, and *Tmem26*. This rFST-induced increase in beige-selective markers in 3T3-L1 cells was also associated with concomitant increase in p38MAPK and ERK1/2 phosphorylation. Furthermore, pharmacological inhibition of their phosphorylation in these cells by either SB023580 or PD98059 resulted in abrogation of rFst-induced upregulation of UCP1 protein expression, suggesting that FST stimulates adipose browning *via* p38MAPK/ERK1/2 pathway. Since FST overexpression in *Fst*-Tg mice displayed distinctly different targets in WAT and BAT tissues, Singh et al. analyzed differential expression of key TGF-β signaling components Smad3/pSmad3 and activin receptor type IIB (Act RIIB) in adipose tissues obtained from WT and Fst-Tg mice. FST overexpression in these *Fst*-Tg mice led to significant inhibition of Smad3/pSmad3 as well as Act RIIB expression in both SC and Epi WAT as well as in BAT (147), suggesting that inhibition of Smad3 signaling may be the common upstream target of FST action that precedes phosphorylation of p38 MAPK/ERK1/2 and activation of Myf5. FST-induced inhibition of TGF-β/Smad3 signaling has also been reported previously in satellite cells and muscle tissues (142, 143). In order to further test the effect of FST overexpression on adipocyte browning in differentiating 3T3-L1 cells, Singh et al. cloned full-length mouse Fst gene in Piggyback Transposon cargo plasmid vector to perform systematic beige/brown adipose gene expression analysis following Fst overexpression (148). Comparative gene expression analysis of Fst-overexpressing 3T3-L1 *Fst* cells with the parental 3T3-L1 cells displayed significantly higher levels of follistatin protein and gene in the cells and in the cell supernatant compared to the 3T3-L1 cells (148). Expression levels of key thermogenic and several adipose browning markers including CD137, Tbx1, and Tmem26 were significantly upregulated following Fst overexpression in differentiating 3T3-L1 cells (148). **Table 1** and **Table 2** summarizes a comprehensive list of proteins and genes respectively that are influenced by increased levels of FST in various cell culture and *Fst* transgenic (*Fst*-Tg) mouse model. *Fst* overexpression also led to significant induction of p38 MAPK and ERK1/2 phosphorylation in-vitro in 3T3-L1 confirming previous findings of induced phosphorylation of these proteins

TABLE 1 | List of proteins targeted by follistatin.

Model System	Protein	Change	Reference
Mouse embryonic fibroblast (MEF) cultures in adipogenic differentiation medium; WT vs. *Fst* KO	UCP1	↓	(144)
	PRDM16	↓	(144)
	aP2	↓	(144)
	PPARγ	↓	(144)
	PGC-1α	↓	(144)
	Cyt C	↓	(144)
Interscapular brown adipose tissue (BAT); WT vs. *Fst*-Tg	UCP1	↑	(147)
	UCP2	↑	(147)
	UCP3	↑	(147)
	PRDM16	↑	(147)
	PGC-1α	↑	(147)
	AdipoQ	↑	(147)
	Myf5	↑	(147)
	pSmad3	↓	(147)
	Smad3	↓	(147)
	ActRIIB	↓	(147)
Epididymal and subcutaneous adipose tissue; WT vs. *Fst*-Tg	UCP1	↑	(147)
	UCP2	↑	(147)
	UCP3	↑	(147)
	PRDM16	↑	(147)
	PGC1α	↑	(147)
	BMP7	↑	(147)
	Glut4	↑	(147)
	CD137	↑	(147)
	pp38 MAPK	↑	(147)
	pERK1/2	↑	(147)
	pSmad3	↓	(147)
	Smad3	↓	(147)
	ActRIIB	↓	(147)
	AdipoQ	↑	(148)
	FGF21	↑	(148)
	pAMPK	↑	(148)
Differentiating 3T3-L1 cells treated with recombinant FST (rFST); Control vs. rFST	UCP1	↑	(147)
	CD137	↑	(147)
	pp38 MAPK	↑	(147)
	pERK1/2	↑	(147)
	AdipoQ	↑	(148)
	AdipoR1	↑	(148)
	FGF21	↑	(148)
	pAMPK	↑	(148)
	PGC-1α	↑	(148)
	SirT1	↑	(148)
Mouse brown adipose tissue (BAT) cells treated with rFST: Con vs. rFST	UCP1	↑	(147)
	Eva1	↑	(147)
	Myf5	↑	(147)
Fst overexpressing stable 3T3-L1 (3T3-L1 *Fst*) cells; 3T3-L1-*Fst* vs. 3T3-L1	UCP1	↑	(148)
	CD137	↑	(148)
	p38 MAPK	↑	(148)
	pERK1/2	↑	(148)
	COX-IV	↑	(148)
	SirT1	↑	(148)
	SirT3	↑	(148)
	AdipoQ	↑	(148)

in both WAT depots of *Fst*-Tg mice. Previous reports have suggested an essential role for p38MAPK in promoting cyclic-AMP-dependent activation of protein kinase A (PKA) and activation of UCP1 transcription (149, 150). Phosphorylation of p38 MAPK following stimulation of beta-adrenergic receptor (β-AR) results in phosphorylation and recruitment of ATF2 and PGC-1α to PPRE and CRF2 motifs within the UCP1 enhancer following their interactions with PPARγ and RXRα to activate the brown adipose thermogenic program (151). Phosphorylation of p38MAPK has also been shown to stimulate adipose browning *via* induction of irisin, a key myokine that can be significantly induced by exercise and PGC1-α (117). Recent data suggest that Fndc5 is also secreted from WAT (152). Since FST is known to induce irisin encoded Fndc5 gene in mouse muscle cells (86), it is possible that induced levels of irisin/Fndc5 will have contributed to increased browning *via* phosphorylation of p38 MAPK and ERK1/2 in *Fst*-Tg mice. Robust activation of FGF21/adiponectin/pAMPK signaling pathway was found in both adipose depots of *Fst*-Tg mice suggest a possible link between *Fst* overexpression and FGF21 activation (147). In order to test the possible intermediate role of β3-AR signaling during FST-induced browning, Singh et al. also tested whether treatment of β3 agonist CL316, 243 would promote BAT activation and adipose browning in *Fst*-Tg compared to the WT mice. The authors were able to show heightened response to β3-AR activation on UCP1 expression in both WAT depots and BAT tissues obtained from *Fst*-Tg mice compared to the WT mice (147).

In order to identify the molecular targets of FST in classical brown fat, Singh et al. also analyzed the effects of exogenous rFST on differentiating mouse brown preadipocyte BAT cultures (147). rFST treatment led to significant increase in BAT-selective UCP1, Eva1, and Myf5 protein and gene expression. They also showed that siRNA-mediated knockdown of mouse Myf5 expression led to significant blockade of FST-induced UCP1 protein and gene expression and two key BAT-selective genes *Lhx8* and *Zic1*. Furthermore, *Fst*-KO embryo sections show decreased Myf5 immunostating compared to the WT, and treatment of differentiating MEF cultures derived from *Fst*-KO embryo with rFST was able to rescue Myf5 protein expression (147). Collectively, these findings obtained from differentiating BAT cells and *Fst* KO primary cultures provide strong evidence that Myf5 acts as an obligatory target of FST in promoting brown adipose characteristics. It appears however, that major action of FST on adipose browning is primarily due to the blocking of TGF-β ligands to inhibit Smad3 signaling as shown in **Figure 1**. A comprehensive list of proteins and genes targeted by FST during adipose browning are also summarized in **Tables 1** and **2** respectively.

Genetic Manipulation of Follistatin Expression and its Relevance to Obesity Related Metabolic Diseases

As adipose tissues are the primary site of energy storage and its mobilization, activation of adipose browning has the potential to positively regulate overall systemic metabolism (153, 154). Adipose browning-induced biochemical changes are implicated

TABLE 2 | List of genes targeted by follistatin.

Model System	Gene	Change	Reference
Mouse brown preadipocyte cells treated with rFST; WT vs. rFST	*Ucp1*	↑	(144)
	Prdm16	↑	(144)
	Pgc1a	↑	(144)
	Fabp3	↑	(144)
Differentiating Mouse embryonic fibroblast (MEF) cultures; WT vs. *Fst* KO	*Ucp1*	↓	(144)
	Prdm16	↓	(144)
	Pgc1a	↓	(144)
	Bmp7	↓	(144)
	Pgc1b	↓	(144)
	Cidea	↓	(144)
	Acsl1	↓	(144)
	AdipoQ	↓	(144)
	Agpat9	↓	(144)
	Cd36	↓	(144)
	Fabp4	↓	(144)
	Mup1	↓	(144)
	Thrsp	↓	(144)
	Apoa2	↓	(144)
	F13a1	↓	(144)
	G2e3	↓	(144)
	Gas5	↓	(144)
	Ifi203	↓	(144)
	Titin	↑	(144)
	Vtn	↓	(144)
	Hp	↓	(144)
	Plg	↓	(144)
	Atpla2	↓	(144)
	Saa1	↓	(144)
	Cps1	↓	(144)
	Serpine 1	↓	(144)
Interscapular brown adipose tissue (BAT); WT vs. *Fst*-Tg	*Ucp1*	↑	(147)
	Prdm16	↑	(147)
	Zic1	↑	(147)
	Myf5	↑	(147)
	Lhx8	↑	(147)
	Acsl1	↑	(147)
	Fabp3	↑	(147)
	Cidea	↑	(147)
	Pgc1a	↑	(147)
	Cox7a1	↑	(147)
	Cox8	↑	(147)
	Glut4	↑	(147)
Epididymal and Subcutaneous adipose tissue; WT vs. *Fst*-Tg	*Ucp1*	↑	(147)
	Prdm16	↑	(147)
	Pgc1a	↑	(147)
	Acsl1	↑	(147)
	Fabp3	↑	(147)
	Cidea	↑	(147)
	Elov3	↑	(147)
	Cox7a1	↑	(147)
	Cox8	↑	(147)
	Cd137	↑	(147)
	Fgf21	↑ (Epi +SC)	(148)
	Egr1	↑ (Epi +SC)	(148)
	c-Fos	↑ (Epi +SC)	(148)
	Fgfr1	↑ (Epi)	(148)
	Fgfr2	↑ (SC)	(148)
	Fgfr3	↑ (SC)	(148)
	Klb	↑ (SC)	(148)
Differentiating 3T3-L1 cells treated with recombinant FST: Control vs. rFST	*Ucp1*	↑	(147)
	Cd137	↑	(147)
	Tbx1	↑	(147)
	Tmem26	↑	(147)
Fst overexpressing stable 3T3-L1 (3T3-L1-*Fst*) cells; 3T3-L1-*Fst* vs. 3T3-L1	*Ucp1*	↑	(148)
	Cd137	↑	(148)
	Pgc1a	↑	(148)
	Fgf21	↑	(148)
	Tbx1	↑	(148)
	Tmem26	↑	(148)
	Ppara	↑	(148)
	Fasn	↓	(148)
	Th	↑	(148)
	Bmp7	↑	(148)
	Ptgs2	↑	(148)
	Cox7a1	↑	(148)
	Cox8b	↑	(148)
	Cpta	↑	(148)
	Mst	↓	(148)

in alterations of several key metabolic pathways that regulate plasma glucose levels and triglyceride metabolism in mice. Beige and brown adipose tissues consume and metabolize nutrients in a specialized way to facilitate weight loss, amelioration of insulin resistance and protection from hyperlipidemia and obesity related metabolic syndromes (155, 156). In order to assess the metabolic consequences of FST-induced adipose browning, Singh et al. performed quantitative analysis of abdominal fat volume, glucose clearance and comprehensive analysis of serum lipid profiles of *Fst*-Tg mice (148). Computerized tomography (CT) scan analysis of Fst-Tg mice revealed significantly lower percentage of abdominal fat mass and increased glucose disposal rate compared to the WT mice (148). Also, serum levels of triglycerides (TG), free fatty acid (FFA), and glucose levels were significantly lower in Fst-Tg mice compared to the WT mice without any significant changes in total cholesterol (TC) and high-density lipoprotein (HDL) levels. Major urinary protein 1 (Mup1), a key regulator of glucose and lipid metabolism (157), and energy expenditure (158) was significantly upregulated in liver and both WAT depots of *Fst*-Tg mice compared to the WT (148). Braga et al. previously reported a significant decrease in Mup1 gene expression in *Fst*-KO MEF differentiating cultures compared to the WT (144). In another recent study, Davey et al. reported that intravascular gene delivery *via* rAAV6-FST 317 to prediabetic *db/db* mice ameliorates progression of hyperglycemia, maintains insulinemia, promote abundance of insulin producing beta cell population, and reduced number of α-like cells (159). The authors also reported that *Fst* gene delivery to older mice with hyperglycemia and declining insulinemia led to significant restoration of

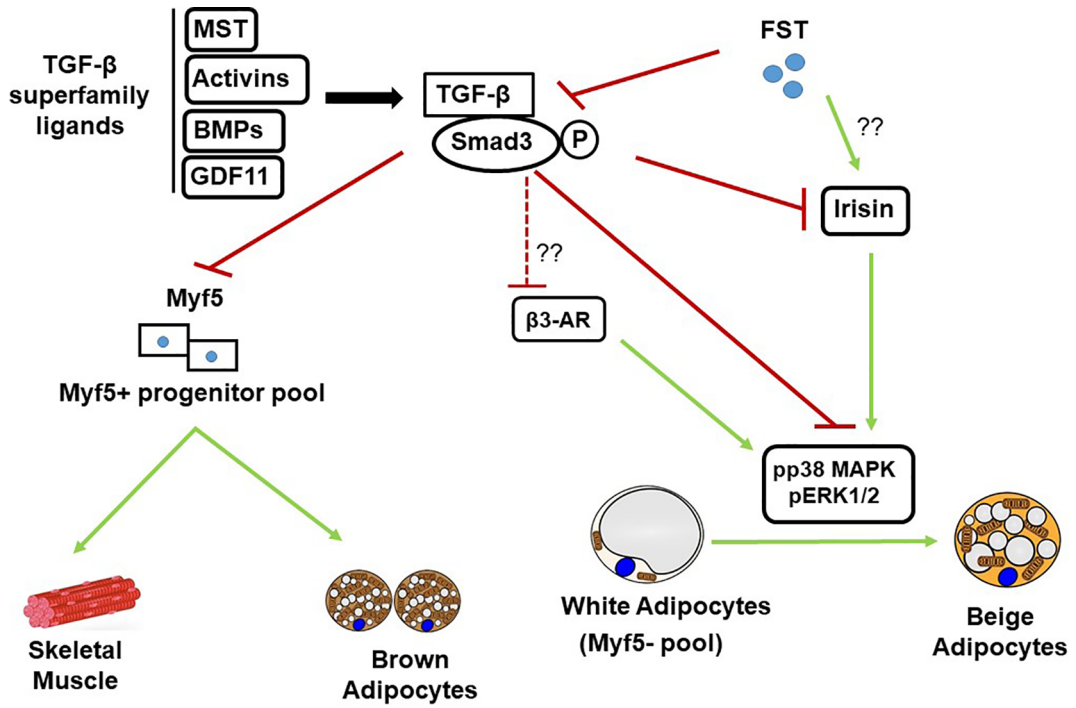

FIGURE 1 | Schematic diagram showing FST modulation of TGF-β/Samd 3 signaling pathway during adipose browning. MST, Myostatin; BMPs, Bone morphogenic proteins; GDF11, Growth and differentiation factor 11; TGF-β, Transforming growth factor beta.

serum insulin concentration. Diabetic *db/db* mice display compromised β-cell function and reduced insulin content. Overexpression of FST in pancreatic-β cells has previously been reported to counter insulin insufficiency and extend the life span of *db/db* mice mainly by inhibition of SMAD pathway and activation of the PI3-kinase/Akt pathway (160). Most recently, Tang et al. also reported significant decrease in body fat percentage in mice on normal diet, and ameliorated the increase in body fat after HFD following AAV-Fst mediated gene delivery (145). In this study, *Fst* gene delivery in the HFD group significantly decreased serum levels of insulin, leptin, resistin, and C-peptide as well as serum glucose, triglycerides, cholesterol, and free FFAs as compared to control group. AAV-*Fst* gene delivery also significantly increased circulating levels of vascular endothelial growth factor (VEGF) and lowered serum levels of inflammatory cytokine IL-1α. In addition, reduced levels of mitochondrial oxidative phosphorylation (OXPHOS) complex subunits in subcutaneous WAT of mice on HFD was normalized following Fst overexpression *via* increased expression of PGC-1α. Although Fst has been reported to promote PGC-1α expression in previous studies (144, 147), the precise mechanism responsible for Fst-induced upregulation of PGC-1α remains unknown. Collectively, these findings provide exciting supporting evidence that Fst gene therapy could elicit beneficial metabolic effects and mitigate HFD-induced obesity. In order to test the effect of FST overexpression on overall lipidomic profiles in differentiating 3T3-L1 cells, Singh et al. performed comparative metabolic profiling of basal 3T3-L1 and Fst overexpressing 3T3-L1 *Fst* cells (148). Increased mitochondrial biogenesis in differentiated 3T3-L1 *Fst* cultures was also confirmed by significantly increased maximal oxygen consumption rate (OCR) (148). Analysis of endogenous lipid metabolites displayed a general reduction in diglycerides (DG), triglycerides (TG), ceramide, FA, phosphatidylcholine (PC), phosphatidylethanolamine (PE), and lysophosphatidylethanolamine (LPE) in FST overexpressing 3T3-L1 Fst cells compared to the basal 3T3-L1 cells (148). On the other hand, levels of several lyosophosphatidylcholines (LPL) such as LPC (16.0), LPC (18.0), and LPC (18.1) were significantly increased in 3T3-L1 *Fst* cells in comparison with the 3T3-L1 cells (148). These *in-vitro* data, thus, provide supporting evidence that genetic manipulation of FST could favorably alter overall lipid metabolites known to be associated with fat mass and promote obesity and associated metabolic conditions (161, 162). *In-vivo* analysis of adipose tissues from *Fst*-Tg mice also show significant differences in several amino acids including leucine, isoleucine, and valine also collectively referred to as branched-chain amino acids (BCAA), key components of urea cycle and arginine metabolism, and components of the Kreb's cycle including citrate, succinylcarnitine, and fumarate were significantly lower compared to the WT tissues. FST overexpression in Fst-Tg mice was associated with significant upregulation of two key BCAA catabolic proteins BCAT2 and BCKDHA in epididymal

WAT (148). Several recent studies have provided convincing evidence in support of a positive association between BCAA levels and insulin resistance and type 2 diabetes as their levels are significantly induced in obese subjects compared to the lean humans (163, 164). Levels of ω-3 polyunsaturated fatty acids (PUFAs), reported to improve obesity-associated chronic inflammation, insulin resistance and dyslipidemia (165), and regulate several aspects of energy and lipid metabolism (166) were significantly increased in the subcutaneous WAT of Fst-Tg mice. Levels of key lysolipids, known metabolic regulators of childhood obesity (167) were significantly elevated in the Epi WAT of *Fst*-Tg compared to the WT mice. Combined together, these findings obtained from comprehensive metabolomic profiling of Fst transgenic mice provide compelling evidence that genetic manipulation of *Fst in-vivo* favorably alters the levels of key metabolites known to influence various aspects of metabolic conditions, and warrant future studies for the use of FST based therapeutic interventions to combat obesity and related diseases (168).

CONCLUSION

Obesity and associated comorbidities resulting from accumulation of dysfunctional white adipose tissues and chronic imbalance between energy intake and energy expenditure represent a growing worldwide problem. Activation of adipose browning characteristics leads to the dissipation of excess stored energy and provide metabolic benefits to combat the burden of obesity and related abnormalities including insulin resistance, hyperlipidemia, type 2 diabetes and cardiovascular diseases. Adipose browning phenomenon in humans has been confirmed based on both morphological, and functional studies (5, 6, 16). Accordingly, new strategies are being explored to identify novel compounds that can promote adipose browning and reduce the development of obesity and associated conditions. Recent reports from several laboratories provide convincing evidence that inhibition of TGF-β signaling pathway provides metabolic protection from obesity and diabetes by regulating glucose and energy homeostasis *via* activation of white adipose browning (13, 59). Genetic inactivation of MST, a key member of TGF-β superfamily not only results in increased muscle mass but also promotes activation of adipose browning and favorably alters several metabolic parameters implicated in the development of metabolic complications (86, 87). Since Fst is a known inhibitor of MST and reported to antagonize overall TGF-β signaling, it is logical to explore the therapeutic potential of FST in regulating key metabolic functions in both adipose depots besides its established role in promoting muscle mass. Recent findings by Braga et al. provided the first evidence that FST enhances the acquisition of beige and brown adipose characteristics by directly targeting Myf5- and Myf5+ populations to promote beige and brown adipose characteristics respectively (142). Since Myf5+ precursor population gives rise to both skeletal muscle and brown fat (20), it is not surprising that FST could selectively target these populations to promote both muscle and BAT mass (147, 169). Additionally, identification of key molecular and cellular targets responsible for FST-induced adipose browning is necessary to develop therapeutic strategies for the treatment of obesity and related diseases. Although activation of p38MAPK and ERK1/2 signaling is necessary for FST-induced adipose browning in both adipose depots (147), it is important to explore the possible role of irisin/Fndc5 during the process as secretion of irisin and subsequent activation of p38 MAPK and ERK1/2 has been reported during exercise (94). Since FST secretion is also induced following exercise (169, 170) and rFST treatment leads to elevated Fndc5 gene expression in muscle (86), it is possible that FST will indirectly affect p38MAPK and ERK1/2 activation *via* increased secretion of irisin. β3-AR signaling has been shown to promote p38 MAPK activation and induce browning of WAT and nonshivering thermogenesis in BAT (150, 171, 172). It is, therefore, possible that FST activates β3-AR signaling to promote p38 MAPK phosphorylation during adipose browning as β3 agonist CL 316,243 treatment elicited additive response in UCP1 levels in both WAT depots as well as in BAT (147). FGF21, another key regulator of adipose browning and a downstream target of β3-AR signaling (173, 174) is upregulated in WAT of Fst transgenic mice, suggesting a possible link between FST and FGF21 signaling during adipose browning. Based on available data, it appears that the beneficial effects of FST on adipose browning, obesity, and related metabolic conditions are mainly due to blocking of TGF-β ligands including MST and inhibition of Smad3 signaling as summarized in **Figure 1**. Finally, data obtained from Fst gene therapy studies in both human and nonhuman primates did not indicate apparent structural or functional aberration in various tissues, suggesting that FST may have therapeutic potential in clinical settings for the treatment of obesity and related diseases.

AUTHOR CONTRIBUTIONS

RS and SP organized and wrote the manuscript. SR edited the manuscript and provided constructive comments. All authors contributed to the article and approved the submitted version.

FUNDING

This work was supported by National Institute of Health grant numbers SC1AG049682 (RS), SC1CA232319 (SP), TRDRP grant number T31IP1551 (RS, SR), Boston Pepper Center P30 AG031679 (RS), UHI NIMHD S21MD000103, and Accelerating Excellence in Translational Sciences (AXIS) Center U54MD007598 to Charles R. Drew University of Medicine and Science.

ACKNOWLEDGMENTS

We thank Azra Tezein Devonshire for language editing.

REFERENCES

1. Tam CS, Lecoultre V, Ravussin E. Brown adipose tissue: mechanisms and potential therapeutic targets. . *Circulation* (2012) 125:2782–91. doi: 10.1161/CIRCULATIONAHA.111.042929
2. *The Toll of America's Obesity*. The New York Times (2018). Available at: https://www.nytimes.com/2018/08/09/opinion/cost-diabetes-obesity-budget.html.
3. Chen Y, Ikeda K, Yoneshiro T, Scaramozza A, Tajima K, Wang Q, et al. Thermal stress induces glycolytic beige fat formation via a myogenic state. *Nature* (2019) 565:180–5. doi: 10.1038/s41586-018-0801-z
4. Oguri Y, Shinoda K, Kim H, Alba DL, Bolus WR, Wang Q, et al. CD81 controls beige fat progenitor cell growth and energy balance via FAK signaling. *Cell* (2020) 182:563–77. doi: 10.1016/j.cell.2020.06.021
5. Cypess AM, Lehman S, Williams G, Tal I, Rodman D, Goldfine AB, et al. Identification and importance of brown adipose tissue in adult humans. *N Engl J Med* (2009) 360(15):1509–17. doi: 10.1056/NEJMoa0810780
6. van Marken Lichtenbelt WD, Vanhommerig JW, Smulders NM, Drossaerts JM, Kemerink GJ, Bouvy ND, et al. Cold-activated brown adipose tissue in healthy men. *N Engl J Med* (2009) 360(15):1500–8. doi: 10.1056/NEJMoa0808718
7. Cao L, Choi EY, Liu X, Martin A, Wang C, Xu X, et al. White to brown fat phenotypic switch induced by genetic and environmental activation of a hypothalamic-adipocyte axis. *Cell Metab* (2011) 14:324–38. doi: 10.1016/j.cmet.2011.06.020
8. Bartelt A, Heeren J. Adipose tissue browning and metabolic health. *Nat Rev Endocrinol* (2014) 10:24–36. doi: 10.1038/nrendo.2013.204
9. Cannon B, Nedergaard J. Brown adipose tissue: function and physiological significance. *Physiol Rev* (2004) 84:277–359. doi: 10.1152/physrev.00015.2003
10. Cohen P, Levy JD, Zhang Y, Frontini A, Kolodin DP, Svensson KJ, et al. Ablation of PRDM16 and beige adipose causes metabolic dysfunction and a subcutaneous to visceral fat switch. *Cell* (2014) 156:304–16. doi: 10.1016/j.cell.2013.12.021
11. Seale P, Conroe HM, Estall J, Kajimura S, Frontini A, Ishibashi J, et al. Prdm16 determines the thermogenic program of subcutaneous white adipose tissue in mice. *J Clin Invest* (2011) 121(1):96–105. doi: 10.1172/JCI44271
12. Zheng Q, Lin J, Huang J, Zhang H, Zhang R, Zhang X, et al. Reconstitution of UCP1 using CRISPR/Cas9 in the white adipose tissue of pigs decreases fat deposition and improves thermogenic capacity. *Proc Natl Acad Sci USA* (2017) 114(45):E9474–82. doi: 10.1073/pnas.1707853114
13. Yadav H, Quijano C, Kamaraju AK, Gavrilova O, Malek R, Chen W, et al. Protection from obesity and diabetes by blockade of TGF-β/Smad3 signaling. *Cell Metab* (2011) 14:67–79. doi: 10.1016/j.cmet.2011.04.013
14. Gilsanz V, Hu HH, Kajimura S. Relevance of brown adipose tissue in infancy and adolescence. *Pediatr Res* (2013) 73:3–9. doi: 10.1038/pr.2012.141
15. Palmer AK, Kirkland JL. Aging and adipose tissue: potential interventions for diabetes and regenerative medicine. *Exp Gerontol* (2016) 86:97–105. doi: 10.1016/j.exger.2016.02.013
16. Sidossis L, Kajimura S. Brown and beige fat in humans: thermogenic adipocytes that control energy and glucose homeostasis. *J Clin Invest* (2015) 125:478–86. doi: 10.1172/JCI78362
17. Atit R, Sgaier SK, Mohamed OA, Taketo MM, Dufort D, Joyner AL, et al. Beta-catenin activation is necessary and sufficient to specify the dorsal dermal fate in the mouse. *Dev Biol* (2006) 296:164–76. doi: 10.1016/j.ydbio.2006.04.449
18. Lepper C, Fan CM. Inducible lineage tracing of Pax7-descendant cells reveals embryonic origin of adult satellite cells. *Genesis* (2010) 48:424–36. doi: 10.1002/dvg.20630
19. Sanchez-Gurmaches J, Hung CM, Sparks CA, Tang Y, Li H, Guertin DA. PTEN loss in the Myf5 lineage redistributes body fat and reveals subsets of white adipocytes that arise from Myf5 precursors. *Cell Metab* (2012) 16:348–62. doi: 10.1016/j.cmet.2012.08.003
20. Seale P, Bjork B, Yang W, Kajimura S, Chin S, Kuang S, et al. PRDM16 controls a brown fat/skeletal muscle switch. *Nature* (2008) 454:961–7. doi: 10.1038/nature07182
21. Kajimura S, Seale P, Spiegelman BM. Transcriptional control of brown fat development. *Cell Metab* (2010) 11:257–62. doi: 10.1016/j.cmet.2010.03.005
22. Harms M, Seale P. Brown and beige fat: development, function and therapeutic potential. *Nat Med* (2013) 19:1252–63. doi: 10.1038/nm.3361
23. Porter C, Chondronikola M, Sidossis LS. The therapeutic potential of brown adipocytes in humans. *Front Endocrinol (Lausanne)* (2015) 6:156. doi: 10.3389/fendo.2015.00156
24. Rodríguez A, Becerril S, Ezquerro S, Méndez-Giménez L, Frühbeck G. Crosstalk between adipokines and myokines in fat browning. *Acta Physiol (Oxf)* (2017) 219:362–81. doi: 10.1111/apha.12686
25. Abdullahi A, Jeschke MG. White adipose tissue browning: a double-edged sword. *Trends Endocrinol Metab* (2016) 27:542–52. doi: 10.1016/j.tem.2016.06.006
26. Long JZ, Svensson KJ, Tsai L, Zeng X, Roh HC, Kong X, et al. A smooth muscle-like origin for beige adipocytes. *Cell Metab* (2014) 19:810–20. doi: 10.1016/j.cmet.2014.03.025
27. Vishvanath L, MacPherson KA, Hepler C, Wang QA, Shao M, Spurgin SB, et al. Pdgfrβ+ mural preadipocytes con-tribute to adipocyte hyperplasia induced by high-fat-diet feeding and prolonged cold exposure in adult mice. *Cell Metab* (2016) 23:350–9. doi: 10.1016/j.cmet.2015.10.018
28. Berry DC, Jiang Y, Graff JM. Mouse strains to study cold-inducible beige progenitors and beige adipocyte formation and function. *Nat Commun* (2016) 7:10184. doi: 10.1038/ncomms10184
29. Lee YH, Petkova AP, Mottillo EP, Granneman JG. *In vivo* identification of bipotential adipocyte progenitors recruited by beta3-adrenoceptor activation and high-fat feeding. *Cell Metab* (2012) 15:480–91. doi: 10.1016/j.cmet.2012.03.009
30. Frontini A, Cinti S. Distribution and development of brown adipocytes in the murine and human adipose organ. *Cell Metab* (2010) 11:253–6. doi: 10.1016/j.cmet.2010.03.004
31. Rosenwald M, Perdikari A, Rülicke T, Wolfrum C. Bi-directional interconversion of brite and white adipocytes. *Nat Cell Biol* (2013) 15:659–67. doi: 10.1038/ncb2740
32. Puigserver P, Wu Z, Park CW, Graves R, Wright M, Spiegelman BM. A cold-inducible coactivator of nuclear receptors linked to adaptive thermogenesis. *Cell* (1998) 92:829–39. doi: 10.1016/s0092-8674(00)81410-5
33. Wu Z, Puigserver P, Andersson U, Zhang C, Adelmant G, Mootha V, et al. Mechanisms controlling mitochondrial biogenesis and respiration through the thermogenic coactivator PGC-1. *Cell* (1999) 98:115–24. doi: 10.1016/S0092-8674(00)80611-X
34. Harms MJ, Ishibashi J, Wang W, Lim HW, Goyama S, Sato T, et al. Prdm16 is required for the maintenance of brown adipocyte identity and function in adult mice. *Cell Metab* (2014) 19(4):593–604. doi: 10.1016/j.cmet.2014.03.007
35. Seale P, Kajimura S, Yang W, Chin S, Rohas LM, Uldry M, et al. Transcriptional control of brown fat determination by PRDM16. *Cell Metab* (2007) 6:38–54. doi: 10.1016/j.cmet.2007.06.001
36. Wu J, Boström P, Sparks LM, Ye L, Choi JH, Giang AH, et al. Beige adipocytes are a distinct type of thermogenic fat cell in mouse and human. *Cell* (2012) 150:366–76. doi: 10.1016/j.cell.2012.05.016
37. Wang W, Kissig M, Rajakumari S, Huang L, Lim HW, Won KJ, et al. Ebf2 is a selective marker of brown and beige adipogenic precursor cells. *Proc Nat Acad Sci USA* (2014) 111:14466–71. doi: 10.1073/pnas.1412685111
38. Lidell ME, Betz MJ, Leinhard OD, Heglind M, Elander L, Slawik M, et al. Evidence for two types of brown adipose tissue in humans. *Nat Med* (2013) 19:631–4. doi: 10.1038/nm.3017
39. Sharp LZ, Shinoda K, Ohno H, Scheel DW, Tomoda E, Ruiz L, et al. Human BAT possesses molecular signatures that resemble beige/brite cells. *PloS One* (2012) 7:e49452. doi: 10.1371/journal.pone.0049452
40. Petrovic N, Walden TB, Shabalina IG, Timmons JA, Cannon B, Nedergaard J. Chronic peroxisome proliferator activated receptor gamma (PPARgamma) activation of epididymally derived white adipocyte cultures reveals a population of thermogenically competent, UCP1- containing adipocytes molecularly distinct from classic brown adipocytes. *J Biol Chem* (2010) 285:7153–64. doi: 10.1074/jbc.M109.053942
41. Jespersen NZ, Larsen TJ, Peijs L, Daugaard S, Homøe P, Loft A, et al. A classical brown adipose tissue mRNA signature partly overlaps with brite in the supraclavicular region of adult humans. *Cell Metab* (2013) 17:798–805. doi: 10.1016/j.cmet.2013.04.011
42. Ussar S, Lee KY, Dankel SN, Boucher J, Haering MF, Kleinridders A, et al. ASC-1, PAT2, and P2RX5 are cell surface markers for white, beige, and brown adipocytes. *Sci Trans Med* (2014) 6:247ra103. doi: 10.1126/scitranslmed.3008490

43. Kim HJ, Cho H, Alexander R, Patterson HC, Gu M, Lo KA, et al. MicroRNAs are required for the feature maintenance and differentiation of brown adipocytes. *Diabetes* (2014) 63:4045–56. doi: 10.2337/db14-0466
44. Hu F, Wang M, Xiao T, Yin B, He L, Meng W, et al. miR-30 promotes thermogenesis and the development of beige fat by targeting RIP140. *Diabetes* (2015) 64:2056–68. doi: 10.2337/db14-1117
45. Sun L, Trajkovski M. MiR-27 orchestrates the transcriptional regulation of brown adipogenesis. *Metabolism* (2014) 63:272–82. doi: 10.1016/j.metabol.2013.10.004
46. Fu T, Seok S, Choi S, Huang Z, Suino-Powell K, Xu HE, et al. MicroRNA 34a inhibits beige and brown fat formation in obesity in part by suppressing adipocyte fibroblast growth factor 21 signaling and SIRT1 function. *Mol Cell Biol* (2014) 34:4130–42. doi: 10.1128/MCB.00596-14
47. Mori M, Nakagami H, Rodriguez-Araujo G, Nimura K, Kaneda Y. Essential role for miR-196a in brown adipogenesis of white fat progenitor cells. *PloS Biol* (2012) 10:e1001314. doi: 10.1371/journal.pbio.1001314
48. Liu W, Bi P, Shan T, Yang X, Yin H, Wang YX, et al. miR-133a regulates adipocyte browning *in vivo*. *PloS Genet* (2013) 9:e1003626. doi: 10.1371/journal.pgen.1003626
49. Budi EH, Duan D, Derynck R. Transforming growth factor-β receptors and Smads: Regulatory complexity and functional versatility. *Trends Cell Biol* (2017) 27:658–72. doi: 10.1016/j.tcb.2017.04.005
50. Shi Y, Massagué J. Mechanisms of TGF-beta signaling from cell membrane to the nucleus. *Cell* (2003) 113:685–700. doi: 10.1016/s0092-8674(03)00432-x
51. Fain JN, Tichansky DS, Madan AK. Transforming growth factor beta1 release by human adipose tissue is enhanced in obesity. *Metabolism* (2005) 54(11):1546–51. doi: 10.1016/j.metabol.2005.05.024
52. Alessi MC, Bastelica D, Morange P, Berthet B, Leduc I, Verdier M, et al. Plasminogen activator inhibitor 1, transforming growth factor-beta 1, and BMI are closely associated in human adipose tissue during morbid obesity. *Diabetes* (2000) 49:1374–80. doi: 10.2337/diabetes.49.8.1374
53. Gordon KJ, Blobe GC. Role of transforming growth factor-beta superfamily. Signaling pathways in human disease. *Biochim Biophys Acta* (2008) 1782:197–228. doi: 10.1016/j.bbadis.2008.01.006
54. Herder C, Zierer A, Koenig W, Roden M, Meisinger C, Thorand B. Transforming growth factor-beta1 and incident type 2 diabetes: results from the MONICA/KORA case-cohort study, 1984-2002. *Diabetes Care* (2009) 32:1921–3. doi: 10.2337/dc09-0476
55. Perry JR, McCarthy MI, Hattersley AT, Zeggini E , Wellcome Trust Case Control Consortium, Weedon MN, et al. Interrogating type 2 diabetes genome-wide association data using a biological pathway-based approach. *Diabetes* (2009) 58(6):1463–7. doi: 10.2337/db08-1378
56. Casalena G, Daehn I, Bottinger E. Transforming growth factor-β, bioenergetics, and mitochondria in renal disease. *Semin Nephrol* (2012) 32:295–303. doi: 10.1016/j.semnephrol.2012.04.009
57. Mishra R, Cool BL, Laderoute KR, Foretz M, Viollet B, Simonson MS. AMP-activated protein kinase inhibits transforming growth factor-beta-induced Smad3-dependent transcription and myofibroblast trans-differentiation. *J Biol Chem* (2008) 283:10461–9. doi: 10.1074/jbc.M800902200
58. Verdin E, Hirschey MD, Finley LW, Haigis MC. Sirtuin regulation of mitochondria: energy production, apoptosis, and signaling. *Trends Biochem Sci* (2010) 35:669–75. doi: 10.1016/j.tibs.2010.07.003
59. Fournier B, Murray B, Gutzwiller S, Marcaletti S, Marcellin D, Bergling S, et al. Blockade of the activin receptor IIb activates functional brown adipogenesis and thermogenesis by inducing mitochondrial oxidative metabolism. *Mol Cell Biol* (2012) 32:2871–9. doi: 10.1128/MCB.06575-11
60. Koncarevic A, Kajimura S, Cornwall-Brady M, Andreucci A, Pullen A, Sako D, et al. A novel therapeutic approach to treating obesity through modulation of TGFβ signaling. *Endocrinology* (2012) 153(7):3133–46. doi: 10.1210/en.2012-1016
61. Elsen MS, Raschke N, Tennagels U, Schwahn T, Jelenik M, Roden T, et al. BMP4 and BMP7 induce the white-to-brown transition of primary human adipose stem cells. *Am J Phys Cell Physiol* (2014) 306:C431–C44. doi: 10.1152/ajpcell.00290.2013
62. Gustafson A, Hammarstedt S, Hedjazifar JM, Hoffmann PA, Svensson J, Grimsby C, et al. BMP4 and BMP antagonists regulate human white and beige adipogenesis. *Diabetes* (2015) 64(5):1670–81. doi: 10.2337/db14-1127
63. Qian SW, Tang Y, Li X, Liu Y, Zhang YY, Huang HY, et al. BMP4-mediated brown fat-like changes in white adipose tissue alter glucose and energy homeostasis. *Proc Natl Acad Sci USA* (2013) 110:E798–807. doi: 10.1073/pnas.1215236110
64. Tang Y, Qian SW, Wu MY, Wang J, Lu P, Li XB, et al. BMP4 mediates the interplay between adipogenesis and angiogenesis during expansion of subcutaneous white adipose tissue. *J Mol Cell Biol* (2016) 8:302–12. doi: 10.1093/jmcb/mjw019
65. Whittle AJ, Carobbio S, Martins L, Slawik M, Hondares E, Vazquez MJ, et al. BMP8B increases brown adipose tissue thermogenesis through both central and peripheral actions. *Cell* (2012) 149:871–85. doi: 10.1016/j.cell.2012.02.066
66. Martins LP, Seoane-Collazo C, Contreras I, Gonzalez-Garcia N, Martinez-Sanchez F, Gonzalez JZ, et al. A functional link between AMPK and orexin mediates the effect of BMP8B on energy balance. *Cell Rep* (2016) 16:2231–42. doi: 10.1016/j.celrep.2016.07.045
67. Tseng YH, Kokkotou E, Schulz TJ, Huang TL, Winnay JN, Taniguchi CM, et al. New role of bone morphogenetic protein 7 in brown adipogenesis and energy expenditure. *Nature* (2008) 454(7207):1000–4. doi: 10.1038/nature07221
68. Thomas M, Langley B, Berry C, Sharma M, Kir S, Bass J, et al. Myostatin, a negative regulator of muscle growth, functions by inhibiting myoblast proliferation. *J Biol Chem* (2000) 275:40235–43. doi: 10.1074/jbc.M004356200
69. Zimmers TA, Davies MV, Koniaris LG, Haynes P, Esquela AF, Tomkinson KN, et al. Induction of cachexia in mice by systemically administered myostatin. *Science* (2002) 296:1486–8. doi: 10.1126/science.1069525
70. Massagué J, Chen YG. Controlling TGFβ signaling. *Genes Dev* (2000) 14(6):627–44.
71. McPherron AC, Lawler AM, Lee SJ. Regulation of skeletal muscle mass in mice by a new TGF-beta superfamily member. *Nature* (1997) 387(6628):83–90. doi: 10.1038/387083a0
72. McPherron AC, Lee SJ. Double muscling in cattle due to mutations in the myostatin gene. *Proc Natl Acad Sci USA* (1997) 94(23):12457–61. doi: 10.1073/pnas.94.23.12457
73. Kambadur R, Sharma M, Smith TP, Bass JJ. Mutations in myostatin (GDF8) in double-muscled Belgian Blue and Piedmontese cattle. *Genome Res* (1997) 7(9):910–6. doi: 10.1101/gr.7.9.910
74. Clop A, Marcq F, Takeda H, Pirottin D, Tordoir X, Bibe B, et al. A mutation creating a potential illegitimate microRNA target site in the myostatin gene affects muscularity in sheep. *Nat Genet* (2006) 38:813–8. doi: 10.1038/ng1810
75. Schuelke M, Wagner KR, Stolz LE, Hubner C, Riebel T, Komen W, et al. Myostatin mutation associated with gross muscle hypertrophy in a child. *N Engl J Med* (2004) 350:2682–8. doi: 10.1056/NEJMoa040933
76. Lebrasseur NK. Building muscle, browning fat and preventing obesity by inhibiting myostatin. *Diabetologia* (2012) 55:13–7. doi: 10.1007/s00125-011-2361-8
77. Bernardo BL, Wachtmann TS, Cosgrove PC, Kuhn M, Opsahl AC, Judkins KM, et al. Postnatal PPAR delta activation and myostatin inhibition exert distinct yet complimentary effects on the metabolic profile of obese insulin-resistant mice. *PloS One* (2010), e113075. doi: 10.1371/journal.pone.0011307
78. Zhang L, Rajan V, Lin E, Hu Z, Han HQ, Zhou X, et al. Pharmacological inhibition of myostatin suppresses systemic inflammation and muscle atrophy in mice with chronic kidney disease. *FASEB J* (2011) 5(6):e11307. doi: 10.1096/fj.10-176917
79. Choi SJ, Yablonka-Reuveni Z, Kaiyala KJ, Ogimoto K, Schwartz MW, Wisse BEIncreased energy expenditure and leptin sensitivity account for low fat mass in myostatin-deficient mice. American Journal of Physiology. *Endocrinol Metab* (2011) 300:E1031–7. doi: 10.1152/ajpendo.00656.2010
80. Kim WK, Choi HR, Park SG, Ko Y, Bae KH, Lee SC. Myostatin inhibits brown adipocyte differentiation via regulation of Smad3-mediated β-catenin stabilization. *Intern J Biochem Cell Biol* (2012) 44:327–34. doi: 10.1016/j.biocel.2011.11.004
81. Braga M, Pervin S, Norris K, Bhasin S, Singh R. Inhibition of in vitro and *in vivo* brown fat differentiation program by myostatin. *Obesity* (2013) 21:1180–8. doi: 10.1002/oby.20117

82. Asterholm IW, Scherer PE. Enhanced metabolic flexibility associated with elevated adiponectin levels. *Am J Pathol* (2010) 176(3):1364–76. doi: 10.2353/ajpath.2010.090647
83. Combs TP, Pajvani UB, Berg AH, Lin Y, Jelicks LA, Laplante M, et al. A transgenic mouse with a deletion in the collagenous domain of adiponectin displays elevated circulating adiponectin and improved insulin sensitivity. *Endocrinology* (2004) 145:367–83. doi: 10.1210/en.2003-1068
84. Zhang C, McFarlane C, Lokireddy S, Masuda S, Ge X, Gluckman PD, et al. Inhibition of myostatin protects against diet-induced obesity by enhancing fatty acid oxidation and promoting a brown adipose phenotype in mice. *Diabetologia* (2012) 55:183–93. doi: 10.1007/s00125-011-2304-4
85. Cai C, Qian L, Jiang S, Sun Y, Wang Q, Ma D, et al. Loss-of-function myostatin mutation increases insulin sensitivity and browning of white fat in Meishan pigs. *Oncotarget* (2017) 8:34911–22. doi: 10.18632/oncotarget.16822
86. Shan T, Liang X, Bi P, Kuang S. Myostatin knockout drives browning of white adipose tissue through activating the AMPK-PGC1α-Fndc5 pathway in muscle. *FASEB J* (2013) 27:1981–9. doi: 10.1096/fj.12-225755
87. Dong J, Dong Y, Dong Y, Chen F, Mitch WE, Zhang L. Inhibition of myostatin in mice improves insulin sensitivity via irisin-mediated cross talk between muscle and adipose tissues. *Int J Obes (Lond)* (2016) 40:434–42. doi: 10.1038/ijo.2015.200
88. Kong X, Banks A, Liu T, Kazak L, Rao RR, Cohen P, et al. IRF4 is a key thermogenic transcriptional partner of PGC-1α. *Cell* (2014) 158:69–83. doi: 10.1016/j.cell.2014.04.049
89. Guo W, Wong S, Bhasin S. AAV-mediated administration of myostatin propeptide mutant in adult Ldlr null mice reduces diet-induced hepatosteatosis and arteriosclerosis. *PloS One* (2013) 8(8):e71017. doi: 10.1371/journal.pone.0071017
90. Berbée JF, Boon MR, Khedoe PP, Bartelt A, Schlein C, Worthmann A, et al. Brown fat activation reduces hypercholesterolaemia and protects from atherosclerosis development. *Nat Commun* (2015) 6:6356. doi: 10.1038/ncomms7356
91. Bartelt A, John C, Schaltenberg N, Berbée JFP, Worthmann A, Cherradi ML, et al. Thermogenic adipocytes promote HDL turnover and reverse cholesterol transport. *Nat Commun* (2017) 8:15010. doi: 10.1038/ncomms15010
92. Hoeke G, Kooijman S, Boon MR, Rensen PC, Berbée JF. Role of brown fat in lipoprotein metabolism and atherosclerosis. *Circ Res* (2016) 118:173–82. doi: 10.1161/CIRCRESAHA.115.306647
93. Pydi SP, Cui Z, He Z, Barella LF, Pham J, Cui Y, et al. Beneficial metabolic role of β-arrestin-1 expressed by AgRP neurons. *Sci Adv* (2020) 6(23):eaaz1341. doi: 10.1126/sciadv.aaz1341
94. Zhang Y, Li R, Meng Y, Li S, Donelan W, Zhao Y, et al. Irisin stimulates browning of white adipocytes through mitogen-activated protein kinase p38 MAP kinase and ERK MAP kinase signaling. *Diabetes* (2014) 63(2):514–25. doi: 10.2337/db13-1106
95. Mahgoub MO, D'Souza C, Al Darmaki RSMH, Baniyas MMYH, Adeghate E. An update on the role of irisin in the regulation of endocrine and metabolic functions. *Peptides* (2018) 104:15–23. doi: 10.1016/j.peptides.2018.03.018
96. Bostrom P, Wu J, Jedrychowski MP, Korde A, Ye L, Lo JC, et al. A PGC1-α-dependent myokine that drives brown-fat-like development of white fat and thermogenesis. *Nature* (2012) 481:463–8. doi: 10.1038/nature10777
97. Lee P, Linderman JD, Smith S, Brychta RJ, Wang J, Idelson C, et al. Irisin and FGF21 are cold-induced endocrine activators of brown fat function in humans. *Cell Metab* (2014) 19:302–9. doi: 10.1016/j.cmet.2013.12.017
98. Moreno-Navarrete JM, Ortega F, Serrano M, Guerra E, Pardo G, Tinahones F, et al. Irisin is expressed and produced by human muscle and adipose tissue in association with obesity and insulin resistance. *J Clin Endocrinol Metab* (2013) 98:E769–78. doi: 10.1210/jc.2012-2749
99. Hojlund K, Bostrom P. Irisin in obesity and type 2 diabetes. *J Diabetes Complicat* (2013) 27:303–4. doi: 10.1016/j.jdiacomp.2013.04.002
100. Zhang HJ, Zhang XF, Ma ZM, Pan LL, Chen Z, Han HW, et al. Irisin is inversely associated with intrahepatic triglyceride contents in obese adults. *J Hepatol* (2013) 59:557–62. doi: 10.1016/j.jhep.2013.04.030
101. Crujeiras AB, Pardo M, Casanueva FF. Irisin: 'fat' or artefact. *Clin Endocrinol* (2015) 82:467–74. doi: 10.1111/cen.12627
102. Raschke S, Eckel J. Adipo-myokines: two sides of the same coin–mediators of inflammation and mediators of exercise. *Mediators Inflamm* (2013) 2013:320724. doi: 10.1155/2013/320724
103. Albrecht E, Norheim F, Thiede B, Holen T, Ohashi T, Schering L, et al. Irisin - a myth rather than an exercise-inducible myokine. *Sci Rep* (2015) 5:8889. doi: 10.1038/srep08889
104. Erickson HP. Irisin and FNDC5 in retrospect: An exercise hormone or a transmembrane receptor? *Adipocyte* (2013) 2:289–93. doi: 10.4161/adip.26082
105. Huh JY, Panagiotou G, Mougios V, Brinkoetter M, Vamvini MT, Schneider BE, et al. FNDC5 and irisin in humans: I. Predictors of circulating concentrations in serum and plasma and II. mRNA expression and circulating concentrations in response to weight loss and exercise. *Metabolism* (2012) 61:1725–38. doi: 10.1016/j.metabol.2012.09.002
106. Timmons JA, Davidsen PK, Atherton PJBK. Is irisin a human exercise gene? *Nature* (2012) 488:E9–10. doi: 10.1038/nature11364
107. Crujeiras AB, Zulet MA, Lopez-Legarrea P, de la Iglesia R, Pardo M, Carreira MC, et al. Association between circulating irisin levels and the promotion of insulin resistance during the weight maintenance period after a dietary weight-lowering program in obese patients. *Metabolism* (2014) 63:520–31. doi: 10.1016/j.metabol.2013.12.007
108. de la Iglesia R, Lopez-Legarrea P, Crujeiras AB, Pardo M, Casanueva FF, Zulet MA, et al. Plasma irisin depletion under energy restriction is associated with improvements in lipid profile in metabolic syndrome patients. *Clin Endocrinol (Oxf)* (2014) 81:1–6. doi: 10.1111/cen.12383
109. Lopez-Legarrea P, de la Iglesia R, Crujeiras AB, Pardo M, Casanueva FF, Zulet MA, et al. Higher baseline irisin concentrations are associated with greater reductions in glycemia and insulinemia after weight loss in obese subjects. *Nutr Diabetes* (2014) 4:e110. doi: 10.1038/nutd.2014.7
110. Park KH, Zaichenko L, Brinkoetter M, Thakkar B, Sahin-Efe A, Joung KE, et al. Circulating irisin in relation to insulin resistance and the metabolic syndrome. *J Clin Endocrinol Metab* (2013) 98:4899–907. doi: 10.1210/jc.2013-2373
111. Pérez-Sotelo D, Roca-Rivada A, Baamonde I, Baltar J, Castro AI, Domínguez E, et al. Lack of Adipocyte-Fndc5/Irisin Expression and Secretion Reduces Thermogenesis and Enhances Adipogenesis. *Sci Rep* (2017) 7(1):16289. doi: 10.1038/s41598-017-16602-z
112. Chen N, Li Q, Liu J, Jia S. Irisin, an exercise-induced myokine as a metabolic regulator: an updated narrative review. *Diabetes Metab Res Rev* (2016) 32(1):51–9. doi: 10.1002/dmrr.2660
113. Vaughan RA, Gannon NP, Barberena MA, Garcia-Smith R, Bisoffi M, Mermier CM, et al. Characterization of the metabolic effects of irisin on skeletal muscle in vitro. *Diabetes Obes Metab* (2014) 16:711–8. doi: 10.1111/dom.12268
114. Arhire LI, Mihalache L, Covasa M. Irisin: A Hope in Understanding and Managing Obesity and Metabolic Syndrome. *Front Endocrinol (Lausanne)* (2019) 10:524. doi: 10.3389/fendo.2019.00524
115. Gao S, Li FL, Huang Y, Liu Y, Chen Y. Effects and molecular mechanism of GST-Irisin on lipolysis and autocrine function in 3T3-L1 adipocytes. *PloS One* (2016) 11:e0147480. doi: 10.1371/journal.pone.0147480
116. Tang HR, Yu S, Liu B, Huwatibieke Z, Li W, Zhang W. Irisin inhibits hepatic cholesterol synthesis via AMPK-SREBP2 signaling. *EBio Med* (2016) 6:139–48. doi: 10.1016/j.ebiom.2016.02.041
117. Duan H, Ma B, Ma X, Wang H, Ni Z, Wang B, et al. Anti-diabetic activity of recombinant irisin in STZ-induced insulin-deficient diabetic mice. *Int J Biol Macromol* (2016) 84:457–63. doi: 10.1016/j.ijbiomac.2015.04.030
118. Xiong XQ, Chen D, Sun HJ, Ding L, Wang JJ, Chen Q, et al. FNDC5 overexpression and irisin ameliorate glucose/lipid metabolic derangements and enhance lipolysis in obesity. *Biochim Biophys Acta* (2015) 1852:1867–75. doi: 10.1016/j.bbadis.2015.06.017
119. Li H, Zhang C, Liu J, Xie W, Xu W, Liang F, et al. Intraperitoneal administration of follistatin promotes adipocyte browning in high-fat diet-induced obese mice. *PloS One* (2019) 14(7):e0220310. doi: 10.1371/journal.pone.0226344
120. Xie C, Zhang Y, Tran DN, Wang H, Li S, George EV, et al. Irisin Controls Growth, Intracellular Ca2+ Signals, and Mitochondrial Thermogenesis in Cardiomyoblasts. *PloS One* (2015) 10(8):e0136816–e0136816. doi: 10.1371/journal.pone.0136816

121. Welt C, Sidis Y, Keutmann HT, Schneyer A. Activins, inhibins and follistatins: from endocrinology to signalling—a paradigm for the new millennium. *Exp Biol Med* (2002) 227:724–52. doi: 10.1177/153537020222700905
122. Sidis Y, Mukherjee A, Keutmann H, Delbaere A, Sadatsuki M, Schneyer A. Biological activity of follistatin isoforms and follistatin-like-3 is dependent on differential cell surface binding and specificity for activin, myostatin, and bone morphogenetic proteins. *Endocrinology* (2006) 147:3586–97. doi: 10.1210/en.2006-0089
123. Amthor H, Nicholas G, McKinnell I, Kemp CF, Sharma M, Kambadur R, et al. Follistatin complexes Myostatin and antagonises Myostatin-mediated inhibition of myogenesis. *Dev Biol* (2004) 270(1):19–30. doi: 10.1016/j.ydbio.2004.01.046
124. Hedger MP, Winnall WR, Phillips DJ, de Kretser DM. The regulation and functions of activin and follistatin in inflammation and immunity. *Vitam Horm* (2011) 85:255–97. doi: 10.1016/B978-0-12-385961-7.00013-5
125. Iemura S, Yamamoto TS, Takagi C, Uchiyama H, Natsume T, Shimasaki S, et al. Direct binding of follistatin to a complex of bone-morphogenetic protein and its receptor inhibits ventral and epidermal cell fates in early Xenopus embryo. *Proc Natl Acad Sci USA* (1998) 95(16):9337–42. doi: 10.1073/pnas.95.16.9337
126. Shimasaki S, Koga M, Esch F, Cooksey K, Mercado M, Koba A, et al. Primary structure of the human follistatin precursor and its genomic organization. *Proc Natl Acad Sci USA* (1988) 85:4218–22. doi: 10.1073/pnas.85.12.4218
127. Inouye S, Guo Y, DePaolo L, Shimonaka M, Ling N, Shimasaki S. Recombinant expression of human follistatin with 315 and 288 amino acids: chemical and biological comparison with native porcine follistatin. *Endocrinology* (1991) 129:815–22. doi: 10.1210/endo-129-2-815
128. Tsuchida K, Arai KY, Kuramoto Y, Yamakawa N, Hasegawa Y, Sugino H. Identification and characterization of a novel follistatin-like protein as a binding protein for the TGF-beta family. *J Biol Chem* (2000) 275:40788–96. doi: 10.1074/jbc.M006114200
129. Schneyer A, Sidis Y, Xia Y, Saito S, del Re E, Lin HY, et al. Differential actions of follistatin and follistatin-like 3. *Mol Cell Endocrinol* (2004) 225(1-2):25–8. doi: 10.1016/j.mce.2004.02.009
130. Schneyer A, Schoen A, Quigg A, Sidis Y. Differential binding and neutralization of activins A and B by follistatin and follistatin like-3 (FSTL-3/FSRP/FLRG). *Endocrinology* (2003) 144:1671–4. doi: 10.1210/en.2002-0203
131. Tortoriello DV, Sidis Y, Holtzman DA, Holmes WE, Schneyer AL. Human follistatin-related protein: a structural homologue of follistatin with nuclear localization. *Endocrinology* (2001) 142:3426–34. doi: 10.1210/endo.142.8.8319
132. Inouye S, Guo Y, Ling N, Shimasaki S. Site-specific mutagenesis of human follistatin. *Biochem Biophys Res Commun* (1991) 179(1):352–8. doi: 10.1016/0006-291x(91)91377-o
133. Brown ML, Bonomi L, Ungerleider N, Zina J, Kimura F, Mukherjee A, et al. Follistatin and follistatin like-3 differentially regulate adiposity and glucose homeostasis. *Obesity (Silver Spring)* (2011) 19(10):1940–9. doi: 10.1038/oby.2011.97
134. Lee YS, Lee SJ. Regulation of GDF-11 and myostatin activity by GASP-1 and GASP-2. *Proc Natl Acad Sci U S A* (2013) 110(39):E3713–22. doi: 10.1073/pnas.1309907110
135. Lee SJ. Extracellular Regulation of Myostatin: A Molecular Rheostat for Muscle Mass. *Immunol Endocr Metab Agents Med Chem* (2010) 10:183–94. doi: 10.2174/187152210793663748
136. Matzuk MM, Lu N, Vogel H, Sellheyer K, Roop DR, Bradley A. Multiple defects and perinatal death in mice deficient in follistatin. *Nature* (1995) 374 (6520):360–3. doi: 10.1038/374360a0
137. Gilson H, Schakman O, Kalista S, Lause P, Tsuchida K, Thissen JP. Follistatin induces muscle hypertrophy through satellite cell proliferation and inhibition of both myostatin and activin. *Am J Physiol Endocrinol Metab* (2009) 297:E157–64. doi: 10.1152/ajpendo.00193.2009
138. Haidet AM, Rizo L, Handy C, Umapathi P, Eagle A, Shilling C, et al. Long-term enhancement of skeletal muscle mass and strength by single gene administration of myostatin inhibitors. *Proc Natl Acad Sci USA* (2008) 105:4318–22. doi: 10.1073/pnas.0709144105
139. Kota J, Handy CR, Haidet AM, Montgomery CL, Eagle A, Rodino-Klapac LR, et al. Follistatin gene delivery enhances muscle growth and strength in nonhuman primates. *Sci Transl Med* (2009) 1(6):6ra15. doi: 10.1126/scitranslmed.3000112
140. Nakatani M, Takehara Y, Sugino H, Matsumoto M, Hashimoto O, Hasegawa Y, et al. Transgenic expression of a myostatin inhibitor derived from follistatin increases skeletal muscle mass and ameliorates dystrophic pathology in mdx mice. *FASEB J* (2008) 22:477–87. doi: 10.1096/fj.07-8673com
141. Mendell JR, Sahenk Z, Malik V, Gomez AM, Flanigan KM, Lowes LP, et al. A phase 1/2a follistatin gene therapy trial for becker muscular dystrophy. *Mol Ther* (2015) 23:192–201. doi: 10.1038/mt.2014.200
142. Singh R, Bhasin S, Braga M, Artaza JN, Pervin S, Taylor WE, et al. Regulation of myogenic differentiation by androgens: cross talk between androgen receptor/beta-catenin and follistatin/transforming growth factor-beta signaling pathways. *Endocrinology* (2009) 150(3):1259–68. doi: 10.1210/en.2008-0858
143. Braga M, Bhasin S, Jasuja R, Pervin S, Singh R. Testosterone inhibits transforming growth factor-β signaling during myogenic differentiation and proliferation of mouse satellite cells: potential role of follistatin in mediating testosterone action. *Mol Cell Endocrinol* (2012) 350(1):39–52. doi: 10.1016/j.mce.2011.11.019
144. Braga M, Reddy ST, Vergnes L, Pervin S, Grijalva V, Stout D, et al. Follistatin promotes adipocyte differentiation, browning, and energy metabolism. *J Lipid Res* (2014) 55(3):375–84. doi: 10.1194/jlr.M039719
145. Tang R, Harasymowicz NS, Wu CL, Collins KH, Choi YR, Oswald SJ, et al. Gene therapy for follistatin mitigates systemic metabolic inflammation and post-traumatic arthritis in high-fat diet-induced obesity. *Sci Adv* (2020) 6 (19):eaaz7492. doi: 10.1126/sciadv.aaz7492
146. Lee SJ, McPherron AC. Regulation of myostatin activity and muscle growth. *Proc Natl Acad Sci USA* (2001) 98(16):9306–11. doi: 10.1073/pnas.151270098
147. Singh R, Braga M, Reddy ST, Lee SJ, Parveen M, Grijalva V, et al. Follistatin Targets Distinct Pathways To Promote Brown Adipocyte Characteristics in Brown and White Adipose Tissues. *Endocrinology* (2017) 158(5):1217–30. doi: 10.1210/en.2016-1607
148. Singh R, Pervin S, Lee SJ, Kuo A, Grijalva V, David J, et al. Metabolic profiling of follistatin overexpression: a novel therapeutic strategy for metabolic diseases. *Diabetes Metab Syndr Obes* (2018) 11:65–84. doi: 10.2147/DMSO.S159315
149. Robidoux J, Cao W, Quan H, Daniel KW, Moukdar F, Bai X, et al. Selective activation of mitogen-activated protein (MAP) kinase kinase 3 and p38alpha MAP kinase is essential for cyclic AMP-dependent UCP1 expression in adipocytes. *Mol Cell Biol* (2005) 25(13):5466–79. doi: 10.1128/MCB.25.13.5466-5479.2005
150. Cao W, Medvedev AV, Daniel KW, Collins S. Beta-adrenergic activation of p38 MAP kinase in adipocytes: cAMP induction of the uncoupling protein 1 (UCP1) gene requires p38 MAP kinase. *J Biol Chem* (2001) 276(29):27077–82. doi: 10.1074/jbc.M101049200
151. Bordicchia M, Liu D, Amri EZ, Ailhaud G, Dessì-Fulgheri P, Zhang C, et al. Cardiac natriuretic peptides act via p38 MAPK to induce the brown fat thermogenic program in mouse and human adipocytes. *J Clin Invest* (2012) 122:1022–36. doi: 10.1172/JCI59701
152. Arturo RR, Cecilia C, Senin LL, Landrove MO, Javier B, Ana BC, et al. FNDC5/irisin is not only a myokine but also an adipokine. *PloS One* (2013) 8 (4):e60563. doi: 10.1371/journal.pone.0060563
153. Hill BG. Insights into an adipocyte whitening program. *Adipocyte* (2015) 4 (1):75–80. doi: 10.4161/21623945.2014.960351
154. Peirce V, Carobbio S, Vidal-Puig A. The different shades of fat. *Nature* (2014) 510(7503):76–83. doi: 10.1038/nature13477
155. Abdullahi A, Jeschke MG. Taming the flames: targeting white adipose tissue browning in hypermetabolic conditions. *Endocr Rev* (2017) 38(6):538–49. doi: 10.1210/er.2017-00163
156. Fabbiano S, Suárez-Zamorano N, Rigo D, Veyrat-Durebex C, Stevanovic DA, Colin DJ, et al. Caloric restriction leads to browning of white adipose tissue through type 2 immune signaling. *Cell Metab* (2016) 24:434–46. doi: 10.1016/j.cmet.2016.07.023
157. Zhou Y, Jiang L, Rui L. Identification of MUP1 as a regulator for glucose and lipid metabolism in mice. *J Biol Chem* (2009) 284(17):11152–9. doi: 10.1074/jbc.M900754200
158. Hui X, Zhu W, Wang Y, Lam KSL, Zhang J, Wu D, et al. Major urinary protein-1 increases energy expenditure and improves glucose intolerance

through enhancing mitochondrial function in skeletal muscle of diabetic mice. *J Biol Chem* (2009) 284(21):14050–7. doi: 10.1074/jbc.M109.001107
159. Davey JR, Estevez E, Thomson RE, Whitham M, Watt KI, Hagg A, et al. Intravascular Follistatin gene delivery improves glycemic control in a mouse model of type 2 diabetes. *FASEB J* (2020) 34(4):5697–714. doi: 10.1096/fj.201802059RRR
160. Zhao C, Qioa C, Tang R-H, Jiang J, Li J, Martin CB, et al. Overcoming insulin insufficiency by forced follistatin expression in β-cells of *db/db* mice. *Mol Ther* (2015) 23:866–74. doi: 10.1038/mt.2015.29
161. Xia JY, Holland WL, Kusminski CM, Sun K, Sharma AX, Pearson MJ, et al. Targeted induction of ceramide degradation leads to improved systemic metabolism and reduced hepatic steatosis. *Cell Metab* (2015) 22(2):266–78. doi: 10.1016/j.cmet.2015.06.007
162. Barber MN, Risis S, Yang C, Meikle PJ, Staples M, Febbraio MA, et al. Plasma lysophosphatidylcholine levels are reduced in obesity and type 2 diabetes. *PloS One* (2012) 7(7):e41456. doi: 10.1371/journal.pone.0041456
163. McCormack SE, Shaham O, McCarthy MA, Deik AA, Wang TJ, Gerszten RE, et al. Circulating branched-chain amino acid concentrations are associated with obesity and future insulin resistance in children and adolescents. *Pediatr Obes* (2013) 8(1):52–61. doi: 10.1111/j.2047-6310.2012.00087.x
164. Lynch CJ, Adams SH. Branched-chain amino acids in metabolic signalling and insulin resistance. *Nat Rev Endocrinol* (2014) 10(12):723–36. doi: 10.1038/nrendo.2014.171
165. Martínez-Fernández L, Laiglesia LM, Huerta AE, Martínez JA, Moreno-Aliaga MJ. Omega-3 fatty acids and adipose tissue function in obesity and metabolic syndrome. *Prostaglandins Other Lipid Mediat* (2015) 121(Pt A):24–41. doi: 10.1016/j.prostaglandins.2015.07.003
166. Kim J, Okla M, Erickson A, Carr T, Natarajan SK, Chung S. Eicosapentaenoic acid potentiates brown thermogenesis through FFAR4-dependent Up-regulation of miR-30b and miR-378. *J Biol Chem* (2016) 291 (39):20551–62. doi: 10.1074/jbc.M116.721480
167. Butte NF, Liu Y, Zakeri IF, Mohney RP, Mehta N, Voruganti VS, et al. Global metabolomic profiling targeting childhood obesity in the Hispanic population. *Am J Clin Nutr* (2015) 102(2):256–67. doi: 10.3945/ajcn.115.111872
168. Singh R, Charles R. (2017). Drew University of Medicine and Science-Assignee; United States Patents, US9682093B2.
169. Li JX, Cummins CL. Getting the Skinny on Follistatin and Fat. *Endocrinology* (2017) 158(5):1109–12. doi: 10.1210/en.2017-00223
170. Hansen J, Brandt C, Nielsen AR, Hojman P, Whitham M, Febbraio MA, et al. Exercise induces a marked increase in plasma follistatin: evidence that follistatin is a contraction-induced hepatokine. *Endocrinology* (2011) 152(1):164–71. doi: 10.1210/en.2010-0868
171. Collins S, Surwit RS. The beta-adrenergic receptors and the control of adipose tissue metabolism and thermogenesis. *Recent Prog Horm Res* (2001) 56:309–28. doi: 10.1210/rp.56.1.309
172. Zheng Z, Liu X, Zhao Q, Zhang L, Li C, Xue Y. Regulation of UCP1 in the Browning of Epididymal Adipose Tissue by β3-Adrenergic Agonist: A Role for MicroRNAs. *Int J Endocrinol* (2014) 2014:530636. doi: 10.1155/2014/530636
173. Douris N, Stevanovic DM, Fisher FM, Cisu TI, Chee MJ, Nguyen NL, et al. Central Fibroblast Growth Factor 21 Browns White Fat via Sympathetic Action in Male Mice. *Endocrinology* (2015) 156(7):2470–81. doi: 10.1210/en.2014-2001
174. Fisher FM, Kleiner S, Douris N, Fox EC, Mepani RJ, Verdeguer F, et al. FGF21 regulates PGC-1alpha and browning of white adipose tissues in adaptive thermogenesis. *Genes Dev* (2012) 26(3):271–81. doi: 10.1101/gad.177857.111

Conflict of Interest: The authors declare that the research was conducted in the absence of any commercial or financial relationships that could be construed as a potential conflict of interest.

frontiers in Endocrinology

REVIEW
published: 19 April 2021
doi: 10.3389/fendo.2021.651763

Brown Adipose Tissue Heterogeneity, Energy Metabolism, and Beyond

Abhijit Babaji Shinde[1], *Anying Song*[1] *and Qiong A. Wang*[1,2]*

[1] Department of Molecular & Cellular Endocrinology, Arthur Riggs Diabetes and Metabolism Research Institute, Beckman Research Institute, City of Hope Medical Center, Duarte, CA, United States, [2] Comprehensive Cancer Center, Beckman Research Institute, City of Hope Medical Center, Duarte, CA, United States

Brown adipocyte in brown adipose tissue (BAT) specializes in expending energy through non-shivering thermogenesis, a process that produces heat either by uncoupling protein 1 (UCP1) dependent uncoupling of mitochondrial respiration or by UCP1 independent mechanisms. Apart from this, there is ample evidence suggesting that BAT has an endocrine function. Studies in rodents point toward its vital roles in glucose and lipid homeostasis, making it an important therapeutic target for treating metabolic disorders related to morbidities such as obesity and type 2 diabetes. The rediscovery of thermogenically active BAT depots in humans by several independent research groups in the last decade has revitalized interest in BAT as an even more promising therapeutic intervention. Over the last few years, there has been overwhelming interest in understanding brown adipocyte's developmental lineages and how brown adipocyte uniquely utilizes energy beyond UCP1 mediated uncoupling respiration. These new discoveries would be leveraged for designing novel therapeutic interventions for metabolic disorders.

Keywords: brown adipocyte development, brown adipocyte heterogeneity, thermogenesis, brown adipocyte energy metabolism, obesity

OPEN ACCESS

Edited by:
Xinran Ma,
East China Normal University, China

Reviewed by:
Craig Porter,
University of Arkansas for Medical Sciences, United States
Rubén Cereijo,
University of Barcelona, Spain
Lawrence Kazak,
McGill University, Canada

***Correspondence:**
Qiong A. Wang
qwang@coh.org

Specialty section:
This article was submitted to Cellular Endocrinology, a section of the journal Frontiers in Endocrinology

Received: *10 January 2021*
Accepted: *18 March 2021*
Published: *19 April 2021*

Citation:
Shinde AB, Song A and Wang QA (2021) Brown Adipose Tissue Heterogeneity, Energy Metabolism, and Beyond. Front. Endocrinol. 12:651763. doi: 10.3389/fendo.2021.651763

INTRODUCTION

Adipose tissue, one of the most plastic organs, is now widely accepted as an essential player in maintaining whole-body energy homeostasis (1, 2). Three different types of adipocytes that exist in mammals are white adipocytes, brown adipocytes, and beige or brite (stands for brown in white) adipocytes (3–6). Brown adipocytes and white adipocytes form a major part of brown adipose tissue (BAT) and white adipose tissue (WAT), respectively. In these adipose tissues, in addition to adipocytes, there are also stem cells, preadipocytes (committed adipocyte precursors), immune cells, fibroblasts, and endothelial cells. Both BAT and WAT appear as several discrete depots located throughout the body (7). Metabolically, WAT specializes in storing energy in the form of triglycerides. BAT expends energy *via* non-shivering thermogenesis, a process that involves dissipation of heat generated *via* uncoupling of mitochondrial respiration mediated by uncoupling protein 1 (UCP1) (8, 9). Morphologically, white adipocytes have unilocular lipid droplets, fewer mitochondria, and no expression of UCP1. Brown adipocytes have multilocular lipid

droplets, high mitochondria content, and high expression of UCP1 (3–5). We recently showed that there are two subpopulations of brown adipocytes which co-exist in the BAT of mice (10). One subpopulation has high thermogenic activity with high UCP1 expression, and the other one has low thermogenic activity with low UCP1 expression. Conversely, beige adipocytes usually appear in the WAT depots in response to external cues such as cold exposure, exercise, or adrenergic stimulation. Although similar to white adipocytes they have low UCP1 expression, with external stimuli they can be activated to increase both UCP1 expression as well as respiration rate. Furthermore, they show a molecular signature that is distinct from either white or brown adipocytes (11, 12).

It is now evident that heterogeneity exists within the thermogenic adipocytes in both rodents and humans. Studying the developmental lineages of this heterogeneous cell population along with the investigation of the key mechanisms involved in the activation and thermoregulation of these adipocytes will enable us to identify novel therapeutic targets to treat metabolic disorders. In this review, we will discuss the developmental origins of BAT along with its heterogeneity followed by its developmental timeline. We will also summarize the recent works on BAT metabolism and fuel selection.

DEVELOPMENTAL ORIGINS AND HETEROGENEITY OF BAT

Early lineage tracing studies suggested that brown adipocytes are closer to skeletal muscles in developmental origin than white adipocytes. Atit et al. showed that cells from mouse embryo central dermomyotome, which express the homeobox transcription factor Engrailed 1 at E9.5 give rise to interscapular BAT (iBAT), dermis, and skeletal muscles (13). After this observation, several other studies were published supporting the same notion that BAT and skeletal muscles share the common progenitors. Using a *Myf5*^{Cre} driver crossed to a cytoplasmic reporter, the Spiegelman group elegantly showed that Myf5^{+} cells contribute to iBAT and skeletal muscles but not to any WAT depots (14). They also demonstrated that PR domain zinc-finger protein 16 (PRDM16) acts as a molecular switch between myoblast and brown fat cell lineages (14). Another study using an inducible Cre under the control of the *Pax7* promoter also showed that Pax7^{+} progenitors labeled at E9.5 give rise to iBAT. They also found that the myogenic restriction of the Pax7^{+} lineage occurs at the later stage in between E9.5 and E12.5 (15). Also, microarray analysis demonstrated that brown preadipocytes show myogenic transcription signature (16). Furthermore, when compared at transcriptome as well as proteome levels, brown fat mitochondria were found to share many similarities with muscle mitochondria (17). Remarkably, several factors including Ewing Sarcoma (EWS), Zinc Finger Protein 516 (ZFP516), Euchromatic Histone Lysine Methyltransferase 1 (EHMT1), early B cell factor-2 (EBF2), TATA-Box Binding Protein Associated Factor 7 Like (TAF7L), and some microRNAs (MyomiR-133, Mir193b-365) have been shown to affect cell fate decision between brown fat and muscle (14, 18–25). Using *Myf5*^{Cre} crossed to *R26R-mTmG* reporter, the Guertin group suggested that brown adipocytes are not exclusively derived from *Myf5* lineage, and this lineage also contributes to white and beige adipocyte populations (26, 27). They also traced a couple of other myoblast-specific markers *viz. Pax3* and *MyoD1* and found that *Pax3* lineage was represented more broadly in the global brown adipocyte population, while *MyoD1*^{Cre} did not trace any of the brown adipocyte population confirming that they do not arise from *MyoD1* lineage (26). Furthermore, some other studies have also reported the heterogeneous adipocyte labeling with *Myf5* lineage (28, 29). Altogether, these studies suggest that brown adipocytes from different depots or even within the same depots could derive from different embryonic lineages. Moreover, another recent report described that only 50% of adipocytes in iBAT derive from Pax7^{+} lineage originating from the central dermomyotome (30); which initially was thought to be a sole source of iBAT.

Several groups have reported the heterogeneous UCP1 expression as well as mitochondrial potential in brown adipocytes (31–34). Spaethling et al. using a single-cell RNA sequencing (scRNA-seq) of nine handpicked mature brown adipocytes showed a transcriptome variability of brown adipocytes. In addition to variability in the expression of well-known brown adipocyte markers such as UCP1 and *Adrb3*, they also identified differential expression of various transporters as well as receptors for neurotransmitters, cytokines, and hormones (32). Similarly, recent work from our lab reported a high degree of functional diversity in the iBAT of mice. More precisely, using a scRNA-seq of mature brown adipocytes we identified two metabolically distinct brown adipocytes; high thermogenic (BA-H) and low thermogenic (BA-L). For thermogenic activity/function, we refer to the ability of the brown adipocyte to get activated to significantly increase substrates oxidization. BA-H is the classical thermogenic population with high UCP1 expression, high mitochondrial content as well as high respiration rate. On the contrary, a novel BA-L population had low UCP1 expression, low mitochondrial content, a respiratory rate that is intermediate between white adipocytes and BA-H, but similar respiration potential (**Figure 1**) (10). Further investigation of the lineage and metabolic functions of this newly identified novel BA-L population will help uncover new cellular mechanisms of thermogenic regulation in BAT. Interestingly, a very recent report, using single nucleus RNA-sequencing (snRNA-seq), identified a unique, rare subpopulation of regulatory brown adipocytes (35). This novel subpopulation that increases in abundance at higher environmental temperature modulates the thermogenic activity of neighboring adipocytes. The higher number of these cells in humans as compared to mice may explain the lower thermogenic capacity of human BAT. It is important to note here that none of these studies (except one by Bertholet et al.) including ours measured mitochondrial respiration in presence of GDP which represents a direct UCP1 dependent respiration. Seahorse Xfe mitochondrial stress test is utilized commonly by researchers to report the

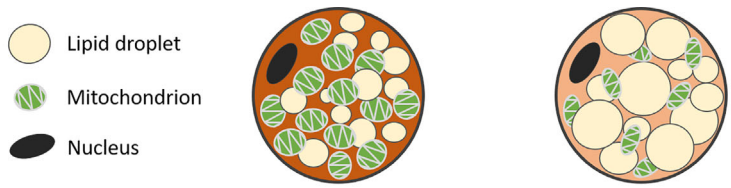

Brown adipocyte type	High thermogenic (BA-H)	Low thermogenic (BA-L)
Ucp1 expression	High	Low
Mitochondrial content	High	Low
Mitochondrial morphology	Round shaped	Oval Shaped
Mitochondrial membrane potential	Low	High
Basal respiration	High	Low
Maximum respiration	High	High
Lipid droplet size	Smaller	Larger
Fatty acid uptake	Low	High

FIGURE 1 | Distinct features of high and low thermogenic adipocytes. Relative to the high thermogenic brown adipocytes (BA-H), the low thermogenic brown adipocytes (BA-L) have lower UCP1 expression, low mitochondrial content, high mitochondrial membrane potential, and distinct mitochondrial morphology. These cells have a lower basal respiration rate, but a similar maximum respiration rate. They also have larger lipid droplets, and a higher fatty acid uptake rate (10).

thermogenic or UCP1 function in brown adipocytes. However, it is not a direct measure of UCP1 activity. Although BA-L population has lower UCP1 protein level, it is not determined if these UCP1 protein has similar activity as UCP1 in the BA-H cells. Our future plan is to use GDP as a direct inhibitor of UCP1 in the mitochondrial stress test to measure UCP1 dependent thermogenic activity (36).

The biggest disadvantage of scRNA-seq is the possible alterations in gene expression because of dissociation and cell isolation procedures used while making single-cell suspensions. Although single-cell/nucleus sequencing technologies can dissect the cellular heterogeneity of the tissue at high resolution, the spatial information however is lost in the process. To help retain such information recent technologies such as spatial transcriptomics (37) and multiplexed *in situ* hybridization (38, 39), or visium spatial gene expression analysis (40) should be utilized along with sn/scRNA-seq. At the moment, even if spatial transcriptomics technologies do not provide a resolution at a single-cell level, progress is being made to achieve it by every passing day. Its application to frozen tissues is one important advantage though, making it a valuable resource for precious samples such as banked human biopsies. Lastly, integrating other omics technologies with sn/scRNA-seq to quantify proteins (41), cell surface epitopes (42) and chromatin accessibility (43) simultaneously will allow us a better understanding not only of the heterogeneity of these cells but also the cellular interactions present in the tissue. Finally, whether these distinct adipocyte types really represent distinct cell types or whether they are just the same cell types under distinct metabolic states remains to be further studied.

In humans, BAT was initially thought to exist only in infants to cope with the cold conditions during and after birth and eventually become metabolically inactive and disappear during adulthood. However, the presence of active BAT has been reported in outdoor workers from northern Finland as early as 1981 (44). Furthermore, there are several reports based on PET/CT scans of pheochromocytoma patients suggesting the presence of active BAT in adult humans (45–47). Later on other dedicated cold exposure as well as retrospective studies confirmed these observations (48–53). A recent report has defined several additional novel brown fat depots in mice, which are anatomically comparable and share molecular similarities with humans (54). An earlier study found the overlap between brown and beige molecular markers in human supraclavicular BAT (55). Later, the Kajimura group, using genetic profiling of clonally derived human brown adipocytes, elegantly showed that their molecular signatures were closely associated with those of mouse beige adipocytes (56, 57). This also led to the identification of human brown adipocyte molecular markers such as potassium channel K3 and mitochondrial tumor suppressor 1, which were found to be essential for beige adipogenesis in mice (56, 57). Using genetic profiling approach for preadipocytes derived from human neck fat, the Tseng group identified CD29 as a surface marker that specifically marks preadipocytes with high thermogenic potential (58). Furthermore, human beige adipocytes derive from the progenitors residing in the capillary network and have been shown to proliferate in response to pro-angiogenic factors (59). Interestingly, a recent study suggested that brown adipocytes, but not beige adipocytes of the physiologically humanized mouse

had the thermogenic potential. They also found that the BAT of these mice closely resembles that of adult humans both morphologically as well as transcriptionally (60). It is important to note here that the difference between this study and the earlier study (57) is that the earlier study used young mice housed in standard conditions and were fed a normal chow diet. In the recent study by the Petrovic laboratory, they used physiologically humanized mice that are middle-aged, have been fed a high-fat diet, and are housed at thermoneutral temperatures. Lately, the housing temperature of mice for the metabolic studies has been questionable as standard conditions represent higher basal metabolic rate (BMR) in mice than that humans show at thermoneutrality. A recent report by Fischer et al. suggested housing mice at higher temperatures such as 30°C to achieve BMR comparable to resting humans (61), however as per Keijer et al. the best temperatures to achieve comparable BMR are between 25.5 – 27.6°C (62). So, it is important to consider housing temperatures and diets while planning and even comparing different mouse studies involving metabolic analyses. Lastly, the fact that only brown adipocytes and not the beige adipocytes of humanized mice retain thermogenic capacity, suggests the decreased thermocapacity of beige adipocytes during aging, thus making BAT an attractive target for therapeutics of metabolic disorders. Nevertheless, these data provide important insights into the heterogeneous nature of both rodent and human thermogenic adipocytes.

In summary, brown adipocytes within BAT represent high heterogeneity, and characterization of these distinct subpopulations will enable us to elucidate BAT thermogenic functions and regulations in detail. BAT's heterogeneous nature offers new critical aspects to consider for future attempts that pursue novel therapeutic targets that activate BAT thermogenesis.

TIMELINE OF BAT DEVELOPMENT

BAT depots appear earlier than WAT depots during embryogenesis (3). Also, most studies reporting such information have studied only a classic BAT depot iBAT. Early studies in rodents like mice and rats using mRNA measurements of mitochondrial markers such as cytochrome oxidase, UCP1, and ATP synthase found clusters of brown adipocytes appearing in the interscapular region around E15-16. UCP1 expression in these cells was hardly detectable during early embryogenesis and was found to be abruptly increased just before the birth around E18-19. This suggests the functional transformation of these cells into thermogenic competent brown adipocytes around E18-19 (63, 64). Another study used immunostaining of master regulator of adipogenesis, PPARγ (65, 66), to identify iBAT depots and found differentiating brown adipocytes as early as E14.5 (28). In a very recent report, in-situ hybridization of another critical factor involved in adipogenesis, C/EBPα (67, 68), demonstrated that the differentiation of adipocytes in iBAT starts at E12.5 and is functionally complete at E17.5 in the mouse embryo (69). Using the AdipoChaser mouse model based on adiponectin promoter (70), we recently suggested that the development of brown adipocytes in the iBAT starts as early as E10, and is most active at E14 (10). The generation of new brown adipocytes finishes by E16, as there were no new brown adipocytes labeled beyond this point. Furthermore, we showed that the heterogeneity in the iBAT cell population is achieved shortly after birth, around two weeks postnatally (10). Apart from the classic iBAT depot, several other BAT depots analogous to those observed in humans have been recently identified and characterized (54, 71). However, it remains unknown if they share a similar developmental timeline.

Postnatally, the BAT is a very plastic tissue and has been shown to undergo dramatic morphological alterations when exposed to different environmental temperatures. When exposed to thermoneutral temperature (30° C) as compared to standard housing conditions (22-24° C), brown adipocytes in mice undergo hypertrophic expansion with lipid droplets coalescing into a unilocular lipid droplet, leading to WAT like morphology as well gene expression profile. However, these cells maintain their molecular identity and are ready to go back to the classical morphology (72, 73). The Granneman group showed that the cold exposure at 4°C could induce brown adipogenesis in mice and their genetic lineage tracing model demonstrated that new adipocytes are derived from PDGFRα$^+$ progenitors. Such *de novo* brown adipogenesis was restricted to the dorsal edge region of the iBAT (74). It remains unknown if long-term cold exposure can induce brown adipocyte recruitment in other BAT depots. Our work showed that cold exposure within a few days alters brown adipocytes' heterogeneity, converting low-thermogenic brown adipocytes into high-thermogenic brown adipocytes (10). Both obesity and aging have been associated with the reduction of BAT thermogenic capacity (75, 76). Interestingly, the phenomenon of dynamic interconversion of BA-L and BA-H was not affected by the high-fat diet (HFD) feeding, but it declined with age (10). These observations provide important insights into the mechanisms of BAT thermoregulation and might help explaining its reduced thermogenic capacity during aging. It will be interesting to investigate the molecular mechanisms that regulate and balance the equilibrium between *de novo* brown adipogenesis and interconversion of high and low thermogenic brown adipocytes after cold exposure.

NON-SHIVERING THERMOGENESIS IN BAT

Adaptive thermogenesis is the most important metabolic function of BAT. There are two types of adaptive thermogenesis: cold-induced thermogenesis (77) and diet-induced thermogenesis (78). Skeletal muscle-based shivering accounts for a portion of cold-induced thermogenesis. However, with the cold adaptation non-shivering thermogenesis in BAT becomes prominent (79). The primary mechanism of BAT non-shivering thermogenesis involves the uncoupling of the mitochondrial respiratory chain, which is mediated *via* UCP1; a proton transporter located on the inner mitochondrial membrane (8, 9, 80–82). This uncoupling

results in increased substrate oxidation and dissipation of energy in the form of heat (83, 84). The rich vascularity of BAT helps in redistributing the generated heat across the body for temperature homeostasis (84). BAT is also highly innervated by sympathetic neurons (85). During cold exposure, activation of β3-adrenergic receptors by norepinephrine leads to lipid catabolism liberating free fatty acids and also induces the expression of UCP1 as well as other pro-thermogenic genes (3, 86). Apart from catecholamines some other non-sympathetic molecules such as triiodothyronine (T3), hepatic bile acids, and various retinoids have also been shown to play a role in the thermogenic activation of brown adipocytes (3). Classical studies performed using isolated BAT mitochondria have suggested an essential role of fatty acids as a regulator of brown adipocyte mitochondrial respiration (87, 88). A recent study using a patch-clamp measurement of UCP1 currents in BAT mitochondria found that fatty acids serve as an anion transporter to transport protons across the inner mitochondrial membrane. Both short-chain fatty acids and long-chain fatty acids are associated with UCP1. However, long-chain fatty acids are unable to dissociate because of hydrophobic interaction (89). Moreover, cold exposure has been shown to increase the activities of several antioxidant enzymes such as superoxide dismutase, catalase, glutathione peroxidases, and glutathione reductase in rat BAT suggesting elevated oxidative stress in BAT during thermogenesis (90).

Interestingly, several recent studies revealed that elevating the levels of reactive oxygen species (ROS), using genetic or pharmacological approaches, increased whole-body energy expenditure and protected against diet-induced obesity, along with increased brown adipocyte mitochondrial respiration (91–94). These observations suggest a critical role of elevated ROS in the thermogenic regulation of brown adipocytes. Furthermore, Cys253 of UCP1 has been recently shown to be sulfenylated by increased mitochondrial ROS in activated brown adipocytes, and this modification was found to be an important regulatory mechanism of UCP1-dependent thermogenesis (95). Moreover, succinylation of lysine residues (K56 and K151) of UCP1 by Sirtuin 5 has been suggested to modulate its stability and activity (96). When there is no thermal stress, UCP1 is usually thought to be functionally inhibited by purine nucleotides (97, 98). A recent report showed that the activation of brown adipocytes by adrenergic stimulation resulted in the degradation of these purine nucleotides in brown adipocytes both *in vivo* and *in vitro*, leading to the activation of UCP1 (99). These observations emphasize an essential role of UCP1 in BAT thermogenesis and further understanding of the regulation of its activity might uncover novel mechanisms of thermoregulation.

Genetic ablation of UCP1 in mice led to fatal hypothermia after cold exposure (100). Interestingly, the cold sensitivity of these mice was dependent on the genetic background. Mice with congenic C57BL/6J and 129/SvImJ backgrounds were cold-sensitive, whereas those on F1 hybrid background were found to be resistant to cold (101). Also, the effects of diet-induced obesity on these mice were found to be temperature-dependent (102, 103). Moreover, when UCP1-null mice were gradually exposed to reduced environmental temperatures, they could regain their ability to acclimatize to cold (104). These findings suggest that UCP1-independent mechanisms of thermogenesis may exist. As an alternate thermogenic mechanism, creatine cycling was initially discovered in the murine beige adipocyte mitochondria (34, 105). Ablation of the creatine synthesis rate-limiting enzyme glycine amidinotransferase in an adipocyte-specific manner in mice resulted in reduced BAT creatine concentration and mild cold intolerance (106). Recently, creatine kinase B (CKB), as the only isoenzyme in brown adipocytes, is proven to be indispensable for the futile creatine cycle-related thermogenesis (107). These studies revealed the critical role of creatine cycling as an alternate thermoregulatory mechanism in brown adipocytes.

BROWN ADIPOCYTE ENERGY METABOLISM

As BAT has exceptionally high energy expenditure, it is not surprising that it is an essential player in whole-body metabolic regulation. As mentioned above, studies done using BAT transplantation approaches suggested a major role of BAT in glucose homeostasis in mice (108–110). Similarly, activating BAT by cold exposure in humans led to improved whole-body glucose homeostasis and insulin sensitivity in both healthy individuals and individuals with type 2 diabetes (111, 112). With Seahorse Analyzers, for the first time, we were able to measure oxygen consumption in primary mature brown adipocytes, which is largely different from BAT tissue chucks, or *in vitro* cultured brown adipocyte differentiated from primary stromal vascular fraction (10). These primary mature brown adipocytes had 5-10 folds higher basal respiration, per cell, compared to the cells in the stromal vascular fraction of the same BAT, or mature white adipocytes from the same mouse (10). This result further validated that brown adipocytes would utilize energy at a much higher rate than other cell types, even at the basal, unstimulated status.

Although BAT is known to have a high rate of glucose uptake, fatty acids are commonly viewed as the primary fuel for mitochondrial uncoupling respiration (49, 51, 52, 54, 113–118). The Jiang group's most recent work used *in vivo* [U-^{13}C] glucose tracing and demonstrated that BAT activation by chronic cold exposure leads to increased glucose oxidation and enhances glucose flux to mitochondrial tricarboxylic acid cycle (119). Such increase in glucose uptake by adrenergic stimulation is, however, found to be independent of UCP1 presence or activity (120). Moreover, BAT has been shown to express pyruvate carboxylase; which can further enhance the glucose uptake by promoting anaplerosis (121). Mitochondrial pyruvate carrier (MPC) connects cytosolic glycolysis and mitochondrial glucose oxidation (122, 123). Most importantly, inhibition of MPC in mice resulted in blockade of cold-induced glucose oxidation in BAT, thereby impairing the body temperature homeostasis (119). In line with this, another group also showed that BAT-selective ablation of mitochondrial pyruvate carrier 1 (MPC1) in mice led to impaired cold sensitivity and

glucose handling (124). Moreover, MPC inhibition in *in vitro* differentiated brown adipocytes, without any adrenergic stimulation, resulted in increased mitochondrial fatty acid oxidation and lipid cycling; thereby increasing the energy expenditure (125). Thus, limiting pyruvate uptake in brown adipocyte mitochondria could be an effective way of increasing the energy expenditure in the absence of adrenergic stimulation. These observations point toward an important role of glucose oxidation in BAT thermogenesis.

Fatty acids and lipolytic agents have been shown to stimulate respiration in brown adipocytes (126). Stimulation of β3-adrenoreceptor results in increased uptake as well as utilization of FFAs in BAT, but not in WAT (127). BAT uses circulating FFAs after hydrolysis of triacylglycerol-rich lipoproteins (TRLs) as a substrate for thermogenesis (128). Notably, lipoprotein lipase (LPL), an enzyme that is required for this hydrolysis, was induced several folds in BAT during cold acclimatization (129). Moreover, this induction has been shown to contribute to vascular lipoprotein homeostasis during cold exposure by channeling TRLs to BAT (130). This effect can also be partly attributed to the downregulation of a secreted protein angiopoietin-like 4 which inhibits LPL activity. This downregulation further potentiates the LPL activity, thereby increasing the uptake of TRLs in BAT, leading to increased systemic triglyceride clearance (131). Intriguingly, BAT volume during thermoneutral or cold exposures was found to be positively correlated to lipolysis, FFA cycling as well as oxidation, and adipose insulin sensitivity in humans (132). Global deletion of adipose triglyceride lipase (ATGL); a rate-limiting enzyme involved in lipolysis of lipid droplet triglycerides, resulted in defective cold adaptation in mice. This suggested an essential role of ATGL in fueling thermogenesis by locally derived FFAs (133). Indeed, adipocyte-specific ablation of ATGL in mice led to the conversion of BAT to WAT-like tissue and resulted in severely impaired thermogenesis (134). However, recent studies using a BAT-specific inhibition of lipolysis using genetic approaches suggested that BAT lipolysis is not essential for cold-induced thermogenesis (135, 136). Cold intolerance previously observed in global ATGL KO mice was attributed to the impaired cardiac function. Another recent study that impaired the triglyceride synthesis and storage in the BAT lipid droplets by BAT-specific deletion of triglyceride synthesis enzymes also suggested that BAT lipid droplets are dispensable for cold-induced thermogenesis (137). While there is no doubt that BAT could utilize a large amount of glucose and fatty acids, it would be fascinating to explore further how brown adipocyte selects the primary fuel for thermogenesis, and how this selection would have a dynamic impact on whole-body glucose and lipid homeostasis.

Apart from FFAs and glucose, branched-chain amino acids (BCAAs) have also been shown to fuel BAT thermogenesis in mice and humans (138). Interestingly, increased blood levels and impaired metabolism of BCAAs, have been linked to the etiology of type 2 diabetes (139, 140). These observations may provide a novel link between impaired BAT thermogenesis and metabolic disorders. Furthermore, the Kajimura group suggested that stimulation of BCAA catabolism by activating BAT may protect against insulin resistance development by preventing the activation of mTOR signaling (138). Moreover, ^{13}C-labeled isotope tracing of preadipocytes and differentiated adipocytes showed increased BCAA catabolism in differentiated adipocytes as compared to proliferating cells, which used glucose and glutamine to fuel the mitochondrial oxidation. Inhibition of BCAA catabolism resulted in impaired adipogenesis, suggesting an important functional role of BCAAs in adipocyte differentiation (141). Additionally, the Chouchani group found a significant accumulation of succinate (92), a tricarboxylic acid cycle intermediates in cold-activated brown adipocytes, which was independent of adrenergic signaling. Interestingly, the administration of succinate to mice also led to the activation of BAT thermogenesis. Mechanistically this effect was dependent on succinate dehydrogenase generated ROS (92). Another recent report showed that FFAs, released from white adipocytes in response to cold exposure, induced hepatocyte nuclear factor 4 alpha mediated acylcarnitine production in the liver (142). This led to increased plasma concentration of acylcarnitines, which were taken up by BAT to fuel the thermogenesis. Most importantly, supplementation with L-carnitine or palmitoylcarnitine rescued the age-dependent cold sensitivity in mice, suggesting an essential role of acylcarnitine metabolism in age-induced impairment of thermogenesis (142). Altogether, brown adipocytes utilize multiple substrates as fuels for thermogenesis (**Figure 2**). Again, how brown adipocytes perform fuel selection among all these substrates remains mostly unknown, and yet it is unclear if there are switches of fuel selections during aging or the development of metabolic disorders.

Lastly, as mentioned earlier, it is important to perform BAT metabolic studies in rodents at thermoneutral temperatures to generate data that is comparable to humans. Although studies in humans have confirmed the presence of thermoactive BAT, one should note that the prevalence of BAT was increased only after cold exposure. In warm conditions little to no BAT was detected in these subjects (50–52). Moreover, overweight, and obese subjects showed significantly lower BAT activity (52). Also, such cold-induced BAT activation was higher during winter as compared to summer (50). Furthermore, Yoneshiro et al. showed that the cold-induced thermoactivation of BAT reduced during aging; as the incidence of cold-activated BAT fell from about 50% in the twenties to less than 10% in the fifties and sixties (75). So, taken together factors such as temperature, age, and dietary compositions should be carefully considered while performing metabolic studies related to BAT or as a matter of fact related to any other metabolically active organ in both rodents and humans.

BAT AS AN ENDOCRINE ORGAN

The WAT is well established as an endocrine organ, secreting adipokines such as adiponectin (143) and leptin (144). There is recently ample evidence supporting the fact that BAT may act as

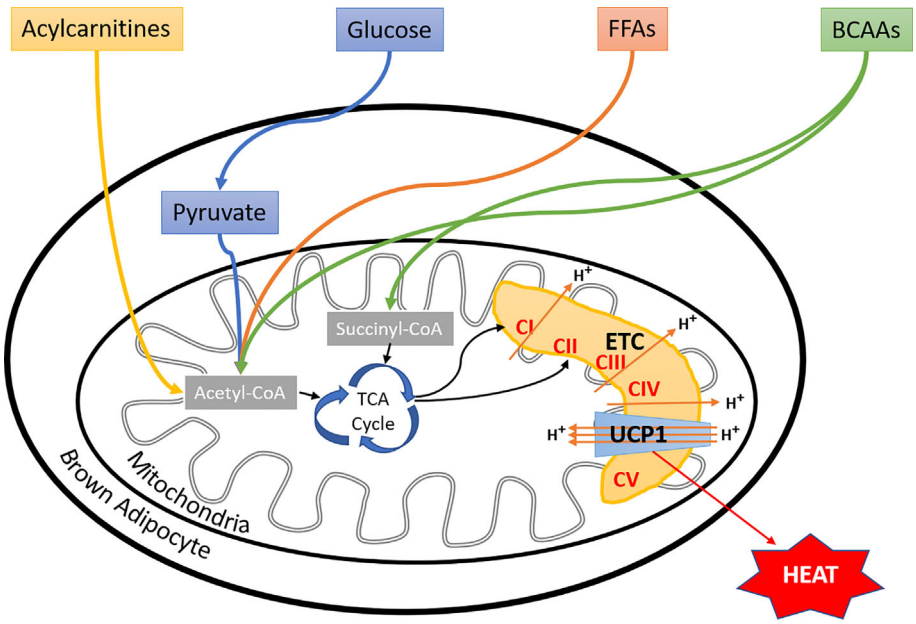

FIGURE 2 | Fuel selection by brown adipocyte. Besides glucose and fatty acids, BAT utilizes a variety of substrates, including BCAAs, succinate, and liver-derived acylcarnitines to fuel thermogenesis, more substrates to be discovered in the near future. However, the regulatory mechanisms of brown adipocyte fuel selection, especially upon environmental temperature changes, and whether aging or metabolic disorders affect these processes remain unknown. FFAs, free fatty acids; BCAAs, branched-chain amino acids; ETC, electron transport chain; CI, complex I; CII, complex II; CIII, complex III; CIV, complex IV; CV, complex V; UCP1, uncoupling protein I.

a unique endocrine organ by secreting some factors, so-referred to as "batokines" (145). In the 1980s, *Silva and Larsen* found that the enzyme type 2 iodothyronine deiodinase (DIO2) is specifically expressed in BAT, and it converts thyroxine (T4) to triiodothyronine (T3) (146). They also showed that its activity is strongly induced during thermogenesis, and BAT serves as an important site for both local and systemic T3 generation (147). Both DIO2 and T3 have essential functions in regulating BAT thermogenesis (148, 149). Fibroblast growth factor-21 (FGF21), an essential player in glucose oxidation in multiple organs, was found to be upregulated in BAT in response to cold exposure as well as adrenergic stimulation (150, 151). Furthermore, cytokine interleukin-6 (IL-6) is induced during thermogenesis in mouse brown adipocytes (152). BAT from healthy mice, when implanted in HFD fed mice, improved glucose homeostasis and insulin sensitivity. This effect was found to be mediated *via* endocrine actions of IL-6 as BAT implantation from IL-6 KO mice failed to show such improvements (108). Likewise, the insulin-independent reversal of type I diabetes (T1D) was achieved when BAT from healthy mice was transplanted in the streptozotocin-induced diabetic mouse model. Such transplantation, if done before the induction, was even able to prevent or significantly delay the development of T1D. This antidiabetic effect of BAT implantation was attributed to insulin-like growth factor-1 (IGF-1), which was upregulated in the tissue transplants. It is supposed to mediate its effects *via* improving the WAT inflammation, adipogenesis, and direct effect on insulin receptors (109, 110). Like many other cell types, brown adipocytes also secrete Vascular endothelial growth factor-A (VEGF-A), a signaling protein that promotes the growth of new blood vessels. VEGF-A is essential for the activation and expansion of BAT (153). Importantly, another brown adipocyte enriched factor neuregulin 4 (*Nrg4*) has been demonstrated by the Lin laboratory to protect against diet-induced insulin resistance as well as hepatic steatosis in mice. This is achieved by negatively regulating the *de novo* lipogenesis in the liver and by activating hepatic fatty acid oxidation (154, 155). *Nrg4* transgenic mice also showed increased energy expenditure and improvement of whole-body glucose metabolism (154, 155). The Kahn laboratory recently discovered BAT-derived circulating miRNAs, which control the gene expression in the liver, especially that of FGF21. Mice lacking miRNA processing enzyme, Dicer, specifically in adipose tissue, had improved glucose tolerance (156). Furthermore, some lipid-derived lipokines, such as 12,13-dihydroxy-9Z-octadecenoic acid (12,13-diHOME) and 12-hydroxyeicosapentaenoic acid (12-HEPE) are secreted specifically by BAT. 12,13-diHOME promotes fatty acid uptake in skeletal muscle and BAT, leading to enhanced cold tolerance and improved systemic triglyceride clearing (157, 158). 12-HEPE, on the other hand, improved the whole-body glucose homeostasis by increasing glucose uptake in skeletal muscle and adipocytes (159). Lastly, secretome analyses of brown adipocytes using modern-day proteomics and transcriptomics approaches have identified several novel batokine candidates including ependymin-related protein 1 (EPDR1) and phospholipid transfer protein (PLTP) (160–162).

EPDR1 was found to be an important commitment factor for brown adipogenesis (161). Whereas, PLTP improved glucose and lipid homeostasis *via* the regulation of liver lipoproteins and bile acids (160). Lastly, recruitment of immune cells in BAT; especially that of activated macrophages has been shown to be associated with the thermogenic activation (163). Chemokine C-X-C motif chemokine ligand-14 (CXCL14) is another example of batokine secreted by BAT in response to adrenergic stimulation and has been shown to play an important role in activation and recruitment of macrophages to BAT during thermogenic activation (164). Taken together, these recent studies highlighted the function of BAT as a unique endocrine organ, playing essential functions in regulating whole-body metabolic homeostasis.

BAT CENTERED THERAPEUTIC APPROACHES AND FUTURE PERSPECTIVES

BAT plays an essential role in energy homeostasis. Upon activation, BAT can function as an effective energy sink, burning and disposing excess lipids and glucose. Unfortunately, BAT activity declines during aging or the development of metabolic disorders (49, 75, 165). Therefore, enhancing BAT thermogenic activity has been an attractive strategy for the treatment of obesity and type 2 diabetes. Indeed, thermogenic activation of BAT either by cold exposure (111, 113, 166, 167) or by adrenergic stimulation *via* β3-adrenoreceptor (AR) agonist Mirabegron (168) showed beneficial metabolic effects such as increased BAT glucose uptake, improved insulin sensitivity, and weight loss in humans. Furthermore, several synthetic molecules acting *via* different mechanisms have recently been shown to activate BAT in mice, increasing whole-body energy expenditure (169–172). The clinical applications of these compounds are being actively evaluated. Although activating BAT might seem an exciting target for treating metabolic disorders, it is worth noting that humans have various responses to the same stimulation regarding BAT activity. BAT mass is negatively correlated with age as well as diabetic status (173), making this approach more challenging in aged as well as diabetic individuals. BAT transplantation studies in mice have shown the vital role of BAT in the regulation of adiposity, glucose homeostasis, and insulin resistance (108–110, 174, 175). Interestingly, brown adipocytes engineered from human fibroblasts or stem cells from human WAT stromal vascular fraction were transplanted in mice in multiple studies (176–178). In general, these transplantations showed beneficial metabolic effects, such as protection from diet-induced adiposity and insulin resistance. A similar approach can be used in humans, in theory, to increase functional BAT mass. Moreover, common dietary supplements such as L-arginine and capsinoids have been shown to increase BAT recruitment and activation, leading to beneficial effects with respect to glucose homeostasis and insulin sensitivity in both mice and humans (179–181). Lastly, as mentioned above several secretory factors having endocrine functions have been recently identified from BAT. These batokines may be considered emerging therapeutic targets for metabolic disorders. For instance, a recent report by Baruch et al. showed that FGF21 mimetic antibody BFKB8488A when injected subcutaneously in overweight/obese human subjects, resulted in a reduction in body weight, improved cardiometabolic parameters, and reduced carbohydrate intake (182). Taking together, the rediscovery of functional BAT depots in humans has undoubtedly sparked a new era of research about the therapeutic targeting of this tissue for its amazing metabolic health benefits. However, a detailed understanding of the basic biology of its development, heterogeneity, and metabolic regulation will surely further aid this cause.

AUTHOR CONTRIBUTIONS

ABS, QW, and AS wrote the manuscript. All authors contributed to the article and approved the submitted version.

FUNDING

QAW was supported by US National Institutes of Health grants R01AG063854, R01HD096152, American Diabetes Association Junior Faculty Development Award 1-19-JDF-023, and City of Hope Caltech-COH Initiative Award.

ACKNOWLEDGMENTS

The authors are grateful to Lei Jiang (COH) and Zhichao Wang (COH) for discussions and comments.

REFERENCES

1. Scherer E. The many secret lives of adipocytes: implications for diabetes. *Diabetologia* (2019) 62(2):223–32. doi: 10.1007/s00125-018-4777-x
2. Kusminski CM, Bickel PE, Scherer PE. Targeting adipose tissue in the treatment of obesity-associated diabetes. *Nat Rev Drug Discovery* (2016) 15 (9):639–60. doi: 10.1038/nrd.2016.75
3. Rosen ED, Spiegelman BM. What we talk about when we talk about fat. *Cell* (2014) 156(1-2):20–44. doi: 10.1016/j.cell.2013.12.012
4. Ikeda K, Maretich P, Kajimura S. The Common and Distinct Features of Brown and Beige Adipocytes. *Trends Endocrinol Metab* (2018) 29(3):191–200. doi: 10.1016/j.tem.2018.01.001
5. Pfeifer A, Hoffmann LS. Brown, beige, and white: the new color code of fat and its pharmacological implications. *Annu Rev Pharmacol Toxicol* (2015) 55:207–27. doi: 10.1146/annurev-pharmtox-010814-124346
6. Waldén TB, Hansen IR, Timmons JA, Cannon B, Nedergaard J. Recruited vs. nonrecruited molecular signatures of brown, "brite," and white adipose tissues. *Am J Physiol Endocrinol Metab* (2012) 302(1):E19–31. doi: 10.1152/ajpendo.00249.2011
7. Gesta S, Tseng YH, Kahn CR. Developmental origin of fat: tracking obesity to its source. *Cell* (2007) 131(2):242–56. doi: 10.1016/j.cell.2007.10.004
8. Aquila H, Link TA, Klingenberg M. The uncoupling protein from brown fat mitochondria is related to the mitochondrial ADP/ATP carrier. Analysis of

sequence homologies and of folding of the protein in the membrane. *EMBO J* (1985) 4(9):2369–76. doi: 10.1002/j.1460-2075.1985.tb03941.x
9. Heaton GM, Wagenvoord RJ, Kemp A Jr, Nicholls DG. Brown-adipose-tissue mitochondria: photoaffinity labelling of the regulatory site of energy dissipation. *Eur J Biochem* (1978) 82(2):515–21. doi: 10.1111/j.1432-1033.1978.tb12045.x
10. Song A, Dai W, Jang MJ, Medrano L, Li Z, Zhao H, et al. Low- and high-thermogenic brown adipocyte subpopulations coexist in murine adipose tissue. *J Clin Invest* (2020) 130(1):247–57. doi: 10.1172/JCI129167
11. Petrovic N, Walden TB, Shabalina IG, Timmons JA, Cannon B, Nedergaard J. Chronic peroxisome proliferator-activated receptor gamma (PPARgamma) activation of epididymally derived white adipocyte cultures reveals a population of thermogenically competent, UCP1-containing adipocytes molecularly distinct from classic brown adipocytes. *J Biol Chem* (2010) 285(10):7153–64. doi: 10.1074/jbc.M109.053942
12. Wu J, Bostrom P, Sparks LM, Ye L, Choi JH, Giang AH, et al. Beige adipocytes are a distinct type of thermogenic fat cell in mouse and human. *Cell* (2012) 150(2):366–76. doi: 10.1016/j.cell.2012.05.016
13. Atit R, Sgaier SK, Mohamed OA, Taketo MM, Dufort D, Joyner AL, et al. Beta-catenin activation is necessary and sufficient to specify the dorsal dermal fate in the mouse. *Dev Biol* (2006) 296(1):164–76. doi: 10.1016/j.ydbio.2006.04.449
14. Seale P, Bjork B, Yang W, Kajimura S, Chin S, Kuang S, et al. PRDM16 controls a brown fat/skeletal muscle switch. *Nature* (2008) 454(7207):961–7. doi: 10.1038/nature07182
15. Lepper C, Fan CM. Inducible lineage tracing of Pax7-descendant cells reveals embryonic origin of adult satellite cells. *Genesis* (2010) 48(7):424–36. doi: 10.1002/dvg.20630
16. Timmons JA, Wennmalm K, Larsson O, Walden TB, Lassmann T, Petrovic N, et al. Myogenic gene expression signature establishes that brown and white adipocytes originate from distinct cell lineages. *Proc Natl Acad Sci USA* (2007) 104(11):4401–6. doi: 10.1073/pnas.0610615104
17. Forner F, Kumar C, Luber CA, Fromme T, Klingenspor M, Mann M, et al. Proteome differences between brown and white fat mitochondria reveal specialized metabolic functions. *Cell Metab* (2009) 10(4):324–35. doi: 10.1016/j.cmet.2009.08.014
18. Yin H, Pasut A, Soleimani VD, Bentzinger CF, Antoun G, Thorn S, et al. MicroRNA-133 controls brown adipose determination in skeletal muscle satellite cells by targeting Prdm16. *Cell Metab* (2013) 17(2):210–24. doi: 10.1016/j.cmet.2013.01.004
19. Trajkovski M, Ahmed K, Esau CC, Stoffel M. MyomiR-133 regulates brown fat differentiation through Prdm16. *Nat Cell Biol* (2012) 14(12):1330–5. doi: 10.1038/ncb2612
20. Sun L, Xie H, Mori MA, Alexander R, Yuan B, Hattangadi SM, et al. Mir193b-365 is essential for brown fat differentiation. *Nat Cell Biol* (2011) 13(8):958–65. doi: 10.1038/ncb2286
21. Zhou H, Wan B, Grubisic I, Kaplan T, Tjian R. TAF7L modulates brown adipose tissue formation. *Elife* (2014) 3:e02811. doi: 10.7554/eLife.02811
22. Rajakumari S, Wu J, Ishibashi J, Lim HW, Giang AH, Won KJ, et al. EBF2 determines and maintains brown adipocyte identity. *Cell Metab* (2013) 17(4):562–74. doi: 10.1016/j.cmet.2013.01.015
23. Ohno H, Shinoda K, Ohyama K, Sharp LZ, Kajimura S. EHMT1 controls brown adipose cell fate and thermogenesis through the PRDM16 complex. *Nature* (2013) 504(7478):163–7. doi: 10.1038/nature12652
24. Dempersmier J, Sambeat A, Gulyaeva O, Paul SM, Hudak CS, Raposo HF, et al. Cold-inducible Zfp516 activates UCP1 transcription to promote browning of white fat and development of brown fat. *Mol Cell* (2015) 57(2):235–46. doi: 10.1016/j.molcel.2014.12.005
25. Park JH, Kang HJ, Kang SI, Lee JE, Hur J, Ge K, et al. A multifunctional protein, EWS, is essential for early brown fat lineage determination. *Dev Cell* (2013) 26(4):393–404. doi: 10.1016/j.devcel.2013.07.002
26. Sanchez-Gurmaches J, Guertin DA. Adipocytes arise from multiple lineages that are heterogeneously and dynamically distributed. *Nat Commun* (2014) 5:4099. doi: 10.1038/ncomms5099
27. Sanchez-Gurmaches J, Hung CM, Sparks CA, Tang Y, Li H, Guertin DA, et al. PTEN loss in the Myf5 lineage redistributes body fat and reveals subsets of white adipocytes that arise from Myf5 precursors. *Cell Metab* (2012) 16(3):348–62. doi: 10.1016/j.cmet.2012.08.003
28. Wang W, Kissig M, Rajakumari S, Huang L, Lim HW, Won KJ, et al. Ebf2 is a selective marker of brown and beige adipogenic precursor cells. *Proc Natl Acad Sci USA* (2014) 111(40):14466–71. doi: 10.1073/pnas.1412685111
29. Shan T, Liang X, Bi P, Zhang P, Liu W, Kuang S, et al. Distinct populations of adipogenic and myogenic Myf5-lineage progenitors in white adipose tissues. *J Lipid Res* (2013) 54(8):2214–24. doi: 10.1194/jlr.M038711
30. Sebo ZL, Jeffery E, Holtrup B, Rodeheffer MS. A mesodermal fate map for adipose tissue. *Development* (2018) 145(17):dev166801. doi: 10.1242/dev.166801
31. Wikstrom JD, Mahdaviani K, Liesa M, Sereda SB, Si Y, Las G, et al. Hormone-induced mitochondrial fission is utilized by brown adipocytes as an amplification pathway for energy expenditure. *EMBO J* (2014) 33(5):418–36. doi: 10.1002/embj.201385014
32. Spaethling JM, Sanchez-Alavez M, Lee J, Xia FC, Dueck H, Wang W, et al. Single-cell transcriptomics and functional target validation of brown adipocytes show their complex roles in metabolic homeostasis. *FASEB J* (2016) 30(1):81–92. doi: 10.1096/fj.15-273797
33. Cinti S, Cancello R, Zingaretti MC, Ceresi E, De Matteis R, Giordano A, et al. CL316,243 and cold stress induce heterogeneous expression of UCP1 mRNA and protein in rodent brown adipocytes. *J Histochem Cytochem* (2002) 50(1):21–31. doi: 10.1177/002215540205000103
34. Bertholet AM, Kazak L, Chouchani ET, Bogaczynska MG, Paranjpe I, Wainwright GL, et al. Mitochondrial Patch Clamp of Beige Adipocytes Reveals UCP1-Positive and UCP1-Negative Cells Both Exhibiting Futile Creatine Cycling. *Cell Metab* (2017) 25(4):811–822.e4 doi: 10.1016/j.cmet.2017.03.002
35. Sun W, Dong H, Balaz M, Slyper M, Drokhlyansky E, Colleluori G, et al. snRNA-seq reveals a subpopulation of adipocytes that regulates thermogenesis. *Nature* (2020) 587(7832):98–102. doi: 10.1038/s41586-020-2856-x
36. Porter C. Quantification of UCP1 function in human brown adipose tissue. *Adipocyte* (2017) 6(2):167–74. doi: 10.1080/21623945.2017.1319535
37. Ståhl PL, Salmén F, Vickovic S, Lundmark A, Navarro JF, Magnusson J, et al. Visualization and analysis of gene expression in tissue sections by spatial transcriptomics. *Science* (2016) 353(6294):78–82. doi: 10.1126/science.aaf2403
38. Anderson R. Multiplex fluorescence in situ hybridization (M-FISH). *Methods Mol Biol* (2010) 659:83–97. doi: 10.1007/978-1-60761-789-1_6
39. Eng CL, Lawson M, Zhu Q, Dries R, Koulena N, Takei Y, et al. Transcriptome-scale super-resolved imaging in tissues by RNA seqFISH. *Nature* (2019) 568(7751):235–9. doi: 10.1038/s41586-019-1049-y
40. Maynard KR, Collado-Torres L, Weber LM, Uytingco C, Barry BK, Williams SR, et al. Transcriptome-scale spatial gene expression in the human dorsolateral prefrontal cortex. *Nat Neurosci* (2021) 24(3):425–36. doi: 10.1038/s41593-021-00817-5
41. Peterson VM, Zhang KX, Kumar N, Wong J, Li L, Wilson DC, et al. Multiplexed quantification of proteins and transcripts in single cells. *Nat Biotechnol* (2017) 35(10):936–9. doi: 10.1038/nbt.3973
42. Stoeckius M, Hafemeister C, Stephenson W, Houck-Loomis B, Chattopadhyay PK, Swerdlow H, et al. Simultaneous epitope and transcriptome measurement in single cells. *Nat Methods* (2017) 14(9):865–8. doi: 10.1038/nmeth.4380
43. Liu L, Liu C, Quintero A, Wu L, Yuan Y, Wang M, et al. Deconvolution of single-cell multi-omics layers reveals regulatory heterogeneity. *Nat Commun* (2019) 10(1):470. doi: 10.1038/s41467-018-08205-7
44. Huttunen P, Hirvonen J, Kinnula V. The occurrence of brown adipose tissue in outdoor workers. *Eur J Appl Physiol Occup Physiol* (1981) 46(4):339–45. doi: 10.1007/BF00422121
45. Yamaga LY, Thom AF, Wagner J, Baroni RH, Hidal JT, Funari MG. The effect of catecholamines on the glucose uptake in brown adipose tissue demonstrated by (18)F-FDG PET/CT in a patient with adrenal pheochromocytoma. *Eur J Nucl Med Mol Imaging* (2008) 35(2):446–7. doi: 10.1007/s00259-007-0538-7
46. Hadi M, Chen CC, Whatley M, Pacak K, Carrasquillo JA. Brown fat imaging with (18)F-6-fluorodopamine PET/CT, (18)F-FDG PET/CT, and (123)I-MIBG SPECT: a study of patients being evaluated for pheochromocytoma. *J Nucl Med* (2007) 48(7):1077–83. doi: 10.2967/jnumed.106.035915

47. Kuji I, Imabayashi E, Minagawa A, Matsuda H, Miyauchi T. Brown adipose tissue demonstrating intense FDG uptake in a patient with mediastinal pheochromocytoma. *Ann Nucl Med* (2008) 22(3):231–5. doi: 10.1007/s12149-007-0096-x
48. Nedergaard J, Bengtsson T, Cannon B. Unexpected evidence for active brown adipose tissue in adult humans. *Am J Physiol Endocrinol Metab* (2007) 293(2):E444–52. doi: 10.1152/ajpendo.00691.2006
49. Cypess AM, Lehman S, Williams G, Tal I, Rodman D, Goldfine AB, et al. Identification and importance of brown adipose tissue in adult humans. *New Engl J Med* (2009) 360(15):1509–17. doi: 10.1056/NEJMoa0810780
50. Saito M, Okamatsu-Ogura Y, Matsushita M, Watanabe K, Yoneshiro T, Nio-Kobayashi J, et al. High incidence of metabolically active brown adipose tissue in healthy adult humans: effects of cold exposure and adiposity. *Diabetes* (2009) 58(7):1526–31. doi: 10.2337/db09-0530
51. Virtanen KA, Lidell ME, Orava J, Heglind M, Westergren R, Niemi T, et al. Functional brown adipose tissue in healthy adults. *N Engl J Med* (2009) 360(15):1518–25. doi: 10.1056/NEJMoa0808949
52. van Marken Lichtenbelt WD, Vanhommerig JW, Smulders NM, Drossaerts JM, Kemerink GJ, Bouvy ND, et al. Cold-activated brown adipose tissue in healthy men. *N Engl J Med* (2009) 360(15):1500–8. doi: 10.1056/NEJMoa0808718
53. Zingaretti MC, Crosta F, Vitali A, Guerrieri M, Frontini A, Cannon B, et al. The presence of UCP1 demonstrates that metabolically active adipose tissue in the neck of adult humans truly represents brown adipose tissue. *FASEB J* (2009) 23(9):3113–20. doi: 10.1096/fj.09-133546
54. Zhang F. An Adipose Tissue Atlas: An Image-Guided Identification ofand Beige Depots in Rodents. *Cell Metab* (2018) 27(1):252–62.e3. doi: 10.1016/j.cmet.2017.12.004
55. Jespersen NZ, Larsen TJ, Peijs L, Daugaard S, Homoe P, Loft A, et al. A classical brown adipose tissue mRNA signature partly overlaps with brite in the supraclavicular region of adult humans. *Cell Metab* (2013) 17(5):798–805. doi: 10.1016/j.cmet.2013.04.011
56. Shinoda K, Luijten IH, Hasegawa Y, Hong H, Sonne SB, Kim M, et al. Genetic and functional characterization of clonally derived adult human brown adipocytes. *Nat Med* (2015) 21(4):389–94. doi: 10.1038/nm.3819
57. Sharp LZ, Shinoda K, Ohno H, Scheel DW, Tomoda E, Ruiz L, et al. Human BAT possesses molecular signatures that resemble beige/brite cells. *PloS One* (2012) 7(11):e49452. doi: 10.1371/journal.pone.0049452
58. Xue R, Lynes MD, Dreyfuss JM, Shamsi F, Schulz TJ, Zhang H, et al. Clonal analyses and gene profiling identify genetic biomarkers of the thermogenic potential of human brown and white preadipocytes. *Nat Med* (2015) 21(7):760–8. doi: 10.1038/nm.3881
59. Min SY, Kady J, Nam M, Rojas-Rodriguez R, Berkenwald A, Kim JH, et al. Human 'brite/beige' adipocytes develop from capillary networks, and their implantation improves metabolic homeostasis in mice. *Nat Med* (2016) 22(3):312–8. doi: 10.1038/nm.4031
60. de Jong JMA, Sun W, Pires ND, Frontini A, Balaz M, Jespersen NZ, et al. Human brown adipose tissue is phenocopied by classical brown adipose tissue in physiologically humanized mice. *Nat Metab* (2019) 1(8):830–43. doi: 10.1038/s42255-019-0101-4
61. Fischer AW, Cannon B, Nedergaard J. Optimal housing temperatures for mice to mimic the thermal environment of humans: An experimental study. *Mol Metab* (2018) 7:161–70. doi: 10.1016/j.molmet.2017.10.009
62. Keijer J, Li M, Speakman JR. What is the best housing temperature to translate mouse experiments to humans? *Mol Metab* (2019) 25:168–76. doi: 10.1016/j.molmet.2019.04.001
63. Houstek J, Kopecky J, Rychter Z, Soukup T. Uncoupling protein in embryonic brown adipose tissue–existence of nonthermogenic and thermogenic mitochondria. *Biochim Biophys Acta* (1988) 935(1):19–25. doi: 10.1016/0005-2728(88)90103-X
64. Giralt M, Martin I, Iglesias R, Vinas O, Villarroya F, Mampel T. Ontogeny and perinatal modulation of gene expression in rat brown adipose tissue. Unaltered iodothyronine 5'-deiodinase activity is necessary for the response to environmental temperature at birth. *Eur J Biochem* (1990) 193(1):297–302. doi: 10.1111/j.1432-1033.1990.tb19336.x
65. Tontonoz P, Hu E, Spiegelman BM. Stimulation of adipogenesis in fibroblasts by PPAR gamma 2, a lipid-activated transcription factor. *Cell* (1994) 79(7):1147–56. doi: 10.1016/0092-8674(94)90006-X
66. Wang QA, Zhang F, Jiang L, Ye R, An Y, Shao M, et al. Peroxisome Proliferator-Activated Receptor γ and Its Role in Adipocyte Homeostasis and Thiazolidinedione-Mediated Insulin Sensitization. *Mol Cell Biol* (2018) 38(10):e00677–17. doi: 10.1128/MCB.00677-17
67. Wu Z, Rosen ED, Brun R, Hauser S, Adelmant G, Troy AE, et al. Cross-regulation of C/EBP alpha and PPAR gamma controls the transcriptional pathway of adipogenesis and insulin sensitivity. *Mol Cell* (1999) 3(2):151–8. doi: 10.1016/S1097-2765(00)80306-8
68. Wang QA, Tao C, Jiang L, Shao M, Ye R, Zhu Y, et al. Distinct regulatory mechanisms governing embryonic versus adult adipocyte maturation. *Nat Cell Biol* (2015) 17(9):1099. doi: 10.1038/ncb3217
69. Mayeuf-Louchart A, Lancel S, Sebti Y, Pourcet B, Loyens A, Delhaye S, et al. Glycogen Dynamics Drives Lipid Droplet Biogenesis during Brown Adipocyte Differentiation. *Cell Rep* (2019) 29(6):1410–1418 e6. doi: 10.1016/j.celrep.2019.09.073
70. Wang QA, Tao C, Gupta RK, Scherer PE. Tracking adipogenesis during white adipose tissue development, expansion and regeneration. *Nat Med* (2013) 19(10):1338–44. doi: 10.1038/nm.3324
71. Mo Q, Salley J, Roshan T, Baer LA, May FJ, Jaehnig EJ, et al. Identification and characterization of a supraclavicular brown adipose tissue in mice. *JCI Insight* (2017) 2(11):e93166. doi: 10.1172/jci.insight.93166
72. Cui X, Nguyen NL, Zarebidaki E, Cao Q, Li F, Zha L, et al. Thermoneutrality decreases thermogenic program and promotes adiposity in high-fat diet-fed mice. *Physiol Rep* (2016) 4(10):e12799. doi: 10.14814/phy2.12799
73. Roh HC, Tsai LTY, Shao M, Tenen D, Shen Y, Kumari M, et al. Warming Induces Significant Reprogramming of Beige, but Not Brown, Adipocyte Cellular Identity. *Cell Metab* (2018) 27(5):1121–1137 e5. doi: 10.1016/j.cmet.2018.03.005
74. Lee YH, Petkova AP, Konkar AA, Granneman JG. Cellular origins of cold-induced brown adipocytes in adult mice. *FASEB J* (2015) 29(1):286–99. doi: 10.1096/fj.14-263038
75. Yoneshiro T, Aita S, Matsushita M, Okamatsu-Ogura Y, Kameya T, Kawai Y, et al. Age-related decrease in cold-activated brown adipose tissue and accumulation of body fat in healthy humans. *Obes (Silver Spring)* (2011) 19(9):1755–60. doi: 10.1038/oby.2011.125
76. Jung RT, Shetty PS, James WP, Barrand MA, Callingham BA. Reduced thermogenesis in obesity. *Nature* (1979) 279(5711):322–3. doi: 10.1038/279322a0
77. Davis TR, Johnston DR, Bell FC, Cremer BJ. Regulation of shivering and non-shivering heat production during acclimation of rats. *Am J Physiol* (1960) 198:471–5. doi: 10.1152/ajplegacy.1960.198.3.471
78. Rothwell NJ, Stock MJ. A role for brown adipose tissue in diet-induced thermogenesis. *Nature* (1979) 281(5726):31–5. doi: 10.1038/281031a0
79. Foster DO, Frydman ML. Tissue distribution of cold-induced thermogenesis in conscious warm- or cold-acclimated rats reevaluated from changes in tissue blood flow: the dominant role of brown adipose tissue in the replacement of shivering by nonshivering thermogenesis. *Can J Physiol Pharmacol* (1979) 57(3):257–70. doi: 10.1139/y79-039
80. Bouillaud F, Weissenbach J, Ricquier D. Complete cDNA-derived amino acid sequence of rat brown fat uncoupling protein. *J Biol Chem* (1986) 261(4):1487–90. doi: 10.1016/S0021-9258(17)35962-8
81. Jacobsson A, Stadler U, Glotzer MA, Kozak LP. Mitochondrial uncoupling protein from mouse brown fat. Molecular cloning, genetic mapping, and mRNA expression. *J Biol Chem* (1985) 260(30):16250–4. doi: 10.1016/S0021-9258(17)36228-2
82. Matthias A, Ohlson KB, Fredriksson JM, Jacobsson A, Nedergaard J, Cannon B. Thermogenic responses in brown fat cells are fully UCP1-dependent. UCP2 or UCP3 do not substitute for UCP1 in adrenergically or fatty scid-induced thermogenesis. *J Biol Chem* (2000) 275(33):25073–81. doi: 10.1074/jbc.M000547200
83. Bargmann W, von Hehn G, Lindner E. [On the cells of the brown fatty tissue and their innervation]. *Z Zellforsch Mikrosk Anat* (1968) 85(4):601–13. doi: 10.1007/BF00324749
84. Smith RE, Roberts JC. Thermogenesis of Brown Adipose Tissue in Cold-Acclimated Rats. *Am J Physiol* (1964) 206:143–8. doi: 10.1152/ajplegacy.1964.206.1.143
85. Wirsen C. Distribution of adrenergic nerve fibers in brown and white adipose tissue. In: AE Renold, GFJ Cahill, editors. *Adipose Tissue Am Physiol Soc*. Washington, DC: Wiley Publishing (1965). p. 197–9.

86. Cannon B, Cannon B, Cannon B, Nedergaard J. Brown adipose tissue: function and physiological significance. *Physiol Rev* (2004) 84(1):277–359. doi: 10.1152/physrev.00015.2003
87. Hittelman KJ, Lindberg O, Cannon B. Oxidative phosphorylation and compartmentation of fatty acid metabolism in brown fat mitochondria. *Eur J Biochem* (1969) 11(1):183–92. doi: 10.1111/j.1432-1033.1969.tb00759.x
88. Locke RM, Rial E, Scott ID, Nicholls DG. Fatty acids as acute regulators of the proton conductance of hamster brown-fat mitochondria. *Eur J Biochem* (1982) 129(2):373–80. doi: 10.1111/j.1432-1033.1982.tb07060.x
89. Fedorenko A, Lishko PV, Kirichok Y. Mechanism of fatty-acid-dependent UCP1 uncoupling in brown fat mitochondria. *Cell* (2012) 151(2):400–13. doi: 10.1016/j.cell.2012.09.010
90. Barja de Quiroga G, Lopez-Torres M, Perez-Campo R, Abelenda M, Paz Nava M, Puerta ML. Effect of cold acclimation on GSH, antioxidant enzymes and lipid peroxidation in brown adipose tissue. *Biochem J* (1991) 277(Pt 1):289–92. doi: 10.1042/bj2770289
91. Schneider K, Valdez J, Nguyen J, Vawter M, Galke B, Kurtz TW, et al. Increased Energy Expenditure, Ucp1 Expression, and Resistance to Diet-induced Obesity in Mice Lacking Nuclear Factor-Erythroid-2-related Transcription Factor-2 (Nrf2). *J Biol Chem* (2016) 291(14):7754–66. doi: 10.1074/jbc.M115.673756
92. Mills EL, Pierce KA, Jedrychowski MP, Garrity R, Winther S, Vidoni S, et al. Accumulation of succinate controls activation of adipose tissue thermogenesis. *Nature* (2018) 560(7716):102–6. doi: 10.1038/s41586-018-0353-2
93. Lee SJ, Kim SH, Park KM, Lee JH, Park JW. Increased obesity resistance and insulin sensitivity in mice lacking the isocitrate dehydrogenase 2 gene. *Free Radic Biol Med* (2016) 99:179–88. doi: 10.1016/j.freeradbiomed.2016.08.011
94. Han YH, Buffolo M, Pires KM, Pei S, Scherer PE, Boudina S. Adipocyte-Specific Deletion of Manganese Superoxide Dismutase Protects From Diet-Induced Obesity Through Increased Mitochondrial Uncoupling and Biogenesis. *Diabetes* (2016) 65(9):2639–51. doi: 10.2337/db16-0283
95. Chouchani ET, Kazak L, Jedrychowski MP, Lu GZ, Erickson BK, Szpyt J, et al. Mitochondrial ROS regulate thermogenic energy expenditure and sulfenylation of UCP1. *Nature* (2016) 532(7597):112–6. doi: 10.1038/nature17399
96. Wang G, Meyer JG, Cai W, Softic S, Li ME, Verdin E, et al. Regulation of UCP1 and Mitochondrial Metabolism in Brown Adipose Tissue by Reversible Succinylation. *Mol Cell* (2019) 74(4):844–57.e7. doi: 10.1016/j.molcel.2019.03.021
97. Rafael J, Ludolph HJ, Hohorst HJ. [Mitochondria from brown adipose tissue: uncoupling of respiratory chain phosphorylation by long fatty acids and recoupling by guanosine triphosphate]. *Hoppe Seylers Z Physiol Chem* (1969) 350(9):1121–31.
98. Klingenberg M, Winkler E. The reconstituted isolated uncoupling protein is a membrane potential driven H+ translocator. *EMBO J* (1985) 4(12):3087–92. doi: 10.1002/j.1460-2075.1985.tb04049.x
99. Fromme T, Kleigrewe K, Dunkel A, Retzler A, Li Y, Maurer S, et al. Degradation of brown adipocyte purine nucleotides regulates uncoupling protein 1 activity. *Mol Metab* (2018) 8:77–85. doi: 10.1016/j.molmet.2017.12.010
100. Enerbäck S, Jacobsson A, Simpson EM, Guerra C, Yamashita H, Harper ME, et al. Mice lacking mitochondrial uncoupling protein are cold-sensitive but not obese. *Nature* (1997) 387(6628):90–4. doi: 10.1038/387090a0
101. Hofmann WE, Liu X, Bearden CM, Harper ME, Kozak LP. Effects of genetic background on thermoregulation and fatty acid-induced uncoupling of mitochondria in UCP1-deficient mice. *J Biol Chem* (2001) 276(15):12460–5. doi: 10.1074/jbc.M100466200
102. Liu X, Rossmeisl M, McClaine J, Riachi M, Harper ME, Kozak LP. Paradoxical resistance to diet-induced obesity in UCP1-deficient mice. *J Clin Invest* (2003) 111(3):399–407. doi: 10.1172/JCI200315737
103. Feldmann HM, Golozoubova V, Cannon B, Nedergaard J. UCP1 ablation induces obesity and abolishes diet-induced thermogenesis in mice exempt from thermal stress by living at thermoneutrality. *Cell Metab* (2009) 9(2):203–9. doi: 10.1016/j.cmet.2008.12.014
104. Golozoubova V, Hohtola E, Matthias A, Jacobsson A, Cannon B, Nedergaard J. Only UCP1 can mediate adaptive nonshivering thermogenesis in the cold. *FASEB J* (2001) 15(11):2048–50. doi: 10.1096/fj.00-0536fje
105. Kazak L, Chouchani ET, Jedrychowski MP, Erickson BK, Shinoda K, Cohen P, et al. A creatine-driven substrate cycle enhances energy expenditure and thermogenesis in beige fat. *Cell* (2015) 163(3):643–55. doi: 10.1016/j.cell.2015.09.035
106. Kazak L, Chouchani ET, Lu GZ, Jedrychowski MP, Bare CJ, Mina AI, et al. Genetic Depletion of Adipocyte Creatine Metabolism Inhibits Diet-Induced Thermogenesis and Drives Obesity. *Cell Metab* (2017) 26(4):660–71.e3. doi: 10.1016/j.cmet.2017.08.009
107. Rahbani JF, Roesler A, Hussain MF, Samborska B, Dykstra CB, Tsai L, et al. Creatine kinase B controls futile creatine cycling in thermogenic fat. *Nature* (2021) 590:480–5. doi: 10.1038/s41586-021-03221-y
108. Stanford KI, Middelbeek RJ, Townsend KL, An D, Nygaard EB, Hitchcox KM, et al. Brown adipose tissue regulates glucose homeostasis and insulin sensitivity. *J Clin Invest* (2013) 123(1):215–23. doi: 10.1172/JCI62308
109. Gunawardana SC, Piston DW. Reversal of type 1 diabetes in mice by brown adipose tissue transplant. *Diabetes* (2012) 61(3):674–82. doi: 10.2337/db11-0510
110. Gunawardana SC, Piston DW. Insulin-independent reversal of type 1 diabetes in nonobese diabetic mice with brown adipose tissue transplant. *Am J Physiol Endocrinol Metab* (2015) 308(12):E1043–55. doi: 10.1152/ajpendo.00570.2014
111. Hanssen MJ, Hoeks J, Brans B, van der Lans AA, Schaart G, van den Driessche JJ, et al. Short-term cold acclimation improves insulin sensitivity in patients with type 2 diabetes mellitus. *Nat Med* (2015) 21(8):863–5. doi: 10.1038/nm.3891
112. Chondronikola M, Volpi E, Borsheim E, Porter C, Annamalai P, Enerback S, et al. Brown adipose tissue improves whole-body glucose homeostasis and insulin sensitivity in humans. *Diabetes* (2014) 63(12):4089–99. doi: 10.2337/db14-0746
113. Ouellet V, Labbe SM, Blondin DP, Phoenix S, Guerin B, Haman F, et al. Brown adipose tissue oxidative metabolism contributes to energy expenditure during acute cold exposure in humans. *J Clin Invest* (2012) 122(2):545–52. doi: 10.1172/JCI60433
114. Blondin DP, Labbe SM, Noll C, Kunach M, Phoenix S, Guerin B, et al. Selective Impairment of Glucose but Not Fatty Acid or Oxidative Metabolism in Brown Adipose Tissue of Subjects With Type 2 Diabetes. *Diabetes* (2015) 64(7):2388–97. doi: 10.2337/db14-1651
115. Wang X, Minze LJ, Shi ZZ. Functional imaging of brown fat in mice with 18F-FDG micro-PET/CT. *J Vis Exp* (2012) 2012(69):4060. doi: 10.3791/4060
116. Townsend KL, Tseng YH. Brown fat fuel utilization and thermogenesis. *Trends Endocrinol Metab* (2014) 25(4):168–77. doi: 10.1016/j.tem.2013.12.004
117. Labbe SM, Caron A, Chechi K, Laplante M, Lecomte R, Richard D. Metabolic activity of brown, "beige," and white adipose tissues in response to chronic adrenergic stimulation in male mice. *Am J Physiol Endocrinol Metab* (2016) 311(1):E260–8. doi: 10.1152/ajpendo.00545.2015
118. Hankir MK, Klingenspor M. Brown adipocyte glucose metabolism: a heated subject. *EMBO Rep* (2018) 19(9):e46404. doi: 10.15252/embr.201846404
119. Wang Z, Ning T, Song A, Rutter J, Wang QA, Jiang L. Chronic cold exposure enhances glucose oxidation in brown adipose tissue. *EMBO Rep* (2020) 21(11):e50085. doi: 10.15252/embr.202050085
120. Olsen JM, Csikasz RI, Dehvari N, Lu L, Sandström A, Öberg AI, et al. β_3-Adrenergically induced glucose uptake in brown adipose tissue is independent of UCP1 presence or activity: Mediation through the mTOR pathway. *Mol Metab* (2017) 6(6):611–9. doi: 10.1016/j.molmet.2017.02.006
121. Cannon B, Nedergaard J. The physiological role of pyruvate carboxylation in hamster brown adipose tissue. *Eur J Biochem* (1979) 94(2):419–26. doi: 10.1111/j.1432-1033.1979.tb12909.x
122. Bricker DK, Taylor EB, Schell JC, Orsak T, Boutron A, Chen YC, et al. A mitochondrial pyruvate carrier required for pyruvate uptake in yeast, Drosophila, and humans. *Science* (2012) 337(6090):96–100. doi: 10.1126/science.1218099
123. Herzig S, Raemy E, Montessuit S, Veuthey JL, Zamboni N, Westermann B, et al. Identification and functional expression of the mitochondrial pyruvate carrier. *Science* (2012) 337(6090):93–6. doi: 10.1126/science.1218530
124. Panic V, Pearson S, Banks J, Tippetts TS, Velasco-Silva JN, Lee S, et al. Mitochondrial pyruvate carrier is required for optimal brown fat thermogenesis. *Elife* (2020) 9:e52558. doi: 10.7554/eLife.52558

125. Veliova M, Ferreira CM, Benador IY, Jones AE, Mahdaviani K, Brownstein AJ, et al. Blocking mitochondrial pyruvate import in brown adipocytes induces energy wasting via lipid cycling. *EMBO Rep* (2020) 12):e49634. doi: 10.1101/841551
126. Reed N, Fain JN. Potassium-dependent stimulation of respiration in brown fat cells by fatty acids and lipolytic agents. *J Biol Chem* (1968) 243(23):6077–83. doi: 10.1016/S0021-9258(18)94462-5
127. Warner A, Kjellstedt A, Carreras A, Bottcher G, Peng XR, Seale P, et al. Activation of beta3-adrenoceptors increases in vivo free fatty acid uptake and utilization in brown but not white fat depots in high-fat-fed rats. *Am J Physiol Endocrinol Metab* (2016) 311(6):E901–10. doi: 10.1152/ajpendo.00204.2016
128. Khedoe PP, Hoeke G, Kooijman S, Dijk W, Buijs JT, Kersten S, et al. Brown adipose tissue takes up plasma triglycerides mostly after lipolysis. *J Lipid Res* (2015) 56(1):51–9. doi: 10.1194/jlr.M052746
129. Carneheim C, Nedergaard J, Cannon B. Beta-adrenergic stimulation of lipoprotein lipase in rat brown adipose tissue during acclimation to cold. *Am J Physiol* (1984) 246(4 Pt 1):E327–33. doi: 10.1152/ajpendo.1984.246.4.E327
130. Bartelt A, Bruns OT, Reimer R, Hohenberg H, Ittrich H, Peldschus K, et al. Brown adipose tissue activity controls triglyceride clearance. *Nat Med* (2011) 17(2):200–5. doi: 10.1038/nm.2297
131. Dijk W, Heine M, Vergnes L, Boon MR, Schaart G, Hesselink MK, et al. ANGPTL4 mediates shuttling of lipid fuel to brown adipose tissue during sustained cold exposure. *Elife* (2015) 4:e08428. doi: 10.7554/eLife.08428
132. Chondronikola M, Volpi E, Borsheim E, Porter C, Saraf MK, Annamalai P, et al. Brown Adipose Tissue Activation Is Linked to Distinct Systemic Effects on Lipid Metabolism in Humans. *Cell Metab* (2016) 23(6):1200–6. doi: 10.1016/j.cmet.2016.04.029
133. Haemmerle G, Lass A, Zimmermann R, Gorkiewicz G, Meyer C, Rozman J, et al. Defective lipolysis and altered energy metabolism in mice lacking adipose triglyceride lipase. *Science* (2006) 312(5774):734–7. doi: 10.1126/science.1123965
134. Ahmadian M, Abbott MJ, Tang T, Hudak CS, Kim Y, Bruss M, et al. Desnutrin/ATGL is regulated by AMPK and is required for a brown adipose phenotype. *Cell Metab* (2011) 13(6):739–48. doi: 10.1016/j.cmet.2011.05.002
135. Shin H, Ma Y, Chanturiya T, Cao Q, Wang Y, Kadegowda AKG, et al. Lipolysis in Brown Adipocytes Is Not Essential for Cold-Induced Thermogenesis in Mice. *Cell Metab* (2017) 26(5):764–77.e5. doi: 10.1016/j.cmet.2017.09.002
136. Schreiber R, Diwoky C, Schoiswohl G, Feiler U, Wongsiriroj N, Abdellatif M, et al. Cold-Induced Thermogenesis Depends on ATGL-Mediated Lipolysis in Cardiac Muscle, but Not Brown Adipose Tissue. *Cell Metab* (2017) 26(5):753–63.e7. doi: 10.1016/j.cmet.2017.09.004
137. Chitraju C, Fischer AW, Farese RVJr., Walther TC. Lipid Droplets in Brown Adipose Tissue Are Dispensable for Cold-Induced Thermogenesis. *Cell Rep* (2020) 33(5):108348. doi: 10.1016/j.celrep.2020.108348
138. Yoneshiro T, Wang Q, Tajima K, Matsushita M, Maki H, Igarashi K, et al. BCAA catabolism in brown fat controls energy homeostasis through SLC25A44. *Nature* (2019) 572(7771):614–9. doi: 10.1038/s41586-019-1503-x
139. Wang TJ, Larson MG, Vasan RS, Cheng S, Rhee EP, McCabe E, et al. Metabolite profiles and the risk of developing diabetes. *Nat Med* (2011) 17(4):448–53. doi: 10.1038/nm.2307
140. Lotta LA, Scott RA, Sharp SJ, Burgess S, Luan J, Tillin T, et al. Genetic Predisposition to an Impaired Metabolism of the Branched-Chain Amino Acids and Risk of Type 2 Diabetes: A Mendelian Randomisation Analysis. *PloS Med* (2016) 13(11):e1002179. doi: 10.1371/journal.pmed.1002179
141. Green CR, Wallace M, Divakaruni AS, Phillips SA, Murphy AN, Ciaraldi TP, et al. Branched-chain amino acid catabolism fuels adipocyte differentiation and lipogenesis. *Nat Chem Biol* (2016) 12(1):15–21. doi: 10.1038/nchembio.1961
142. Simcox J, Geoghegan G, Maschek JA, Bensard CL, Pasquali M, Miao R, et al. Global Analysis of Plasma Lipids Identifies Liver-Derived Acylcarnitines as a Fuel Source for Brown Fat Thermogenesis. *Cell Metab* (2017) 26(3):509–22.e6. doi: 10.1016/j.cmet.2017.08.006
143. Scherer PE, Williams S, Fogliano M, Baldini G, Lodish HF. A Novel Serum Protein Similar to C1q, Produced Exclusively in Adipocytes (*). *J Biol Chem* (1995) 270(45):26746–9. doi: 10.1074/jbc.270.45.26746
144. Zhang Y, Proenca R, Maffei M, Barone M, Leopold L, Friedman JM. Positional cloning of the mouse obese gene and its human homologue. *Nature* 372:425–32 (1994). doi: 10.1038/372425a0
145. Villarroya F, Cereijo R, Villarroya J, Giralt M. Brown adipose tissue as a secretory organ. *Nat Rev Endocrinol* (2017) 13(1):26–35. doi: 10.1038/nrendo.2016.136
146. Silva JE, Larsen PR. Adrenergic activation of triiodothyronine production in brown adipose tissue. *Nature* (1983) 305(5936):712–3. doi: 10.1038/305712a0
147. Silva JE, Larsen PR. Potential of brown adipose tissue type II thyroxine 5'-deiodinase as a local and systemic source of triiodothyronine in rats. *J Clin Invest* (1985) 76(6):2296–305. doi: 10.1172/JCI112239
148. Bianco AC, Silva JE. Intracellular conversion of thyroxine to triiodothyronine is required for the optimal thermogenic function of brown adipose tissue. *J Clin Invest* (1987) 79(1):295–300. doi: 10.1172/JCI112798
149. de Jesus LA, Carvalho SD, Ribeiro MO, Schneider M, Kim SW, Harney JW, et al. The type 2 iodothyronine deiodinase is essential for adaptive thermogenesis in brown adipose tissue. *J Clin Invest* (2001) 108(9):1379–85. doi: 10.1172/JCI200113803
150. Hondares E, Iglesias R, Giralt A, Gonzalez FJ, Giralt M, Mampel T, et al. Thermogenic activation induces FGF21 expression and release in brown adipose tissue. *J Biol Chem* (2011) 286(15):12983–90. doi: 10.1074/jbc.M110.215889
151. Chartoumpekis DV, Habeos IG, Ziros PG, Psyrogiannis AI, Kyriazopoulou VE, Papavassiliou AG. Brown adipose tissue responds to cold and adrenergic stimulation by induction of FGF21. *Mol Med* (2011) 17(7-8):736–40. doi: 10.2119/molmed.2011.00075
152. Burysek L, Houstek J. beta-Adrenergic stimulation of interleukin-1alpha and interleukin-6 expression in mouse brown adipocytes. *FEBS Lett* (1997) 411(1):83–6. doi: 10.1016/S0014-5793(97)00671-6
153. Sun K, Kusminski CM, Luby-Phelps K, Spurgin SB, An YA, Wang QA, et al. Brown adipose tissue derived VEGF-A modulates cold tolerance and energy expenditure. *Mol Metab* (2014) 3(4):474–83. doi: 10.1016/j.molmet.2014.03.010
154. Wang GX, Zhao XY, Meng ZX, Kern M, Dietrich A, Chen Z, et al. The brown fat-enriched secreted factor Nrg4 preserves metabolic homeostasis through attenuation of hepatic lipogenesis. *Nat Med* (2014) 20(12):1436–43. doi: 10.1038/nm.3713
155. Chen Z, Wang GX, Ma SL, Jung DY, Ha H, Altamimi T, et al. Nrg4 promotes fuel oxidation and a healthy adipokine profile to ameliorate diet-induced metabolic disorders. *Mol Metab* (2017) 6(8):863–72. doi: 10.1016/j.molmet.2017.03.016
156. Thomou T, Mori MA, Dreyfuss JM, Konishi M, Sakaguchi M, Wolfrum C, et al. Adipose-derived circulating miRNAs regulate gene expression in other tissues. *Nature* (2017) 542(7642):450–5. doi: 10.1038/nature21365
157. Stanford KI, Lynes MD, Takahashi H, Baer LA, Arts PJ, May FJ, et al. 12,13-diHOME: An Exercise-Induced Lipokine that Increases Skeletal Muscle Fatty Acid Uptake. *Cell Metab* (2018) 27(6):1357. doi: 10.1016/j.cmet.2018.04.023
158. Lynes MD, Leiria LO, Lundh M, Bartelt A, Shamsi F, Huang TL, et al. The cold-induced lipokine 12,13-diHOME promotes fatty acid transport into brown adipose tissue. *Nat Med* (2017) 23(5):631–7. doi: 10.1038/nm.4297
159. Leiria LO, Wang CH, Lynes MD, Yang K, Shamsi F, Sato M, et al. 12-Lipoxygenase Regulates Cold Adaptation and Glucose Metabolism by Producing the Omega-3 Lipid 12-HEPE from Brown Fat. *Cell Metab* (2019) 30(4):768–83.e7. doi: 10.1016/j.cmet.2019.07.001
160. Sponton CH, Hosono T, Taura J, Jedrychowski MP, Yoneshiro T, Wang Q, et al. The regulation of glucose and lipid homeostasis via PLTP as a mediator of BAT-liver communication. *EMBO Rep* (2020) 21(9):e49828. doi: 10.15252/embr.201949828
161. Deshmukh AS, Peijs L, Beaudry JL, Jespersen NZ, Nielsen CH, Ma T, et al. Proteomics-Based Comparative Mapping of the Secretomes of Human Brown and White Adipocytes Reveals EPDR1 as a Novel Batokine. *Cell Metab* (2019) 30(5):963–75.e7. doi: 10.1016/j.cmet.2019.10.001

162. Ali Khan A, Hansson J, Weber P, Foehr S, Krijgsveld J, Herzig S, et al. Comparative Secretome Analyses of Primary Murine White and Brown Adipocytes Reveal Novel Adipokines. *Mol Cell Proteomics* (2018) 17 (12):2358–70. doi: 10.1074/mcp.RA118.000704
163. Villarroya J, Cereijo R, Gavaldà-Navarro A, Peyrou M, Giralt M, Villarroya F. New insights into the secretory functions of brown adipose tissue. *J Endocrinol* (2019) 243(2):R19–27. doi: 10.1530/JOE-19-0295
164. Cereijo R, Gavaldà-Navarro A, Cairó M, Quesada-López T, Villarroya J, Morón- Ros S, et al. CXCL14, a Brown Adipokine that Mediates Brown-Fat-to-Macrophage Communication in Thermogenic Adaptation. *Cell Metab* (2018) 28(5):750–63.e6. doi: 10.1016/j.cmet.2018.07.015
165. Leitner BP, Huang S, Brychta RJ, Duckworth CJ, Baskin AS, McGehee S, et al. Mapping of human brown adipose tissue in lean and obese young men. *Proc Natl Acad Sci USA* (2017) 114(32):8649–54. doi: 10.1073/pnas.1705287114
166. van der Lans AA, Hoeks J, Brans B, Vijgen GH, Visser MG, Vosselman MJ, et al. Cold acclimation recruits human brown fat and increases nonshivering thermogenesis. *J Clin Invest* (2013) 123(8):3395–403. doi: 10.1172/JCI68993
167. Lee P, Smith S, Linderman J, Courville AB, Brychta RJ, Dieckmann W, et al. Temperature-acclimated brown adipose tissue modulates insulin sensitivity in humans. *Diabetes* (2014) 63(11):3686–98. doi: 10.2337/db14-0513
168. Cypess AM, Weiner LS, Roberts-Toler C, Franquet Elia E, Kessler SH, Kahn PA, et al. Activation of human brown adipose tissue by a beta3-adrenergic receptor agonist. *Cell Metab* (2015) 21(1):33–8. doi: 10.1016/j.cmet.2014.12.009
169. Galmozzi A, Sonne SB, Altshuler-Keylin S, Hasegawa Y, Shinoda K, Luijten IHN, et al. ThermoMouse: an in vivo model to identify modulators of UCP1 expression in brown adipose tissue. *Cell Rep* (2014) 9(5):1584–93. doi: 10.1016/j.celrep.2014.10.066
170. Beiroa D, Imbernon M, Gallego R, Senra A, Herranz D, Villarroya F, et al. GLP-1 agonism stimulates brown adipose tissue thermogenesis and browning through hypothalamic AMPK. *Diabetes* (2014) 63(10):3346–58. doi: 10.2337/db14-0302
171. Reilly SM, Chiang SH, Decker SJ, Chang L, Uhm M, Larsen MJ, et al. An inhibitor of the protein kinases TBK1 and IKK-varepsilon improves obesity-related metabolic dysfunctions in mice. *Nat Med* (2013) 19(3):313–21. doi: 10.1038/nm.3082
172. Hoffmann LS, Etzrodt J, Willkomm L, Sanyal A, Scheja L, Fischer AWC, et al. Stimulation of soluble guanylyl cyclase protects against obesity by recruiting brown adipose tissue. *Nat Commun* (2015) 6:7235. doi: 10.1038/ncomms8235
173. Ouellet V, Routhier-Labadie A, Bellemare W, Lakhal-Chaieb L, Turcotte E, Carpentier AC, et al. Outdoor temperature, age, sex, body mass index, and diabetic status determine the prevalence, mass, and glucose-uptake activity of 18F-FDG-detected BAT in humans. *J Clin Endocrinol Metab* (2011) 96 (1):192–9. doi: 10.1210/jc.2010-0989
174. Zhu Z, Spicer EG, Gavini CK, Goudjo-Ako AJ, Novak CM, Shi H. Enhanced sympathetic activity in mice with brown adipose tissue transplantation (transBATation). *Physiol Behav* (2014) 125:21–9. doi: 10.1016/j.physbeh.2013.11.008
175. Liu X, Zheng Z, Zhu X, Meng M, Li L, Shen Y, et al. Brown adipose tissue transplantation improves whole-body energy metabolism. *Cell Res* (2013) 23 (6):851–4. doi: 10.1038/cr.2013.64
176. Kajimura S, Seale P, Kubota K, Lunsford E, Frangioni JV, Gygi SP, et al. Initiation of myoblast to brown fat switch by a PRDM16-C/EBP-beta transcriptional complex. *Nature* (2009) 460(7259):1154–8. doi: 10.1038/nature08262
177. Kishida T, Ejima A, Yamamoto K, Tanaka S, Yamamoto T, Mazda O. Reprogrammed Functional Brown Adipocytes Ameliorate Insulin Resistance and Dyslipidemia in Diet-Induced Obesity and Type 2 Diabetes. *Stem Cell Rep* (2015) 5(4):569–81. doi: 10.1016/j.stemcr.2015.08.007
178. Ahfeldt T, Schinzel RT, Lee YK, Hendrickson D, Kaplan A, Lum DH, et al. Programming human pluripotent stem cells into white and brown adipocytes. *Nat Cell Biol* (2012) 14(2):209–19. doi: 10.1038/ncb2411
179. Jobgen W, Meininger CJ, Jobgen SC, Li P, Lee MJ, Smith SB, et al. Dietary L-arginine supplementation reduces white fat gain and enhances skeletal muscle and brown fat masses in diet-induced obese rats. *J Nutr* (2009) 139 (2):230–7. doi: 10.3945/jn.108.096362
180. Lucotti P, Setola E, Monti LD, Galluccio E, Costa S, Sandoli EP, et al. Beneficial effects of a long-term oral L-arginine treatment added to a hypocaloric diet and exercise training program in obese, insulin-resistant type 2 diabetic patients. *Am J Physiol Endocrinol Metab* (2006) 291(5):E906–12. doi: 10.1152/ajpendo.00002.2006
181. Yoneshiro T, Aita S, Matsushita M, Kayahara T, Kameya T, Kawai Y, et al. Recruited brown adipose tissue as an antiobesity agent in humans. *J Clin Invest* (2013) 123(8):3404–8. doi: 10.1172/JCI67803
182. Baruch A, Wong C, Chinn LW, Vaze A, Sonoda J, Gelzleichter T, et al. Antibody-mediated activation of the FGFR1/Klothoβ complex corrects metabolic dysfunction and alters food preference in obese humans. *Proc Natl Acad Sci USA* (2020) 117(46):28992–9000. doi: 10.1073/pnas.2012073117

Conflict of Interest: The authors declare that the review was construed in the absence of any commercial or financial relationships that could be constructed as a potential conflict of interest.

frontiers in Endocrinology

ORIGINAL RESEARCH
published: 10 May 2021
doi: 10.3389/fendo.2021.618037

Emodin Improves Glucose and Lipid Metabolism Disorders in Obese Mice *via* Activating Brown Adipose Tissue and Inducing Browning of White Adipose Tissue

Long Cheng[1], *Shuofeng Zhang*[1], *Fei Shang*[2], *Yibo Ning*[1], *Zhiqi Huang*[1], *Runcheng He*[1], *Jianning Sun*[1] *and Shifen Dong*[1*†]

[1] School of Chinese Materia Medica, Beijing University of Chinese Medicine, Beijing, China, [2] Analytical and Testing Center, Beijing University of Chemical Technology, Beijing, China

OPEN ACCESS

Edited by:
Xinran Ma,
East China Normal University, China

Reviewed by:
Damasia Becu-Villalobos,
CONICET Instituto de Biología y Medicina Experimental (IBYME), Argentina
André Sarmento Cabral,
Maimonides Biomedical Research Institute of Cordoba (IMIBIC), Spain
Yingfei Li,
Institute of Chinese Materia Medica, China Academy of Chinese Medical Sciences, China

***Correspondence:**
Shifen Dong
dongshifen@bucm.edu.cn

[†]Present address:
Shifen Dong,
Department of Pharmacology of Chinese Medicine, School of Chinese Materia Medica, Beijing University of Chinese Medicine,
Beijing, China

Specialty section:
This article was submitted to Translational Endocrinology, a section of the journal Frontiers in Endocrinology

Received: 20 October 2020
Accepted: 06 April 2021
Published: 10 May 2021

Citation:
Cheng L, Zhang S, Shang F, Ning Y, Huang Z, He R, Sun J and Dong S (2021) Emodin Improves Glucose and Lipid Metabolism Disorders in Obese Mice via Activating Brown Adipose Tissue and Inducing Browning of White Adipose Tissue. Front. Endocrinol. 12:618037. doi: 10.3389/fendo.2021.618037

Background: Adipose tissue (e.g. white, brown and brite) plays a critical role in modulating energy metabolism. Activating brown adipose tissue (BAT) and inducing browning in white adipose tissue (WAT) has been proposed to be a potential molecular target for obesity treatment. Emodin is a natural anthraquinone derivative that exhibits variety of pharmacologic effects including lowering lipids and regulating glucose utilization. However, the underlying mechanism of action is still unclear. In the present study, we investigated whether emodin could alleviate obesity *via* promoting browning process in adipose tissue.

Methods: C57BL/6J mice were fed with high fat diet to induce obesity. Emodin at the doses of 40 and 80 mg/kg were orally given to obesity mice for consecutive 6 weeks. Parameters including fasting blood glucose, oral glucose tolerance, blood lipids, and the ratios of subcutaneous white adipose tissue (scWAT) or BAT mass to body weight, and morphology of adipose tissue were observed. Besides, the protein expression of uncoupling protein 1 (UCP1) and prohibitin in BAT and scWAT was determined by immunohistochemistry method. Relative mRNA expression of *Cd137*, transmembrane protein 26 (*Tmem26*) and *Tbx1* in scWAT was analyzed using qRT-PCR. And the protein expression of UCP1, CD36, fatty acid transporter 4 (FATP4), peroxisome proliferator-activated receptor alpha (PPARα) and prohibitin of scWAT and BAT were analyzed using western blotting. In addition, ultra-high-performance liquid chromatography with electrospray ionization tandem mass spectrometry was utilized to detect the small lipid metabolites of scWAT and BAT.

Results: Emodin decreased the body weight and food intake in HFD-induced obesity mice, and it also improved the glucose tolerance and reduced the blood lipids. Emodin treatment induced beiging of WAT, and more multilocular lipid droplets were found in scWAT. Also, emodin significantly increased markers of beige adipocytes, e.g. *Cd137*, *Tmem26* and *Tbx1* mRNA in scWAT, and UCP1, CD36, FATP4, PPARα and prohibitin

protein expression in scWAT and BAT. Furthermore, emodin perturbed the lipidomic profiles in scWAT and BAT of obese mice. Emodin increased total ceramides (Cers), lysophosphatidylcholines (LPCs), lyso-phosphatidylcholines oxygen (LPCs-O), and phosphatidylethanolamines oxygen (PEs-O) species concentration in scWAT. Specifically, emodin significantly up-regulated levels of Cer (34:1), LPC (18:2), LPC-(O-20:2), PC (O-40:7), PE (O-36:3), PE (O-38:6), PE (O-40:6), and sphingolipid (41:0) [SM (41:0)], and down-regulated PC (O-38:0), PE (O-40:4), PE (O-40:5) in scWAT of obesity mice. In terms of lipid matabolites of BAT, the emodin remarkably increased the total PCs levels, which was driven by significant increase of PC (30:0), PC (32:1), PC (32:2), PC (33:4) and PC (38:0) species. In addition, it also increased species of LPCs, e.g. LPC (20:0), LPC (20:1), LPC (22:0), LPC (22:1), LPC (24:0), and LPC (24:1). Especially, emodin treatment could reverse the ratio of PC/PE in HFD-induced obese mice.

Conclusions: These results indicated that emodin could ameliorate adiposity and improve metabolic disorders in obese mice. Also, emodin could promote browning in scWAT and activate the BAT activities. In addition, emodin treatment-induced changes to the scWAT and BAT lipidome were highly specific to certain molecular lipid species, indicating that changes in tissue lipid content reflects selective remodeling in scWAT and BAT of both glycerophospholipids and sphingolipids in response to emodin treatment.

Keywords: emodin, obesity, brown adipose tissue, white adipose tissue, browning of white adipose tissue, lipid metabolic signature

BACKGROUND

White adipose tissue (WAT) and brown adipose tissue (BAT) play a critical role in modulating energy metabolism (1). The adipocytes within WAT store large amounts of triglycerides as chemical energy in unilocular droplets, which are released into circulation as needed. WAT also functions to produce hormones and cytokines, regulates immune system and supports local tissue frame (2). Increases in WAT mass are directly associated with increased rates of metabolic diseases such as obesity and type 2 diabetes (3). BAT is specialized for energy expenditure, which is characterized by small multi-atrial lipid droplets, abundant mitochondria and expresses uncoupling protein 1 (UCP1) (4, 5). BAT dissipates energy as heat and stores energy for use of non-shivering thermogenesis, which also plays a significant role in energy regulation (5, 6). It has been confirmed that when the body is stimulated by cold exposure (7) or activated by β-adrenoceptors agonist (8), brown-like phenotypic adipocytes (e.g. beige adipocytes) can be detected in WAT, which are characterized by an increased number of mitochondria and increased expression of brown fat marker genes (e.g. *Ucp1*, *Pgc-1α*, *Prdm16*). The above process is called browning of WAT. Recent studies showed that increasing metabolic activity of brown and beige adipose tissue might be a novel way to ameliorate glucose and lipid metabolism in obese patients (9–12). Furthermore, changes in tissue lipid content reflects selective remodeling in scWAT and BAT of both phospholipids and glycerol lipids in response to specific conditions such as exercise training (1).

Emodin (1,3,8-trihydroxy-6-methylanthraquinone) is a natural anthraquinone derivative, and is the main component of *Rheum palmatum* L (13). It has been reported to exhibit anti-inflammatory, anti-bacterial, anti-cancer, anti-diabetic, anti-ulcerogenic, immunosuppressive, pro-apoptotic and chemopreventive activities (14–18). It has been found that the emodin can regulate glucose utilization and lower lipids in epididymal WAT by activating AMP activated protein kinase (AMPK) pathway (19, 20). In addition, the emodin could inhibit adipocyte differentiation and enhances osteoblast differentiation from bone marrow mesenchymal stem cells (BMSCs) (21). And it could improve the inactive glucocorticoid-induced adipose tissue dysfunction by selective inhibition on 11β-hydroxysteroid dehydrogenase type 1 (11β-HSD1) in 3T3-L1 adipocyte (22). Our previous research also showed that emodin could inhibit the accumulation of white adipocytes and inducing browning of WAT in apolipoprotein E knockout ($ApoE^{-/-}$) mice (23). However, the effect of emodin on the lipid metabolic signature of scWAT and BAT has not been investigated. Here, we report the effect of emodin on adipose tissue in high fat diet-induced obese mice, as well as a comprehensive analysis of lipid composition in scWAT and BAT.

Abbreviations: WAT, white adipose tissue; BAT, brown adipose tissue; HFD, high-fat diet; scWAT, subcutaneous white adipose tissue; UCP1, uncoupling protein 1; PPARα, Peroxisome proliferator-activated receptor alpha; PGC-1α, Peroxisome proliferator activated receptor γ coactivator-1α; PRDM16, positive regulatory domain-containing 16; PHB, prohibitin; AMPK, AMP activated protein kinase; SREBP, sterol regulatory element-binding protein; Tmem26, Transmembrane protein 26; TC, total cholesterol; TG, triglyceride; HDL-c, high-density lipoprotein cholesterol; LDL-c, low-density lipoprotein cholesterol; FFA, free fatty acid; AUC, area under circle; IR, insulin resistance; LCFA, long-chain fatty acids; FATP 4, Fatty acid transporter 4; PC, Phosphatidylcholine; PE, phosphatidylethanolamine; PS, phosphatidylserine; SM, sphingolipid; Cer, ceramides; LPC, lyso-phosphatidylcholine; LPE, lyso-phosphatidylethanolamine.

MATERIALS AND METHODS

Chemicals and Reagents

Emodin (purity 95%) was purchased from Shanghai Yuanye Biotechnology Co., Ltd. CL 316243 disodium salt was purchased from APExBIO Technology LLC (Houston, USA). Biochemical kits of serum total cholesterol (TC), triglyceride (TG), high-density lipoprotein cholesterol (HDL-c), and low-density lipoprotein cholesterol (LDL-c) were purchased from Nanjing Jiancheng Bioengineering Institute (Nanjing, China). Free fatty acid (FFA) ELISA assay kit was purchased from Jiangsu Kete Biotechnology Co., Ltd. (Jiangsu, China). Leptin ELISA assay kit and adiponectin ELISA assay kit were purchased from cloud-clone Corp. Wuhan (Wuhan, China).

Animals and Experimental Protocol

Eight-week-old male C57BL/6J mice weighing 18-22g were purchased from Sibeifu (Beijing) Biotechnology Co., Ltd (grade SPF, Certificate No: SCXK (jing) 2016-0002). Mice were maintained at 23 ± 1°C and 60-70% humidity with a 12h light/dark cycle. The regular diet was a standard chow diet containing 3.65 kcal/g. And the high fat diet was 60% of kilocalories from fat containing 5.24 kcal/g. Normal diet is purchased from SBF (Beijing) Biotechnology Co., Ltd (Beijing, China, 0817SH08200438C). High fat diet was purchased from Beijing huafukang Biotechnology Co., Ltd (Beijing, China, 20180376).

Mice were randomly divided into two groups according to weight and fed with normal control diet (n=8) or fed with high fat diet (HFD) for 8 weeks to induce hyperlipidemia. After 8 weeks of HFD, mice were randomly divided into four groups as follows (n=8/group): HFD group, emodin 40 mg/kg group, and emodin 80 mg/kg group, and CL 316243 1 mg/kg group. Mice in normal control group and HFD group were administrated with equal amount of 0.1% carboxymethyl cellulose-Na (CMC-Na). Mice in emodin 40 and 80 mg/kg groups were taken emodin (dissolved in 0.1% CMC-Na) by intragastric administration for consecutive 6 weeks. Before dissection, mice in CL 316243 1 mg/kg treatment group were intraperitoneally injected with 1mg/kg/day of CL 316243 disodium salt for 3 days. All the animal studies were in accordance with ethics standards of the Animal Care and Welfare Committee of Beijing University of Chinese Medicine (Certificate No. BUCM-04-2018070603-3015).

Oral Glucose Tolerance Test

After 6 weeks of intervention, the mice were fed by oral gavage with 50% D-glucose (2.0 g/kg) after overnight (12 h) fasting. Blood samples were taken from the tail 0, 30, 60, 90 and 120 min after oral gavage, and glucose levels were measured by the One Touch Ultra blood glucose monitoring system (ONETOUCH Ultra Easy).

Measurement of Lee's Index

At the end of the treatment, the body mass of the mice was accurately weighed, and the body length (the distance from the tip of the nose to the anus) was accurately measured, and then the Lee's index was calculated according to the reference (24).

Measurement of Adipose Tissue Mass/Body Weights

Subcutaneous WAT (scWAT) mass and scapular brown adipose tissues (BAT) mass were accurately weighed. The ratios of scWAT mass to body weight (BW) and BAT mass to body weight (BW) were calculated.

Serum Biochemical Analysis

Serum TC, TG, HDL-c and LDL-c levels were measured with the method of biochemical kits (Nanjing Jiancheng, China). The levels of FFA were determined by the Mouse FFA ELISA kit (Kete, China). Serum leptin and adiponectin levels were analyzed using the mouse leptin and adiponectin ELISA kit respectively (Cloud-clone, China).

Histological and Immunohistochemical Analysis

BAT and scWAT were fixed with 10% formalin, dehydrated, embedded in paraffin and sectioned. For histological analysis, sections were deparaffinized and stained with hematoxylin and eosin. The expression of UCP1 (1:500, ab10983, Abcam) and prohibitin (1:500, ab75766, Abcam) in mouse BAT and scWAT was determined by immunohistochemistry. All images were acquired with the microscope (Leica, Germany). The expression level of UCP1 and prohibitin in BAT and scWAT of the mice was quantified by using Image Pro Plus 6.0.

Quantitative Real-Time PCR Analysis

Total RNA of scWAT was extracted with Trizol® Reagent (Ambion, USA). Reverse transcription of total RNA (1 μg) was performed with Revert Aid First Stand cDNA Synthesis Kit (Thermo Scientific, USA). Real-time quantitative PCR (qRT-PCR) was performed with a SYBR Green Master Mix (Novoprotein, China). The PCR reaction was operated in triplicate for each sample using the Step One Real-Time PCR System (Applied Biosystems, USA). After standardizing the expression level of internal control actin in each sample, the data were expressed in arbitrary units. The sequences of primer in this study were shown in **Table 1**.

Western Blot Analysis

The homogenates of scWAT and BAT were dissolved in RIPA lysate and protease inhibition for protein extraction. Sample protein concentrations were measured using the bicinchoninic acid (BCA) method (Beyotime). Total protein (10μg/Lane) was separated on a 12% acrylamide/acrylamide gel using sodium dodecyl sulfate-polyacrylamide gel electrophoresis (SDS-PAGE)

TABLE 1 | Primer sequences were used for quantitative real-time reverse transcription polymerase chain reaction (qRT-PCR).

Gene name	Forward (5'-3')	Reverse (5'-3')
Cd137	GGTGGACAGCCGAACTGTAA	GCTGCTCCAGTGGTCTTCTT
Tmem26	AGTGTGAGCAAGAACTCGGG	GATGGCCGGAGAAAGCCATT
Tbx1	CGCTACCGGTATGCTTTCCA	GTCTTTTCGAGGGGCCACAT
β-actin	GGTGGGAATGGGTCAGAAGG	GTTGGCCTTAGGGTTCAGGG

and transferred to polyvinylidene difluoride (PVDF) membranes. PVDF membranes containing protein were incubated with specific anti-alpha tubulin antibody (1:5000, ab18251, Abcam), anti-UCP1 antibody (1:1000, ab10983, Abcam), anti-Prohibitin antibody (1:10000, ab75766, Abcam), anti-PPAR α antibody (1:2000, ab8934, Abcam), anti-CD36 antibody (1:5000, ab133625, Abcam), anti-slc27a4/FATP4 antibody (1:1000, ab200353, Abcam), respectively. Then membranes were incubated with HRP-conjugated Affinipure Goat Anti-Mouse IgG (H+L) (1:5000, 20000175, proteintech) or HRP-conjugated Affinipure Goat Anti-Rabbit IgG (H+L) (1:5000, 20000174, proteintech). Protein bands were visualized using the ECL kit (EMD millipore). Image was analyzed using Image-Pro-Plus 6.0.

Targeted Lipidomics Analysis

Tissue Sample Preparation

BAT and scWAT tissue samples were thawed on ice. Samples were accurately weighed and then homogenized in the 1.5 mL centrifuge tube using a Speed Mill Plus. Internal standards were dissolved in 300μL of methanol [SPLASH® II LIPIDOMIX® Mass Spec Standard (330709), Cer/Sph Mixture I (LM6002, Avanti), 12:0-13:0 PC (LM1000, Avanti), 12:0-13:0 PE (LM1100, Avanti)] and added to each sample, and then extracted with 1mL of methyl tert-butyl ether (MTBE) for 1 hour. The extraction was added 250 μL of water and pelleted in a 4℃ centrifuge at 12,000 rpm for 5 min. 100 μL of the MTBE layer was transferred to a new 1.5 mL centrifuge tube and dried in a Savant™ SpeedVac™ High Capacity Concentrator. The dried sample was reconstituted with 400 μL of isopropanol/acetonitrile (1:1) and shaken for 40s. And the dissolved matter was centrifuged at 12,000 for 5 min, and then 100 μL of the supernatant was transferred to a 200 μL vial insert for liquid chromatography-mass spectrometry analysis.

Chromatography

ACQUITY Ultra Performance Liquid Chromatography (UPLC) I-Class System (Waters, USA) with ACQUITY UPLC BEH C_8 Column (2.1 mm×100 mm, 1.7 μm) was used to perform the UPLC separation. For C_8 separation, mobile phase A is acetonitrile/water (60/40) and mobile phase B is acetonitrile/isopropanol (90/10), and both A and B contain 0.1% formic acid and 5 mM ammonium acetate (formate). The gradient conditions were shown in **Tables 2** and **3**.

Quality Control

Five QC samples of adipose tissue were continuously injected at the beginning of the sequence to monitor the UPLC-MS system stability by the Overlay Graphs method using Mass Lynx software. And QC samples were run at regular intervals (8 samples) throughout the entire sequence.

Mass Spectrometry

Electrospray ionization tandem mass spectrometry (XEVO TQ-S Micro, Waters, USA) was used for mass spectrometry. And the conduct conditions of ESI^+ and ESI^- showed in **Table 4**. Masslyxn4.1 was used for mass spectrometry data acquisition.

TABLE 2 | The gradient conditions for reversed phase C_8 separation for lipids.

Time(min)	A (v%)	B (v%)
0	68	32
1.5	68	32
15.5	15	85
15.6	3	97
18	3	97
18.1	68	32
20	68	32

TABLE 3 | The gradient conditions for reversed phase C_8 separation for fatty acids.

Time(min)	A(v%)	B(v%)
0	90	10
1.5	90	10
8	3	97
13	3	97
13.1	90	10
15	90	10

Statistical Analysis

The data of target metabolism group were operated by skyline 19.1. The parameters were set as follows: the quality extraction error was 5 ppm and the allowable retention time error was 15s. Other data were statistically analyzed using SAS 8.2 software. All data were expressed as means ± SE. Two-way analysis of variance for repeated measures was used for body weight analysis (for the effects of treatment and time). Other statistics was performed using the one-way analysis of variance (ANOVA) followed by SNK-*q* test. *P*-value<0.05 was considered as statistically significant.

RESULTS

Emodin Can Inhibit Obesity and Appetite and Reduce Fat Mass in HFD Induced Obese Mice

The HFD treated mice showed characteristics of obesity. When compared with the control mice, parameters including body weight, food intake, Lee's index and scWAT/BW ratio were significantly increased in HFD treated mice (by 51.6%, 41.1%, 8.5% and 39.1%, respectively). Emodin at the dose of 40 mg/kg caused a significant reduction in body weight at week 5 and 6 (by 13.0% and 15.7%, respectively), and emodin 80 mg/kg caused a remarkable reduction in body weight at week 3, 4, 5, 6 (by 11.1%,

TABLE 4 | Analysis condition of positive and negative electrospray ionization.

Parameter	ESI^+	ESI^-
Capillary voltage	3200V	2000V
Desolvation temperature	500°C	500℃
Source temperature	120°C	120℃
Desolvation gas flow	1000 L/h	1000L/h
Cone gas flow	150 L/h	150 L/h
Nebuliser gas	7.0 bar	7.0 bar
Collision gas flow	0.13 L/h	0.13 L/h

12.6%, 12.6% and 13.9%, respectively), when compared with HFD mice (**Figure 1A**).

Emodin (40 mg/kg, 80 mg/kg) significantly decreased the food intake by 9.8% and 7.3%, respectively, when compared with the obese mice (P <0.01 or P <0.05) (**Figure 1B**).

Lee's index can be used as an indicator to evaluate the degree of obesity in adult obese model mice (25). Emodin at the doses of 40 and 80 mg/kg and CL316243 (1 mg/kg) treatment group could significantly reduce the Lee's index, when compared with HFD mice (P <0.01) (**Figure 1C**).

The ratio of scWAT to BW in mice treated with emodin (40mg/kg, 80mg/kg) and CL316243 (1mg/kg) was significantly decreased (by 39.1%, 46.4% and 40.9%, respectively), when compared with the HFD mice (P < 0.01 or P < 0.05). (**Figure 1D**).

The function of BAT is consuming glucose and lipids, mediating the thermogenic effects of non-shivering, thereby increasing energy expenditure (26). Interestingly, compared with HFD mice, emodin (80 mg/kg) and CL 316243 (1 mg/kg) treatment significantly decreased the ratio of BAT/BW (by 22.5% and 47.5%, respectively (**Figure 1E**).

Emodin Ameliorates Abnormal Blood Glucose and Blood Lipid in Mice Fed With HFD

In this study, we investigated whether emodin improved glucose tolerance in obese mice. The results indicated an impaired glucose tolerance in HFD mice, and high fat diet significantly increased AUC index, when compared with control mice (P <0.01). Emodin at the doses of 40 and 80 mg/kg and CL316243 (1 mg/kg) treatment significantly decreased AUC value (31.1%, 35.3% and 45.1% respectively), when compared with HFD mice (P <0.01) (**Figures 2A, B**). These results suggested that emodin could ameliorate glucose metabolism in obese mice.

To investigate whether emodin improved hyperlipidemia in obese mice, blood lipid parameters were measured. When compared with control mice, serum TC, TG, LDL-c, HDL-c and FFA levels were significantly increased in obese mice (P <0.01). When compared with obese mice, emodin (40 mg/kg, 80 mg/kg) could remarkably decrease serum TC, TG and LDL-c by 15.1%-16.3%, 19.6%-34.0%, 52.9%-54.3%, respectively (P <0.01 or P <0.05) (**Figures 2C–E**), and emodin (80 mg/kg) could remarkably decrease serum FFA levels (**Figure 2G**), but there was no significant difference in the content of HDL in serum (**Figure 2F**).

Leptin plays an important role in maintaining energy metabolism and regulating adipose ratio (27). It was demonstrated that the serum leptin content of HFD mice was significantly increased by 574.3%, when compared with control mice (P <0.01). Emodin (40 mg/kg, 80 mg/kg) and CL316243 (1 mg/kg) caused significant reduction in leptin levels (by 40.7%, 54.6% and 41.5%, respectively), when compared with HFD mice (P <0.01) (**Figure 2H**).

As an endogenous insulin sensitizer secreted by adipose tissue, reduction of adiponectin is an independent risk factor for hyperlipidemia and diabetes (28). When compared with control mice, serum adiponectin in HFD mice was significantly decreased (P <0.01). Emodin (40 mg/kg, 80 mg/kg) treatment

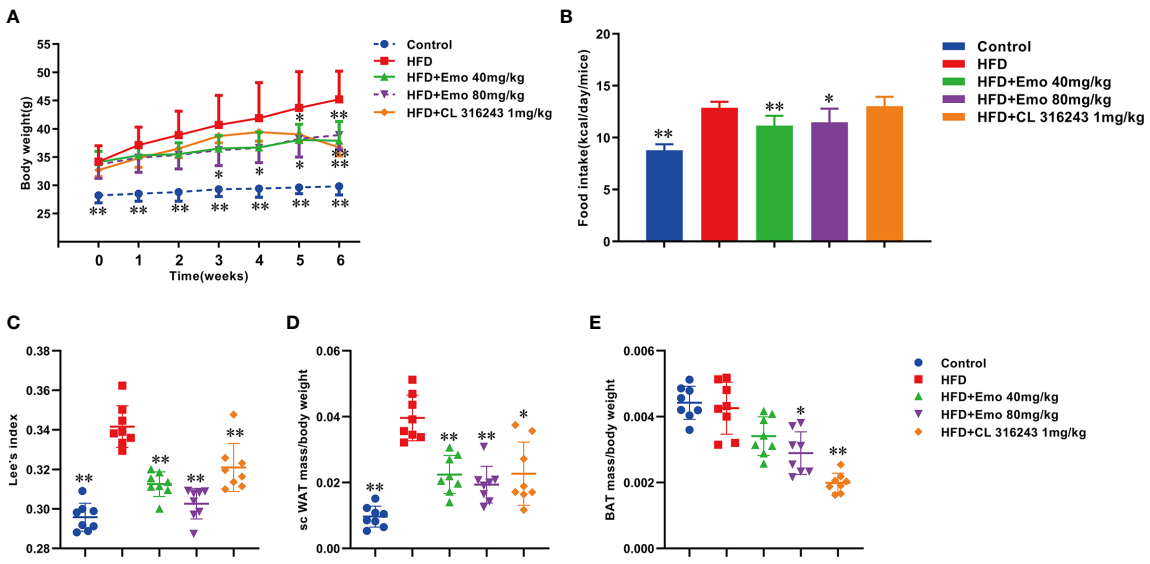

FIGURE 1 | Effects of emodin on body weight, food intake and Lee's index in HFD mice. Mice were fed with high fat diet (HFD) containing 5.24 kcal/g for 8 weeks to induce hyperlipidemia. The mice in HFD+Emo group were intragastrically administered with emodin at the doses of 40 and 80 mg/kg/day respectively for consecutive 6 weeks. The mice in HFD+CL 316243 group were intraperitoneally injected with 1mg/kg/day of CL 316243 disodium salt for 3 days just before detecting time point. **(A)** Body weight. **(B)** Food intake. **(C)** Lee's index. **(D)** The ratio of scWAT mass/BW. **(E)** The ratio of BAT mass/BW. HFD, high fat diet; Emo, emodin. Data are expressed as mean ± SE, with n = 8. *P < 0.05, **P < 0.01 *vs.* HFD group.

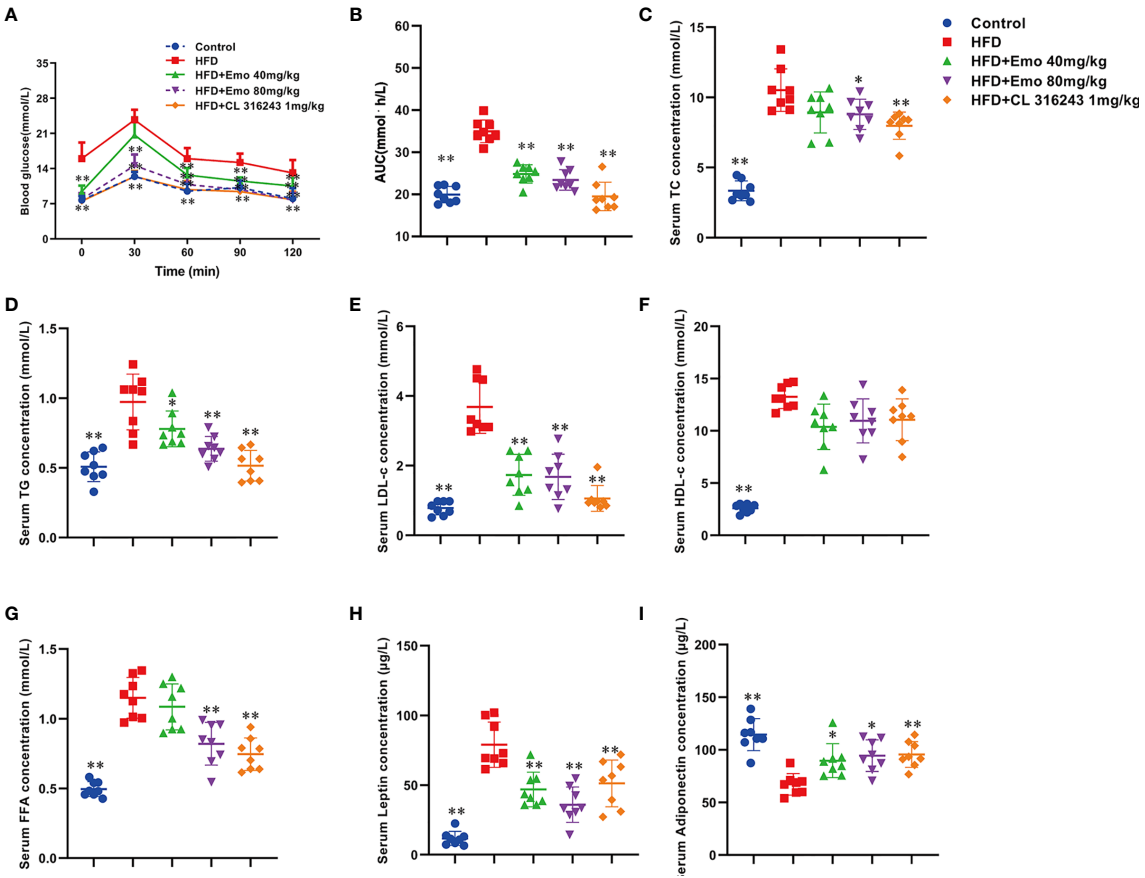

FIGURE 2 | Effects of emodin on blood glucose and lipids in HFD mice. **(A)** Oral glucose tolerance test (OGTT). The mice were fasted for 12 h, and then 2 g/kg glucose was given oral gavage. Glucose levels were tested before (0) and after fed glucose at 30, 60, 90, and 120 min. **(B)** Quantification of AUC from the OGTT. **(C–F)** Serum TC, TG, LDL-c, HDL-c concentration. **(G)** Serum free fatty acids concentration. **(H)** Serum leptin concentration. **(I)** Serum adiponectin concentration. HFD, high fat diet; Emo, emodin. Data are expressed as mean ± SE, with n = 8. *$P < 0.05$, **$P < 0.01$ *vs.* HFD group.

could significantly increase the serum adiponectin levels in HFD mice (by 28.6% and 42.9%, respectively), when compared with HFD mice (P <0.01 or P <0.05) (**Figure 2I**).

Emodin Induces Browning of scWAT in Mice Fed With HFD

We analyzed the morphology of scWAT and the expression of thermogenic protein UCP1 and mitochondrial membrane protein prohibitin in scWAT (**Figure 3A**). When compared with the control mice, the diameter of fat cells in HFD mice increased and the number of cells per unit area decreased. When compared with HFD mice, the adipocytes of the mice in the emodin (40 mg/kg, 80 mg/kg) groups are small and tightly arranged, with obvious nuclei. As an important thermogenic protein, UCP1 is specifically expressed in BAT (6, 29). Prohibitin, mainly located in the inner membrane of mitochondria, plays an important role in maintaining mitochondrial morphology, function and regulating energy metabolism (30). Therefore, we measured the expression of UCP1 and prohibitin protein in scWAT (**Figure 3B**). The expression of UCP1 and prohibitin protein in scWAT of emodin 80 mg/kg-treated group was significantly increased (P <0.01), Compared with HFD mice. We also evaluated the mRNA expression of beige adipocyte marker genes, such as *Cd137*, Transmembrane protein 26 (*Tmem26*) and *Tbx1*. As expected, the expression of several beige adipocyte marker genes, including *Cd137*, *Tmem26* and *Tbx1*, was significantly upregulated in scWAT after emodin (80 mg/kg) and CL316243 (1 mg/kg) treatment (**Figure 3C**).

In order to confirm whether emodin can induce the browning of scWAT, we measured thermogenic protein and fatty acid transporter (**Figure 3D**). The expression of UCP1, prohibitin, CD36, FATP4 and PPARα protein in scWAT of emodin (80 mg/kg) and CL316243 (1 mg/kg) treatment group increased significantly, when compared with HFD mice (P <0.05 or P <0.01) (**Figures 3E–I**). These results suggested that emodin could induce the browning of scWAT in HFD mice.

Emodin Activates Brown Adipose Tissue in Mice Fed With HFD

We also analyzed the morphology of BAT and the expression of thermogenic protein UCP1 and mitochondrial membrane

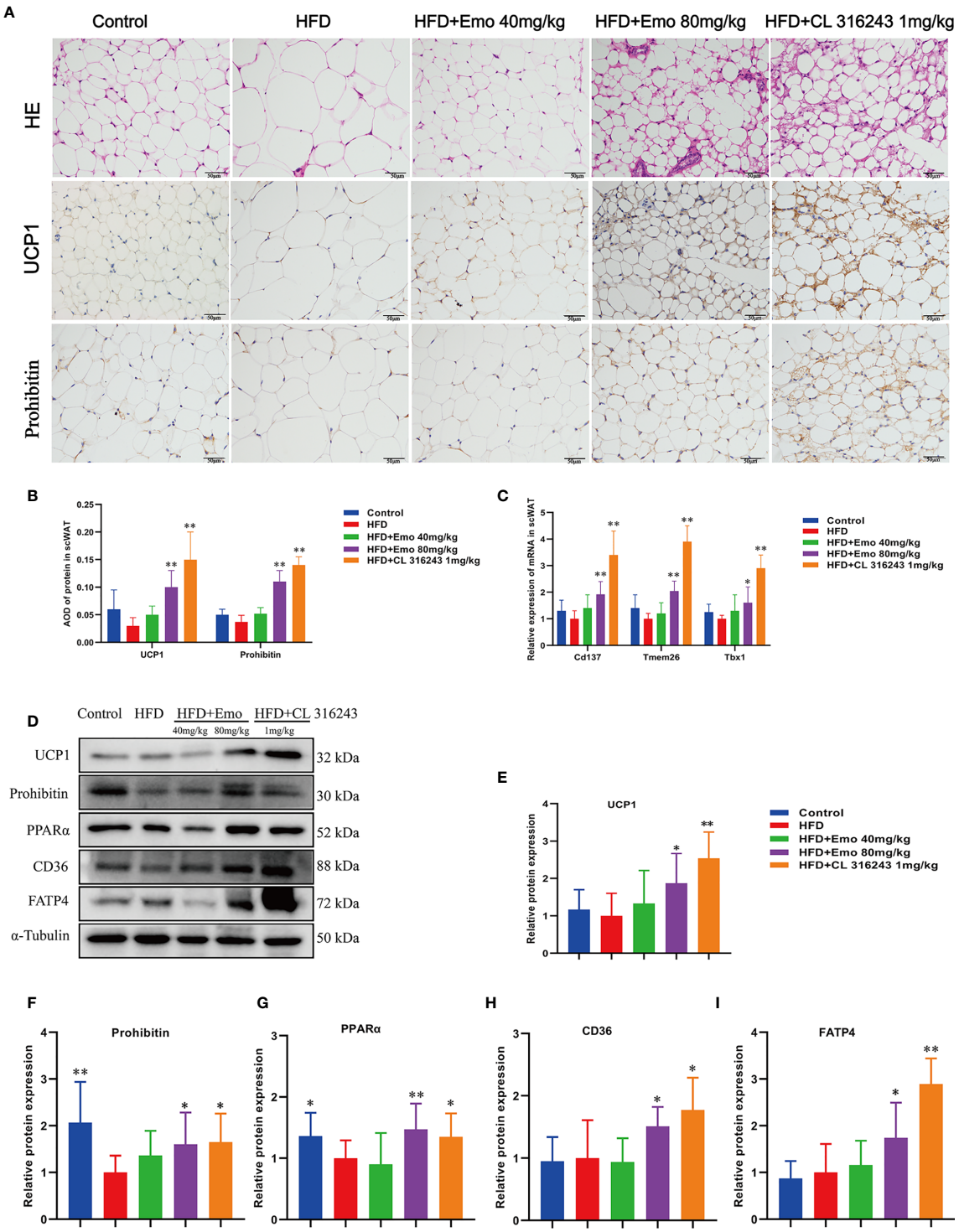

FIGURE 3 | Effects of emodin on the morphology and function of scWAT in HFD mice. **(A)** H&E and immunohistochemical staining of scWAT. **(B)** Relative expression of UCP1 and Prohibitin protein in scWAT. **(C)** Relative expression of *Cd137*, *Tmem26* and *Tbx1* mRNA in scWAT. **(D)** Protein expression of UCP1, prohibitin, PPAR α, CD36 and FATP4 in scWAT using western blotting. **(E)** Protein expression of UCP1. **(F)** Protein expression of prohibitin. **(G)** Protein expression of PPAR α. **(H)** Protein expression of CD36. **(I)** Protein expression of FATP4. HFD, high fat diet; Emo, emodin. Data are expressed as mean ± SE. $^{*}P < 0.05$, $^{**}P < 0.01$ *vs.* HFD group.

protein prohibitin in BAT (**Figures 4A–C**). When compared with control mice, the diameter of fat cells in BAT of HFD mice was significantly increased, the number of cells per unit area decreased, and the number of white fat cells increased. This indicates that long-term HFD feeding results in so-called 'whitening' of BAT. When compared with HFD mice, the adipocytes of the mice in the emodin (40 mg/kg, 80 mg/kg) groups are small and tightly arranged, with large and obvious nuclei. We also measured the expression of UCP1 and prolibitin protein in BAT. The expression of UCP1 and prohibitin protein in BAT of emodin and CL316243-treated group was significantly increased (P <0.05 or P <0.01), when compared with HFD mice.

To confirm that emodin can activate BAT of HFD mice, we measured thermogenic protein and fatty acid transporter (**Figure 4D**). The expression of UCP1, prohibitin, CD36, FATP4 and PPARα protein in BAT of emodin and CL316243-treated group increased significantly, when compared with HFD mice (P <0.05 or P <0.01) (**Figures 4E–I**). These results suggested that emodin could activate BAT in HFD mice.

Phospholipid Metabolism Is Altered in scWAT With Emodin Treatment

Based on the above experimental results, we analyzed scWAT by targeted metabolomics. We selected the biomarkers that have changed and created a heat map (**Figures 5A–E**). The lipidomics data show that emodin treatment can perturb the lipidomics profile in HFD mice, and several phospholipid species (e.g. Cer, LPC, LPC-O, and PE-O) are remarkably increased in scWAT, indicating a remodeling of phospholipids after emodin 80 mg/kg treatment. Specifically, when compared with HFD mice, concentration of Cer (34:2), LPC (18:2), LPC-(O-20:2), PC (O-40:7), PE (O-36:3), PE (O-38:6), PE (O-40:6), and SM (41:0) was significantly up-regulated in emodin-treated group. Otherwise, levels of PC (O-38:6), PE (O-40:4), PE (O-40:5) were significantly reduced in emodin-treated group, when compared with HFD mice.

Phospholipid Metabolism Is Altered in BAT With Emodin Treatment

In addition, we also analyzed BAT by targeted metabolomics. We selected the biomarkers that have changed and created a heat map (**Figures 6A–E**). In BAT, the lipidomics indicated a significant reduction of PEs and PCs in BAT of HFD mice. And emodin treatment caused a significant increase of PEs and PCs in BAT, when compared with HFD mice. The increase in total PC was driven by significant increase of PC (30:0), PC (32:1), PC (32:2), PC (33:4) and PC (38:0) species, as well as species of LPC [e.g. LPC (20:0), LPC (20:1), LPC (22:0), LPC (22:1), LPC (24:0), LPC (24:1)] with emodin treatment. In addition, when compared with the control mice, the ratio of PC/PE was significantly increased in HFD-induced mice (P <0.05 or P <0.01). And emodin at the doses of 40 and 80 mg/kg and CL 316243 significantly decreased the ratio of PC/PE compared with HFD-induced mice.

DISCUSSION

Emodin ameliorates adiposity and improves whole-body metabolic balance in obese mice. In this study, we demonstrated that emodin could decrease the body weight and food intake in high fat diet induced obese mice, also it could improve the glucose tolerance and reduce the blood lipids, which was consistent with the results of previous studies *in vivo* (22, 31, 32). The regulating of white adipose tissue and brown adipose tissue acts a critical role in combating obesity and metabolic disease. As a thermogenic tissue, BAT is innervated by both sympathetic and sensory nerves. The activity and metabolism of BAT could be influenced by cold exposure and exercise (33), as well as some natural product extracts or compounds, such as rose hip supplement (34), black raspberry (35), green tea extract (36), genistein (37), pentamethylquercetin (38), and etc. Here, we first proved that emodin could promote browning in scWAT. The white adipose tissue mass was decreased after emodin treatment. After treatment of emodin, more multilocular lipid droplets were found in scWAT, the mRNA expression of browning markers including *Cd137*, *Tmem26* and *Tbx1* was increased in scWAT, and the protein expression of browning markers including UCP1 and prohibitin was increased in scWAT of obese mice. Meanwhile, the protein expression of UCP1, prohibitin, PPARα was increased in BAT of obese mice after emodin treatment. PPAR α is the key factor of BAT thermogenesis, which can regulate lipid catabolism and thermogenic gene expression in coordination with *Pgc-1α* and *Prdm16* (39). PPAR α can enhance the expression of PGC-1α and UCP-1 by increasing the activity of erythropoietin (EPO). PPAR α also plays a coordinating role with SIRT1 activated by EPO and jointly regulates the level of NAD^+ to heighten the metabolic activity (40). The mitochondria are involved in the metabolic control of brown adipocytes. Mitochondrial function is related to the endocrine function of adipocytes. In addition, brown adipocytes rely on mitochondria to maintain intracellular metabolism. Located in mitochondrial inner membrane, prohibitin plays a critical role in maintaining the shape and function of mitochondria and regulating energy metabolism (30, 41). The results of western blotting demonstrated that emodin increased the protein expression of PPAR α and prohibtin of scWAT and BAT in obese mice. As a fatty acid translocase, CD36 acts a pivotal part in the uptake and transport of long-chain fatty acids (LCFA) in heart and adipose tissues (42, 43). It was found that cold exposure drastically accelerated plasma clearance of triglycerides as a result of increased uptake into BAT, a process crucially dependent on local LPL activity and transmembrane receptor CD36 (44). Fatty acid transporter 4 (FATP 4) is a member of the fatty acid transport proteins (FATPs), which plays a significant role in the transport of long-chain fatty acids with more effectively compared with FATP1. It was found that FAT/CD36 and FATP4 were the most effective fatty acid transporters (45, 46). In this study, emodin accelerated the transport and consumption of fatty acids and improved the disorder of lipid metabolism by increasing the expression of CD36 and FATP4 protein in both scWAT and BAT of HFD-induced mice.

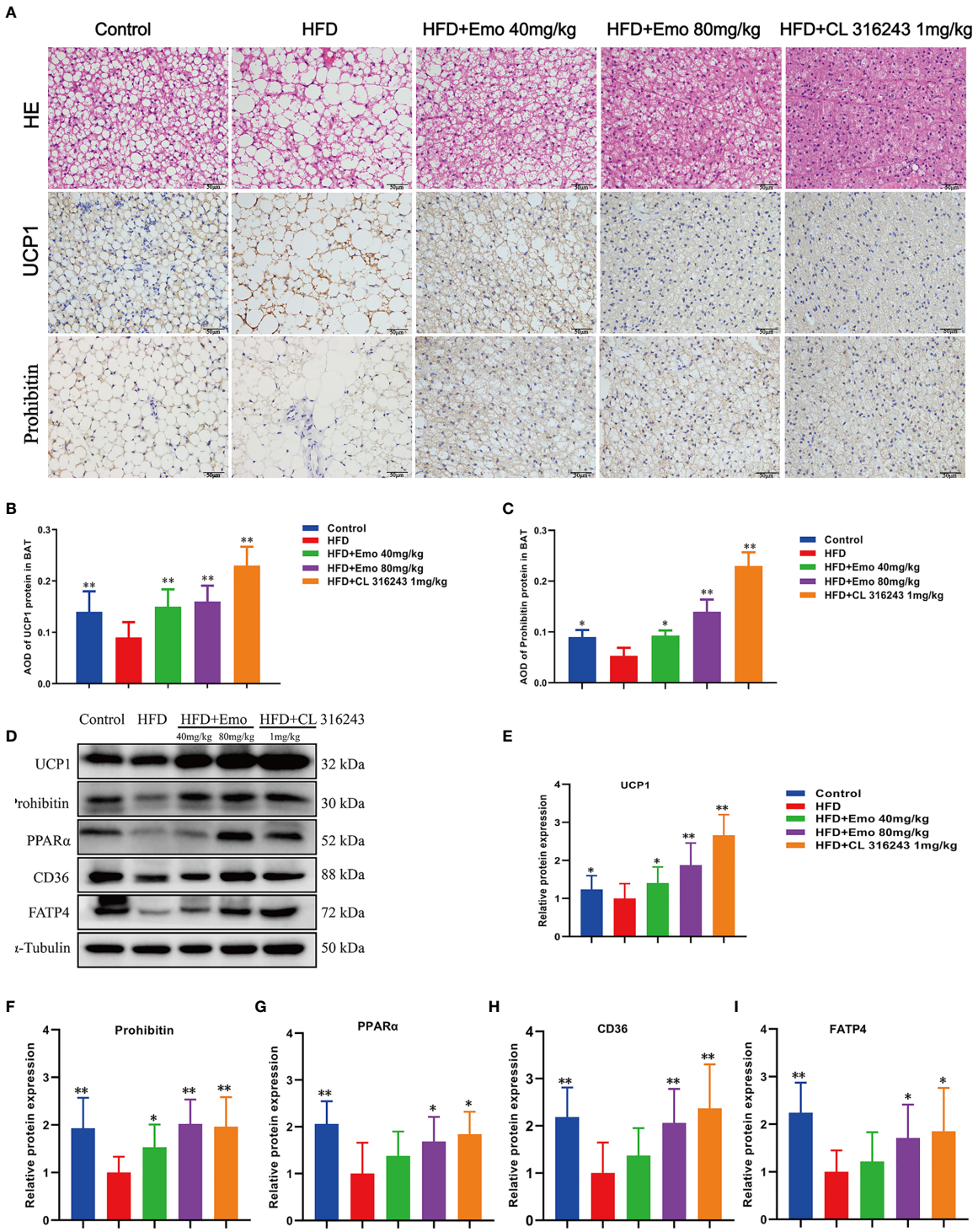

FIGURE 4 | Effects of emodin on the morphology and function of BAT in HFD mice. **(A)** H&E and immunohistochemical staining of BAT. **(B)** Relative expression of UCP1 in BAT. **(C)** Relative expression of prohibitin in BAT. **(D)** Protein expression of UCP1, prohibitin, PPAR α, CD36 and FATP4 in BAT using western blotting. **(E)** Protein expression of UCP1. **(F)** Protein expression of prohibitin. **(G)** Protein expression of PPAR α. **(H)** Protein expression of CD36. **(I)** Protein expression of FATP4. HFD, high fat diet; Emo, emodin. Data are expressed as mean ± SE. $^{*}P < 0.05$, $^{**}P < 0.01$ *vs.* HFD group.

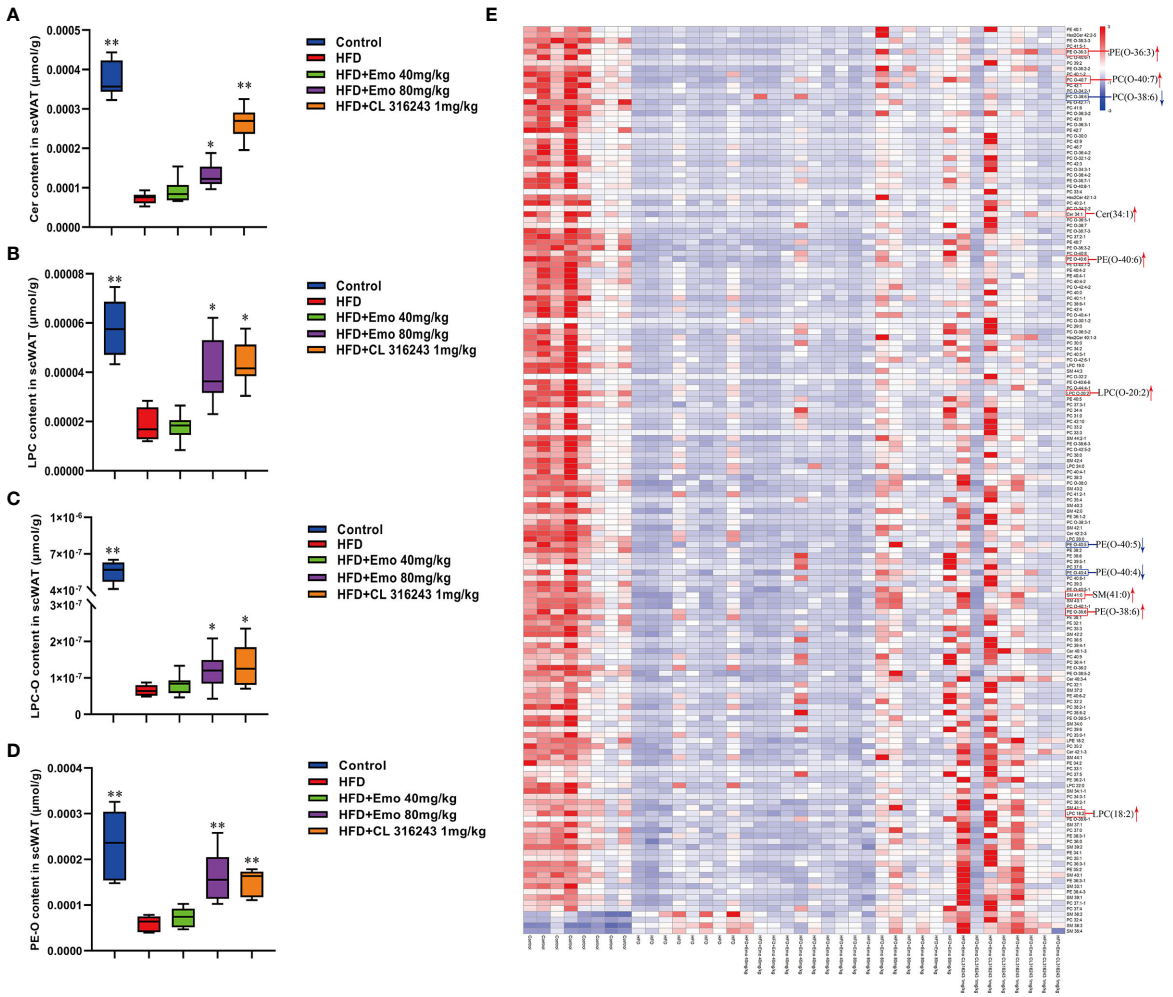

FIGURE 5 | Effects of emodin on the lipid metabolites in scWAT of HFD mice. **(A)** The content of Cer in scWAT. **(B)** The content of LPC in scWAT. **(C)** The content of LPC-O in scWAT. **(D)** The content of PE-O in scWAT. **(E)** Heat map. Only metabolites with VIP >1 and P <0.05 were selected in heat map, and different shades of color present the concentration (red, white and blue presented the high, normal and low concentration). The red up arrow indicates up regulation or promotion, and the blue down arrow indicates down regulation or inhibition. HFD, high fat diet; Emo, emodin; PC, phosphatidylcholine; PE, phosphatidylethanolamine; Cer, ceramides; LPC, lyso-phosphatidylcholine. Data are expressed as mean ± SE. *P < 0.05, **P < 0.01 *vs.* HFD group.

White and brown adipocytes exhibit different lipid metabolic signature, which reflect their distinct organelle composition and cell functions. The neutral lipids in the lipid droplets core are surrounded by a monolayer of phospholipids (47). PCs, PEs and CLs make up 89% of the phospholipids in BAT, which are increased in response to cold exposure and exercise (48). It was confirmed that regulation and metabolism of PCs, PSs and PEs prevented inflammation of adipose tissue, hyperlipidemia and obesity (49). Exercise can increase specific molecular species of PCs and PEs in brown adipocytes. It has been reported that after exercise, the increase in total PC was driven by the significant increase of the highly abundant PC (36:2) species, as well as increases in numerous species of PC and PC-O. However, there was no overall change in abundance of PE after exercise in BAT (1). Our recent study manifested that the lipidomic profile of adipocytes was remolded with high fat diets, and emodin treatment could perturb the profile and reverse some small lipid metabolites of HFD mice.

Furthermore, the relative abundance of PCs and PEs on the surface of LDs is important for their dynamics (50). An increase in the relative amount of PEs on the surface of lipid droplets can promote fusion of smaller droplets into larger ones (51). Inhibition of PCs biosynthesis can promote TG storage increases the size of the lipid droplets presumably (52, 53). Either abnormally high, or abnormally low cellular PC : PE molar ratios can influence energy metabolism in various organelles (50). It has been shown that both PC amount and PC : PE molar ratio tend to increase, and palmitate- and stearate-containing LPC species were upregulated in 16-week-old Lep$^{ob/ob}$ adipose tissue macrophage, which related to WAT inflammation and contribute to the development of insulin resistance in obesity (54). It has been proved the different composition of

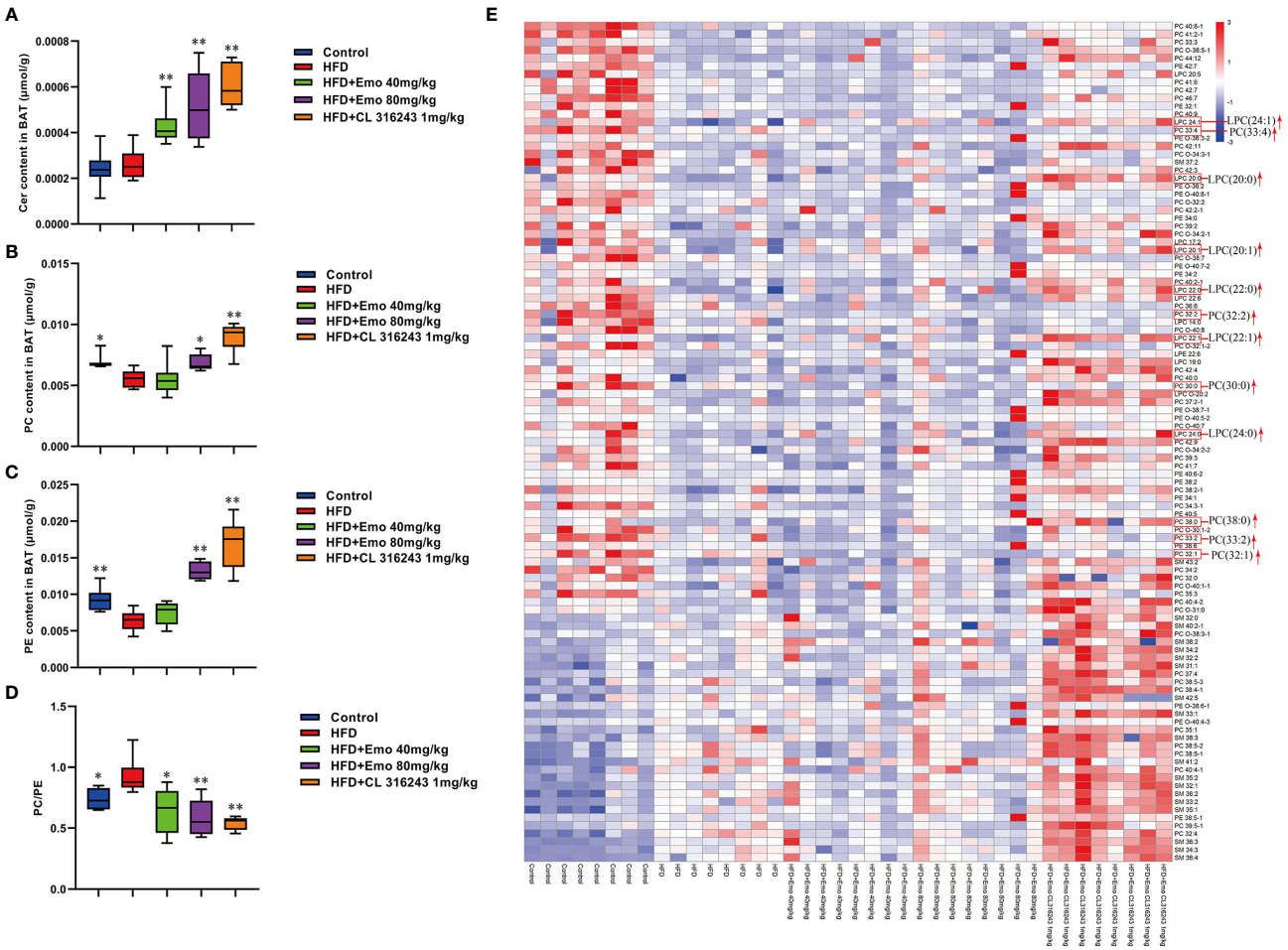

FIGURE 6 | Effects of emodin on the lipid metabolites in BAT of HFD mice. **(A)** The content of Cer in BAT. **(B)** The content of PC in BAT. **(C)** The content of PE in BAT. **(D)** The ratio of PC : PE in BAT. **(E)** Heat map. Only metabolites with VIP >1 and P <0.05 were selected in heat map, and different shades of color present the concentration (red, white and blue presented the high, normal and low concentration). The red up arrow indicates up regulation or promotion. HFD, high fat diet; Emo, emodin; PC, Phosphatidylcholine; PE, phosphatidylethanolamine; Cer, ceramides. Data are expressed as mean ± SE. *P < 0.05, **P < 0.01 *vs.* HFD group.

phospholipids in white and brown adipocyte, and thermogenic adipocytes possess higher abundance of PCs and PEs, with longer (C >36) and more polyunsaturated species (55). Our results also indicated that the ratio of PC : PE was significantly increased in brown adipose tissue but not scWAT in HFD-induced mice compared with control mice. Interestingly, emodin 40 and 80 mg/kg treatment and CL 316243 could significantly increase abundance of PCs and PEs, and decrease the PC : PE ratio in BAT of obesity mice. Specifically, emodin significantly up-regulated levels of Cer (34:2), LPC (18:2), LPC-(O-20:2), PC (O-40:7), PE (O-36:3), PE (O-38:6), PE (O-40:6), and SM (41:0), and down-regulated PC (O-38:6), PE (O-40:4), PE (O-40:5) in scWAT compared with HFD mice. And in BAT, the remarkable increase in total PCs was driven by significant increase of PC (30:0), PC (32:1), PC (32:2), PC (33:4) and PC (38:0) species with emodin treatment. In addition, emodin significantly increased species of LPC (e.g. LPC (20:0), LPC (20:1), LPC (22:0), LPC (22:1), LPC (24:0), when compared with HFD mice.

CONCLUSION

These results indicated that emodin could ameliorate adiposity and improve metabolic disorders in obese mice. Also, emodin could promote browning in scWAT and activate the BAT activities. In addition, emodin treatment-induced changes to the scWAT and BAT lipidome were highly specific to certain molecular lipid species, indicating that changes in tissue lipid content reflects selective remodeling in scWAT and BAT of both glycerophospholipids and sphingolipids in response to emodin treatment.

DATA AVAILABILITY STATEMENT

The raw data supporting the conclusions of this article will be made available by the authors, without undue reservation.

ETHICS STATEMENT

All the animal studies were in accordance with ethics standards of the Animal Care and Welfare Committee of Beijing University of Chinese Medicine [Certificate No. BUCM-04-2018070603-3015].

AUTHOR CONTRIBUTIONS

JS and SD designed experiments. LC, SZ, FS, YN, ZH, RH, and SD performed experiments. FS and LC performed UPLCQ-MS/MS analysis. LC and SD performed statistical analysis. LC wrote the paper. All authors contributed to the article and approved the submitted version.

FUNDING

This paper was supported by the National Natural Science Foundation of China (Grant No. 81503287, 81430094), Natural Science Foundation of Beijing Municipality (Grant No. 7144222, 7174312), and Doctoral Program Foundation of Institutions of Higher Education of China (Grant No. 20130013120002).

REFERENCES

1. May FJ, Baer LA, Lehnig AC, So K, Chen EY, Gao F, et al. Lipidomic Adaptations in White and Brown Adipose Tissue in Response to Exercise Demonstrate Molecular Species-Specific Remodeling. *Cell Rep* (2017) 18:1558–72. doi: 10.1016/j.celrep.2017.01.038
2. Tran TT, Kahn CR. Transplantation of Adipose Tissue and Stem Cells: Role in Metabolism and Disease. *Nat Rev Endocrinol* (2010) 6:195–213. doi: 10.1038/nrendo.2010.20
3. Wang C, Li JX, Xue HF, Li Y, Huang JF, Mai JZ, et al. Type 2 Diabetes Mellitus Incidence in Chinese: Contributions of Overweight and Obesity. *Diabetes Res Clin Pract* (2015) 107:424–32. doi: 10.1016/j.diabres.2014.09.059
4. Nicholls DG, Locke RM. Thermogenic Mechanisms in Brown Fat. *Physioll Rev* (1984) 64:1–64. doi: 10.1152/physrev.1984.64.1.1
5. Fedorenko A, Lishko PV, Kirichok Y. Mechanism of Fatty-Acid-Dependent UCP1 Uncoupling in Brown Fat Mitochondria. *Cell* (2012) 151:400–13. doi: 10.1016/j.cell.2012.09.010
6. Carpentier AC, Blondin DP, Virtanen KA, Richard D, Haman F, Turcotte ÉE. Brown Adipose Tissue Energy Metabolism in Humans. *Front Endocrinol* (2018) 9:447. doi: 10.3389/fendo.2018.00447
7. De Matteis R, Lucertini F, Guescini M, Polidori E, Zeppa S, Stocchi V, et al. Exercise as a New Physiological Stimulus for Brown Adipose Tissue Activity. *Nutr Metab Cardiovasc Dis* (2013) 23:582–90. doi: 10.1016/j.numecd.2012.01.013
8. Ghorbani M, Claus TH, Himmshagen J. Hypertrophy of Brown Adipocytes in Brown and White Adipose Tissues and Reversal of Diet-Induced Obesity in Rats Treated With a beta3-adrenoceptor Agonist. *Biochem Pharmacol* (1997) 54:121–31. doi: 10.1016/S0006-2952(97)00162-7
9. Cypess AM, Lehman S, Williams G, Tal I, Rodman D, Goldfine AB, et al. Identification and Importance of Brown Adipose Tissue in Adult Humans. *N Engl J Med* (2009) 360:1509–17. doi: 10.1056/NEJMoa0810780
10. Loyd C, Obici S. Brown Fat Fuel Use and Regulation of Energy Homeostasis. *Curr Opin Clin Nutr Metab Care* (2014) 17:368–72. doi: 10.1097/MCO.0000000000000063
11. Schrauwen P, van Marken Lichtenbelt WD, Spiegelman BM. The Future of Brown Adipose Tissues in the Treatment of Type 2 Diabetes. *Diabetologia* (2015) 58:1704–07. doi: 10.1007/s00125-015-3611-y
12. Kaisanlahti A, Glumoff T. Browning of White Fat: Agents and Implications for Beige Adipose Tissue to Type 2 Diabetes. *J Physiol Biochem* (2019) 75:1–10. doi: 10.1007/s13105-018-0658-5
13. Dong X, Fu J, Yin X, Cao S, Li X, Lin L, et al. Emodin: A Review of its Pharmacology, Toxicity and Pharmacokinetics. *Phytother Res* (2016) 30:1207–18. doi: 10.1002/ptr.5631
14. Heo SK, Yun HJ, Park WH, Park SD. Emodin Inhibits TNF-α-Induced Human Aortic Smooth-Muscle Cell Proliferation Via Caspase and Mitochondrial-Dependent Apoptosis. *J Cell Biochem* (2008) 105:70–80. doi: 10.1002/jcb.21805
15. Subramaniam A, Shanmugam MK, Ong TH, Li F, Perumal E, Chen L, et al. Emodin Inhibits Growth and Induces Apoptosis in an Orthotopic Hepatocellular Carcinoma Model by Blocking Activation of STAT3. *Br J Pharmacol* (2013) 170:807–21. doi: 10.1111/bph.12302
16. Zhu XF, Zeng K, Qiu Y, Yan FH, Lin CZ. Therapeutic Effect of Emodin on Collagen-Induced Arthritis in Mice. *Inflammation* (2013) 36:1253–9. doi: 10.1007/s10753-013-9663-6
17. Izhaki I. Emodin-a Secondary Metabolite With Multiple Ecological Functions in Higher Plants. *New Phytol* (2002) 155:205–17. doi: 10.1046/j.1469-8137.2002.00459.x
18. Hwang SY, Heo K, Kim JS, Im JW, Lee SM, Cho M, et al. Emodin Attenuates Radio-Resistance Induced by Hypoxia in HepG2 Cells Via the Enhancement of PARP1 Cleavage and Inhibition of JMJD2B. *Oncol Rep* (2015) 33:1691–8. doi: 10.3892/or.2015.3744
19. Tzeng TF, Lu HJ, Liou SS, Chang CJ, Liu IM. Emodin Protects Against High-Fat Diet-Induced Obesity Via Regulation of AMP-activated Protein Kinase Pathways in White Adipose Tissue. *Planta Med* (2012) 78:943–50. doi: 10.1055/s-0031-1298626
20. Song P, Kim JH, Ghim J, Yoon JH, Lee A, Kwon Y, et al. Emodin Regulates Glucose Utilization by Activating AMP-activated Protein Kinase. *J Biol Chem* (2013) 288:5732–42. doi: 10.1074/jbc.M112.441477
21. Yang F, Yuan PW, Hao YQ, Zheng ML. Emodin Enhances Osteogenesis and Inhibits Adipogenesis. *BMC Complement Altern Med* (2014) 14:74. doi: 10.1186/1472-6882-14-74
22. Wang YJ, Huang SL, Feng Y, Ning MM, Leng Y. Emodin, an 11β-Hydroxysteroid Dehydrogenase Type 1 Inhibitor, Regulates Adipocyte Function In Vitro and Exerts Anti-Diabetic Effect in Ob/Ob Mice. *Acta Pharmacol Sin* (2012) 33:1195–203. doi: 10.1038/aps.2012.87
23. Cheng L, Dong SF, Yuan YY, Ma D, Song JY, Sun JN, et al. Effect of Emodin on Adipose Browning in ApoE Knockout Mice. *Chin J Comp Med* (2018) 28:8–14. doi: 10.3969/j.issn.1671-7856
24. Bunyan J, Murrell EA, Shah PP. The Induction of Obesity in Rodents by Means of Monosodium Glutamate. *Br J Nutr* (1976) 35:25–39. doi: 10.1079/BJN19760005
25. Bernardis LL, Patterson BD. Correlation Between Lee Index' and Carcass Fat Content in Weanling and Adult Female Rats With Hypothalamic Lesions. *J Endocrinol* (1968) 40:527–28. doi: 10.1677/joe.0.0400527
26. Okla M, Kim J, Koehler K, Chung S. Dietary Factors Promoting Brown and Beige Fat Development and Thermogenesis. *Adv Nutr* (2017) 8:473–83. doi: 10.3945/an.116.014332
27. Dodd GT, Decherf S, Loh K, Simonds SE, Wiede F, Balland E, et al. Leptin and Insulin Act on POMC Neurons to Promote the Browning of White Fat. *Cell* (2015) 160:88–104. doi: 10.1016/j.cell.2014.12.022
28. Ziemke F, Mantzoros CS. Adiponectin in Insulin Resistance: Lessons From Translational Research. *Am J Clin Nutr* (2010) 91:258S–61S. doi: 10.3945/ajcn.2009.28449C
29. Lowell BB, Spiegelman BM. Towards a Molecular Understanding of Adaptive Thermogenesis. *Nature* (2000) 404:652–60. doi: 10.1038/35007527
30. Artal-Sanz M, Tavernarakis N. Prohibitin and Mitochondrial Biology. *Trends Endocrinol Metab* (2009) 20:394–401. doi: 10.1016/j.tem.2009.04.004
31. Feng Y, Huang SL, Dou W, Zhang S, Chen JH, Shen Y, et al. Emodin, a Natural Product, Selectively Inhibits 11b-Hydroxysteroid Dehydrogenase Type 1 and Ameliorates Metabolic Disorder in Diet-Induced Obese Mice. *Br J Pharmacol* (2010) 161:113–26. doi: 10.1111/j.1476-5381.2010.00826.x
32. Li J, Ding L, Song B, Xiao X, Qi M, Yang QL, et al. Emodin Improves Lipid and Glucose Metabolism in High Fat Diet-Induced Obese Mice Through

Regulating SREBP Pathway. *Eur J Pharmacol* (2016) 770:99–109. doi: 10.1016/j.ejphar.2015.11.045
33. Peres Valgas da Silva C, Hernández-Saavedra D, White JD, Stanford KI. Cold and Exercise: Therapeutic Tools to Activate Brown Adipose Tissue and Combat Obesity. *Biology* (2019) 8:9. doi: 10.3390/biology8010009
34. Cavalera M, Axling U, Berger K, Holm C. Rose Hip Supplementation Increases Energy Expenditure and Induces Browning of White Adipose Tissue. *Nutr Metab* (2016) 13:91. doi: 10.1186/s12986-016-0151-5
35. Park WY, Choe SK, Park J, Um JY. Black Raspberry (Rubus Coreanus Miquel) Promotes Browning of Preadipocytes and Inguinal White Adipose Tissue in Cold-Induced Mice. *Nutrients* (2019) 11:2164. doi: 10.3390/nu11092164
36. Chen LH, Chien YW, Liang CT, Chan CH, Fan MH, Huang HY. Green Tea Extract Induces Genes Related to Browning of White Adipose Tissue and Limits Weight-Gain in High Energy Diet-Fed Rat. *Food Nutr Res* (2017) 61:1347480. doi: 10.1080/16546628.2017.1347480
37. Zhou L, Xiao X, Zhang Q, Zheng J, Li M, Deng MQ. A Possible Mechanism: Genistein Improves Metabolism and Induces White Fat Browning Through Modulating Hypothalamic Expression of Ucn3, Depp, and Stc1. *Front Endocrinol* (2019) 10:478. doi: 10.3389/fendo.2019.00478
38. Han Y, Wu JZ, Shen JZ, Chen L, He T, Jin MW, et al. Pentamethylquercetin Induces Adipose Browning and Exerts Beneficial Effects in 3T3-L1 Adipocytes and High-Fat Diet-Fed Mice. *Sci Rep* (2017) 7:1123. doi: 10.1038/s41598-017-01206-4
39. Hondares E, Rosell M, Díaz-Delfín J, Olmos Y, Monsalve M, Iglesias R, et al. Peroxisome Proliferator-Activated Receptor α (Pparα) Induces Pparγ Coactivator 1α (Pgc-1α) Gene Expression and Contributes to Thermogenic Activation of Brown Fat: Involvement of PRDM16. *J Biol Chem* (2011) 286:43112–22. doi: 10.1074/jbc.M111.252775
40. Wang L, Teng RF, Di LJ, Rogers H, Wu H, Kopp JB, et al. Pparα and Sirt1 Mediate Erythropoietin Action in Increasing Metabolic Activity and Browning of White Adipocytes to Protect Against Obesity and Metabolic Disorders. *Diabetes* (2013) 62:4122–31. doi: 10.2337/db13-0518
41. Vessal M, Mishra S, Moulik S, Murphy LJ. Prohibitin Attenuates Insulin-Stimulated Glucose and Fatty Acid Oxidation in Adipose Tissue by Inhibition of Pyruvate Carboxylase. *FEBS J* (2006) 273:568–76. doi: 10.1111/j.1742-4658.2005.05090.x
42. Habets DD, Coumans WA, Voshol PJ, Boer MA, Febbraio M, Bonen A, et al. AMPK-Mediated Increase in Myocardial Long-Chain Fatty Acid Uptake Critically Depends on Sarcolemmal CD36. *Biochem Biophys Res Commun* (2007) 355:204–10. doi: 10.1016/j.bbrc.2007.01.141
43. Wan Z, Matravadia S, Holloway GP, Wright DC. FAT/CD36 Regulates PEPCK Expression in Adipose Tissue. *Am J Physiol Cell Physiol* (2013) 304:C478–84. doi: 10.1152/ajpcell.00372.2012
44. Bartelt A, Bruns OT, Reimer R, Hohenberg H, Ittrich H, Peldschus K, et al. Brown Adipose Tissue Activity Controls Triglyceride Clearance. *Nat Med* (2011) 17:200–5. doi: 10.1038/nm.2297
45. Nickerson JG, Alkhateeb H, Benton CR, Lally J, Nickerson J, Han XX, et al. Greater Transport Efficiencies of the Membrane Fatty Acid Transporters FAT/CD36 and FATP4 Compared With FABPpm and FATP1 and Differential Effects on Fatty Acid Esterification and Oxidation in Rat Skeletal Muscle. *J Biol Chem* (2009) 284:16522–30. doi: 10.1074/jbc.M109.004788
46. Stahl A, Gimeno RE, Tartaglia LA, Lodish HF. Fatty Acid Transport Proteins: A Current View of a Growing Family. *Trends Endocrinol Metab* (2001) 12:266–73. doi: 10.1016/S1043-2760(01)00427-1
47. Pol A, Steven PG, Parton RG. Review: Biogenesis of the Multifunctional Lipid Droplet: Lipids, Proteins, and Sites. *J Cell Biol* (2014) 204:635–46. doi: 10.1083/jcb.201311051
48. Senault C, Yazbeck J, Goubern M, Portet R, Vincent M, Gallay J. Relation Between Membrane Phospholipid Composition, Fluidity and Function in Mitochondria of Rat Brown Adipose Tissue. Effect of Thermal Adaptation and Essential Fatty Acid Deficiency. *Biochim Biophys Acta* (1990) 1023:283–9. doi: 10.1016/0005-2736(90)90424-M
49. Body DR. The Lipid Composition of Adipose Tissue. *Prog Lipid Res* (1988) 27:39–60. doi: 10.1016/0163-7827(88)90004-5
50. van der Veen JN, Kennelly JP, Wan S, Vance JE, Vance DE, Jacobs RL. The Critical Role of Phosphatidylcholine and Phosphatidylethanolamine Metabolism in Health and Disease. *Biochim Biophys Acta Biomembr* (2017) 1859:1558–72. doi: 10.1016/j.bbamem.2017.04.006
51. Hafez IM, Cullis PR. Roles of Lipid Polymorphism in Intracellular Delivery. *Adv Drug Delivery Rev* (2001) 47:139–48. doi: 10.1016/S0169-409X(01)00103-X
52. Guo Y, Walther TC, Rao M, Stuurman N, Goshima G, Terayama K, et al. Functional Genomic Screen Reveals Genes Involved in Lipid-Droplet Formation and Utilization. *Nature* (2008) 453:657–61. doi: 10.1038/nature06928
53. Aitchison AJ, Arsenault DJ, Ridgway ND. Nuclear-Localized CTP: Phosphocholine Cytidylyltransferase α Regulates Phosphatidylcholine Synthesis Required for Lipid Droplet Biogenesis. *Mol Biol Cell* (2015) 26:2927–38. doi: 10.1091/mbc.E15-03-0159
54. Petkevicius K, Virtue S, Bidault G, Jenkins B, Çubuk C, Morgantini C, et al. Accelerated Phosphatidylcholine Turnover in Macrophages Promotes Adipose Tissue Inflammation in Obesity. *Elife* (2019) 8:e47990. doi: 10.7554/eLife.47990
55. Leiria LO, Tseng YH. Lipidomics of Brown and White Adipose Tissue: Implications for Energy Metabolism. *Biochim Biophys Acta Mol Cell Biol Lipids* (2020) 1865:158788. doi: 10.1016/j.bbalip.2020.158788

Conflict of Interest: The authors declare that the research was conducted in the absence of any commercial or financial relationships that could be construed as a potential conflict of interest.

frontiers in Endocrinology

REVIEW
published: 25 May 2021
doi: 10.3389/fendo.2021.652246

The Role of Brown Adipose Tissue Dysfunction in the Development of Cardiovascular Disease

Hong-Jin Chen[1,2], *Ting Meng*[3], *Ping-Jin Gao*[1,2] *and Cheng-Chao Ruan*[1,2,3*]

[1] Department of Cardiovascular Medicine, State Key Laboratory of Medical Genomics, Shanghai Key Laboratory of Hypertension, Department of Hypertension, Ruijin Hospital, Shanghai, China, [2] Shanghai Institute of Hypertension, Shanghai Jiao Tong University School of Medicine, Shanghai, China, [3] Shanghai Key Laboratory of Bioactive Small Molecules, Department of Physiology and Pathophysiology, School of Basic Medical Sciences, Fudan University, Shanghai, China

Brown adipose tissue (BAT), consisted of brown adipocytes and stromal vascular fraction, which includes endothelial cells, lymphocytes, fibroblasts and stem cells, plays a vital role in regulating cardiovascular health and diseases. As a thermogenic organ, BAT can influence body through strengthening energy expenditure by promoting glucose and lipid metabolism. In addition, BAT is also an endocrine organ which is able to secret adipokines in an autocrine and/or paracrine fashion. BAT plays a protective role in cardiovascular system through attenuating cardiac remodeling and suppressing inflammatory response. In this review, we summarize the advances from the discovery of BAT to the present and provide an overview on the role of BAT dysfunction in cardiovascular diseases.

Keywords: brown adipose tissue, cardiovascular diseases, obesity, adipokines, adipocyte

OPEN ACCESS

Edited by:
Xinran Ma,
East China Normal University, China

Reviewed by:
Rita De Matteis,
University of Urbino Carlo Bo, Italy
Giulia Cantini,
University of Florence, Italy

****Correspondence:***
Cheng-Chao Ruan
ruancc@fudan.edu.cn

Specialty section:
This article was submitted to Cellular Endocrinology, a section of the journal Frontiers in Endocrinology

Received: *12 January 2021*
Accepted: *03 May 2021*
Published: *25 May 2021*

Citation:
Chen H-J, Meng T, Gao P-J and Ruan C-C (2021) The Role of Brown Adipose Tissue Dysfunction in the Development of Cardiovascular Disease. Front. Endocrinol. 12:652246. doi: 10.3389/fendo.2021.652246

INTRODUCTION

Since 2000, the prevalence of obesity has risen sharply around the world. According to the research, a total of 108 million children and 604 million adults had been obese by 2015. Obesity accounted for 2.4 million deaths globally, and more than two thirds of deaths were due to cardiovascular disease (CVD), including hypertension, coronary heart disease and stroke (1). In particular, the accumulation of visceral fat can greatly increase the risk of death from CVD (2). These patients experience systemic changes, especially the change of white adipose tissue (WAT). WAT is a vital organ in energy storage, which can excessively accumulate in obese patients (3). The increase of WAT is the result of both hyperplasia and hypertrophy of adipocytes (4). In addition to WAT, there are two types of adipose tissue: brown adipose tissue (BAT) and beige adipose tissue. BAT merely represents 1–2% of fat, consisting of brown adipocytes and stromal vascular fraction (SVF), but it is vital in maintaining homeostasis. BAT has a crucial capacity for non-shivering thermogenesis in mammals, which is essential for survival in cold environment and consumption of excessive energy. Recently, research has found that BAT is not only significant in maintaining cardiovascular stability, but also recognized as a novel target to deal with obesity and other metabolic diseases, which attracts more and more attention. In this article, we review the development of BAT in animal models and human, discussing its relevance to cardiovascular damage.

DISCOVERY AND LOCATION OF BAT

Early in 1551, BAT was first discovered in the scapula of a groundhog by Swiss naturalist Konrad Gessner, which was thought to be a gland associated with hibernation. It was not until twentieth century that BAT was considered as a mature tissue with certain component. Later, through necropsy studies, Heaton found BAT mainly located in (1) cervical/axillary (2), perirenal/adrenal, and (3) around blood vessels. In addition, BAT was also found in the scapula of infants, which was the major location in rodents (5). In infants, BAT accounts for about 2–5% of body weight, while in adults, it only accounts for 0.05–0.1%. The amount of BAT will decline with age, but it remains in specific areas of human body all the time. There are some researches showing that individuals exposed to cold will possess more BAT (6–8). However, lacking valid non-intervention means, the studies on BAT *in vivo* have been greatly limited for a long time. It was not until the application of positron emission tomography (PET) in combination with computer tomography (CT) that rekindled people's interest in BAT research. In 2009, three papers published in NEJM confirmed the presence of functional BAT in healthy humans, and the location was consistent with previous autopsy findings (9–11). Virtanen's research found a 15-fold increase in glucose intake in the cervical and supraclavicular regions of five participants exposed to cold (9). Cypess et al. reported that women possessed more BAT than men (10). According to the research, except for classic BAT, some BAT is mixed with WAT rather than presents alone (12). The aforementioned beige adipose tissue is also contained in WAT. Beige adipocytes intersperse within WAT, which can transforming into brown-like adipocytes under the certain stimulation such as cold exposure and beta adrenaline (13, 14). This process is named browning.

THE ORIGIN OF BAT

There was a research that researchers removed 40% BAT from young male rats surgically showing that the total mass, the oxidative and thermogenic capacity of BAT in experimental group was identical to control group after 9 days (15). There may be two possibilities. One is the functional compensation of remaining BAT. The other reason may be the differentiation of preadipocytes. A variety of researches have focused on the origin of BAT over the past decade. It is well-accepted that brown adipocytes share the same lineage with skeletal muscle cells. Pax3 and Pax7-expressing cells are confirmed to be the progenitor cells of skeletal muscle (16). And the function of Pax3 can be replaced by Pax7 mostly (17). Later in 2010, Pax7+ cells at embryonic day 9.5 (E9.5) can give rise to brown adipose tissue. While after E11.5, the Pax7 marked cells reduced drastically in BAT and then disappeared in E12.5 (18). As the embryo develops, Pax7-expressing cells become restricted to muscle-specific fate. Myf5 is also proved to be expressed in skeletal myogenic precursors previously, which plays an important role in myogenic determination (19). Then Myf5-expressing cells were confirmed by Seale et al. that they could give rise to brown adipocytes in the development of classic BAT, beige adipocytes not included, while Myf5 mRNA was not found in mature BAT (20). Brown adipocytes arise from multiple lineages. Classic brown adipocytes are mentioned above that they are broadly believed from Pax7/Myf5 progenitor cells, while these genes just expressing transiently in the development of BAT. Activated beige adipocytes are similar to brown adipocytes. They are distributed in many areas, including WAT, PVAT and so on. Thereinto, SM22α is reported to take part in the development of perivascular adipocytes transiently (21). Recent research shows that the adipocytes in thoracic aorta perivascular adipose tissue (T-PVAT) have different cell lineages. In this research, T-PVAT is divided into anterior T-PVAT (A-T-PVAT) and lateral T-PVAT (L-T-PVAT), and the results suggest that A-T-PVAT adipocytes are derived from SM22α progenitors while L-T-PVAT adipocytes are originated from cells containing both SM22α and Myf5 (22). Different sources of adipose cells may indicate they will play different roles in maintaining body homeostasis.

FUNCTIONS OF BAT

Metabolic Function of BAT

Since its discovery, BAT, as a thermogenesis organ, has been linked to heat production, which is regulated by the sympathetic nervous system. Thermogenesis is a manifestation of metabolic process containing shivering thermogenesis and non-shivering thermogenesis. Thereinto, shivering thermogenesis is the main contributor to heat generation under the circumstance of extreme cold. It is the result of involuntary contraction of skeletal muscles (23), and this process requires a lot of energy, causing discomfort and fatigue. Non-shivering thermogenesis under cold stimulation is to activate sympathetic nervous system to promote BAT heat production (24). Inhibiting the thermogenic function of BAT by using nicotinic acid led to increased muscle contraction against cold temperature, which demonstrated that BAT plays an important role in maintaining a normal body temperature in cold (25). Brown adipocytes with multilocular lipid droplets, are rich in mitochondria, and can significantly express uncoupling protein 1 (UCP1), PGC1α, PR domain-containing protein 16 (PRDM16) (26, 27), β3-adrenoceptor and other genes related to thermogenesis. Activated BAT expresses β3 adrenoreceptors which mediate the sympathetic drive to mobilize and upregulate UCP1 to promote a large amount of energy loss in the form of heat energy (28). Thus BAT plays a vital role in body energy expenditure through increasing glucose metabolism and lipid metabolism, which may be a valuable therapeutic approach to metabolism-related diseases, such as obesity. According to the research, nearly 40 g totally activated BAT in man could correspond to as much as 20% of body energy expenditure over a year, which is equivalent to 20 kg of body weight (29). Hence BAT is an important regulator not only in energy metabolism, but in the lipid and glucose metabolism and these two aspects are interrelated. Free fatty acids are the main source of oxidation in BAT to produce heat which is from the lipolysis of the triglyceride (TG) in lipid droplets in adipocytes. With the oxidation of fatty acids, reduced TG needs to be restored through the uptake of glucose and albumin-bound free fatty acid in the plasma (30) in order to provide the source of mitochondrial

oxidation. Thus activated BAT has its place in the clearance of glucose and TG in the plasma (31, 32). According to the research, the utilize of glucose in BAT accounts for nearly 1% of the total body glucose use, and that is about 5g of glucose in a healthy individual (33). Disordered glucose and lipid metabolism including decreased high-density lipoprotein (HDL-C), increased triglyceride-rich lipoprotein and insulin resistance are important risk factors for CVD (34). As mentioned above, BAT accounts for 0.05–0.1% of body weight in adults. Thus a healthy adult possesses nearly 40 g BAT, which plays a vital role in balancing body energy, lipid and glucose metabolism.

Secretion Function of BAT

Apart from thermogenesis, BAT has gradually attracted more attention as a secretory organ. Before that, a number of WAT-secreted molecules, which are called adipokines, have been identified in recent years, including inflammatory cytokines, leptin and so on. However, these adipokines are rarely expressed in BAT, which led the researchers to think that BAT has limited function of secretion (35). Recent years, the application of proteomics analysis in BAT researches provides researchers with an effective method to discover new cytokines. Ail et al. found fibroblast growth factor 21 (FGF21), interleukin-6 (IL-6), neuregulin-4 (NRG4) and vascular endothelial growth factor A (VEGFA), expressed in BAT will involve in thermogenesis, angiogenesis and the browning of WAT in an autocrine and/or paracrine fashion (36–40). Brown adipokines, they mainly act on different tissues or target organs to protect or regulate the cardiovascular system. For example, FGF21 is shown to have an important protective effect on the heart (41); IL-6, whose concentration is usually considered as indication of inflammatory response (42), has a positive function on regulating the glucose metabolism of BAT working together with FGF21 (43, 44) and the function of anti-inflammation (45). In addition, IL-6 can perform completely different function depending on cell type and context; bone-morphogenetic protein 8b (BMP8b) takes part in the neurovascular remolding (46); NRG4 has a negative relation with acute coronary syndrome (ACS) (47); C-X-C motif chemokine ligand-14 (CXCL14) and growth differentiation factor 15 (GDF15) participate in anti-inflammation process (48, 49). Furthermore, there are several bioactive lipid termed lipokines from both WAT and BAT, which also play an important role in the regulation of cardiovascular health. Recently, a novel lipokine derived from BAT, 12,13-dihydroxy-9Z-octadecenoic acid (12,13-diHOME), has been confirmed to play a positive role in cardiac function (50). However, further research is needed on the discovery and characteristics of the new cytokines derived from brown adipocytes. The important factors, which have been found discovered so far, are listed in **Table 1**.

BAT AND CARDIOVASCULAR DISEASES

The relationship between obesity and cardiovascular diseases has received much attention since last century (51). Multiple epidemiological investigations indicate that obesity is the major determinant of cardiovascular diseases especially in adolescents (52). More than 75% high blood pressure is caused by obesity directly (53). A large number of studies have reported that there are structural and functional heart abnormalities in obese subjects, such as left atrium enlargement and left ventricular hypertrophy (54–56). There are also some researches showing that the activity of BAT will decline in obesity (57), which may reveal that BAT plays a positive role in health maintaining (**Figure 1**). Active BAT may promote cardiac metabolic health through the combustion of triglycerides and glucose derived free fatty acids, thus preventing adipose tissue dysfunction, obesity and insulin resistance (58). As early as the twentieth century, Cittadini et al. developed obese mice based on the ablation of BAT by transgenic technology to study the relationship between BAT and CVD. In their research, they found these knockout mice had decreased energy-expenditure, and hyperphagia leading to obesity, composed with decreased body temperature and metabolic rate. Their follow-up research showed that in addition to the development of obesity and insulin resistance, the ablation of BAT led to the elevation of blood pressure, left ventricular hypertrophy with an eccentric remodeling pattern and increased interstitial tissue (59). In clinical research, Richard and his group's data obtained from the follow-up investigation of 443 patients indicated that the activity of BAT had a negative relationship with vascular inflammation and CVD (60). And the beneficial effects of BAT on improving blood glucose, TG and HDL play an significant role in promoting cadiometabolic health (61). The next question for the researchers is how BAT is involved into the occurrence and development of CVD.

BAT and Vascular Injury

Vascular injury refers to the structural damage or dysfunction of blood vessel caused by mechanical or chemical stimulation *in vitro* or *in vivo*. And atherosclerosis and aorta aneurysm, considered as the two most common and dangerous human diseases, are given serious attention.

Atherosclerosis is associated with a chronic inflammation reaction, including the accumulation of lipid, infiltration of inflammatory cells, proliferation, migration of smooth muscle cells, oxidative stress and neovascularization. Obesity is a recognized risk factor for atherosclerosis. Adipose tissue, including WAT,BAT and thoracic and abdominal PVAT, play an important role in the occurrence and development of atherosclerosis. It is traditionally believed that the increased low density lipoprotein (LDL) in the blood of obese people, which is deposited on the wall of blood vessels, then swallowed by macrophage and finally forms the foam cells, is the key step in the formation and development of atherosclerosis (62). However, recent researches show that the formation of atherosclerotic plaque is initially due to endothelial dysfunction, which is associated with infiltration of inflammatory cells, caused by the pro-inflammatory factor secreted by adipose tissue (63, 64). In animal studies, researchers use beta-adrenaline to induce browning of adipose tissue. Increased BAT can slow the development of hypercholesterolaemia and atherosclerosis in hyperlipidemia mice (65). Mitochondria are abundant in BAT, which can synthesize and release peroxisome proliferator-activated receptor gamma coactivator-1α (PGC-1α) to assist carbon monoxide to complete vasodilation. The decreased BAT results in the insufficient synthesis

TABLE 1 | Major factors expressed by adipose tissue and their important and putative functions.

Factors	Origin		Regulation	Putative functions
	WAT	BAT		
Leptin	+	+	Increased AT mass↑ Fasting↓ β-adrenergic activator↓ Obesity↑	**In physiological conditions:** Decrease atherosclerosis Decrease insulin secretion Increase energy expenditure In pathological conditions: Increase insulin resistance Hyperglycemia Decrease thyroid hormone Increase neointima formation
FGF21 ☆	–	+	β-adrenergic activator↑ Cold exposure↑ Obesity↑	**In physiological conditions:** Increase insulin sensitivity Increase browning of AT In pathological conditions: Decrease cardiac hypertrophy Decrease cardiac fibrosis
IL-6	+	+	Psychological stress↑ β-adrenergic activator↑ BAT transplantation↑	**In physiological conditions:** Decrease inflammation Increase energy expenditure Increase lipolysis Increase insulin sensitivity In pathological conditions: Increase inflammation Increase insulin resistance
NRG4	–	+	Obesity↓ Increased carotid intima-media thickness↓ Increased atherosclerotic plague↓	**In physiological conditions:** Improve insulin resistance Decrease lipogenesis Increase cardiomyocyte proliferation Decrease inflammation Decrease apoptosis of endothelial cell Decrease apoptosis and necrosis In pathological conditions: Increase insulin resistance Increase inflammation
VEGFA	+	+	Cold exposure↑	**In physiological conditions:** Increase angiogenesis Improve metabolic dysfunction Increase browning of AT Increase energy expenditure Decrease inflammation In pathological conditions: Increase inflammation
CXCL14	–	+	Cold exposure↑ Norepinephrine↑ cAMP↑ Obesity↓	**In physiological conditions:** Promote the recruitment of M2-type macrophage Increase browning of AT In pathological conditions: Decrease glucose tolerance Increase inflammation
GDF15☆	+	+	Cold exposure↑ CVD↑ Cancer↑	**In physiological conditions:** Increase lipolysis Improve insulin resistance In pathological conditions: Decrease inflammation
PGC-1α	–	+	Cold exposure↑ Norepinephrine↑ Aging↓	**In physiological conditions:** Improve vascular senescence Decrease inflammation Decrease oxidative stress Regulate mitochondrial biogenesis In pathological conditions: Increase inflammation Increase oxidative stress
PRDM16	+	+	Aging↓	**In physiological conditions:** Increase browning of AT Regulate thermogenesis Suppress fibrogenesis Increase lipolysis Increase ketogenesis In pathological conditions: Increase browning of AT
Adiponectin	+	+	obesity↓ β-adrenergic activator↑ Calorie restriction↑ Increased bone marrow adipose tissue mass↑ Coronary artery diseases↓	**In physiological conditions:** Decrease inflammation Increase insulin sensitivity Decrease atherosclerosis In pathological conditions: Increase β-cell apoptosis
12,13-diHOME	–	+	BAT transplantation↑ Heart diseases↓	**In physiological conditions:** Regulate calcium cycling Increase mitochondrial respiration In pathological conditions: Decrease cardiac protection

– represents this factor is not expressed or rare expressed in the tissue; + represents this factor is expressed in physical condition or certain conditions. Most factors listed above play a protective role in physiological conditions, and their expression decrease in pathological conditions which leads to bad results as showed in "in pathological conditions" column. "" means the expression of these factors will increase early in pathological conditions and then exert protective effects.*

of PGC-1α and then impairs vasodilation seriously (66). In addition, PGC-1α plays a vital role in the biosynthesis and function of mitochondria, and the dysfunction of mitochondria will cause a series of problems including telomere dysfunction, DNA damage and oxidative stress (67). There are also evidence showing that PGC-1α can regulate vascular senescence negatively (68). In the study of atherosclerosis, there are researches showing that the BAT-derived exosome can inhibit the increase of miR-324-5p, which is the specific biomarker of the development of atherosclerosis (69). There are also many other BAT-derived cytokines involved in vascular health. Adiponectin, for example, which is produced by adipose tissue and enters into the circulation, was suggested to fight against atherosclerosis through suppressing endothelial inflammation and VSMC proliferation. Besides, it can restrain the transformation of macrophage to foam cells (70). Apart from BAT, the adipose tissue around vessels, which is called perivascular adipose tissue (PVAT), also plays a vital role in protecting vessels. PVAT, especially thoracic PVAT, similar to BAT, is a thermogenesis organ, which is crucial for maintenance of intravascular temperature. The activation of PVAT can attenuate the development of atherosclerosis, through preventing intravascular temperature loss which can directly maintenance the function of endothelial. Furthermore, thermogenic activation of

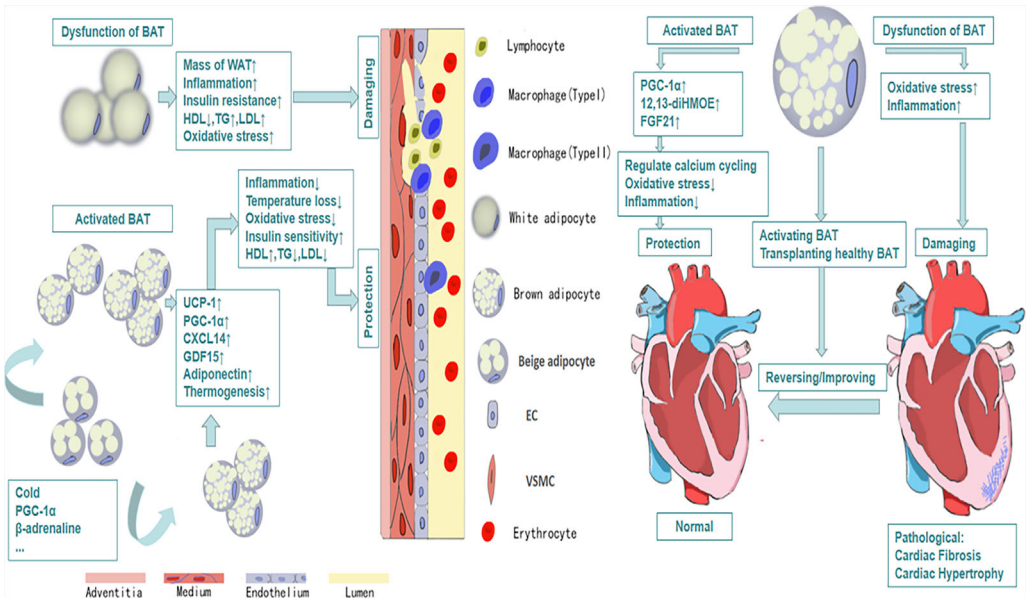

FIGURE 1 | The protective efforts of BAT on vessels and heart. Activated BAT, including classic BAT and the BAT derived from the browning of beige adipocytes under the condition of cold exposure, beta-adrenaline stimulation and so on, plays a protective role through its metabolic function and secretion function, which leads to decreased inflammation, decreased oxidative stress response and increased HDL, increased uptake of glucose and so on. And all of these contribute to cardiovascular health and vice versa.

PVAT can enhance the clearance of total lipid. While this protection will disappear when PVAT is removed (21). In addition, there is an underestimated type of adipose tissue, called epicardial adipose tissue (EAT), increasing of whose mass is considered as a risk factor for the development of coronary artery diseases (71). EAT is considered as a type of beige adipose tissue with overexpression of UCP-1, the marker of brown adipose tissue, relative to WAT (72). Akin to PVAT, EAT possesses significant thermogenic capacity, sharing a negative association with temperature, and plays an important role in protecting cardiovascular health. α2A-adrenergic receptor (ADRA2A) is an inhibitory α-adrenergic receptor, which is at a lower level compared to WAT and it may contribute to the higher signaling *via* β-adrenergic receptors in EAT. Besides, through adding conditioned media which was collected from EAT treated with isoproterenol to primary human cardiac endothelial cell and then culturing it for 24 h, significant down-regulation of the expression of adhesion markers such as Icam1 and Vcam1 in endothelial cells were detected compared to control group (73). Thus abnormal EAT affected the function of endothelial cells seriously which is considered as the initial pathological process in the development of atherosclerosis. What's more, research reported that activated EAT was associated with decreased circulating TG levels and increased HDL-C levels which had protective effect on atherosclerosis (72). In conclusion, in obesity, increased fatty acid release by WAT and decreased lipid combustion by BAT and thoracic PVAT lead to hyperlipidemia, which contributes to atherosclerosis development. Besides, obese WAT and abdominal PVAT release pro-inflaammatory factors that further promote atherosclerosis (74).

Aortic aneurysm (AA), defined as a pathological and progressive dilation of a segment of a blood vessel, is a common and dangerous vascular disease, especially abdominal aortic aneurysm (AAA). There is still lacking effective means of medical treatments. For the pathogenesis of AA, the mainstream view is that decreased smooth muscle cells, the degradation of cell matrix and infiltration of inflammatory cells in the blood vessel result in the thinning of adventitia and media jointly (75). The high risk of cardiovascular-related death in obesity is due to the AA partly (76). In the research, researchers found obesity could increase the morbidity of AngII-induced AA and exacerbate perivascular infiltration of macrophage and expression of MCP-1, IL-6, chemotactic factors and so on. In addition, they found there were more brown adipocytes around thoracic aorta, while more white adipocytes around abdominal aorta. Thus they finally draw the conclusion that in obesity, the high incidence of AA, especially AAA, is critically due to the decreased BAT which aggravates vascular inflammation rather than changes cholesterol concentration, distribution of lipoprotein and insulin resistance in blood (77). Dowal and his group confirm that BAT has ability to repress the inflammatory action of macrophage (78). Further research shows that BAT can inhibit inflammation to protect blood vessels through following two aspects at least. On the one hand, BAT-derived CXCL14 can recruit M2 macrophage possessing anti-inflammation ability (48). On the other hand, BAT can secrete GDF15 which acts on M1 macrophage to inhibit its pro-inflammation response (49).

In summary, the capacity of BAT in vascular protection is now widely recognized to be multifaceted from its original thermogenic function to its powerful endocrine function and metabolic function. And its anti-inflammation function and the ability to improve lipid, glucose metabolism can prevent of reverse vascular diseases directly or indirectly.

BAT and Heart Diseases

Heart failure, as the terminal state of kinds of heart diseases, with high mortality and bad prognosis, is a clinical syndrome caused by the structural or functional abnormalities of the heart. It is a progressive disease, from initial myocardial damage to the damage of ventricular filling and cardiac ejection, and then to ventricular remolding finally. Recent research shows that adipose tissue-derived cytokines take part in the regulation of heart diseases (79). In animal study, removing BAT in the body will aggravate cardiac remolding, which appears BAT may play a role in cardiac protection in some way. FGF21, as one of the first proven cytokines from BAT, has a protective effect on the heart. And in the follow-up study, activation of adenosine 2A (A2A) receptor in BAT can mediate BAT secrete FGF21, which can attenuate hypertensive cardiac remolding (80). In addition, mice with UCP-1 knockout had severe myocardial injuries, fibrosis and ventricular remolding when they were given heart injury in experiments, and their survival rate was significant reducing. However, transplanting BAT from healthy mice could reverse heart damage and improve survival (81). As is mentioned above, PGC-1α plays an important role in vascular protection. It is essential for heart protection as well. The dysfunction of BAT results in the decrease of PGC-1α synthesis. In some patients with cardiac hypertrophy caused by hypertension or heart failure, it was found that reduced PGC-1α would lead to the decrease of the oxidation of fatty acid and the suppression in mitochondrial oxidative phosphorylation (82). While the exact mechanisms have not been elucidated. Some researches show that BAT can inhibit NF-κB through SIRT1-PGC1α-PPARγ pathway to suppress inflammation (83). What's more, Pinckard et al. found that the transplantation of BAT could reverse cardiac dysfunction and cardiac remodeling caused by high-fat diet through increase the expression of 12,13-diHOME. Further research showed that 12,13-diHOME together with NOS1 could enhance cardiac function by regulating the calcium cycling (50). In addition, the dysfunction of adipose tissue has been discussed on a variety of cardiac disorders in many researches (84).

The Negative Effect of BAT

There are a number of studies showing that BAT plays a positive role in cardiovascular damage. While some researches show that activated BAT and increased browning of WAT may exacerbate atherosclerosis (85, 86). Activated BAT and increased beige adipose tissue can elevate lipolysis and thermogenesis, then increase bio-synthesis of cholesterol and mobilization of low density lipoprotein (LDL) and very low density lipoprotein (VLDL), which promotes the growth of atherosclerotic plague. In their further study, they found genetic deletion of UCP1 in ApoE(−/−) mice, which is the specific marker of BAT, could prevent the occurrence of the above phenomenon.

CONCLUSION

It is widely accepted that obesity can induce and accelerate the progression of CVD. Traditionally, the accumulation of WAT in obese people was considered as the major factor that increases the morbidity of CVD, while the role of BAT in obesity has been paid much more attention recently. In the past, due to the lack of accurate detection methods, the clinic value of BAT has been greatly underestimated. With the development of technology, such as the application of PET/CT, BAT is strongly associated with health. After kinds of studies, BAT is considered as not only a thermogenic organ, but also a endocrine organ. It has a powerful anti-inflammatory effect which plays an important role in cardiovascular protection. As a bridge between CVD and metabolic diseases, BAT will provide new ideas for the treatment. While recent researches show activated BAT is not as good as we thought before, which can accelerate the formation of atherosclerosis. So BAT might be a double-edged sword in the development of CVD and the exact mechanism of BAT has not been understood yet. Thus developing its positive function fully and reducing its possible negative effects are the direction we should strive for in the future, and it needs further elaboration of its possible mechanism in the development of CVD.

AUTHOR CONTRIBUTIONS

C-CR and H-JC designed the study and wrote the manuscript. TM and P-JG performed critical revision of the manuscript. All authors contributed to the article and approved the submitted version.

FUNDING

This work was supported by the National Natural Science Foundation of China (81922004, 81770495, 91739303, 81870180 and 81700433) and the Natural Science Foundation of Shanghai, China (19JC1414600).

REFERENCES

1. GBD 2015 Obesity Collaborators, Afshin A, Forouzanfar MH, Reitsma MB, Sur P, Estep K, et al. Health Effects of Overweight and Obesity in 195 Countries Over 25 Years. *N Engl J Med* (2017) 377(1):13–27. doi: 10.1056/NEJMoa1614362
2. Després JP, Moorjani S, Lupien PJ, Tremblay A, Nadeau A, Bouchard C. Regional Distribution of Body Fat, Plasma Lipoproteins, and Cardiovascular Disease. *Arteriosclerosis* (1990) 10(4):497–511. doi: 10.1161/01.atv.10.4.497
3. Rosen ED, Spiegelman BM. Adipocytes as Regulators of Energy Balance and Glucose Homeostasis. *Nature* (2006) 444(7121):847–53. doi: 10.1038/nature05483
4. Hirsch J, Batchelor B. Adipose Tissue Cellularity in Human Obesity. *Clin Endocrinol Metab* (1976) 5(2):299–311. doi: 10.1016/s0300-595x(76)80023-0
5. Heaton JM. The Distribution of Brown Adipose Tissue in the Human. *J Anat* (1972) 112(Pt 1):35–9.
6. Huttunen P, Hirvonen J, Kinnula V. The Occurrence of Brown Adipose Tissue in Outdoor Workers. *Eur J Appl Physiol Occup Physiol* (1981) 46 (4):339–45. doi: 10.1007/BF00422121
7. van Ooijen AM, van Marken Lichtenbelt WD, van Steenhoven AA, Westerterp KR. Seasonal Changes in Metabolic and Temperature Responses to Cold Air in Humans. *Physiol Behav* (2004) 82(2-3):545–53. doi: 10.1016/j.physbeh.2004.05.001

8. Nishimura T, Motoi M, Egashira Y, Choi D, Aoyagi K, Watanuki S. Seasonal Variation of Non-Shivering Thermogenesis (NST) During Mild Cold Exposure. *J Physiol Anthropol* (2015) 34(1):11. doi: 10.1186/s40101-015-0051-9
9. Virtanen KA, Lidell ME, Orava J, Heglind M, Westergren R, Niemi T, et al. Functional Brown Adipose Tissue in Healthy Adults. *N Engl J Med* (2009) 360 (15):1518–25. doi: 10.1056/NEJMoa0808949
10. Cypess AM, Lehman S, Williams G, Tal I, Rodman D, Goldfine AB, et al. Identification and Importance of Brown Adipose Tissue in Adult Humans. *N Engl J Med* (2009) 360(15):1509–17. doi: 10.1056/NEJMoa0810780
11. van Marken Lichtenbelt WD, Vanhommerig JW, Smulders NM, Drossaerts JM, Kemerink GJ, Bouvy ND, et al. Cold-Activated Brown Adipose Tissue in Healthy Men. *N Engl J Med* (2009) 360(15):1500–8. doi: 10.1056/NEJMoa0808718
12. Cypess AM, White AP, Vernochet C, Schulz TJ, Xue R, Sass CA, et al. Anatomical Localization, Gene Expression Profiling and Functional Characterization of Adult Human Neck Brown Fat. *Nat Med* (2013) 19 (5):635–9. doi: 10.1038/nm.3112
13. Granneman JG, Li P, Zhu Z, Lu Y. Metabolic and Cellular Plasticity in White Adipose Tissue I: Effects of Beta3-Adrenergic Receptor Activation. *Am J Physiol Endocrinol Metab* (2005) 289(4):E608–16. doi: 10.1152/ajpendo.00009.2005
14. Himms-Hagen J, Melnyk A, Zingaretti MC, Ceresi E, Barbatelli G, Cinti S. Multilocular Fat Cells in WAT of CL-316243-Treated Rats Derive Directly From White Adipocytes. *Am J Physiol Cell Physiol* (2000) 279(3):C670–81. doi: 10.1152/ajpcell.2000.279.3.C670
15. Rothwell NJ, Stock MJ. Surgical Removal of Brown Fat Results in Rapid and Complete Compensation by Other Depots. *Am J Physiol* (1989) 257(2 Pt 2): R253–8. doi: 10.1152/ajpregu.1989.257.2.R253
16. Relaix F, Rocancourt D, Mansouri A, Buckingham M. A Pax3/Pax7-Dependent Population of Skeletal Muscle Progenitor Cells. *Nature* (2005) 435(7044):948–53. doi: 10.1038/nature03594
17. Relaix F, Rocancourt D, Mansouri A, Buckingham M. Divergent Functions of Murine Pax3 and Pax7 in Limb Muscle Development. *Genes Dev* (2004) 18 (9):1088–105. doi: 10.1101/gad.301004
18. Lepper C, Fan CM. Inducible Lineage Tracing of Pax7-Descendant Cells Reveals Embryonic Origin of Adult Satellite Cells. *Genesis* (2010) 48(7):424–36. doi: 10.1002/dvg.20630
19. Tallquist MD, Weismann KE, Hellström M, Soriano P. Early Myotome Specification Regulates PDGFA Expression and Axial Skeleton Development. *Development* (2000) 127(23):5059–70. doi: 10.1242/dev.127.23.5059
20. Seale P, Bjork B, Yang W, Kajimura S, Chin S, Kuang S, et al. PRDM16 Controls a Brown Fat/Skeletal Muscle Switch. *Nature* (2008) 454(7207):961–7. doi: 10.1038/nature07182
21. Chang L, Villacorta L, Li R, Hamblin M, Xu W, Dou C, et al. Loss of Perivascular Adipose Tissue on Peroxisome Proliferator-Activated Receptor-Γ Deletion in Smooth Muscle Cells Impairs Intravascular Thermoregulation and Enhances Atherosclerosis. *Circulation* (2012) 126(9):1067–78. doi: 10.1161/CIRCULATIONAHA.112.104489
22. Ye M, Ruan CC, Fu M, Xu L, Chen D, Zhu M, et al. Developmental and Functional Characteristics of the Thoracic Aorta Perivascular Adipocyte. *Cell Mol Life Sci* (2019) 76(4):777–89. doi: 10.1007/s00018-018-2970-1
23. Haman F, Blondin DP. Shivering Thermogenesis in Humans: Origin, Contribution and Metabolic Requirement. *Temperature (Austin)* (2017) 4 (3):217–26. doi: 10.1080/23328940.2017.1328999
24. SMITH RE, ROBERTS JC. Thermogenesis of Brown Adipose Tissue in Cold-Acclimated Rats. *Am J Physiol* (1964) 206:143–8. doi: 10.1152/ajplegacy.1964.206.1.143
25. Blondin DP, Frisch F, Phoenix S, Guérin B, Turcotte ÉE, Haman F, et al. Inhibition of Intracellular Triglyceride Lipolysis Suppresses Cold-Induced Brown Adipose Tissue Metabolism and Increases Shivering in Humans. *Cell Metab* (2017) 25(2):438–47. doi: 10.1016/j.cmet.2016.12.005
26. Seale P, Kajimura S, Yang W, Chin S, Rohas LM, Uldry M, et al. Transcriptional Control of Brown Fat Determination by PRDM16. *Cell Metab* (2007) 6(1):38–54. doi: 10.1016/j.cmet.2007.06.001
27. Wang W, Ishibashi J, Trefely S, Shao M, Cowan AJ, Sakers A, et al. A PRDM16-Driven Metabolic Signal From Adipocytes Regulates Precursor Cell Fate. *Cell Metab* (2019) 30(1):174–89.e5. doi: 10.1016/j.cmet.2019.05.005
28. Bhatt PS, Dhillo WS, Salem V. Human Brown Adipose Tissue-Function and Therapeutic Potential in Metabolic Disease. *Curr Opin Pharmacol* (2017) 37:1–9. doi: 10.1016/j.coph.2017.07.004
29. Rothwell NJ, Stock MJ. Luxuskonsumption, Diet-Induced Thermogenesis and Brown Fat: The Case in Favour. *Clin Sci (Lond)* (1983) 64(1):19–23. doi: 10.1042/cs0640019
30. Maliszewska K, Kretowski A. Brown Adipose Tissue and Its Role in Insulin and Glucose Homeostasis. *Int J Mol Sci* (2021) 22(4):1530. doi: 10.3390/ijms22041530
31. Wu MV, Bikopoulos G, Hung S, Ceddia RB. Thermogenic Capacity is Antagonistically Regulated in Classical Brown and White Subcutaneous Fat Depots by High Fat Diet and Endurance Training in Rats: Impact on Whole-Body Energy Expenditure. *J Biol Chem* (2014) 289(49):34129–40. doi: 10.1074/jbc.M114.591008
32. Burcelin R, Kande J, Ricquier D, Girard J. Changes in Uncoupling Protein and GLUT4 Glucose Transporter Expressions in Interscapular Brown Adipose Tissue of Diabetic Rats: Relative Roles of Hyperglycaemia and Hypoinsulinaemia. *Biochem J* (1993) 291(Pt 1):109–13. doi: 10.1042/bj2910109
33. Blondin DP, Labbé SM, Noll C, Kunach M, Phoenix S, Guérin B, et al. Selective Impairment of Glucose But Not Fatty Acid or Oxidative Metabolism in Brown Adipose Tissue of Subjects With Type 2 Diabetes. *Diabetes* (2015) Jul64(7):2388–97. doi: 10.2337/db14-1651
34. Eckel RH, York DA, Rössner S, Hubbard V, Caterson I, St Jeor ST, et al. American Heart Association. Prevention Conference VII: Obesity, a Worldwide Epidemic Related to Heart Disease and Stroke: Executive Summary. *Circulation.* (2004) 110 (18):2968–75. doi: 10.1161/01.CIR.0000140086.88453.9A
35. Cannon B, Nedergaard J. Brown Adipose Tissue: Function and Physiological Significance. *Physiol Rev* (2004) 84(1):277–359. doi: 10.1152/physrev.00015.2003
36. Ali Khan A, Hansson J, Weber P, Foehr S, Krijgsveld J, Herzig S, et al. Comparative Secretome Analyses of Primary Murine White and Brown Adipocytes Reveal Novel Adipokines. *Mol Cell Proteomics* (2018) 17 (12):2358–70. doi: 10.1074/mcp.RA118.000704
37. Burýsek L, Houstek J. Beta-Adrenergic Stimulation of Interleukin-1alpha and Interleukin-6 Expression in Mouse Brown Adipocytes. *FEBS Lett* (1997) 411 (1):83–6. doi: 10.1016/s0014-5793(97)00671-6
38. Bersell K, Arab S, Haring B, Kühn B. Neuregulin1/Erbb4 Signaling Induces Cardiomyocyte Proliferation and Repair of Heart Injury. *Cell.* (2009) 138 (2):257–70. doi: 10.1016/j.cell.2009.04.060
39. Schumacher MA, Hedl M, Abraham C, Bernard JK, Lozano PR, Hsieh JJ, et al. Erbb4 Signaling Stimulates Pro-Inflammatory Macrophage Apoptosis and Limits Colonic Inflammation. *Cell Death Dis* (2017) 8(2):e2622. doi: 10.1038/cddis.2017.42
40. Tie G, Yan J, Yang Y, Park BD, Messina JA, Raffai RL, et al. Oxidized Low-Density Lipoprotein Induces Apoptosis in Endothelial Progenitor Cells by Inactivating the Phosphoinositide 3-Kinase/Akt Pathway. *J Vasc Res* (2010) 47 (6):519–30. doi: 10.1159/000313879
41. Planavila A, Redondo I, Hondares E, Vinciguerra M, Munts C, Iglesias R, et al. Fibroblast Growth Factor 21 Protects Against Cardiac Hypertrophy in Mice. *Nat Commun* (2013) 4:2019. doi: 10.1038/ncomms3019
42. Kotch C, Barrett D, Teachey DT. Tocilizumab for the Treatment of Chimeric Antigen Receptor T Cell-Induced Cytokine Release Syndrome. *Expert Rev Clin Immunol* (2019) Aug15(8):813–22. doi: 10.1080/1744666X.2019.1629904
43. Stanford KI, Middelbeek RJ, Townsend KL, An D, Nygaard EB, Hitchcox KM, et al. Brown Adipose Tissue Regulates Glucose Homeostasis and Insulin Sensitivity. *J Clin Invest* (2013) Jan123(1):215–23. doi: 10.1172/JCI62308
44. Qing H, Desrouleaux R, Israni-Winger K, Mineur YS, Fogelman N, Zhang C, et al. Origin and Function of Stress-Induced IL-6 in Murine Models. *Cell.* (2020) 182(2):372–87.e14. doi: 10.1016/j.cell.2020.05.054
45. Nandi D, Mishra MK, Basu A, Bishayi B. Protective Effects of Interleukin-6 in Lipopolysaccharide (LPS)-Induced Experimental Endotoxemia are Linked to Alteration in Hepatic Anti-Oxidant Enzymes and Endogenous Cytokines. *Immunobiology* (2010) 215(6):443–51. doi: 10.1016/j.imbio.2009.08.003
46. Pellegrinelli V, Peirce VJ, Howard L, Virtue S, Türei D, Senzacqua M, et al. Adipocyte-Secreted BMP8b Mediates Adrenergic-Induced Remodeling of the Neuro-Vascular Network in Adipose Tissue. *Nat Commun* (2018) 9(1):4974. doi: 10.1038/s41467-018-07453-x

47. Rahimzadeh M, Farshidi N, Naderi N, Farshidi H, Montazerghaem H. Clinical Significance of Serum Concentrations of Neuregulin-4, in Acute Coronary Syndrome. *Sci Rep* (2020) 10(1):5797. doi: 10.1038/s41598-020-62680-x
48. Cereijo R, Gavaldà-Navarro A, Cairó M, Quesada-López T, Villarroya J, Morón-Ros S, et al. CXCL14, a Brown Adipokine That Mediates Brown-Fat-to-Macrophage Communication in Thermogenic Adaptation. *Cell Metab* (2018) 28(5):750–63. doi: 10.1016/j.cmet.2018.07.015
49. Campderrós L, Moure R, Cairó M, Gavaldà-Navarro A, Quesada-López T, Cereijo R, et al. Brown Adipocytes Secrete GDF15 in Response to Thermogenic Activation. *Obes (Silver Spring)* (2019) 27(10):1606–16. doi: 10.1002/oby.22584
50. Pinckard KM, Shettigar VK, Wright KR, Abay E, Baer LA, Vidal P, et al. A Novel Endocrine Role for the BAT-Released Lipokine 12,13-Dihome to Mediate Cardiac Function. *Circulation* (2021) 143(2):145–59. doi: 10.1161/CIRCULATIONAHA.120.049813
51. Barrett-Connor EL. Obesity, Atherosclerosis, and Coronary Artery Disease. *Ann Intern Med* (1985) 103(6(6 (Pt 2):1010–9. doi: 10.7326/0003-4819-103-6-1010
52. Yeh TL, Chen HH, Tsai SY, Lin CY, Liu SJ, Chien KL. The Relationship Between Metabolically Healthy Obesity and the Risk of Cardiovascular Disease: A Systematic Review and Meta-Analysis. *J Clin Med* (2019) 8 (8):1228. doi: 10.3390/jcm8081228
53. Krauss RM, Winston M, Fletcher BJ, Grundy SM. Obesity : Impact on Cardiovascular Disease. *Circulation.* (1998) 98(14):1472–6. doi: 10.1161/01.CIR.98.14.1472
54. Warnes CA, Roberts WC. The Heart in Massive (More Than 300 Pounds or 136 Kilograms) Obesity: Analysis of 12 Patients Studied At Necropsy. *Am J Cardiol* (1984) 54(8):1087–91. doi: 10.1016/s0002-9149(84)80149-6
55. de Divitiis O, Fazio S, Petitto M, Maddalena G, Contaldo F, Mancini M. Obesity and Cardiac Function. *Circulation* (1981) 64(3):477–82. doi: 10.1161/01.cir.64.3.477
56. de Simone G, Devereux RB, Mureddu GF, Roman MJ, Ganau A, Alderman MH, et al. Influence of Obesity on Left Ventricular Midwall Mechanics in Arterial Hypertension. *Hypertension* (1996) 28(2):276–83. doi: 10.1161/01.hyp.28.2.276
57. Betz MJ, Enerbäck S. Human Brown Adipose Tissue: What We Have Learned So Far. *Diabetes* (2015) 64(7):2352–60. doi: 10.2337/db15-0146
58. Franssens BT, Hoogduin H, Leiner T, van der Graaf Y, Visseren FLJ. Relation Between Brown Adipose Tissue and Measures of Obesity and Metabolic Dysfunction in Patients With Cardiovascular Disease. *J Magn Reson Imaging* (2017) 46(2):497–504. doi: 10.1002/jmri.25594
59. Cittadini A, Mantzoros CS, Hampton TG, Travers KE, Katz SE, Morgan JP, et al. Cardiovascular Abnormalities in Transgenic Mice With Reduced Brown Fat: An Animal Model of Human Obesity. *Circulation* (1999) 100(21):2177–83. doi: 10.1161/01.cir.100.21.2177
60. Takx RA, Ishai A, Truong QA, MacNabb MH, Scherrer-Crosbie M, Tawakol A. Supraclavicular Brown Adipose Tissue 18F-FDG Uptake and Cardiovascular Disease. *J Nucl Med* (2016) 57(8):1221–5. doi: 10.2967/jnumed.115.166025
61. Becher T, Palanisamy S, Kramer DJ, Eljalby M, Marx SJ, Wibmer AG, et al. Brown Adipose Tissue is Associated With Cardiometabolic Health. *Nat Med* (2021) 27(1):58–65. doi: 10.1038/s41591-020-1126-7
62. Moore KJ, Sheedy FJ, Fisher EA. Macrophages in Atherosclerosis: A Dynamic Balance. *Nat Rev Immunol* (2013) 13(10):709–21. doi: 10.1038/nri3520
63. Huh JY, Park YJ, Ham M, Kim JB. Crosstalk Between Adipocytes and Immune Cells in Adipose Tissue Inflammation and Metabolic Dysregulation in Obesity. *Mol Cells* (2014) 37(5):365–71. doi: 10.14348/molcells.2014.0074
64. Wang H, Wang Q, Venugopal J, Wang J, Kleiman K, Guo C, et al. Obesity-Induced Endothelial Dysfunction is Prevented by Neutrophil Extracellular Trap Inhibition. *Sci Rep* (2018) 8(1):4881. doi: 10.1038/s41598-018-23256-y
65. Berbée JF, Boon MR, Khedoe PP, Bartelt A, Schlein C, Worthmann A, et al. Brown Fat Activation Reduces Hypercholesterolaemia and Protects From Atherosclerosis Development. *Nat Commun* (2015) 6:6356. doi: 10.1038/ncomms7356
66. Nisoli E, Clementi E, Paolucci C, Cozzi V, Tonello C, Sciorati C, et al. Mitochondrial Biogenesis in Mammals: The Role of Endogenous Nitric Oxide. *Science* (2003) 299(5608):896–9. doi: 10.1126/science.1079368
67. Wenz T. Mitochondria and PGC-1α in Aging and Age-Associated Diseases. *J Aging Res* (2011) 2011:810619. doi: 10.4061/2011/810619
68. Xiong S, Salazar G, Patrushev N, Ma M, Forouzandeh F, Hilenski L, et al. Peroxisome Proliferator-Activated Receptor Γ Coactivator-1α is a Central Negative Regulator of Vascular Senescence. *Arterioscler Thromb Vasc Biol* (2013) 33(5):988–98. doi: 10.1161/ATVBAHA.112.301019
69. Xing X, Li Z, Yang X, Li M, Liu C, Pang Y, et al. Adipose-Derived Mesenchymal Stem Cells-Derived Exosome-Mediated Microrna-342-5p Protects Endothelial Cells Against Atherosclerosis. *Aging (Albany NY)* (2020) 12(4):3880–98. doi: 10.18632/aging.102857
70. Okamoto Y, Kihara S, Ouchi N, Nishida M, Arita Y, Kumada M, et al. Adiponectin Reduces Atherosclerosis in Apolipoprotein E-Deficient Mice. *Circulation* (2002) 106(22):2767–70. doi: 10.1161/01.cir.0000042707.50032.19
71. Raggi P. Epicardial Adipose Tissue as a Marker of Coronary Artery Disease Risk. *J Am Coll Cardiol* (2013) 61(13):1396–7. doi: 10.1016/j.jacc.2012.12.028
72. Chechi K, Blanchard PG, Mathieu P, Deshaies Y, Richard D. Brown Fat Like Gene Expression in the Epicardial Fat Depot Correlates With Circulating HDL-Cholesterol and Triglycerides in Patients With Coronary Artery Disease. *Int J Cardiol* (2013) 167(5):2264–70. doi: 10.1016/j.ijcard.2012.06.008
73. Chechi K, Voisine P, Mathieu P, Laplante M, Bonnet S, Picard F, et al. Functional Characterization of the Ucp1-Associated Oxidative Phenotype of Human Epicardial Adipose Tissue. *Sci Rep* (2017) 7(1):15566. doi: 10.1038/s41598-017-15501-7
74. van Dam AD, Boon MR, Berbée JFP, Rensen PCN, van Harmelen V. Targeting White, Brown and Perivascular Adipose Tissue in Atherosclerosis Development. *Eur J Pharmacol* (2017) 816:82–92. doi: 10.1016/j.ejphar.2017.03.051
75. Sakalihasan N, Michel JB, Katsargyris A, Kuivaniemi H, Defraigne JO, Nchimi A, et al. Abdominal Aortic Aneurysms. *Nat Rev Dis Primers* (2018) 4(1):34. doi: 10.1038/s41572-018-0030-7
76. Nieves DJ, Cnop M, Retzlaff B, Walden CE, Brunzell JD, Knopp RH, et al. The Atherogenic Lipoprotein Profile Associated With Obesity and Insulin Resistance is Largely Attributable to Intra-Abdominal Fat. *Diabetes* (2003) 52(1):172–9. doi: 10.2337/diabetes.52.1.172
77. Police SB, Thatcher SE, Charnigo R, Daugherty A, Cassis LA. Obesity Promotes Inflammation in Periaortic Adipose Tissue and Angiotensin II-Induced Abdominal Aortic Aneurysm Formation. *Arterioscler Thromb Vasc Biol* (2009) 29(10):1458–64. doi: 10.1161/ATVBAHA.109.192658
78. Dowal L, Parameswaran P, Phat S, Akella S, Majumdar ID, Ranjan J, et al. Intrinsic Properties of Brown and White Adipocytes Have Differential Effects on Macrophage Inflammatory Responses. *Mediators Inflamm* (2017) 2017:9067049. doi: 10.1155/2017/9067049
79. Mechanick JI, Zhao S, Garvey WT. The Adipokine-Cardiovascular-Lifestyle Network: Translation to Clinical Practice. *J Am Coll Cardiol* (2016) 68 (16):1785–803. doi: 10.1016/j.jacc.2016.06.072
80. Ruan CC, Kong LR, Chen XH, Ma Y, Pan XX, Zhang ZB, et al. A2A Receptor Activation Attenuates Hypertensive Cardiac Remodeling Via Promoting Brown Adipose Tissue-Derived FGF21. *Cell Metab* (2020) 632(4):689. doi: 10.1016/j.cmet.2020.08.018
81. Thoonen R, Ernande L, Cheng J, Nagasaka Y, Yao V, Miranda-Bezerra A, et al. Functional Brown Adipose Tissue Limits Cardiomyocyte Injury and Adverse Remodeling in Catecholamine-Induced Cardiomyopathy. *J Mol Cell Cardiol* (2015) 84:202–11. doi: 10.1016/j.yjmcc.2015.05.002
82. Sihag S, Cresci S, Li AY, Sucharov CC, Lehman JJ. PGC-1alpha and Erralpha Target Gene Downregulation is a Signature of the Failing Human Heart. *J Mol Cell Cardiol* (2009) 46(2):201–12. doi: 10.1016/j.yjmcc.2008.10.025
83. Planavila A, Iglesias R, Giralt M, Villarroya F. Sirt1 Acts in Association With Pparα to Protect the Heart From Hypertrophy, Metabolic Dysregulation, and Inflammation. *Cardiovasc Res* (2011) 90(2):276–84. doi: 10.1093/cvr/cvq376
84. Lv J, Deng C, Jiang S, Ji T, Yang Z, Wang Z, et al. Blossoming 20: The Energetic Regulator's Birthday Unveils Its Versatility in Cardiac Diseases. *Theranostics* (2019) 9(2):466–76. doi: 10.7150/thno.29130
85. Dong M, Yang X, Lim S, Cao Z, Honek J, Lu H, et al. Cold Exposure Promotes Atherosclerotic Plaque Growth and Instability Via UCP1-Dependent Lipolysis. *Cell Metab* (2013) 18(1):118–29. doi: 10.1016/j.cmet.2013.06.003
86. Sui W, Li H, Yang Y, Jing X, Xue F, Cheng J, et al. Bladder Drug Mirabegron Exacerbates Atherosclerosis Through Activation of Brown Fat-Mediated

Lipolysis. *Proc Natl Acad Sci USA* (2019) 116(22):10937–42. doi: 10.1073/pnas.1901655116

Conflict of Interest: The authors declare that the research was conducted in the absence of any commercial or financial relationships that could be construed as a potential conflict of interest.

frontiers in Endocrinology

ORIGINAL RESEARCH
published: 04 August 2021
doi: 10.3389/fendo.2021.642000

Combination Usage of AdipoCount and Image-Pro Plus/ImageJ Software for Quantification of Adipocyte Sizes

Yepeng Hu[1†], Jian Yu[2†], Xiangdi Cui[2], Zhe Zhang[2], Qianqian Li[1], Wenxiu Guo[2], Cheng Zhao[2], Xin Chen[2], Meiyao Meng[2], Yu Li[2], Mingwei Guo[2], Jin Qiu[2], Fei Shen[3], Dongmei Wang[2], Xinran Ma[1,2], Lingyan Xu[1,2], Feixia Shen[1*] and Xuejiang Gu[1*]*

[1] Department of Endocrine and Metabolic Diseases, The First Affiliated Hospital of Wenzhou Medical University, Wenzhou, China, [2] Shanghai Key Laboratory of Regulatory Biology, Institute of Biomedical Sciences and School of Life Sciences, East China Normal University, Shanghai, China, [3] Key Laboratory of Adolescent Health Assessment and Exercise Intervention of Ministry of Education, College of Physical Education and Health, East China Normal University, Shanghai, China

OPEN ACCESS

Edited by:
Jiqiu Wang,
Shanghai Jiao Tong University, China

Reviewed by:
Rita De Matteis,
University of Urbino Carlo Bo, Italy
Delobel Pierre,
INRA UMR Dynamique Musculaire et Métabolisme, France
Cen Xie,
Chinese Academy of Sciences, China
Cheng-Chao Ruan,
Shanghai Jiao Tong University, China

***Correspondence:**
Lingyan Xu
lyxu@bio.ecnu.edu.cn
Feixia Shen
shenfeixia@wmu.edu.cn
Xuejiang Gu
guxuejiang@wmu.edu.cn

[†]These authors have contributed equally to this work

Specialty section:
This article was submitted to Cellular Endocrinology, a section of the journal Frontiers in Endocrinology

Received: 15 December 2020
Accepted: 14 July 2021
Published: 04 August 2021

Citation:
Hu Y, Yu J, Cui X, Zhang Z, Li Q, Guo W, Zhao C, Chen X, Meng M, Li Y, Guo M, Qiu J, Shen F, Wang D, Ma X, Xu L, Shen F and Gu X (2021) Combination Usage of AdipoCount and Image-Pro Plus/ImageJ Software for Quantification of Adipocyte Sizes. Front. Endocrinol. 12:642000. doi: 10.3389/fendo.2021.642000

In recent decades, the prevalence of obesity has been rising. One of the major characteristics of obesity is fat accumulation, including hyperplasia (increase in number) and hypertrophy (increase in size). After histological staining, it is critical to accurately measure the number and size of adipocytes for assessing the severity of obesity in a timely fashion. Manual measurement is accurate but time-consuming. Although commercially available adipocyte counting tools, including AdipoCount, Image-Pro Plus, and ImageJ were helpful, limitations still exist in accuracy and time consuming. In the present study, we introduced the protocol of combined usage of these tools and illustrated the process with histological staining slides from adipose tissues of lean and obese mice. We found that the adipocyte sizes quantified by the tool combination were comparable as manual measurement, whereas the combined methods were more efficient. Besides, the recognition effect of monochrome segmentation image is better than that of color segmentation image. Overall, we developed a combination method to measure adipocyte sizes accurately and efficiently, which may be helpful for experimental process in laboratory and also for clinic diagnosis.

Keywords: adipocyte sizes, AdipoCount, Image-Pro Plus, ImageJ, obesity

INTRODUCTION

Obesity results from energy intake in excess of energy expenditure, and surplus energy is stored in adipocytes as a form of triglycerides, which results in adipocyte hyperplasia and hypertrophy (1, 2). When the capacity of adipocytes cannot meet the demand for lipid storage, excess lipids will be ectopically deposited in the muscles, liver, and pancreas, causing metabolic abnormalities, such as insulin resistance (3, 4). Therefore, quantification of the number and size of adipocytes is essential for assessing the severity of obesity and providing the reference for the choice of treatment (5).

As technology advances, image processing software have been developed for the measurement of adipocytes (6–8). ImageJ and Image-Pro Plus (IPP) are both the open-software platform image

processing tools for scientific image analysis and have been widely used in life sciences (9, 10). Area of interest (AOI) and measurement threshold of adipose tissue slides can be set to screen out objects that meet the requirements automatically (11, 12). However, because adipocytes are membrane-stained, and clear contrast or threshold is difficult to be set by these tools, the automatic counting of adipocyte sizes on adipose tissue slides may result in severe measurement errors. Meanwhile, drawing the adipocyte boundaries manually by IPP and ImageJ is accurate but time-consuming and intractable to large-scale investigations.

Researchers have been committed to developing software that can identify adipocytes accurately and efficiently (13, 14). However, these automatic methods may require programming knowledge or plug-ins, and the counting results also rely on slide quality, software recognition, so the accuracy is often unsatisfactory (15–18). Recently, a freely available counting software for adipocyte numbers, AdipoCount, is reported to be convenient and has powerful capability to recognize adipocyte boundaries and segment images with simple operations for further analysis (19). During our operation, we found that adipocytes with empty holes, cell debris, and cells adhesion edges may also be mistakenly counted by AdipoCount software. Besides, AdipoCount software lacks threshold settings and one-step area measurement function, thus the counting mistake could not be adjusted, and final results have to be calculated.

In the present study, we combined AdipoCount with IPP/ImageJ to measure the size of adipocytes while considering the following reasons: 1) IPP and ImageJ could not identify contours of adipocytes clearly but they could provide accurate results with clear segmentation and perform threshold setting to screen out unreasonable data; 2) AdipoCount could recognize adipocyte boundaries and export segmentation images, although without area measurement and threshold setting functions. Therefore, we took advantage of AdipoCount and IPP/ImageJ and designed the combination protocol for adipocyte sizes counting. By comparison of the combined method to manual method, we confirmed its accuracy and time saving characteristic, which suggested the advantage of applying AdipoCount and IPP/ImageJ combination for adipocyte size measurement.

MATERIALS AND METHODS

Animal Studies

Mouse studies were performed according to the guidelines of the East China Normal University Animal Care and Use Committee. C57BL/6J male mice, purchased from Shanghai Research Center for Model Organisms, were housed at 23 ± 1°C on a 12-h light/12-h dark cycle with free access to food and water. 8-week-old male mice (n=5 per group) were fed with normal chow diet (NCD) (Research Diet, D10012G) or high fat diet (HFD) (Research Diet, D12492). All mice were sacrificed 3 months later and epididymal fat (eWAT) and inguinal fat (iWAT) tissues were dissected for histological analysis.

Histology Processing and Image Capture

Adipose tissues were fixed in 10% buffered formalin for 12 h and dehydrated following a standard procedure. Then, the tissues were embedded in paraffin wax and sections (5-μm thick) were cut. Hematoxylin and eosin (H&E) staining was performed as previous report (17). Images were captured by a Nikon microscope instrument (MODEL ECLIPSE Ci-L) with a 20× objective using a Sony camera(DS-2000P, 20Mp 1" Color Sony Exmor CMOS SENSOR).

Software

A 32/64-bit operating system (Windows7-10) was required for the established protocol. AdipoCount (version 1.0), a free open access software (http://www.csbio.sjtu.edu.cn/bioinf/AdipoCount/), was used to segment the membranes of adipocytes. Image-Pro Plus (version 6.0.0.260, Media Cybernetics Corporation, USA) and ImageJ (version 1.52a, NIH, USA) were used as image analysis software. These softwares (AdipoCount, ImageJ, IPP) have good compatibility in Windows7-10 system.

Manual Measurement With IPP/ImageJ

IPP

Open Base Image

The image of interest was imported through "File → Open" option on the tool bar.

Set Scale

An image with a known linear scale bar was opened firstly. Image was calibrated by clicking on "Measure → Calibration → Spatial Calibration". In the pop-up window, "μm" was selected as unit, and "image" was clicked to show the "position line", which was dragged to make it completely coincide with the known linear scale bar. Subsequently, the known length of scale bar was input in the box to finish the calibration.

Measurement

The measurement scale was selected firstly through "Measure →Calibration → Select Spatial Calibration". The adipocyte areas were depicted manually using "Measure → Count/Size", then clicking "Edit → Draw/Merge Objects" in the tool bar of pop-up window. During the measurement, the image should be enlarged by 50%, which would make the segmentation results more accurate. In this process, the following objects were excluded: objects whose sizes were not in the range of 240 to 15,000 μm^2, cells adhesion edges, empty holes without clear structure, and cell debris.

"View → Measurement Data" was selected to show the measurement results.

ImageJ

Open Base Image

The image of interest was imported through "File → Open" option in the tool bar.

Set Scale

An image with a known linear scale bar was opened firstly. The "Straight line" tool was chosen in the tool bar to draw a line,

which was as long as the known linear scale bar. "Analyze → Set scale" option was clicked and the distance of known linear scale was displayed in the "Known distance" box of the "Set Scale" window. The pixel aspect ratio was set to 1. The known distance of the linear scale bar was entered into the "Known Distance" box. The unit was dependent on the scale bar (such as μm). The "Global" option was selected to maintain the calibration for all subsequent image analysis if all images were taken at the same magnification.

Subtract Background

To help clarify the image for subsequent analysis, the backgrounds of images were corrected. "Process → Subtract Background" was selected from the task bar. "Rolling Ball Radius" should be set to 50 pixels. "Light Background" and "Sliding Paraboloid" should be checked. When all of the parameters were set, "OK" was clicked.

Measurement

The image should also be enlarged by 50%. The "Wand" (tracing tool) in the tool bar was chosen to select the individual adipocytes. However, this tool could not identify adipocytes accurately sometimes. For example, partial membranes of adipocytes were lost. Then, the "Polygon Selection" tool was select from the task bar to depict the adipocyte areas. Every time when a cell was depicted, "M" was pressed in keyboard, and the selected area would be measured. To avoid repeated measurements, "Backspace" was pressed to mark the cells which had been counted. Above operations were repeated until the last cell. The exclusion criteria were the same as IPP measurement.

General Measurement (Identifying Adipocytes by IPP/ImageJ Directly)

IPP

Open Base Image and Set Scale

Same as described in "Manual measurement with IPP/ImageJ (2.4.1.)".

Threshold Images

"Count/Size" option was selected under "File" drop-down menu. In the "Count/Size" window, the "Manual → Select Ranges" was clicked to show segmentation menu. "Histogram Based" option was selected in segmentation menu. The "HSI" was selected. In "H" and "S" channels, the first and second sliding bars were set to 0 and 255 respectively. As for "I" channel, the first sliding bar was set to 0, the second sliding bar was set to make the red highlight maximally cover the areas defined as adipocytes without impact on the membrane areas.

Measurement

The threshold of area was set through "Measure → Select measurements" in the "Count/Size" window. The filter range of area was set starting from 240 μm^2 and ending at 15000 μm^2. "Apply Filter Ranges" option was selected to apply the settings. Clicking "Count", the software would measure the areas of objects.

ImageJ

Open Base Image, Set Scale, and Subtract Background

Same as described in "Manual measurement with IPP/ImageJ (2.4.2)".

Threshold Images

The images were converted into 8-bit using "Image → Type → 8-bit" option. Then the "Image → Adjust → Threshold" was selected from the tool bar. The first sliding bar was set to 0, the second sliding bar was set to make the red highlight maximally covering the areas defined as adipocytes without impact on the membrane areas.

Measurement

The areas were measured through "Analyze → Analyze Particles". In the pop-up window, the threshold of area, 240 to 15,000 μm^2, was input into "Size" box. The options of "Display results", "Exclude on edges" were selected. Clicking "OK", the software would detect the areas.

Adipocyte Boundary Segmentation by AdipoCount

The adipocytes were segmented by AdipoCount as previously described (19). Briefly, the image was imported through "File → Input image". The "Re-segment" option was selected to improve accuracy, and then "Process" button was clicked to get preliminary segmentation image (**Supplementary Figure 1B**). The segmentation results could be further corrected manually. Missing membrane segments were added and false membrane segments were deleted. Moreover, holes with large areas should be separated into several small holes by "Add line", then these small holes could be excluded in further detection through area threshold. Finally, two different segmentation images (monochrome and color) were exported by clicking "Counting → Save" in "Counting" box (**Supplementary Figures 1C, D**).

Combined Methods for Measurement

Combination Usage of AdipoCount and IPP

Open Images and Select Calibrated Scale Bar

The monochrome and color segmentation images exported by AdipoCount were imported into IPP and the measure scale was selected as described above.

Threshold Images

"Count/Size" option was selected under "File" drop-down menu. In the "Count/Size" window, the "Manual → Select Ranges" was clicked to show segmentation menu.

The next steps were slightly different about monochrome and color segmentation images. For monochrome segmentation images, the first sliding bar was set to 52 (this varied until the red highlight covered all the empty space defined as adipocytes), the second sliding bar was set to 255. For color segmentation images, "Histogram Based" option was selected in segmentation menu. The "HSI" was selected. In "H" and "S" channels, the first and second sliding bars were set to 0 and 255, respectively. As for "I" channel, the first sliding bar was set to 0, the second sliding bar was set to make the red highlight maximally

covering the areas defined as adipocytes without impact on the membrane areas.

Measurement

"Rectangular AOI" tool in task bar was selected to choose the area, which only contained intact cells. Then the "Options" was clicked, and "All Borders" was selected in "Clean Borders" box. In this way, the cells touching edge of the field would be excluded in next detections.

The threshold setting and the following operations were same as described in "General measurement (Identifying adipocytes by IPP/ImageJ directly) (2.5.1)".

Combination Usage of AdipoCount and ImageJ

Before measurement, the quality of the slices needs to be manually checked: the cell boundaries in the slices are clear and there are enough cells for the measurement. In this study, we ensured that the number of cells in each field was not less than 25.

Open Images and Set Scale

The monochrome and color segmentation images were imported into ImageJ and the measure scale was set as described above.

Threshold Images

The images were converted into 8-bit using "Image → Type → 8-bit" option. Then the "Image → Adjust → Threshold" was selected from the tool bar.

The next steps were slightly different about monochrome and color segmentation images. For monochrome segmentation images, the first sliding bar was set to 52 (this varied until the red highlight covered all the empty space defined as adipocytes), the second sliding bar was set to 255. For color segmentation images, the first sliding bar was set to 0, the second sliding bar was set to 240 (this varied to make the red highlight maximally covering the areas defined as adipocytes without impact on the membrane areas).

After these steps, membranes and adipocytes areas were filled by white and black respectively.

Measurement

To exclude the cells touching edge of the field, "Rectangle" tool in task bar was used to select the area, which only contained intact cells (the area of rectangle would change to contain all intact cells). The areas were measured through "Analyze → Analyze Particles". In the pop-up window, the threshold of area, 240-15000 μm^2, was input into "Size" box. The options of "Display results" and "Exclude on edges" were selected. Clicking "OK", the software would detect the areas.

The results would be presented in "Results" window.

Note: The Steps (2–3) could be automated by creating a macro. "Plugins → New → Macro" was selected and the computer script as following was pasted into a new screen. The new macro was saved by clicking "File → Save". Then the subsequent image analysis could be performed easily using the created macro by clicking "Plugins → Macros → Run".

The macro was different for monochrome and color segmentation images.

For monochrome segmentation images:

```
run("8-bit");
setAutoThreshold("Default");
//run("Threshold…");
setThreshold(52, 255);
run("Convert to Mask");
//setTool("rectangle");
makeRectangle(48, 32, 5336, 3552);
run("Analyze Particles…," "size=240-15000 show=[Bare Outlines] display exclude summarize add in_situ");
```

For color segmentation images:

```
run("8-bit");
setAutoThreshold("Default");
//run("Threshold…");
setThreshold(0, 240);
setOption("BlackBackground," false);
run("Convert to Mask");
//setTool("rectangle");
makeRectangle(48, 40, 5352, 3576);
run("Analyze Particles…," "size=240-15000 show=[Bare Outlines] display exclude summarize add in_situ");
```

Note: The area of "Rectangle" should be adjusted and recorded when size of image changes. Then this new area should be used in macro to replace the old one. By this way, the macro could work when the size of images changed.

Videos were made to describe the details of the combined methods (**Supplementary Video**).

Statistical Analysis

The number and size of adipocytes were measured by IPP or ImageJ. 2 slides were collected for each mouse, and 4 different fields were counted for each slide. Any objects with an area below 240 μm^2 or above 15000 μm^2 were excluded. In this study, the number of adipocytes for different tissues counted by each method was shown in **Supplementary Tables 1–4**. The frequency distribution of size was calculated from 240 to 15000 μm^2 (this range might change for different animal model and tissue) in 500 increments. The number of adipocytes within the distribution was counted and the result was transformed to a percentage of total adipocytes in each group. A Student *t* test was performed to compare between two groups. Two-way ANOVA followed by a Bonferroni *post hoc* analysis was used for multiple comparisons in Prism 8 (GraphPad Software Inc.).

RESULTS

General Measurement Results of IPP and ImageJ Are Not Accurate

In this study, two eWAT histological slides were selected to evaluate whether IPP or ImageJ could detect the area of

adipocytes accurately using general methods. H&E staining of eWAT was measured by manual and general methods respectively with IPP/ImageJ. As shown in **Figures 1A–D**, IPP and ImageJ could not identify and segment adipocytes accurately by themselves, compared with manual methods. In detail, there was no significant difference between manual measurement results of IPP and ImageJ (**Figure 1E**), whereas the area measured by general methods was significantly smaller than the manual measurement result (**Figures 1F, G**). These results indicated that the general methods of IPP and ImageJ were unable to measure the area of adipocytes accurately.

AdipoCount Cannot Recognize Empty Holes, Cell Debris, and Adhesion Edges

AdipoCount is a software designed for adipocyte counting, which is powerful to segment adipocyte and export the image, although it only gives numbers but not areas directly. Thus, we next examined whether dividing the total area of the eWAT image previously tested by the number of cells could get an accurate area. An original image was imported into AdipoCount (**Figure 2A**), and the segmentation image revealed that empty holes, cell debris, and adipocyte adhesion edges were counted mistakenly (**Figure 2B**). Because the software could not set the

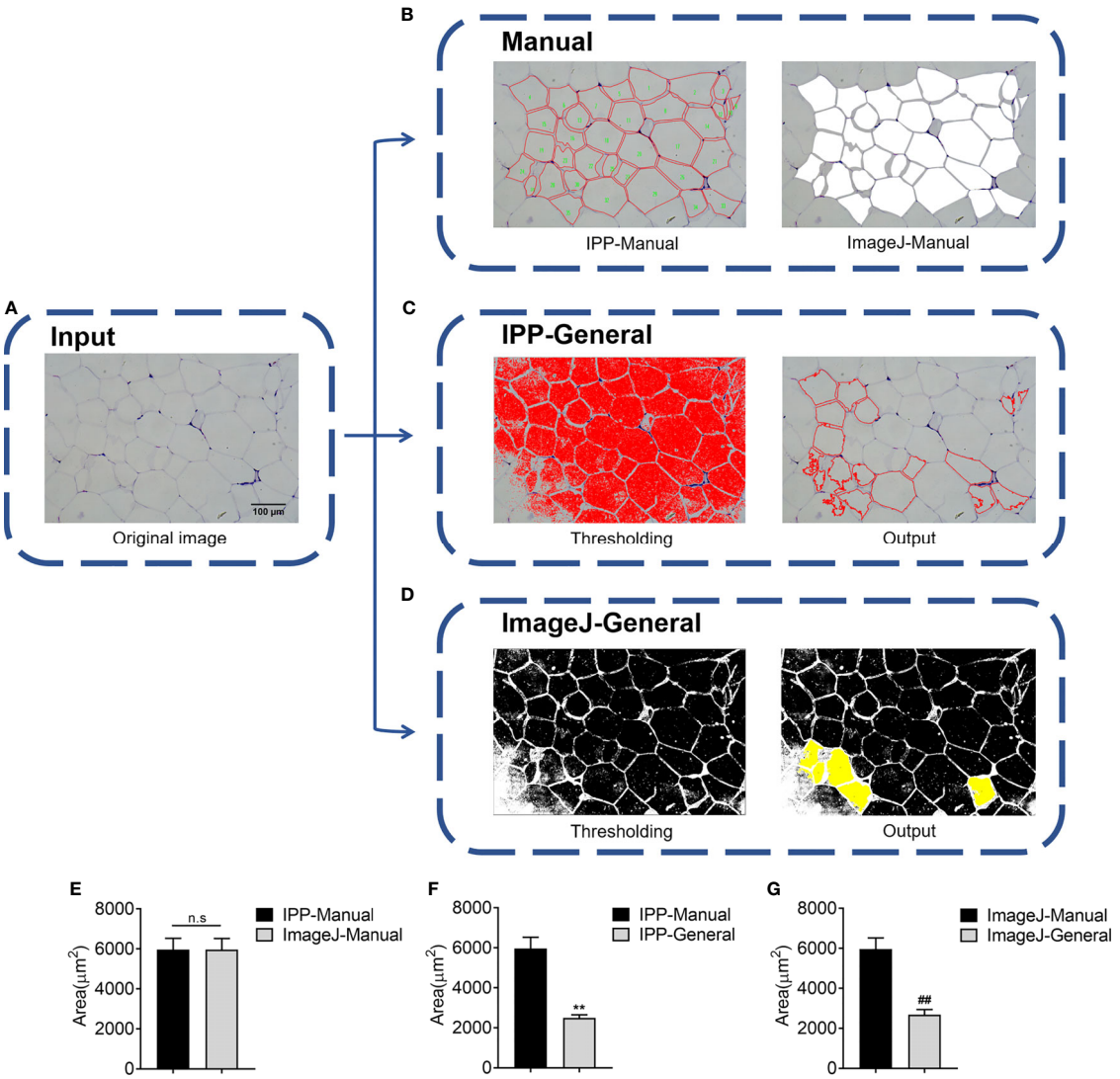

FIGURE 1 | Adipocyte sizes measured by manual and general methods respectively with IPP/ImageJ. **(A)** Original image of adipocytes. **(B)** Manual segmentation results of IPP (left) and ImageJ (right). **(C)** General segmentation results of IPP, the image after threshold adjustment (left), and the output image, where the red circles represented identified adipocytes (right). **(D)** General segmentation results of ImageJ, the image after threshold adjustment (left), and the output image, where the identified adipocytes were filled with yellow (right). **(E)** Adipocyte sizes measured by manual methods with IPP and ImageJ. **(F)** Adipocyte sizes measured by manual and general methods with IPP. **(G)** Adipocyte sizes measured by manual and general methods with ImageJ. Data are presented as mean ± SEM and $^{**}P < 0.01$ compared to IPP manual measurement group. $^{\#\#}P < 0.01$ compared to ImageJ manual measurement group. n.s., not significant; IPP, Image-Pro Plus.

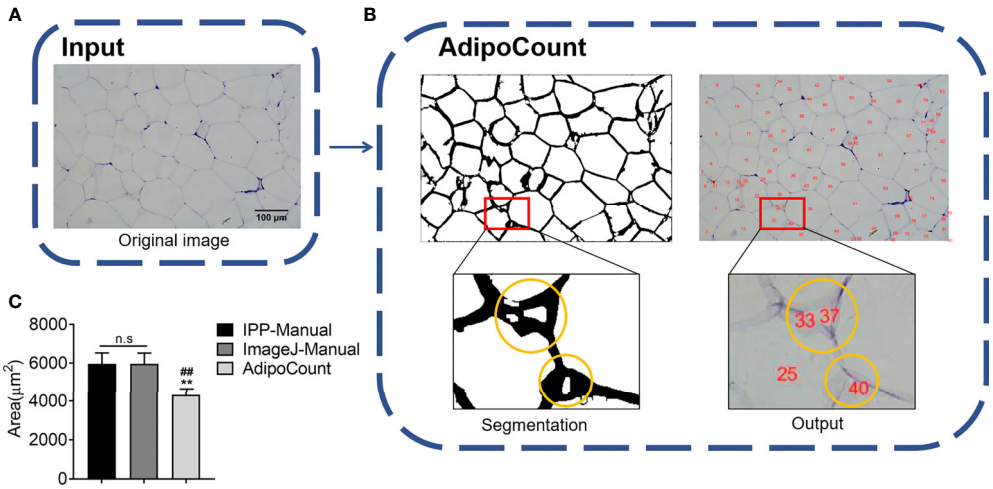

FIGURE 2 | AdipoCount cannot recognize empty holes, cell debris, and adhesion edges. **(A)** Original image of adipocytes. **(B)** The segmentation image of AdipoCount (left), and the labeled image with cell numbers (right); what in the yellow circles were cell debris or empty holes (left), which were counted as cells mistakenly by AdipoCount (right). **(C)** Adipocyte sizes measured by manual methods with IPP and ImageJ, or calculated with AdipoCount. Data are presented as mean ± SEM and $^{**}P < 0.01$ compared to IPP manual measurement group. $^{\#\#}P < 0.01$ compared to ImageJ manual measurement group. n.s., not significant; IPP, Image-Pro Plus.

threshold and manual calibration could not eliminate the errors, the counting number result was significantly more than the actual number. So, the adipocyte areas achieved was significantly underestimated (**Figure 2C**). These results suggested that there was still improvement space for AdipoCount to better calculate the adipocyte area.

Combination of AdipoCount and IPP/ImageJ Identifies and Segments Adipocytes Accurately

Via the above tests, we found that IPP/ImageJ could set the threshold and had the area measurement function, although the ability to recognize adipocyte boundaries was poor during general measurement. On the other hand, AdipoCount had no measurement functions and threshold settings, although it could segment adipocytes with a high accuracy. Indeed, a preliminary segmentation image was generated by AdipoCount, which could be further corrected manually (**Supplementary Figure 1B**). Besides, from two different segmentation images (monochrome and color segmentation image) exported from AdipoCount, we could clearly see that adipocytes had clear boundaries in both two segmentation images (**Supplementary Figures 1C, D**). In addition, the size of segmentation images exported by AdipoCount was same as the original image. Images analyzed by the different software remained their original size of 5440 × 3648 pixels, suggesting that AdipoCount processing did not compress the image, and the calibration scale of original image could be used for segmentation image.

We next imported both monochrome and color segmentation images into IPP and ImageJ to measure the adipocyte size. Of note, adipocytes in segmentation images could be identified accurately using general methods of IPP/ImageJ. Moreover, empty holes, cell debris, and adhesion edges were eliminated by setting threshold to area of interest (AOI) (**Figures 3A–C**). These results suggested that combination of AdipoCount and IPP/ImageJ might be a better method to measure the adipocyte sizes accurately.

The Combined Methods Can Measure the Area Accurately and Take Less Time

Next, manual methods and combined methods were performed to examine the adipocyte sizes in eWAT and iWAT of obese mice. The average adipocyte sizes and size distributions in eWAT measured by combined methods were comparable with the manual measurement results (**Figures 4A, C**). Besides, there were no obvious differences between the measurement results of monochrome and color segmentation images (**Figures 4A, C**). Of note, the combined methods could significantly save measurement time (**Figure 4B**). In addition, the measurement results in iWAT were similar as those in eWAT (**Figures 4D–F**).

Then, the combined methods were used to measure adipocyte sizes in eWAT and iWAT of lean mice. Similar to the results in obese mice, the combined methods could count the areas and size distributions accurately in lean mice, but saved time significantly (**Figures 5A–F**). Interestingly, we noticed that the manual measurement of ImageJ took more time than IPP, which was because of the different operating procedures of these two softwares (**Figures 5B, E**).

Very small adipocytes may lead to increased incidence of miscounting, thus we further analyzed the size distributions in range of 0 to 1000 μm^2. The results showed that the size distributions measured by the combined methods were comparable as the manual methods (**Supplementary Figures 2A–D**).

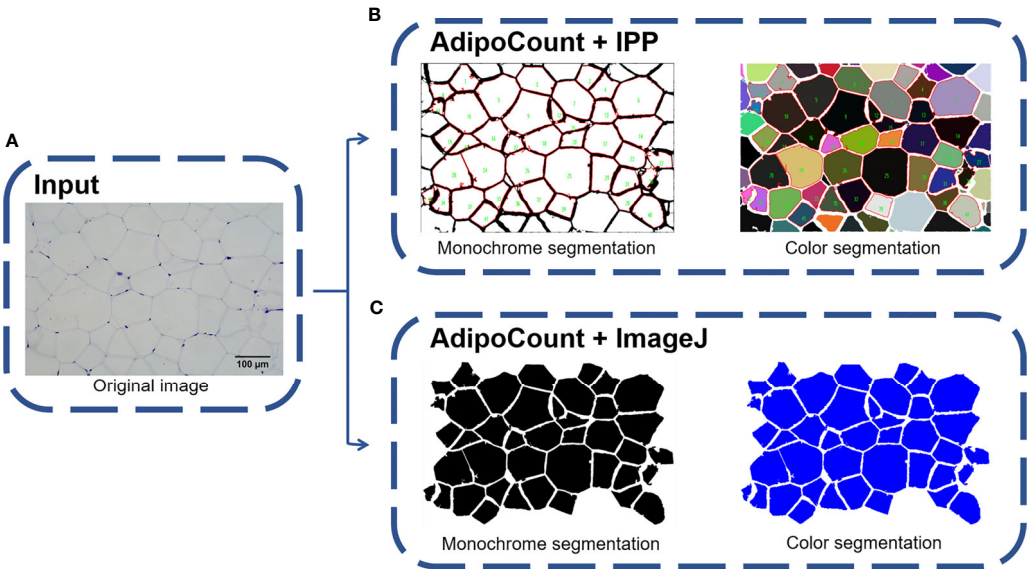

FIGURE 3 | Combination of AdipoCount and IPP/Image identifies adipose cells accurately. **(A)** Original image of adipocytes. **(B)** Combination of AdipoCount and IPP, the identification results of monochrome segmentation image (left), and color segmentation image (right). **(C)** Combination of AdipoCount and ImageJ, the identification results of monochrome segmentation image (left), and color segmentation image (right). IPP, Image-Pro Plus.

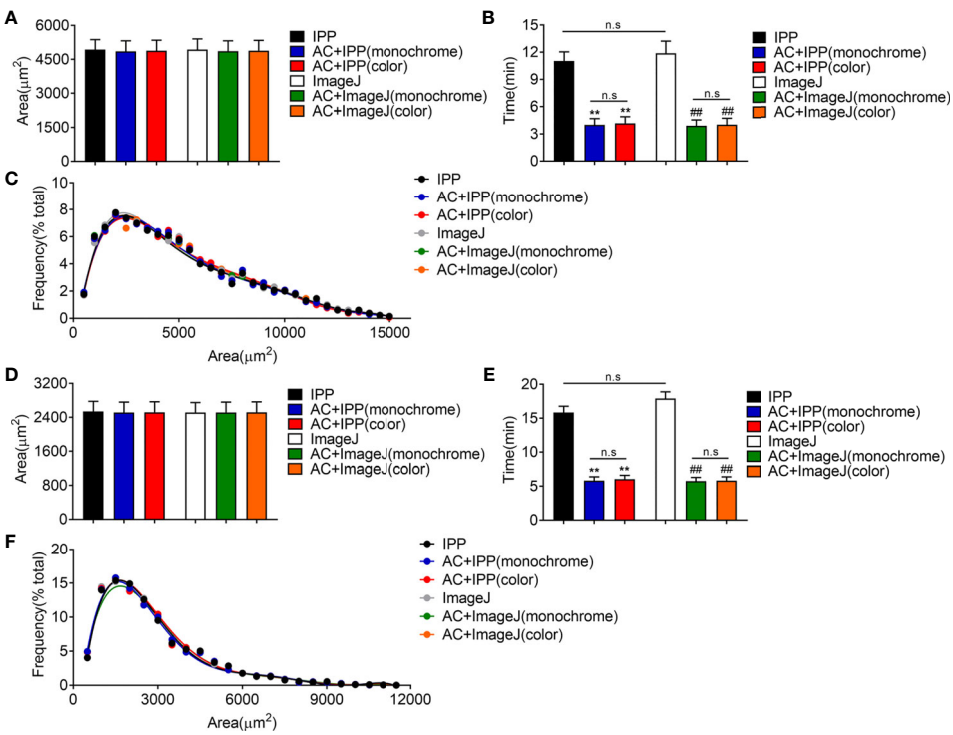

FIGURE 4 | The combined methods can measure the area accurately and take less time in eWAT and iWAT of obese mice. **(A–C)** The measurement results of eWAT, adipocyte sizes derived from manual and combined methods **(A)**, measurement time **(B)**, adipocyte size distributions measured by manual and combined methods **(C)**. **(D–F)** The measurement results of iWAT. Data are presented as mean ± SEM and $^{**}P < 0.01$ compared to IPP manual measurement group. $^{\#\#}P < 0.01$ compared to ImageJ manual measurement group. n.s., not significant; IPP, Image-Pro Plus; AC, AdipoCount.

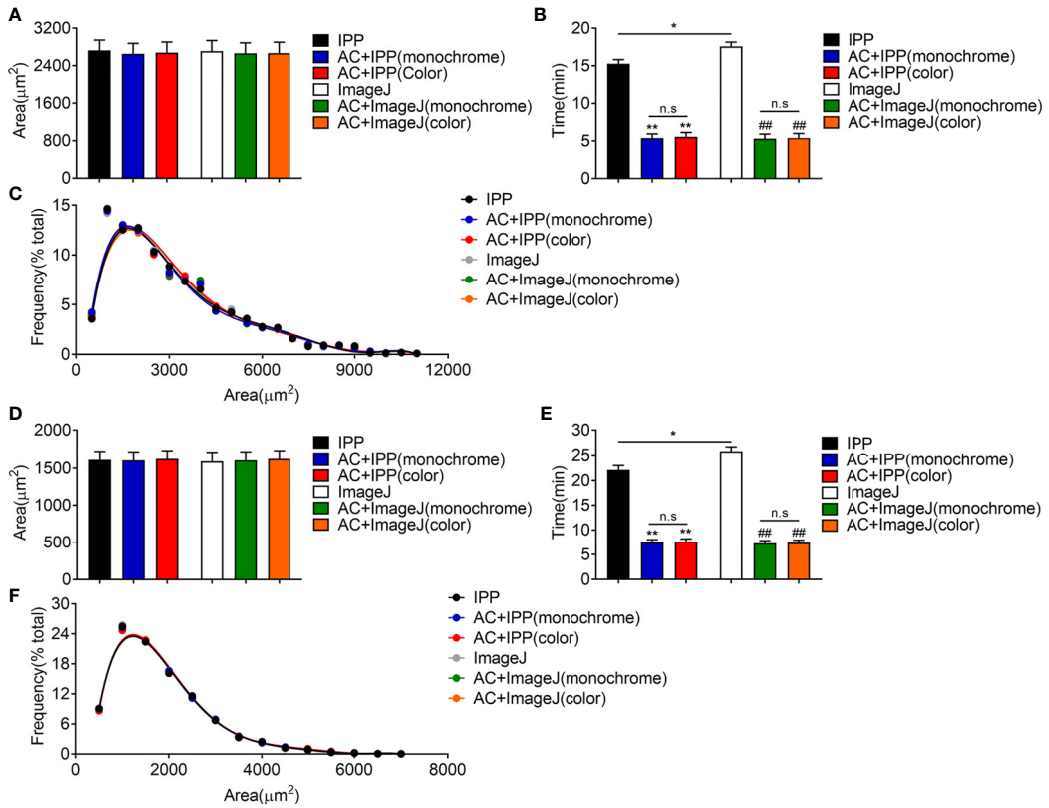

FIGURE 5 | The combined methods can measure the area accurately and take less time in eWAT and iWAT of lean mice. **(A–C)** The measurement results of eWAT, adipocyte sizes derived from manual and combined methods **(A)**, measurement time **(B)**, adipocyte size distributions measured by manual and combined methods **(C)**. **(D–F)** The measurement results of iWAT. Data are presented as mean ± SEM and $^{*}P < 0.05$, $^{**}P < 0.01$ compared to IPP manual measurement group. $^{\#\#}P < 0.01$ compared to ImageJ manual measurement group. n.s, no significant. IPP, Image-Pro Plus; AC, AdipoCount.

Limitation and Suggestion of the Combined Measurement

During the operation, we noticed that there were small adipocytes with the size close to the lower limit of threshold exclusion in iWAT of lean mice. The result of UCP-1 immunostaining indicated the small adipocytes might be caused by the process called "browning of white fat", which was important for lipid mobilization and thermogenesis (**Supplementary Figure 3**). These adipocytes were counted when using the manual measurement of IPP but excluded while the combined method was performed (**Figures 6A, B**), which might be due to the slight loss of area during segmentation by AdipoCount and the setting of the intensity thresholding. Of note, the combined measurement results were comparable to manual measurements, suggesting that individual cell misidentification had little effect on the overall result.

In a color segmentation image, if boundary between two adjacent adipocytes was thin and was filled with similar color, then the two adipocytes might be identified as one adipocyte in subsequent measurements. Although the area could be split in two manually, it would take more time. Thus, the monochrome segmentation image was better recognized and recommended (**Figures 6C, D**).

Adipocyte Counting by the Combined Methods Yields Comparable Data as Manual Methods But Is More Efficient

Finally, the combined methods using monochrome segmentation images were performed to measure the adipocyte sized in lean and obese mice. Both manual and combined methods identified a significant increase of adipocyte sizes and frequency of large adipocyte in fat tissues isolated from obese mice compared with lean mice (**Figures 7A–D**), with comparable area counting results, suggesting that the combined methods yielded the accurate results as manual methods with more efficiency.

CONCLUSION

The measurement of adipocyte sizes is important for obesity research. In the present study, we provided an easy and

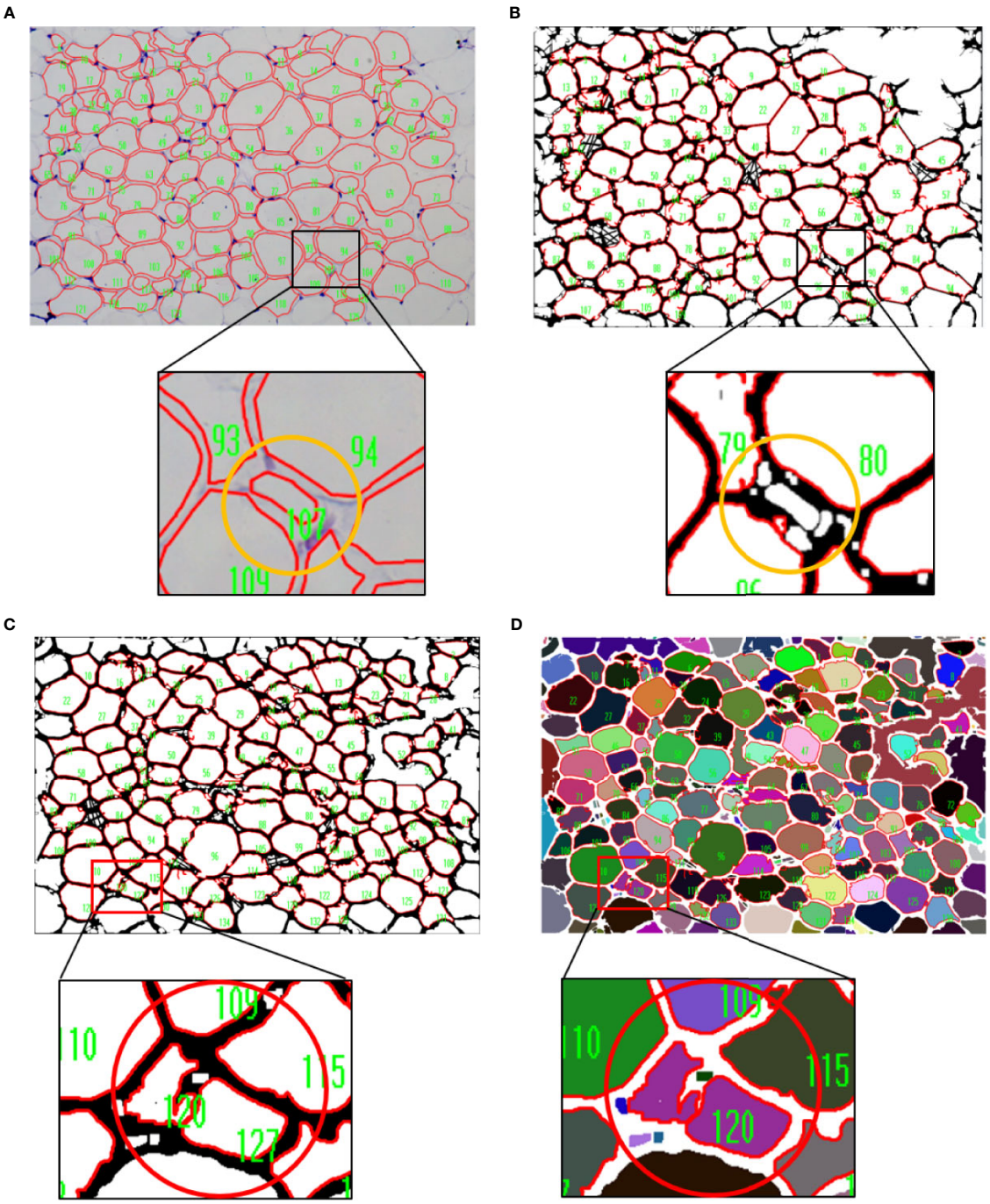

FIGURE 6 | Limitation of the combined measurement. **(A, B)** The results of manual and combined measurement. The cell numbered 107 in yellow circle was counted when using manual measurement **(A)**,whereas it was excluded when the combined method was performed **(B)**. **(C, D)** Comparison of measurement results of two different segmentation images. Two cells inside the red circle could be distinguished in monochrome segmentation image **(C)**, but not in color segmentation image **(D)**.

semiautomated method by taking advantage of AdipoCount and IPP/ImageJ software to accurately and efficiently quantify adipocyte sizes. Briefly, adipocytes from H&E staining slides are segmented by AdipoCount, and clear segmentation images are exported. IPP or ImageJ is then performed to analyze segmentation images with threshold setting and one-step quantification. It has to be noticed that the monochrome image is more accurate than colored one. For the simple operation protocol, no programming experience is

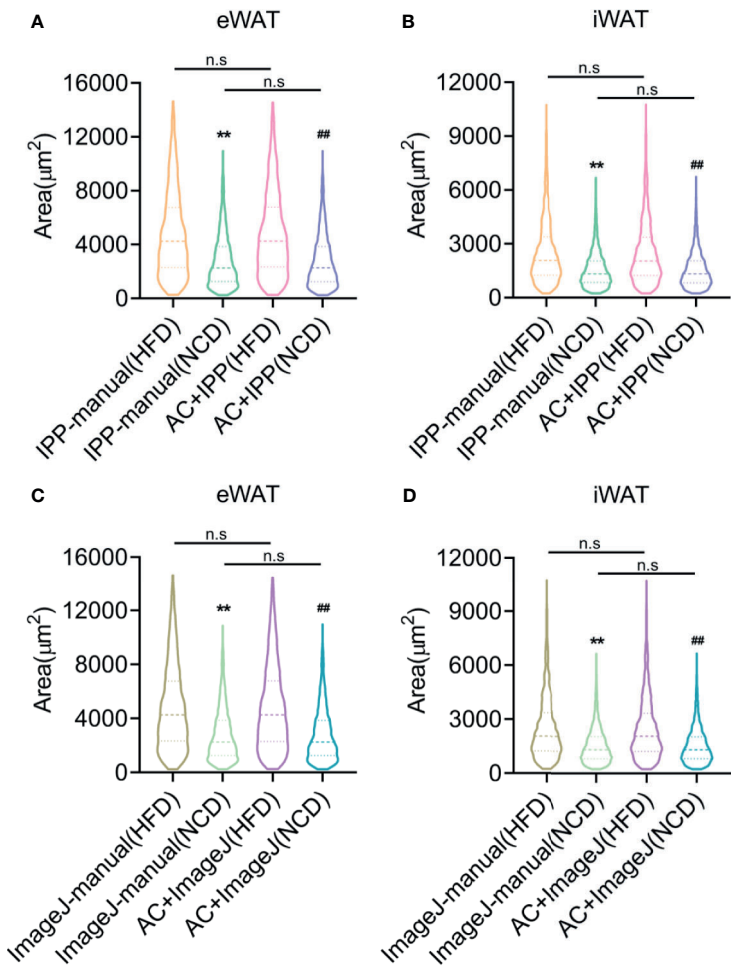

FIGURE 7 | Adipocyte counting by the combined methods yields comparable data as manual methods but saves more time. **(A, B)** Adipocyte sizes measured by manual methods with IPP and combined methods with IPP and AdipoCount, in eWAT **(A)** and iWAT **(B)**. **(C, D)** Adipocyte sizes measured by manual methods with ImageJ and combined methods with ImageJ and AdipoCount, in eWAT **(C)** and iWAT **(D)**. Data are presented as mean ± SEM and $^{**}P < 0.01$ compared to manual methods group. $^{\#\#}P < 0.01$ compared to combined methods group. n.s, no significant. IPP, Image-Pro Plus; AC, AdipoCount.

required. However, this method is not yet fully automated and still requires some manual manipulation, especially the manual correction of segmentation images from AdipoCount. The quality of slides, such as clear cell staining and complete membrane, is also important to get the accurate results, especially slides with small adipocytes. Further adjustment of the exclusion range and intensity threshold is required to improve the accuracy of the measurement. Theoretically, the combined method can be used for images with clear cell boundaries. More efforts will be made to explore whether this method can be applied besides adipocytes in the future.

DATA AVAILABILITY STATEMENT

The original contributions presented in the study are included in the article/**Supplementary Material**. Further inquiries can be directed to the corresponding authors.

ETHICS STATEMENT

The animal study was reviewed and approved by the East China Normal University Animal Care and Use Committee.

AUTHOR CONTRIBUTIONS

XG, FeixiaS and LX conceived the project and designed the experiments. YH and JY carried out most of the experiments. XCu, ZZ, QL, and WG assisted in histology processing and image capture. CZ, XCh, MM, and YL provided rodent biological samples for association analysis. MG, JQ, FeiS, DW, and XM assisted in software manipulation and technical support. XG, FeixiaS and LX wrote and edited the paper.

All authors contributed to the article and approved the submitted version.

FUNDING

This project is supported by fundings from Key Research and Development Project of Zhejiang Province (2021C03069), Natural Science Foundation of Zhejiang Province (LY20H070003), National Key Research and Development Program of China (2019YFA0904500), National Natural Science Foundation of China (31800989, 32071148, 81902980), and ECNU public platform for Innovation (011), the Instruments Sharing Platform of School of Life Sciences, East China Normal University.

REFERENCES

1. Ghaben AL, Scherer PE. Adipogenesis and Metabolic Health. *Nat Rev Mol Cell Biol* (2019) 20:242–58. doi: 10.1038/s41580-018-0093-z
2. Haczeyni F, Bell-Anderson KS, Farrell GC. Causes and Mechanisms of Adipocyte Enlargement and Adipose Expansion. *Obes Rev* (2018) 19:406–20. doi: 10.1111/obr.12646
3. Girousse A, Virtue S, Hart D, Vidal-Puig A, Murgatroyd PR, Mouisel E, et al. Surplus Fat Rapidly Increases Fat Oxidation and Insulin Resistance in Lipodystrophic Mice. *Mol Metab* (2018) 13:24–9. doi: 10.1016/j.molmet.2018.05.006
4. Karpe F, Dickmann JR, Frayn KN. Fatty Acids, Obesity, and Insulin Resistance: Time for a Reevaluation. *Diabetes* (2011) 60:2441–9. doi: 10.2337/db11-0425
5. Muir LA, Neeley CK, Meyer KA, Baker NA, Brosius AM, Washabaugh AR, et al. Adipose Tissue Fibrosis, Hypertrophy, and Hyperplasia: Correlations With Diabetes in Human Obesity. *Obes (Silver Spring)* (2016) 24:597–605. doi: 10.1002/oby.21377
6. Chen HC, Farese RVJr. Determination of Adipocyte Size by Computer Image Analysis. *J Lipid Res* (2002) 43:986–9. doi: 10.1016/S0022-2275(20)30474-0
7. Maguire AS, Woodie LN, Judd RL, Martin DR, Greene MW, Graff EC. Whole-Slide Image Analysis Outperforms Micrograph Acquisition for Adipocyte Size Quantification. *Adipocyte* (2020) 9:567–75. doi: 10.1080/21623945.2020.1823139
8. Wiggenhauser PS, Kuhlmann C, Blum J, Giunta RE, Schenck T. Influence of Software Parameters on Measurements in Automatized Image-Based Analysis of Fat Tissue Histology. *Acta Histochem* (2020) 122:151537. doi: 10.1016/j.acthis.2020.151537
9. Schindelin J, Rueden CT, Hiner MC, Eliceiri KW. The ImageJ Ecosystem: An Open Platform for Biomedical Image Analysis. *Mol Reprod Dev* (2015) 82:518–29. doi: 10.1002/mrd.22489
10. Mei Y, Tang Z, Li Z, Yang X. Repeatability and Reproducibility of Quantitative Corneal Shape Analysis After Orthokeratology Treatment Using Image-Pro Plus Software. *J Ophthalmol* (2016) 2016:1732476. doi: 10.1155/2016/1732476
11. Rawlinson A, Elcock C, Cheung A, Al-Buhairi A, Khanna S, Walsh TF, et al. An in-Vitro and in-Vivo Methodology Study of Alveolar Bone Measurement Using Extra-Oral Radiographic Alignment Apparatus, Image Pro-Plus Software and a Subtraction Programme. *J Dent* (2005) 33:781–8. doi: 10.1016/j.jdent.2005.01.013
12. Egan KP, Brennan TA, Pignolo RJ. Bone Histomorphometry Using Free and Commonly Available Software. *Histopathology* (2012) 61:1168–73. doi: 10.1111/j.1365-2559.2012.04333.x
13. Mersmann HJ, MacNeil MD. Variables in Estimation of Adipocyte Size and Number With a Particle Counter. *J Anim Sci* (1986) 62:980–91. doi: 10.2527/jas1986.624980x
14. Hassanlou L, Meshgini S, Alizadeh E. Evaluating Adipocyte Differentiation of Bone Marrow-Derived Mesenchymal Stem Cells by a Deep Learning Method for Automatic Lipid Droplet Counting. *Comput Biol Med* (2019) 112:103365. doi: 10.1016/j.compbiomed.2019.103365
15. Stern MP, Conrad F. An Automated, Direct Method for Measuring Adipocyte Cell Size. *Clin Chim Acta* (1975) 65:29–37. doi: 10.1016/0009-8981(75)90331-9
16. Lee JH, Kirkham JC, McCormack MC, Medina MA, Nicholls AM, Randolph MA, et al. A Novel Approach to Adipocyte Analysis. *Plast Reconstr Surg* (2012) 129:380–7. doi: 10.1097/PRS.0b013e31823aea29
17. Parlee SD, Lentz SI, Mori H, MacDougald OA. Quantifying Size and Number of Adipocytes in Adipose Tissue. *Methods Enzymol* (2014) 537:93–122. doi: 10.1016/B978-0-12-411619-1.00006-9
18. Osman OS, Selway JL, Kępczyńska MA, Stocker CJ, O'Dowd JF, Cawthorne MA, et al. A Novel Automated Image Analysis Method for Accurate Adipocyte Quantification. *Adipocyte* (2013) 2:160–4. doi: 10.4161/adip.24652
19. Zhi X, Wang J, Lu P, Jia J, Shen HB, Ning G. AdipoCount: A New Software for Automatic Adipocyte Counting. *Front Physiol* (2018) 9:85. doi: 10.3389/fphys.2018.00085

SUPPLEMENTARY MATERIAL

The Supplementary Material for this article can be found online at: https://www.frontiersin.org/articles/10.3389/fendo.2021.642000/full#supplementary-material

Supplementary Figure 1 | Two different segmentation images of AdipoCount. **(A)** Original image of adipocytes. **(B)** Preliminary segmentation image without correction. **(C)** Monochrome segmentation image after correction. **(D)** Color segmentation image after correction.

Supplementary Figure 2 | The combined methods measured the size of very small adipocyte accurately. **(A-D)** The size distributions of adipocytes (range of 240-1000μm2, in 100 increments) measured by manual and combined methods, in eWAT of obese mice **(A)**, in iWAT of obese mice **(B)**, in eWAT of lean mice **(C)**, in iWAT of lean mice **(D)** IPP, Image-Pro Plus; AC, AdipoCount.

Supplementary Figure 3 | UCP-1 immunostaining of iWAT in lean mice.

Conflict of Interest: The authors declare that the research was conducted in the absence of any commercial or financial relationships that could be construed as a potential conflict of interest.

Publisher's Note: All claims expressed in this article are solely those of the authors and do not necessarily represent those of their affiliated organizations, or those of the publisher, the editors and the reviewers. Any product that may be evaluated in this article, or claim that may be made by its manufacturer, is not guaranteed or endorsed by the publisher.

frontiers in Endocrinology

ORIGINAL RESEARCH
published: 28 September 2021
doi: 10.3389/fendo.2021.739021

Role of Ubiquilins for Brown Adipocyte Proteostasis and Thermogenesis

Carolin Muley[1], *Stefan Kotschi*[1] *and Alexander Bartelt*[1,2,3,4]*

[1] Institute for Cardiovascular Prevention (IPEK), Ludwig-Maximilians-University, Munich, Germany, [2] German Center for Cardiovascular Research, Partner Site Munich Heart Alliance, Technische Universität München, Munich, Germany, [3] Institute for Diabetes and Cancer (IDC), Helmholtz Center Munich, German Research Center for Environmental Health, Neuherberg, Germany, [4] Department of Molecular Metabolism & Sabri Ülker Center, Harvard T.H. Chan School of Public Health, Boston, MA, United States

The acclimatization of brown adipose tissue (BAT) to sustained cold exposure requires an adaptive increase in proteasomal protein quality control. Ubiquilins represent a recently identified family of shuttle proteins with versatile functions in protein degradation, such as facilitating substrate targeting and proteasomal degradation. However, whether ubiquilins participate in brown adipocyte function has not been investigated so far. Here, we determine the role of ubiquilins for proteostasis and non-shivering thermogenesis in brown adipocytes. We found that *Ubqln1, 2* and *4* are highly expressed in BAT and their expression was induced by cold and proteasomal inhibition. Surprisingly, silencing of ubiquilin gene expression (one or multiple in combinations) did not lead to aggravated ER stress or inflammation. Moreover, ubiquitin level and proteasomal activity under basal conditions were not impacted by loss of ubiquilins. Also, non-shivering thermogenesis measured by norepinephrine-induced respiration remained intact after loss of ubiquilins. In conclusion, ubiquilin proteins are highly abundant in BAT and regulated by cold, but they are dispensable for brown adipocyte proteostasis and thermogenesis.

Keywords: ubiquilins, brown adipose tissue, cold adaptation, thermogenesis, proteostasis, ubiquitin-proteasome-system

OPEN ACCESS

Edited by:
Xinran Ma,
East China Normal University, China

Reviewed by:
Craig Porter,
University of Arkansas for Medical Sciences, United States
Tao Nie,
Jinan University, China

***Correspondence:**
Alexander Bartelt
alexander.bartelt@med.uni-muenchen.de

Specialty section:
This article was submitted to Cellular Endocrinology, a section of the journal Frontiers in Endocrinology

Received: *09 July 2021*
Accepted: *14 September 2021*
Published: *28 September 2021*

Citation:
Muley C, Kotschi S and Bartelt A (2021) Role of Ubiquilins for Brown Adipocyte Proteostasis and Thermogenesis. Front. Endocrinol. 12:739021. doi: 10.3389/fendo.2021.739021

INTRODUCTION

Brown adipose tissue (BAT) is a unique organ that transforms chemical energy from nutrients into heat in response to cold, a process called non-shivering thermogenesis (NST) (1). While acute cold exposure activates the existing thermogenic potential, sustained cold induces the recruitment of thermogenic capacity. This process of cold adaptation requires tremendous remodeling of the cells and tissue, which involves both differentiation of new thermogenic adipocytes and increasing metabolic activity of the existing ones (1). Paradoxically, despite the catabolic nature of NST, long-term adaptation to cold is an anabolic process that involves enhanced *de novo* synthesis of lipids, proteins and organelles (2). Brown adipocytes engage protein quality control mechanisms to

Abbreviations: BAT, Brown adipose tissue; GWAT, Gonadal white adipose tissue; imBAT, Immortalized brown pre-adipocyte cell line; NST, Non-shivering thermogenesis; SCAT, Subcutaneous adipose tissue; UBA, Ubiquitin-associated domain; UBL, Ubiquitin-like domain; WAT, White adipose tissue.

maintain cellular homeostasis under these stressful metabolic conditions (3) and we have demonstrated that NST requires an adaptive increase in proteasomal activity (4). The increase in transcription of proteasomal subunits was regulated by the ER-localized transcription factor nuclear factor erythroid 2–like 1 (Nfe2l1, also known as Nrf1 or TCF11). Interestingly, even in light of increased proteasomal protein degradation, cold adaptation resulted in enhanced protein ubiquitination (4), suggesting that the overall set point of the ubiquitin-proteasome system (UPS) is shifted in BAT after cold acclimatization. This probably also involves the machinery and regulators of ubiquitination itself.

The family of ubiquilin (*Ubqln*) proteins has recently emerged as versatile components of protein quality control. Ubiquilins are shuttle proteins that assist protein folding as chaperones, as well as facilitate degradation of ubiquitinated substrates through the UPS, endoplasmic reticulum-associated protein degradation (ERAD), and autophagy (5–7). To this date, five mammalian ubiquilins have been identified, 1, 2, 3, 4 and L, of which *Ubqln3* and *UbqlnL* are exclusively found in the testis (8, 9). *Ubqln1*, *2* and *4* are known to share a similar domain structure, which comprises a carboxy-terminal Ubiquitin-associated domain (UBA), heat-shock-chaperonin-binding motifs and an amino-terminal Ubiquitin-like domain (UBL). The UBA-UBL construct enables the interaction of ubiquilins with ubiquitinated proteins and the proteasome, which allows them to act as multifaceted adaptor molecules (10).

Based on the dynamic nature of UPS regulation in BAT during cold adaptation, it is likely that there are additional mechanisms supporting the function of Nfe2l1. In that vein, the role of ubiquilins in BAT has not been investigated so far. We hypothesized that Ubiquilins, with their function of targeting ubiquitinated proteins and facilitating their degradation by the UPS, could play a significant role in maintaining proteostasis in brown adipocytes. Here we investigate the role of ubiquilins for proteostasis and NST in immortalized and primary brown adipocytes.

MATERIAL & METHODS

Mice

All animal experiments were performed according to procedures approved by the animal welfare committees of the government of Upper Bavaria, Germany (ROB-55.2-2532.Vet_02-20-32) and performed in compliance with German Animal Welfare Laws. Animals were housed in individually ventilated cages at room temperature (22°C) with a 12-h light–dark cycle. All mouse housing and husbandry occurred on standard chow diet (Ssniff). We used 12 weeks old C57BL/6J (Janvier) wild-type mice, which we housed at 30°C for 7 days for thermoneutral acclimatization. For cold exposure and cold adaptation, mice were housed at 4°C for 24 h and 1 week, respectively.

Cell Culture and Treatments

We used an immortalized brown preadipocyte cell line (imBAT) (11), which we differentiated into mature brown adipocytes *in vitro*. The cells were induced at confluence for 2 days and differentiated for 2 days followed by 1 day of cultivation in standard medium [DMEM GlutaMax (Gibco), 10% fetal bovine serum (Sigma-Aldrich), 1% penicillin-streptomycin (Sigma-Aldrich)]. For induction the standard medium was supplemented with 850 nM human insulin (Sigma-Aldrich), 1 µM dexamethasone (Sigma-Aldrich, in 100% ethanol), 1 µM T3 (Sigma-Aldrich, in 1 M NaOH), 1 µM rosiglitazone (Cayman Chemicals, in 100% DMSO), 500 nM IBMX (Sigma-Aldrich, in 100% DMSO) and 125 nM indomethacin (Sigma-Aldrich, in 100% ethanol). The differentiation medium contained 1 µM T3 and 1 µM rosiglitazone. All treatments were performed on the 5th day of differentiation. Proteasome inhibitors bortezomib (Selleckchem), epoxomicin (Millipore) and MG-132 (Calbiochem) were used at 100 nM in 100% DMSO and incubated for 6 h. For β3-adrenergic stimulation, cells were treated with 1 µM CL316,243 (Tocris, in distilled H_2O) for 6 h.

Primary Cell Preparation and Culture

For primary cell experiments, mature adipocytes were differentiated from preadipocytes, isolated from the stromal-vascular fraction of adipose tissue of 4 weeks old C57BL/6J (Janvier) wild-type mice. The mice were sacrificed by cervical dislocation, the respective adipose tissues were harvested and pooled. The tissues were minced, weighted and digested in DMEM/F-12 (Sigma-Aldrich), 1% PenStrep (Sigma-Aldrich), 15 mg/mL fatty acid free BSA (Sigma-Aldrich), 1 mg/mL collagenase type 2 (Worthington) and 0.1 mg/mL DNase 1 (Roche) for 30 – 45 min at 37°C. For BAT, the digestion mix was supplemented with 1.2 U/mL Dispase (Roche). The digestion was stopped by adding DMEM/F-12 (+10% FBS, +1% PenStrep) in a 1:5 ratio. The digest was filtered through a 100 µm strainer and centrifuged at room temperature for 10 min at 500 xg. The mature adipocyte and the supernatant were aspirated, the pellet suspended in DMEM/F-12 (+10% FBS, +1% PenStrep) and filtered through a 70 µm strainer. After another centrifugation step at room temperature for 10 min at 500 xg, the pellet was again suspended in DMEM/F-12 (+10% FBS, +1% PenStrep), filtered through a 30 µm strainer and eventually plated in T75 flasks. The medium was changed the next day, to remove debris from the digestion and then every other day until the cells reached confluency. To differentiate the preadipocytes into mature adipocytes, cells were induced for 2 days and differentiated for 2 days followed by 1 day cultivation in standard medium. The induction medium consisted of DMEM/F-12 (+10% FBS, +1% PenStrep) supplemented with 340 nM human insulin (Sigma-Aldrich), 1 µM dexamethasone (Sigma-Aldrich, in 100% ethanol), 1 µM T3 (Sigma-Aldrich, in 1 M NaOH), 1 µM rosiglitazone (Cayman Chemicals, in 100% DMSO), 500 nM IBMX (Sigma-Aldrich, in 100% DMSO). The differentiation medium for white adipocytes from gonadal white adipose tissue (GWAT) consisted of DMEM/F-12 (+10% FBS, +1% PenStrep) with 10 nM human insulin and 2 µM T3. For beige and brown adipocytes from subcutaneous adipose tissue (SCAT) and BAT, respectively, DMEM/F-12 (+10% FBS, +1% PenStrep) was supplemented with 10 nM human insulin, 2 µM T3 and 1 µM rosiglitazone.

Reverse Transfection and RNAi

For RNA interference experiments, we reverse transfected imBAT and primary brown adipocytes with SMARTpool siRNA (Dharmacon) on the 3rd day of differentiation. Lipofectamine™ RNAiMAX transfection reagent (Thermo Fisher Scientific) was used according to manufacturer's instructions. SMARTpool siRNAs for *Nfe2l1*, *Ubqln1, 2* and *4* were used in a final concentration of 30 nM for single knockdowns. For double and triple knockdown of *Ubqln1*, *2* and *4* SMARTpool siRNAs were mixed in an equimolar ratio with final concentrations of 60 nM and 90 nM, respectively. After 24 h the transfection mix was replaced with the standard medium and the cells were incubated for another 24 h, after which we treated or directly harvested them.

RNA Extraction, cDNA Synthesis and RT-qPCR

To extract total RNA from frozen adipose tissue and cells we used the NucleoSpin® RNA kit (Macherey-Nagel) according to the manufacturer's instructions. RNA concentrations were measured on a NanoDrop spectrophotometer (Thermo Fisher Scientific). To synthesize complementary DNA (cDNA), we reverse-transcribed 500 ng RNA with the Maxima™ H Master Mix 5x (Thermo Fisher Scientific) in a total volume of 10 µl. cDNA was diluted 1:40 with RNase-free H_2O. Relative gene expression was quantified using quantitative real time-PCR. Each reaction contained 4 µL cDNA, 5 µL PowerUp™ SYBR Green Master Mix (Applied Biosystems) and 1 µL of 5 µM primer stock (full primer list in **Supplementary Table 1**). We used standard run conditions for Applied Biosystems SYBR Green Gene Expression Assays (2:00 min 50°C, 10:00 min 95°C, 40 cycles of 0:15 min 95°C, 1:00 min 60°C). Cycle thresholds (Cts) of genes of interest were normalized to *TATA-box binding protein (Tbp)* levels by the ΔΔCt-method and displayed as relative copies per *Tbp* or relative expression normalized to experimental control groups.

Oil Red O Staining

To visualize and quantify lipid content in adipocytes, we used Oil Red O staining. Confluent cells were harvested 48 h after transfection, washed once with DPBS and incubated with zinc formalin solution (Merck) for 5 min at room temperature. Afterwards, zinc formalin was replaced with fresh zinc formalin and the cells were fixed for 48 h at 4°C. Adipocytes were washed with 100% isopropanol and dried at 37°C. Cells were stained with 0.5 ml 60% vol/vol Oil Red O solution (Sigma), 40% vol/vol distilled H_2O for 1 h at room temperature and immediately washed 4x with distilled H_2O afterwards. Pictures from each well were taken with a digital camera as well as with a microscope at 200x magnification before ORO stain was eluted with 100% isopropanol and transferred into a clear 96-well plate. To quantify the staining, absorption of the eluates was measured at 500 nm on a Tecan plate reader. Absorption was normalized by subtracting the absorbance of 100% isopropanol and displayed as fold change to *Scramble*.

Extracellular Flux Analysis (Seahorse)

For extracellular flux analysis, we reverse transfected imBAT and plated them at 25,000 cells per well in a 24-well Seahorse plate in two independent experiments. To ensure even distribution, cells were seeded in 50 µl of medium and kept for 2 h at room temperature. Then, 175 µl medium were added, and the cells were allowed to fully attach at 37°C overnight. On the day before the experiment, Seahorse cartridges with the sensors were equilibrated in XF calibrant solution (Agilent) at 37°C in a non-CO2 chamber overnight. The experiment was performed on the 5th day of differentiation. Cells were treated with 100 nM bortezomib for 6 h or the corresponding amount of DMSO (Sigma-Aldrich) as a control treatment. XF DMEM pH 7.4 medium (Agilent) was supplemented fresh on the day of the experiment with 10 mM glucose, 1 mM pyruvate and 2 mM L-glutamine (Seahorse medium, all reagents from Agilent). Cells were carefully washed 2x with 1 ml Seahorse medium before incubating them with 500 µl of Seahorse medium for approximately 45 min at 37°C without CO_2. During the measurement norepinephrine (Sigma-Aldrich), oligomycin (Sigma-Aldrich), FCCP (Sigma-Aldrich) and rotenone–antimycin A (Sigma-Aldrich) were injected *via* the port of the Seahorse cartridge. Final concentrations were 1 µM norepinephrine (in 100% H_2O), 1 µM oligomycin, 4 µM FCCP and 0.5 µM rotenone–antimycin A (all in 100% DMSO). The protocol was 3 min mix, 2 min wait and 3 min measure for each time point. For normalization of respiration to live cell count, the cell plate was retrieved after the run, and we quantified the cell count using the CyQUANT® Cell Proliferation Assay Kit (Thermo Fisher Scientific) according to manufacturer's instructions.

Protein Extraction and Western Blotting

We lysed cells in RIPA buffer [150 mM NaCl (Merck), 5 mM EDTA (Merck), 50 mM Tris pH 8 (Merck), 0.1% wt/vol SDS (Carl Roth), 1% wt/vol IGEPAL® CA-630 (Sigma-Aldrich), 0.5% wt/vol sodium deoxycholate (Sigma-Aldrich)] freshly supplemented with protease inhibitors (Sigma-Aldrich) in a 1:100 ratio. The lysate was centrifuged at 4°C for 30 min at 21,000xg, to clear the lysate from debris and lipids. Protein concentrations were determined using the Pierce BCA Protein Assay (Thermo Fisher Scientific) according to the manufacturer's instructions. For western blotting, lysates were adjusted to a final concentration of 0.85 µg/µl in 1x Bolt™ LDS Sample buffer (Thermo Fisher Scientific) supplemented with 5% vol/vol 2-mercaptoethanol (Sigma-Aldrich). For SDS-PAGE we used Bolt™ 4–12% Bis-Tris gels (Thermo Fisher Scientific) with Bolt™ MOPS SDS running buffer. After separation, proteins were transferred onto a 0.2 µm PVDF membrane (Bio-Rad) using the Trans-Blot® Turbo™ system (Bio-Rad) at 12 V, 1.4 A for 16 min. The membrane was briefly stained with Ponceau S (Sigma-Aldrich) to verify successful transfer and blocked in 1x Roti-Block (Carl Roth) for 1 h at room temperature. Primary antibodies (Cell signaling) were used in a 1:1,000 ratio in 1x Roti-Block overnight at 4°C. After washing 4× for 10 min with TBS-T (200 mM Tris (Merck), 1.36 mM NaCl (Merck), 0.1% vol/vol Tween 20 (Sigma)), secondary antibodies (Santa Cruz) were applied in a 1:10,000 ratio in Roti-Block for 1 h at room temperature. Then membranes were washed again 3× for 10 min in TBS-T and developed using SuperSignal West Pico PLUS Chemiluminescent Substrate (Thermo Fisher Scientific) and a Chemidoc imager (Bio-Rad). We analyzed the digital images

with the Image Lab software (Bio-Rad). Uncropped images can be found in (**Supplementary Figure 1**).

Proteasomal Activity Assay

For the proteasomal activity assay, we lysed cells with a buffer containing 40 mM TRIS pH 7.2 (Merck), 50 mM NaCl (Merck), 5 mM $MgCl_2$(hexahydrate) (Merck) and 10% vol/vol glycerol (Sigma-Aldrich) freshly supplemented with 2 mM β-mercaptoethanol (Sigma-Aldrich) and 2 mM ATP (Sigma-Aldrich). To measure chemotrypsin-like, trypsin-like and caspase-like activity, we used the Proteasome Activity Fluorometric Assay (UBP Bio) according to the manufacturer's instructions. For the normalization of proteasomal activity to total protein content, we used the Bio-Rad Protein Assay Kit II to determine protein concentration in our samples.

Statistics

Data were expressed as the mean ± standard error of the mean (SEM). For comparing three and more groups we used one-way ANOVA with Bonferroni post-hoc test as indicated in the figure legends. For comparing two variables we used two-way ANOVA with Bonferroni post-hoc test. Analysis was performed using R, Microsoft Excel and/or GraphPad Prism. $P < 0.05$ was considered significant, as indicated by asterisks and letters in the figures legends.

RESULTS

Ubqln1 Is Expressed in Adipose Tissue and Induced by Cold and Proteasome Inhibition

As nothing is known about ubiquilins in BAT, we first investigated their gene expression levels in primary and immortalized adipocytes as well as in BAT ex vivo and second how these are impacted by cold and proteasome inhibition. In primary cells from intrascapular brown, inguinal subcutaneous and gonadal white adipose tissue (WAT), *Ubqln1, 2* and *4* expression was found to be expressed whereas *Ubqln3* was undetectable (**Figure 1A**). *Ubqln2* and *Ubqln4* were expressed at similar levels in all three adipocyte types. Interestingly, *Ubqln1* was approximately higher expressed compared to *Ubqln2* and *4* with highest expression in adipocytes from the subcutaneous WAT. In BAT from 12-week-old mice, which were kept at 4°C for 24 h (cold exposure) and 7 days (cold adaptation), we found that *Ubqln1* and *Ubqln4* expression was higher compared to mice kept at 30°C (thermoneutrality) (**Figure 1B**). We confirmed that the cold challenge was successful by increased expression of thermogenic markers *Ucp1* and *Ppargc1a* (**Supplementary Figures 2A, B**). Compared to primary brown adipocytes, we found a similar expression pattern in imBAT, which remained unchanged upon stimulation with beta3-agonist CL316,243 (**Figure 1C**). Proteasome inhibition with epoxomicin, MG132 or bortezomib respectively, resulted in higher *Ubqln1* expression compared to DMSO treated controls (**Figure 1D**). We were unable to detect *Ubqln3* mRNA in any of our samples, which is in line with a previous report that *Ubqln3* is specific to testis (9). Thus, *Ubqln1, 2* and *4* are expressed in adipose tissue, yet only *Ubqln1* is positively regulated by cold and proteasome inhibition.

Silencing of *Ubqln1*, *2* and *4* Does Not Cause ER Stress or Inflammation

Next, we determined the significance of ubiquilins in brown adipocyte homeostasis. We used RNA interference to silence the gene expression of *Ubqln1, 2* and *4* in immortalized and primary adipocytes to investigate their functional relevance. We explored established surrogate markers of stress responses and adipocyte function linked to BAT proteostasis (4). While our RNAi strategy was efficient, knockdown of any of the *Ubqln* genes did not result in changes in the mRNA expression of surrogate stress markers, *Ddit3* and *Ccl2* (**Figures 2A, B**). Knockdown of *Ubqln2* resulted in lower *Adipoq* expression in both immortalized and primary brown adipocytes, which suggests that adipocyte health is affected under these conditions. Since *Ubqln1, 2* and *4* share the same domain structure and their sequences are highly similar, we hypothesized that they could compensate for each other (12). This was also supported by upregulation of *Ubqln2* after knockdown of *Ubqln1* in primary brown adipocytes (**Figure 2B**). To circumvent this effect, we studied all possible combinations of *Ubqln1, 2* and *4* siRNAs in single, double and triple *Ubqln* knockdown experiments in imBAT (**Figure 2C**). This resulted in lower *Adipoq* expression in conditions with *Ubqln2* knockdown compared to the control cells (**Figure 2D**). *Ddit3* and *Ccl2* expression remained largely unaffected. Hence, loss of *Ubqln1, 2* or *4* did not increase ER stress or inflammation marker genes, alone or in combination.

Silencing of Ubiquilins Does Not Impair Adipocyte Health and Non-Shivering Thermogenesis

As we observed a reduction in *Adipoq* mRNA levels in both immortalized and primary brown adipocytes, we next investigated how loss of ubiquilins impacts adipocyte health. To our surprise, the expression levels of other adipocyte marker genes such as *Pparg*, *Plin1*, *Fabp4*, *Fasn* and *Cebpa* remained unchanged by *Ubqln* single or triple knockdown (**Figure 3A**. However, compared to the control cells we observed a lower lipid content in imBAT (**Figures 3B, C** and **Supplementary Figure 3**). Next, we investigated if loss of ubiquilins impacts NST. We analyzed norepinephrine-induced respiration and mitochondrial stress tests as the gold standard of measuring NST in cells. Neither single nor triple knockdown affected basal cellular respiration, the response to norepinephrine stimulation or maximal respiratory capacity (**Figures 3D, E**). To investigate if ubiquilins participate in the coordinated cellular response to proteasome inhibition, which has been shown to impair mitochondrial function in brown adipocytes (4), we treated imBAT cells with the compound bortezomib. While pretreatment with bortezomib led to lower levels of respiration, this response was independent of single or triple knockdown of ubiquilins (**Figures 3F, G**).

Ubiquilins Are Dispensable for Proteostasis in Brown Adipocytes

As we found that *Ubqln1* expression in brown adipocytes is strongly induced by proteasome inhibition, we hypothesized that Ubiquilins are involved in maintaining proteostasis. Indeed, knockdown of *Ubqln1, 2* and *4* resulted in higher *Atf3* gene expression, albeit the effect was small but significant

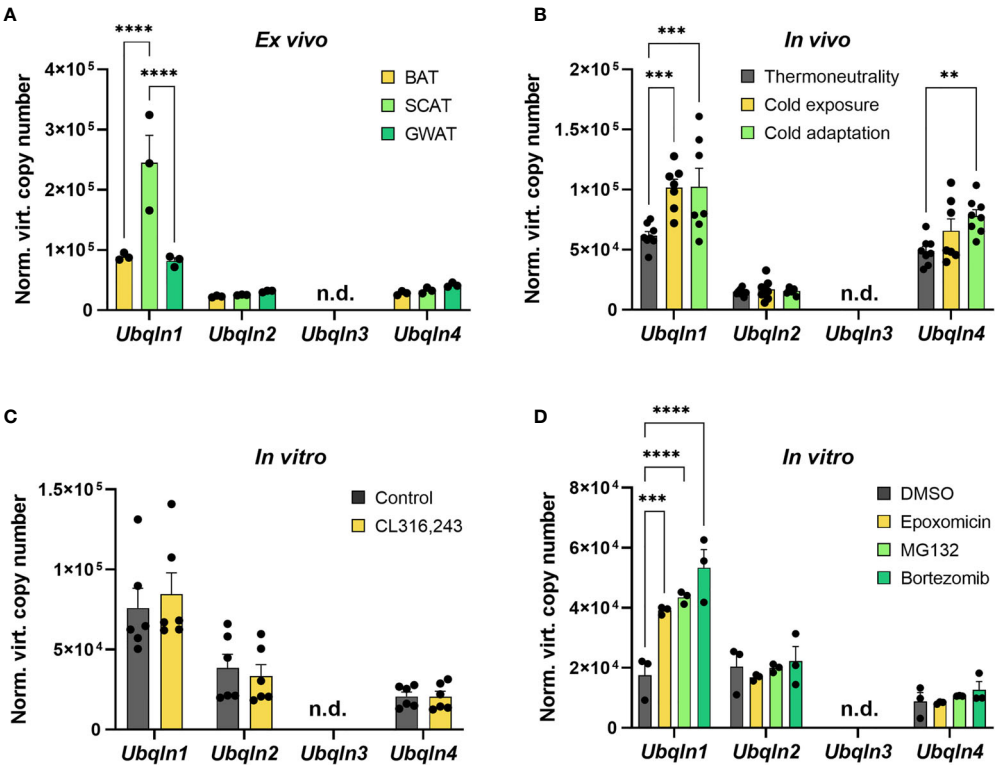

FIGURE 1 | *Ubqln1* is highly expressed in adipose tissue and induced by cold & proteasome inhibition. Absolute mRNA expression calculated from Ct values of *Ubqln1*, *Ubqln2, Ubqln3* & *Ubqln4* in **(A)** Primary adipocytes from BAT, SCAT & GWAT (n = 3 technical replicates). **(B)**, BAT from mice kept at 30°C for 7 days (thermoneutrality), 4°C for 24 h (cold exposure) and 4°C for 7 days (cold adaptation) (n = 8 biological replicates). **(C)** imBAT untreated or treated with 1 µM CL316,243 for 6 h (n = 6 technical replicates from 2 independent experiments). **(D),** imBAT treated with DMSO (control), 100 nM epoxomicin, 100 nM MG132 or 100 nM bortezomib for 6 h (n = 6 technical replicates from 2 independent experiments). Throughout, data are mean ± SEM. *P_{adj} < 0.05, **P_{adj} < 0.01, ***P_{adj} < 0.001, ****P_{adj} < 0.0001 by two-way ANOVA with Bonferroni *post-hoc* test **(A–D)**. n.d., not detected; SCAT, subcutaneous white adipose tissue; GWAT, gonadal white adipose tissue.

(**Figure 4A**). Other stress markers related to accumulation of misfolded proteins or ER stress such as *Atf4*, *Atf6* and s*Xbp1* were unchanged and *Hspa5* was only higher in the triple knockdown condition. Another important player for brown fat proteostasis is the transcription factor *Nfe2l1*, which activates the transcription of proteasomal subunits in a bounce-back-mechanism in response to proteasomal inhibition and cold (4). It is conceivable that *Nfe2l1* counteracts accumulation of misfolded proteins and ER stress as a consequence of diminished *Ubqln* expression through increased proteasome formation. However, we neither observed differences in *Nfe2l1* expression nor in the expression of two of its downstream targets *Psma1* and *Psmb1*. We also tested whether, the induction of *Atf3* in response to *Ubqln* knockdown was mediated by *Nfe2l1*, but *Atf3* expression was unchanged by *Ubqln* triple knockdown in combination with Nfe2l1 knockdown (**Supplementary Figure 4**). In line with these findings, single *Ubqln* knockdown (**Supplementary Figure 5**) or triple *Ubqln* knockdown neither affected the levels of ubiquitinated proteins nor Nfe2l1 protein levels, neither under basal conditions nor after proteasome inhibition (**Figure 4B**). Triple knockdown did also not result in lower proteasomal activity (**Figure 4C**). Thus, ubiquilins are dispensable to maintain proteostasis in brown adipocytes under basal and proteasome inhibited conditions and their absence is not linked to Nfe2l1 activation.

DISCUSSION

The adaptation to sustained cold is a challenging process for thermogenic adipocytes. These cells undergo extensive remodeling for enhanced and sustainable oxidative metabolism, which involves the synthesis of new proteins, lipids and entire organelles (2). We have previously shown that this process requires enhanced proteasomal protein quality control, transcriptionally mediated by Nfe2l1 (4). However, even with increased proteasomal degradation, cold adaptation still results in increased protein ubiquitination (4). The mechanisms dynamically coupling ubiquitination of proteins to proteasomal degradation in brown adipocytes remain elusive. Here, we investigated the role of ubiquilins for proteostasis and NST in brown adipocytes.

Ubiquilins are multifaceted shuttling proteins, which have an amino-terminal UBL and a carboxy-terminal UBA domain, which enable them to interact with both mono- and poly-ubiquitinated cargo as well as facilitate their degradation through the UPS. This

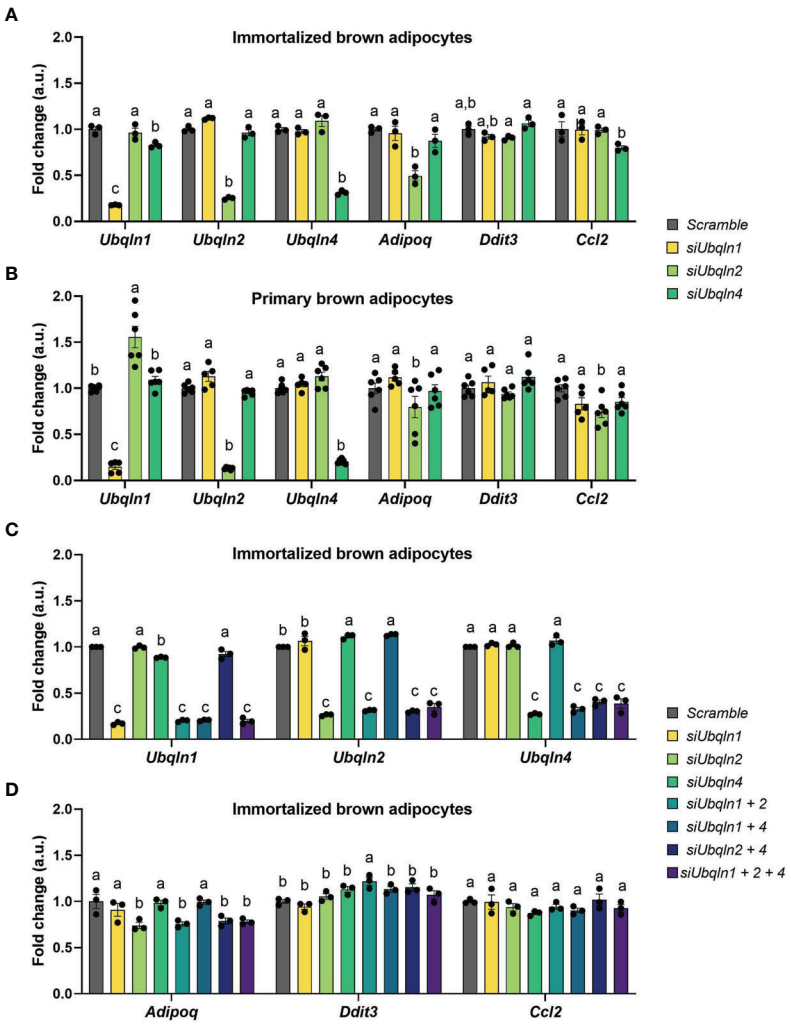

FIGURE 2 | Silencing of *Ubqln1, 2 and 4* in brown adipocytes does not cause ER stress or inflammation. Ubiquilins were silenced by siRNA-mediated knockdown in imBAT and primary brown adipocytes. Relative gene expression measured by qPCR in: **(A)**, imBAT (*n* = 3 technical replicates). **(B)**, primary brown adipocytes (*n* = 5-6 technical replicates from 2 independent experiments). **(C, D),** imBAT (n = 3 technical replicates). Throughout, data are mean ± SEM. Statistical testing was done by two-way ANOVA with Bonferroni post-hoc test. Different small letters indicate differences in mean compared to *Scramble* with at least $P_{adj} < 0.05$.

role seems to be their predominant function, as it is conserved from yeast to humans (10). We show that *Ubqln1, 2* and *4* are highly expressed in BAT and that their expression, most notably of *Ubqln1* is induced by cold and proteasomal inhibition. *Ubqln1*, *2* and *4* are highly homologous and share a similar domain structure. It is therefore likely that they share similar functions and might compensate for the loss of each other (13). However, silencing of one or the combination of ubiquilins by RNAi did neither impact ubiquitin levels nor proteasomal activity under basal conditions or after treatment with proteasome inhibitors. Consequently, except for mildly upregulated expression of *Atf3*, a stress marker in response to various physiological stressors, no changes in ER stress or inflammation were observed under these conditions.

We could speculate that *Nfe2l1* as the major regulator of proteostasis in brown adipocytes, is involved in upregulation of *Atf3* upon knockdown of ubiquilins. However, we did not investigate this in an epistasis-type of experiment, since we did not find any changes in Nfe2l1 gene and protein expression. Another limitation of this study is that we only silenced *Ubqln1*, *2* and *4* by RNAi. Presumably, knockout of one or all ubiquilins would have a stronger effect on proteostasis and NST. In mice, transgenic knockout of *Ubqln1* in neurons aggravated brain injury and delayed functional recovery after ischemic stroke. Ubiquitous overexpression of *Ubqln1*, however, resulted in reduced neuronal damage (14). Similarly, cardiomyocyte-specific knockout of *Ubqln1* in a mouse model of myocardial ischemia-reperfusion injury resulted in enlarged infarct size and late-onset cardiomyopathy, whereas overexpression of *Ubqln1* resulted in reduced infarct size (15). Moreover, in humans, mutations in *Ubqln1, 2* and *4* are strongly associated with the onset of neurodegenerative diseases

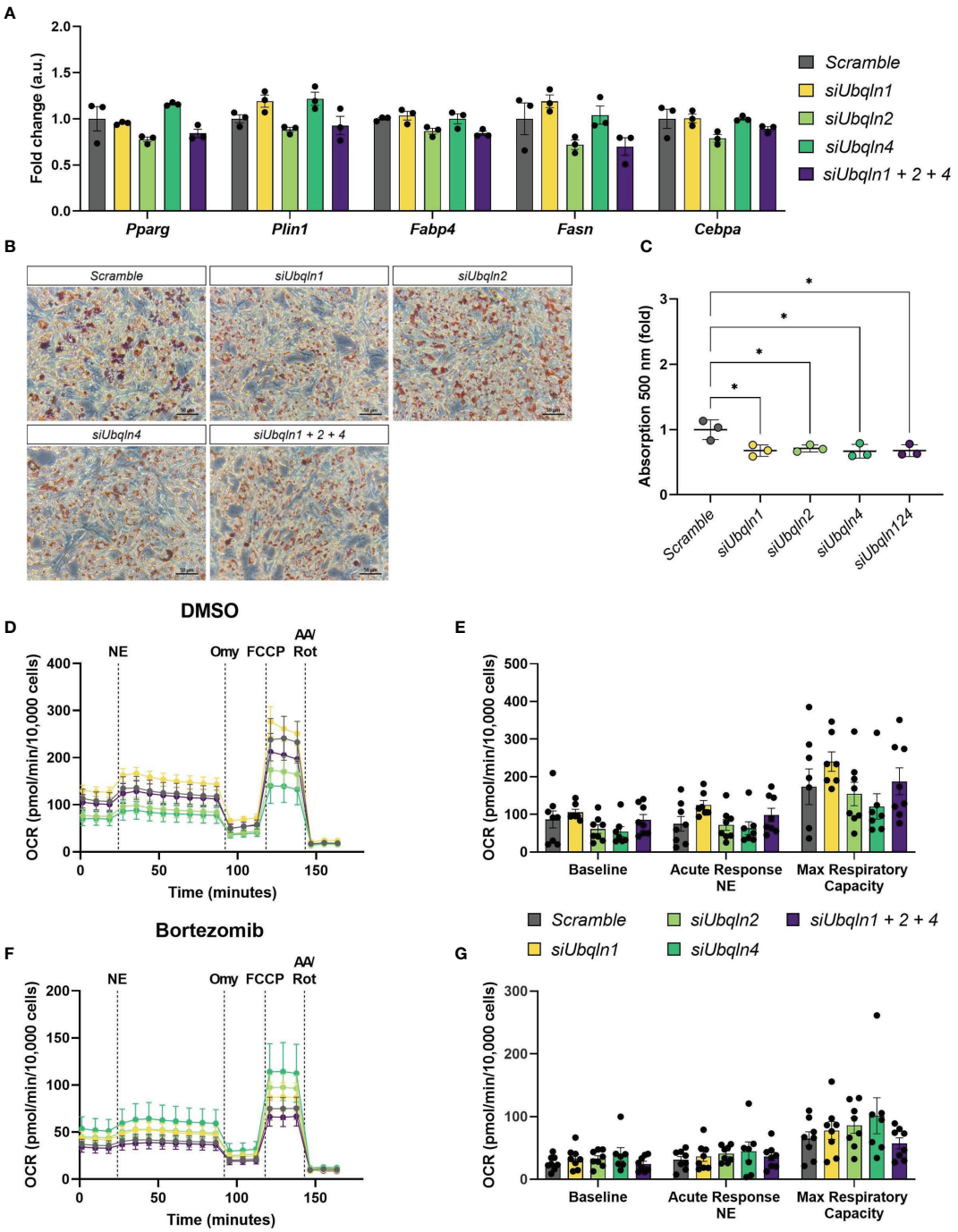

FIGURE 3 | Silencing of *Ubqln1, 2 and 4* lowers lipid content but does not impair adipocyte health. Ubiquilins were silenced by siRNA-mediated knockdown in imBAT. **(A)**, Relative gene expression measured by qPCR (n = 3 technical replicates mean ± SEM). **(B, C)**, Oil red O staining and quantification. **(D, E),** Oxygen consumption rate (OCR) of imBAT treated with DMSO (control) or **(F, G)**, 100 nM bortezomib for 6 h. Data are mean ± SEM. (n = 7-8 technical replicates of 2 independent experiments). *P_{adj}<0.05, **P_{adj} < 0.01, ***P_{adj} < 0.001, ****P_{adj} < 0.0001 by two-way ANOVA *versus Scramble* with Bonferroni post-hoc test **(A, C, E, G)**.

such as dementia, Alzheimer's disease and amyotrophic lateral sclerosis (12, 16–18). These data strongly suggest that impairment or loss of function of ubiquilins are associated with numerous pathologies in both humans and rodents.

In Drosophila loss of Ubqn, the homologue of mammalian ubiquilins, results in ER expansion and activation of the PKR-like ER kinase (PERK) pathway, one branch of the unfolded protein response (5). According to our original hypothesis that

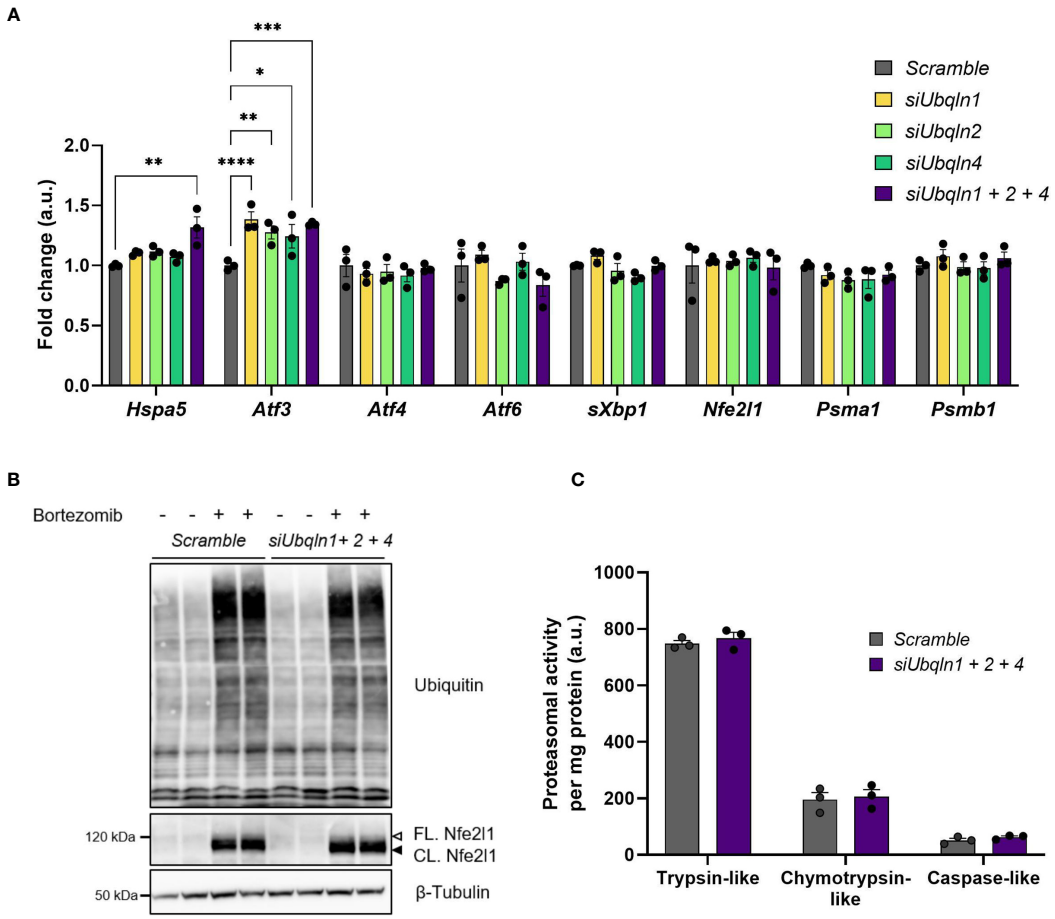

FIGURE 4 | *Ubqln1, 2 and 4* are not required for maintaining proteostasis in brown adipocytes. Ubiquilins were silenced by siRNA-mediated knockdown in imBAT. **(A)**, Relative gene expression measured by qPCR (n = 3 technical replicates mean ± SEM). *P_{adj} < 0.05, **P_{adj} < 0.01 and ***P_{adj} < 0.001 by one-way ANOVA with Bonferroni post-hoc test. **(B),** Representative ubiquitin immunoblot, imBAT treated with DMSO (control) or 100 nM bortezomib for 6 h (n = 2 technical replicates, representative blot of 2 independent experiments). **(C)**, Proteasomal activity (n = 3 technical replicates, mean ± SEM). *P_{adj} < 0.05, ***P_{adj} < 0.001 by one-way **(A)** or two-way **(D)** ANOVA *versus Scramble* with Bonferroni post-hoc test **(A, C)**.

ubiquilins might be involved in ubiquitination of proteins and their proteasomal degradation during NST, we measured norepinephrine-induced respiration but NST was intact despite the loss of ubiquilins. However, we found reduced lipid content compared to control cells. Lipogenesis and lipid droplet biosynthesis takes place in the ER and ER stress, even if driven by proteotoxic stressors disrupt lipid homeostasis (3). In light of the absence of overt ER stress upon loss of ubiquilins, the changes in lipid content point to a more specific role of ubiquilins in lipid metabolism beyond proteostasis. While this warrants further investigation, we did not observe any functional change in NST.

Yeast has only one ubiquilin isoform Dsk2, but other UBL/UBA proteins such as Rad23. None of these individual proteins are essential in yeast, but combined loss of Rad23, Dsk2 and the proteasome ubiquitin receptor Rpn10/S5a results in mitotic arrest (19). This suggests that, at least in yeast, UBL/UBA proteins are redundant and may have overlapping substrate specificity. In future, it will be important finding those UBL/UBA proteins that participate in ubiquitination in brown adipocytes. In summary, in this study, we investigated the role of ubiquilins for brown adipocyte proteostasis and thermogenesis. We found that despite high expression levels of *Ubqln 1, 2* and *4*, these ubiquilins are only minor regulators of brown adipocyte function.

DATA AVAILABILITY STATEMENT

The raw data supporting the conclusions of this article will be made available by the authors, without undue reservation.

ETHICS STATEMENT

The animal study was reviewed and approved by Government of Upper Bavaria, Germany (ROB-55.2-2532.Vet_02-20-32).

AUTHOR CONTRIBUTIONS

CM performed experiments and analyzed data. SK provided samples and assisted with experiments. CM and AB conceptually designed the study, interpreted the data and wrote the manuscript. All authors contributed to the article and approved the submitted version.

FUNDING

AB and this work was supported by the Deutsche Forschungsgemeinschaft Sonderforschungsbereich 1123 (B10), the Deutsches Zentrum für Herz-Kreislauf-Forschung Junior Research Group Grant, and the European Research Council Starting Grant Proteofit.

ACKNOWLEDGMENTS

We thank the members of Bartelt Lab for the enjoyable atmosphere and stimulating discussions. The authors thank Maude Giroud for technical advice, Sajjad Khani for sharing R codes, and Nienke Willemsen for critically reading the manuscript. We thank Siegfried Ussar for providing the immortalized brown preadipocyte cell line.

SUPPLEMENTARY MATERIAL

The Supplementary Material for this article can be found online at: https://www.frontiersin.org/articles/10.3389/fendo.2021.739021/full#supplementary-material

REFERENCES

1. Cannon B, Nedergaard J. Brown Adipose Tissue: Function and Physiological Significance. *Physiol Rev* (2004) 84:277–359. doi: 10.1152/physrev.00015.2003
2. Bartelt A, Widenmaier SB. Proteostasis in Thermogenesis and Obesity. *Biol Chem* (2020) 401:1019–30. doi: 10.1515/hsz-2019-0427
3. Lemmer IL, Willemsen N, Hilal N, Bartelt A. A Guide to Understanding Endoplasmic Reticulum Stress in Metabolic Disorders. *Mol Metab* (2021) 47:101169. doi: 10.1016/j.molmet.2021.101169
4. Bartelt A, Widenmaier SB, Schlein C, Johann K, Goncalves RLS, Eguchi K, et al. Brown Adipose Tissue Thermogenic Adaptation Requires Nrf1-Mediated Proteasomal Activity. *Nat Med* (2018) 24:292–303. doi: 10.1038/nm.4481
5. Şentürk M, Lin G, Zuo Z, Mao D, Watson E, Mikos AG, et al. Ubiquilins Regulate Autophagic Flux Through mTOR Signalling and Lysosomal Acidification. *Nat Cell Biol* (2019) 21:384–96. doi: 10.1038/s41556-019-0281-x
6. Lim PJ, Danner R, Liang J, Doong H, Harman C, Srinivasan D, et al. Ubiquilin and P97/VCP Bind Erasin, Forming a Complex Involved in ERAD. *J Cell Biol* (2009) 187:201–17. doi: 10.1083/jcb.200903024
7. Hjerpe R, Bett JS, Keuss MJ, Solovyova A, McWilliams TG, Johnson C, et al. UBQLN2 Mediates Autophagy-Independent Protein Aggregate Clearance by the Proteasome. *Cell* (2016) 166:935–49. doi: 10.1016/j.cell.2016.07.001
8. Yuan S, Swiggin HM, Zheng H, Yan W. A Testis-Specific Gene, *Ubqlnl*, Is Dispensable for Mouse Embryonic Development and Spermatogenesis. *Mol Reprod Dev* (2015) 82:408–9. doi: 10.1002/mrd.22504
9. Conklin D, Holderman S, Whitmore TE, Maurer M, Feldhaus AL. Molecular Cloning, Chromosome Mapping and Characterization of UBQLN3 a Testis-Specific Gene That Contains an Ubiquitin-Like Domain. *Gene* (2000) 249:91–8. doi: 10.1016/S0378-1119(00)00122-0
10. Zheng T, Yang Y, Castañeda CA. Structure, Dynamics and Functions of UBQLNs: At the Crossroads of Protein Quality Control Machinery. *Biochem J* (2020) 477:3471–97. doi: 10.1042/BCJ20190497
11. Pramme-Steinwachs I, Jastroch M, Ussar S. Extracellular Calcium Modulates Brown Adipocyte Differentiation and Identity. *Sci Rep* (2017) 7:1–10. doi: 10.1038/s41598-017-09025-3
12. Deng HX, Chen W, Hong ST, Boycott KM, Gorrie GH, Siddique N, et al. Mutations in UBQLN2 Cause Dominant X-Linked Juvenile and Adult-Onset ALS and ALS/Dementia. *Nature* (2011) 477:211–5. doi: 10.1038/nature10353
13. Madsen L, Schulze A, Seeger M, Hartmann-Petersen R. Ubiquitin Domain Proteins in Disease. *BMC Biochem* (2007) 8. doi: 10.1186/1471-2091-8-S1-S1
14. Liu Y, Lü L, Hettinger CL, Dong G, Zhang D, Rezvani K, et al. Ubiquilin-1 Protects Cells From Oxidative Stress and Ischemic Stroke Caused Tissue Injury in Mice. *J Neurosci* (2014) 34:2813–21. doi: 10.1523/JNEUROSCI.3541-13.2014
15. Hu C, Tian Y, Xu H, Pan B, Terpstra EM, Wu P, et al. Inadequate Ubiquitination-Proteasome Coupling Contributes to Myocardial Ischemia-Reperfusion Injury. *J Clin Invest* (2018) 128:5294–306. doi: 10.1172/JCI98287
16. Bertram L, Hiltunen M, Parkinson M, Ingelsson M, Lange C, Ramasamy K, et al. Family-Based Association Between Alzheimer's Disease and Variants in UBQLN1. *N Engl J Med* (2005) 352:884–94. doi: 10.1056/NEJMoa042765
17. Renaud L, Picher-Martel V, Codron P, Julien JP. Key Role of UBQLN2 in Pathogenesis of Amyotrophic Lateral Sclerosis and Frontotemporal Dementia. *Acta Neuropathol Commun* (2019) 7:1–11. doi: 10.1186/s40478-019-0758-7
18. Halloran M, Ragagnin AMG, Vidal M, Parakh S, Yang S, Heng B, et al. Amyotrophic Lateral Sclerosis-Linked UBQLN2 Mutants Inhibit Endoplasmic Reticulum to Golgi Transport, Leading to Golgi Fragmentation and ER Stress. *Cell Mol Life Sci* (2020) 77:3859–73. doi: 10.1007/s00018-019-03394-w
19. Wilkinson CRM, Seeger M, Hartmann-Petersen R, Stone M, Wallace M, Semple C, et al. Proteins Containing the UBA Domain are Able to Bind to Multi-Ubiquitin Chains. *Nat Cell Biol* (2001) 3:939–43. doi: 10.1038/ncb1001-939

Conflict of Interest: The authors declare that the research was conducted in the absence of any commercial or financial relationships that could be construed as a potential conflict of interest.

Publisher's Note: All claims expressed in this article are solely those of the authors and do not necessarily represent those of their affiliated organizations, or those of the publisher, the editors and the reviewers. Any product that may be evaluated in this article, or claim that may be made by its manufacturer, is not guaranteed or endorsed by the publisher.

Advantages of publishing in Frontiers

OPEN ACCESS
Articles are free to read for greatest visibility and readership

FAST PUBLICATION
Around 90 days from submission to decision

HIGH QUALITY PEER-REVIEW
Rigorous, collaborative, and constructive peer-review

TRANSPARENT PEER-REVIEW
Editors and reviewers acknowledged by name on published articles

Frontiers
Avenue du Tribunal-Fédéral 34
1005 Lausanne | Switzerland

Visit us: www.frontiersin.org
Contact us: frontiersin.org/about/contact

REPRODUCIBILITY OF RESEARCH
Support open data and methods to enhance research reproducibility

DIGITAL PUBLISHING
Articles designed for optimal readership across devices

FOLLOW US
@frontiersin

IMPACT METRICS
Advanced article metrics track visibility across digital media

EXTENSIVE PROMOTION
Marketing and promotion of impactful research

LOOP RESEARCH NETWORK
Our network increases your article's readership